Small-molecule induced degradation of fascin as a strategy for metastasis prevention

Sarah Memarzadeh

Thesis submitted in fulfilment of the requirements

for the degree of Doctor of Philosophy.

School of Chemistry

College of Science and Engineering

University of Glasgow

January 2022

Abstract

The risk of being diagnosed with cancer during our lifetime is estimated to be around 50%, and – although survival rates have vastly improved over the last few decades – cancer remains the second leading cause of death worldwide. Metastasis, the ability of cancer cells to spread and colonise throughout the body, is the major contributor to cancer mortality. Identification of suitable targets for the development of anti-metastatic therapeutics is challenging due to the complex nature of the metastatic process. Cancer cell motility and formation of invasive actin structures are vital for a multitude of steps in this metastatic cascade. The actin-bundling protein fascin has been found to be crucial for the formation of those invasive membrane protrusions and its expression correlates with aggressive metastatic cancers, however, fascin is not found in healthy epithelial tissue. Despite representing an attractive target, disruption of protein–protein interactions of structural proteins with traditional small-molecule drugs remains a difficult task in drug discovery. Therefore, this project aims at overcoming this challenge by recruiting the cell's natural protein degradation mechanism to the scaffold protein in order to induce its targeted degradation by means of proteolysis-targeting chimeras (PROTACs). Selective degradation of the pro-metastatic target could impede assembly of invasive membrane protrusions, reduce invasiveness of cancer cells and thereby prevent formation of metastases.

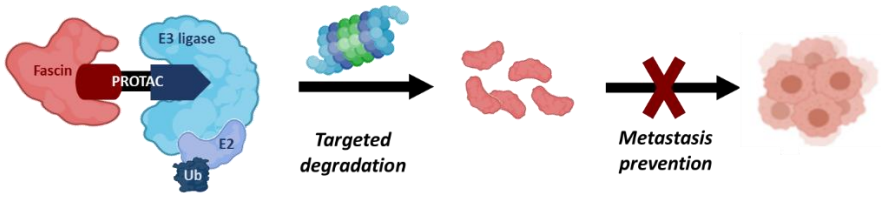

Chapter 1 discusses the process of metastasis and the role of cancer cell motility in the metastatic cascade. It goes on to describe actin-based cell membrane protrusions implicated with cell migration and invasion, and fascin's involvement in the formation of invasive actin structures and cancer cell metastasis. Drug discovery efforts to develop a small molecule capable of inhibiting the actin-bundling activity of fascin are mentioned. The second part of Chapter 1 details the mechanisms behind cellular protein degradation and how it can be exploited therapeutically using PROTACs. Considerations to be taken into account when designing bi-functional degrader molecules are explained, and evaluation of

physicochemical properties of PROTACs are discussed. The last part of Chapter 1 briefly summarises the project's aims and hypotheses.

Chapter 2 describes the development of a HaloTag-based model system used to prove the concept for targeted protein degradation of fascin. The first part of Chapter 2 reports the modular design and synthesis of active compounds and mono-functional controls. The second part of Chapter 2 details biological assays used to determine compound activity as well as experiments assessing the effect on cell function and phenotype, emphasising the importance of using cell lines suitable for evaluating proposed outcomes.

Chapter 3 details the design and synthesis of three series of fascin-targeting PROTACs based on different fascin ligands, as well as evaluation of physicochemical properties of the degrader molecules. The second part of Chapter 3 describes biological assays carried out to test activity of the compounds in different cell lines and their binding to fascin. It highlights difficulties encountered with cell permeability and attempted strategies to overcome these challenges.

Chapter 4 concludes on the findings of the PhD project and proposes future work to be carried out.

Chapter 5 describes experimental protocols for the biological and chemical components of this project.

The appendix contains compound characterisation data as well as supplementary experimental data for biological experiments.

Table of contents

Acknowledgements

I would thank Dr David France for giving me the opportunity to join his research group and his invaluable assistance with all aspects of this multifaceted project. Thank you for all your support – in science as in life, for being an amazing mentor and for keeping me happy and sane with wisdom and beer.

I would also like to thank Prof Laura Machesky for giving me the chance to carry out the biological work for this project in her lab and for her advice on the cancer science part of this research. I am very grateful for the assistance on the medicinal chemistry aspects of this project I received from Prof Justin Bower, Charlie Parry and Stuart Francis. Thank you also to Dr Nikki Paul for the support in the lab and for providing microscopy images for this thesis. In addition, would like to thank Dr Jamie Whitelaw for assisting me with CRIPSR; Dr Anh Le for his help with the wound healing assays; Dr Katie Pollock for the SPR experiments and Dr Claire Wilson for X-ray crystallography carried out for this project. I would like to extend my appreciation to the support staff at the School of Chemistry, in particular Analytical Services and Stores, as well as Central Services at the Beatson.
I would also like to express my gratitude to Cancer Research UK for having given me the opportunity to carry out this research by funding my project.

A big thank you also goes to my fellow France Group companions: Stuart for being a great teacher and an even greater inventor of useful lab gadgets; Glen for enduring my love for order in the lab and a somewhat intrusive bike trip; Claire for the freezing of stress-relief equipment and emer-ghers; Lorna for silly Tuesdays and scrolly-rollies; Liam for all the support as the more senior PostDoc and for lab art exhibitions; Chara for sharing the pain of yeast-infested cells; Charlotte for being accepting of my vial-geddon; Anna, Skye, Anusha, Mirjam and Jane for being great students. Thank you to the Henderson lab family for making the lab so enjoyable: ma chère poo-poule Albane for sharing tout le fish&chips&cheese and bacon roooooolls avec moi; Gregor for all the Pintlis in the Publi and an unforgettable Onesie-Christmas; Arwa for giving me cookies when I burn mine in the microwave and for making sure I'm comfy; Myron and Venky for being the best late-night and weird-hours team; old-people-club member Alistair for being a great convenor for all two-wheel-related issues, no matter the time; Mikey P, Jim, Angus, Dan, Jess, Jimy,

Hibah, Sophie, Justin, Emily, New Jess, Matt 1 and Matt 2. I am grateful for everyone who made life in Jo Black so much more bearable: Selma for being the best co-parent to our Salamander boy; Jake for scaring me in the lab late at night and for all the crust; Alin for countless coffees together and the rest of the smoking team Laura, Tom, Bart, Mike and Michele.

I'd also like to thank my second lab family at the Beatson for adopting me and answering all my weird chemist questions: Nikki for teaching a chemist how to "do biology", patiently explaining the bio world to me and proof-reading half of my thesis; Anh for showing me the torture device and bubble tea; Dr S for endless blotting madness together; Peggy, Pete, Hakem and Elaine for companionship at random hours in the lab; Savvas for sharing bench and gels with me; Heather, Amelie, Jamie, James, Sonia, Sophie and Dominika.

I am also very thankful for everyone who made me feel at home in Glasgow: Annie & Pete for making Shields Road my home; Olgui & Isabella for being the best viudas negras and for all the kitchen table reunions; Norma & Rachel for being amazing flatmates; Chris, Michal, Ian & Lou and Sarah & Dave for all the crazy adventures together.
Ein riesiges Dankeschön to Sonieta, Virgi, Roxi, Nilsi, Jule, Alex, Silke and Caro for believing in me and providing me with support and supplies from Germany, and giving me shelter when I was on Heimaturlaub.

I would also like to thank my parents for supporting me in whichever path I choose to take. Thank you for being there for me, for inspiring me and for making me the person I am. Samira, thank you for being my amazing little big sister and for giving me a different perspective on life – I am so proud of you.

And the biggest thanks of all deserves Falk, for his endless support, his unconditional love and all the beers. Thank you for being you and for being in my life – I could not have done this without you.

This thesis is dedicated to

Tante Anneliese

(16. January 1946 – 29. May 2019)

Author's declaration

This thesis represents the original work of Sarah Memarzadeh, unless otherwise explicitly stated in the text. The research was conducted at the University of Glasgow, either within the School of Chemistry in the Henderson and Chemical Biology Labs under the supervision of Dr David France, or at the Beatson Institute for Cancer Research in the R02 Lab under the supervision of Prof Laura Machesky. Research was conducted during the period of October 2017 to December 2021.

List of abbreviations

Abbreviations and acronyms used in this thesis are in agreement with the standard list of abbreviations and acronyms published by The Journal of Organic Chemistry. Non-standard abbreviations and acronyms used in this thesis are listed here.

2D	two-dimensional
3D	three-dimensional
BSA	bovine serum albumin
BRET	bioluminescent resonance energy transfer
bRo5	beyond rule-of-5
BRSM	based on recovered starting material
CDC	cholesterol-dependent cytolysin
CDI	*N,N'*-carbonyldiimidazole
cLogP	calculated partition coefficient
CRBN	cereblon
CRISPR	clustered regularly interspaced short palindromic repeats
Ctrl	control
CuAAC	copper-catalysed azide–alkyne cycloaddition
Da	Dalton
DegS	degradation score
DIPEA	*N,N'*-diisopropylethylamine
DMEM	Dulbecco's Modified Eagle Medium
DMFDMA	*N,N*-dimethylformamide dimethyl acetal
DMP	Dess–Martin periodinane
ds	double-stranded
ECM	extracellular matrix
EDC	1-ethyl-3-(3-dimethylaminopropyl)carbodiimide
EMT	epithelial–mesenchymal transition
FACS	fluorescence-activated cell sorting
FCS	foetal calf serum

FDA	Food and Drug Administration
FSCN	fascin
GAPDH	glyceraldehyde 3-phosphate dehydrogenase
GDN	glycodiosgenin
GFP	green fluorescent protein
gRNA	guide RNA
HATU	hexafluorophosphate azabenzotriazole tetramethyl uronium
HBA	hydrogen bond acceptor
HBD	hydrogen bond donor
HIF1α	hypoxia-inducible factor 1α
His	histidine
HIV-1	human immunodeficiency virus-1
HOAt	1-hydroxy-7-azabenzotriazole
HOBt	1-hydroxybenzotriazole
HP	HaloPROTAC
HSP	heat shock protein
HTL	HaloTag ligand
HyT	hydrophobic tag
Hyp	hydroxyproline
IAP	inhibitor of apoptosis
IC_{50}	half-maximal inhibitory concentration
IgG	immunoglobulin G
ITC	isothermal titration calorimetry
K_D	dissociation constant
KO	knock-out
k_{off}	rate of dissociation
k_{on}	rate of association
LB	Luria broth
LCMS	liquid chromatography–mass spectrometry
LC/MS/MS	liquid chromatography/tandem mass spectrometry
LiHMDS	lithium bis(trimethylsilyl)amide
LLS	longest linear sequence
logP	partition coefficient

MDM2	mouse double minute-2
MET	mesenchymal–epithelial transition
MMP	matrix metalloprotease
MOPS	4-morpholinepropanesulfonic acid
MT	microtubule
MW	molecular weight
NB	not binding
NMI	*N*-methylimidazole
NRotB	number of rotatable bonds
ns	not significant
PAM	protospacer adjacent motif
PAMPA	parallel artificial membrane permeability assay
PBS	phosphate buffered saline
PCR	polymerase chain reaction
PDB	Protein Data Bank
PE	PBS-EDTA
PEG	polyethylene glycol
PenStrep	Penicillin Streptomycin
PFA	paraformaldehyde
P-gp	P-glycoprotein
Phe	phenylalanine
POI	protein of interest
PPI	protein–protein interaction
PROTAC	proteolysis-targeting chimera
RISC	RNA-inducing silencing complex
RIPA	radioimmuno-precipitation assay
RNAi	RNA interference
Ro5	rule-of-5
RP-HPLC	reverse-phase high-performance liquid chromatography
RSB	reducing sample buffer
SDS	sodium dodecyl sulfate
SDS–PAGE	sodium dodecyl sulfate–polyacrylamide gel electrophoresis
SEM	standard error of the mean

SFM	serum-free medium
siRNA	small interfering RNA, silencing RNA
SLO	streptolysin O
S_NAr	nucleophilic aromatic substitution
SOC	super optimal broth
SPR	surface plasmon resonance
$t_{1/2}$	half-life
T3P	propanephosphonic acid anhydride
TAE	tris-acetate-EDTA
TBS-T	tris-buffered saline with Tween20
TCFH	chloro-*N,N,N',N'*-tetramethylformamidinium hexafluorophosphate
tPSA	topological polar surface area
t_R	retention time
Ub	ubiquitin
UPS	ubiquitin–proteasome system
VHL	von Hippel–Lindau
WB	western blotting
WT	wild-type

1 Introduction

1.1 Cancer and metastasis

1.1.1 Metastasis as major cause of cancer mortality

During 2019, the year prior to the ongoing COVID-19 pandemic, around 18% of global deaths accounting for 10 million fatalities were attributed to cancer, making it the second leading cause of death worldwide after cardiovascular diseases (Figure 1.1 a).[1,2] What is commonly referred to as cancer comprises of a large group of multifactorial diseases which are characterised by abnormal cell growth and can affect almost any part of the body (Figure 1.1 b).[3]

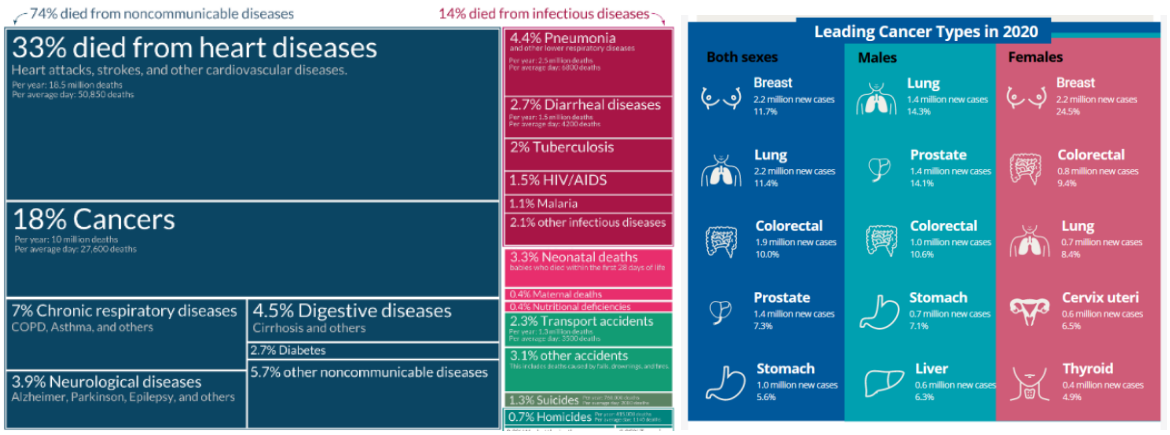

Figure 1.1: a) Global causes of death recorded in 2019[1] and b) leading cancer types in 2020.[4]

It is estimated that around 1 in 2 people will be diagnosed with cancer during their lifetime,[5] however, detection and treatment of cancer have vastly improved over the last decades. Although survival rates vary between different types of cancer, around 50% of all cancer patients across Europe survive for 10 or more years after diagnosis, compared to only 24% of patients 40 years ago.[6] Metastasis, the ability of cancer cells from a primary tumour to invade and colonise at a distal site in the body, is a critical step in cancer progression and represents the primary cause of cancer mortality.[7] Survival rates of cancer patients drop severely for all types of cancer when diagnosed in stage 4, once it has started metastasising (Figure 1.2).

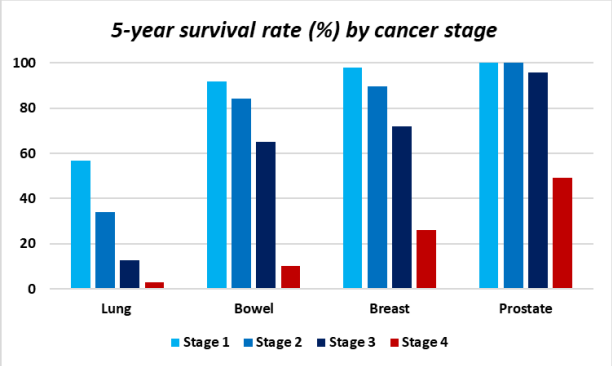

Figure 1.2: 5-year survival rate for cancer patients by stage diagnosed for lung, bowel, breast and prostate cancer.[6]

Despite extensive research efforts aimed at elucidating biological mechanisms behind metastasis and its drivers at molecular level, those efforts have failed to translate into successful therapeutic strategies for treatment and prevention of metastasis.[8-11] This discrepancy is illustrated by an analysis revealing that less than 4% of the annual number of publications about cancer treatment between 1997 and 2017 were associated with anti-metastatic therapeutics (Figure 1.3).[12] In addition, anti-metastatic agents reaching the clinical trial stage run the risk of being perceived as not sufficiently efficient due to regulatory requirement being aimed more at cytotoxic drugs by prioritising decrease in tumour size rather than the ability to prevent formation of metastases.[13,14]

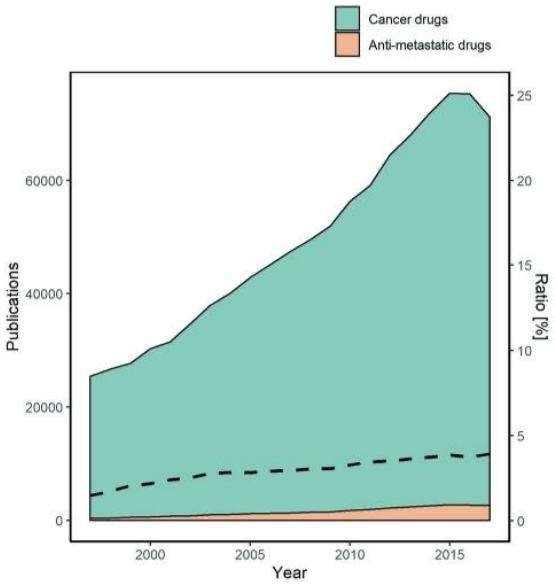

Figure 1.3: Comparison of annual publications associated with cancer drugs vs publications about anti-metastatic drugs (1997–2017).[12]

In search for a suitable therapeutic target great care needs to be taken in order to identify a process common to metastasis, and at the same time not affecting any pathways crucial for healthy cells.[15] This is further complicated by the genetically unstable and heterogeneous nature of metastatic cells, which can possess characteristics of the tissue of the primary tumour site, the invaded tissue as well as properties common to cancer and metastatic cells.[16] Previously, metastasis was thought to only occur in late stages of disease progression, however, there is evidence that cancer cells can also detach early in the development of primary tumours.[8] This emphasises the need for anti-metastatic therapeutics which can be administered in combination with cytotoxic agents. As such cancer growth can be inhibited at the same time as preventing metastasis, in order to improve survival rates of patients suffering from metastatic diseases.[17,18]

1.1.2 Metastatic cascade

The metastatic cascade describes the complex process by which cancer cells disseminate from the primary tumour into the adjacent tissue, travel through the circulatory or lymphatic system to then colonise at a distal site in the body, forming a secondary tumour (Figure 1.4).[3] Many interdependent mechanisms are at play during metastasis: For cancer cells to be able to detach from the primary tumour (Figure 1.4 a), cells undergo epithelial–mesenchymal transition (EMT), a process during which characteristics of adherent (epithelial) cells are lost and stem cell (mesenchymal)-like properties are acquired.[8] As a result of this transition, cancer cells gain the ability to dissociate from neighbouring cells and the extracellular matrix (ECM) and develop structural features allowing for degradation of the surrounding tissue and invasion through the matrix away from the primary tumour (Figure 1.4 b).[10] Invasion into connective tissue and the basement membrane, which acts as a mechanical barrier between the blood and lymphatic vessels, can either be achieved by individual cells or by cell clusters with cells at the leading edges “paving the way” for the trailing cell cohort.[10] Once intravasation into the blood or lymphatic system is achieved, cells circulate throughout the body (Figure 1.4 c and d). However, circulation is highly inefficient and therefore rate-limiting for the formation of metastases: Of millions of cells disseminated from the primary tumour entering the blood or lymphatic vessels, only about 0.01% are successful in surviving and colonising at a distal site.[17] Upon dissociation from the matrix, circulatory cells are not able to facilitate intercellular communication essential for their growth and survival, which could lead to anoikis, programmed cell death upon loss

of cell–matrix interactions.[18] In addition, hydrostatic shear forces of the circulatory system as well as recognition and elimination by components of the immune system pose further challenges circulating cancer cells need to withstand.[10] However, by adhering to healthy cells, such as platelets, cancer cells can evade detection.[19] This interaction with platelets is also thought to aid in the initial adhering of cancer cells to the walls of the vascular system, a process necessary for extravasation out of the circulatory system (Figure 1.4 e).[18] Upon successful extravasation, colonisation in the surrounding tissue requires cancer cells to undergo mesenchymal–epithelial transition (MET) to revert to a more adherent phenotype (Figure 1.4 f). The regained ability to interact with the surrounding tissue and neighbouring cells activates cell proliferation and survival pathways essential for metastasis growth.[10]

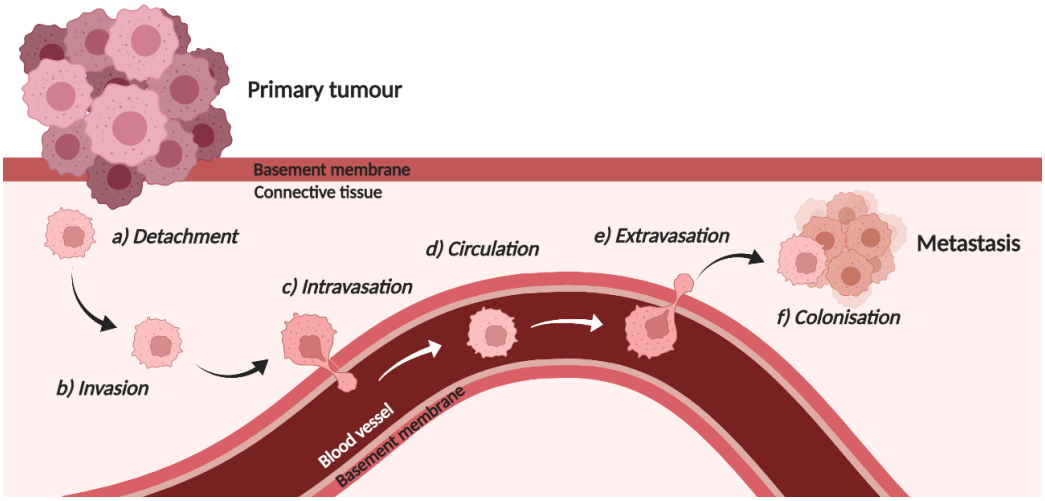

Figure 1.4: Metastatic cascade: a) Detachment of cancer cell from primary tumour, b) invasion into surrounding tissue, c) intravasation into circulatory system, d) circulation through body, e) extravasation and f) colonisation to form metastasis - adapted from [9].

Although the metastatic cascade is a complex process, and interdependencies between the different stages are not yet fully elucidated, cell migration and invasion are key to multiple steps in metastasis. Similar cellular motility and functional transition processes can be observed for physiological activities, such as embryogenesis, wound healing and inflammation, indicating tumour cell invasion and migration to be regular cellular behaviours occurring in a dysregulated environment.[20-22]

1.1.3 Actin structures in cell migration and invasion

Movement of cancer cells is mediated by the highly dynamic actin cytoskeleton and associated regulatory and structural proteins. Actin forms dynamic fibres (F-actin) through polymerisation of actin monomers (G-actin) at the (+) end of the filament and depolymerisation at the (-) end (Figure 1.5).[23]

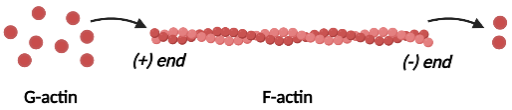

Figure 1.5: Actin polymerisation and depolymerisation.

Whilst non-invasive membrane protrusions (lamellipodia, filopodia and podosomes) are also formed by healthy epithelial cells for cellular processes requiring cellular motility, such as embryonic development and tissue regeneration, metastatic cancer cells additionally develop invasive protrusions (invadopodia). The underlying arrangement of actin filaments by different actin-associated proteins determine the morphology of the membrane protrusions.[24] Lamellipodia (Figure 1.6 a) are localised at the leading edges of cells and mediate cell locomotion and cell spreading by interacting with and attaching to their environment *via* adhesion proteins and pull the cell body forward when migrating. The thin sheet-like protrusions are formed by a mesh of actin filaments. Those highly branched structures are mediated by an actin nucleation protein which attaches to existing mother filaments and promotes formation of daughter filaments at a 70 ° angle.[25] Thinner finger-like structures, filopodia (Figure 1.6 b), can project out from lamellipodia at the leading edges and function as sensory organ detecting external signals like nutrient and chemoattractants.[26] Filopodial protrusions are formed through elongating parallel actin filaments, which are cross-linked by actin-bundling proteins.[27] Podosomes (Figure 1.6 c) are short-lived dot-like actin clusters at the ventral surface. Although little is known about the precise function of podosomes, they are thought to play a role in adhesion and transfer of membrane tension when lamellipodia extend forward.[28] Pathological invadopodia (Figure 1.6 d), which are localised at the ventral side of metastatic cancer cells, are long-lived stiff membrane protrusions capable of penetrating deep into the matrix and degrading surrounding tissue. Their main function is to facilitate invasion through the extracellular matrix by use of matrix metalloprotease (MMP) activity or mechanical force, and are considered to be crucial for several steps in the metastatic cascade.[29]

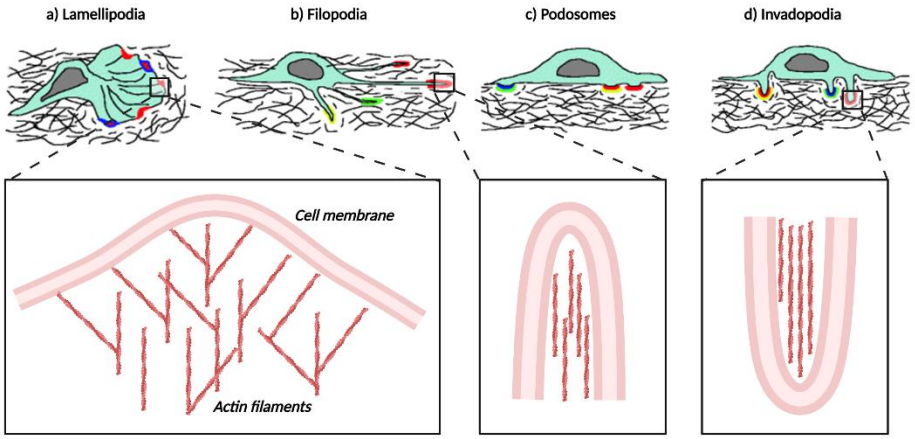

Figure 1.6: Cellular membrane protrusions and underlying actin structures: a) lamellipodia, b) filopodia, c) podosomes and d) invadopodia.[30]

When migrating in response to external stimuli, cancer cells dynamically generate interconvertible actin structures underneath the cell membrane, leading to formation of lamellipodia and filopodia at the leading edge of the cell (Figure 1.7 a). The directional force generated by those structures, together with adhesion of leading cell edges to the cell surroundings, push the cell membrane into a forward direction (Figure 1.7 b). The cell body and the nucleus are then translocated by formation of stress fibres (Figure 1.7 c), before the trailing edge of the cell is pulled forward by retraction fibres (Figure 1.7 d).[26]

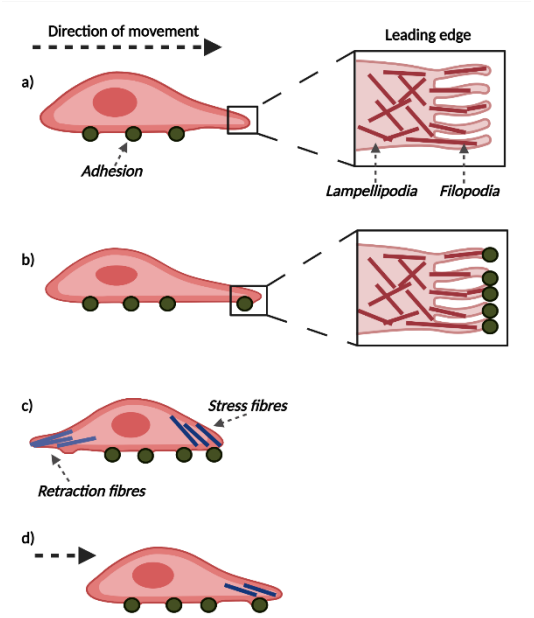

Figure 1.7: Membrane protrusions and actin structures involved in cell migration: a) formation of protrusive structures (lamellipodia and filopodia) at leading edges of cell, b) adhesion of leading edges to surface, c) movement of cell body and nucleus through formation of stress fibres and d) retraction of trailing edge of cell by formation of retraction fibres – adapted from [26].

However, tumour cell invasion occurs in a three-dimensional (3D) environment, requiring cancer cells to move through the surrounding matrix. Metastatic cells achieve this invasive movement in two independent but interconvertible ways of migration, depending on the physical constitution of the surrounding matrix: through mesenchymal motility in stiffer matrices or through amoeboid motility in softer tissue (Figure 1.8 a).[31] Mesenchymal-like cells display a more elongated morphology, which aligns with the direction of movement, and form invasive actin structures, such as invadopodia. The motility is path-generating through MMP-mediated degradation of the surrounding tissue as well as tractile force generated by contractability of the cell's cytoskeleton and adhesion to the matrix.[32] Amoeboid-type motility, on the other hand, is protease-independent. Cells displaying an amoeboid-like morphology are more rounded and deformable, which allows them to squeeze through pores in the surrounding tissue, hence migrating in a path-finding manner (Figure 1.8 b). Due to weaker and more dynamic adhesion to the matrix, cell movement can proceed at a higher speed through amoeboid-type than with mesenchymal-type motility.[33] Changes in matrix environment or in cell functionality, such as inhibition of protease activity, can trigger a transition in phenotype, hence allowing for compensatory escape through morphological plasticity.[34]

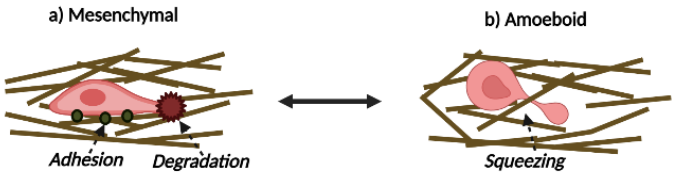

Figure 1.8: Mesenchymal and amoeboid migration – adapted from [32].

Invadopodia are solely found in invasive cancer cells and correlate with increased invasiveness and formation of metastasis. The invasive membrane protrusions drive metastatic spread through their essential function in several processes of the metastatic cascade, namely invasion, intravasation and extravasation.[35] Preventing the formation or inhibiting the function of those structures could impede dissemination of cancer cells throughout the body and colonisation at a distal site.[36] There is a set of components unique to invadopodia and crucial to their formation and function, which represent appealing targets for therapeutic interventions.[37-40] However, identification of a suitable target is far from trivial, which is illustrated by the initially promising strategy of inhibiting invadopodia-specific proteases. After extensive efforts to develop MMP inhibitors and favourable pre-

clinical data, around 50 compounds failed during clinical trials, displaying considerable toxicity due to lack of protease specificity. Instead, the results indicated that inhibition of MMPs could even promote cancer metastasis due to overlapping functions of the proteases.[41] Impeding formation of invadopodia by targeting processes associated with the actin cytoskeleton could be an anti-metastatic strategy alternative to inhibition of the proteolytic function.[42] However, since actin-rich structures are also essential for motile processes in healthy cells, such as inflammation and wound healing, identification of components specific to invadopodia is imperative in order to prevent potential disastrous side effects.[48] The actin-bundling protein, fascin, has been shown to have a unique role in actin cytoskeleton reorganisation and cell motility in invasive tumour cells hence could be a suitable drug target for anti-metastatic therapeutics.[43]

1.1.4 Actin-bundling protein fascin as a potential drug target

Fascins are structural proteins that bind and bundle actin filaments, forming dynamic and stable membrane protrusions and other specialised structures. In mammalian cells, three isoforms of fascin are known: fascin-1 (hereafter called fascin) which has been found to be crucial for invadopodia formation in epithelial cancer cells, retinal fascin-2 which is involved in formation of photoreceptor cells and testis-specific fascin-3 with unknown function in sperm-heads of late-stage spermatozoa.[44] Fascin is only expressed in neuronal and connective tissue during embryonic development when cell motility is important but expression levels in healthy adult epithelial cells are negligible. It is highly upregulated in various types of cancers, and is used as a prognostic marker for metastasis. Expression levels of fascin correlate with aggressive, metastatic cancers exhibiting poor survival prognosis and have been implicated with cancer progression and metastasis.[45]

Fascin is a 55 kD globular protein and consists of four β-trefoil domains.[44] Two domains possess actin-binding sites (Figure 1.9 a), one at the N-terminus and one further towards the C-terminus. Fascin also binds microtubules (MT binding site in Figure 1.9 a) and is thought to contribute to focal adhesion dynamics and cell migration speed.[46] Whilst phosphorylation usually activates protein function and signalling pathways, in the case of fascin, phosphorylation of the N-terminal binding site deactivates actin-binding. This negative regulation by phosphorylation is common to actin-binding proteins.[30] Positively charged arginine and lysine residues in those actin-binding sites interact with negatively

charged actin filaments electrostatically.[47] The interactions can be regulated by mono-ubiquitination at the lysine residues within the actin binding sites, which sterically interferes with actin binding.[48] Binding of actin by fascin is cooperative and the two actin-binding sites are conformationally connected – binding of one actin filament likely stabilises the active configuration of fascin, enhancing binding of another actin filament at the other binding site. Similarly, impairment of one actin binding site leads to a conformational change that disables the other actin binding site.[49] By binding to two adjacent actin filaments, fascin cross-links the filaments, forming rigid parallel bundles (Figure 1.9 b).[46] Bundling of about 10 to 30 actin filaments results in formation of membrane protrusions of about 60 to 200 nm in size (Figure 1.9 c).[49]

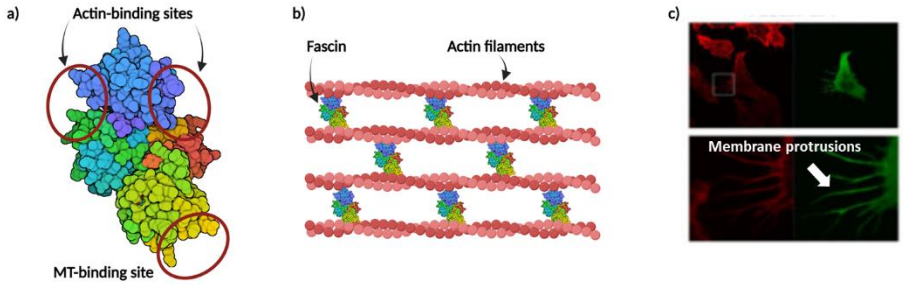

Figure 1.9: a) Fascin structure and actin-binding sites, c) actin cross-linking and c) membrane protrusions formed by GFP-fascin.[47]

In healthy cells, fascin is responsible for the formation of filopodia by cross-linking adjacent actin filaments that allow for cell communication and motility during embryonic development.[50] In cancer cells, this bundling activity plays a crucial role in regulation of adhesion, migration and invasion by formation of filopodia as well as invadopodia. Fascin has been found to be particularly stable and exchange more slowly at invadopodia compared to other actin-based membrane protrusions, hence result in more stable structures capable of invading through the ECM.[51] Knock-down of fascin resulted in cells forming fewer, smaller and more short-lived invadopodia, indicating that fascin is vital for invadopodia numbers and size, as well as their stability and lifetime.[29] Non-cancerous epithelial cells transfected with fascin developed spikey membrane protrusions and reduced cell–cell contact was observed (Figure 1.10 a), whereas fascin-deficient cells exhibited a more rounded morphology with a smooth surface, and clustering of cells (Figure 1.10 b). Fascin-transfected cells also show greatly enhanced motility compared to their fascin-deficient counterparts.[43] Similarly, overexpression of fascin in fascin-negative cancer cells augments their motility and ability to metastasise.[44] It has been shown that

cancer cells acquire fascin during EMT, allowing them to change their morphology and increase motility and invasiveness.[52]

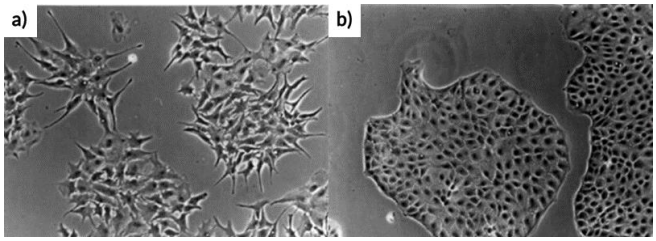

Figure 1.10: Pig kidney epithelial cells: a) transfected with fascin and b) fascin-deficient.[43]

Fascin expression levels are negligible in non-cancerous adult cells and genetic knock-down experiments have not been reported to cause significant growth or survival defects. Moreover, fascin was shown to have a key role in cell motility and adhesion in invasive cancer cells, and inhibition of its actin-bundling activity causes a dramatic decrease in formation of invadopodia and reduction in tumour cell invasion and proliferation.[15] Taken together, those finding suggest fascin to present a promising target for anti-metastatic therapeutics.

1.1.5 Inhibition of fascin's actin-bundling activity

A series of different compounds were developed to inhibit fascin's actin-bundling activity. Initially, migrastatin, a macrolide natural product isolated from *Streptomyces*, and its synthetic analogue macroketone (Figure 1.11), were shown to inhibit tumour cell migration *in vitro* without knowledge of their biological target.[53] *In vivo* studies carried out in mice showed reduction in metastases after treatment with macroketone, though metabolic instability of the compound was observed.[53] Further studies identified macroketone and other analogues to inhibit fascin's actin-bundling activity,[54] however, the exact binding mode and mechanism remained somewhat elusive.[55] Structural modifications of synthetic analogues in order to improve anti-metastatic activity as well as metabolic stability are the subject of further investigations.[56,57]

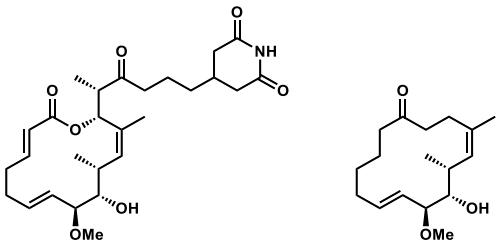

Figure 1.11: Migrastatin and synthetic analogue macroketone.

FSCN-A (1.4) and **FSCN-B (1.5)** were developed as part of a drug development project at the Drug Discovery Unit at the Beatson Institute for Cancer Research, which was aimed at identifying compounds capable of inhibiting fascin's actin-bundling activity. Using a fragment-based drug design approach, a virtual library of around two million fragments were screened and 1000 promising compounds were selected for assessment of binding affinities for fascin, yielding 53 hits.[58,59] Hit fragment **1.1** was observed to bind in the same pocket as previously identified compound **1.2** (Figure 1.12).[60] A virtual screen of commercial compounds and an in-house library identified analogues of compound **1.2**. Binding to fascin of 100 promising compounds was assessed by surface plasmon resonance (SPR) and compound **1.3** was selected for further optimisation. Combining structural features of **1.2** and **1.3** and further modifications to improve fascin binding yielded **FSCN-A (1.4)** and **FSCN-B (1.5)**.[58,61]

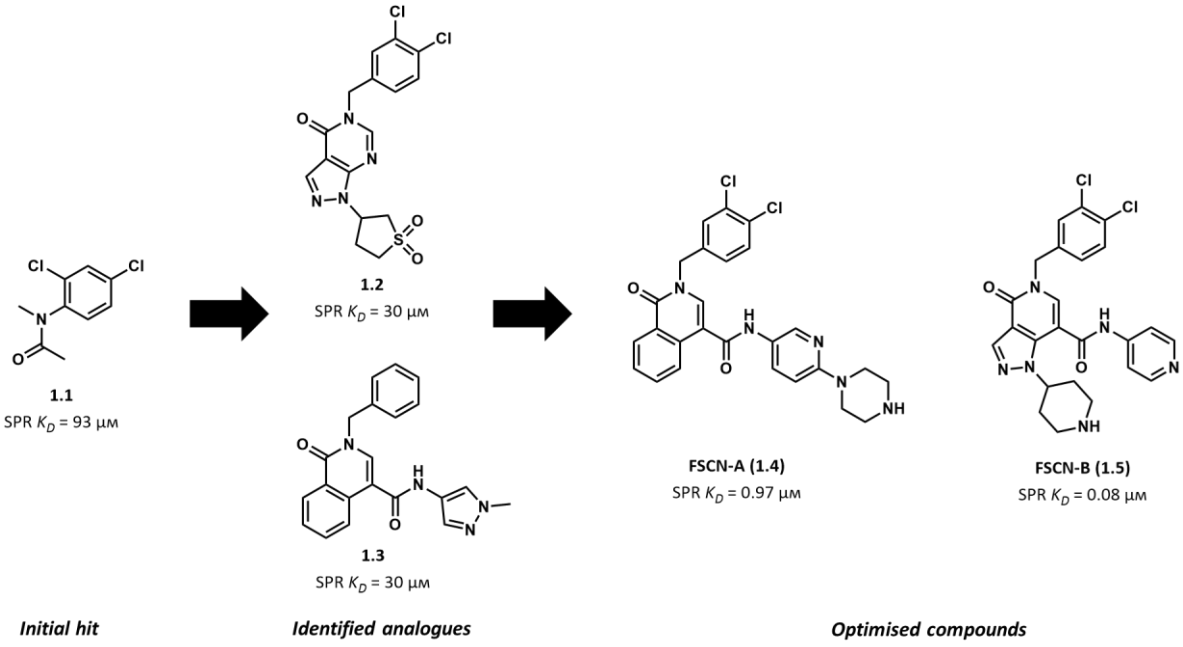

*Figure 1.12: Initial hit fragment **1.1**, analogues **1.2** and **1.3** and optimised compounds **FSCN-A (1.4)** and **FSCN-B (1.5)**.*

Co-crystal structures with fascin revealed both compounds, **FSCN-A (1.4)** and **FSCN-B (1.5)**, to bind to the same actin-binding site (Figure 1.13). Due to cooperativity between the two actin-binding sites (Chapter 1.1.4), binding of the compounds induces a global conformational change, thereby preventing fascin from binding to actin filaments and inhibiting its actin-bundling activity.[59]

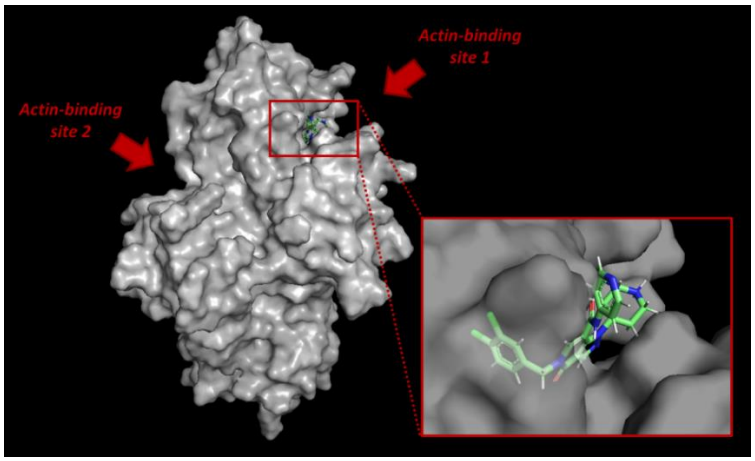

*Figure 1.13: Co-crystal structure of fascin with **FSCN-B (1.5)** (PDB ID 6i18).*

FSCN-B (1.5), which displayed a higher affinity for fascin when assessed by SPR, also showed improved inhibition of actin bundling whilst being less cytotoxic, compared to **FSCN-A (1.4)** (Table 1.1). **FSCN-B (1.5)** was also shown to inhibit tumour cell invasion *in vitro*.[61]

	Fascin binding SPR K_D (μM)	***Inhibition of actin bundling IC_{50} (μM)***	***Toxicity (μM)***
FSCN-A (1.4)	0.97	1.40	> 1
FSCN-B (1.5)	0.08	0.24	> 30

*Table 1.1: Activity of **FSCN-A (1.4)** and **FSCN-B (1.5)**.* [59,61]

FSCN-C (1.7) and analogues (Figure 1.14) were identified at Weill Cornell Medical College by screening chemical libraries for compounds capable of inhibiting fascin's actin-bundling activity. Out of around 165,000 screened compounds, 15 were identified to display reproducible IC_{50} values of less than 10 μM, and **1.6** was selected for further optimisation due to its drug-like structure.[62] Generation of analogues of **1.6** by exploration of different head groups afforded **FSCN-C (1.7)**, between others, which was then also tested *in vitro* and *in vivo*.[63]

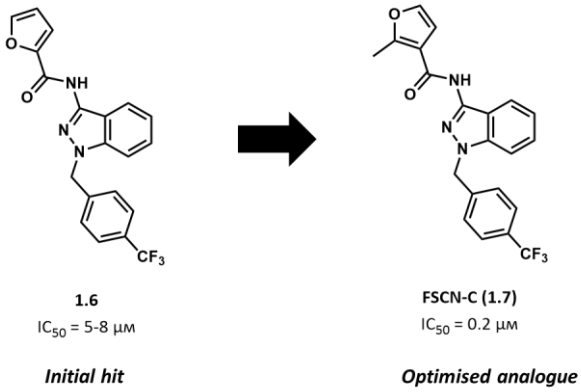

*Figure 1.14: Optimisation of **FSCN-C (1.7)**.*

FSCN-C (1.7) showed improved activity over initial hit **1.6** *in vitro* when assessed in actin-bundling and invasion assays, and decreased formation of metastases by around 95% at 100 mg/kg in mice (Table 1.2). Co-crystal structures of **FSCN-C (1.7)** and analogues with fascin confirmed binding to the same actin-binding site as **FSCN-A (1.4)** and **FSCN-B (1.5)** (Figure 1.13).[64] Further *in vivo* studies revealed that **FSCN-C (1.7)** not only inhibits tumour metastasis but also decreases tumour growth of certain cancer types in mice.[65,66]

	Fascin binding ITC K_D (µM)	***Inhibition of actin bundling IC_{50} (µM)***	***Inhibition of invasion IC_{50} (µM)***	***Decrease of metastasis* in vivo at 100 mg/kg**
1.6	2 to 20	5 to 8	50 to 100	~ 95%
FSCN-C (1.7)	NR	0.2	~10	~ 95%

*Table 1.2: Activity of initial hit **1.6** and optimised analogue **FSCN-C (1.7)**.*[62,63]

A recent *in silico* screen of around 1000 Food and Drug Administration (FDA)-approved and experimental drugs against fascin identified potential inhibitors for fascin's activity.[67,68] Two FDA-approved drugs, raltegravir, an inhibitor of human immunodeficiency virus-1 (HIV-1) integrase, and imipramine, an antidepressant (Figure 1.15), were selected for further *in vitro* actin-bundling and invasion assays, as well as *in vivo* assays using a Zebrafish larvae model, in which they showed promising preliminary activity.

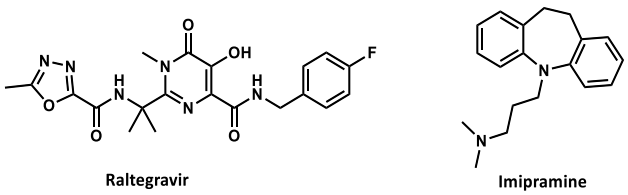

Figure 1.15: Raltegravir and imipramine.

However, despite extensive research efforts and promising results *in vitro* and in animal models, no anti-metastatic targeting the scaffold protein fascin has yet reached the clinical trials. One major challenge with drugging structural proteins is achieving inhibition of protein–protein interactions with a small-molecule drug.

1.2 Targeted protein degradation

1.2.1 Challenges in targeting protein–protein interactions

Despite vital roles of structural proteins in healthy and pathological processes, targeting scaffold proteins, such as fascin, and modulating their protein–protein interactions (PPIs) using small-molecule drugs remains an ongoing challenge in drug discovery.[69] Classical drug targets, like enzymes or receptors, possess of well-defined binding sites with specific interactions that can be exploited when modulating a protein's function *via* a small molecule (Figure 1.16 a). PPIs, on the other hand, occur through contact of two or more proteins over large shallow surfaces, making it difficult for a small-molecule drug to disrupt this binding over a large interactive surface. Moreover, the cumulative affinity of protein–protein binding is high due to the numerous interactions between the amino acids of the two proteins, further complicating disruption of this high-affinity interaction with a small molecule (Figure 1.16 b).[70]

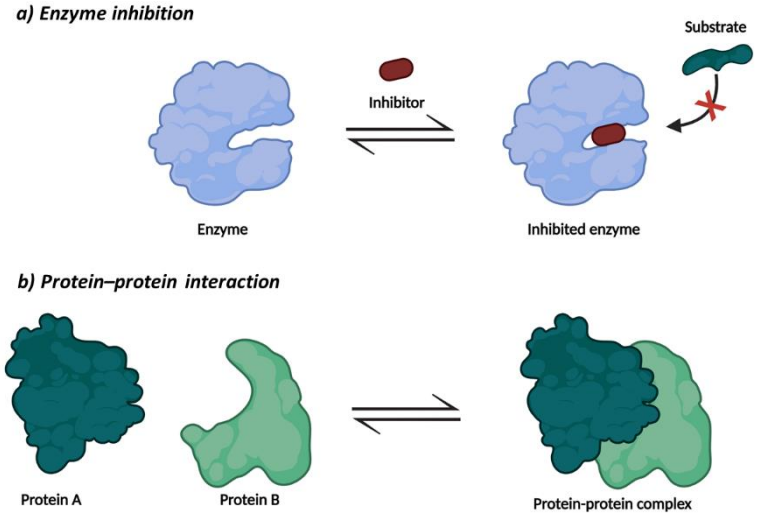

Figure 1.16: a) Inhibition of enzyme with small-molecule drug and b) protein–protein interaction.

More recently, with the development of novel non-small-molecule therapeutics such as antibodies or peptides,[71] several PPI-modulating drugs have reached clinical trials and some even the market.[72] However, poor oral availability and adverse immune reactions

remain inherent challenges with these non-traditional therapeutic agents.[69] Another potential therapeutic modality for structural proteins is targeted protein degradation. This strategy does not rely on inhibiting PPIs but instead induces degradation of a protein of interest (POI) through the cell's natural protein degradation mechanism. Since the POI can be recruited for degradation by binding anywhere on the target, no functional binding site is required. In addition, by permanently degrading the POI, the therapeutic effect does not rely on transient and reversible inhibition of the PPI. Targeted protein degradation can therefore be used to access protein targets otherwise considered "undruggable" with small-molecule drugs, such as scaffolding proteins.[73] Although this approach is widely explored for a variety of targets in the context of cancer[74,75] and has recently reached the clinical trial stage,[76,77] only few structural proteins have been targeted to date.[78,79]

1.2.2 Natural degradation of endogenous proteins

To maintain proper cell function, quality and quantity of the protein content within the cell needs to be regulated, and protein degradation plays a vital role in achieving cellular homeostasis. Degradation of surplus and aberrant proteins occurs through two major mechanisms: either the lysosomal pathway, through which proteins are degraded by hydrolytic enzymes in the acidic interior of the lysosome, or the ubiquitin–proteasome system (UPS), for which proteins are tagged for proteasomal degradation through an enzymatic cascade.[80,81] Since targeted protein degradation takes advantage of the UPS, only this pathway will be described herein.

To trigger the UPS cascade leading to protein degradation, a ubiquitin-activating enzyme (E1) activates ubiquitin, a small highly-conserved protein which serves as a cofactor for a variety of cellular processes, by catalysing the reaction between ubiquitin's C-terminal carboxylate and adenosine triphosphate (ATP) to form a ubiquitin adenylate (Figure 1.17 a). This ubiquitin adenylate then reacts with a cysteine residue of E1 to form a thioester. Through transthioesterification ubiquitin is transferred from E1 to a ubiquitin-conjugating enzyme (E2) (Figure 1.17 b). The ubiquitin ligase (E3) binds to the target protein and facilitates transfer of the activated ubiquitin from E2 to a lysine residue on the substrate by formation of an isopeptide bond with ubiquitin's C-terminal glycine (Figure 1.17 c).[82] This ubiquitin transfer occurs several times, building up a poly-ubiquitin chain on the protein (Figure 1.17 d), which is then recognised by the proteasome as a degradation signal. The

proteasome, a multi-subunit protease complex, subsequently unfolds and degrades the protein into non-functional peptide fragments (Figure 1.17 e).[83]

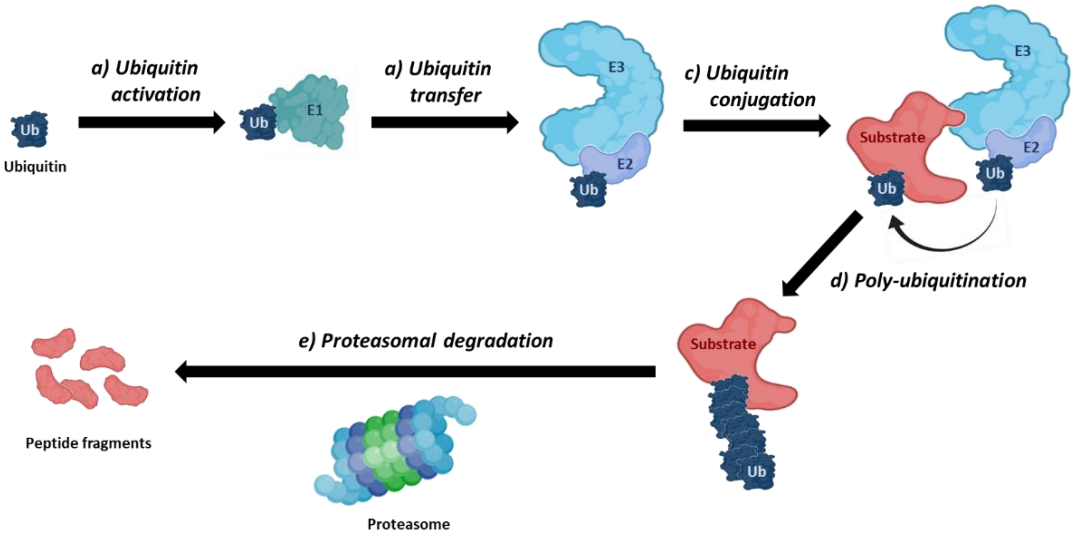

Figure 1.17: Endogenous protein degradation through the ubiquitin-proteasome system (UPS): a) E1 ubiquitin activation, b) ubiquitin transfer to E2, c) ubiquitin conjugation to protein, d) poly-ubiquitination and d) proteasomal degradation of ubiquitinated protein.

Whereas only two E1 enzymes conjugate ubiquitin to around 40 E2 enzymes, substrate specificity is achieved through the interaction of E3 ligases with the target protein. Hundreds of different E3 ligases are encoded in the human genome and their expression is tissue-specific and can vary depending on the cellular context, conferring selectivity to the degradation process.[84]

1.2.3 Targeted protein degradation

Targeted protein degradation diverts the UPS-mediated degradation mechanism to a target protein by use of proteolysis-targeting chimeras (PROTACs) or molecular glues. PROTACs, which act as an adapter between the POI and the E3 ligase, are heterobifunctional molecules, consisting of two ligands, one for the E3 ligase and one for the POI, connected through a linker. By recruitment of both the POI and the E3 ligase, and formation of a ternary complex, the E3 ligase is brought in close proximity to the POI, inducing ubiquitination of the target and subsequent proteasomal degradation through the UPS pathway (Figure 1.18). The PROTAC, on the other hand, is released and can re-enter the catalytic degradation cycle by recruiting another copy of the POI.[85] Recruitment of the UPS to a target protein can also be mediated *via* molecular glues. These small molecules are capable of stabilising interactions between two proteins that would not normally

interact, in this case the POI and an E3 ligase. Discovery of molecular glues for a specific target is currently still somewhat serendipitous, making it more difficult to achieve substrate specificity compared to PROTAC development.[86]

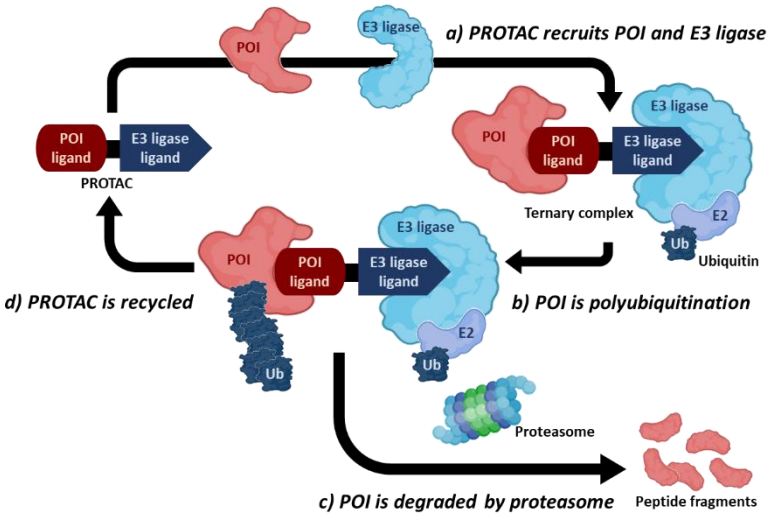

Figure 1.18: PROTAC-mediated targeted protein degradation: a) PROTAC recruits POI and E3 ligase to form ternary complex, b) POI is polyubiquitinated, c) POI is degraded by the proteasome and d) PROTAC is recycled and can recruit more copies of the POI.

Targeted protein degradation potentially offers advantages over traditional inhibitory small-molecule drugs. Since PROTACs are recycled and can act catalytically by recruiting several copies of the POI, lower systemic concentrations of the compound might be needed for therapy, reducing the risk of adverse off-target effects.[87] Additionally, permanent degradation of the target leads to depletion of protein levels over time, and re-synthesis of the protein is required in order to restore its function, possibly leading to longer-lasting therapeutic effects when compared to transient inhibition of the target.[88] As PROTACs do not modulate protein function but only require binding to the POI in order to initiate the ubiquitination cascade leading to proteasomal degradation, identification of an active site on the protein or development of a strongly binding ligand are not necessarily needed. Therefore, proteins previously deemed "undruggable" due to lack of well-defined pockets can be targeted.[89,90] Target selectivity can be achieved through the choice of recruited E3 ligase as well as adaptation of linker length to obtain optimal interaction between the POI and the E3 ligase.[91,92]

1.2.4 Considerations for PROTAC design

The mechanisms by which targeted protein degradation proceed are complex and success is influenced by interdependencies of various factors, such as the target protein and the tissue type. Therefore, components involved in the development of PROTACs and their impact on inducing targeted degradation need to be carefully considered.

E3 ligase ligands

Even though more than 600 E3 ligases are found in the human body, only a handful are expressed in a wide range of tissues and for very few E3 ligases small-molecule ligands known to bind with high affinity and specificity are available.[93] In the context of targeted protein degradation, particularly four E3 ligases have been exploited, namely von Hippel–Lindau (VHL), cereblon (CRBN), mouse double minute-2 (MDM2) and inhibitor of apoptosis (IAP).[94] However, identification of additional E3 ligases and development of suitable small-molecule ligands for incorporation into PROTACs are currently heavily investigated.[95,96] To date, the vast majority of successful PROTACs reported in literature target VHL and CRBN (Figure 1.19),[97-100] hence for the purpose of this work, only ligands for VHL and CRBN E3 ligases are discussed.

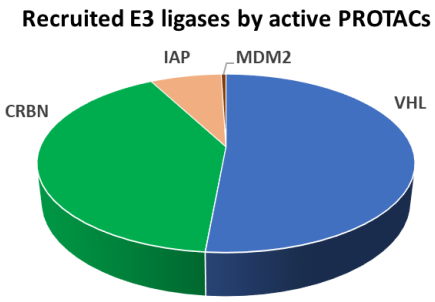

Figure 1.19: Analysis of E3 ligases recruited by active PROTACs – based on [100].

The ligand for VHL stems from a structure-guided design of a small molecule able to disrupt the interaction with its primary endogenous substrate hypoxia-inducible factor 1α (HIF1α). HIF1α is a transcription factor for regulating several genes related to sensing oxygen and hypoxic response. In its hydroxylated form, HIF1α is recognised by VHL, ubiquitinated and proteasomally degraded, hence the development of an inhibitor was centred around the hydroxyproline moiety crucial for HIF1α binding (Figure 1.20).[101,102] Further structure-activity relationship (SAR) studies produced **VHL ligand 1** which is now widely incorporated

in PROTACs by attachment of a linker through the nitrogen atom at the *tert*-leucine moiety.[102-104] Further optimisation of the ligand by incorporation of a cyclopropyl group to increase binding affinity yielded **VH101**, which allows for linker attachment through the phenol moiety.[105-107] Although the VHL binding affinity for **VH101** was determined to be higher than for **VHL ligand 1**, head-to-head comparisons between PROTACs featuring the two VHL ligands revealed that the efficacy of the E3 ligase recruiter is target-dependent.[103,104]

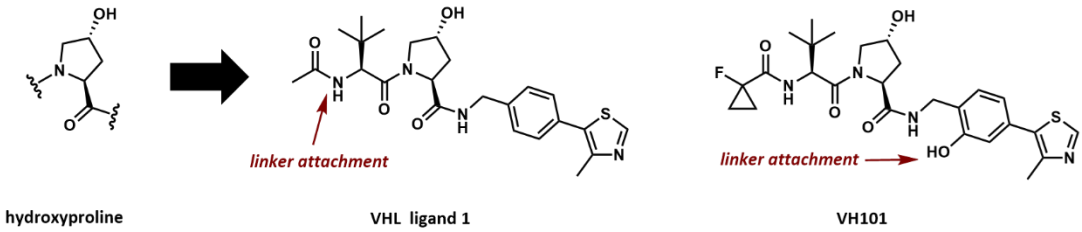

Figure 1.20: Development of VHL ligands based on hydroxyproline moiety crucial for on HIF1α binding.

Decades after the pharmaceutical disaster leading to devastating developmental defects caused by thalidomide, a drug used to treat morning sickness in pregnant women, research directed towards elucidating the teratogenic mechanisms led to the discovery of thalidomide binding to CRBN E3 ligase.[108] Furthermore, it was determined that phthalimide-based drugs racemise rapidly *in vivo*, implicating the *in vivo*-generated (*S*)-thalidomide for the observed teratogenicity.[109,110] However, both enantiomers bind to the CRBN E3 ligase and different phthalimide-based ligands, such as pomalidomide or lenalidomide, are currently successfully used in PROTAC design (Figure 1.21).[99,111,112] Recent studies suggest that linker attachment through a phenolic linkage compared to the pomalidomide nitrogen atom could improve solubility and reduce off-target effects caused by the immunomodulatory activity reported for phthalimide-based drugs (Figure 1.21).[113-115]

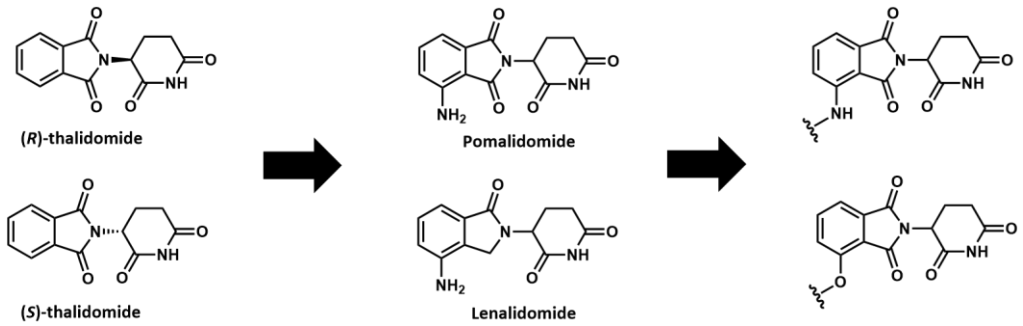

Figure 1.21: Phthalimide-based compounds: thalidomide, pomalidomide, lenalidomide and CRBN-binding moieties.

In direct comparisons of CRBN- and VHL-recruiting PROTACs, the CRBN E3 ligase seemed to be more promiscuous than the VHL E3 ligase, inducing degradation of a wider spectrum of targets.[116] However, the choice of the E3 ligase also depends on the availability and expression levels in the different cell lines to be targeted. Varying the E3 ligase ligand could also provide the opportunity to modulate selectivity of a PROTAC towards a particular target.[92,97]

Hydrophobic tags (HyTs)

A strategy alternative to recruiting E3 ligases to induce targeted protein degradation, is conjugation of a hydrophobic tag (HyT) to a target protein. By binding of the PROTAC to the POI and exposure of the lipophilic residue, partial misfolding of the protein is mimicked.[117] Ubiquitination and subsequent degradation through the UPS is triggered by recruitment of a small molecule chaperone of the heat shock protein (HSP70) family which recognises exposed hydrophobic residues of denatured proteins.[118] Several HyTs can be used for this approach, with adamantyl moieties being most widely explored (Figure 1.22).[50,51]

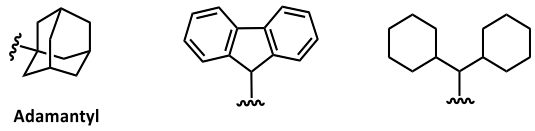

Figure 1.22: Lipophilic moieties used as hydrophobic tags.

Linkers

The primary and most obvious function of the linker is to connect the POI and the E3 ligase ligands und bring the two proteins together once bound to the PROTAC. However, length and orientation of the linker functionality have been shown to greatly impact on the interaction between the two proteins and ultimately the efficacy to induce protein degradation.[98] By bringing the POI and the E3 ligase into close proximity, the linker can stabilise protein–protein interaction for optimal presentation of the POI for ubiquitination to occur.[119] Through this positive cooperativity, effective PROTACs can be developed based on compounds that only weakly bind to the POI.[120] Additionally, linker choice can modulate target selectivity, to the extent of preferential degradation of one isoform of a target protein over another.[114]

The “hook effect”, a phenomenon inherent to three-component systems, is typically observed for high PROTAC concentrations. Preferential formation of unproductive binary (E3 ligase–PROTAC and PROTAC–POI) over ternary (E3 ligase–PROTAC–POI) complexes needed to induce degradation leads to reduced efficacy at higher compound concentrations (Figure 1.23). This effect can likely be mitigated through cooperative binding between the two proteins mediated by a suitable linker.[121,122]

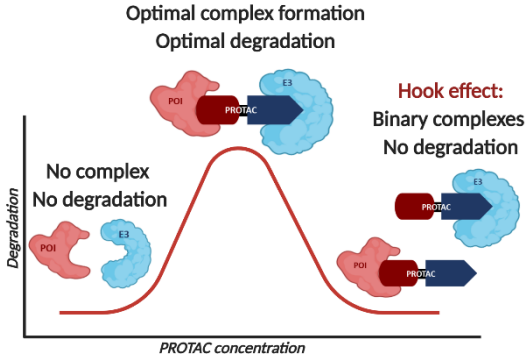

Figure 1.23: “Hook effect” at high PROTAC concentrations.

Optimal linker length and composition are highly dependent on the individual system thus requires experimental optimisation.[123] If the chosen linker is too short, steric clash between the two proteins, POI and E3 ligase, would impede interaction or even prevent both proteins from binding to the PROTAC at the same time. A linker that is too long would introduce a high degree of flexibility into the three-component system, disfavouring ubiquitination of the POI through the E3 ligase.[124] By far, polyethylene glycol (PEG) and alkyl chains are most commonly used in PROTAC design due to their synthetic accessibility and the ease to adjust linker length. This tuneability allows for systematic determination of optimal linker size and conjugation sites on both ligands for a given target.[125] Once a suitable linker length has been established, substitution of a flexible chain by more rigid bridging structures can have a favourable effect on PROTAC efficacy, essentially by locking the PROTAC into its optimal conformation and increasing selectivity for desired interactions with the proteins over other, unproductive interactions.[105,126]

Linker composition may also impact on cell permeability and solubility, with the potential to improve bioavailability of the PROTAC.[98] Despite the synthetic utility of PEG and alkyl chains (Figure 1.24), they may contribute to toxicity and metabolic instability of the compounds.[127] More rigid moieties, such as alkynes, or saturated nitrogen heterocycles,

like piperazines and piperidines, could alleviate those issues at the same time as increasing solubility.[128,129]

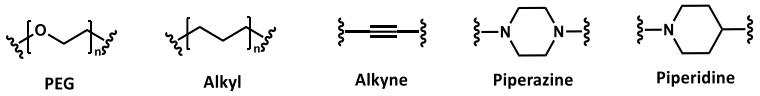

Figure 1.24: Commonly used linker motifs in PROTAC design.

1.2.5 Evaluation of physicochemical properties

The functionalities needed for PROTAC design inevitably result in a higher molecular weight compared to small-molecule drugs, and impact on properties and behaviour of the degraders. In an attempt to predict if compounds are likely to be cell permeable and orally bioavailable therapeutics prior to subjecting them to expensive and time-consuming *in vitro* and *in vivo* assays, different physicochemical properties can be evaluated:

- *Molecular weight (MW)* = molecular mass of compounds in daltons (Da). A high molecular weight can impact negatively on other physicochemical properties and could complicate passive cellular uptake of the compound.
- *Calculated partition coefficient (cLogP)* = measure of compound lipophilicity. Lipophilicity contributes to a compound's ability to cross the cell membrane, however, high lipophilicity can impact negatively on aqueous solubility and could result in enhanced oxidative metabolism.[94]
- *Hydrogen bond donors* (*HBD)* = number of hydrogen atoms bonded to either nitrogen or oxygen atoms and *hydrogen bond acceptors (HBA)* = number of oxygen and nitrogen atoms in delocalised systems. HBD and HBA contribute to the polar surface area of a compound. A large number of HBD and HBA can lead to a high cost of desolvation of complexed water molecules necessary for passive transport across the cell membrane.[130]
- *Number of rotatable bonds (NRotB)* = single, acyclic bonds with both atoms bonded to at least one other non-terminal heavy atom. A high number of NRotB are considered unfavourable due to an increased entropic cost of binding. However, they can also have a favourable impact by conferring compounds the ability to selectively display of different polarities depending on environment (chameleonic effect).[131]

- *Topological polar surface area (tPSA)* = measure of compound polarity or hydrophilicity. A large tPSA can impact negatively on passive cell membrane permeability, however, also contributes positively to compound solubility.[130,132]

Several metrics have been developed, with one of the most well-known being Lipinski's "rule-of-5" (Ro5),[133] which was developed as a guideline to define the chemical space in which drug-like molecules fall. The Ro5 was determined by assessing physicochemical properties associated with orally bioavailable drugs, such as MW, HBD, HBA and partition coefficient (logP) as a measure of compound lipophilicity (Table 1.3). Veber *et al.*[130] analysed a large set of drug candidates with oral bioavailability in rats, and found that properties such as NRotB and tPSA would be more meaningful indicators for predicting oral bioavailability (Table 1.3). However, both, Lipinski's and Veber's "rules", mostly apply to traditional small-molecule drugs with a molecular weight under 500 Da. Owing to their necessary functionalities, essentially two small-molecule ligands conjugated by a linker, PROTACs fall far outwith those values, rendering the application of Lipinski's and Veber's guidelines to predict compound properties and behaviour difficult. More recently, as more non-traditional therapeutics, such as peptidomimetics and macrocycles, are developed and reach the market, Kihlberg's "beyond rule-of-5" (bRo5)[134,135] expanded the range of physicochemical properties to approved therapeutics and clinical candidates with molecular weights over 500 Da (Table 1.3). Although not designed as a set of "rules" but more specific to the context of targeted protein degradation, Maple *et al.*[100] evaluated PROTACs reported in literature by their ability to induce degradation of the targeted proteins using a normalised degradation score (DegS). In doing so, analysis of physicochemical properties of the highest scoring PROTACs were analysed and could aid in the determination of optimal properties in degrader development. The average physicochemical properties for highest scoring PROTACs (Maple set, PROTACs with DegS ≥ 4) fall in the space between the Lipinski's Ro5/Veber's and Kihlberg's bRo5 (Table 1.3), indicating those average values could be a good starting point to compare properties of newly developed PROTACs against.

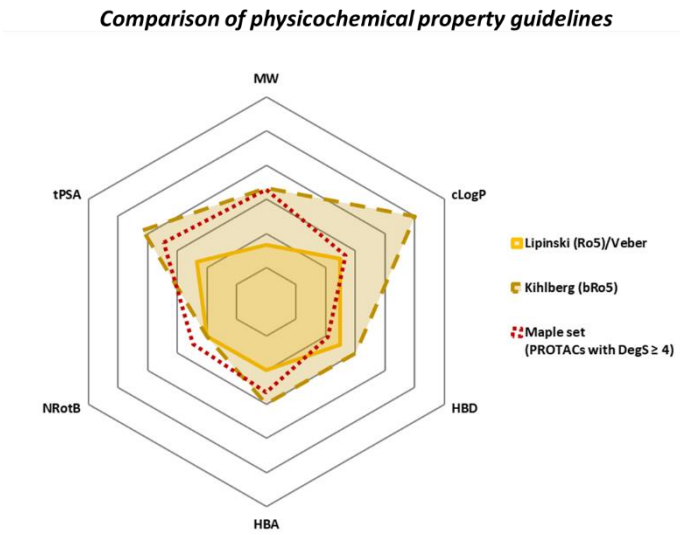

	MW (Da)	cLogP	HBD	HBA	NRotB	tPSA (Å²)
Lipinski (Ro5)[133] / Veber[130]	≤ 500	≤ 5	≤ 5	≤ 10	≤ 10	≤ 140
Kihlberg (bRo5)[134,135]	≤ 1000	-2 ≤ x ≤ 10	≤ 6	≤ 15	≤ 20	≤ 250
Maple set (PROTACs with DegS ≥ 4)[100]	985	5.36	4.13	13.3	24.6	208

Table 1.3: Optimal physicochemical properties as defined by Lipinski/Veber, Kihlberg and Maple.

Despite potential challenges with respect to oral bioavailability, several PROTACs have reached phase I and even phase II of human clinical trials, with more in the pipeline approaching the clinic.[136] Structural detail of those compounds could further contribute to understanding optimal physicochemical properties for PROTAC development, however, most structures have not been disclosed to the public yet. Recently, Arvinas revealed structures of two PROTACs currently in phase II clinical trials: **ARV-110**, a CBRN-recruiting androgen receptor degrader, and **ARV-471**, a CBRN-recruiting oestrogen receptor degrader (Figure 1.25).[76,77]

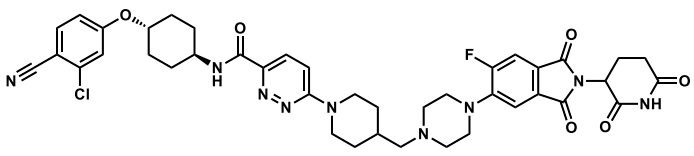

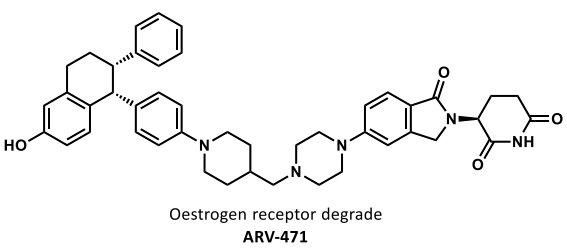

Figure 1.25: Arvinas PROTACs in clinical trials.[76,77]

When comparing physicochemical properties of **ARV-110** and **ARV-471** with the average values of PROTACs with DegS ≥ 4 (Maple set), it is noticeable that the values for the clinical PROTACs lie well below the values reported for the Maple set, even complying with Lipinski's/Veber's guidelines for drug-like small molecules for all parameters despite their molecular weights (Table 1.4 a). Though it should be noted that both Arvinas PROTACs target CRBN, and CRBN-recruiting PROTACs display on average lower cLogP values, fewer NRotB and HBD compared to VHL-recruiting PROTACs (Table 1.4 b),[100] mostly due to more favourable physicochemical properties of the CRBN ligand compared to the VHL ligand. This general difference in physicochemical properties between CRBN-recruiting and VHL-recruiting PROTACs highlights one of the major challenges in PROTAC development: Properties of the degraders are partially dictated by inherent properties of the ligands involved, somewhat restricting improvement of overall properties of the compounds.[94]

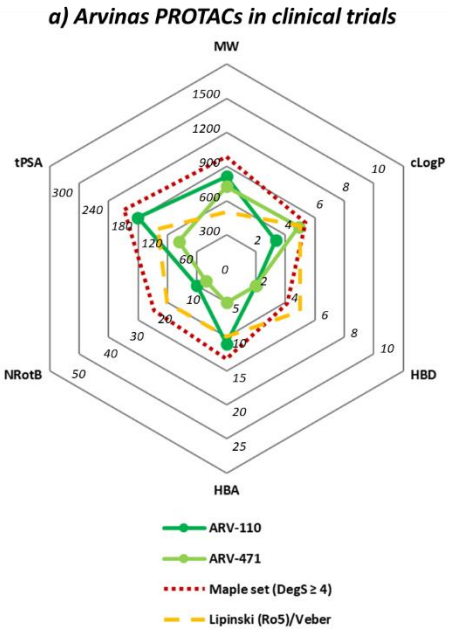

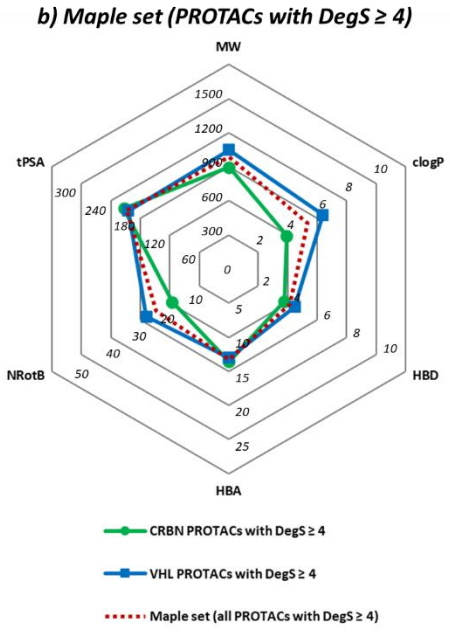

	MW (Da)	cLogP	HBD	HBA	NRotB	tPSA (Å²)
a) Arvinas PROTACs in clinical trials						
ARV-110[76]	812	3.34	2	11	10	181
ARV-471[77]	724	4.92	2	5	7	96
b) Maple set (PROTACs with DegS ≥ 4)[100]						
All PROTACs	985	5.36	4.13	13.3	24.6	208
CRBN PROTACs	1047	6.36	4.46	13.0	28.0	205
VHL PROTACs	896	3.91	3.77	13.6	19.3	213

Table 1.4: Comparison of a) Arvinas PROTACs in clinical trials and b) Maple set PROTACs with DegS ≥ 4.

Despite progress in computational methods to model interactions between proteins and PROTAC and a growing knowledge base on targeted protein degradation, compound development relies on experimental optimisation informed by structural insights since optimal PROTAC design is highly dependent on the protein target and tissue type.

1.3 Project aims and hypotheses

The overall aim of this project was to develop PROTACs capable of inducing degradation of fascin. A library of PROTACs based on different fascin ligands would be synthesised and their biological activity assessed (Figure 1.26). Different *in vitro* assays would be used to confirm binding of the PROTAC to fascin, engagement of the UPS and selective degradation of the target through the PROTAC mechanism. The effect of degrading fascin on invasive and migratory ability of cancer cells would be probed with different functional and phenotype assays. It was hypothesised that through targeted degradation of fascin, formation of invasive cellular structures by bundling of actin filaments would be abolished, and cancer cell invasion could be prevented. Development of a PROTAC able to induce selective degradation of fascin could pave the way in the development of a therapeutic capable of containing metastatic spread.

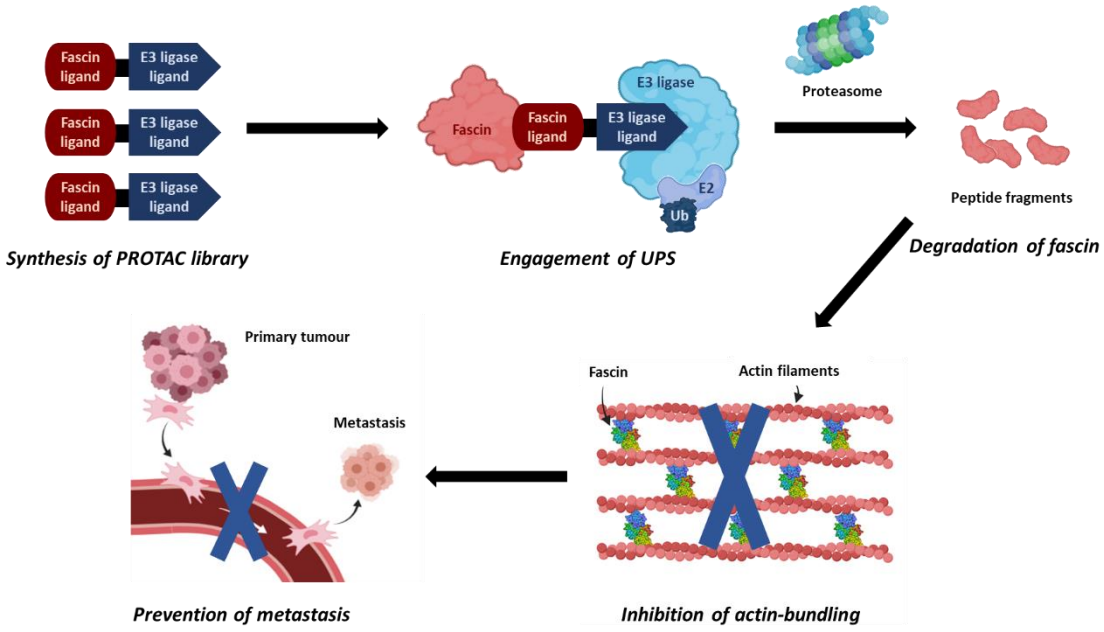

Figure 1.26: Summary of project aims and hypotheses.

2 HaloTag model system: proof-of-concept for targeted protein degradation of a fascin fusion protein using HaloPROTACs

In order to probe the possibility of engaging the UPS to fascin and induce protein degradation *via* the PROTAC mechanism, a proof-of-concept with a model system based on a tagged version of fascin was carried out. The well-studied[103,137,138] high-affinity and high-specificity interaction of the protein tag, HaloTag, with the corresponding synthetic ligand would allow for validation of fascin as a suitable target for selective protein degradation prior to development of fascin-targeting PROTACs.[139]

2.1 HaloTag model system

2.1.1 HaloTag as high-affinity protein tag

The HaloTag protein was developed from the bacterial dehalogenase DhaA, which catalyses hydrolytic cleavage of carbon–halogen bonds of aliphatic halogenated compounds.[140] The enzyme was modified to irreversibly bind to a haloalkane ligand, by substituting the histidine residue (His272) (Figure 2.1 a) to a phenylalanine residue (Phe272) thereby rendering the enzyme unable to regenerate its catalytic triad in the active site and trapping the intermediate as irreversible covalent adduct (Figure 2.1 b).[141]

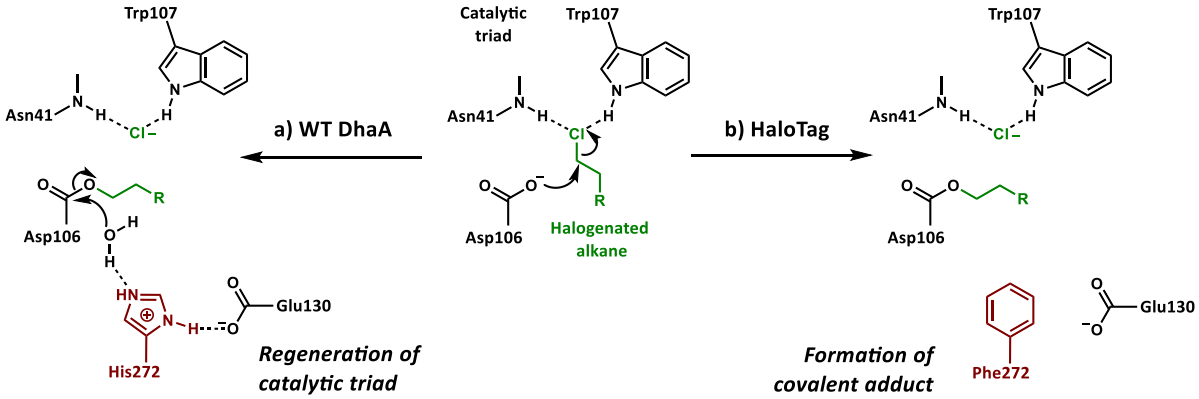

Figure 2.1: Hydrolytic cleavage of carbon–halogen bond of halogenated alkane in active site of bacterial dehalogenase with catalytic triad (Trp107, Asn41 and Asp106) with a) regeneration of catalytic triad through His272 in wild-type dehalogenase (WT DhaA) and b) trapping of intermediate as irreversible covalent adduct by substituting His272 for Phe272 in modified HaloTag.[141]

The high specificity of the relatively small protein tag HaloTag (33 kDa) is attributed to its enzymatic mode of action, which is not found in mammalian cells, and the unique shape of the binding pocket (Figure 2.2 a).[141] HaloTag can easily be fused to different POIs (Figure 2.2 b), and the HaloTag ligand (HTL) can be incorporated in a variety of chemical probes, allowing for this high-affinity system to be used for different biorthogonal purposes, such as labelling with fluorescent probes, protein purification by pull-down or studying interactions between proteins and in protein complexes.[142]

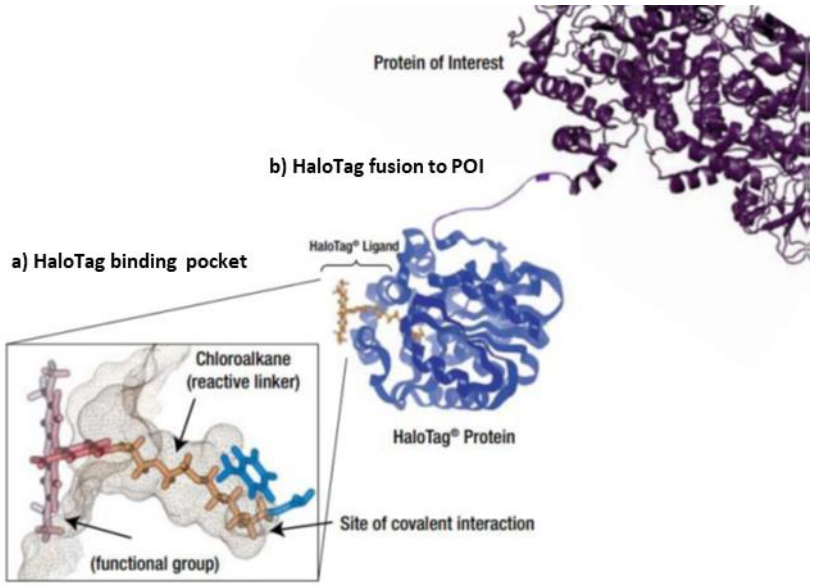

Figure 2.2: HaloTag a) binding pocket with covalently attached chloroalkane ligand and b) fusion to POI.[141]

2.1.2 Targeted degradation of HaloTag-fascin fusion protein

In this project, the HaloTag functionality was used to probe targeted degradation of a HaloTag–fascin fusion protein induced by HaloPROTACs (HPs). Instead of binding to the POI *via* a small-molecule ligand, HaloPROTACs carry a haloalkane moiety which would covalently attach to the HaloTag portion of the fusion protein. Then – analogous to the PROTAC mechanism previously described (Chapter 1.2.3) – recruitment of the UPS through the E3 ligase ligand would induce poly-ubiquitination of the fusion protein and subsequent degradation by the proteasome (Figure 2.3). Due to covalent attachment of HaloPROTAC to fusion protein, the HaloPROTAC would not be recycled and the catalytic nature of the mechanism would be lost.[103]

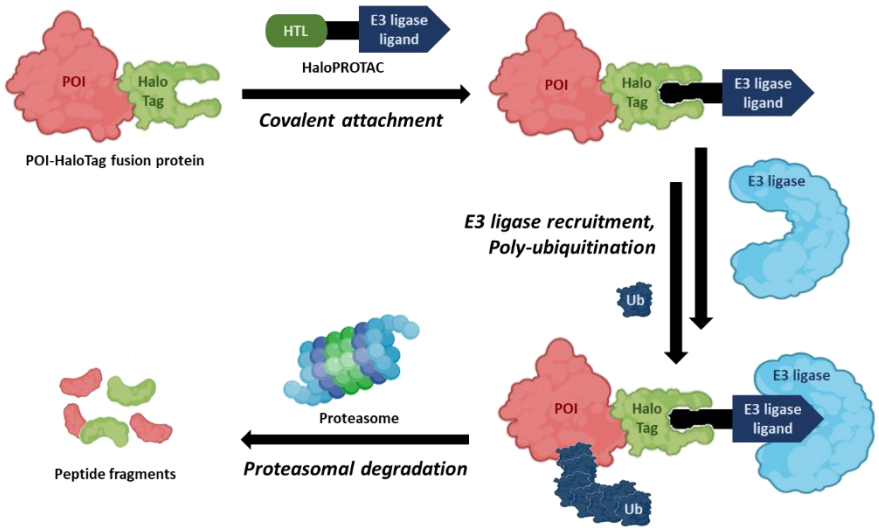

Figure 2.3: Targeted degradation of HaloTag fusion protein induced by HaloPROTAC.

2.2 Design and synthesis of HaloPROTACs

2.2.1 Design of HaloPROTACs and mono-functional controls

The design of the compounds was based on HaloPROTACs reported to induce degradation of green fluorescent protein (GFP)–HaloTag fusion proteins, either by recruiting the VHL E3 ligase[103] or by acting as a hydrophobic tag (HyT).[138] The compounds were comprised of three components: the HaloTag ligand (HTL) which covalently binds to the HaloTag portion of the fusion protein, a ligand recruiting the cellular degradation machinery and a linker connecting the two ligands (Figure 2.4). The HTL moiety, a hexyl chloride, would be conserved across all HaloPROTAC compounds since it was developed specifically for the HaloTag system.[141] To allow for direct comparison between the activity of the compounds, linkers of similar length and composition would be chosen for conjugation of the two ligands. It was decided to incorporate PEG-based linkers due to their flexibility, permitting optimal orientation of the proteins for ubiquitination, and their composition which could potentially aid with cell permeability as well as solubility of the compounds (Chapter 1.2.4).[98] A range of ligands recruiting the cellular degradation machinery would be selected in order to assess any differences in activity, depending on which degradation pathway would be targeted. Therefore, different ligands which were developed to recruit either VHL or CRBN E3 ligase, or an adamantyl moiety acting as a HyT were chosen (Chapter 1.2.4).

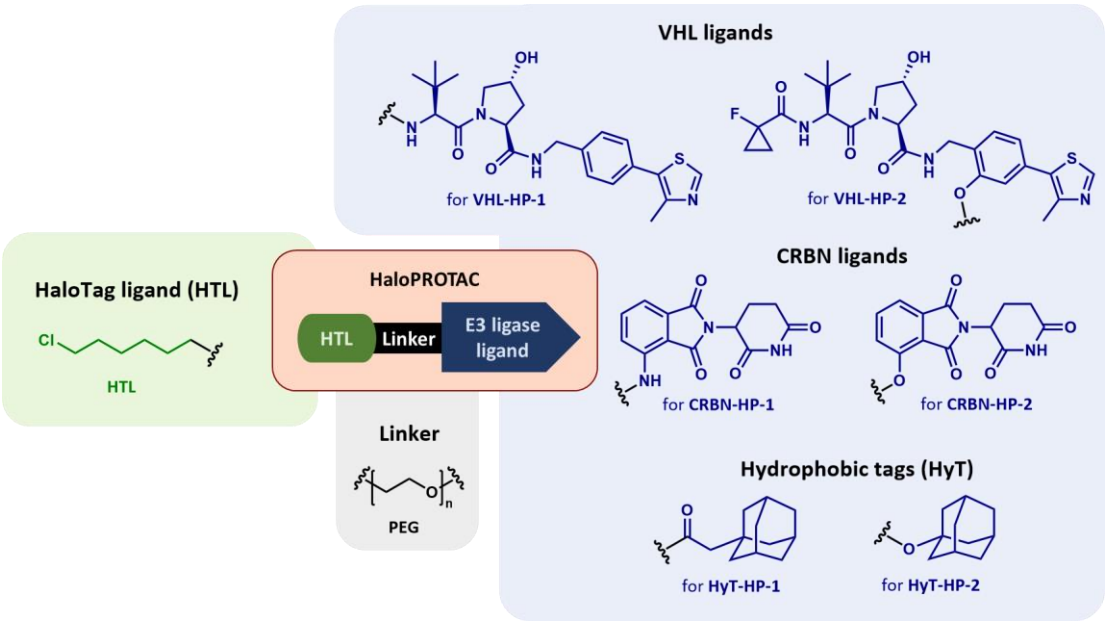

Figure 2.4: Design of HaloPROTACs.

To be able to carry out control experiments verifying that any potential degradation is induced through the PROTAC mechanism, a library of mono-functional control compounds would be synthesised (Figure 2.5). Mono-functional HaloTag control compounds would feature active E3 ligase ligands, however, lack the chlorine atom on HTL, in order to demonstrate covalent attachment to HaloTag was required for degradation. Mono-functional E3 ligase control compounds, on the other hand, would be able to bind to HaloTag through the HTL but would carry inactive E3 ligase control ligands to probe that engagement of the E3 ligases was needed to induce degradation. For VHL, the inactive control would be *cis*-hydroxyproline epimers of the active ligands and for CRBN a methylated version of the active ligand – both of which are widely used for control experiments in the PROTAC context.[120,143]

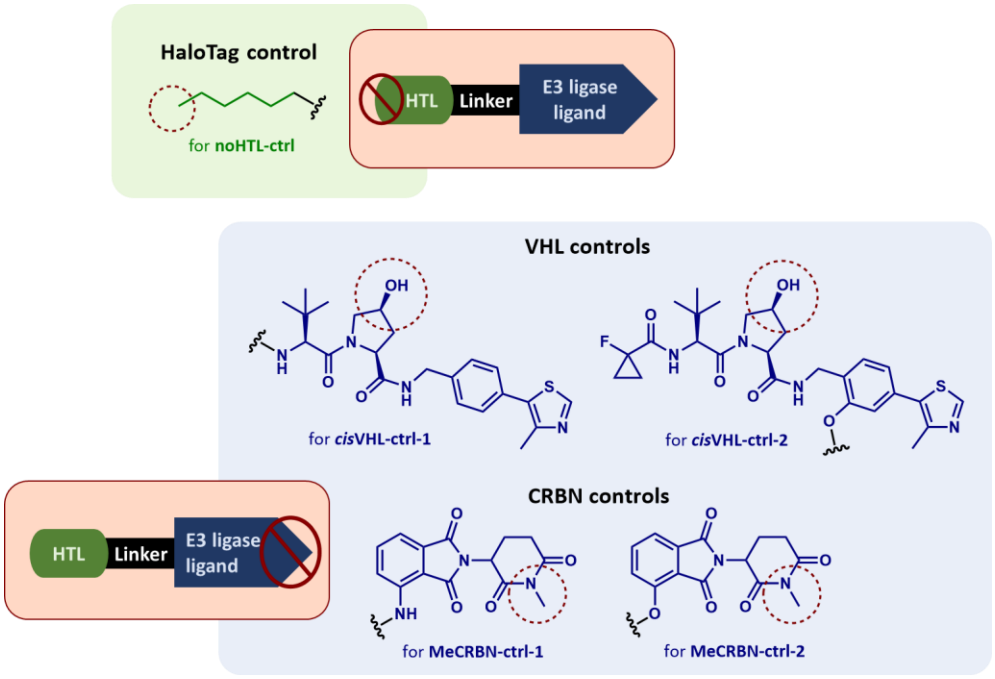

Figure 2.5: Design of mono-functional controls.

2.2.2 Synthetic strategy

The envisioned synthetic strategy was centred around a modular synthesis by which active HaloPROTACs and mono-functional controls could be easily accessed through reliable reactions from common intermediates. The combination of different modular components, such as HTL–linker fragments, would result in a diverse but also comparable compound library. In order to achieve this, first desymmetrisation of a PEG linker by mono-addition of HTL or its inactive equivalent (noHTL) would yield common linker fragments (Figure 2.6). Through functionalisation of the alcohol, different handles could be introduced, allowing for subsequent coupling to active E3 ligase ligands, HyT or negative control ligands.

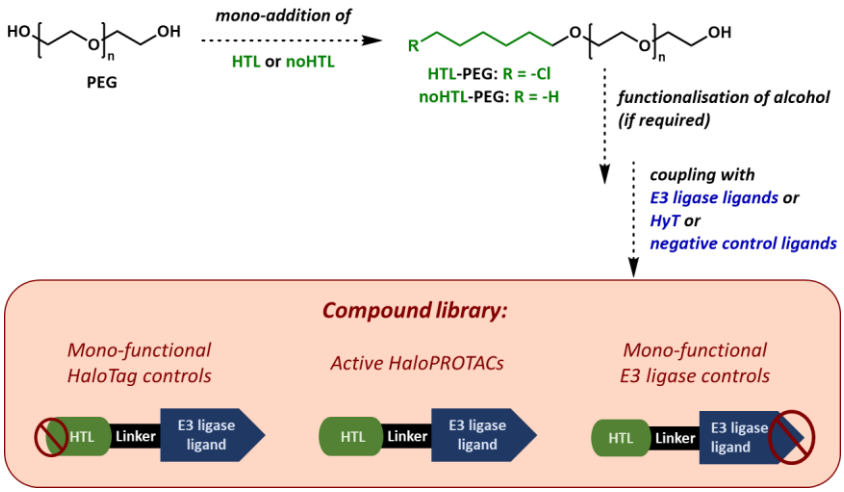

Figure 2.6: Proposed modular synthesis of HaloPROTACs and mono-functional controls.

2.2.3 Synthesis of E3 ligase ligands and inactive control ligands

Before establishing the HaloPROTAC library using aforementioned approach, the required E3 ligase ligands and their corresponding inactive control ligands needed to be synthesised.

VHL ligands and inactive epimer controls

Whereas VHL ligand **VHL-1 (2.1)** was commercially obtained, the inactive epimer control ***cis*VHL-1 (2.2)** (Figure 2.7) had been synthesised by another member of the group. Adapting a literature procedure[102] for active ligand **VHL-1 (2.1)** by incorporating *cis*- instead of *trans*-4-hydroxy-L-proline resulted in the desired inactive *cis*-hydroxyproline configuration of the control ligand ***cis*VHL-1 (2.2)**. Active VHL ligand **VHL-2 (2.3)** and the corresponding inactive epimer control ***cis*VHL-2 (2.4)** (Figure 2.7) were prepared following a route similar to the literature precedent.[105]

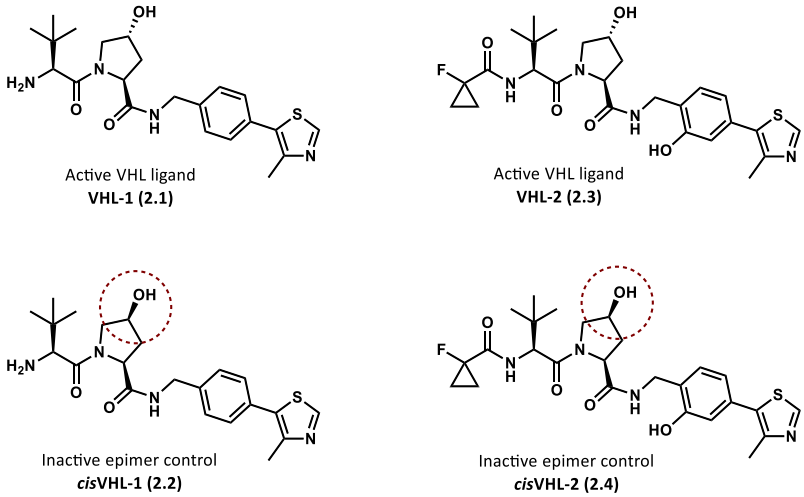

*Figure 2.7: Active VHL ligands **VHL-1 (2.1)** and **VHL-2 (2.3)** and corresponding inactive control ligands **cis*VHL-1 (2.2)** and **cis*VHL-2 (2.4).***

Common precursor amine **2.6** for active VHL ligand **VHL-2 (2.3)** and the corresponding inactive control ligand ***cis*VHL-2 (2.4)** were synthesised following a modified literature precedent.[105] Nitrile **2.5** was accessed from 4-bromo-2-hydroxybenzonitrile and 4-methylthiazole through a palladium-catalysed carbon–hydrogen activation reaction (Table 2.1). Subsequently, nitrile **2.5** was reduced to amine **2.6** using lithium aluminium hydride. Although TLC analysis of the reaction mixture indicated complete consumption of the starting material, the isolated yield of 62% after basic aqueous work-up and purification by column chromatography was lower than expected (entry 1 in Table 2.1). Recovery of the product from the aqueous phase as well as subsequent purification by column chromatography proved to be challenging due to the highly polar nature of amine **2.6**,

hence different work-up conditions were attempted. It was hypothesised that the orientation of the amine and the phenol moieties could result in metal ion chelation by **2.6**, complicating extraction and purification. Therefore, addition of potassium sodium tartrate (Rochelle's salt, entry 2 in Table 2.1) could be able to counteract any possible chelating activity. Although this strategy increased the crude yield to 89%, TLC analysis of the crude product indicated purification by column chromatography was necessary, lowering the isolated yield to 54%. Next, careful dropwise addition of accurate amounts of water and 15% aqueous sodium hydroxide solution to quench the remaining lithium aluminium hydride (Fieser work-up,[144] entry 3 in Table 2.1), followed by removal of the inorganic precipitate by filtration through celite was attempted. TLC and nuclear magnetic resonance (NMR) analysis confirmed satisfactory purity, however, only 70% of the product was obtained. This was thought to be due to the celite and the inorganic precipitate forming a dense pad through which filtration was difficult. By using the same method for work-up method, however, filtering the precipitate through a small amount of cotton wool (Fieser work-up[144], entry 4 in Table 2.1), a quantitative yield of the product was obtained and adequate purity was confirmed by TLC and NMR analysis.

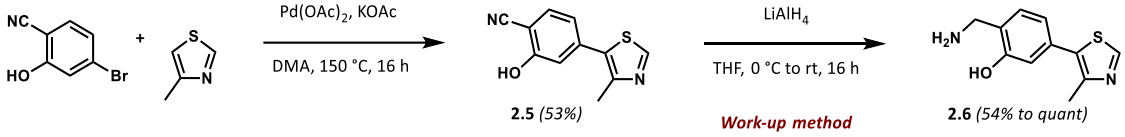

	Work-up method	Filtration	2.6 yield (crude)	2.6 yield (column)
1	Basic aqueous work-up[105]	Celite pad	75%	62%
2	Rochelle's salt	None	89%	54%
3	Fieser work-up[144]	Celite pad	70%	Not required
4	Fieser work-up[144]	Cotton wool	Quantitative	Not required

*Table 2.1: Optimisation of work-up for reduction of nitrile **2.5** to amine **2.6**.*

From common intermediate **2.6**, active VHL ligand **VHL-2 (2.3)** and inactive control ligand ***cis*VHL-2 (2.4)** were synthesised through a sequence of deprotection and amide coupling reactions (Scheme 2.1). The conditions employed for the amide coupling reactions – using hexafluorophosphate azabenzotriazole tetramethyl uronium (HATU) as amide coupling reagent and ethyl 2-cyano-2-(hydroxyimino)acetate (OxymaPure) as additive – were previously optimised within the group in order to reduce the formation of undesired side product formed by competitive nucleophilic attack of the phenol moiety of intermediate

2.6.[145] OxymaPure is an additive used in carbodiimide-mediated peptide bond formation as a safer alternative developed to replace traditional benzotriazole-based additives which were reported to display potentially explosive properties.[146] Using this strategy, common amine intermediate **2.6** was coupled with *N*-Boc-*trans*-4-hydroxy-L-proline *(trans*-Hyp) to obtain *trans* fragment **2.7a** and with *N*-Boc-*cis*-4-hydroxy-L-proline *(cis*-Hyp) for *cis* fragment **2.7b**, with both coupling reactions yielding around 50%. Acidic deprotection of the *tert*-butyl carbamate to give the corresponding amine salts was followed by coupling to the carboxylic acid of *N*-Boc-L-*tert*-leucine, affording the *trans* fragment **2.8a** and the *cis* fragment **2.8b** in comparable yields. After another iteration of acidic deprotection of the *tert*-butyl carbamate and coupling to 1-fluorocyclopropanecarboxylic acid, both the active VHL ligand **VHL-2 (2.3)** and its inactive counterpart ***cis*VHL-2 (2.4)** were isolated in good yields, 74% and 62%, respectively. The HATU/OxymaPure-mediated amide coupling reactions afforded slightly improved yields compared to yields reported in literature using HATU/benzotriazole-based additives (55%)[105] and HATU without additive (52%).[103]

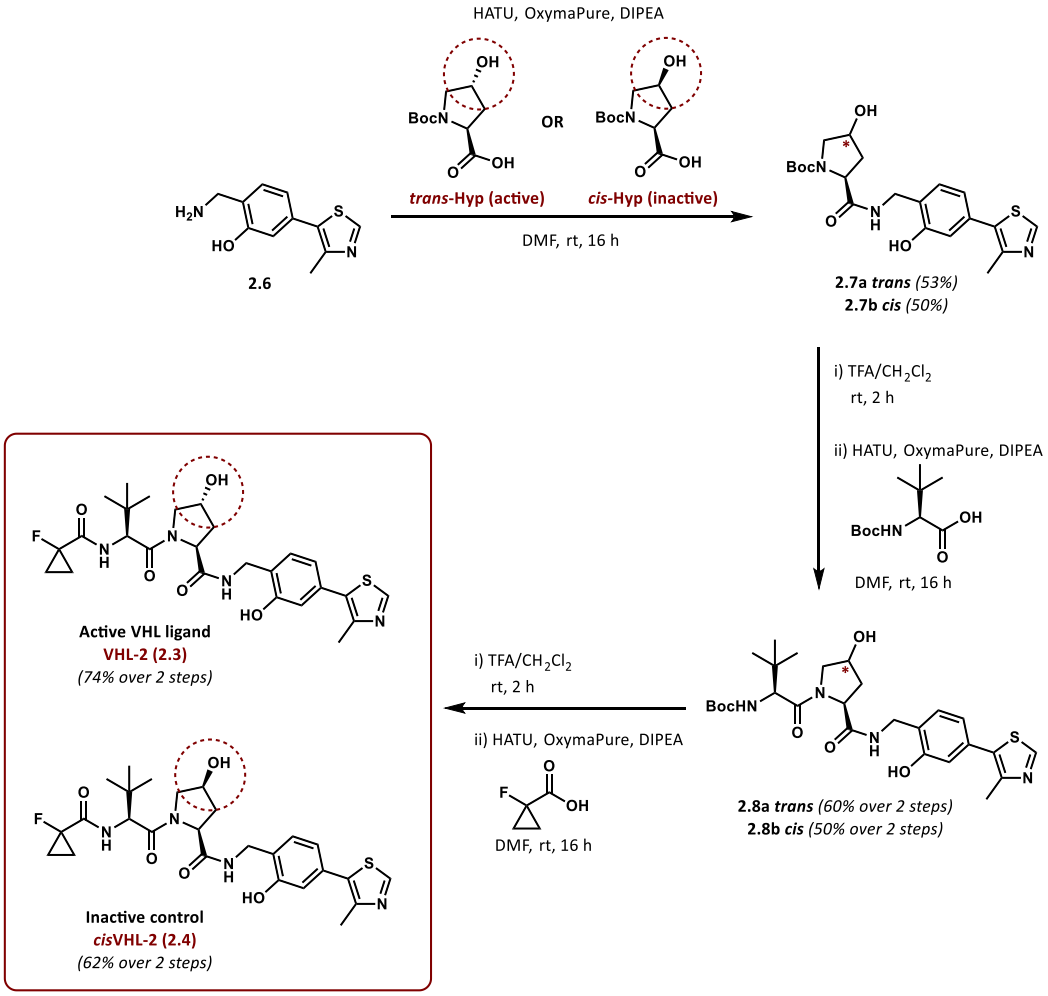

*Scheme 2.1: Synthesis of active VHL ligand **VHL-2 (2.3)** and inactive epimer control ligand **cis**VHL-2 (2.4) from common intermediate **2.6**.*

CRBN ligands and inactive methylated controls

Both active CRBN ligands **CRBN-1 (2.9)** and **CRBN-2 (2.11)** (Figure 2.8) were synthesised over two steps following slightly differing procedures. Subsequent *N*-methylation of the glutarimide yielded inactive control ligands **MeCRBN-1 (2.10)** and **MeCRBN-2 (2.12)**.

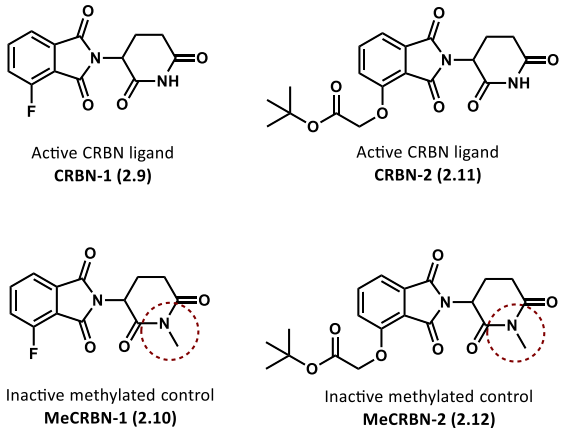

*Figure 2.8: Active CRBN ligands **CRBN-1 (2.9)** and **CRBN-2 (2.11)** and corresponding inactive control ligands **MeCRBN-1 (2.10)** and **MeCRBN-2 (2.12).***

Complete consumption of 3-fluorophthalic anhydride and L-glutamine, as well as formation of a single new product was confirmed by TLC after heating the reaction to 90 °C for 16 hours (Table 2.2). However, addition of 4 M aqueous hydrochloric acid, stirring of the solution for a further 16 hours at room temperature and subsequent filtration of the precipitate – as described in the precedented procedure[99] – afforded phthalimide **2.13** in only around 40% yield. Liquid chromatography–mass spectrometry (LCMS) analysis of the aqueous filtrate confirmed considerable amounts of phthalimide **2.13** remained in the aqueous phase. In an attempt to extract the remaining product, solid lithium chloride (5% w/w) was added to the aqueous filtrate and left to stir for an additional 16 hours at room temperature, resulting in further precipitation of phthalimide **2.13** and increasing the overall yield up to around 70%. Alternatively, extracting the aqueous phase with ethyl acetate after filtration of the precipitate resulted in a similar increase in yield.

Initially, the cyclisation reaction of phthalimide **2.13** to obtain the glutarimide product **CRBN-1 (2.9)** was carried out following the procedure reported in literature,[99] using *N,N'*-carbonyldiimidazole (CDI) as coupling reagent and catalytic amounts of 4-dimethylaminopyridine (DMAP). However, monitoring of the reaction by TLC showed formation of two major product which were identified as the desired active CRBN ligand **CRBN-1 (2.9)** and undesired imidazole adduct **2.9b** in (entry 1 in Table 2.2) and isolated in equal yields. Attempting to suppress the formation of side product **2.9b**, the cyclisation

reaction was carried out at a higher concentration, however, this approach resulted in increased formation of side product **2.9b** instead (entry 2 in Table 2.2). The increased reaction concentration favoured an intermolecular nucleophilic aromatic substitution (S_NAr) reaction with displacement of the fluorine atom of the fluorophthalimide of **CRBN-1 (2.9)** by imidazole which is generated as by-product in CDI-mediated coupling reactions. Similarly, increasing DMAP loading led to considerable formation of side product **2.9b**, however, low yields of product **CRBN-1 (2.9)** (entry 3 in Table 2.2), possibly due accelerated release of imidazole. Finally, with decreased DMAP loading and careful monitoring of the reaction by TLC for formation of side product **2.9b**, an increase of the isolated yield of product **CRBN-1 (2.9)** to 55%, whilst minimising formation of the imidazole adduct **2.9b,** was achieved. With this approach, it was possible to increase the yield to 55%, from 25% reported in literature.[99]

Through optimisation of extraction methods and reaction conditions, CRBN ligand **CRBN-1 (2.9)** was synthesised in a 40% yield over two steps compared to a 13% yield precedented in literature.[99] Although L-glutamine was employed in the reaction, epimerisation during the synthesis could not be ruled out. However, due to previously described *in vivo* racemisation of phthalimide compounds (Chapter 1.2.4) inclusion of the ligand as a mixture of enantiomers into PROTACs was considered to be inconsequential.

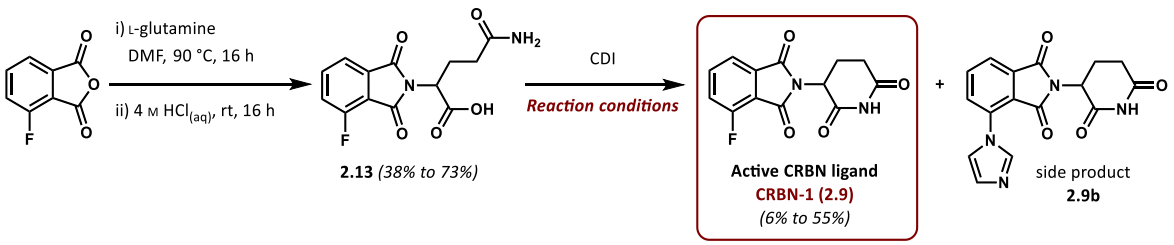

	Reaction conditions	CRBN-1 (2.9) yield	2.9b yield	Ratio 2.9 : 2.9b
1	DMAP (10 mol%), MeCN (1.0 M), reflux, 16 h	39%	38%	1 : 1
2	DMAP (10 mol%), MeCN (**1.6 M**), reflux, 16 h.	10%	52%	1 : 6
3	DMAP (**20 mol%**), MeCN (1.0 M), reflux, 16 h.	6%	49%	1 : 9
4	DMAP (**4 mol%**), MeCN (1.0 M), reflux, **6 h (monitored by TLC/LCMS)**	55%	20%	3 : 1

*Table 2.2: Optimisation of cyclisation reaction conditions to reduce formation of side product **2.9b**.*

The corresponding inactive methylated control ligand **MeCRBN-1 (2.10)** was by *N*-methylation of the glutarimide functionality of **CRBN-1 (2.9)** using iodomethane and potassium carbonate as base following a literature precedent (Scheme 2.2).[147]

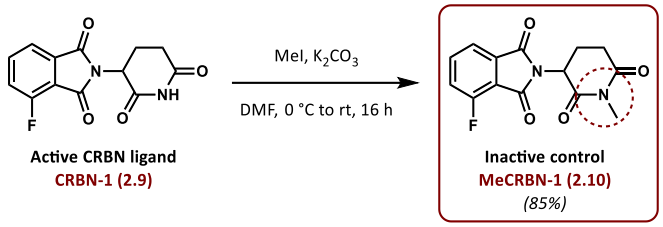

*Scheme 2.2: Synthesis of inactive methylated control ligand **MeCRBN-1 (2.10)**.*

Although it was possible to achieve a three-fold increase of the overall yield for the synthesis of **CRBN-1 (2.9)** compared to the literature procedure, a higher yielding and more convenient alternative route was sought for the **CRBN-2 (2.11)**. Adapting a literature precedent,[114] commercially available cyclised analogue of glutamine, aminoglutarimide, was employed in the synthesis (Scheme 2.3). Acidic deprotection of the *tert*-butyl carbamate, followed by condensation with 4-hydroxyisobenzofuran-1,3-dione afforded phenol intermediate **2.14** in 93% yield over two steps. This was a significant increase in yield compared to the glutamine-based synthesis of **CRBN-1 (2.9)**. Through alkylation of phenol **2.14** with *tert*-butyl bromoacetate active CRBN ligand **CRBN-2 (2.11)** was afforded.

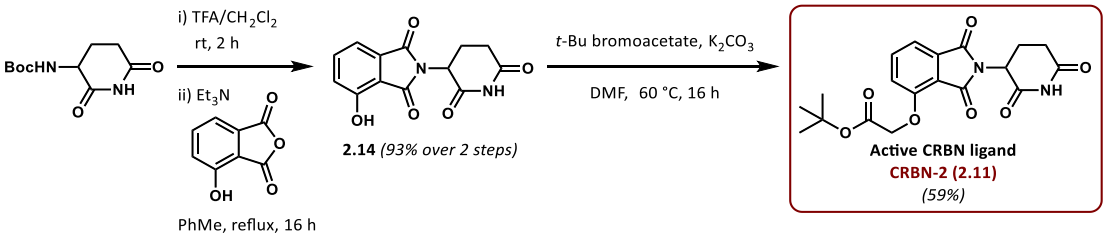

*Scheme 2.3: Synthesis of active CRBN ligand **CRBN-2 (2.11)**.*

The corresponding inactive methylated control **MeCRBN-2 (2.12)** was prepared by *N*-methylation of the glutarimide employed previously to generate inactive methylated control **MeCRBN-1 (2.10)** in excellent yield (Scheme 2.4).

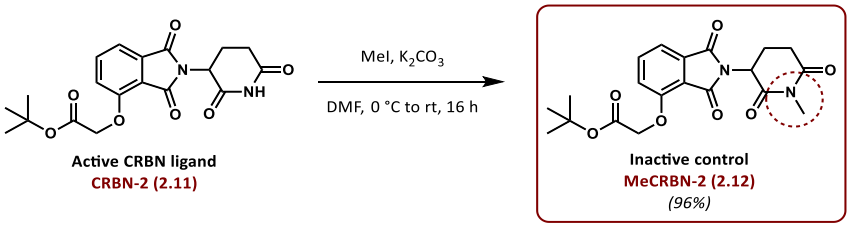

*Scheme 2.4: Synthesis of inactive methylated control ligand **MeCRBN-2 (2.12)**.*

2.2.4 Synthesis of HaloPROTACs and mono-functional controls

VHL HaloPROTACs and mono-functional controls

With the active ligands and the inactive control ligands in hand, HaloPROTACs and corresponding mono-functional controls could be synthesised. The synthesis of the VHL HaloPROTACs and mono-functional controls was based on modified procedures reported in literature.[103,137] Firstly, common linker fragments were generated by mono-functionalisation of pentaethylene glycol (Scheme 2.5 a). This was achieved by mono-alkylation with either 1-chloro-6-iodohexane to afford active HTL–linker fragment **2.15a** or with 1-bromohexane for the inactive noHTL–linker fragment **2.15b**. By employing five equivalents of pentaethylene glycol to favour mono-alkylation, the yield for HTL-linker fragment **2.15a** could be increased from 30% to 79%. Using the same strategy, quantitative yield was achieved for noHTL–linker fragment **2.15b**. The alcohol of fragments **2.15a** and **2.15b** allowed for introduction of different functional handles, either by oxidation to the carboxylic acid for coupling to the amine moiety on VHL ligand **VHL-1 (2.1)** and inactive control ligand ***cis*VHL-1 (2.2)** (Scheme 2.5 b) or activation for alkylation at the phenol moeity of VHL ligand **VHL-2 (2.3)** and inactive control ligand ***cis*VHL-2 (2.4)** (Scheme 2.5 c). With a two-step oxidation protocol (Scheme 2.5 b) alcohols **2.15a** and **2.15b** were converted to the corresponding carboxylic acids **2.17a** and **2.17b** in good yields *via* aldehydes **2.16a** and **2.16b**, without the need for purification of the intermediates. Subsequent HATU-mediated amide coupling reactions of the carboxylic acid linker fragments **2.17a** or **2.17b** with the amine moiety of active VHL ligand **VHL-1 (2.1)** or inactive control ligand ***cis*VHL-1 (2.2)** afforded active VHL HaloPROTAC **VHL-HP-1 (2.18)** in 77% yield, mono-functional epimer control ***cis*VHL-ctrl-1 (2.19)** in 51% yield and mono-functional HTL control **noHTL-VHL-ctrl-1 (2.20)** in 68% yield. For cellular testing, the compounds were further purified using semi-preparative reverse-phase high-performance liquid chromatography (RP-HPLC) resulting in final yields of 30% to 40%.

For alkylation at the phenol moiety of VHL ligand **VHL-2 (2.3)** and inactive control ligand ***cis*VHL-2 (2.4)** (Scheme 2.5 c), the alcohol of linker fragments **2.15a** and **2.15b** was activated by mesylation to afford mesylates **2.21a** and **2.21b** in excellent yields. Subsequent ether formation with **VHL-2 (2.3)** and ***cis*VHL-2 (2.4)** was carried out using a carbonate base to afford active VHL HaloPROTAC **VHL-HP-2 (2.22)** in 47% yield prior to purification with RP-HPLC, mono-functional epimer control ***cis*VHL-ctrl-2 (2.23)** in 92% yield and mono-functional HTL control **noHTL-VHL-ctrl-2 (2.24)** in 89% yield. Since recovery of the active VHL HaloPROTAC **VHL-HP-2 (2.22)** from the aqueous phase proved difficult, it was decided

to avoid aqueous work-up conditions for the two mono-functional control compounds ***cis*VHL-ctrl-2 (2.23)** and **noHTL-VHL-ctrl-2 (2.24)**. Instead, volatile components were removed *in vacuo* and the residues were purified by column chromatography, followed by semi-preparative RP-HPLC, resulting in yields comparable to the first set of compounds.

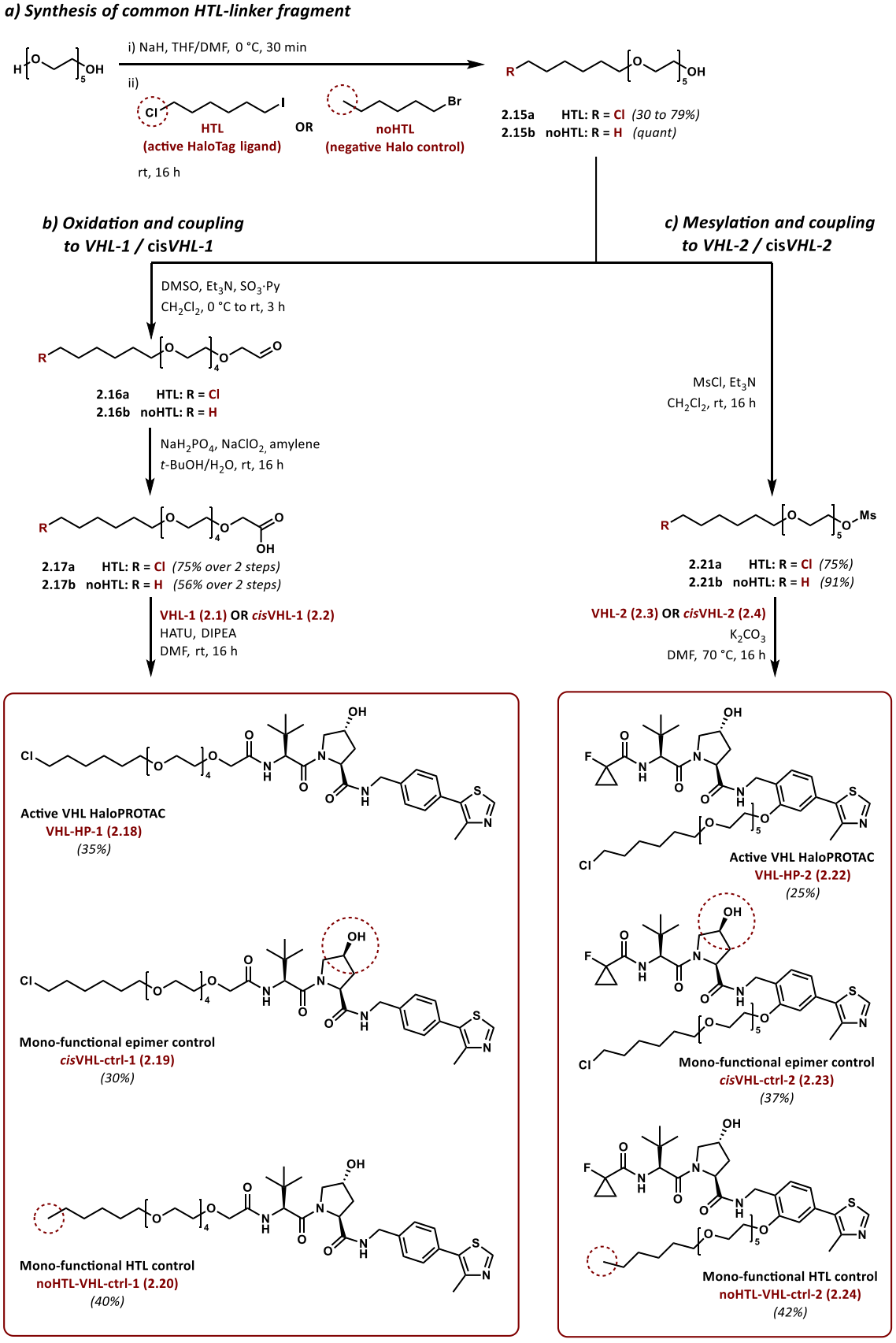

Scheme 2.5: Synthesis of VHL HaloPROTACs and mono-functional controls.

CRBN HaloPROTACs and mono-functional controls

Azido-tetraethylene glycol intermediate **2.25** was readily available in sufficient quantities, hence the synthesis of CRBN HaloPROTACs and corresponding mono-functional controls was based on this building block. As for the synthesis of the VHL-recruiting compounds, common linker fragments were synthesised as a first step (Scheme 2.6 a). Azide **2.25** was reduced using palladium-catalysed hydrogenation to yield aminoalcohol linker **2.26** in excellent yield. The amine was protected using di-*tert*-butyl dicarbonate yielding carbamate **2.27** prior to alkylation of the alcohol with either 1-chloro-6-iodohexane for HTL–linker fragment **2.28a** and with 1-bromo-hexane for noHTL–linker fragment **2.28b**. Both alkylation reactions proceeded in moderate yields, 33% for HTL–linker fragment **2.28a** and 28% for noHTL–linker fragment **2.28b**, possibly due to *N*-alkylation at the amide functionality of protected linker fragment **2.27** leading to the formation of a di-alkylated side product. As sufficient quantities of the desired products were obtained any further optimisation of this transformation was deprioritised.

After acidic deprotection of the carbamates **2.28a** and **2.28b** to the corresponding amine salts, those could be employed for S_NAr reactions with the fluorinated CRBN ligand **CRBN-1 (2.9)** and the methylated control ligand **MeCRBN-1 (2.10)** (Scheme 2.6 b), as well as for amide coupling reactions with deprotected CRBN ligand **CRBN-2 (2.11)** and the corresponding control ligand **MeCRBN-2 (2.12)** (Scheme 2.6 c). S_NAr reactions with CRBN ligand **CRBN-1 (2.9)** and the methylated control ligand **MeCRBN-1 (2.10)** afforded active CRBN HaloPROTAC **CRBN-HP-1 (2.29)**, mono-functional methylated control **MeCRBN-ctrl-1 (2.30)** and mono-functional HTL control **noHTL-CRBN-ctrl-1 (2.31)** in moderate yields, and further purification with semi-preparative RP-HPLC yielded the compounds in 7% to 29% (Scheme 2.6 b). HATU-mediated amide coupling reactions with **CRBN-2 (2.11)** and the corresponding control ligand **MeCRBN-2 (2.12)** proceeded good yields, and after further semi-preparative RP-HPLC purification afforded active CRBN HaloPROTAC **CRBN-HP-2 (2.32)**, mono-functional methylated control **MeCRBN-ctrl-2 (2.33)** and mono-functional HTL control **noHTL-CRBN-ctrl-2 (2.34)** in final yields between 34% and 62%.

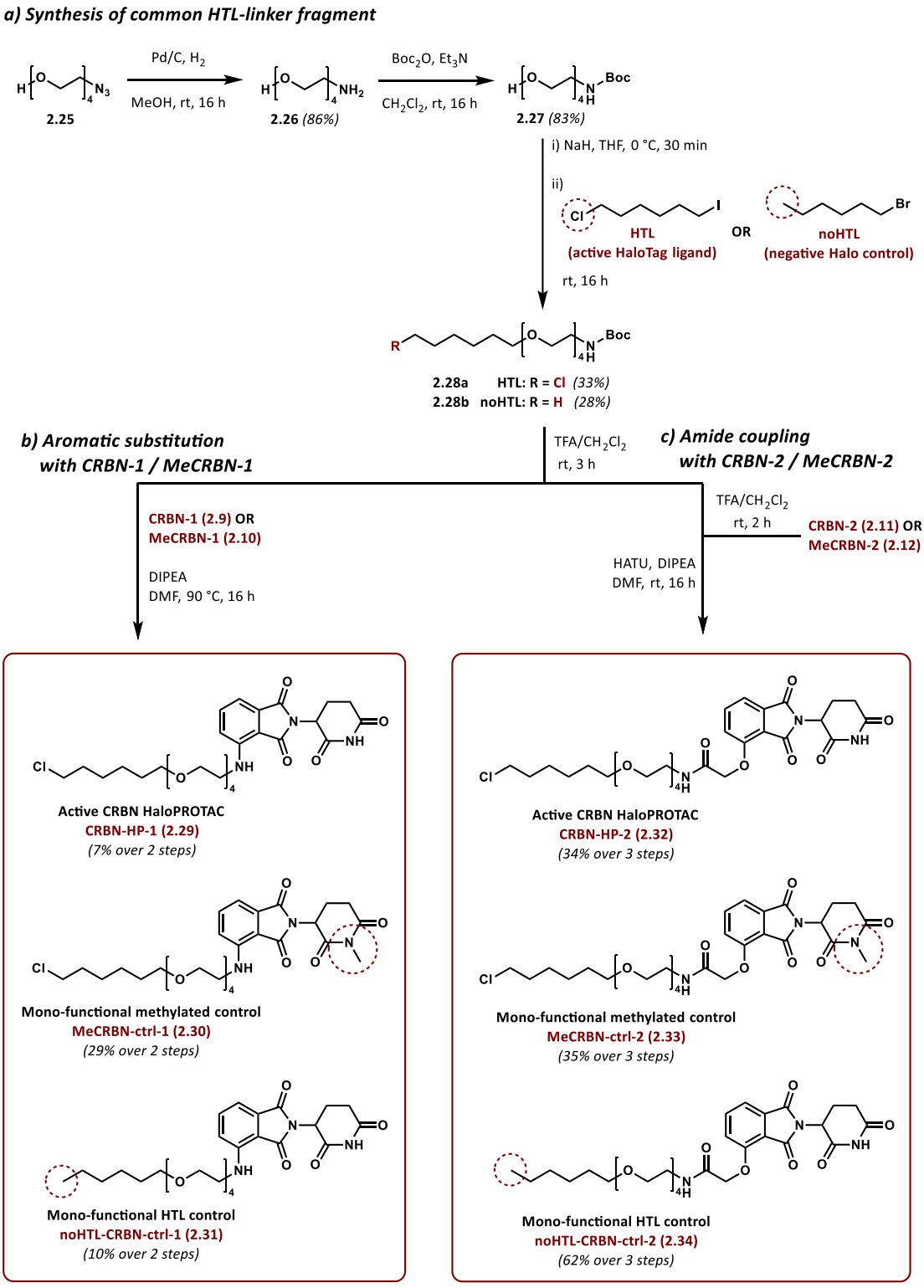

Scheme 2.6: Synthesis of CRBN HaloPROTACs and mono-functional controls.

HyT HaloPROTACs

Active HyT HaloPROTAC **HyT-HP-1 (2.36)** was accessed by mono-functionalising tetraethylene glycol *via* substitution of 1-bromoadamantane using triethylamine and catalytic amounts of 1,8-diazabicyclo[5.4.0]undec-7-ene (DBU) to afford Hyt–linker fragment **2.35** (Scheme 2.7), following a literature precedent.[148] The chlorohexane moiety was introduced analogously to the previously described syntheses of HTL–linker fragments, affording HyT HaloPROTAC **HyT-HP-1 (2.36)** in a 41% yield. HyT HaloPROTAC **HyT-HP-2 (2.37)** (Scheme 2.7) had been previously synthesised within the group.[149]

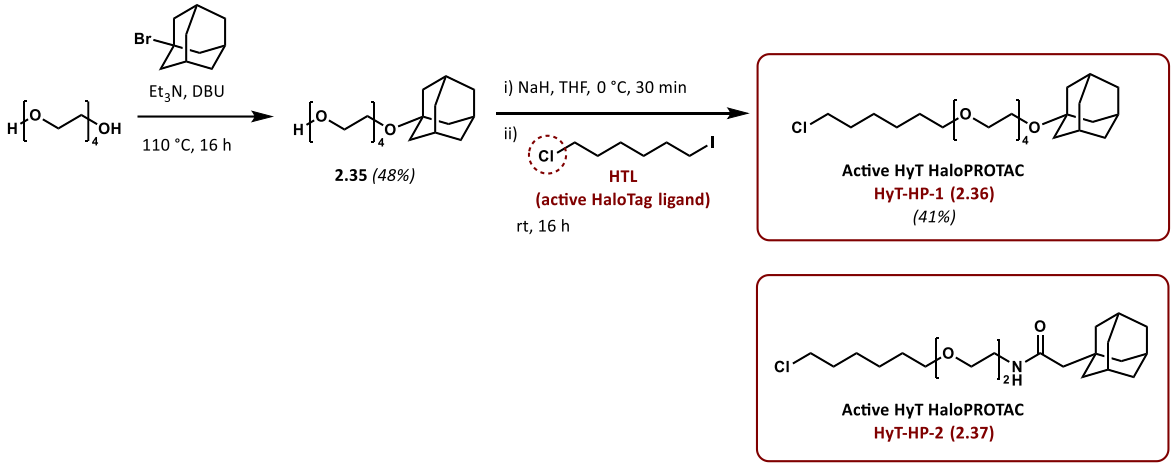

Scheme 2.7: Synthesis of HyT HaloPROTAC.

2.3 Biological testing of HaloPROTACs

2.3.1 Cloning of HaloTag–fascin fusion protein

Before carrying out biological testing assessing activity of the synthesised HaloPROTACs, a plasmid for the expression of a HaloTag–fascin fusion protein in different cell lines needed to be designed and constructed. It was decided to append HaloTag at the N-terminus of fascin (Figure 2.9) since N-terminal fusion was shown to not interfere with the actin-binding activity of fascin of a GFP–fascin fusion protein previously established and used in functional assays.[29]

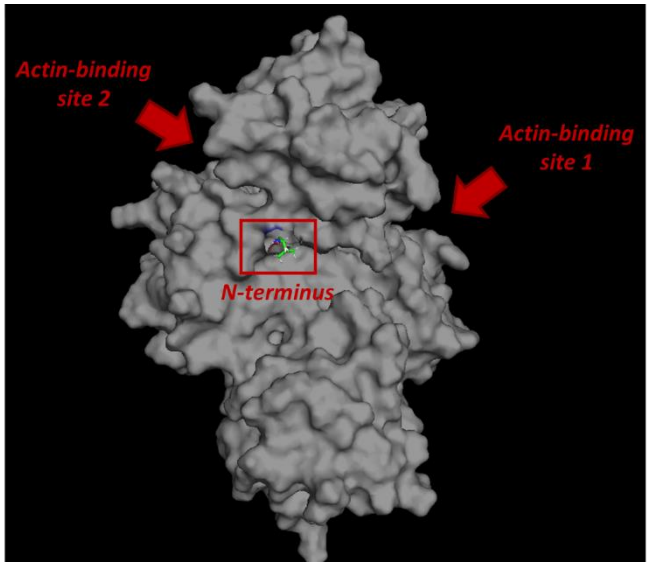

Figure 2.9: Fascin's N-terminus and actin-binding sites (PDB ID 6i18).

Based on a collaborator's results obtained with a HaloTag7 fusion protein,[150] it was decided to employ the same destination vector to construct the HaloTag–fascin fusion. HaloTag7 was initially developed as an optimised protein tag with improved solubility and expression for protein purification,[151] however, HaloTag7 is also widely employed in HaloPROTAC-mediated protein degradation studies.[103,117,137] The desired plasmid was established using In-Fusion cloning, a technique which is used for high-throughput screening applications due to its high accuracy and efficiency.[152] Compared to traditional cloning, no restriction enzymes or ligation is required: Polymerase chain reaction (PCR) amplification with specifically designed primers introduced complementary 15 base pair (bp) extensions on both, the insert and the linearised vector, allowing for direct annealing of the homologous ends (Figure 2.10). Generated clones were screened using agarose gel electrophoresis and clones of the correct size were submitted for sequencing, before bacterial transformation and purification of the plasmids for expression in different cells lines.

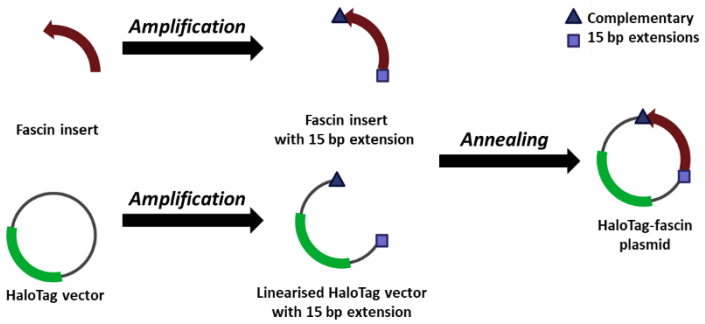

Figure 2.10: In-Fusion cloning process.

2.3.2 Cell line selection and expression of HaloTag–fascin fusion protein

Different cell lines were then selected, and expression of the necessary E3 ligases, namely VHL (~ 18 kDa) and CRBN (~ 55 kDa), was confirmed using western blot analysis (Figure 2.11). The human ovarian cancer cell line SK-OV-3 was selected since PROTAC-mediated degradation recruiting both CRBN and VHL has been reported in literature in this cell line.[128,153] Human fibrosarcoma cell line, HT-1080, is commonly used in functional assays to study invasive and migratory behaviour,[154,155] experiments which were planned to be conducted for this project as well. MIA-PaCa-2, a human pancreatic cancer cell line, was one of the cell lines employed for assessment of fascin activity in the Machesky Lab and was known to form pronounced filopodia, hence deemed appropriate for use. Although not a cancer cell line, mouse embryonic fibroblasts, MEF, were selected since they had previously been used to establish a fascin knock-out cell line and to study the actin cytoskeleton in phenotype assays in the Machesky Lab.

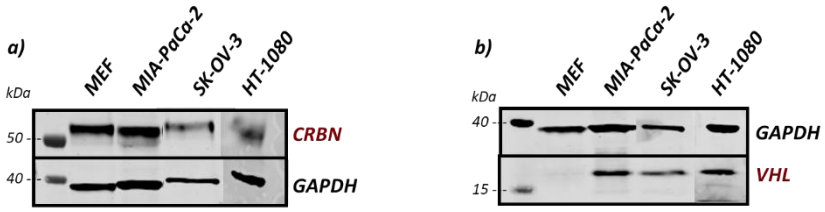

Figure 2.11: Western blot analysis of MEF, MIA-PaCa-2, SK-OV-3 and HT-1080 cell lysates to confirm expression of a) CRBN E3 ligase (~ 55 kDa) and b) VHL E3 ligase (~ 18 kDa) with GAPDH (~36 kDa) as loading control.

Cells were then transfected with the HaloTag–fascin plasmid using electroporation, incubated overnight to allow for expression of the fusion protein, lysed and the cell lysate was analysed by western blotting to confirm protein levels were adequate for further experiments. Since a primary antibody for fascin was used for visualisation, the blots revealed two bands – one for the fusion protein and one for the endogenous protein, confirming expression of the latter in the selected cell lines at the same time (Figure 2.12). It has to be noted that transfection with the plasmid was tolerated less well by MIA-PaCa-2 and MEF cells compared to SK-OV-3 and HT-1080 cells.

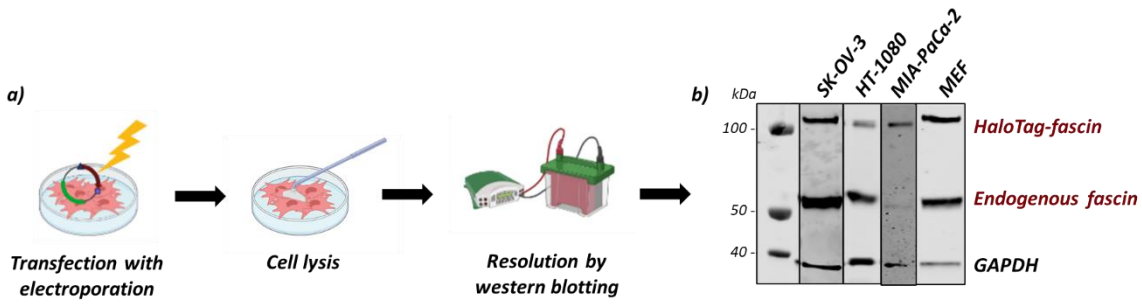

Figure 2.12: Western blot analysis to confirm HaloTag–fascin expression in different cell lines: a) workflow of western blot analysis and b) western blot analysis of MEF, MIA-PaCa-2, SK-OV-3 and HT-1080 cell lysates confirming expression of HaloTag–fascin fusion protein (~ 110 kDa) and endogenous fascin (~ 55 kDa) with GAPDH (~36 kDa) as loading control

All four cell lines were then used to carry out degradation assays in order to assess any potential differences, as cell line- and tissue-specific degradation profiles have been reported in the literature.[156,157] Additionally, due to their differences in phenotype and function, each cell line could prove useful for different aspects of the project.

2.3.3 HaloTag–fascin degradation assays with HaloPROTACs

Dose-response assays

To assess activity of the synthesised HaloPROTACs, degradation assays were carried out. Cells were transfected with the plasmid and incubated overnight to allow for expression of the fusion protein (Figure 2.13). Cells were then treated with the compounds at concentrations ranging from 0.01 μM to 10 μM, similar to degradation experiments reported in the literature.[103,137,158] After a 24-hour incubation period, cells were lysed and the lysate was resolved by western blotting. Treatment with appropriate primary antibodies for fascin and glyceraldehyde 3-phosphate dehydrogenase (GAPDH) as a loading control, and fluorescent secondary antibodies allowed for visualisation and quantification of protein levels.

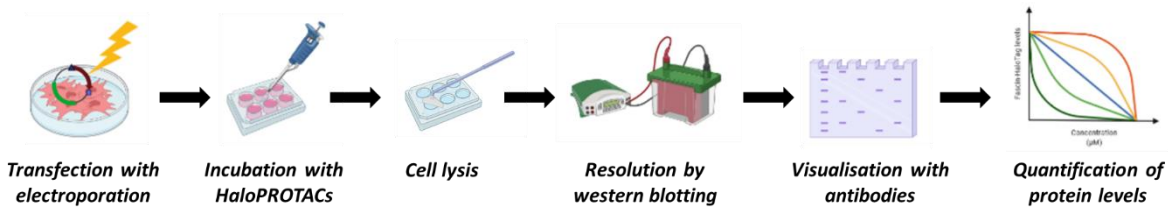

Figure 2.13: Degradation assay workflow: transfection of cells with plasmid by electroporation, treatment with HaloPROTACs at different concentrations, cell lysis, resolution of lysate by western blotting, visualisation by treatment with appropriate antibodies and quantification of protein levels.

Treatment with both VHL HaloPROTACs, **VHL-HP-1 (2.18)** and **VHL-HP-2 (2.22)**, resulted in a decrease in protein levels compared to the DMSO-treated control treated in SK-OV-3 and HT-1080 cells (Figure 2.14). VHL HaloPROTAC **VHL-HP-1 (2.18)** appeared to be slightly more active in both cells lines with reaching maximum degradation of around 70% at 1 μM in SK-OV-3 cells and 80% at 0.1 μM in HT-1080 cells. Protein levels were observed to increase at higher concentrations (10 μM) due to the "hook effect" observed for degrader compounds (Chapter 1.2.4).[103] For MIA-PaCa-2 and MEF cells, no decrease in protein levels could be observed, and the results were inconsistent, potentially due to those cell lines not tolerating transfection with the plasmid well.

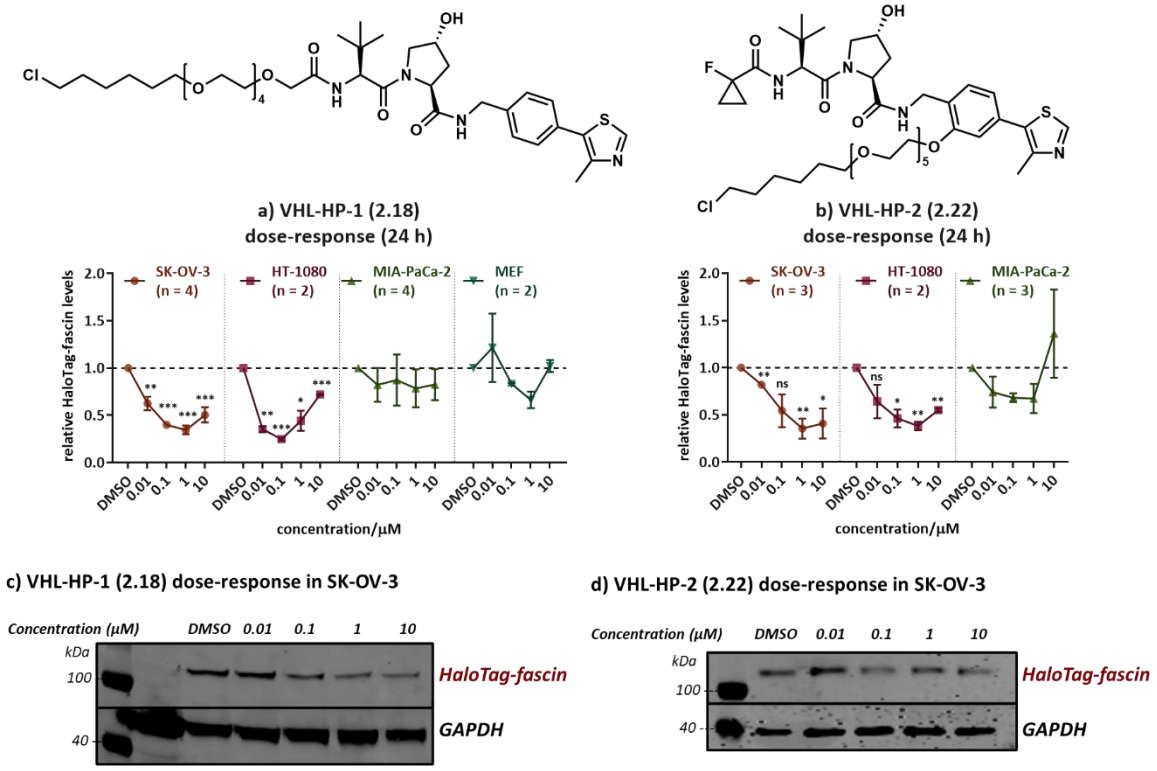

*Figure 2.14: Quantification of western blot analysis - HaloTag–fascin levels 24 hours after treatment with increasing concentrations of VHL HaloPROTACs a) **VHL-HP-1 (2.18)** and b) **VHL-HP-2 (2.22)**. Examples of western blots of dose-response assays in SK-OV-3 cells with c) **VHL-HP-1 (2.18)** and d) **VHL-HP-2 (2.22)**. Error bars represent SEM, unpaired t-test was applied (ns: $p > 0.05$, *: $p \leq 0.05$, **: $p \leq 0.01$, ***: $p \leq 0.001$).*

Results obtained for dose-response assays with CRBN HaloPROTACs **CRBN-HP-1 (2.29)** and **CRBN-HP-2 (2.32)** were irreproducible with no clear indication of a decrease in protein levels in any of the cell lines (Figure 2.15). Solely higher concentrations of **CRBN-HP-1 (2.29)** in MIA-PaCa-2 cells resulted in a slight decrease in protein levels, albeit by less than 30%.

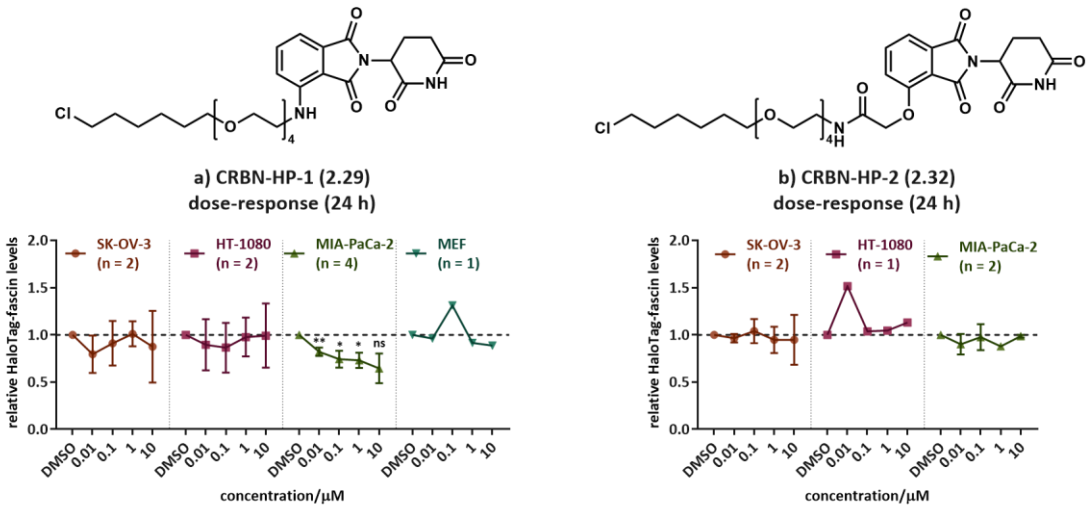

Figure 2.15: Quantification of western blot analysis - HaloTag–fascin levels 24 hours after treatment with increasing concentrations of CRBN HaloPROTACs a) ***CRBN-HP-1 (2.29)*** *and b)* ***CRBN-HP-2 (2.32)****.*
*Error bars represent SEM, unpaired t-test was applied (ns: p > 0.05, *: p ≤ 0.05, **: p ≤ 0.01, ***: p ≤ 0.001).*

The lack of activity of HyT HaloPROTAC **HyT-HP-1 (2.36)** was clearly observable in all tested cell lines (Figure 2.16). It was hypothesised that the polar oxygen atom adjacent to the adamantyl moiety could interfere with the ability of **HyT-HP-1 (2.36)** acting as a HyT. Hyt HaloPROTAC **HyT-HP-2 (2.37)**, which features an additional methylene group between the adamantyl moiety and the polar amide, appeared to induce a decrease in protein levels by around 30% at 0.1 µM concentration in SK-OV-3 cells and around 20% at 1 µM in MIA-PaCa-2 cells, however, the decrease was not statistically significant.

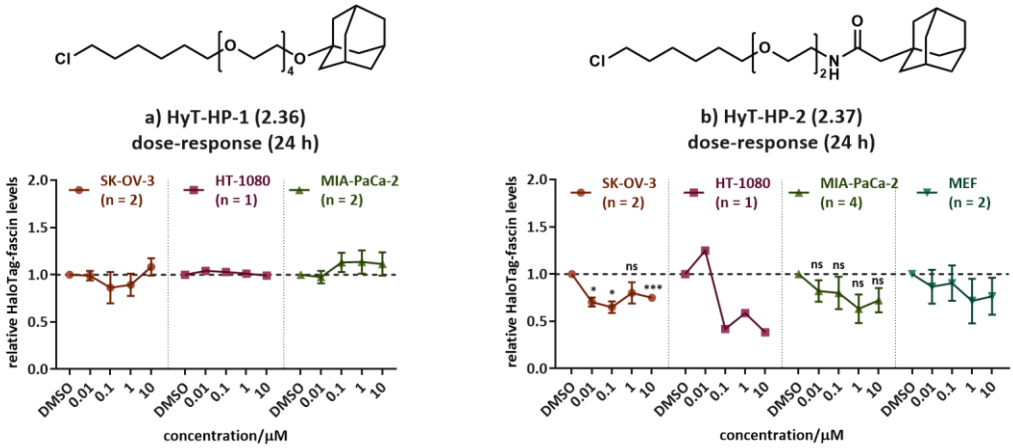

Figure 2.16: Quantification of western blot analysis - HaloTag–fascin levels 24 hours after treatment with increasing concentrations of HyT HaloPROTACs a) ***HyT-HP-1 (2.36)*** *and b)* ***HyT-HP-2 (2.37)****.*
*Error bars represent SEM, unpaired t-test was applied (ns: p > 0.05, *: p ≤ 0.05, **: p ≤ 0.01, ***: p ≤ 0.001).*

Since no activity for any of the compounds was observed in MEF cells, the cell line was abandoned, and for the remaining three cell lines, time-course assays were carried out to assess the timeframe of degradation of the fusion protein. When transiently transfecting

cells with plasmid DNA, the genetic material is not integrated into the cell's genome. Due to decay of the plasmid and loss of the genetic material as cells proliferate, expression of the fusion protein is temporary and protein levels decrease over time.[159] To determine how long the fusion protein would be expressed, protein levels were analysed 24 hours after transfection until 96 hours post-transfection (Figure 2.17). Whereas after 48 hours, around 50% of protein levels could be detected in SK-OV-3 cells, expression level decreased more rapidly in HT-1080 and MIA-PaCa-2 cells, with only around 20% to 25% protein detectable. This more rapid decrease in protein levels in HT-1080 and MIA-PaCa-2 cells could be explained by a faster proliferation rate of those two cell lines compared to SK-OV-3 cells. However, sufficient quantities of the fusion protein were observable 96 hours post-transfection in all cell lines, albeit at low levels, hence it was deemed appropriate to carry out time-course assays up to 96 hours after transfection.

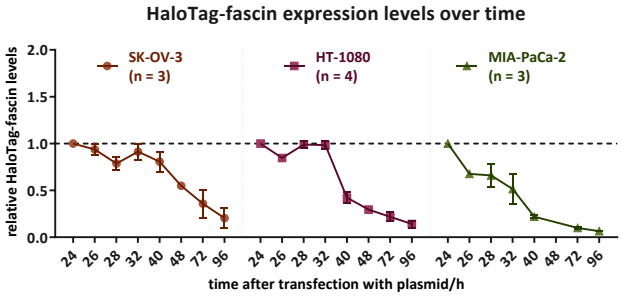

Figure 2.17: Quantification of western blot analysis – HaloTag–fascin expression levels in different cell lines over time after transfection with plasmid.
Error bars represent SEM.

Cells were transfected with the plasmid, as previously described, and incubated with 1 μM of the compounds for indicated times, ranging from 2 hours to 72 hours. Protein levels were determined and normalised against a DMSO-treated control for each time point to account for decrease in expression levels of the fusion protein over time. Both VHL HaloPROTACs, **VHL-HP-1 (2.18)** and **VHL-HP-2 (2.22)**, induced degradation of HaloTag–fascin after 4 to 8 hours in SK-OV-3 cells (Figure 2.18), whereas in HT-1080 cells degradation commenced later, after 16 to 24 hours (Figure 2.18). In both cell lines, both VHL HaloPROTACs induced sustained degradation up to 90% beyond 72 hours. For MIA-PaCa-2 cells, a decrease in protein levels was not observed until 72 hours and, similar to dose-response assays, the results were inconsistent, possibly due difficulties with tolerability of transfection with the plasmid.

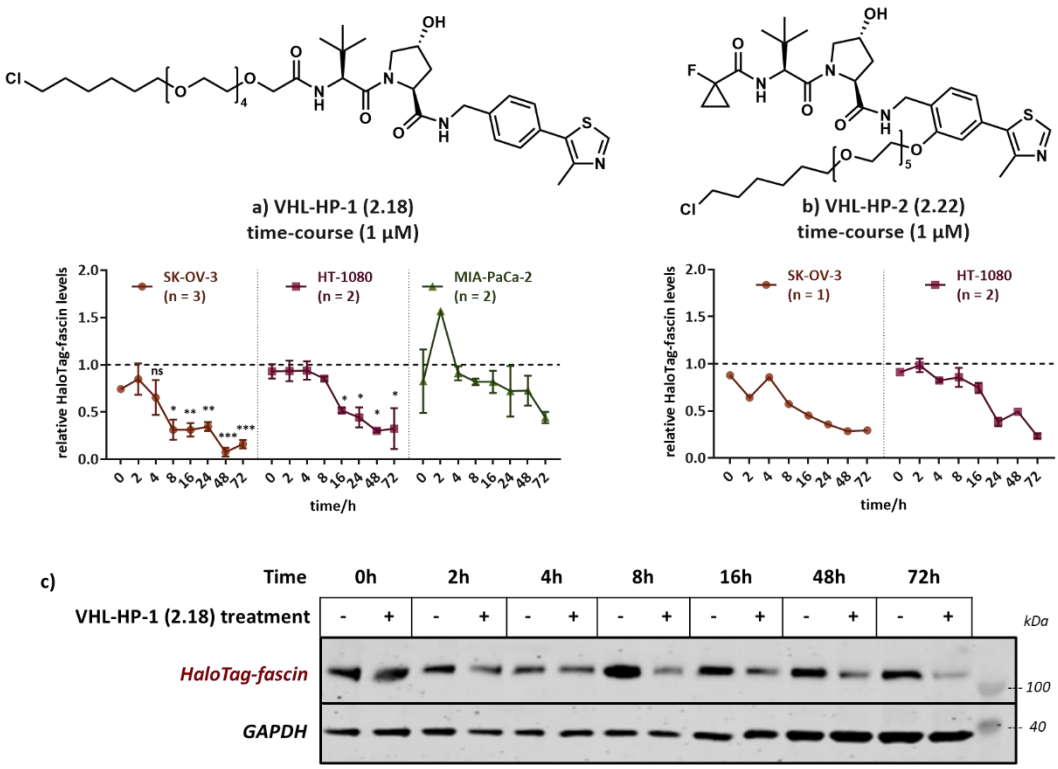

*Figure 2.18: Quantification of western blot analysis - HaloTag–fascin levels at different time points after treatment with 1 µM of VHL HaloPROTACs a) **VHL-HP-1 (2.18)** and b) **VHL-HP-2 (2.22)**; c) Example of western blot of time-course assay with **VHL-HP-1 (2.18)** in SK-OV-3 with DMSO control (-) and treated cells (+) for each time point.*
*Error bars represent SEM, unpaired t-test was applied (ns: $p > 0.05$, *: $p \leq 0.05$, **: $p \leq 0.01$, ***: $p \leq 0.001$).*

Despite the lack of activity of CRBN HaloPROTACs **CRBN-HP-1 (2.29)** and **CRBN-HP-2 (2.32)** for any concentration in dose-response assays, time-course assays were attempted in order to determine if degradation would occur at a later time point. Alternatively, potential metabolic instability of the compounds could have led to recovery of protein levels after 24 hours.[92] However, as for dose-response assays, no reproducible decrease in protein levels was observed in any of the cell lines at the tested concentrations. (Figure 2.19).

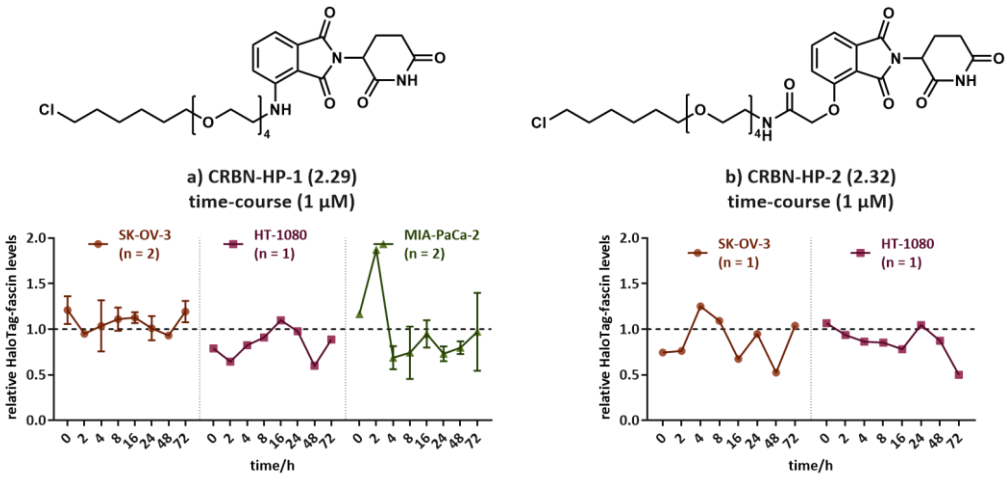

*Figure 2.19: Quantification of western blot analysis - HaloTag–fascin levels at different time points after treatment with 1 µM of CRBN HaloPROTACs a) **CRBN-HP-1 (2.29)** and b) **CRBN-HP-2 (2.32)**.*
Error bars represent SEM.

Similarly, activity of HyT PROTAC **HyT-HP-2 (2.37)**, for which inconclusive results were obtained in the dose-response assays, was assessed in time-course studies. Unfortunately, data obtained did again not offer clear indication of a decrease in protein levels for any of the cell lines tested (Figure 2.20). Due to the clear lack of activity of HyT PROTAC **HyT-HP-1 (2.36)** in dose-response assays, time-course experiments for this compound were deprioritised.

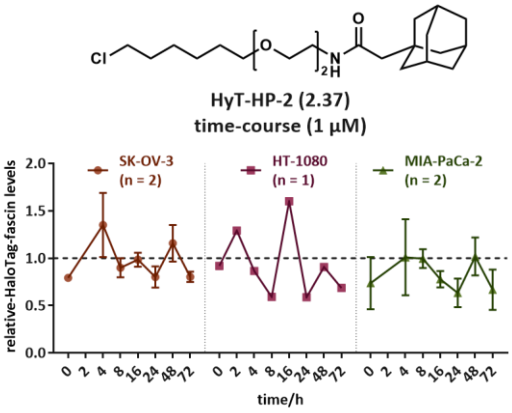

*Figure 2.20: Quantification of western blot analysis - HaloTag–fascin levels at different time points after treatment with 1 µM of HyT HaloPROTAC **HyT-HP-2 (2.37)**.*
Error bars represent SEM.

2.3.4 Intracellular engagement assays

Attempting to elucidate if the underlying cause for the lack of activity of CRBN and HyT HaloPROTACs could be found with lack of cell permeability of the compounds, competition assays with active VHL HaloPROTAC **VHL-HP-1 (2.18)** were carried out. It was hypothesised that if the inactive compounds were cell permeable, they would bind to the HaloTag portion of the fusion protein, essentially inhibiting it, thereby preventing active HaloPROTAC **VHL-HP-1 (2.18)** from binding and inducing protein degradation, which would result in a rescue of protein levels. Hence if after co-treatment with 1 µM of active **VHL-HP-1 (2.18)** and increasing concentrations from 0.1 µM to 100 µM of the inactive HaloPROTACs, protein levels would be rescued, this would provide some evidence for the inactive compounds being cell permeable and the lack of activity would be caused by other factors. Treatment with active **VHL-HP-1 (2.18)** expectedly decreased protein levels by 70% to 80%, in line with previous dose-response assays (Figure 2.21). Titration of CRBN HaloPROTACs **CRBN-HP-1 (2.29)** and **CRBN-HP-2 (2.32)**, and HyT HaloPROTACs **HyT-HP-1 (2.36)** and **HyT-HP-2 (2.37)** resulted in rescue of HaloTag–fascin levels at higher concentrations, with reaching full recovery of protein levels at the highest concentration of 100 µM. Based on the obtained results, cell permeability was ruled out as a constraint for activity of CRBN and

HyT HaloPROTACs. Other factors could impede activity, such as suboptimal linker lengths which could hinder recruitment of the E3 ligase or prevent optimal exposure of the HyT necessary to induce degradation of the POI.[120,138]

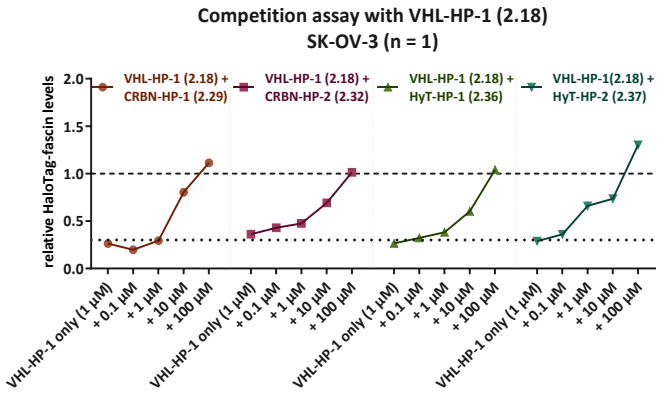

*Figure 2.21: Quantification of western blot analysis – HaloTag–fascin levels for intracellular engagement assay by co-treatment of 1 µM **VHL-HP-1 (2.18)** and increasing concentrations of CRBN HaloPROTACs **CRBN-HP-1 (2.29)** and **CRBN-HP-2 (2.32)**, and HyT HaloPROTACs **HyT-HP-1 (2.36)** and **HyT-HP-2 (2.37)***

It was decided to proceed with further experiments using the two VHL HaloPROTACs which showed activity in SK-OV-3 and HT-1080 cells, based on the reproducible results and consistent degradation obtained for those compounds and the ease of handling of the two selected cell lines.

2.3.5 Control assays to confirm PROTAC-mediated mechanism

Next, control assays were carried out in order to confirm that the observed decrease of HaloTag–fascin protein levels after treatment with VHL HaloPROTACs **VHL-HP-1 (2.18)** and **VHL-HP-2 (2.22)** was indeed mediated by the proposed PROTAC mechanism resulting in proteasomal degradation of the fusion protein.

Competition with mono-functional controls

Similar to the competition assays carried out to confirm intracellular engagement of the inactive HaloPROTACs (Chapter 2.3.4), control assays with mono-functional control compounds were performed. Two sets of control compounds had previously been synthesised for each active compound: Mono-functional VHL epimer controls ***cis*VHL-ctrl-1 (2.19)** and ***cis*VHL-ctrl-2 (2.23)** which would bind to the HaloTag portion of the fusion protein but not the VHL E3 ligase (Figure 2.22 a), blocking the active HaloPROTACs from binding to the fusion protein. Mono-functional HaloTag control compounds **noHTL-VHL-**

ctrl-1 (2.20) and **noHTL-VHL-ctrl-2 (2.24)**, on the other hand, would recruit the VHL E3 ligase but not bind to the fusion protein (Figure 2.22 b), essentially inhibiting the E3 ligase.

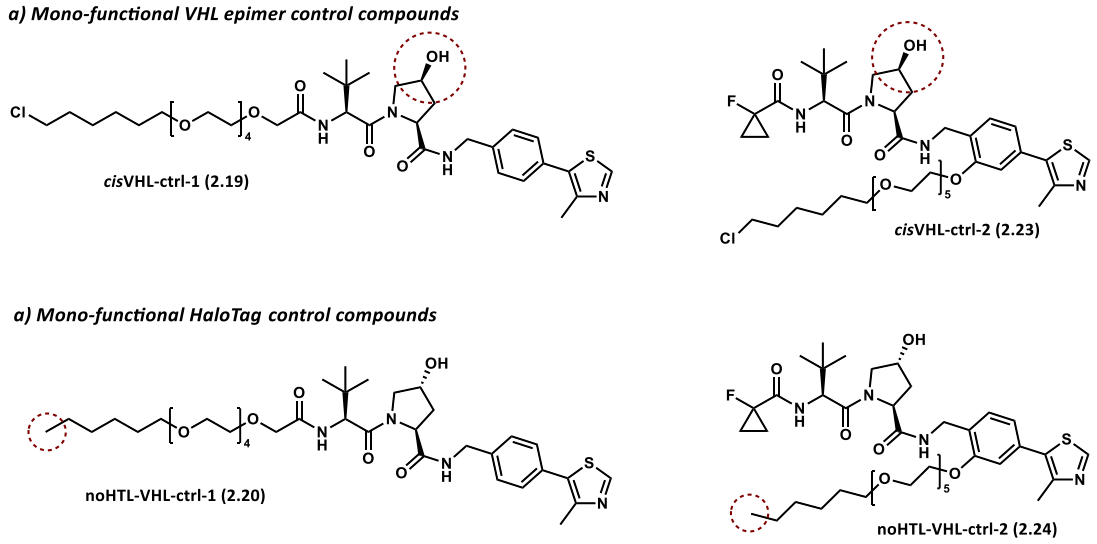

Figure 2.22: a) Mono-functional VHL epimer control compounds **cis*VHL-ctrl-1 (2.19)*** *for* ***VHL-HP-1 (2.18)*** *and* **cis*VHL-ctrl-2 (2.23)*** *for* ***VHL-HP-2 (2.22)***
b) Mono-functional HaloTag control compounds ***noHTL-VHL-ctrl-1 (2.20)*** *for* ***VHL-HP-1 (2.18)*** *and* ***noHTL-VHL-ctrl-2 (2.24)*** *for* ***VHL-HP-2 (2.22)****.*

First, confirmation that the mono-functional control compounds themselves would not induce any decrease in fusion protein levels at the concentrations tested was obtained (Figure 2.23). Compound concentrations above 10 µM were not tolerated by the cell lines tested.

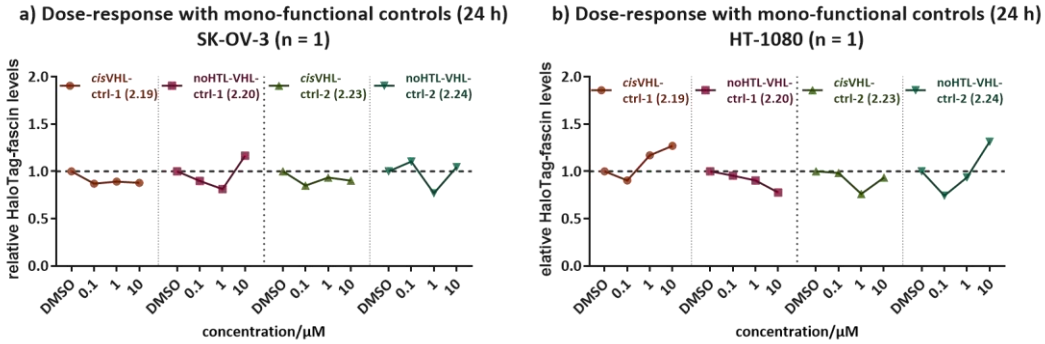

Figure 2.23: Quantification of western blot analysis - HaloTag–fascin levels 24 hours after treatment with increasing concentrations of mono-functional controls **cis*VHL-ctrl-1 (2.19)*****,** **cis*VHL-ctrl-2 (2.23)*****,** ***noHTL-VHL-ctrl-1 (2.20)*** *and* ***noHTL-VHL-ctrl-2 (2.24)*** *in a) SK-OV-3 cells and b) HT-1080 cells.*

Then, cells were incubated with 1 µM of the active VHL HaloPROTACs, **VHL-HP-1 (2.18)** or **VHL-HP-2 (2.22)**, and increasing concentrations from 0.1 µM to 10 µM of the corresponding mono-functional control compound before analysing protein levels by western blotting after 24 hours (Figure 2.24). Each mono-functional control for either of the active VHL HaloPROTACs was able to rescue of protein levels. Interestingly, rescue of protein levels

was more pronounced for VHL epimer control compounds ***cis*VHL-ctrl-1 (2.19)** and ***cis*VHL-ctrl-2 (2.23)**. This can be explained by the covalent attachment of the control compounds to HaloTag, thereby permanently impeding the active HaloPROTACs from binding. HaloTag control compounds **noHTL-VHL-ctrl-1 (2.20)** and **noHTL-VHL-ctrl-2 (2.24)**, on the other hand, reversibly inhibit the VHL E3 ligase, allowing for recruitment of VHL to the covalent PROTAC–fusion protein complex and its subsequent degradation to occur.

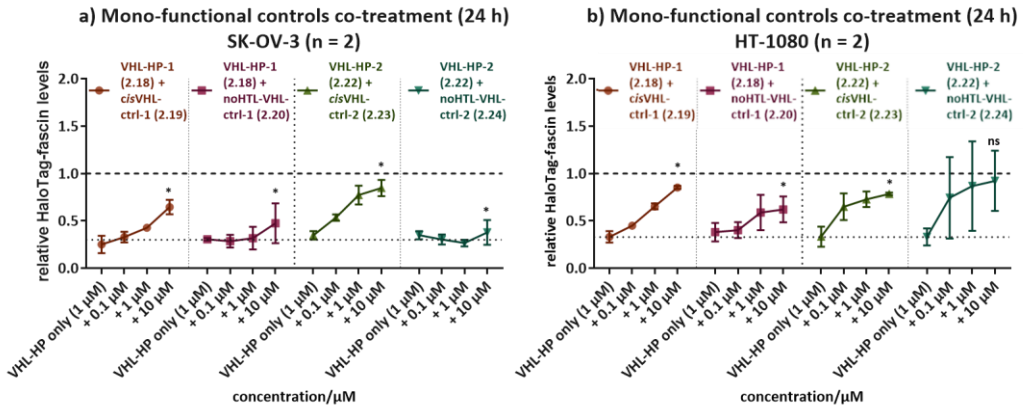

*Figure 2.24: Quantification of western blot analysis – HaloTag–fascin levels 24 hours after co-treatment of 1 µM of active VHL HaloPROTACs **VHL-HP-1 (2.18)** and **VHL-HP-2 (2.22)** and increasing concentrations of mono-functional VHL epimer controls **cis*VHL-ctrl-1 (2.19)*** and **cis*VHL-ctrl-2 (2.23)*** and mono-functional HaloTag controls **noHTL-VHL-ctrl-1 (2.20)** and **noHTL-VHL-ctrl-2 (2.24)** in a) SK-OV-3 and b) HT-1080 cells. Error bars represent SEM, unpaired t-test was applied (ns: $p > 0.05$, *: $p \leq 0.05$, **: $p \leq 0.01$, ***: $p \leq 0.001$).*

Inhibition of proteasome

PROTAC-induced protein degradation is mediated by the proteasome (Chapter 1.2.3), hence rescue of protein levels through inhibition of the proteasome would confirm degradation to proceed *via* the PROTAC mechanism.[128,160] Different proteasome inhibitors are available, each of which acting through a distinct mechanism.[161] MG132 (Cbz-Leu-Leu-Leucinal), a synthetic peptide aldehyde, is a well-studied reversible and cell-permeable proteasome inhibitor. It acts by forming a hemiacetal with the hydroxyl moiety of the proteasome's N-terminal threonine, which is the catalytic nucleophile in the active site crucial for the proteasome's peptide cleavage activity (Figure 2.25).[162]

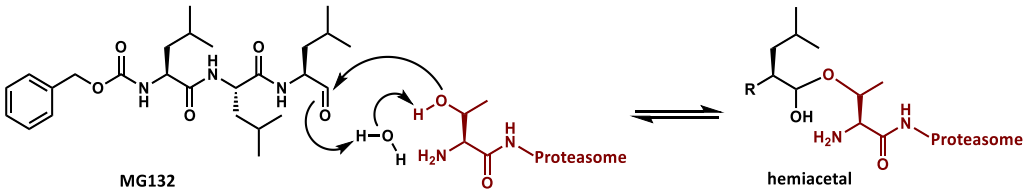

Figure 2.25: Proteasome inhibitor MG132 and its mechanism of action.[161]

For the control assays, the proteasome was inhibited by pre-treating SK-OV-3 and HT-1080 cells with 0.5 μM of MG132 for 4 hours, before addition of 1 μM of active VHL HaloPROTACs, **VHL-HP-1 (2.18)** or **VHL-HP-2 (2.22)**, and analysis of protein levels after a 24-hour incubation period. Higher concentrations of MG132 were not tolerated by the cells, indicating that proteasome function is crucial for cell survival.[163] Pre-treatment with the proteasome inhibitor rescued protein levels in both cell lines for both VHL HaloPROTACs (Figure 2.26), confirming degradation was mediated proteasomally. Interestingly, increased HaloTag–fascin levels were observed after treatment with the inhibitor compared to the DMSO-treated control, providing evidence for significant degradation of the fusion protein through the proteasomal pathway even without PROTAC treatment.

Taken together, the control experiments confirmed degradation of the HaloTag–fascin fusion protein proceeded *via* the PROTAC mechanism through recruitment of the UPS by VHL HaloPROTACs **VHL-HP-1 (2.18)** and **VHL-HP-2 (2.22)** and subsequent proteasomal degradation of the fusion protein. Next, the effect of PROTAC-mediated degradation of the fusion protein could be determined with functional and phenotype assays.

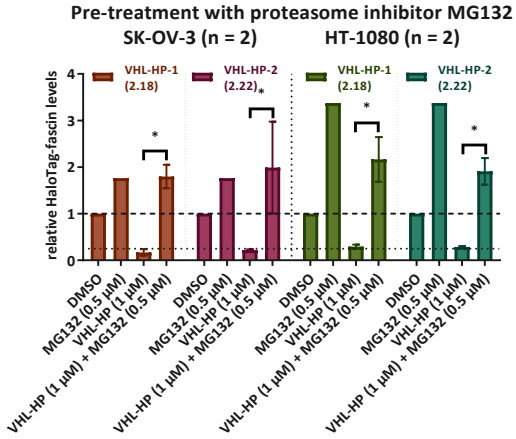

*Figure 2.26: Quantification of western blot analysis – HaloTag–fascin levels 24 hours after inhibition of proteasome with MG132 and treatment with 1 μM of active VHL HaloPROTACs **VHL-HP-1 (2.18)** and **VHL-HP-2 (2.22)** or DMSO in SK-OV-3 and HT-1080 cells.*
*Error bars represent SEM, unpaired t-test was applied (ns: $p > 0.05$, *: $p \leq 0.05$, **: $p \leq 0.01$, ***: $p \leq 0.001$).*

2.3.6 Fascin knock-down trials

Due to presence of endogenous fascin in the cell lines employed for the experiments, a fascin knock-out cell line needed to be established in order to determine the effect of absence of the endogenous protein. In addition, expression of the HaloTag–fascin fusion protein in a fascin knock-out cell line would allow for assessment of functionality of the fusion protein, and the effect of its selective degradation on cell function and phenotype. As an initial trial, transient genetic knock-down using small interfering RNA (or silencing

RNA, siRNA) was carried out to probe the effect on cell function, specifically on the migratory and invasive ability of the cells, in order to then establish which cell line might be suitable for generation of a stable knock-out cell line. siRNA, double-stranded (ds) non-coding RNA of 20 to 24 bp length, acts through the RNA interference (RNAi) pathway.[164] Essentially, it interferes with expression of the targeted gene by inducing degradation of messenger RNA (mRNA) after transcription, thus preventing its translation (Figure 2.27). Assembly of the ds siRNA with RNA-inducing silencing complex (RISC) activates the complex. Through unwinding of the ds siRNA and cleavage of the sense strand, the anti-sense strand can now bind to the target mRNA, inducing its cleavage and degradation. However, the effect is of temporary nature, and expression of the HaloTag–fascin fusion protein would not be possible due to interference with its transcription through the same pathway.[165]

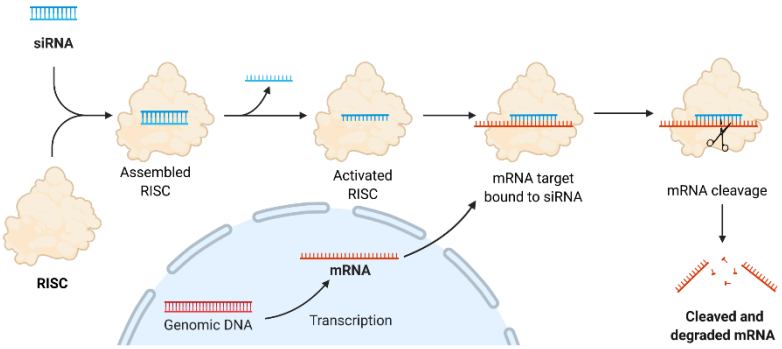

Figure 2.27: RNA interference pathway.

SK-OV-3 and HT-1080 cells were treated with four commercially obtained siRNAs and a non-targeting siRNA control, and fascin levels were analysed with western blotting 48 hours after treatment. Three out of the four siRNAs resulted in a knock-down of fascin of over 80% compared to the untreated control in both cell lines (Figure 2.28), and siRNA07 and siRNA08 were chosen for further assays.

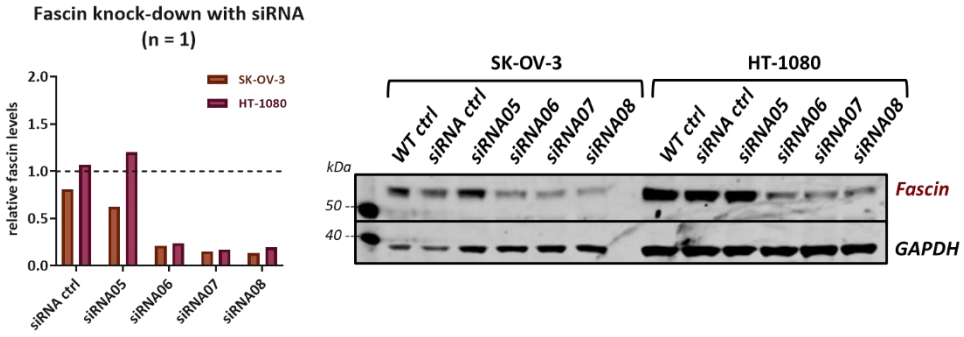

Figure 2.28: Western blot analysis to confirm fascin knock-down with siRNAs in SK-OV-3 and HT-1080 cells.

Functional assays were then carried out to assess the impact of fascin knock-down on cell functionality. Following a protocol employed by the Drug Discovery Unit at the Beatson Institute for Cancer Research to assess activity of the compounds developed as part of their drug discovery projects,[59,61] cells were treated with siRNA07 and siRNA08 as well as with fascin ligand B **FSCN-B (1.5)** for which inhibition of invasion was reported.

Proliferation assay

First, the impact of the different treatments on cell proliferation was assessed since impairment of cell growth could impact on migratory and invasive behaviour of the cells. For proliferation assays, SK-OV-3 and HT-1080 cells were seeded at low density and then treated with siRNA control, siRNA07 and siRNA08, as well as 10 μM and 30 μM of fascin ligand B **FSCN-B (1.5)**. Proliferation was monitored hourly over 70 hours on an automated microscope, and the rate of proliferation of treated cells was compared against untreated control cells (Figure 2.29). Cell confluence, the percentage of well surface covered by cells, was used as a measure for proliferation, and the normalised proliferation index was determined by normalising cell confluence at the respective time points against initial cell confluence to account for any variability in initial cell seeding. For SK-OV-3 cells (Figure 2.29 a and b), treatment with siRNA08 impacted negatively on proliferation, resulting in a significantly slower cell growth compared to cells treated with the siRNA control. All other conditions were tolerated well by SK-OV-3 cells, and did not result in slowed proliferation. HT-1080 cells (Figure 2.29 c and d) were observed to be faster proliferating than SK-OV-3 cells, however, tolerated treatment less well: All conditions, including treatment with the siRNA control, resulted in slower cell growth. The impact after treatment with fascin ligand B **FSCN-B (1.5)** was less pronounced than siRNA treatment, with siRNA08 again resulting in the most significant impairment of cell growth.

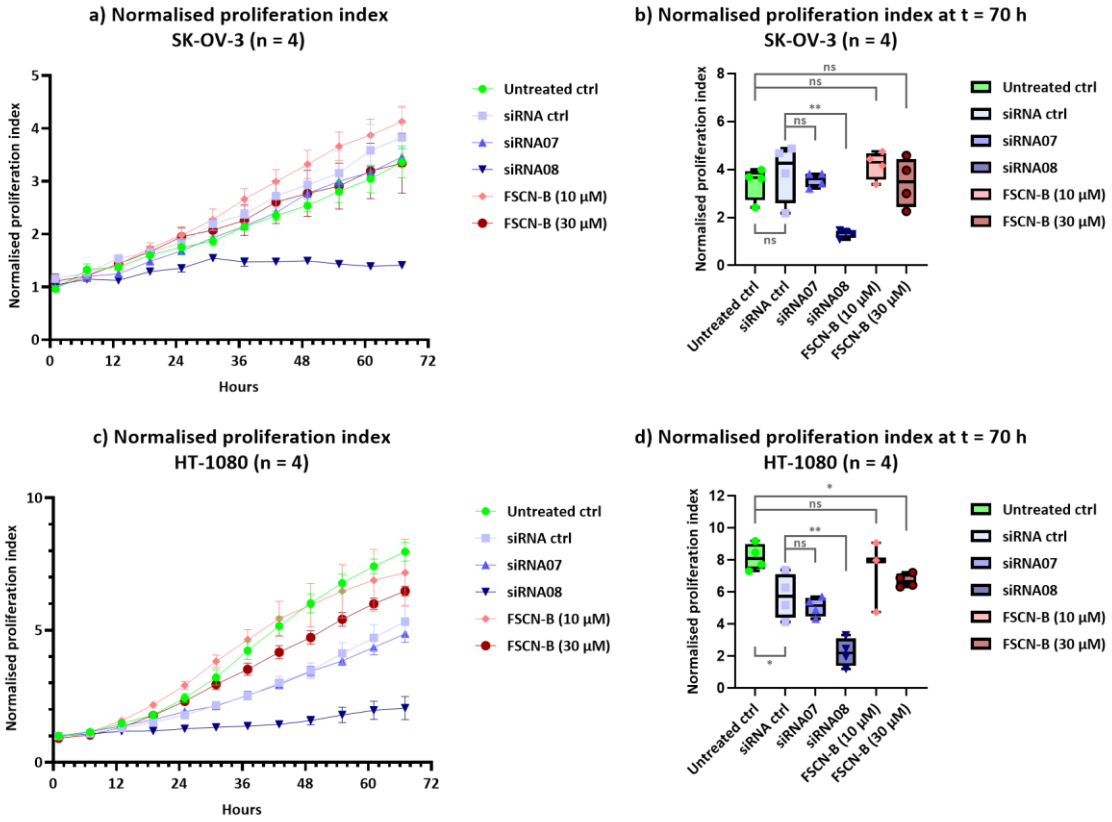

Figure 2.29: Normalised proliferation index based on cell confluence a) over 70 hours for SK-OV-3 cells, b) at t = 70 h for SK-OV-3 cells: untreated ctrl
c) over 70 hours for HT-1080 cells and b) at t = 70 h for HT-1080 cells.
*Error bars in a) and c) represent SEM. Whiskers in b) and d) represent minimum and maximum. Unpaired t-test was applied (ns: $p > 0.05$, *: $p \leq 0.05$, **: $p \leq 0.01$, ***: $p \leq 0.001$).*
Normalised proliferation index at t = 70 h calculated as mean ± SEM (Appendix 1).

Wound healing assays

Next, wound healing assays were carried out in order to assess the ability of the cells to migrate or invade into a wound to close it. For the assays, cells were seeded at full confluency and grown until forming a uniform monolayer of cells, before a wound was scratched into the cell layer (Figure 2.30).[166] For invasion assays, a matrix overlay was inserted into the wound through which the cells would invade, whereas for migration assays no overlay was added. Cells were treated and monitored over time to then analyse wound closure for the different conditions compared to a control condition.

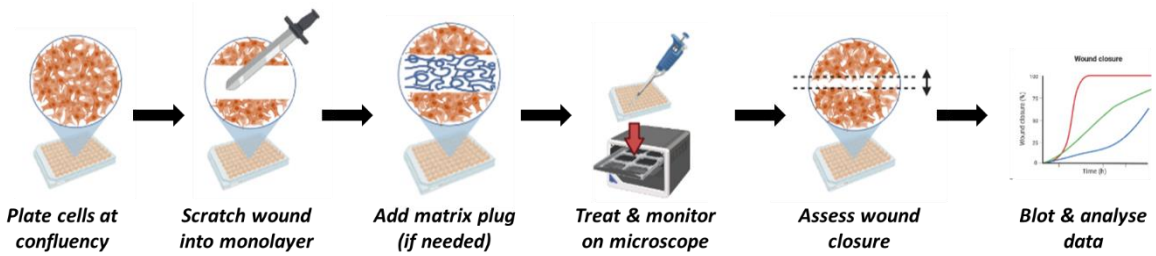

Figure 2.30: Wound scratch assay workflow.

Wound closure can then be assessed by the rate by which the wound closes or by the increase in relative wound density over time.[167] Wound closing rates are established as a function of changes in wound width over time, hence assessing how fast cell boundaries move towards each other into the wound to close it. However, this cell movement is not always uniform and cell boundaries, and therefore wound width, can be difficult to determine. This is particularly important for invasion assays for which cells move through a three-dimensional matrix, potentially displaying changes in morphology or forming invasion tracts or networks through the matrix, making it difficult to establish wound boundaries. Relative wound density is a measure that not only assesses the wound area but also takes into account any changes that occur outside of the wound as a results of cell movement. As such, it is self-normalising for overall changes in cell density or cell morphology and can be used as a robust metric to assess wound healing.

In wound healing assays assessing cell migration, HT-1080 cells generally displayed a faster increase in relative wound density over time (Figure 2.31 c and d), and a faster wound closing rate, compared to SK-OV-3 cells (Figure 2.31 a and b). This could be explained by faster proliferation of HT-1080 cells compared to SK-OV-3 cells, as also observed in aforementioned proliferation assays. Treatment with siRNA08 slowed wound closure by round 30% for SK-OV-3 from 52 ± 0.67 µm/h for the untreated control cell to 38 ± 1.1 µm/h, however, the slower rate for siRNA08 treatment was not significant when compared to siRNA control treatment (Figure 2.31 d). For HT-1080 cells, siRNA08 treatment slowed wound closure by around 20%, from 110 ± 6.6 µm/h for the untreated control to 89 ± 2.4 µm/h (Figure 2.31 d). Treatment of HT-1080 cells with 30 µM of fascin ligand B **FSCN-B (1.5)** resulted in a small decrease in wound closing rate of around 10%. Taken together, the findings obtained from the migration assay were in line with the effects observed for proliferation.

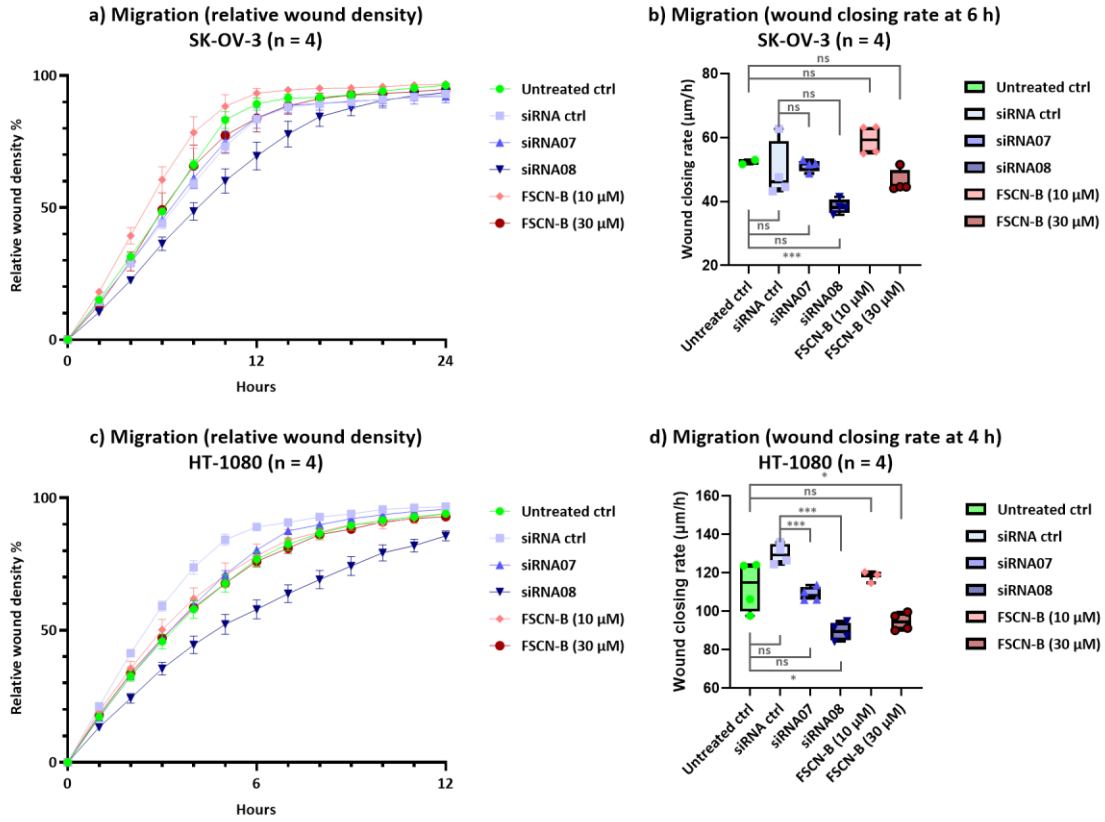

Figure 2.31: Wound healing assay – migration: a) relative wound density (%) over time for SK-OV-3 cells, b) wound closing rate (µm/h) at t = 6 h for SK-OV-3 cells, c) relative wound density (%) over time for HT-1080 cells, b) wound closing rate (µm/h) at t = 4 h for HT-1080 cells.
*Error bars in a) and c) represent SEM. Whiskers in b) and d) represent minimum and maximum. Unpaired t-test was applied (ns: $p > 0.05$, *: $p \leq 0.05$, **: $p \leq 0.01$, ***: $p \leq 0.001$). Wound closing rate calculated as mean ± SEM (Appendix 1).*

For invasion assays, a matrix overlay was inserted into the wound through which cells would need to invade in order to close the wound. Since fascin has been shown to modulate the invasive ability of cancer cells, inhibition of its function or its knock-down would be expected to slow invasion through the matrix.[61] Matrigel is commonly used as matrix to model the basement membrane when evaluating invasiveness of cancer cells.[168,169] Whereas untreated HT-1080 cells achieved full wound closure after 24 hours (Figure 2.32 c), full closure was not observed for untreated SK-OV-3 even after 72 hours (Figure 2.32 a). Since this effect appeared to be greater than the effect observed for migration assays, it was hypothesised to not only be due to a slower proliferation rate but due to a reduced invasiveness of SK-OV-3 cells compared to HT-1080 cells. Despite this, treatment with siRNA07 and fascin ligand B **FSCN-B (1.5)** showed a greater effect upon wound closure rate for SK-OV-3 than for HT-1080 cells. Other than treatment with siRNA08, which exhibited unexpected effects in previous assays, inhibition of fascin's activity or its knock-down did not result in any significant change in wound closure rate for HT-1080 cells (Figure 2.32 d).

For SK-OV-3 cells, wound closure decreased significantly by around 45% after treatment with siRNA07, from 14 ± 3.9 µm/h for the untreated control to 7.6 ± 2.1 µm/h, whereas treatment with 10 µM of fascin ligand B **FSCN-B (1.5)** slowed wound closure by 60% to 5.7 ± 1.8 µm/h.

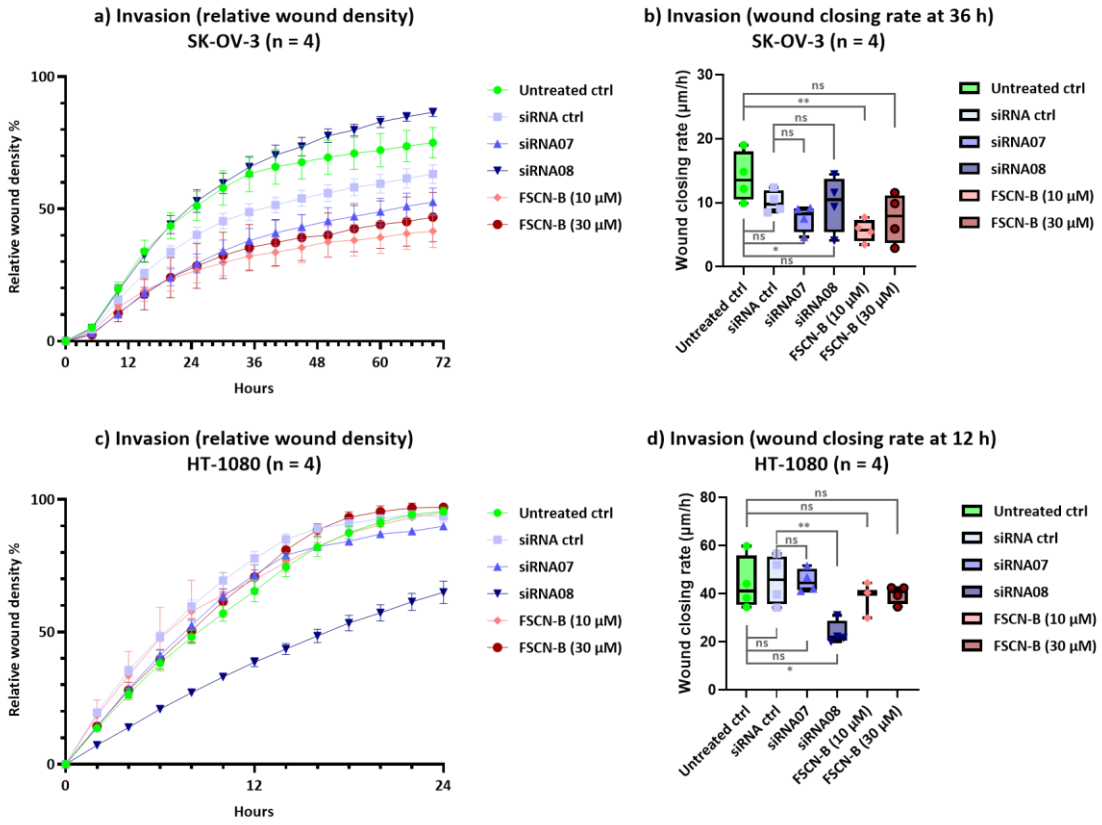

Figure 2.32: Wound healing assay – invasion: a) relative wound density (%) over time for SK-OV-3 cells, b) wound closing rate (µm/h) at t = 36 h for SK-OV-3 cells, c) relative wound density (%) over time for HT-1080 cells, b) wound closing rate (µm/h) at t = 12 h for HT-1080 cells.
*Error bars in a) and c) represent SEM. Whiskers in b) and d) represent minimum and maximum. Unpaired t-test was applied (ns: p > 0.05, *: p ≤ 0.05, **: p ≤ 0.01, ***: p ≤ 0.001). Wound closing rate calculated as mean ± SEM (Appendix 1).*

Despite their seemingly less invasive phenotype, SK-OV-3 cells were deemed appropriate for generation of a fascin knock-out cell line to be used for further experiments with the HaloTag model system. This was based on the results obtained for SK-OV-3 cells indicating that inhibition of fascin's activity or its absence would impact on the cells' functionality, an effect which was not observed for the more invasive HT-1080 cells.

2.3.7 Generation of fascin knock-out cell line

Individual genes can be permanently deactivated, or knocked-out, using different techniques, however, for this project, it was decided to use the CRISPR (clustered regularly interspaced short palindromic repeats)-Cas9 gene editing system due to its ease of

execution. Emmanuelle Charpentier and Jennifer Doudna were awarded the 2020 Nobel Prize in Chemistry for their work on this method which has undoubtedly revolutionised gene editing.[170] CRISPR-Cas9 was discovered as be part of the bacterial adaptive immune response to infections by viruses (bacteriophages), and has been adapted for use in gene editing to induce ds breaks at specific sites in the DNA.[171] Relying on RNA–DNA recognition, the interaction is highly specific, can be adapted to virtually any genomic target and potential off-target effects can be predicted more easily.[172] Cas9, a nuclease, is complexed with synthetic guide RNA (gRNA) specific for the target DNA sequence to be cleaved by the nuclease (Figure 2.33 a). Through RNA–DNA recognition, the nuclease is guided to the site of cleavage, and induces a ds break in the DNA. Repair of this ds break can now proceed in one of two ways (Figure 2.33 b). Non-homologous joining of ends is mediated *via* the cell's natural repair mechanisms and is prone to result in insertion or deletion of nucleotides. Such insertions or deletions would shift codons which, by either encoding for incorrect amino acids or prematurely introducing stop codons, would result in production of a non-functional protein and as such disrupting, or knocking out, the gene. By supplying the cell's natural repair mechanisms with donor DNA to be used as a repair template, additional genetic information can be added *via* homology-directed repair, thereby repairing a gene or introducing a novel gene function (knock-in).[173]

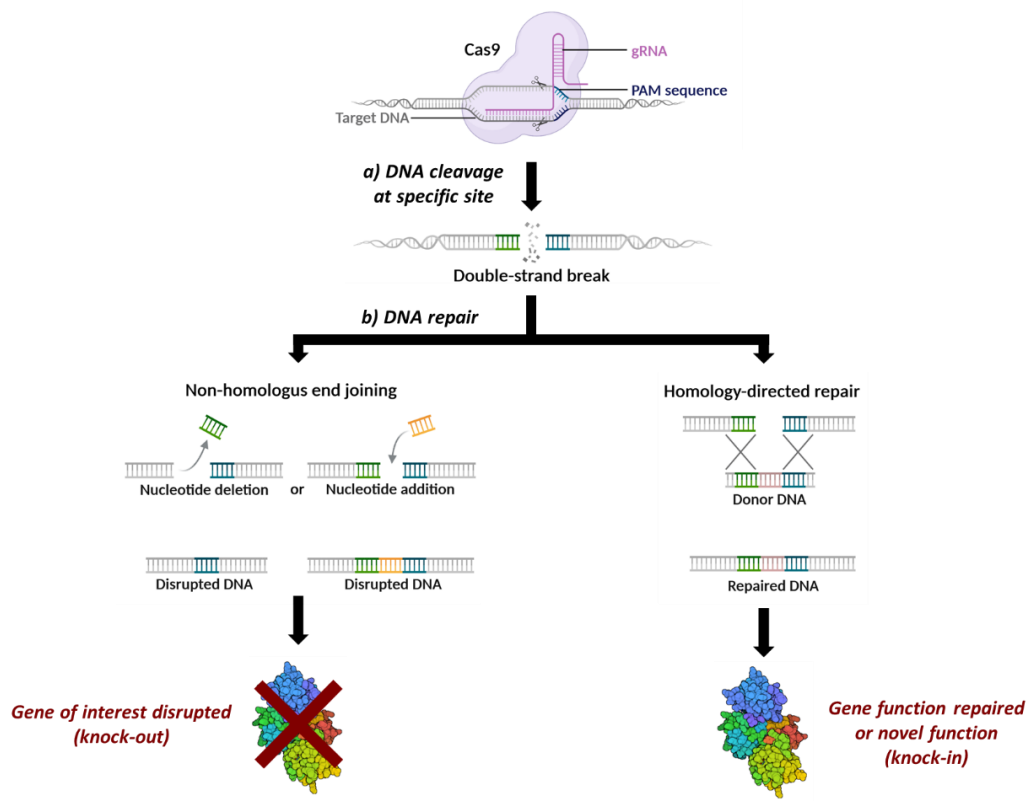

Figure 2.33: Gene editing through a) CRISPR-Cas9 inducing a double-strand break in the DNA and b) subsequent repair by either non-homologous end joining (knock-out) or homology-directed repair (knock-in) – adapted from [173].

For the design of a gRNA sequence for successful genetic knock-out, several considerations have to be taken into account. The targeted region on the gene to be knocked out should be protein coding (exon) in order to prevent it being spliced out, or removed. To obtain the best results, the region should be at either the start of the gene towards the 5' end so that disruption of the entire sequence is induced, or it should code for an essential domain of the protein in order to render it non-functional. In addition, the region needs to be adjacent to a protospacer adjacent motif (PAM) sequence which is necessary for Cas9 to initiate, and it should be unique compared to the remainder of the genome to avoid any off-target effects.[174]

The common approach to deliver Cas9 and the gRNA into the cell is *via* viral vectors, usually resulting in integration into the cell's genome and stable expression of Cas9. This method was deemed unpractical for the purpose of this project since a permanently expressed Cas9 would also target the introduced plasmid DNA due to homology with the endogenous protein, thereby preventing expression of the HaloTag–fascin fusion protein.[175] However, through transient transfection with a plasmid specially designed to express the necessary components for CRISPR–Cas9 gene editing, knock-out of only the gene encoding for endogenous fascin could be achieved.[176] Due to the transient nature of plasmid DNA, Cas9 would essentially disappear over time, which would make it possible to express the fusion protein once knock-out of the endogenous protein was achieved. Moreover, this approach would prevent the nuclease from interfering with cell function through potentially prolonged off-target activity, an issue occasionally encountered with stably expressed Cas9.[176]

Using this approach, appropriate gRNA oligonucleotides would be cloned into a Cas9–GFP vector, and the obtained plasmid DNA would be transformed in bacteria. Generated clones would be submitted for sequencing to confirm insertion of the gRNA, before bacterial transformation and purification of the plasmids for expression (Figure 2.34). Cells would be transfected with the plasmid and allowed to express GFP as selection marker before submitting them for fluorescence-activated cell sorting (FACS) and collection of cells displaying appropriate fluorescence. From the collected pool, individual cells would be grown into single clone populations before confirming knock-out by western blotting.[176]

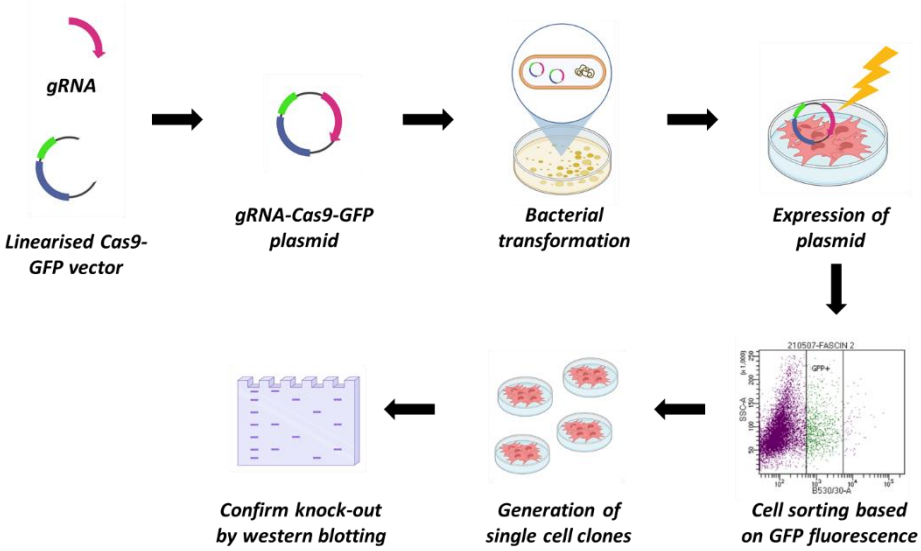

Figure 2.34: CRISPR–Cas9 workflow of generating a fascin knock-out cell line using gRNA–Cas9–GFP plasmids.

The plasmid for transient expression of Cas9 was established by cloning two suitable gRNA oligonucleotides which had previously been designed and successfully employed in the Machesky Lab, into a Cas9–GFP vector. Cas9 and GFP marker would be expressed as individual proteins, to ensure full function of the nuclease once assembled with gRNA after expression in the cells.[176]

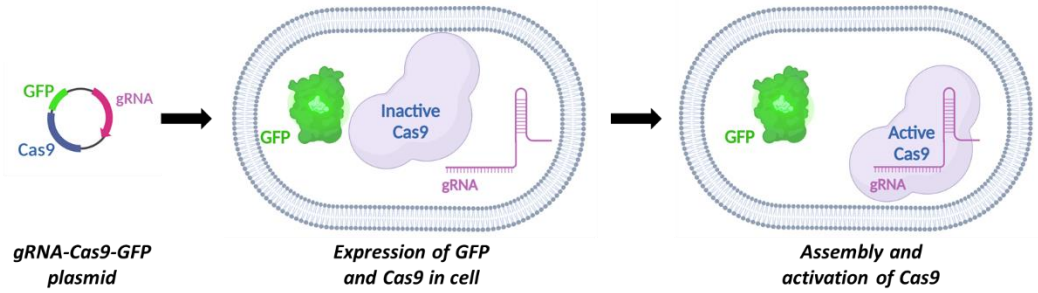

Figure 2.35: gRNA–Cas9–GFP plasmid expression in cell with subsequent assembly and activation of Cas9.

From cells transfected with either of the two plasmids, populations displaying appropriate fluorescence compared to the GFP-only control ("GFP+" in Figure 2.36 a) were used to generation of single cells clones. Out of the eleven clone populations, only one was determined to exhibit complete fascin knock-out (#9 in Figure 2.36 b) and was selected for further experiments. Unexpectedly, one clone population displayed 200% fascin protein levels compared to the wild-type control (#8 in Figure 2.36 b), possibly due to genomic rearrangement after the ds break was induced,[177] and was also chosen for subsequent assays to assess impact of fascin overexpression. Fascin levels of the selected clone populations were verified by western blotting before conducting experiments.

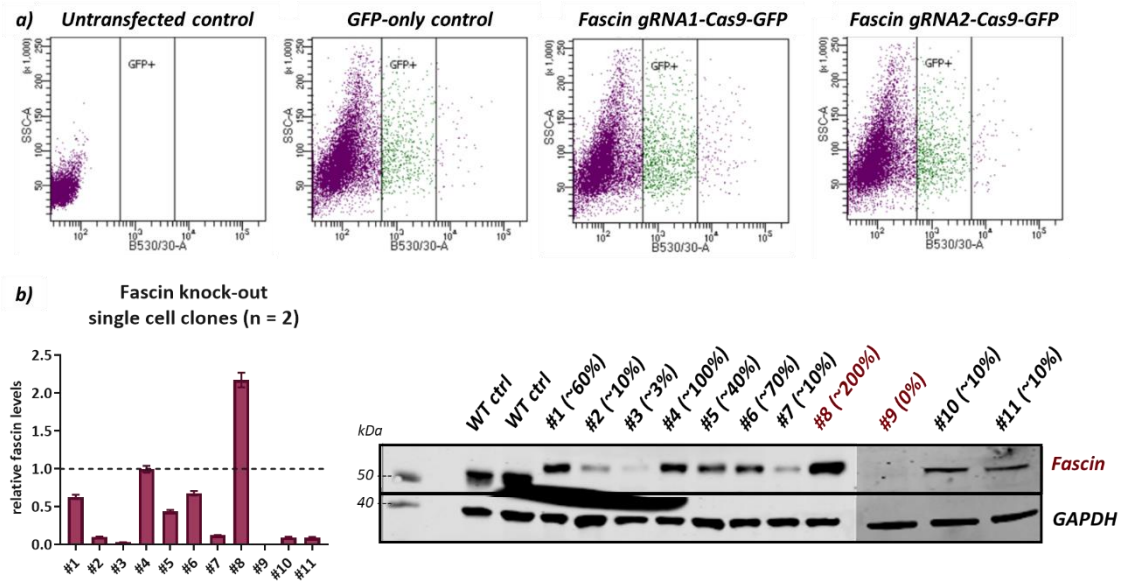

Figure 2.36: a) FACS (GFP fluorescence vs. side scatter) of untransfected control cells, control cells transfected with GFP–Cas9 plasmid, cells transfected with fascin gRNA1–Cas9–GFP plasmid and with fascin gRNA2–Cas9–GFP plasmid. Cells in "GFP+" range were collected to generate single cell clones and b) Western blot analysis to determine fascin levels of single cell clone populations.

Analogous to the assays for fascin knock-down using siRNA, proliferation and wound healing assays were carried out with the generated fascin knock-out cell line and the cell line expressing 200% fascin to assess the impact of absence and overexpression of the endogenous protein, respectively. Additionally, effects of expressing the HaloTag–fascin fusion protein as well as its degradation using VHL HaloPROTAC **VHL-HP-1 (2.18)** were assessed.

Proliferation assay

For the proliferation assays, wild-type SK-OV-3 cells, fascin knock-out cells, cells expressing 200% fascin as well as cells transfected with the HaloTag–fascin fusion protein were seeded at a low density, and treated with VHL HaloPROTAC **VHL-HP-1 (2.18),** as indicated (Figure 2.37). Unlike the proliferation assay carried out for the fascin knock-down trials, cells were treated with a cell permeable nuclear dye to be able to assess cell count instead of relying on confluence as a measure for proliferation. Cell count is a more accurate metric for proliferation since, compared to confluence, it is not impacted by any changes in morphology or size of the cells which could be caused by absence of fascin or presence of the fusion protein.[178] Cells were then monitored hourly over 94 hours on an automated microscope and the normalised proliferation index was determined by normalising cell numbers at the respective time points against initial cell numbers. Overexpression of fascin

significantly increased proliferation by around 40%, whereas knock-out of fascin did not impact on cell growth compared to the wild-type control cells (Figure 2.37 b). Interestingly, expression of HaloTag–fascin in fascin knock-out cells slowed proliferation by around 30% compared to knock-out cells not expressing the fusion protein, which could be an indication of the fusion protein not being fully functional or even interfering with cell function. Treatment with 1 μM of VHL HaloPROTAC **VHL-HP-1 (2.18)** did not exert any significant effect.

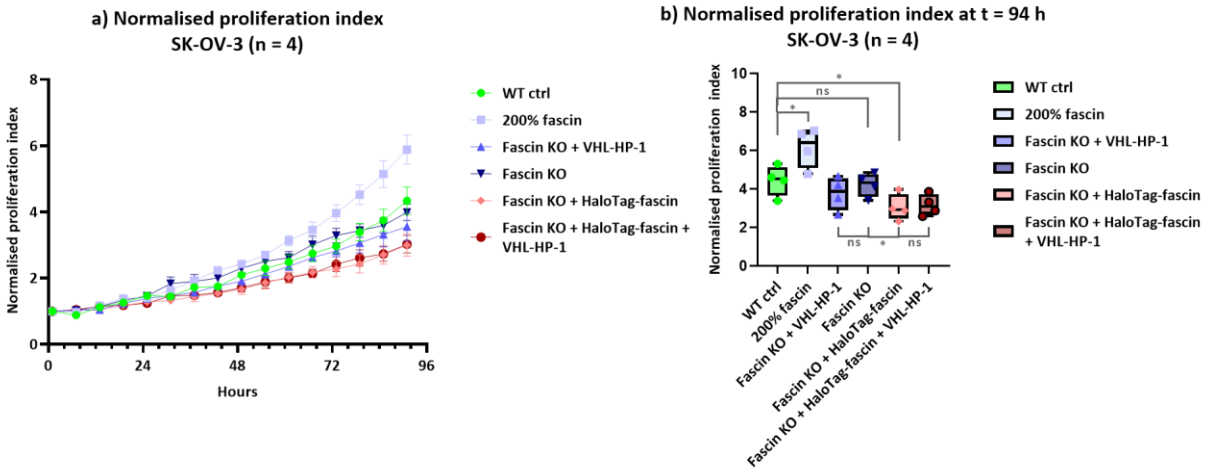

*Figure 2.37: Normalised proliferation index based on cell numbers a) over 94 hours and b) at t = 94 h for SK-OV-3 WT cells, cells overexpressing fascin and fascin KO cells, transfected with the HaloTag–fascin fusion protein and treated with 1 μM of **VHL-HP-1 (2.18),** as indicated.*
*Error bars in a) represent SEM. Whiskers in b) represent minimum and maximum. Unpaired t-test was applied (ns: $p > 0.05$, *: $p \leq 0.05$, **: $p \leq 0.01$, ***: $p \leq 0.001$). Normalised proliferation index calculated as mean ± SEM (Appendix 1).*

Random migration

In addition, movement of individual cells was tracked hourly over 24 hours to reveal if any condition would confer a motility advantage, which could in turn impact on wound closure. To compare the cells' intrinsic migratory ability non-directed random migration (Figure 2.39 a) as well as migration velocity (Figure 2.39 b) were determined.[179] Although overexpression of fascin did not impact on velocity, the cells displayed a more motile behaviour in terms of their distance travelled from the initial start point. Knock-out of fascin resulted in a 35% increase in velocity compare to wild-type control cells, and expression of HaloTag–fascin resulted in a further increase of around 20%. However, knock-out of the endogenous protein and expression of the fusion protein did not noticeably impact on the cells' migratory patterns. Treatment with 1 μM of VHL HaloPROTAC **VHL-HP-1 (2.18)** reduced motility and velocity, however, only in cells not transfected with the fusion

protein. For cells transfected with the fusion protein and then treated with **VHL-HP-1 (2.18)** this effect was not observable.

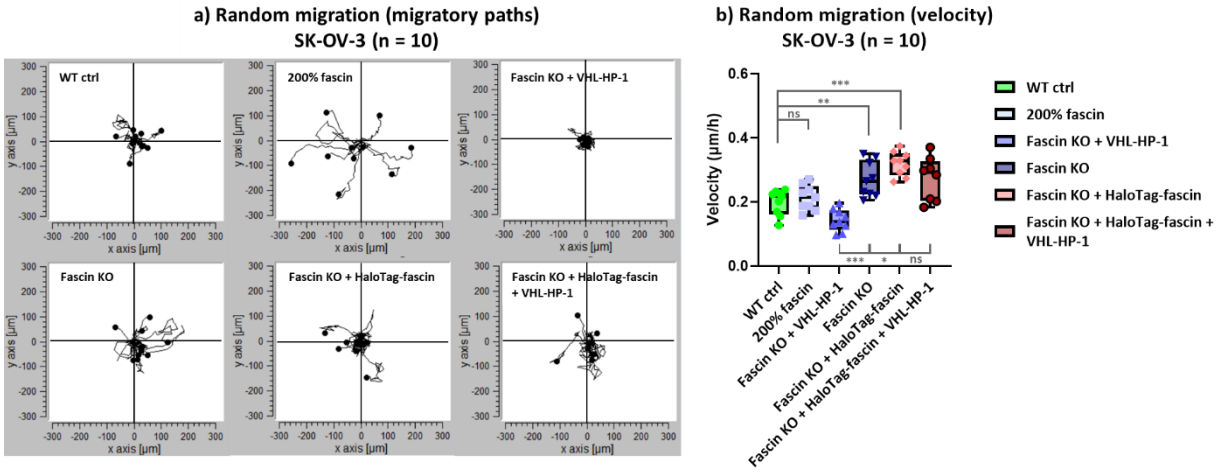

*Figure 2.38: Random migration for 10 individual cells over 24 hours: a) migratory paths from common starting point and b) migratory velocity for SK-OV-3 WT cells, cells overexpressing fascin and fascin KO cells, transfected with the HaloTag–fascin fusion protein and treated with 1 µM of **VHL-HP-1 (2.18),** as indicated. Whiskers represent minimum and maximum. Unpaired t-test was applied (ns: $p > 0.05$, *: $p \leq 0.05$, **: $p \leq 0.01$, ***: $p \leq 0.001$). Velocity calculated as mean ± SEM (Appendix 1).*

Wound healing assays

Similar to the proliferation assays, in the wound healing assays assessing cell migration (Figure 2.39), cells overexpressing fascin displayed a faster increase in relative wound density, with the wound closing rate showing a boost of 30% compared to the wild-type control cells (Figure 2.39 a), which could be explained by a faster rate of proliferation. However, conversely to results from the proliferation and random migration assays, knock-out of the endogenous protein exerted a significant effect, leading to a 40% decrease in wound closing rate. Pleasingly, expression of HaloTag–fascin resulted in rescue of some migratory activity – the wound closing rate increased by 35% compared to knock-out cells but remained 20% slower than the wild-type control. Again, treatment with 1 µM of VHL HaloPROTAC **VHL-HP-1 (2.18)** did not impact on wound closure.

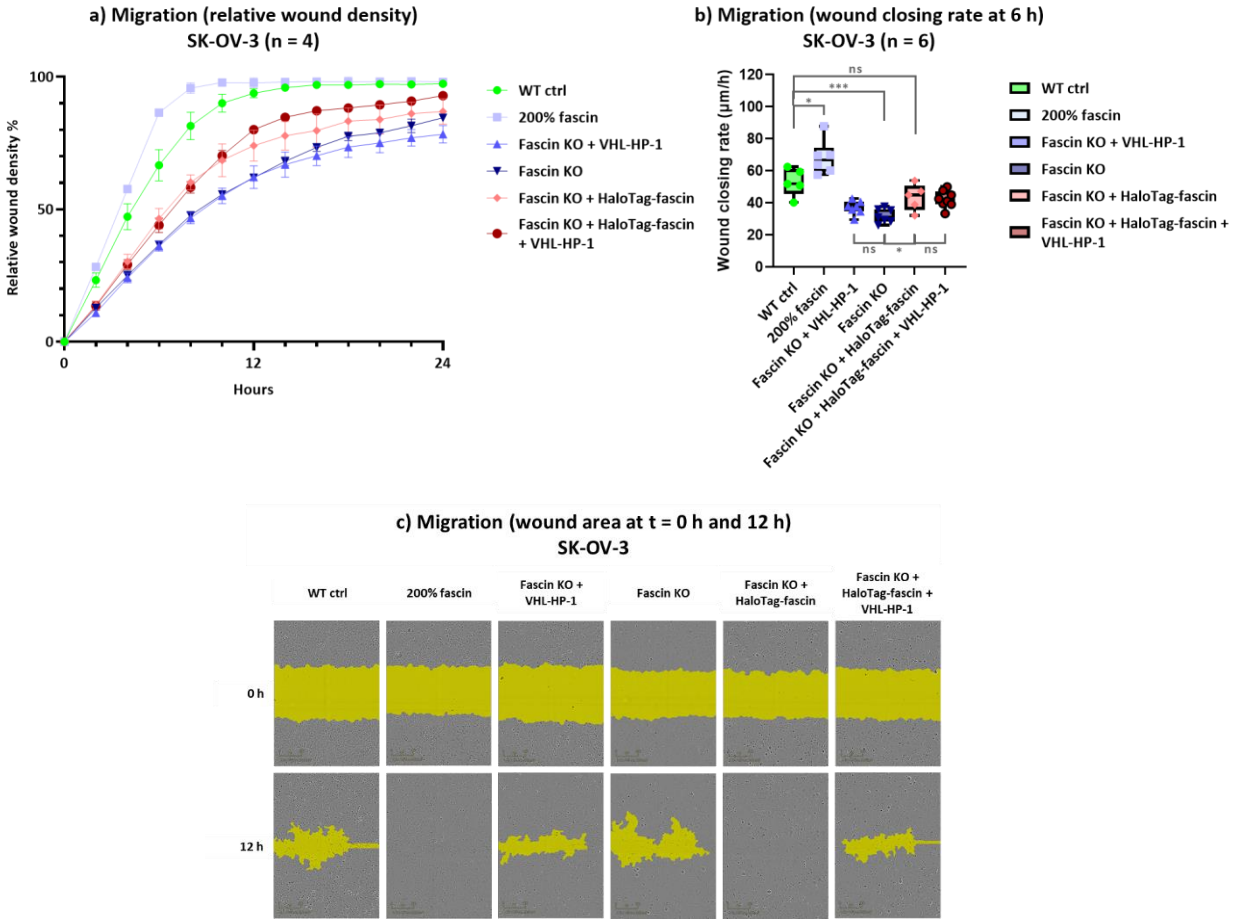

*Figure 2.39: Wound healing assay – migration: a) relative wound density (%) over time, b) wound closing rate (µm/h) at t = 6 h and c) images of wound area at t = 0 h and 12 h for SK-OV-3 WT cells, cells overexpressing fascin and fascin KO cells, transfected with the HaloTag–fascin fusion protein and treated with 1 µM of **VHL-HP-1 (2.18),** as indicated.*
*Error bars in a) and c) represent SEM. Whiskers in b) and d) represent minimum and maximum. Unpaired t-test was applied (ns: $p > 0.05$, *: $p \leq 0.05$, **: $p \leq 0.01$, ***: $p \leq 0.001$). Wound closing rate calculated as mean ± SEM (Appendix 1).*

For wound healing assays assessing invasiveness of the cells, a Matrigel overlay (4 mg/mL) was inserted into the wound and wound closure was monitored hourly over 94 hours (Figure 2.40). The effect of fascin overexpression was striking, with a wound closing rate being 250% higher than for the wild-type cells (Figure 2.40 b), showcasing increased levels of fascin did indeed confer invasive ability, even to a less invasive cell line. Although it was hypothesised that knock-out of fascin would slow invasive ability of the cells, surprisingly, an increase in wound closing rate by around 60% compared to the wild-type cells was observed. Expression of the fusion protein accelerated wound closure further, leading to 150% faster wound closure compared to the wild-type control. Unfortunately, treatment with VHL HaloPROTAC **VHL-HP-1 (2.18)** did not significantly impact on wound closure.

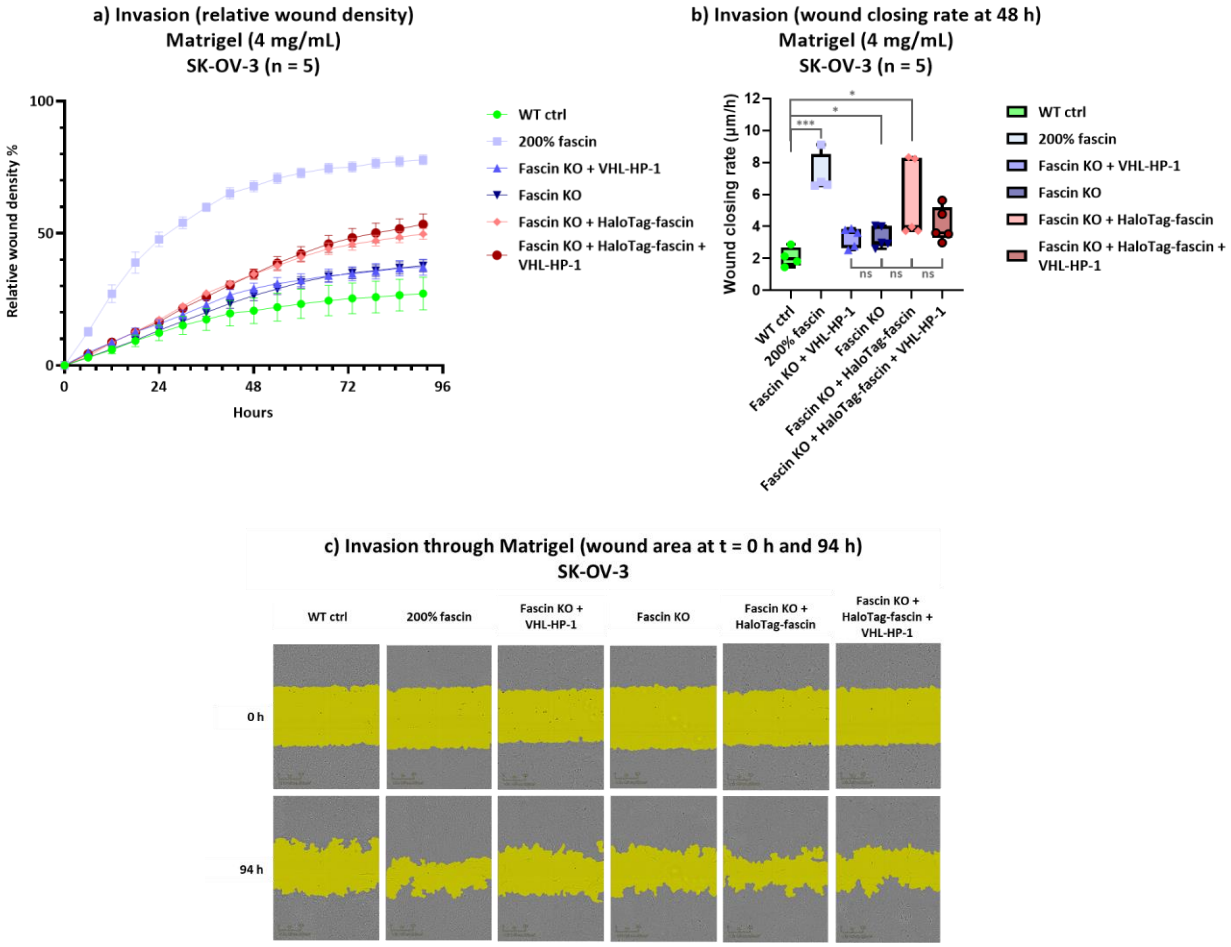

*Figure 2.40: Wound healing assay – invasion with Matrigel overlay (4 mg/mL): a a) relative wound density (%) over time and b) wound closing rate (µm/h) at t = 48 h and c) images of wound area at t = 0 h and 94 h for SK-OV-3 WT cells, cells overexpressing fascin and fascin KO cells, transfected with the HaloTag–fascin fusion protein and treated with 1 µM of **VHL-HP-1 (2.18),** as indicated.*
*Error bars in a) and b) represent SEM. Whiskers in b) represent minimum and maximum. Unpaired t-test was applied (ns: $p > 0.05$, *: $p \leq 0.05$, **: $p \leq 0.01$, ***: $p \leq 0.001$). Wound closing rate calculated as mean ± SEM (Appendix 1).*

A second wound healing assay assessing cell invasion was carried out, however, using a Matrigel/collagen I mixture as matrix overlay through which cells would migrate (Figure 2.41). Whereas Matrigel can be used to mimic the softer basement membrane, collagen I is a surrogate for the stiffer stromal portion of the extracellular matrix. Reports in literature suggested that collagen I would be a preferred matrix for ovarian cancer cells to adhere to,[180] even promoting a more mesenchymal-like invasive behaviour by providing a stiffer environment (Chapter 1.1.3).[181] However, the contrary outcome was observed: even though the same general pattern as for the previous invasion assay was noticeable, wound closing of wild-type cells, cells overexpressing fascin and fascin knock-out cells proceeded at a 30% to 40% slower rate through the Matrigel/collagen I overlay compared to the rates observed for the assay using solely Matrigel. The rates of wound closure for cells expressing HaloTag–fascin, however, were comparable between the two matrices.

A study assessing invasive behaviour of different ovarian cancer cell lines found SK-OV-3 cells to be one of the two most invasive cell line in assays using a Matrigel matrix, however, SK-OV-3 cells did not to invade into a matrix containing collagen I.[182] For invasion through collagen I, MMP activity, specifically collagenase MT1-MMP, is required, and SK-OV-3 cells were shown to have very low expression levels of this particular MMP, explaining the lack of invasiveness observed.[155] For invasion through Matrigel, MMPs are not required since the cells can move through the matrix by physical force without the need for degradation of the surrounding tissue.[183] Those literature reports support the observed significant drop in wound closing rate when switching from Matrigel to a Matrigel/collagen I mixture for the wound healing assays with SK-OV-3 cells.

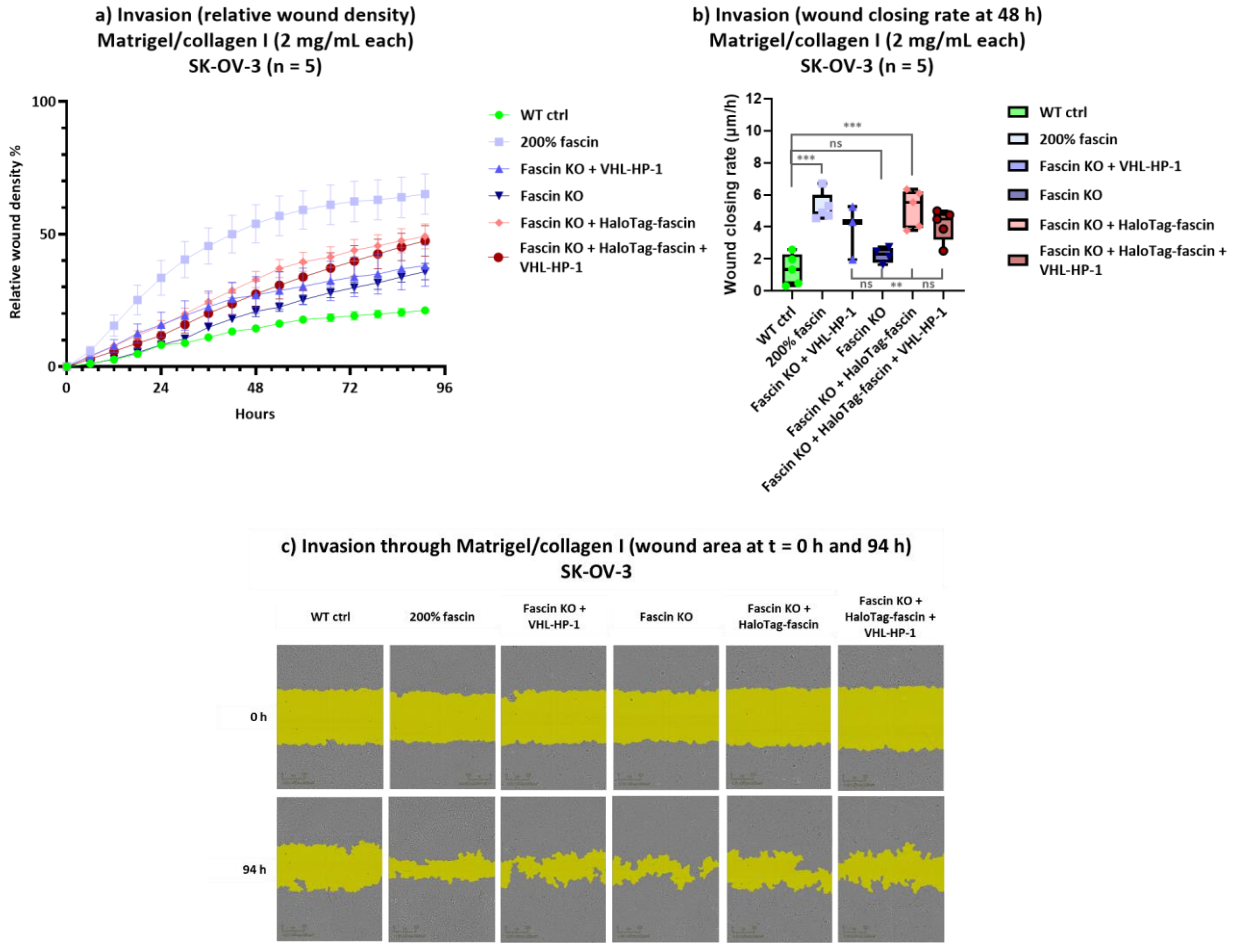

Figure 2.41: Wound healing assay – invasion with Matrigel/collagen I overlay (2 mg/mL each): a) relative wound density (%) over time and b) wound closing rate (µm/h) at t = 48 h and c) images of wound area at t = 0 h and 94 h for SK-OV-3 WT cells, cells overexpressing fascin and fascin KO cells, transfected with the HaloTag–fascin fusion protein and treated with 1 µM of ***VHL-HP-1 (2.18),*** *as indicated.*
*Error bars in a) and b) represent SEM. Whiskers in b) represent minimum and maximum. Unpaired t-test was applied (ns: p > 0.05, *: p ≤ 0.05, **: p ≤ 0.01, ***: p ≤ 0.001). Wound closing rate calculated as mean ± SEM (Appendix 1).*

Phenotype studies

In an attempt to gain more insights into the results obtained through aforementioned functional assays, phenotype studies were carried out. Firstly, to assess changes in morphology, fluorescence microscopy images of cells stained with phalloidin to reveal actin structures were obtained by Nikki Paul at the Beatson Institute for Cancer Research (Figure 2.42). In SK-OV-3 wild-type cells, filopodia protruding out of lamellipodia at the leading edges and retraction fibres at the retracting edges of the cells were observed (Figure 2.42 a). Overexpression of fascin resulted in formation of a higher number of filopodia but also an increased amount of stress fibres was visible, with cells generally appearing larger compared to wild-type cells (Figure 2.42 b). This could be an indication for overexpression of fascin resulting in a higher cell tension which could increase the tractile force of the cells. This stiffer morphology could contribute to a more mesenchymal-like motility,[32] leading to an improved ability to move through matrices (Chapter 1.1.3) – this would explain the observations of increased invasiveness obtained from functional assays. Fascin knock-out cells appeared to display a more disordered and less rounded morphology (Figure 2.42 c) which could be an indication of a more amoeboid-like phenotype.[33] This change in morphology could also offer an explanation for the unexpectedly faster wound closing rate compared to the wild-type control observed in functional assays: this increased invasiveness could stem from a more amoeboid-type motility (Chapter 1.1.3). Fascin knock-out cells expressing the HaloTag–fascin fusion protein also seemed to display a more disordered phenotype than the wild-type control, however, appearing to form a higher number of filopodia (Figure 2.42 d) which disappear upon treatment with VHL HaloPROTAC **VHL-HP-1 (2.18)** (Figure 2.42 e).

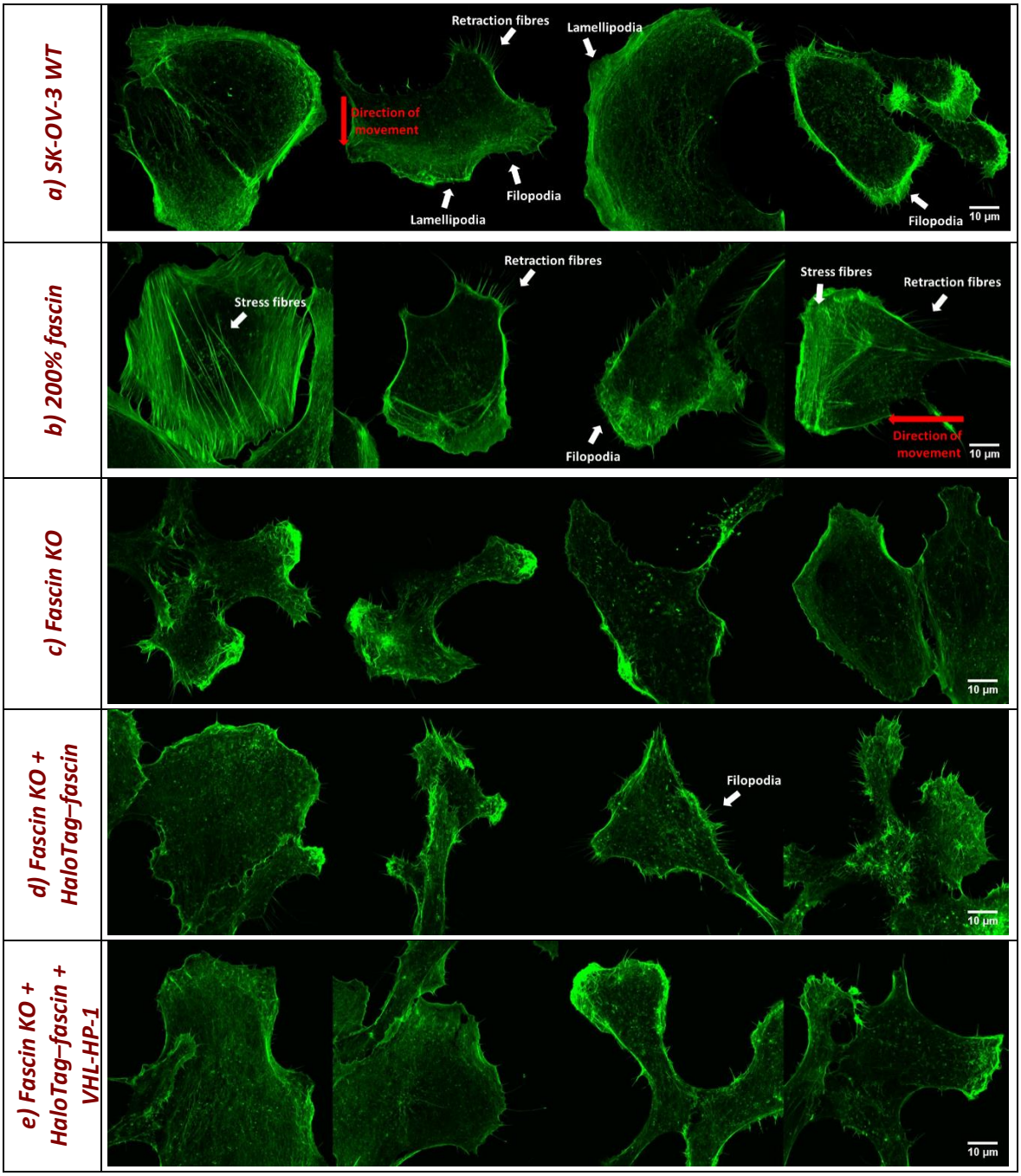

Figure 2.42: Fluorescence microscope images with actin staining: a) SK-OV-3 WT, b) 200% fascin, c) fascin KO, d) fascin KO expressing HaloTag–fascin, e) fascin KO expressing HaloTag–fascin treated with VHL-HP-1.

Then, to determine localisation of fascin in wild-type cells and of the HaloTag–fascin fusion protein in transfected fascin knock-out cells, fluorescence microscopy with fascin staining was performed by Nikki Paul at the Beatson Institute for Cancer Research (Figure 2.43). Fascin was localised to filopodia formed at the leading edges of SK-OV-3 wild-type cells, though SK-OV-3 cells exhibited a low number of filopodia in general (Figure 2.43 a). Overexpression of fascin also resulted in formation of more and thicker filopodia, and the cells appeared to be bigger in size compared to wild-type cells (Figure 2.43 b). Images of fascin knock-out cells expectedly only displayed autofluorescence or secondary antibody

background (Figure 2.43 c). Some fluorescence was detected in knock-out cells transfected with HaloTag–fascin, although the fusion protein did not seem to localise at the cell edges and significant localisation at filopodia was not observed (Figure 2.43 d). The lack of localisation could either indicate that the fusion did not displaying the same functionality as the endogenous protein, or that expression levels were insufficient for adequate visualisation. For knock-out cells transfected with HaloTag–fascin and treated with **VHL-HP-1 (2.18)** only background fluorescence of the cells was observed (Figure 2.43 e), providing further evidence for degradation of the fusion protein by the HaloPROTAC.

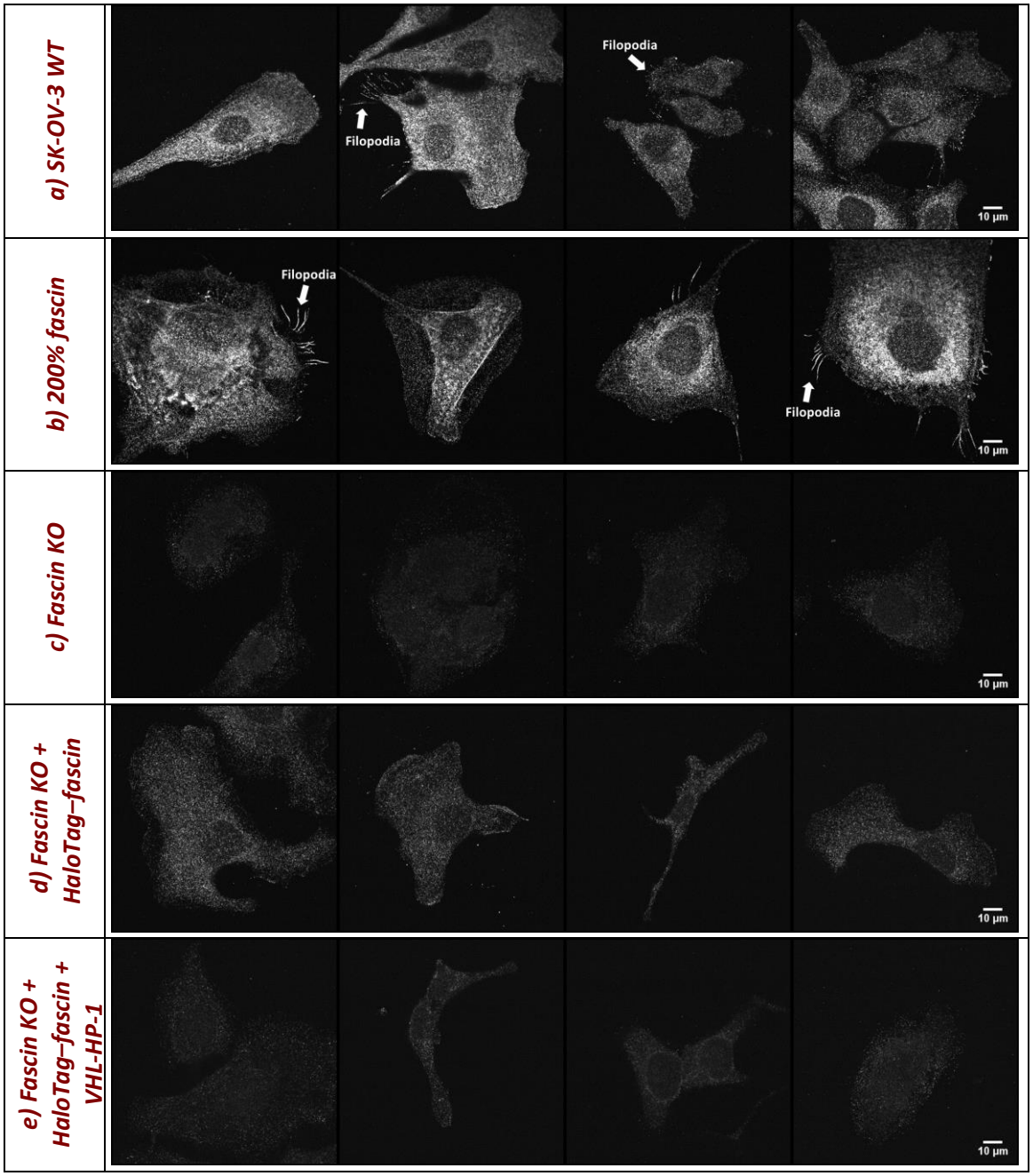

Figure 2.43: Fluorescence microscope images with fascin staining: a) SK-OV-3 WT, b) 200% fascin, c) fascin KO, d) fascin KO expressing HaloTag–fascin, e) fascin KO expressing HaloTag–fascin treated with VHL-HP-1.

2.4 Summary of HaloTag model system

Prior to attempting to degrade endogenous fascin, in order to probe the possibility of engaging the UPS to fascin and induce protein degradation *via* the PROTAC mechanism, a proof-of-concept using a HaloTag model system was carried out. For this model system, a series of HaloPROTACs and corresponding mono-functional control were synthesised and a HaloTag–fascin fusion protein was cloned. Using different biological assays, activity of the compounds as well as effect of degradation of the fusion protein on cell function and phenotype were assessed.

2.4.1 Synthetic summary

E3 ligase ligands

Active VHL ligand **VHL-2 (2.3)** and inactive control ligand ***cis*VHL-2 (2.4)** were synthesised over seven steps with overall yields of 12% and 8%, respectively, from commercially available starting materials *via* common amine intermediate **2.6** (Figure 2.44).

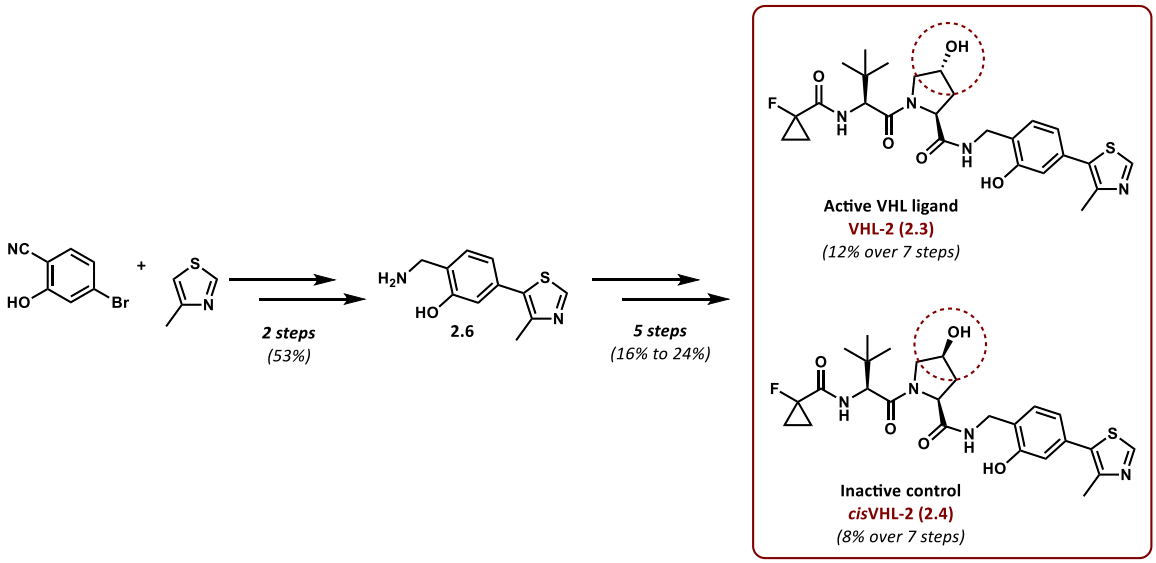

Figure 2.44: Summary of the synthesis of active VHL ligand and inactive control ligand.

Through optimisation of reaction conditions, active CRBN ligand **CRBN-1 (2.9)** was generated from L-glutamine and fluorophthalic anhydride in improved yields (40% over two steps) compared to yields reported in literature.[99] In an attempt to increase yields further, the cyclised glutamine analogue aminoglutarimide was employed in the synthesis of active CRBN ligand **CRBN-2 (2.11)** – resulting in an improved overall yield of 55% over two steps (Figure 2.45). The corresponding inactive methylated control ligands **MeCRBN-1 (2.10)** and

MeCRBN-2 (2.12) were generated in excellent yields of 85% and 96%, respectively, from the active counterparts.

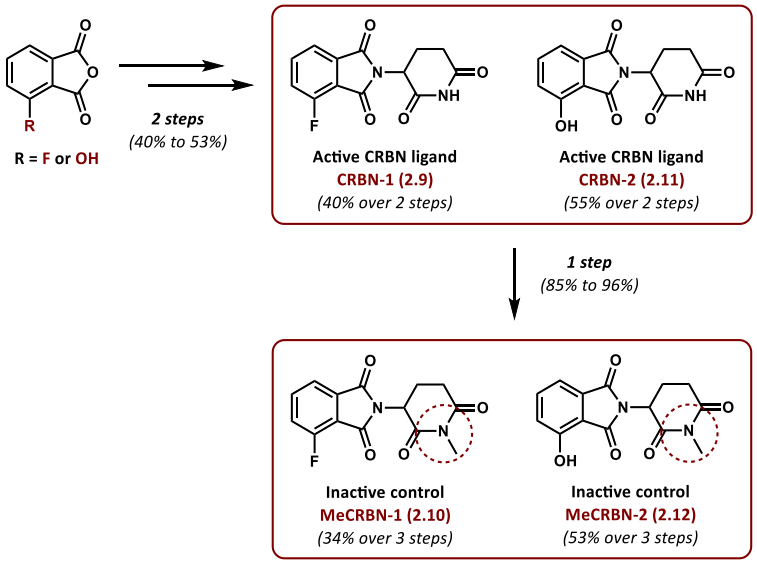

Figure 2.45: Summary of the synthesis of active CRBN ligands and inactive control ligands.

HaloPROTACs

A total of five active HaloPROTACs and eight mono-functional control compounds were synthesised using a modular approach. For the VHL-recruiting compounds, common linker fragments **2.15a** and **2.15b** were accessed from pentaethylene glycol in excellent yields (Figure 2.46). Differential functionalisation of the common intermediates and subsequent coupling with active ligands as well as inactive control ligands generated two active VHL-targeting HaloPROTACs and the four corresponding mono-functional control compounds with overall yields of 15% to 38%.

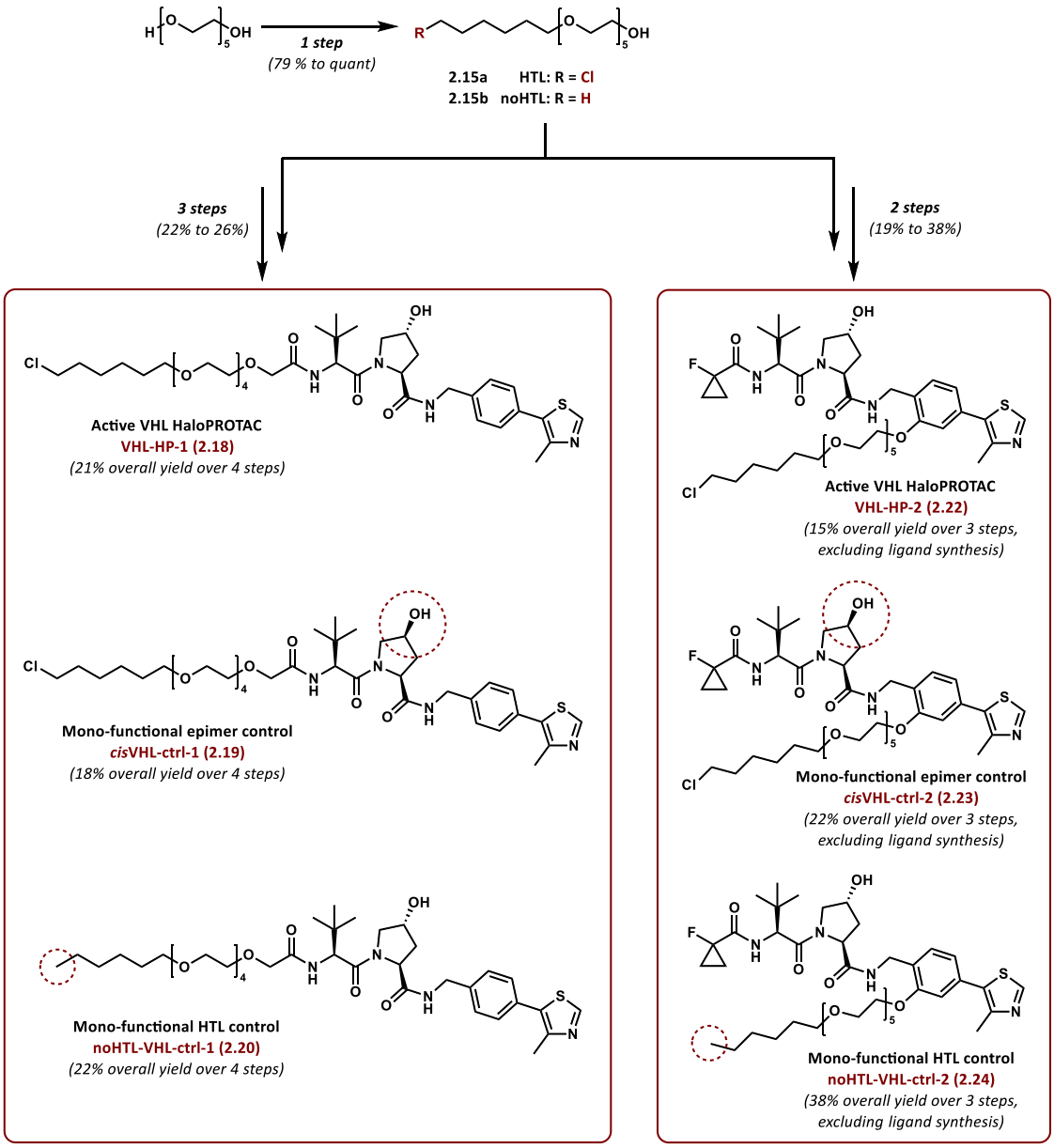

Figure 2.46: Summary of the synthesis of VHL HaloPROTACs and mono-functional control compounds.

Similarly, for CRBN-recruiting compounds intermediates **2.28a** and **2.28b** were prepared over three steps in 20% to 24% yield (Figure 2.47). Two active CRBN HaloPROTACs and four mono-functional control compounds were accessed in 2% to 12% overall yields from the common intermediates.

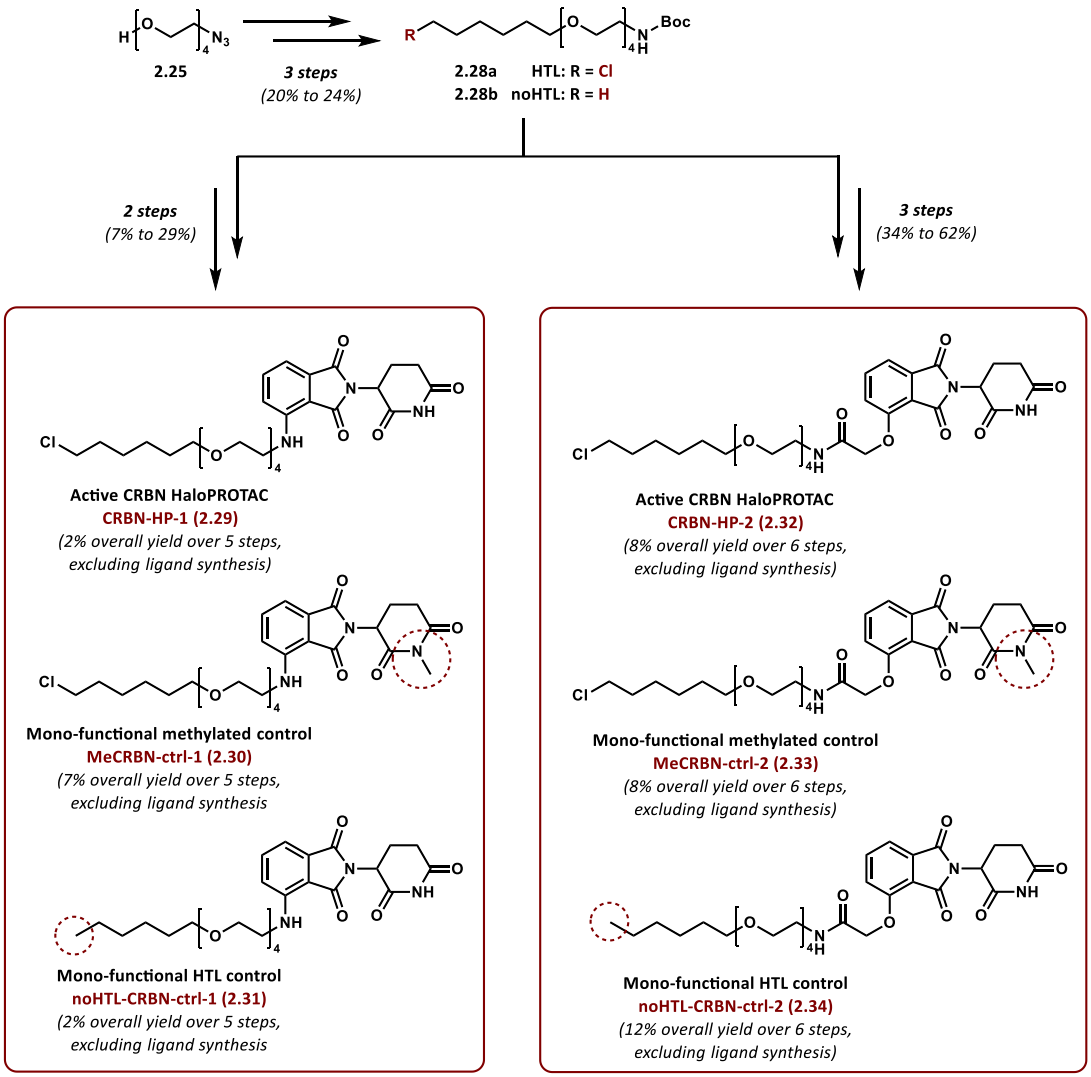

Figure 2.47: Summary of the synthesis of CRBN HaloPROTACs and mono-functional control compounds.

In addition, HyT HaloPROTAC **HyT-HP-1 (2.36)** was synthesised over two steps in a 20% overall yield (Figure 2.48).

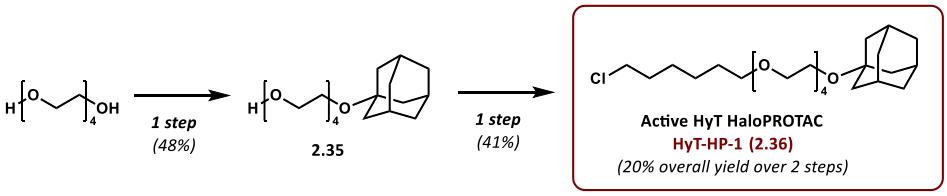

Figure 2.48: Summary of the synthesis of HyT HaloPROTAC.

2.4.2 Summary of biological testing

In order to assess the activity of the synthesised HaloPROTACs, a plasmid for a HaloTag–fascin protein was cloned and expressed in different cell lines. Degradation assays with increasing concentrations of the compounds as well as time-course assays were carried out. Both VHL HaloPROTACs **VHL-HP-1 (2.18)** and **VHL-HP-2 (2.22)** were found to induce reproducible and sustained degradation of the fusion protein in two cell lines, SK-OV-3 and HT-1080 (Figure 2.49 a and b). Control assays with the corresponding mono-functional control compounds and proteasome inhibition confirmed degradation of the fusion protein was mediated *via* the PROTAC mechanism.

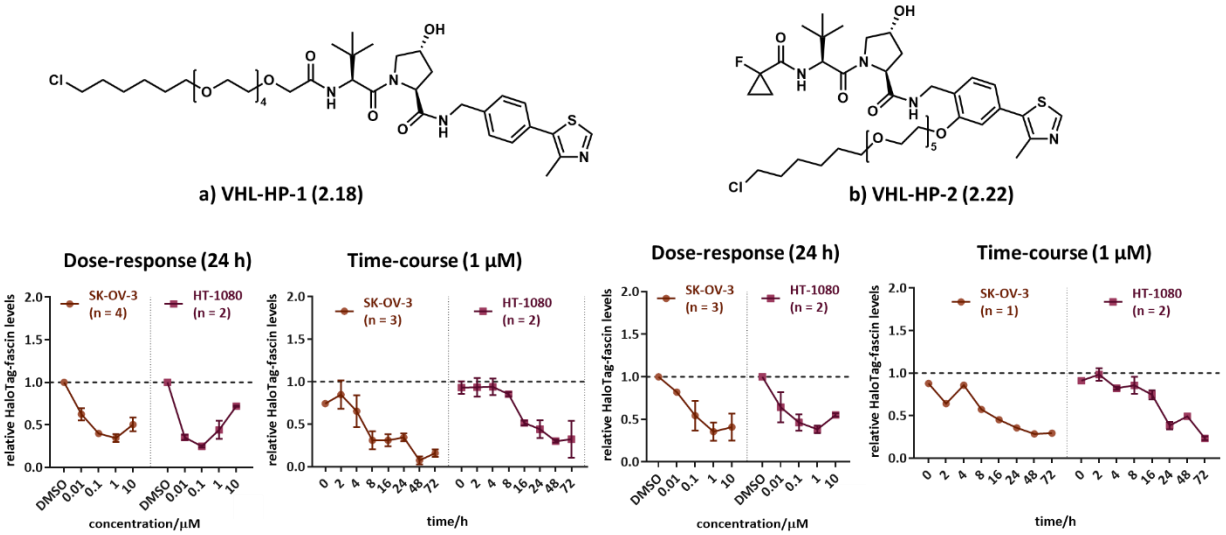

*Figure 2.49: Quantification of western blot analysis - HaloTag–fascin levels for dose-response and time-course assays in SK-OV-3 and HT-1080 cells for a) **VHL-HP-1 (2.18)** and b) **VHL-HP-2 (2.22)**.*

Prior to generation a fascin knock-out cell line for further functional and phenotype assays, fascin knock-down trials using siRNAs were carried out with SK-OV-3 and HT-1080 cells. The results indicated that the impact of absence of the endogenous protein would be more pronounced for SK-OV-3 than for HT-1080 cells. Based on these findings, a SK-OV-3 fascin knock-out cell line was established using the CRISPR–Cas9 technique. By cloning and expression of two CRISPR–Cas9 plasmids containing GFP as selection marker and subsequent generation of single clone cell populations, SK-OV-3 fascin knock-out cells and cells overexpressing fascin were obtained. Functional assays assessing invasive properties of fascin knock-out cells, knock-out cells expressing the HaloTag–fusion protein and cells overexpressing the endogenous protein provided unexpected results in wound-healing experiments. Although it was expected that knock-out of endogenous fascin would impair invasion through matrices, a faster wound closure rate was observed for fascin knock-out cells compared to wild-type control cells. It was hypothesised that knock-out of the

structural protein would lead to an amoeboid-type mode of migration through a 3D environment, thereby increasing the invasive ability of the fascin knock-out cells (Figure 2.50). Expression of the HaloTag–fusion protein further augmented the observed invasiveness, similar to overexpression the endogenous protein. Degradation of the fusion protein induced by treatment with VHL HaloPROTAC **VHL-HP-1 (2.18)** did not seem to exert any significant effect on cell invasion.

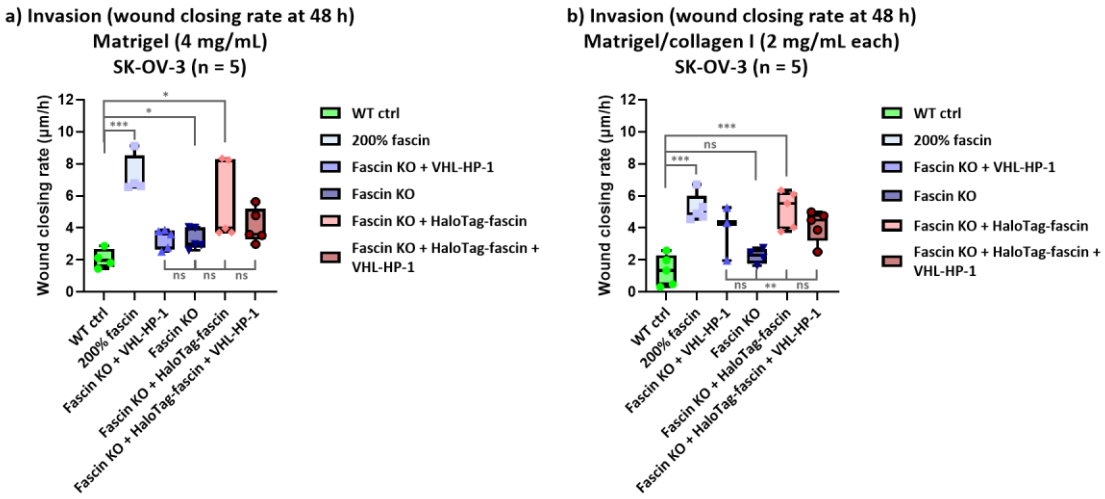

*Figure 2.50: Wound healing assay – wound closing rate(µm/h) at t = 48 h for SK-OV-3 WT cells, cells overexpressing fascin and fascin KO cells, transfected with the HaloTag–fascin fusion protein and treated with 1 µM of **VHL-HP-1 (2.18),** as indicated: a) through Matrigel overlay (4 mg/mL) and b) through Matrigel/collagen I overlay (2 mg/mL each).*

Fluorescence images visualising the actin cytoskeleton of the cells showed that fascin knock-out cells displayed a more disordered and less rounded phenotype, which provided further evidence for an amoeboid-type morphology of the cells (Figure 2.51 a). Based on the results obtained, it was hypothesised that overexpression of the endogenous protein as well as its knock-out resulted in generation of more invasive cells compare to wild-type control cells through two different mechanisms. Overexpression of fascin would lead to a mesenchymal-like stiffer morphology, whereas knock-out would results in an amoeboid-like flexible phenotype of the cells (Chapter 1.1.3), both of which would confer an advantage to invade through the matrices used in the assays compared to the WT control cells.[32] Expression of the fusion protein resulted in formation of pronounced actin structures, which disappeared after treatment with VHL HaloPROTAC **VHL-HP-1 (2.18)**. Fluorescence images to determine localisation of fascin also supported the aforementioned findings. Additionally, no clear localisation of the fusion protein could be determined for the transfected cells which could indicate low expression levels of the protein after transient transfection (Figure 2.51 b).

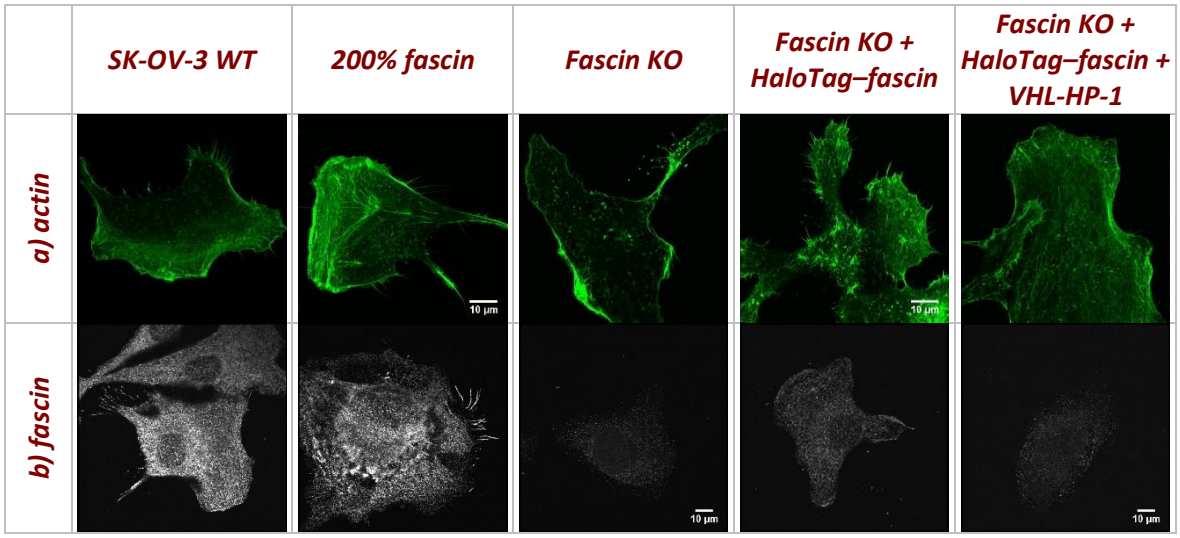

Figure 2.51: Fluorescence microscope images with a) actin and b) fascin staining of SK-OV-3 WT, 200% fascin, fascin KO, fascin KO expressing HaloTag–fascin, fascin knock-out expressing HaloTag–fascin treated with VHL-HP-1. Images obtained by Nikki Paul.

3 Fascin-targeting PROTACs: compound design, chemical synthesis and evaluation of biological activity

3.1 PROTAC design

3.1.1 Design of compounds

For the design of fascin-targeting PROTACs, a similar strategy as for the HaloPROTACs was planned (Figure 3.1). Different compound series would be based on previously described fascin ligands **FSCN-A (1.4)**, **FSCN-B (1.5)** and **FSCN-C (1.7)** (Chapter 1.1.5) as fascin-recruiting components. Although best results were obtained for VHL-recruiting HaloPROTACs in the model system, it was decided to generate both, compounds recruiting CRBN E3 ligase and VHL E3 ligase, as well as HyTs, as degradation could be modulated by distinct E3 ligases in different cell lines (Chapter 1.2.4).[92,97] Similarly, since the linker can impact on interactions between the POI and the E3 ligase (Chapter 1.2.4) and optimal length and composition need to be determined experimentally,[98] different PEG-based linkers would be explored within each compound series.

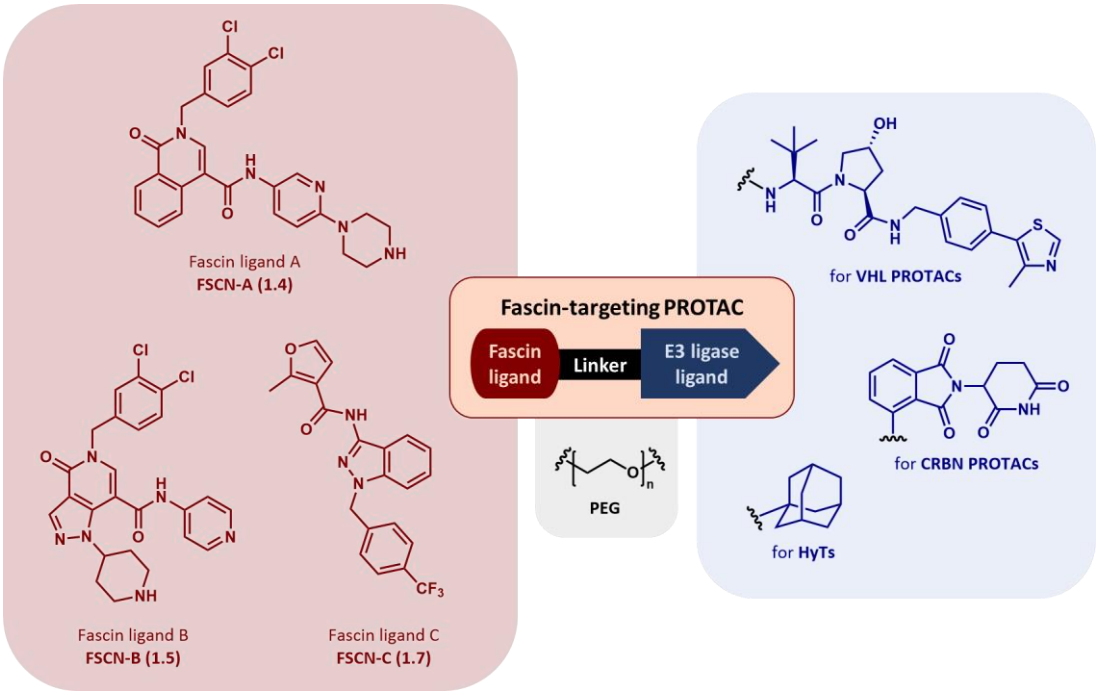

Figure 3.1: Design of fascin-targeting PROTACs.

3.1.2 Evaluation of physicochemical properties

In order to evaluate physicochemical properties of potential PROTACs assessing their likelihood to be cell permeable, a set of guidelines was developed based on an analysis of active PROTACs reported in literature (Chapter 1.2.5).[14] Physicochemical properties were calculated in line with the analysis prepared by Maple *et al.*[14] to allow for direct comparison with highest scoring, *i.e.* most active, PROTACs ("Maple set (PROTACs with DegS ≥ 4)" in Table 3.1). Similarly, the classification boundaries ("good" (green), "acceptable" (yellow) and "bad" (red) in Table 3.1) were defined based on the results of the analysis and on recommendations for optimal physicochemical properties of PROTACs.[94,100]

	MW (Da)	***cLogP***	***HBD***	***HBA***	***NRotB***	***tPSA (Å²)***
Maple set (PROTACs with DegS ≥ 4)[100]	985	5.36	4.13	13.3	24.6	208
Metrics for evaluation of physicochemical properties						
Good (green)	< 900	< 4	< 4	< 10	< 20	< 200
Acceptable (yellow)	900 - 1100	4 - 6	4 - 6	10 - 15	20 - 28	200 - 250
Bad (red)	> 1100	> 6	> 6	> 15	> 28	> 250
NB: MW, HBD, HBA, NRotB and tPSA were determined using ChemDraw v20.1 and cLogP was calculated using SwissADME, with molecules submitted in their neutral form.[184]						

Table 3.1: Metrics used to evaluate calculated physicochemical properties.

It should be noted that physicochemical properties of PROTACs will be partially dictated by the properties of both involved ligands, which already display properties of traditional small-molecule drugs, hence only limited optimisation of properties may be possible.[94] Other factors, like ternary complex formation and cooperativity effects, are crucial for PROTAC activity and can drive compound efficacy (Chapter 1.2.4), however, the impact of those effects can only be determined experimentally.[185] Therefore, evaluation of physicochemical properties should only be regarded as a rough guideline in the design of PROTACs.

3.2 1st series PROTACs (based on FSCN-A (1.4))

The 1st series of PROTACs was based on **FSCN-A (1.4)** due to availability of the ligand, which was kindly provided by the Drug Discovery Unit of the Beatson Institute for Cancer Research. As part of a previous drug discovery programme,[186] fluorescent probes were generated by functionalisation at the piperazine moiety, a modification which was shown to not interfere with the fascin-binding ability of the compound, hence it was decided to attach the linker at this position. This was supported by computational docking studies of fascin ligand A **FSCN-A (1.4)** into actin-binding site 1 of a fascin co-crystal structure (PDB ID 6i18), showing the piperazine moiety to be protruding outwards of the protein (Figure 3.2). Moreover, the piperazine could be easily functionalised by either alkylation or amide bond formation.

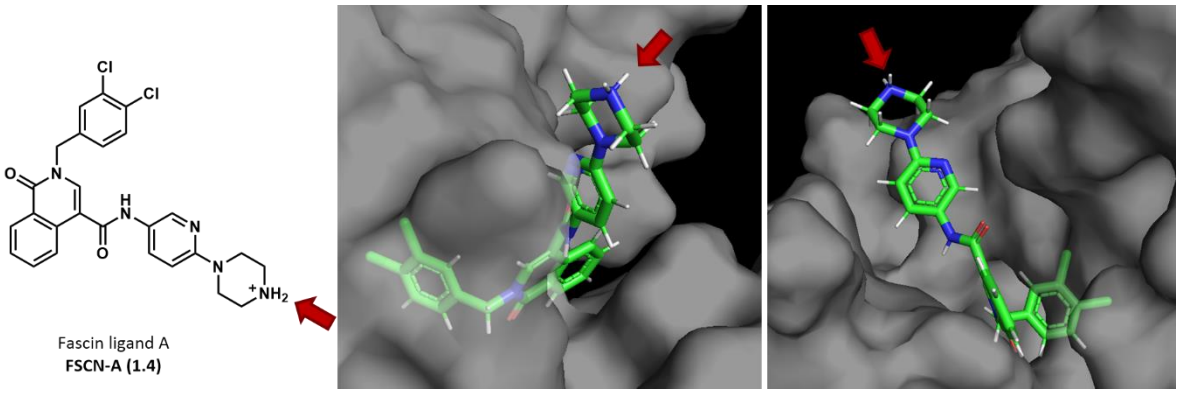

*Figure 3.2: Potential linker attachment point for **FSCN-A (1.4)** docked into fascin crystal structure PDB ID 6i18.*

3.2.1 Synthetic strategy for 1st series PROTACs

The synthetic strategy was based on a convergent synthesis using a modular approach to generate an inventory of E3 ligase ligand–linker fragments (Figure 2.6). The fragments could then be functionalised and coupled to different POI ligands, allowing for a fast synthesis of a diverse library of PROTACs. To achieve this, different commercially available PEG-based linkers would be desymmetrised and coupled to CRBN and VHL ligands. Further functionalisation of the fragments would allow for coupling to fascin ligand A **FSCN-A (1.4),** generating the 1st series of fascin-targeting PROTACs.

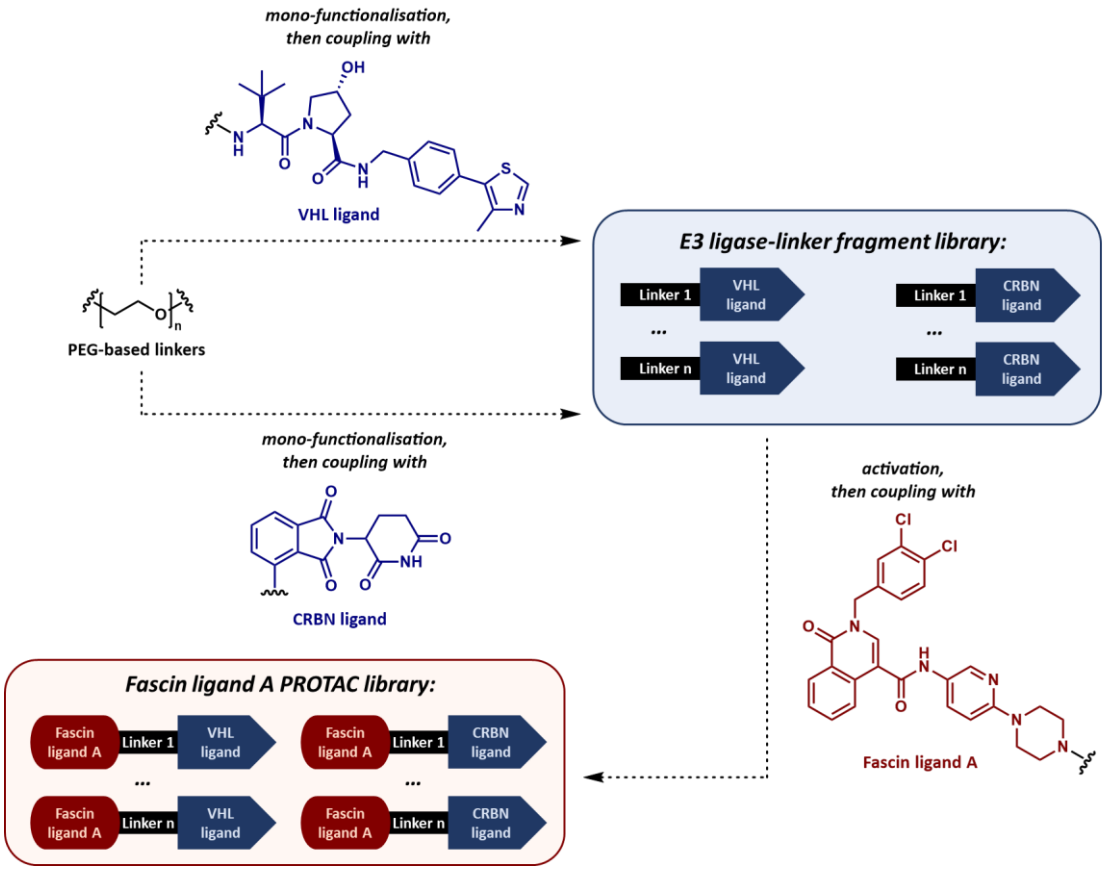

Figure 3.3: Proposed modular synthesis of E3-ligase ligand–linker library and 1st series PROTACs.

3.2.2 Synthesis of 1st series amide PROTACs

E3 ligase ligand–linker fragments

For the first set of compounds, mono-protected diamine linkers **3.1a** and **3.1b** of different lengths, which were readily available in sufficient quantities, were used (Figure 3.4).

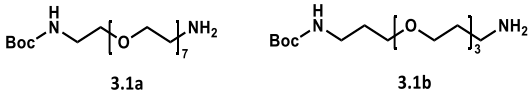

3.1a 3.1b

Figure 3.4: Linkers used to generate E3 ligase ligand-linker library.

To access VHL ligand–linker fragments **3.3a** and **3.3b**, mono-protected diamine linkers **3.1a** and **3.1b** were extended by opening of succinic anhydride, generating longer linker fragment **3.2a** in a 96% yield (Scheme 3.1 a). Shorter linker fragment **3.2b** had previously been synthesised using a similar protocol in a 95% yield. The generated carboxylic acid functionalities of linker fragments **3.2a** and **3.2b** were then available for HATU-mediated amide coupling with the amine of VHL ligand **VHL-1 (2.1)**, affording shorter VHL ligand-linker fragment **3.3a** in a 21% yield. Longer VHL–linker fragment **3.3b** had previously been synthesised in a 50% yield. To obtain CRBN ligand–linker fragments **3.4a** and **3.4b**, mono-

protected diamine linkers **3.1a** and **3.1b** were reacted with fluorinated CRBN ligand **CRBN-1 (2.9)** *via* S_NAr alkylation to generate longer CRBN ligand–linker fragment **3.4a** in 42% and shorter CRBN ligand-linker fragment **3.4b** in 53% yield, respectively (Scheme 3.1 b).

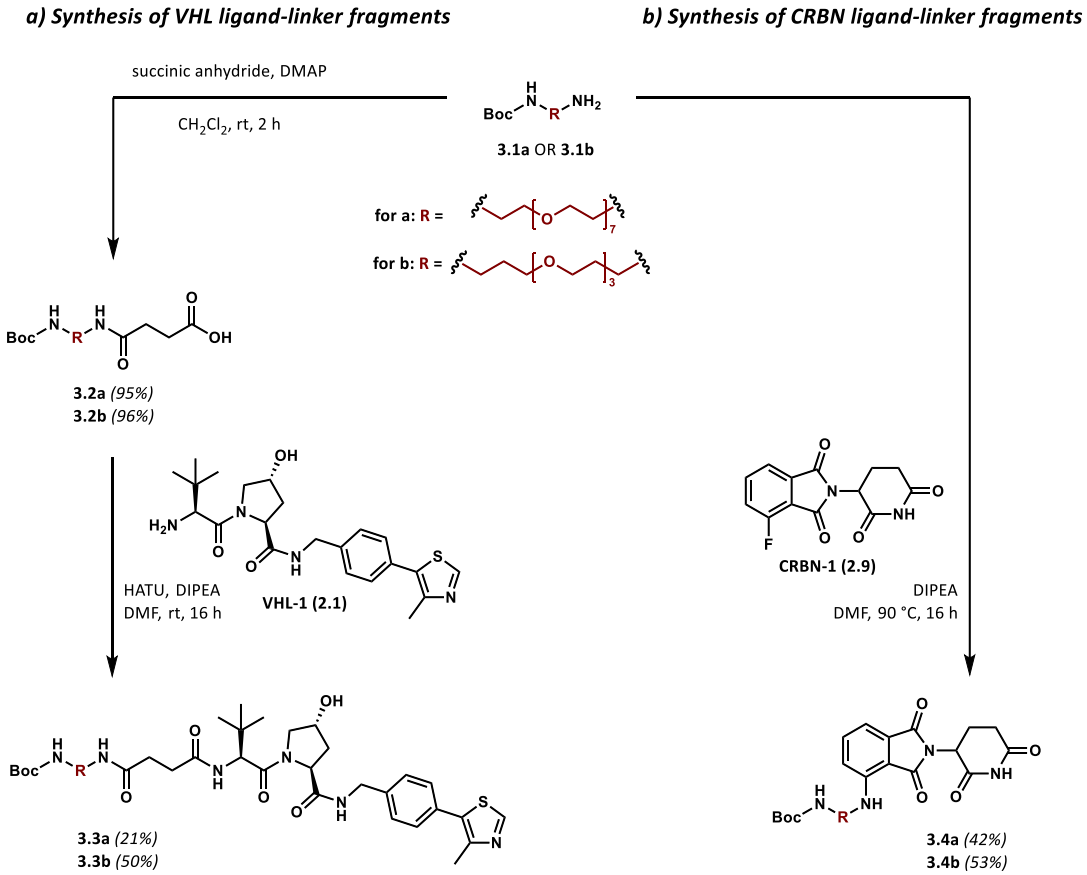

Scheme 3.1: Synthesis of E3 ligase ligand–linker fragment library.

Fascin ligand A fragment

Fascin ligand A fragment **3.5** was accessed by extending the piperazine moiety of fascin ligand A **FSCN-A (1.4)** *via* opening of succinic anhydride (Scheme 3.2).[187] The obtained carboxylic acid could then be coupled with the amine moiety of the previously generated E3 ligase ligand–linker fragments. To assess the impact of functionalisation through an amide bond at the piperazine moiety on binding to fascin, fascin ligand A control **FSCN-A-ctrl (3.6)** was synthesised by capping the carboxylic acid as a methyl amide in a 25% yield. The control compound was purified using semi-preparative RP-HPLC, and the trifluoroacetate anion was exchanged to obtain the hydrochloride salt compatible with biological testing.

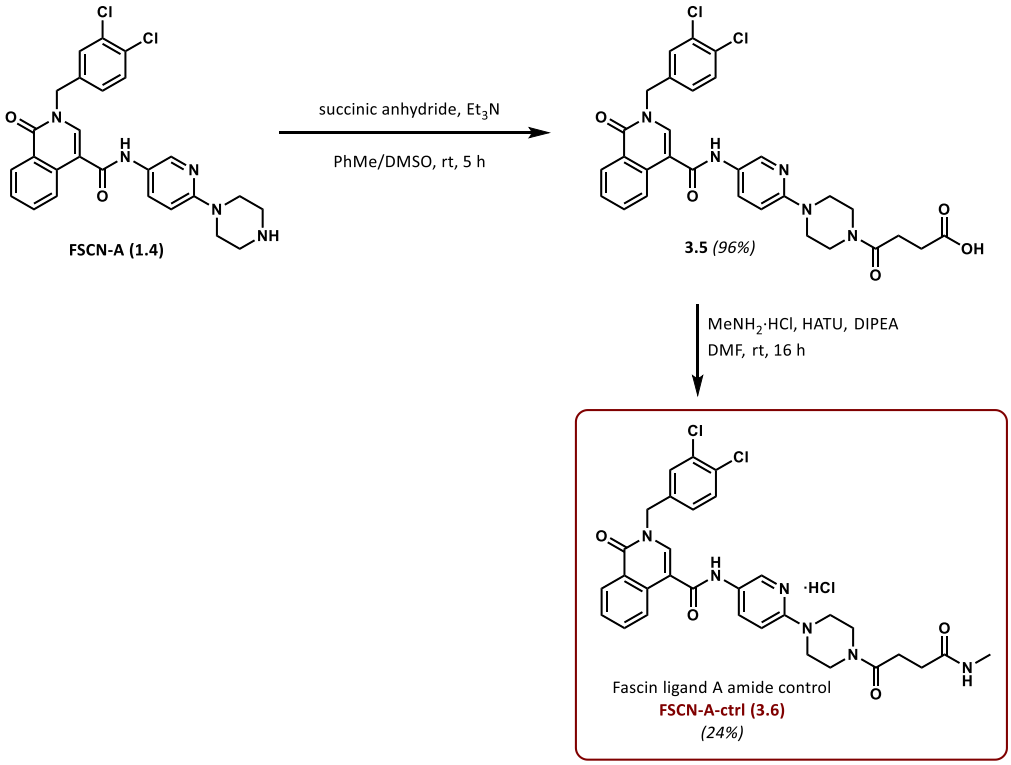

*Scheme 3.2: Synthesis of fascin ligand A fragment **3.5** and control **FSCN-A-ctrl (3.6)**.*

1st series amide PROTACs

The *tert*-butyl carbamate protecting groups on the E3 ligase ligand–linker fragments **3.3a**, **3.3b**, **3.4a** and **3.4b** were removed under acidic conditions. The corresponding amine salts were then coupled with fascin ligand A fragment **3.5** using HATU-mediated amide coupling conditions (Scheme 3.3). Subsequent purification by semi-preparative RP-HPLC and exchange of trifluoroacetate for chloride anions yielded the 1st series amide PROTACs. Whereas fascin ligand A amide VHL PROTAC 1 **FSCN-A-VHL-1 (3.7)** was obtained in a 23% yield, fascin ligand A amide VHL PROTAC 2 **FSCN-A-VHL-2 (3.8)** was not generated in sufficient quantities for full characterisation and subsequent biological testing due to poor mass recovery after purification. Re-synthesis of the compound was not attempted due to unavailability of linker **3.1b**. It was decided to carry out initial testing of the remaining 1st series PROTACs, and in case of successful results, **FSCN-A-VHL-2 (3.8)** would be re-synthesised. Fascin ligand A amide CRBN PROTACs **FSCN-A-CRBN-1 (3.9)** and **FSCN-A-CRBN-2 (3.10)** were generated in yields of 11% and 6% after purification with semi-preparative RP-HPLC and anion exchange, respectively.

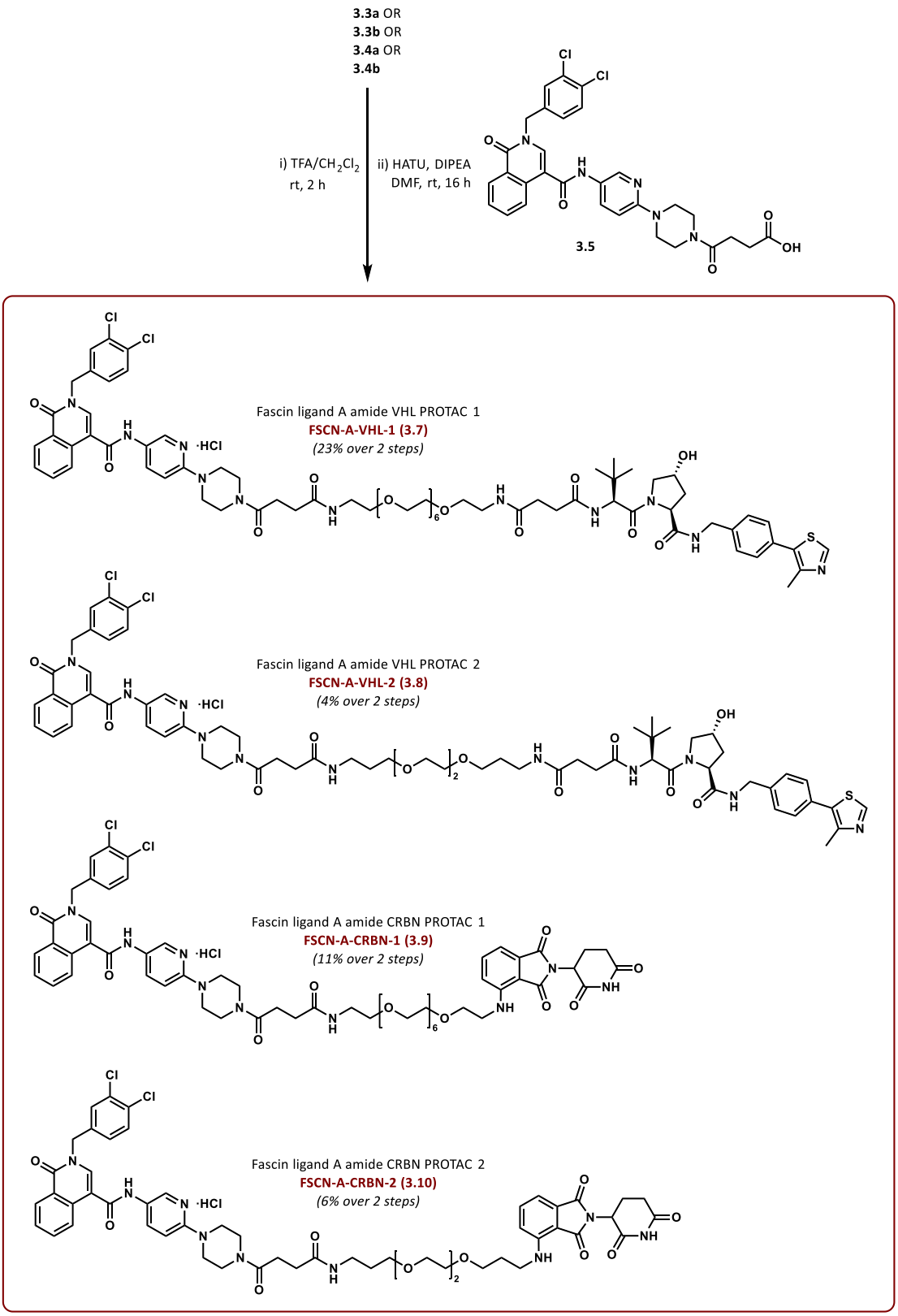

Scheme 3.3: Synthesis of 1st series amide PROTACs.

During synthesis and purification of the 1st series amide PROTACs, poor aqueous solubility of the compounds was observed. Additionally, it was hypothesised that the high number of amide bonds present in the compounds could impact negatively on cell permeability and

intracellular stability,[14] hence alternative approaches to synthesise analogues with potentially improved properties were sought.

3.2.3 Synthesis of 1st series alkylation PROTACs

Instead of functionalisation of the piperazine through formation of an amide bond, alkylation of piperazine nitrogen atom was proposed. This strategy would decrease the number of amide bonds in the compounds at the same time as potentially improving aqueous solubility.

Fascin ligand A alkylation VHL PROTACs

Following a modified literature procedure,[98] mono-protected linker **3.11** was synthesised from pentaethylene glycol by dropwise addition of *tert*-butyl bromoacetate to an excess of the diol to promote mono-substitution, introducing a *tert*-butyl ester as masked carboxylic acid (Scheme 3.4). Subsequent activation the alcohol of mono-protected linker **3.11** by mesylation afforded mono-protected mesylated linker **3.12** in excellent yield. Alkylation of the piperazine moiety of fascin ligand A **FSCN-A (1.4)** with activated linker **3.12** yielded protected fragment **3.13**. After deprotection under acidic conditions to expose the carboxylic acid and subsequent HATU-mediated amide coupling with the amine of VHL ligand **VHL-1 (2.1)**, the crude product was purified by column chromatography on silica gel and semi-preparative RP-HPLC. Anion exchange afforded fascin ligand A alkylation VHL PROTAC **FSCN-A-VHL-3 (3.14)** as a *bis*-hydrochloride salt in 25% yield.

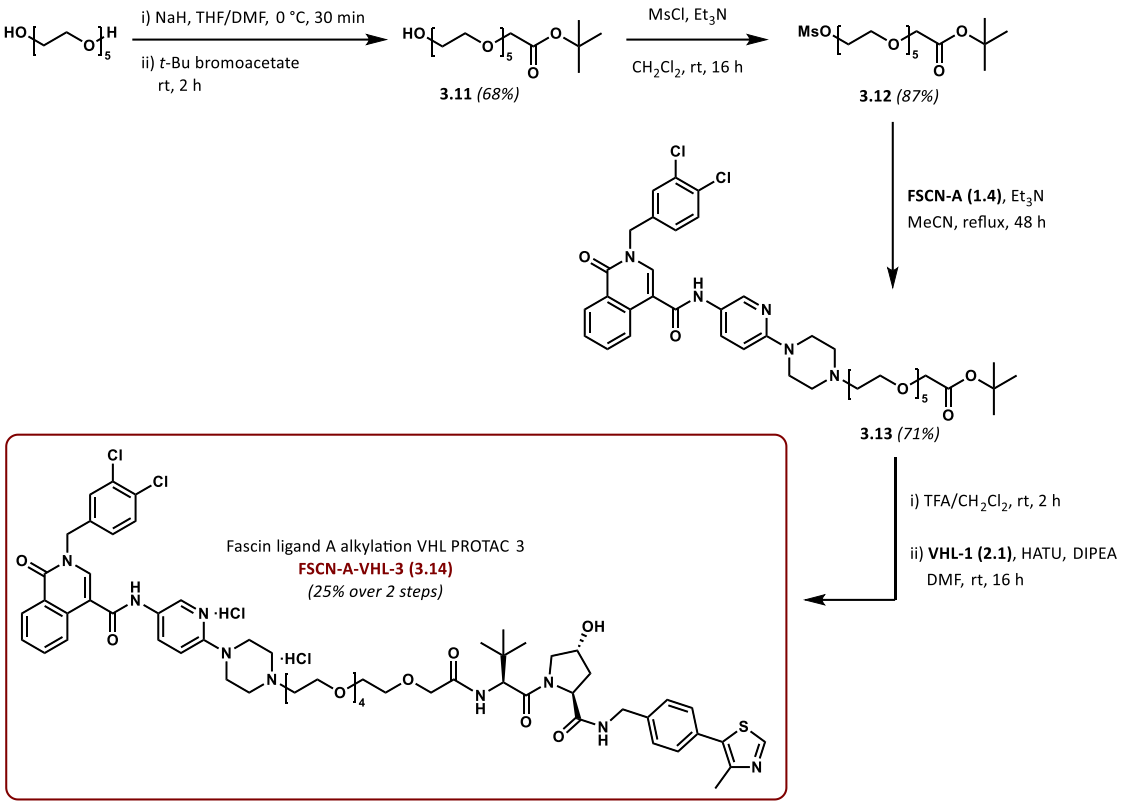

*Scheme 3.4: Synthesis of fascin ligand A alkylation VHL PROTAC **FSCN-A-VHL-3 (3.14)**.*

Click chemistry, such as copper-catalysed azide–alkyne cycloaddition (CuAAC), can be used as a potential approach to quickly establish diverse compound libraries.[188] In order to probe the feasibility of this strategy, fascin ligand A alkylation VHL PROTAC **FSCN-A-VHL-4 (3.19)** was synthesised from fascin ligand A–azide fragment **3.17** and VHL ligand–alkyne fragment **3.18** (Scheme 3.5). Following a modified literature procedure,[188] azide fragment **3.17** was synthesised over three steps from ethylene glycol. Di-tosylation of ethylene glycol proceeded in almost quantitative yield to afford di-tosylate **3.15** and subsequent mono-substitution with sodium azide yielded azide **3.16**. Although the mono-substitution was low-yielding and some of the di-tosylate starting material was recovered, a sufficient quantity of the product was obtained to proceed with the synthesis and optimisation of the reaction was deprioritised. *N*-alkylation of the piperazine moiety of fascin ligand A **FSCN-A (1.4)** afforded azide fragment **3.17** in excellent yield. For alkyne fragment **3.18**, HATU-mediated amide bond formation between the amine of VHL ligand **VHL-1 (2.1)** and the carboxylic acid of the commercially obtained alkyne linker was carried out. Click reaction between azide fragment **3.16** and alkyne fragment **3.18** was performed under standard CuAAC conditions, using catalytic amounts of copper(II) sulfate powder and sodium L-ascorbate for its activation. A small amount of water was added to

tetrahydrofuran as solvent for better solubilisation of the copper catalyst.[188] Purification by semi-preparative RP-HPLC and subsequent anion exchange of the resulting trifluoroacetate salt afforded fascin ligand A alkylation VHL PROTAC **FSCN-A-VHL-4 (3.19)** as *bis*-hydrochloride salt in 29% yield.

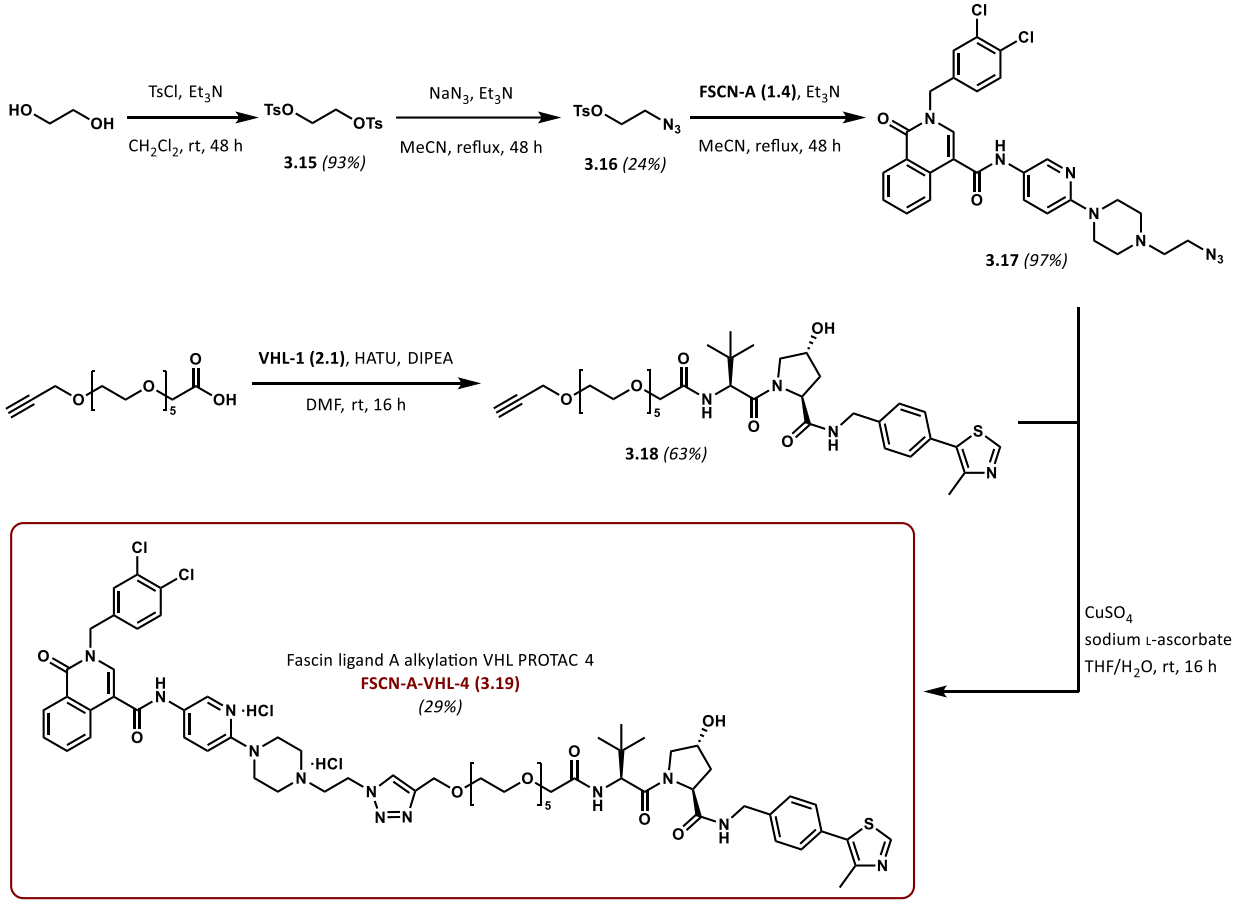

*Scheme 3.5: Synthesis of fascin ligand A alkylation VHL PROTAC **FSCN-A-VHL-4 (3.19)**.*

Fascin ligand A alkylation CRBN PROTAC

For fascin ligand A alkylation CRBN PROTAC **FSCN-A-CRBN-3 (3.22)**, a mono-protected aminoalcohol linker was activated to generate mesylate **3.20**, which was subsequently used for *N*-alkylation at the piperazine moiety of fascin ligand A **VHL-1 (2.1)** (Scheme 3.6). Acidic deprotection of both fascin ligand A–linker fragment **3.21** and CBRN ligand **CRBN-2 (2.11)**, unmasked the amine and carboxylic acid, which were then subjected to HATU-mediated amide coupling conditions. Fascin ligand A alkylation CRBN PROTAC **FSCN-A-CRBN-3 (3.22)** was generated as *bis*-hydrochloride salt in 17% yield after purification by semi-preparative RP-HPLC and anion exchange.

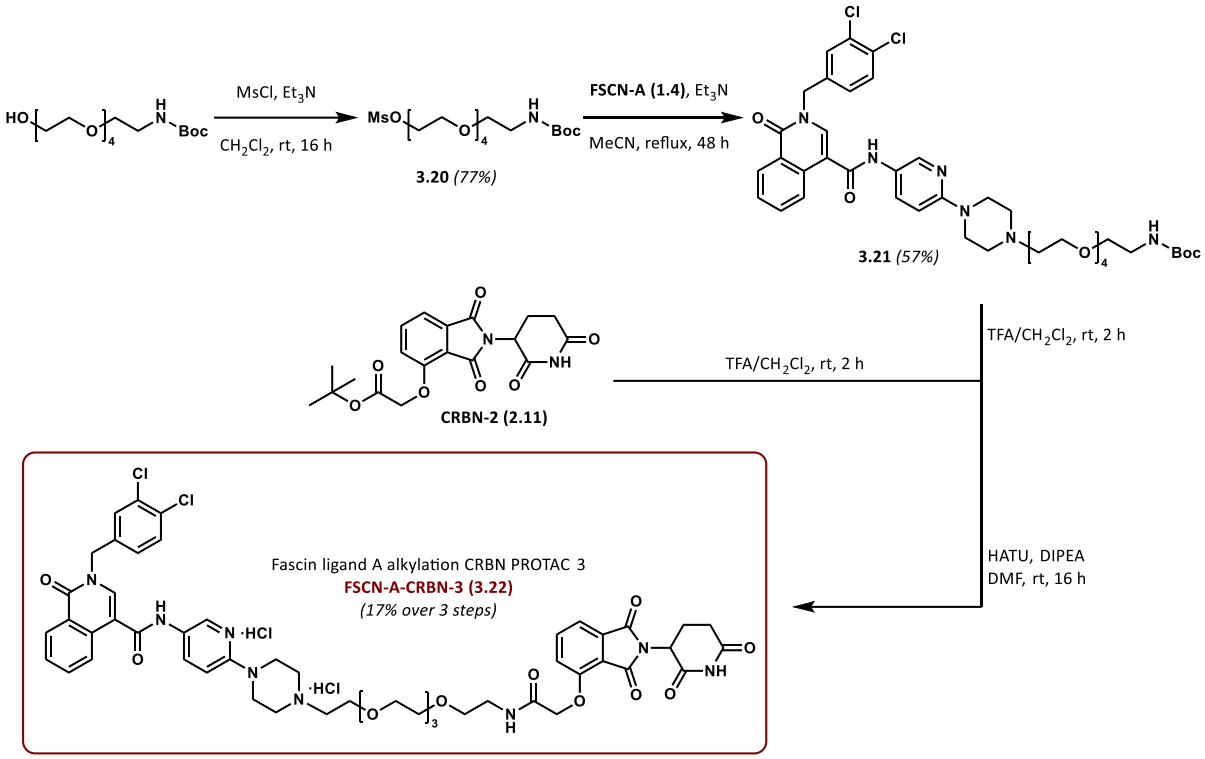

*Scheme 3.6: Synthesis of fascin ligand A alkylation CRBN PROTAC **FSCN-A-CRBN-3 (3.22)**.*

Fascin ligand A alkylation HyT PROTAC

HyT-linker fragment **2.35**, which had previously been generated for the synthesis of HyT HaloPROTAC **HyT-HP-1 (2.36)**, was activated by mesylation to obtain fragment **2.35**, followed by alkylation of the piperazine nitrogen of fascin ligand A **FSCN-A (1.4)** (Scheme 3.7). Fascin ligand A alkylation HyT PROTAC **FSCN-A-HyT-1 (3.24)** was afforded in 32% yield as *bis*-hydrochloride salt after purification by semi-preparative RP-HPLC and anion exchange.

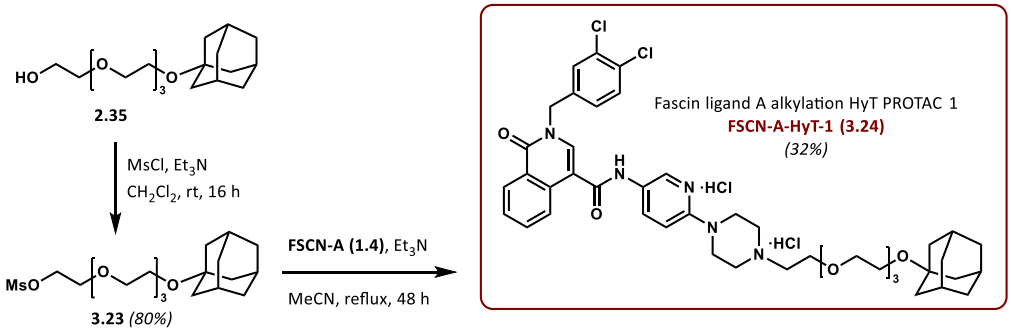

*Scheme 3.7: Synthesis of fascin ligand A alkylation HyT PROTAC **FSCN-A-HyT-1 (3.24)**.*

3.2.4 Physicochemical properties of 1st series PROTACs

Generally, calculated physicochemical properties for the 1st series PROTACs were suboptimal, especially for the initial set of amide PROTACs (Table 3.2). Particularly

noteworthy is the high tPSA and large number of HBA, due to the large number of amide bonds present in the molecules. Decrease of the number of amide bonds in the alkylation series resulted in a lower tPSA, as anticipated. A shorter linker length led to a decrease in NRotB but also an improved tPSA, which can be seen by comparing properties of longer linker amide PROTAC **FSCN-A-CRBN-1 (3.9)** and shorter linker amide analogue **FSCN-A-CRBN-2 (3.10)**. This can be explained by fewer polar and flexible ethylene glycol units in shorter-length linkers. The lipophilicity of all compounds was in the acceptable range, with CRBN PROTACs **FSCN-A-CRBN-1 (3.9)** and **FSCN-A-CRBN-3 (3.22)** displaying excellent values, showcasing the effect the E3 ligase ligand can exert upon PROTAC properties.

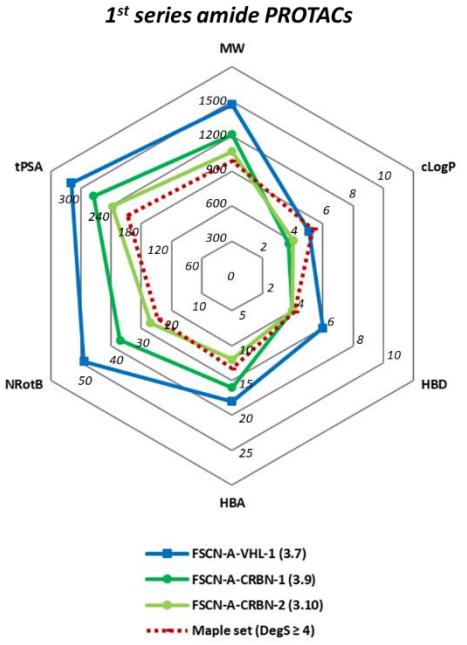

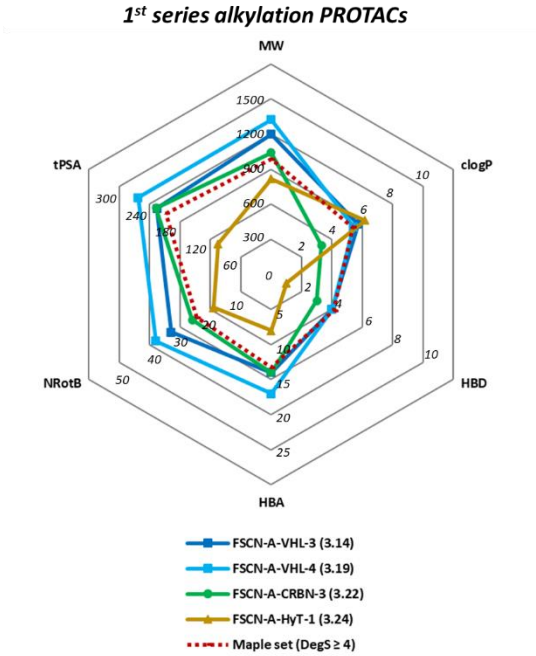

	MW (Da)	cLogP	HBD	HBA	NRotB	tPSA (Å²)
FSCN-A (1.4)	508	3.74	2	5	6	77
1st series amide PROTACs						
FSCN-A-VHL-1 (3.7)	1472	5.07	6	18	49	319
FSCN-A-CRBN-1 (3.9)	1215	3.73	4	16	37	275
FSCN-A-CRBN-2 (3.10)	1067	4.05	4	12	27	238
1st series alkylation PROTACs						
FSCN-A-VHL-3 (3.14)	1199	5.71	4	14	33	226
FSCN-A-VHL-4 (3.19)	1324	5.42	4	17	38	263
FSCN-A-CRBN-3 (3.22)	1042	3.32	3	14	26	227
FSCN-A-HyT-1 (3.24)	819	6.17	1	8	19	105
Good (green): MW < 900, cLogP < 4, HBD < 4, HBA < 10, NRotB < 20, tPSA < 200 *Bad (red): MW > 1100, cLogP > 6, HBD > 6, HBA > 15, NRotB > 28, tPSA > 250*						

Table 3.2: Physicochemical properties of 1st series PROTACs.

3.3 2nd series PROTACs (based on FSCN-B (1.5))

With the intent of synthesising compounds with more favourable properties, attention was shifted to fascin ligand B **FSCN-B (1.5)**. It was hypothesised that incorporating **FSCN-B (1.5)** as fascin-recruiting component could impact positively on PROTAC properties since the ligand was shown to have considerably higher solubility and affinity for fascin, whilst displaying lower cellular toxicity, compared to fascin ligand A **FSCN-A (1.4)** (Chapter 1.1.5).[59] Again, leveraging insights from the development of fluorescent probes based on fascin ligand B **FSCN-B (1.5)**,[186] and supported by a co-crystal structure of the ligand with fascin (Figure 3.5), linker attachment at the solvent-exposed piperidine was rationalised.

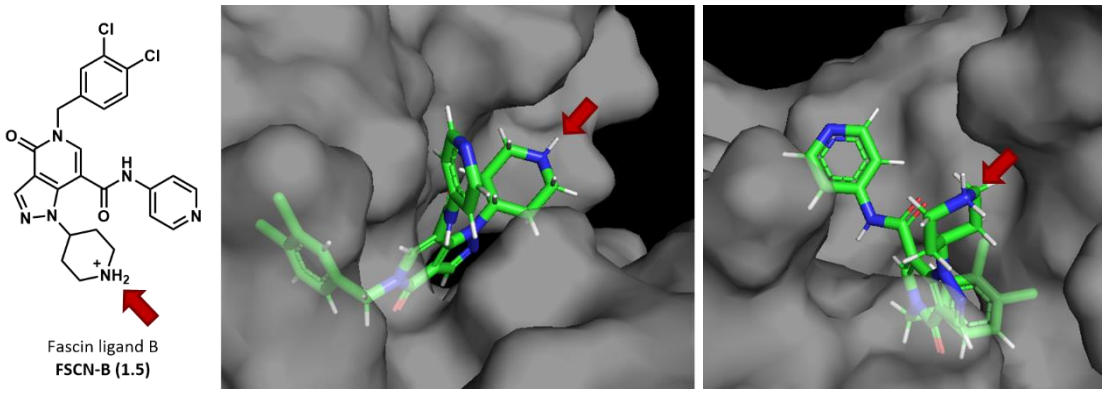

*Figure 3.5: Potential linker attachment point for **FSCN-B (1.5)** co-crystallised with fascin (PDB ID 6i18).*

3.3.1 Synthetic strategy for 2nd series PROTACs

Based on the overall higher yielding synthetic routes of the 1st series alkylation PROTACs compared to the 1st series amide PROTACs, it was decided to follow a similar approach for the 2nd series PROTACs. First, a fascin ligand B–linker fragment library would be generated by activating PEG-based linkers, followed by alkylation of fascin ligand B **FSCN-B (1.5)** (Figure 3.6). The fragments could then be coupled to E3 ligase ligands and HyTs to obtain a library of fascin ligand B-based PROTACs.

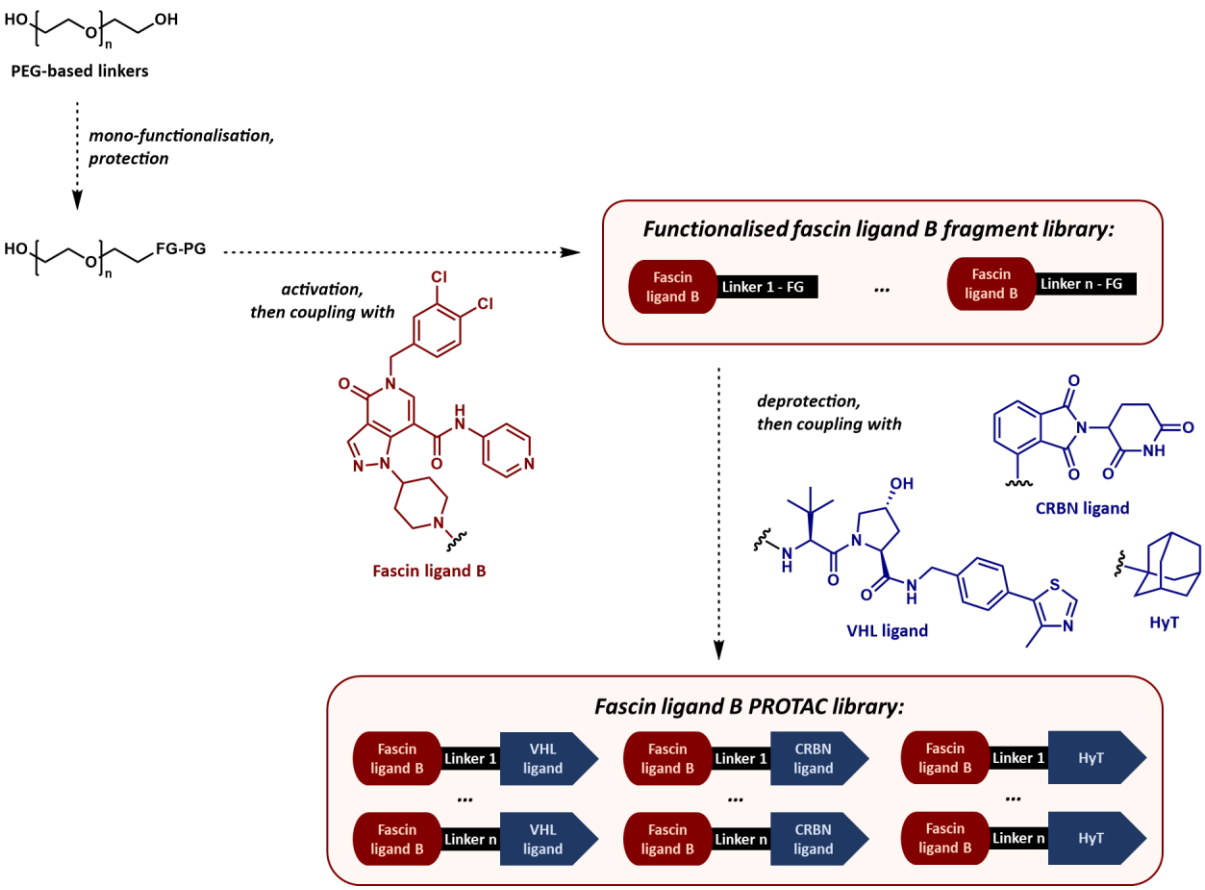

Figure 3.6: Proposed modular synthesis of fascin ligand B–linker library and 2nd series PROTACs.

3.3.2 Synthesis of fascin ligand B FSCN-B (1.5)

As a first step, fascin ligand B **FSCN-B (1.5)** needed to be synthesised following a modified literature precedent.[59] Enaminone **3.25** was accessed as a 1:1 mixture of *E* and *Z* isomers in adequate yield by reacting *N,N*-dimethylformamide dimethyl acetal (DMFDMA) with dimethyl 3-oxoglutarate (Scheme 3.8). *Tert*-butyl 4-hydrazinopiperidine-1-carboxylate hydrochloride was neutralised *in situ* before addition of enaminone **3.25** to the reaction mixture. One major product was obtained in 68% to 82% yield, however, it could not be established with certainty if desired pyrazole regioisomer **3.26a** or undesired regioisomer **3.26b** was obtained. Formation of pyridone **3.26c**, as reported in literature,[189] was however not observed. LCMS analysis of the crude material displayed one major and one minor peak, both containing the same molecular weight corresponding to pyrazoles **3.26a** and **3.26b**. 2D NOESY NMR analysis provided some evidence for the desired regiosomer **3.26a**, indicating that the protons of the methylene group were close in space to the piperidine protons, however, the analysis was not finally conclusive. It was rationalised that formation of pyrazole regioisomer **3.26a** would proceed through a thermodynamically favoured pathway with the non-substituted nitrogen of the hydrazine reacting first.[190] Despite the

structural uncertainty, it was decided to proceed with the synthesis of fascin ligand B **FSCN-B (1.5)** with the aim of fully elucidating the structure at a later stage in the synthesis.

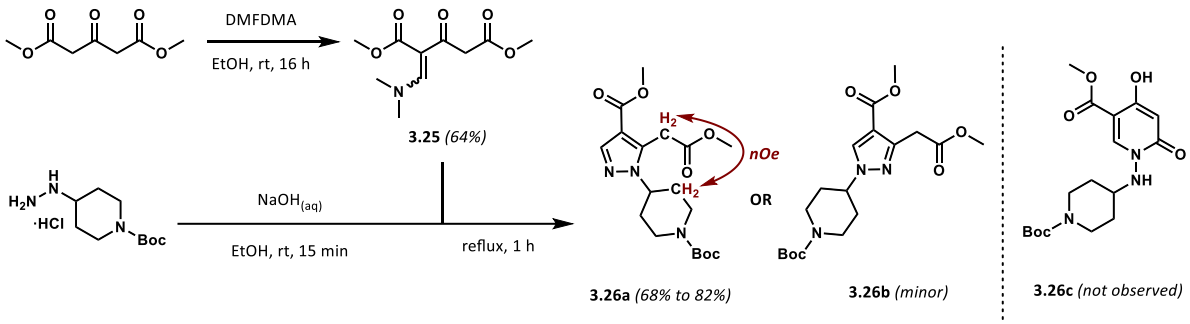

*Scheme 3.8: Synthesis of pyrazole **3.26a** or **3.26b**.*

Reaction of Bredereck's reagent with pyrazole **3.26a** afforded enaminone **3.27** in quantitative yield (Scheme 3.9). Subsequent addition of 3,4-dichlorobenzylamine under acidic catalysis resulted in the substitution product **3.28** in 63% yield but, unexpectedly, the annulated product **3.29** was also obtained in 28% yield. Full annulation was achieved by subjecting substitution product **3.28** to sodium methoxide in methanol under reflux for 2 hours. Ester saponification of **3.29** unmasked the carboxylic acid of **3.30** which was then coupled to 4-aminopyridine using a HATU-mediated amide coupling protocol to afford protected fascin ligand B **3.31** in excellent yield. Fascin ligand B **FSCN-B (1.5)** was obtained in quantitative yield after deprotection of the piperidine under acidic conditions, followed by neutralisation of the resultant salt.

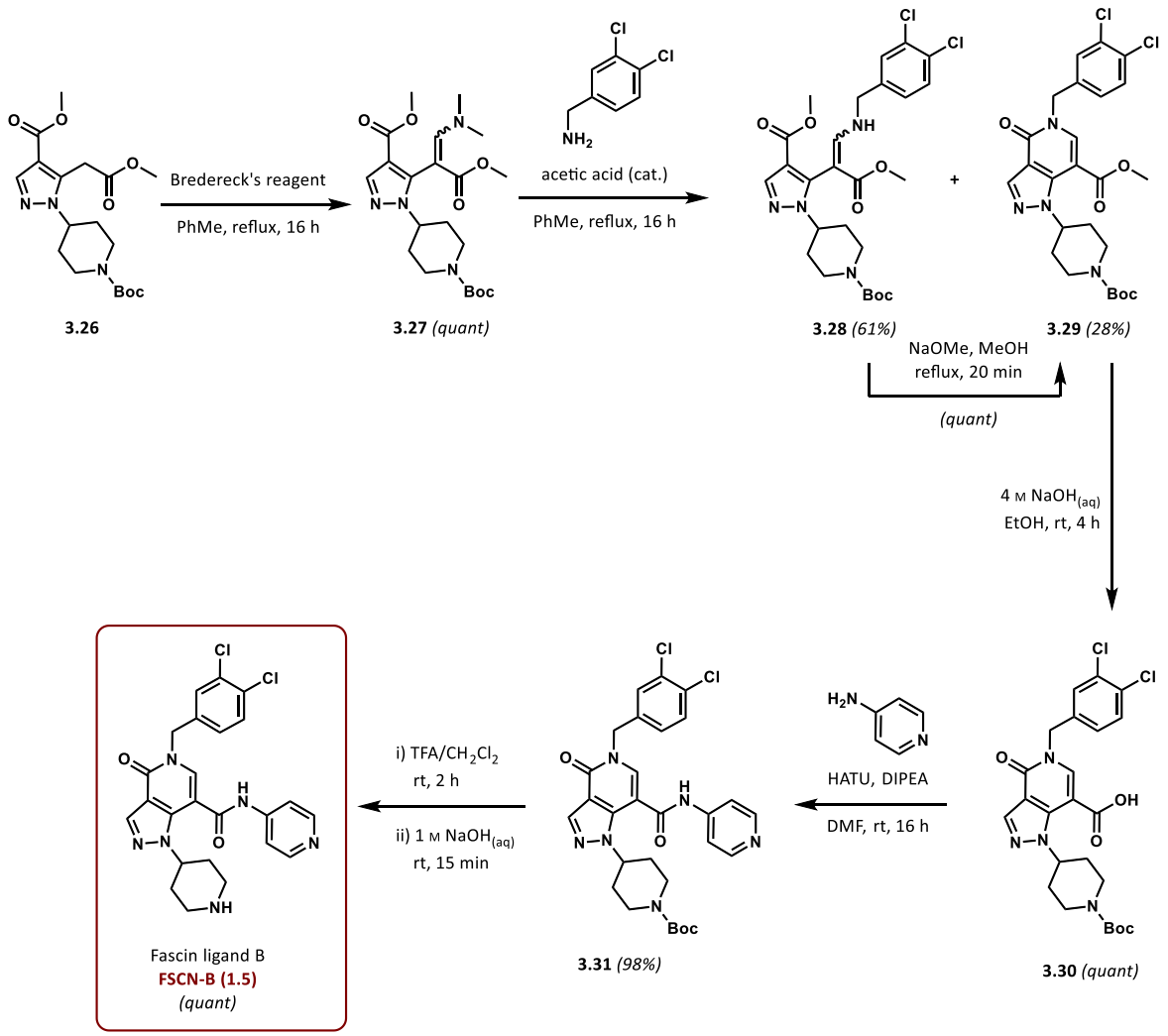

*Scheme 3.9: Synthesis of fascin ligand B **FSCN-B (1.5)**.*

In order to conclusively confirm the structure of fascin ligand B **FSCN-B (1.5)**, the compound was purified by semi-preparative RP-HPLC, followed exchange of trifluoroacetate to chloride anions. Crystals were generated using a two-solvent recrystallisation. Subsequent analysis by X-ray diffraction confirmed the correct pyrazole regioisomer was in fact obtained (Figure 3.7).

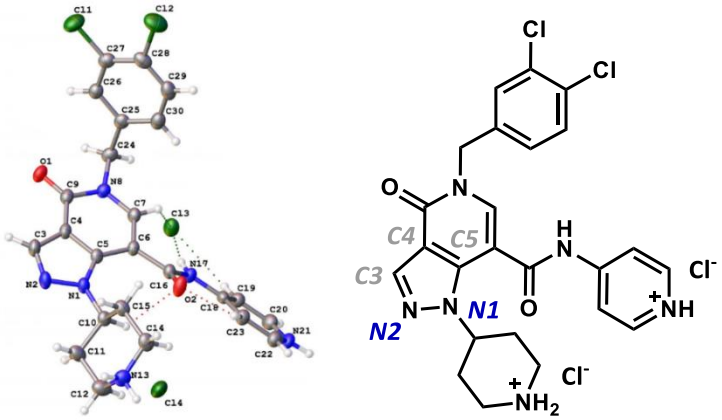

*Figure 3.7: X-ray model of fascin ligand B **FSCN-B (1.5)**.*

With fascin ligand B **FSCN-B (1.5)** in hand, synthesis of the 2nd series PROTACs could commence. It was envisioned to generate matched pairs of each, VHL-recruiting and CRBN-recruiting PROTACs, as well as a matched pair of HyTs, featuring a shorter and a longer linker, in order to probe the impact of linker length on the ability to induce targeted fascin degradation.

3.3.3 Synthesis of 2nd series PROTACs

VHL PROTACs

First, attention was turned to VHL-recruiting PROTACs. Whereas longer mono-protected activated linker **3.12** was available from the synthesis of 1st series VHL PROTAC **FSCN-A-VHL-3 (3.14)**, shorter analogue **3.33** was synthesised using the same protocol (Scheme 3.10). Diethylene glycol was mono-functionalised with *tert*-butyl bromoacetate affording mono-*tert*-butyl ester **3.32** in a yield comparable to the longer linker analogue **3.11**. This was followed by activation of the alcohol by mesylation affording linker fragment **3.33** in excellent yield. Subsequently, the piperidine nitrogen of fascin ligand B **FSCN-B (1.5)** was alkylated with activated longer linker **3.12** and activated shorter linker **3.33**, generating fascin ligand–linker fragments **3.34a** and **3.34b** in comparable yields. After acidic deprotection to expose the corresponding carboxylic acids, which were thencoupled to the amine moiety of VHL ligand **VHL-1 (2.1)** using HATU-mediated amidation. Purification by semi-preparative RP-HPLC and anion exchange yielded longer linker PROTAC **FSCN-B-VHL-1 (3.35)** in 44% and shorter linker PROTAC **FSCN-B-VHL-2 (3.36)** in 32% as *bis*-hydrochloride salts.

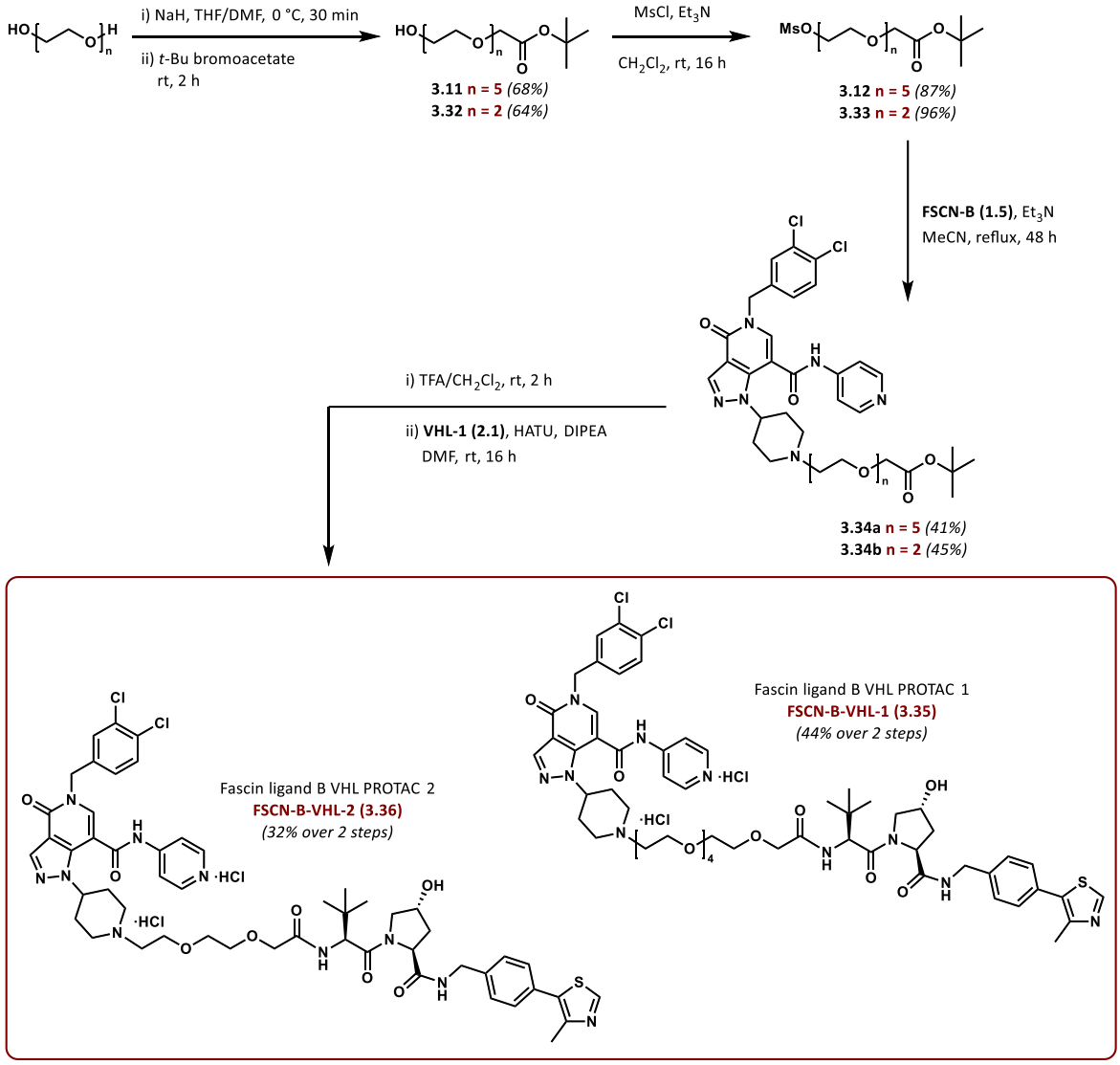

*Scheme 3.10: Synthesis of fascin ligand B VHL PROTACs **FSCN-B-VHL-1 (3.35)** and **FSCN-B-VHL-2 (3.36)**.*

CRBN PROTACs

For the corresponding CRBN-recruiting PROTACs and HyTs, aminoalcohol linkers were required. Shorter linker **3.39** was commercially available, however, longer linker analogue **3.38** needed to be synthesised by converting a mono-activated PEG linker into azide **3.37**, followed by hydrogenation of the azide to obtain aminoalcohol linker **3.38** in excellent yield (Scheme 3.11).

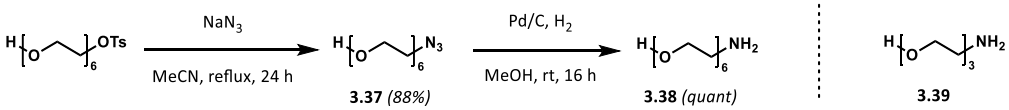

*Scheme 3.11: Synthesis of aminoalcohol linker **3.38** and commercial aminoalcohol linker **3.39** used for synthesis of CRBN and HyT PROTACs.*

Initially, it was planned to synthesise fascin ligand B–linker fragments which could then be coupled to both, CRBN ligand **CRBN-1 (2.9)** *via* S_NAr and adamantylacetic acid through amide coupling reactions. To do so, the amine moiety of aminoalcohol linker **3.38** was protected using di-*tert*-butyl dicarbonate to yield protected linker **3.39**. Then the alcohol was activated by mesylation to allow for subsequent *N*-alkylation of the piperidine of fascin ligand B **FSCN-B (1.5)** (Scheme 3.12 a). After acidic deprotection of fragment **3.41**, S_NAr at CRBN ligand **CRBN-1 (2.9)** was attempted. However, the reaction failed to generate sufficient quantities of CRBN PROTAC **FSCN-B-CRBN-1 (3.42)** for full characterisation and biological testing. Instead of optimising attempted route A, an alternative synthesis was pursued for which protection and deprotection of the amine moiety of aminoalcohol linker **3.38** was to be avoided, aiming to improve the overall yield (Scheme 3.12 b). Therefore, CRBN ligand–linker fragment **3.43** was established *via* S_NAr reaction of CRBN ligand **CRBN-1 (2.9)** with aminoalcohol linker **3.38**. However, this reaction proceeded in low yield, with recovery of some of the unreacted CRBN ligand **CRBN-1 (2.9)**. Since sufficient amounts of CRBN ligand–linker fragment **3.43** was generated, the synthesis was carried forward by activation of the alcohol moiety *via* mesylation which proceeded in moderate yield to afford activated fragment **3.44**. Subsequent *N*-alkylation of fascin ligand B **FSCN-B (1.5)**, followed by purification by semi-preparative RP-HPLC and anion exchange afforded CRBN PROTAC **FSCN-B-CRBN-1 (3.42)** as *bis*-hydrochloride salt in adequate yield.

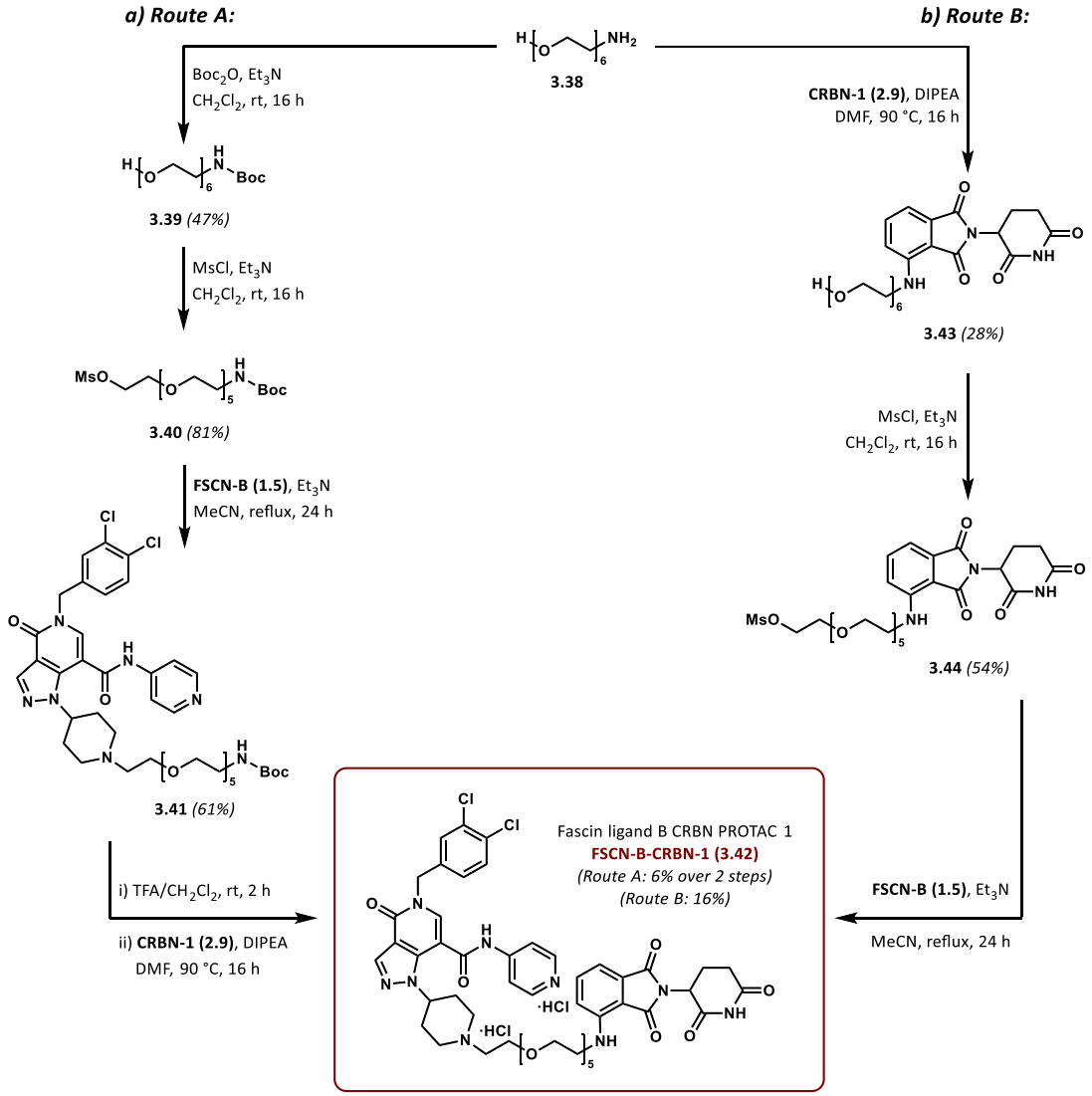

*Scheme 3.12: Synthesis of fascin ligand B CRBN PROTAC **FSCN-B-CRBN-1 (3.42)**.*

Due to the low-yielding S_NAr reactions encountered in the synthesis of longer linker CRBN PROTAC **FSCN-B-CRBN-1 (3.42)**, a different strategy was pursued for the synthesis of shorter linker analogue **FSCN-B-CRBN-2 (3.47)** (Scheme 3.13). After acidic deprotection to expose the carboxylic acid of CRBN ligand **CRBN-2 (2.11)** and HATU-mediated amide coupling with aminoalcohol linker **3.39**, CRBN ligand–linker fragment **3.45** was generated in acceptable yield. The alcohol was activated through mesylation for subsequent alkylation of fascin ligand **FSCN-B (1.5)**, generating the shorter linker CRBN PROTAC analogue. Purification of semi-preparative RP-HPLC and anion exchange yielded **FSCN-B-CRBN-2 (3.47)** as *bis*-hydrochloride salt in 9%.

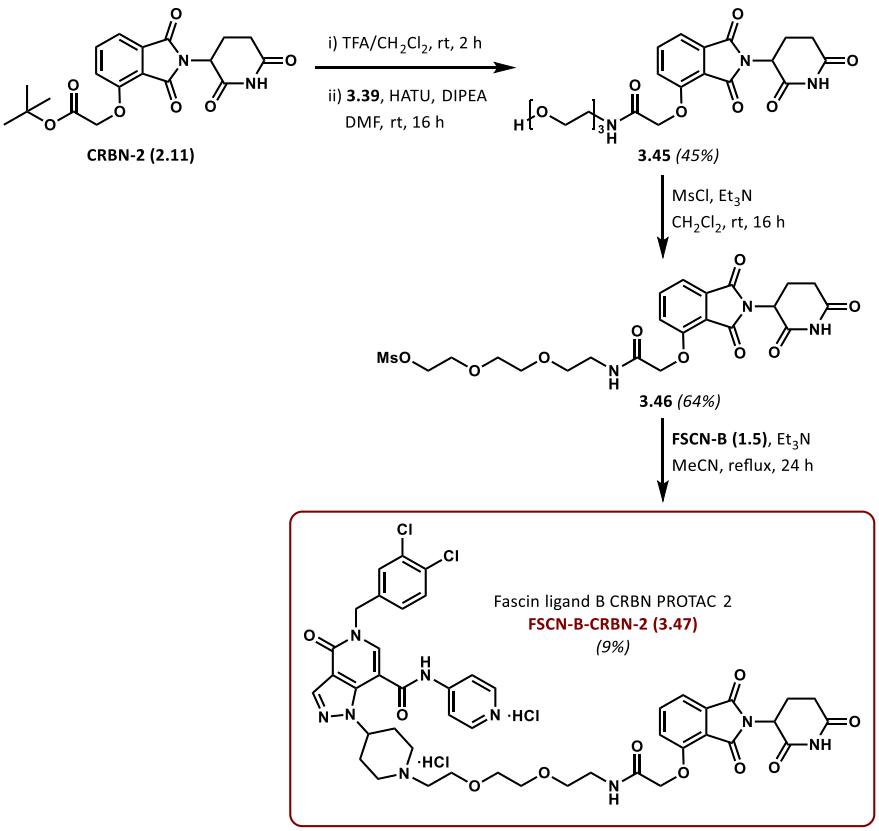

*Scheme 3.13: Synthesis of fascin ligand B CRBN PROTAC **FSCN-B-CRBN-2 (3.47)**.*

HyT PROTACs

The amine moiety of fascin ligand B–linker fragment **3.41**, which had been generated previously in the synthesis of CRBN PROTAC **FSCN-B-CRBN-1 (3.42)**, was deprotected under acidic conditions. Coupling with 1-adamantylacetic acid using HATU and subsequent purification by semi-preparative RP-HPLC and anion exchange, afforded longer linker HyT PROTAC **FSCN-B-HyT-1 (3.48)** as a *bis*-hydrochloride salt in 29% yield (Scheme 3.14).

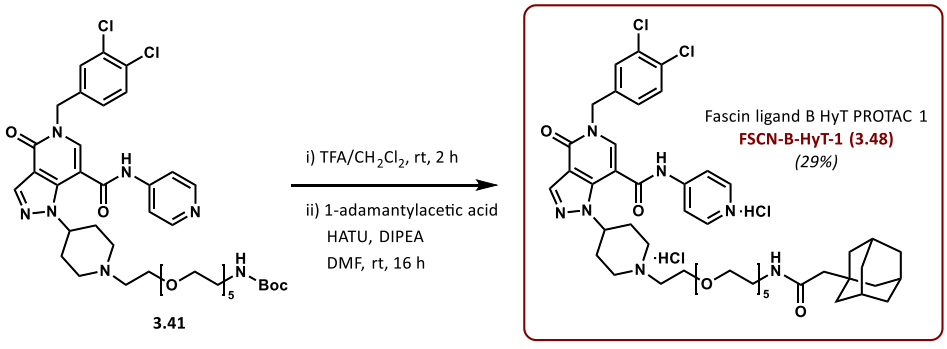

*Scheme 3.14: Synthesis of fascin ligand B HyT PROTAC **FSCN-B-HyT-1 (3.48)**.*

For the shorter linker analogue, HyT–linker fragment **3.49** was generated first by coupling of aminoalcohol linker **3.39** with adamantylacetic acid in order to avoid protection-deprotection of the amine moiety (Scheme 3.15). This was followed by mesylation of the alcohol to yield activated fragment **3.50** which could then be used for alkylation of the piperidine moiety of fascin ligand B **FSCN-B (1.5)**. Shorter linker HyT PROTAC **FSCN-B-HyT-2 (3.51)** was yielded in 38% as *bis*-hydrochloride salt after purification with semi-preparative RP-HPLC and anion exchange.

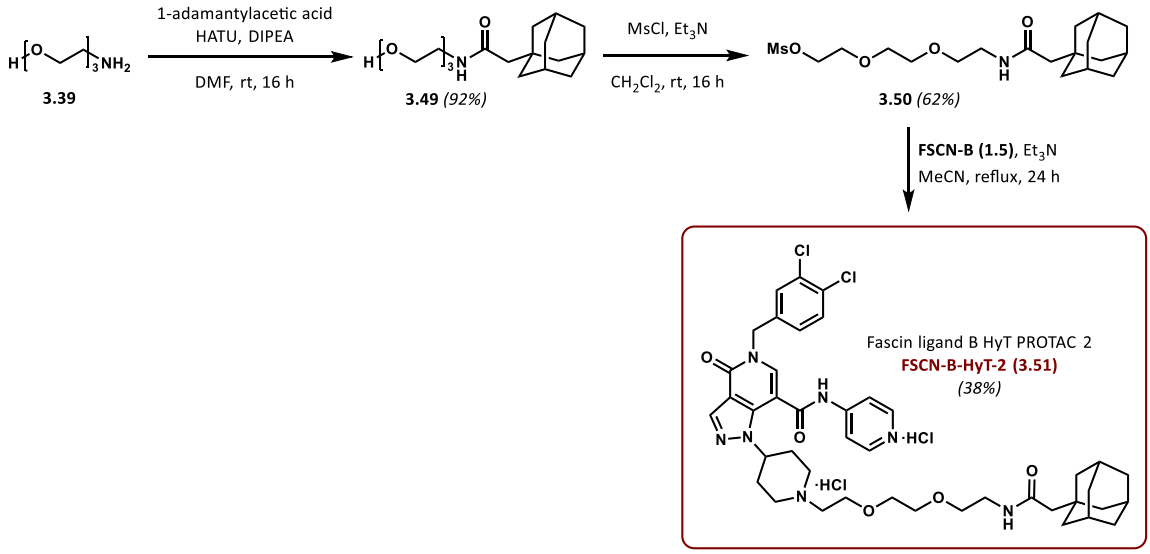

*Scheme 3.15: Synthesis of fascin ligand B HyT PROTAC **FSCN-B-HyT-2 (3.51)**.*

3.3.4 Physicochemical properties of 2nd series PROTACs

The physicochemical properties of the 2nd series PROTACs were comparable, albeit slightly improved, to those of the 1st series alkylation PROTACs (Table 3.3). This can be explained by both parent compounds, fascin ligand A **FSCN-A (1.4)** and fascin ligand B **FSCN-B (1.5)**, displaying similar properties, with fascin ligand B **FSCN-B (1.5)** exhibiting marginally lower lipophilicity. Interestingly, although fascin ligand B **FSCN-B (1.5)** was calculated to have a higher tPSA than fascin ligand A **FSCN-A (1.4)**, the 2nd series PROTACs displayed generally lower tPSA values. Expectedly, the shorter linker PROTAC set featured slightly fewer HBA, a smaller tPSA and fewer NRotB compared to the longer linker analogues due to a reduced number ethylene glycol units. A similar trend as for the 1st series PROTACs could be observed, with CRBN-recruiting PROTACs **FSCN-B-CRBN-1 (3.42)** and **FSCN-B-CRBN-2 (3.47)** displaying improved lipophilicity due to the inherent properties of the CRBN ligand itself. Overall, properties of the 2nd series PROTACs, especially those of the shorter linker analogues, seemed to be in the range of properties reported for active PROTACs (Maple set), indicating that this series could be cell-permeable.

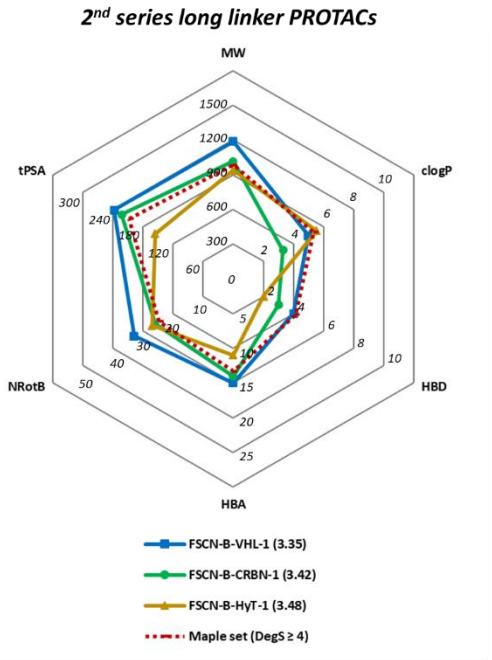

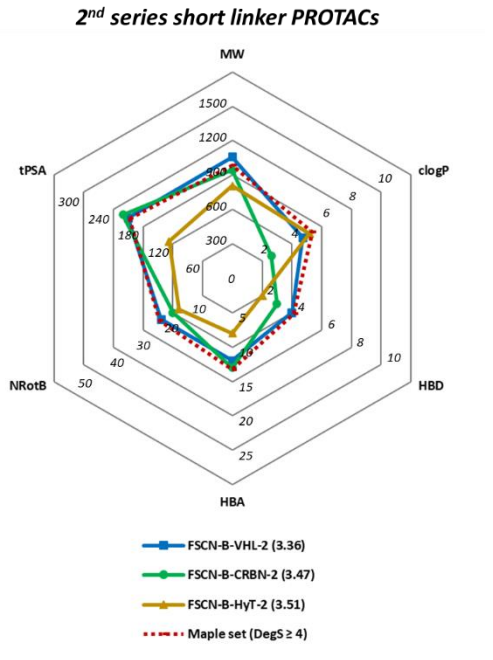

	MW (Da)	cLogP	HBD	HBA	NRotB	tPSA (Å²)
FSCN-B (1.5)	497	2.95	2	6	6	89
2nd series long linker PROTACs						
FSCN-B-VHL-1 (3.35)	1188	4.98	4	15	33	238
FSCN-B-CRBN-1 (3.42)	1017	3.32	3	14	26	222
FSCN-B-HyT-1 (3.48)	937	5.53	2	11	27	156
2nd series short linker PROTACs						
FSCN-B-VHL-2 (3.36)	1056	4.72	4	12	24	210
FSCN-B-CRBN-2 (3.47)	943	2.62	3	13	20	221
FSCN-B-HyT-2 (3.51)	805	5.18	2	8	18	128
Good (green): MW < 900, cLogP < 4, HBD < 4, HBA < 10, NRotB < 20, tPSA < 200 *Bad (red): MW > 1100, cLogP > 6, HBD > 6, HBA > 15, NRotB > 28, tPSA > 250*						

Table 3.3: Physicochemical properties of 2nd series PROTACs.

3.4 3rd series PROTACs (based on FSCN-C (1.7))

The 3rd series PROTACs were based on a different set of fascin ligands which were reported to display *in vitro*[63] as well as *in vivo*[65,66] activity against fascin (Chapter 1.1.5). Occupying the same actin-binding site as the previous two ligands, co-crystal structures showed that fascin ligand C **FSCN-C (1.7)** can adopt two different conformations in the binding site.[64] Since no experimental data for functionalisation of the ligand was available, *in silico* docking studies were carried out to rationalise potential linker attachment points (Figure 3.8). For both conformations, the 5-position of the furan moiety as well as 5-position of the indazole moiety (red arrows in Figure 3.8) appeared to be solvent-exposed in the docking results as well as the reported co-crystal structures of analogues of the compound, providing some

evidence that linker attachment at those two positions would likely not interfere with the fascin-binding ability of the ligand.

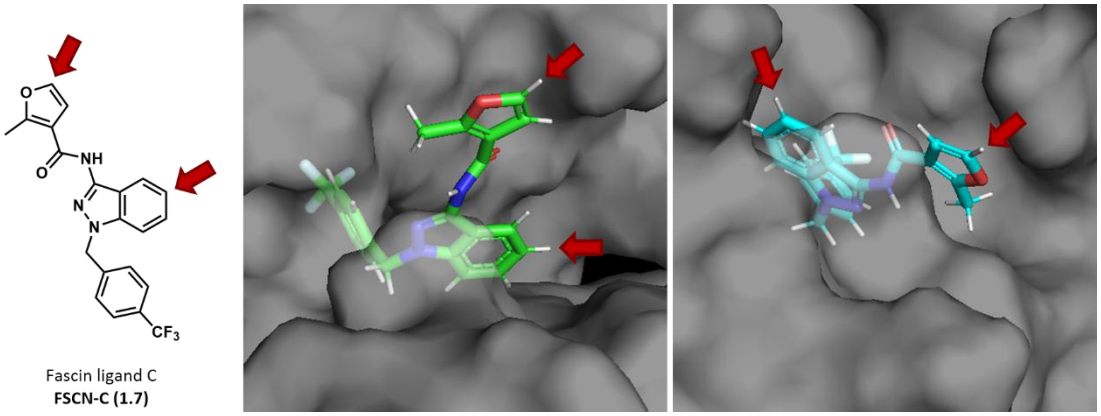

*Figure 3.8: Potential linker attachment points for both binding conformations of **FSCN-C (1.7)** docked into fascin (PDB ID 6i18).*

3.4.1 Synthetic strategy for 3rd series PROTACs

In contrast to the synthetic strategies employed for the previous two series, the proposed synthesis for the 3rd series PROTACs would be based on linker attachment at two different positions of the ligand. Functionalisation of the 5-position at the furan moiety or at the 5-position of the indazole moiety would introduce handles for linker attachment (Figure 3.9). Subsequent coupling to different PEG-based linkers would afford a set of fascin ligand C–linker modules. Attachment of E3 ligase ligands or HyTs would results in a diverse 3rd series of fascin-targeting PROTACs. With linker attachment at different positions, the impact on binding and activity of the compounds could be directly compared and the optimal attachment point and linker length could be determined.

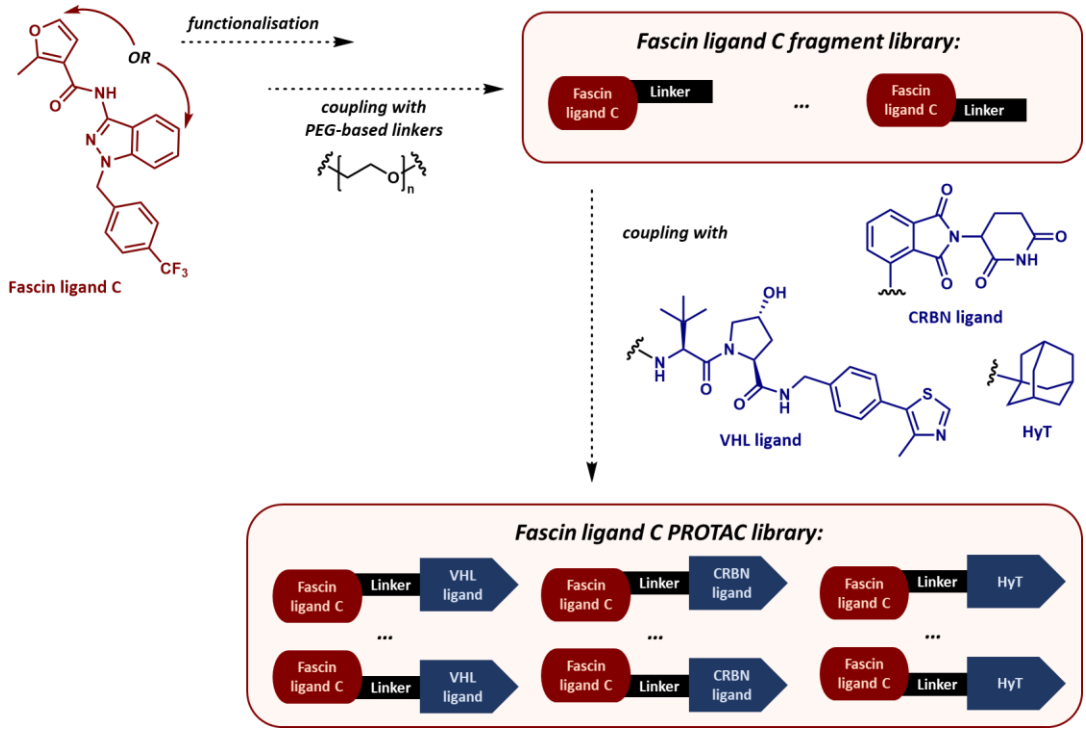

*Figure 3.9: Proposed functionalisation of **FSCN-C (1.7)** and modular synthesis of 3rd series PROTACs.*

3.4.2 Synthesis of fascin ligand C and functionalised analogues

Since direct introduction of handles on parent compound **FSCN-C (1.7)** was deemed unpractical, functionalised analogues would be generated to allow for linker attachment (Figure 3.10): Analogue **3.52** would feature a furfuryl alcohol moiety for subsequent alkylation and bromo-analogue **3.53** could be used for palladium-catalysed carbon–nitrogen bond formation at the indazole moiety.

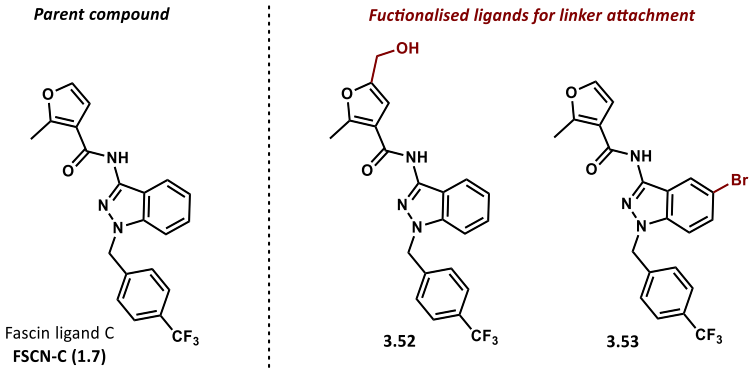

*Figure 3.10: Parent compound fascin ligand C **FSCN-C (1.7)** and functionalised analogues **3.52** and **3.53**.*

Following a modified literature procedure,[191] the alcohol handle for analogue **3.52** was introduced by subjecting methyl 2-methylfuran-3-carboxylate to Vilsmeier–Haack conditions and the resulting furfural **3.54** was reduced using sodium borohydride to afford alcohol **3.55** in excellent yield (Scheme 3.16). Methyl ester **3.55** was then saponified

yielding furoic acid **3.56a**. The non-functionalised analogue **3.56b**, which would be used for synthesis of parent compound **FSCN-C (1.7)** and bromo-analogue **3.53**, was generated by direct saponification of the methyl 2-methylfuran-3-carboxylate starting material in quantitative yield.

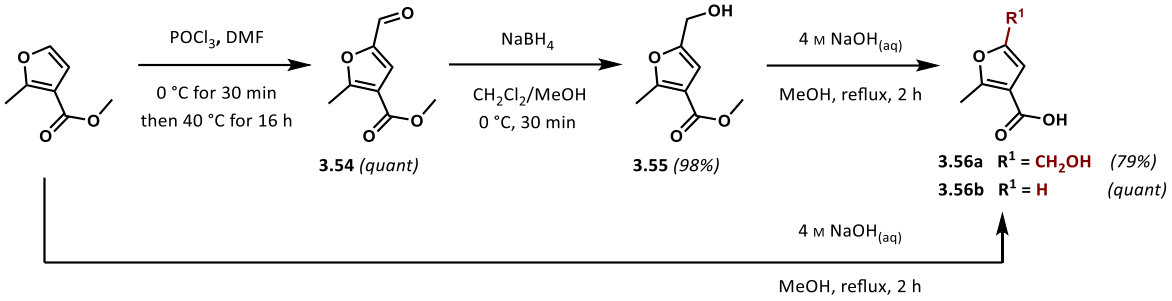

*Scheme 3.16: Synthesis of furoic acids **3.56a** and **3.56b**.*

Alkylation of 1*H*-indazol-3-amine or 5-bromo-1*H*-indazol-3-amine with 4-(trifluoromethyl)benzyl bromide was carried out following a modified literature precedent.[64] Deprotonation of the indazole was achieved by use of potassium hydroxide and the desired mono-alkylated products **3.57a** and **3.57b** were afforded in good yields following slow dropwise of 4-(trifluoromethyl)benzyl bromide (Scheme 3.17). Hastier addition of 4-(trifluoromethyl)benzyl bromide resulted in formation of significant amounts of undesired di-alkylated side product **3.57c**.

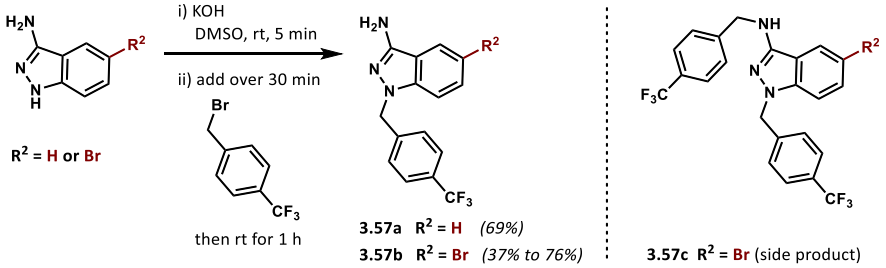

*Scheme 3.17: Synthesis of mono-alkylation fragments **3.57a** and **3.57b**.*

Amidation reactions of acids **3.56a** and **3.56b** with amines **3.57a** and **3.57b** to obtain parent compound **FSCN-C (1.7)** as well as the functionalised analogues **3.52** and **3.53** were first attempted for parent compound **FSCN-C (1.7)** using propanephosphonic acid anhydride (T3P) as coupling agent (entry 1 in Table 3.4).[64] Although only 30% of the product was obtained, with recovery of most of the unreacted amine starting material **3.57a**, sufficient quantity of parent compound **FSCN-C (1.7)** material was generated for purification by semi-preparative RP-HPLC and biological testing. For functionalised analogue **3.52**, HATU-mediated amide coupling conditions were trialled (entry 2 in Table 3.4), resulting in a slight

improvement in yield to 43%, again with recovery of the majority of the unreacted amine starting material **3.57a**. TLC analysis indicated disappearance of the acid starting material **3.56a**, suggesting formation of the activated ester was taking place. Due to the inactivated nature of the amine nucleophile **3.57a**, competing attack by the alcohol of **3.56a** was hypothesised to occur. However, when subjecting acid **3.56b** lacking the alcohol moiety and amine **3.57b** to the same HATU-mediated amide coupling conditions, bromo-analogue **3.53** was obtained in a comparable yield (entry 3 in Table 3.4). This suggested that competing attack of the alcohol was inconsequential, and the root cause of the low yields was to be found with the unreactive nature of the amine, hence further amide coupling conditions were trialled.

An amide coupling protocol reported in literature[192] using EDC·HCl, HOBt and DMAP which was developed for deactivated amines was attempted (entry 4 in Table 3.4). Theoretically, initial reaction of the carboxylic acid with EDC·HCl and HOBt would form a reactive HOBt ester, and subsequent attack of DMAP would generate a highly reactive acyl iminium intermediate which would then be sufficiently activated for attack by electron-deficient amines. However, subjecting acid **3.56b** and amine **3.57b** to these conditions afforded amide **3.53** in only 25% yield, hence was lower yielding than the previously attempted HATU-mediated coupling conditions. Next, a borate ester-based amide coupling protocol which was reported to afford high yields for highly functionalised substrates and challenging coupling reactions was tried.[193,194] Using borate ester $B(OCH_2CF_3)_3$ and elevated temperatures, it was possible to improve the yield of product **3.53** (entry 5 in Table 3.4), however, purification by column chromatography proved difficult due to the acid starting material eluting together with the product, requiring several purification steps to obtain the product in a 59% yield in adequate purity.

Finally, a recent addition to the amide coupling reagent repertoire, chloro-*N,N,N',N'*-tetramethylformamidinium hexafluorophosphate (TCFH) and *N*-methylimidazole (NMI),[195] was attempted. Reaction of TCFH and NMI with the carboxylic acid would generate a highly reactive acyl imidazolium intermediate which was reported to display high reactivity towards non-nucleophilic amines. Subjecting acid **3.56b** and amine **3.57b** to the formadinium-based amidation conditions afforded product **3.53** in quantitative yield, along with recovery of unreacted amine starting material **3.57b** which was added in a slight excess. Using acetonitrile as solvent allowed for facile work-up of the reaction by removal of volatile components *in vacuo*, removing the need for a lengthy aqueous work-up

involving several washes with aqueous lithium chloride solution as needed for reactions carried out in DMF.

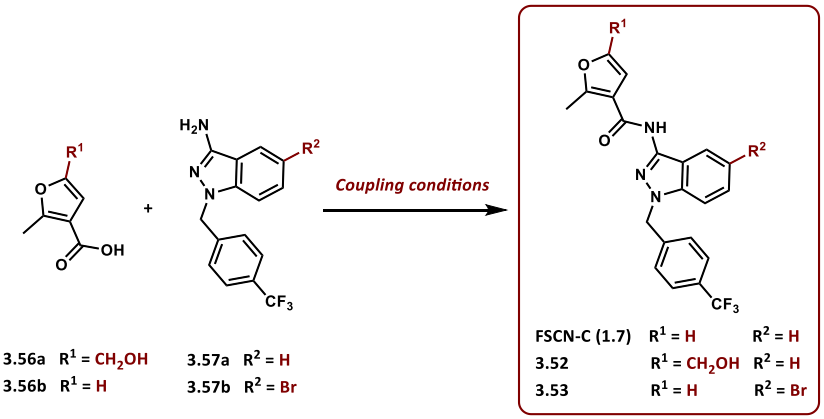

	Acid	Amine	Coupling conditions	Product (yield / yield BRSM)	Ref
1	3.56b	3.57a	T3P (50% in ethyl acetate), Et_3N CH_2Cl_2, rt, 16 h	**FSCN-C (1.7)** *(30% / 90% BRSM)*	64
2	3.56a	3.57a	HATU, DIPEA DMF, rt, 16 h	**3.52** *(43% / 90% BRSM)*	
3	3.56b	3.57b	HATU, DIPEA DMF, rt, 16 h	**3.53** *(43% / 91% BRSM)*	
4	3.56b	3.57b	EDC·HCl, HOBt, DMAP, DIPEA MeCN, 40 °C, 16 h	**3.53** *(25% / 70% BRSM)*	192
5	3.56b	3.57b	$B(OCH_2CF_3)_3$ MeCN, 100 °C, 16 h	**3.53** *(59% / 80% BRSM)*	193,194
6	3.56b	3.57b	TCFH, NMI MeCN, rt, 16 h	**3.53** *(quant)*	195

Table 3.4: Optimisation of amidation conditions.

3.4.3 Synthesis of 3rd series PROTACs

VHL PROTACs

Alkylation of functionalised fascin ligand C analogue **3.52** with activated linker **3.12**, which was previously synthesised, was initially attempted using triethylamine, however, the reaction failed to proceed. The use of a slight excess of the much stronger base sodium hydride in order to deprotonate the alcohol moiety of **3.52** prior to addition of activated linker **3.12** was also unfruitful. Increasing the equivalents of sodium hydride resulted in the formation of a major product, which was, however, not the expected protected fascin ligand C–linker fragment **3.58** (Scheme 3.18). Analysis by NMR and LCMS confirmed deprotected fragment **3.59** was instead afforded in 28% yield. It was hypothesised that protected fragment **3.58** was obtained in the reaction, with deprotection occurring when the remaining sodium hydride was quenched by slow addition of water, generating

hydroxide anions capable of hydrolysing the *tert*-butyl ester to expose the corresponding carboxylic acid. Having obtained carboxylic acid fragment **3.59** directly, it could then be coupled to the amine moiety of VHL ligand **VHL-1 (2.1)**, yielding fascin ligand C VHL PROTAC **FSCN-C-VHL-1 (3.60)** in 32% after purification by semi-preparative RP-HPLC.

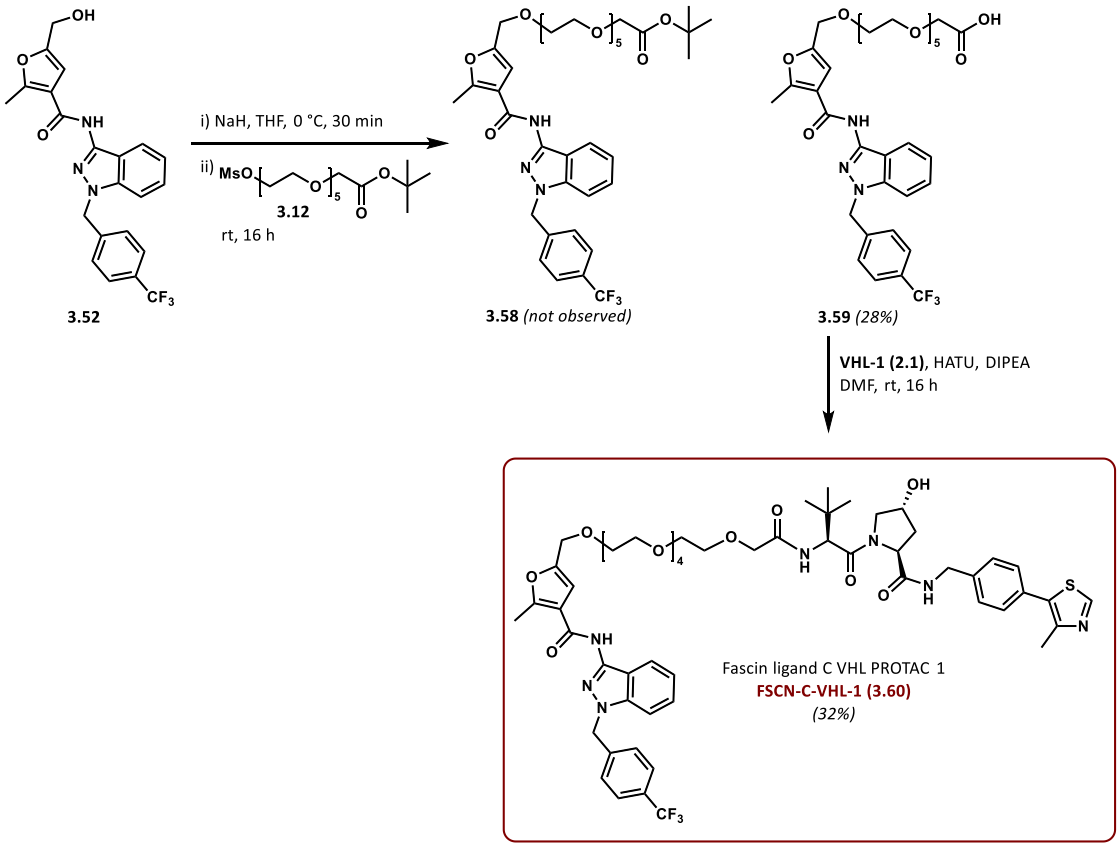

*Scheme 3.18: Synthesis of fascin ligand C VHL PROTAC **FSCN-C-VHL-1 (3.60)**.*

Attachment of an aminoalcohol linker through the bromoindazole functionality of fascin ligand C analogue **3.53** was first attempted with Ullmann-type coupling conditions reported for aryl halide compounds using catalytic amounts of copper(I) iodide and diethylene glycol as ligand,[196,197] however, formation of product **3.61a** was not observed (entry 1 in Table 3.5). Palladium-catalysed carbon–nitrogen cross-coupling reactions have been extensively studied for a variety of different substrates, and the BrettPhos Pd G3 precatalyst has been reported to show improved yields for cross-coupling reactions between aryl halides and amine substrates featuring alcohol functionalities.[198,199] Following a modified literature procedure,[200] bromide **3.53** and the aminoalcohol linker were subjected to palladium-catalysed cross-coupling conditions using lithium bis(trimethylsilyl)amide (LiHMDS) as base, however, only decomposition of the starting materials was observed (entry 2 in Table 3.5). Literature suggested that optimisation of the cross-coupling conditions might be necessary, depending on the nature of the substrate.[198,201] Hence, the use of sodium *tert*-

butoxide as base was attempted instead, which yielded cross-coupled product **3.61b** in 11% (entry 3 in Table 3.5). Intending to improve the yield further, a solvent screen (entries 4, 5 and 6 in Table 3.5) was carried out, hoping to increase solubilisation of the *tert*-butoxide base. As expected, more polar solvents, DMA and *tert*-butanol (entries 5 and 6 in Table 3.5) resulted in slightly improved yields of the product. Next, attention was turned to the base used in the cross-coupling reaction. According to optimisation of the reaction conditions for highly-functionalised substrates, a milder inorganic base, such as caesium carbonate, could be beneficial.[200] An additional solvent screen using caesium carbonate as base was carried out (entries 7, 8 and 9 in Table 3.5), and expectedly, more polar solvents, such as DMA and *tert*-butanol (entries 8 and 9 in Table 3.5), again performed better – most likely due to higher solubility of the base in those solvents. Despite a further slight improvement, the yields remained far from optimal.

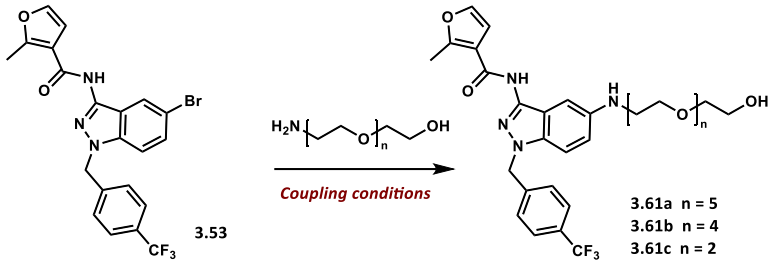

	Catalyst / Ligand	Base	Solvent / Temperature	Product *(yield)*	Ref
1	**CuI** (5 mol%) **Diethylene glycol** (2 equiv)	K_3PO_4 (2 equiv)	*i*-PrOH [0.5 M] 80 °C	**3.61a** *(not observed)*	196,197
2	**BrettPhos Pd G3** (5 mol%) **BrettPhos** (5 mol%)	**LiHMDS** (3.4 equiv)	Dioxane [0.3 M] 100 °C	**3.61a** *(not observed)*	200
3	BrettPhos Pd G3 (5 mol%) BrettPhos (5 mol%)	**NaO*t*-Bu** (2.4 equiv)	Dioxane [0.2 M] 100 °C	**3.61b** *(11%)*	198
4	BrettPhos Pd G3 (5 mol%) BrettPhos (5 mol%)	NaO*t*-Bu (2.4 equiv)	**Toluene** [0.2 M] 110 °C	**3.61b** *(4%)*	198
5	BrettPhos Pd G3 (5 mol%) BrettPhos (5 mol%)	NaO*t*-Bu (2.4 equiv)	**DMA** [0.2 M] 110 °C	**3.61c** *(9%)*	201
6	BrettPhos Pd G3 (5 mol%) BrettPhos (5 mol%)	NaO*t*-Bu (2.4 equiv)	***t*-BuOH** [0.2 M] 110 °C	**3.61c** *(18%)*	201
7	BrettPhos Pd G3 (5 mol%) BrettPhos (5 mol%)	**Cs_2CO_3** (2.4 equiv)	Toluene [0.2 M] 110 °C	**3.61c** *(traces)*	200
8	BrettPhos Pd G3 (5 mol%) BrettPhos (5 mol%)	Cs_2CO_3 (2.4 equiv)	**DMA** [0.2 M] 110 °C	**3.61c** *(13%)*	200
9	BrettPhos Pd G3 (5 mol%) BrettPhos (5 mol%)	Cs_2CO_3 (2.4 equiv)	***t*-BuOH** [0.2 M] 110 °C	**3.61c** *(21%)*	200

Table 3.5: Optimisation of carbon–nitrogen cross-coupling.

A sufficient quantity of fascin ligand C–linker fragment **3.61c** was obtained to proceed with the synthesis. Initially, a two-step oxidation protocol was planned to convert the alcohol of **3.61c** to the corresponding carboxylic acid. The carboxylic acid could then be used for amide coupling with the amine moiety of VHL ligand **VHL-1 (2.1)** to obtain proposed VHL PROTAC **3.63** (Scheme 3.19). However, subjecting alcohol **3.61c** to Parikh–Doering oxidation conditions failed to yield the expected aldehyde **3.62** and decomposition of the starting material was observed. Oxidation attempts using Dess–Martin periodinane (DMP) were also unfruitful, with almost complete recovery of starting material **3.61c**.

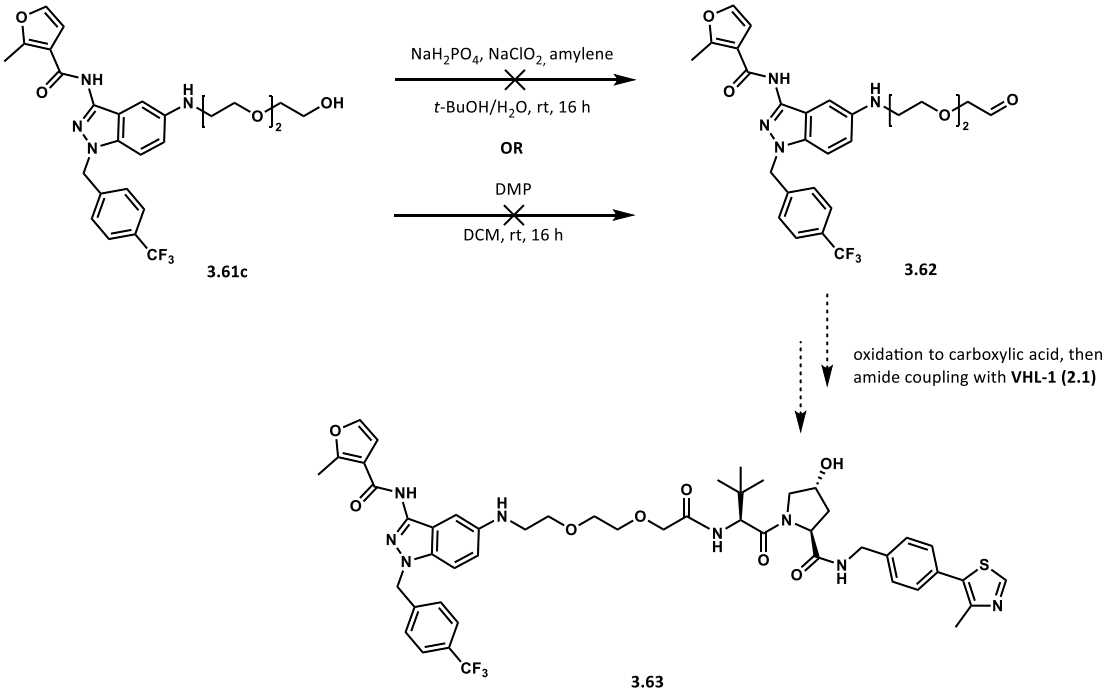

*Scheme 3.19: Attempted oxidation of alcohol **3.61c** to obtain aldehyde **3.62** and proposed route to VHL PROTAC **3.63**.*

Failing to oxidise alcohol **3.61c** to aldehyde **3.62**, an alternative route was sought: Activation of the alcohol **3.61c** could generate mesylate **3.64** which could then be used for ether formation with the phenol moiety of VHL ligand **VHL-2 (2.3)** to afford proposed VHL PROTAC **3.65** (Scheme 3.20). Attempts to activate alcohol **3.61c**, however, failed to produce mesylate **3.64**, resulting in decomposition of the starting material instead. Ultimately, it was not possible to obtain proposed VHL PROTAC **3.65** due the challenges of the carbon–nitrogen cross-coupling reaction and the difficulties in subsequent alcohol functionalisation.

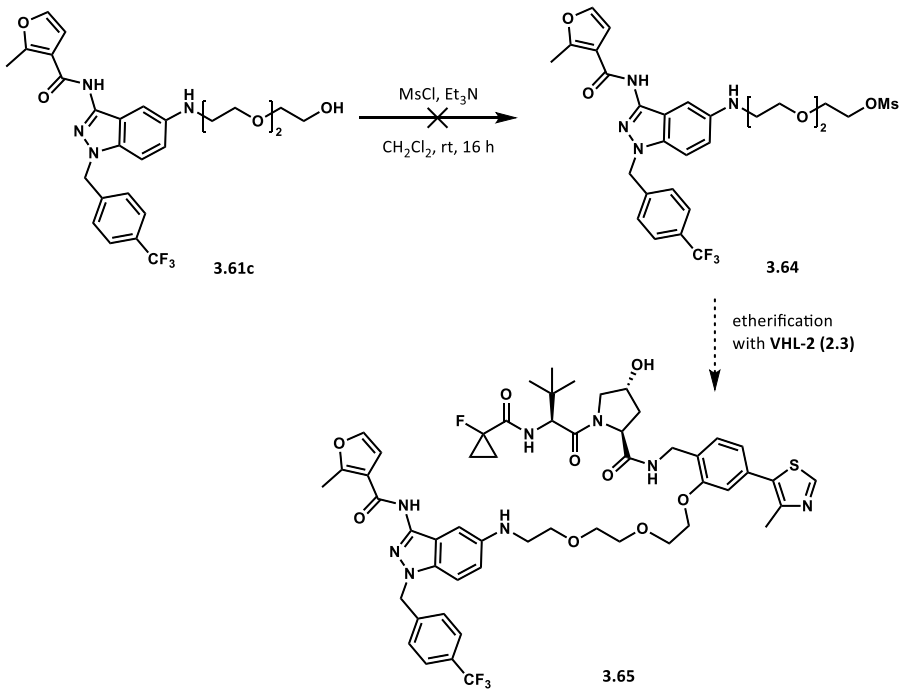

*Scheme 3.20: Attempted activation of alcohol **3.61c** to obtain mesylate **3.64** and proposed route to VHL PROTAC **3.65**.*

3.4.4 Physicochemical properties of 3rd series PROTAC

Calculated physicochemical properties

Physicochemical properties of the 3rd series PROTAC **FSCN-C-VHL-1 (3.60)** were comparable to the 2nd series long linker VHL PROTAC **FSCN-B-VHL-2 (3.36)** owing to a similar linker length (Table 3.6). Due to increased lipophilicity of the parent compound **FSCN-C (1.7)**, the corresponding PROTAC also displayed a higher cLogP value compared to the 2nd series PROTACs. Overall, although properties were suboptimal, they were still close to the values reported for active PROTACs.

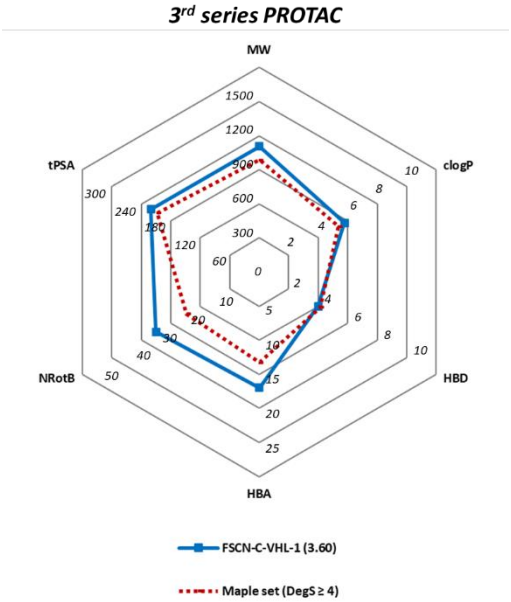

	MW (Da)	cLogP	HBD	HBA	NRotB	tPSA (Å²)
FSCN-C (1.7)	399	4.44	1	7	6	54
3rd series PROTAC						
FSCN-C-VHL-1 (3.60)	1106	5.79	4	17	35	220
Good (green): MW < 900, cLogP < 4, HBD < 4, HBA < 10, NRotB < 20, tPSA < 200 Bad (red): MW > 1100, cLogP > 6, HBD > 6, HBA > 15, NRotB > 28, tPSA > 250						

Table 3.6: Physicochemical properties of 3rd series PROTAC.

3.5 Biological testing of fascin-targeting PROTACs

3.5.1 Chemical structures of tested PROTACs

In total, 14 fascin-targeting PROTACs based on three fascin ligands were synthesised and subjected to biological assays to assess their activity *in vitro*. The chemical structures of PROTACs from all three series are summarised here: 1st series PROTACs based on **FSCN-A (1.4)** (Figure 3.11), 2nd series PROTACs based on **FSCN-B (1.5)** (Figure 3.12) and 3rd series PROTAC based on **FSCN-C (1.7)** (Figure 3.13).

1st series amide PROTACs

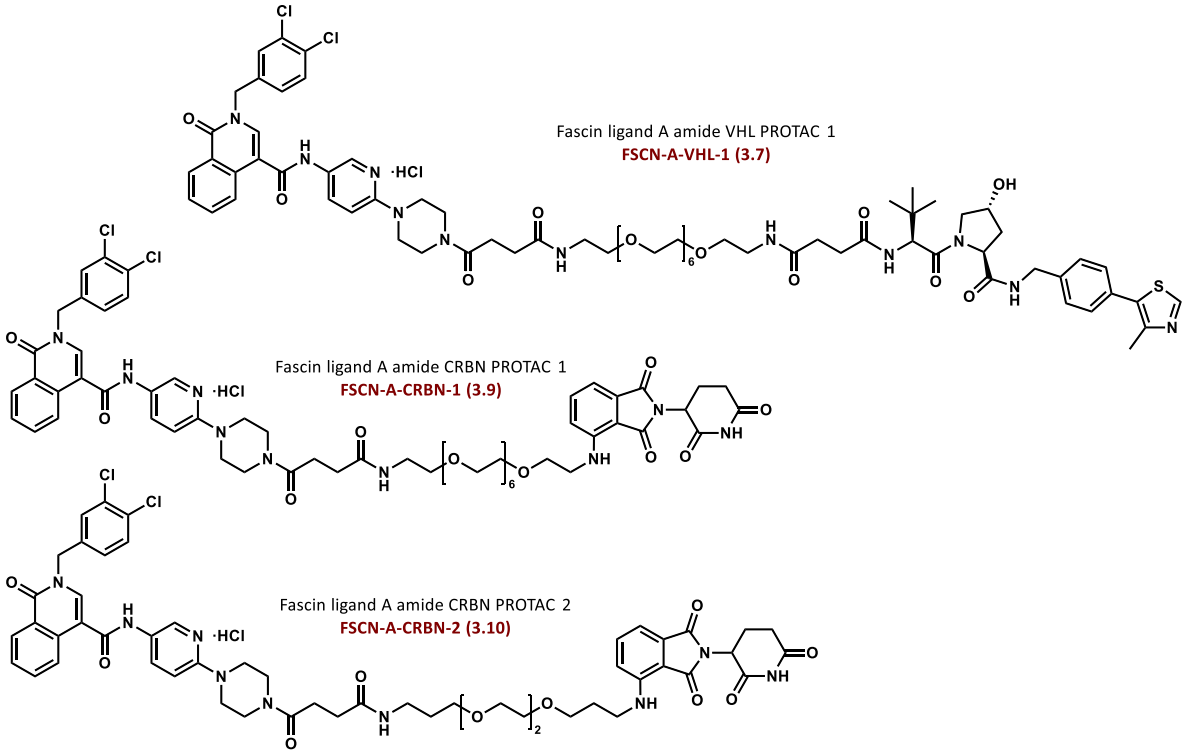

1st series alkylation PROTACs

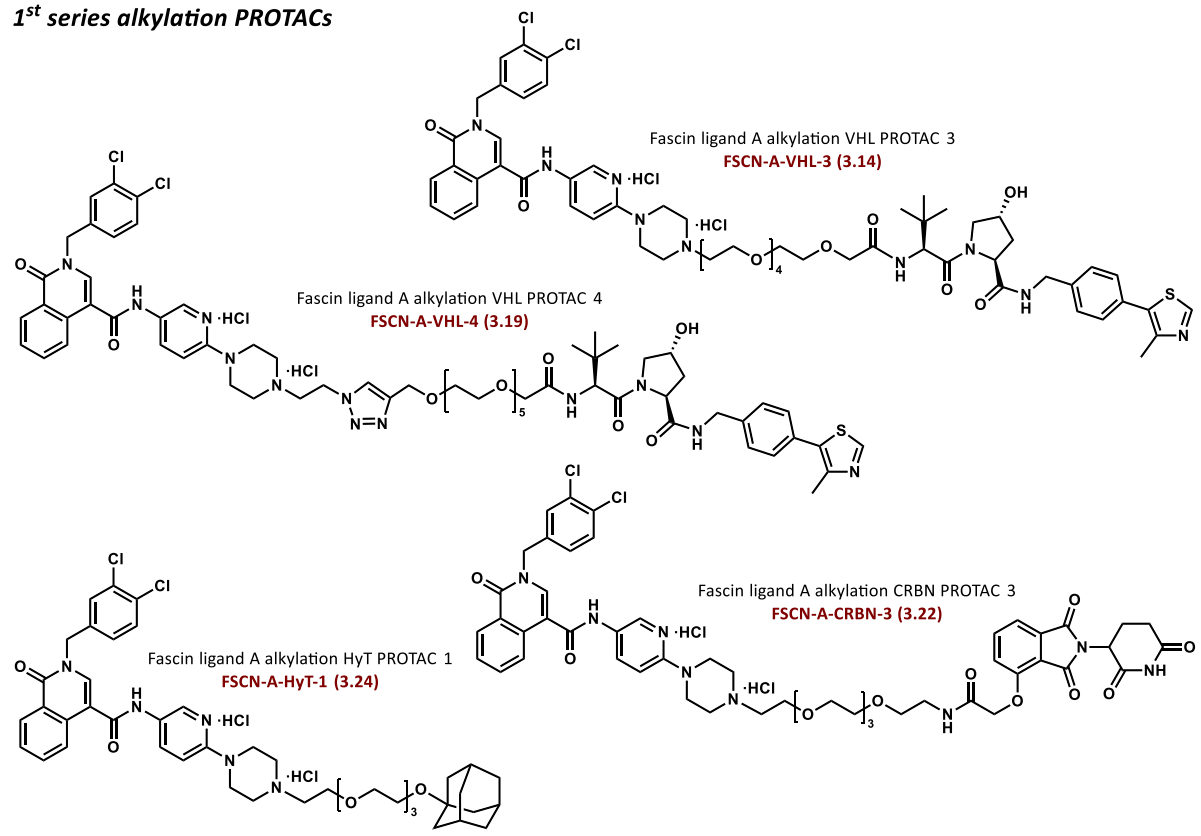

*Figure 3.11: 1st series PROTACs based on **FSCN-A (1.4)**.*

2nd series PROTACs

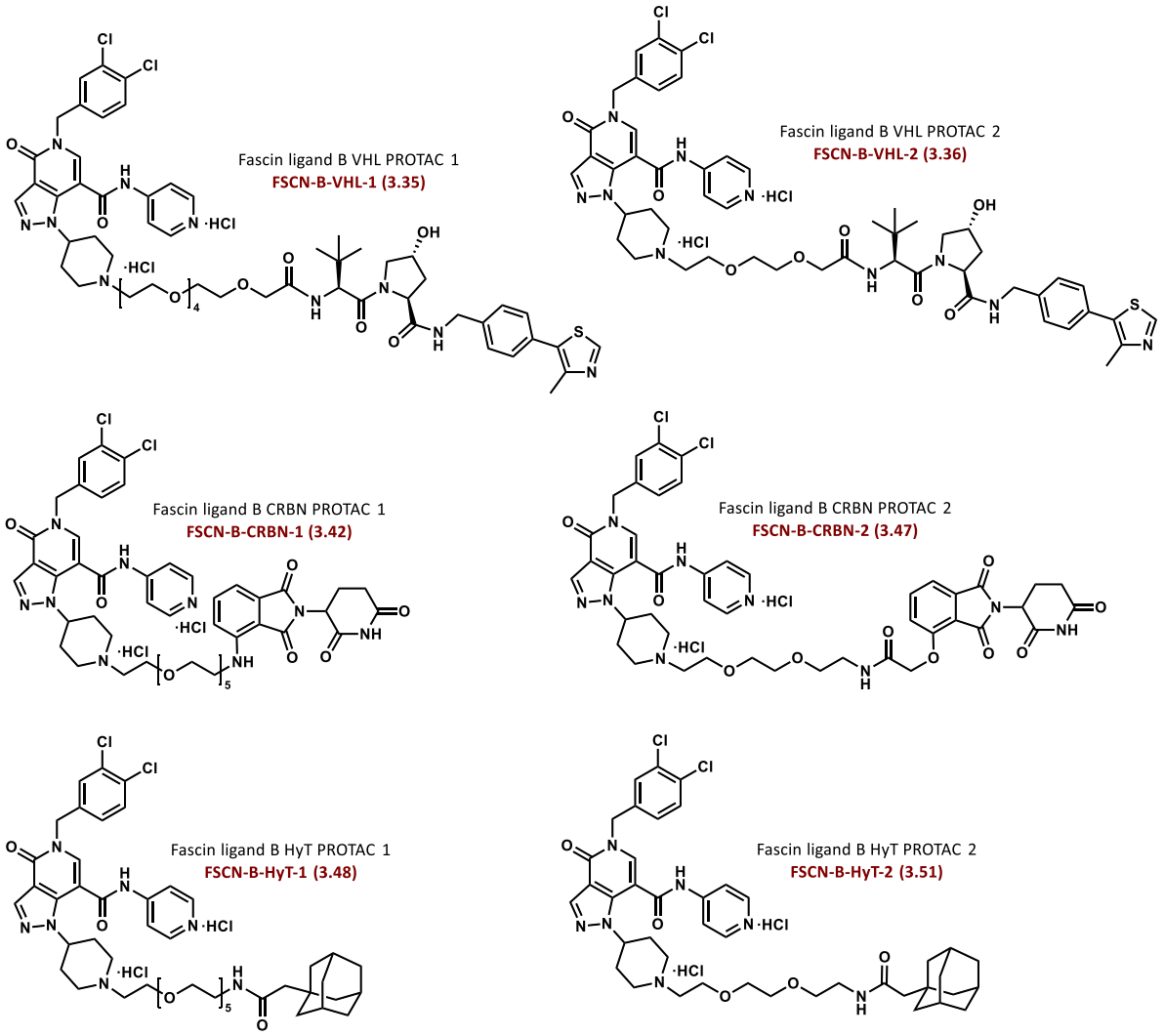

*Figure 3.12: 2nd series PROTACs based on **FSCN-B (1.5)**.*

3rd series PROTAC

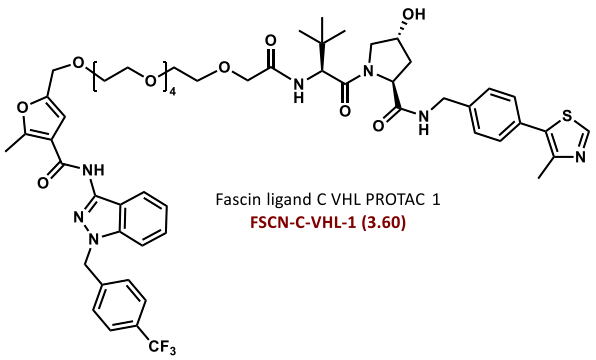

*Figure 3.13: 3rd series PROTAC based on **FSCN-C (1.7)**.*

3.5.2 Determination of fascin's half-life

Since the turnover of the target protein through endogenous cellular mechanisms influences PROTAC efficacy, estimating a protein's half-life can be beneficial.[202] Protein half-lives can be approximated by inhibiting protein synthesis and comparing protein levels against control cells.[203] Inhibition of protein synthesis can be achieved by treating cells with cycloheximide, a bacterial fungicide, which interferes with the translocation step, *i.e.* the movement of tRNA and mRNA in relation to the ribosome, and essentially stalls elongation of the polypeptide produced by the ribosome (Figure 3.14).[204] However, it has to be noted that cycloheximide-mediated inhibition of protein synthesis also impacts on components involved in the natural degradation of the POI, as well as on synthesis and degradation of the loading control protein used to normalise protein levels, hence data obtained through this method should be treated as a rough approximation of the protein half-life observed under normal growth conditions.[205]

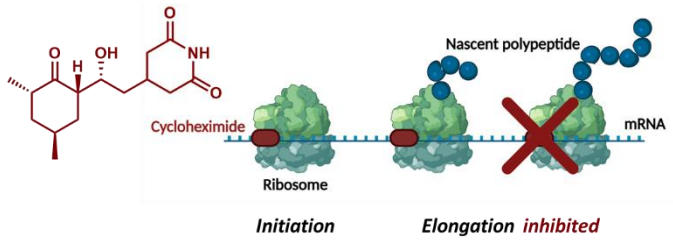

Figure 3.14: Cycloheximide structure and mode of action - adapted from [206].

To obtain an approximation of fascin's half-life, SK-OV-3 and HT-1080 cells were treated with cycloheximide at concentrations ranging from 10 µg/mL to 1 mg/mL for 24 hours to determine the optimal concentration for inhibition of protein synthesis whilst not impairing cell viability (Figure 3.15 a). Whereas decrease in fascin levels was only observed at higher concentration of cycloheximide (500 µg/mL and 1 mg/mL) in SK-OV-3 cells, a decrease was noticeable for concentrations of 50 µg/mL and above in HT-1080 cells. Concentrations higher than 1 mg/mL were not tolerated by either cell line, hence it was decided to carry out a time-course assay with 1 mg/mL of cycloheximide to estimate fascin's half-life in both cell lines (Figure 3.15 b). For SK-OV-3 cells, a reduction in fascin levels was observed to occur between 6 to 8 hours, though for HT-1080 cells a decrease in protein levels was observed to commence later, after between 8 and 24 hours. For both cell lines, around 50% protein levels were reached after 24 hours, indicating that the protein turnover would be adequate for targeted protein degradation.

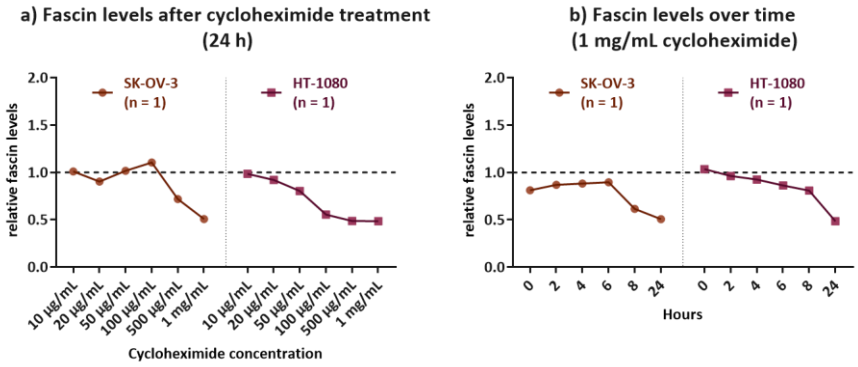

Figure 3.15: Quantification of western blot analysis - protein synthesis inhibition with cycloheximide to estimate fascin's half-life: fascin protein levels a) 24 hours after treatment with different cycloheximide concentrations and b) over time after treatment with 1 mg/mL of cycloheximide.

3.5.3 Cell viability assay

In studies carried out by the Drug Discovery Unit at the Beatson Institute for Cancer Research, fascin ligand A **FSCN-A (1.4)** displayed cytotoxicity at concentrations above 1 µM. In order to determine if PROTACs based on this ligand would exhibit comparable cytotoxicity, a preliminary viability experiment with the 1st series alkylation PROTACs was carried out prior to subjecting them to dose-response assays. For this experiment, SK-OV-3 cells were incubated at a range of concentrations from 1 nM to 10 µM with the parent compound **FSCN-A (1.4)**, fascin ligand A control **FSCN-A-ctrl (3.6)** and PROTACs **FSCN-A-VHL-1 (3.7)**, **FSCN-A-CRBN-1 (3.9)** and **FSCN-A-CRBN-2 (3.10)**. Cell confluence was monitored hourly over 72 hours using an automated microscope (Figure 3.16). As expected, cell confluence increased over time for cells treated with DMSO (Figure 3.16 a). For cells incubated with the parent compound **FSCN-A (1.4)** (Figure 3.16 b) reduced proliferation could be observed at 3 µM and virtually no cell growth at the highest concentration of 10 µM, confirming previously observed cytotoxicity at higher concentrations. The highest concentration of fascin ligand A control **FSCN-A-ctrl (3.6)** also resulted in reduced cell growth (Figure 3.16 c). However, for cells treated with PROTACs **FSCN-A-VHL-1 (3.7)**, **FSCN-A-CRBN-1 (3.9)**, **FSCN-A-CRBN-2 (3.10)** (Figure 3.16 d, e and f), no impairment of cell growth could be observed, indicating that the compounds would likely not display cytotoxicity at concentrations up to 10 µM. Based on those preliminary viability results, it was decided to carry out dose-response assays up to compound concentrations of 10 µM.

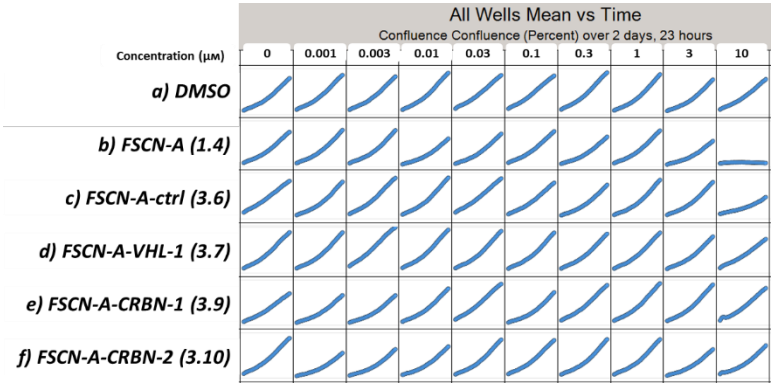

Figure 3.16: Confluence over time of SK-OV-3 cells treated with a) DMSO, b) parent compound ***FSCN-A (1.4)****, c) fascin ligand A control* ***FSCN-A-ctrl (3.6)*** *and PROTACs d)* ***FSCN-A-VHL-1 (3.7)****, e)* ***FSCN-A-CRBN-1 (3.9)*** *and f)* ***FSCN-A-CRBN-2 (3.10)*** *at different concentrations over 72 hours.*

3.5.4 Fascin degradation assays with fascin-targeting PROTACs

Analogous to dose-response degradation assays carried out with HaloPROTACs (Chapter 2.3.3), cells were incubated with fascin-targeting PROTACs (Chapter 3.5.1) at concentrations ranging from 0.01 µM to 10 µM for 24 hours, before fascin levels were analysed using western blotting. Most assays were carried out with SK-OV-3 and HT-1080 cells based on their tolerability of treatment and the robust results obtained with the HaloTag model system.

1st series PROTACs

No decrease in fascin levels was observed after treatment with 1st series amide PROTACs in SK-OV-3 cells (Figure 3.17 a) and with 1st series alkylation PROTACs in SK-OV-3 and HT-1080 cells (Figure 3.17 b and c). Despite the initial viability assay suggesting higher concentrations of the 1st series amide PROTACs were tolerated well, precipitation of the compounds at concentrations higher than 1 µM and some cell death were observed, indicating poor solubility of this set of compounds. Precipitation at higher concentrations was not observed for the 1st series alkylation PROTACs, confirming that attachment of the linker *via* alkylation rather than amide bond formation did indeed impact positively on compound properties, such as solubility.

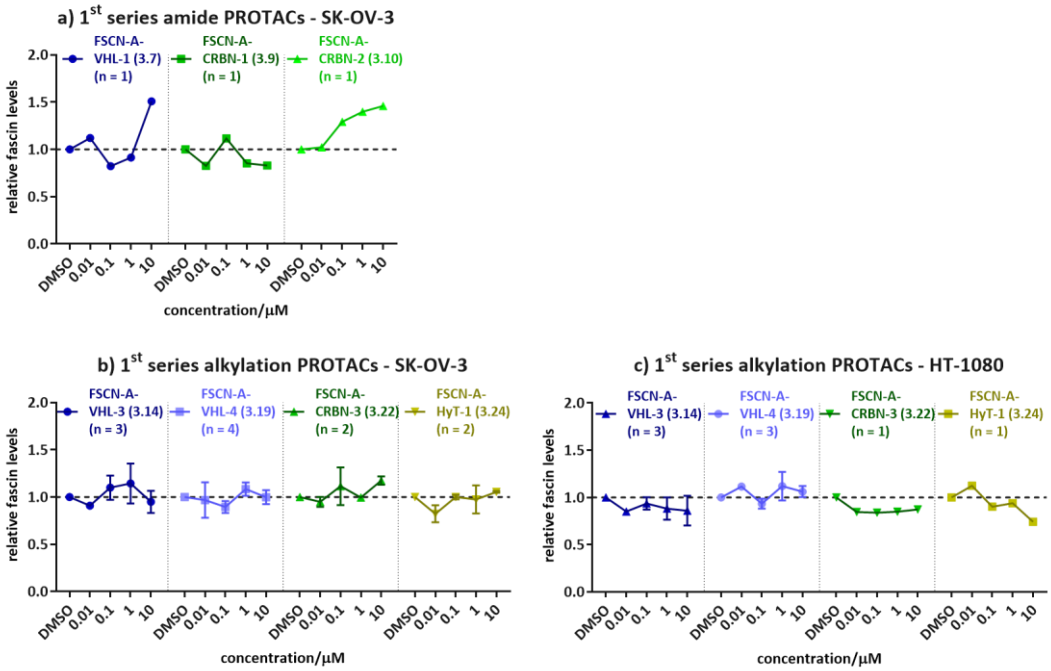

Figure 3.17: Quantification of western blot analysis - fascin levels 24 hours after treatment with increasing concentrations of fascin ligand A-based PROTACs: a) 1st series amide PROTACs in SK-OV-3 cells and b) 1st series alkylation PROTACs in SK-OV-3 cells and c) 1st series alkylation PROTACs in HT-1080 cells. Error bars represent SEM.

2nd series PROTACs

Similarly, no significant decrease in fascin levels was observed after treatment with the 2nd series PROTACs, which were based on fascin ligand B **FSCN-B (1.5)**, at any concentration of the longer linker analogues (Figure 3.18 a and b) and the shorter linker analogues (Figure 3.18 c and d). The slight decrease in protein levels observed for **FSCN-B-CRBN-1 (3.42)** in SK-OV-3 cells (Figure 3.18 a) and for **FSCN-B-CRBN-2 (3.47)** in HT-1080 cells (Figure 3.18 d) was determined not to be statistically significant.

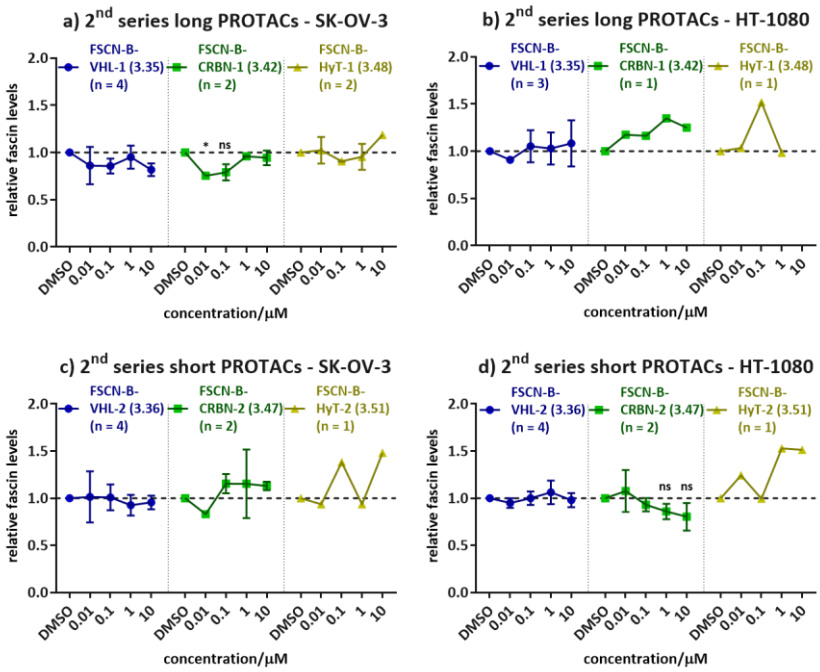

Figure 3.18: Quantification of western blot analysis - fascin levels 24 hours after treatment with increasing concentrations of fascin ligand B-based PROTACs: a) 2nd series long linker PROTACs in SK-OV-3 cells, b) 2nd series long linker PROTACs in HT-1080 cells, c) 2nd series short linker PROTACs in SK-OV-3 and d) 2nd series short linker PROTACs in HT-1080 cells.
*Error bars represent SEM, unpaired t-test was applied (ns: $p > 0.05$, *: $p \leq 0.05$, **: $p \leq 0.01$, ***: $p \leq 0.001$)*

3rd series PROTAC

The 3rd series VHL PROTAC **FSCN-C-VHL-1 (3.60)** was also tested in SK-OV-3 and HT-1080 cells. Again, no decrease in fascin levels could be observed in either cell line (Figure 3.19). Seemingly, HT-1080 cells tolerated treatment less well compared to SK-OV-3 cells.

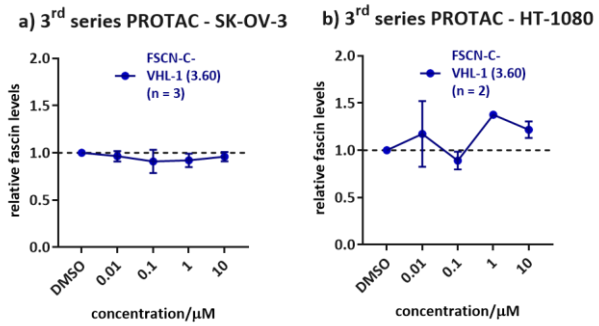

Figure 3.19: Quantification of western blot analysis - fascin levels 24 hours after treatment with increasing concentrations of fascin ligand C-based PROTAC: a) in SK-OV-3 cells and b) in HT-1080 cells.
Error bars represent SEM.

3.5.5 Intracellular VHL engagement assay

It was hypothesised that cell permeability of the compounds due to their suboptimal physicochemical properties (Chapter 3.2.4, Chapter 3.3.4 and Chapter 3.4.4) could be a potential limiting factor to their actvitiy. Especially the high molecular weight and tPSA

could impact negatively on the ability of the compounds to cross the cell membrane.[158] Different assays can be carried out to determine if compounds are able to cross cell membranes,[207-209] measure intracellular concentrations of compounds after treatment,[210] or confirm target engagement inside the cell.[160,211]

In order to devise a rapid assay without the need for lengthy optimisation, the competition assay with active VHL HaloPROTAC **VHL-HP-1 (2.18)** and inactive CRBN and HyT HaloPROTACs for the HaloTag model system (Chapter 2.3.3) was adapted to assess intracellular engagement of VHL by the VHL-recruiting PROTACs. Cells were transfected with the HaloTag–fascin fusion protein and treated with 1 µM of VHL HaloPROTAC **VHL-HP-1 (2.18)** which was shown to degrade the fusion protein. If addition of increasing concentrations of the VHL-recruiting PROTACs that were designed to degrade endogenous fascin would rescue fusion protein levels, this could offer an indication for cellular permeability of the endogenous fascin-targeting degraders and intracellular engagement of the E3 ligase. Treatment with active **VHL-HP-1 (2.18)** expectedly decreased protein levels by 70% to 80% (Figure 3.20); however, titration of VHL-recruiting fascin PROTACs up to 10 µM did not result in any rescue of HaloTag–fascin levels in SK-OV-3 or HT-1080 cells. At PROTAC concentrations higher than 10 µM some indication of HaloTag–fascin levels was observed, for example for **FSCN-A-VHL-3 (3.14)** and **FSCN-B-VHL-2 (3.36)** (Figure 3.20 b) in SK-OV-3 (Figure 3.20 a) and HT-1080 cells (Figure 3.20 b), however, precipitation of the compounds and cell death were apparent at such high concentrations. On the other hand, even low concentrations of 3rd series VHL PROTAC **FSCN-C-VHL-1 (3.60)** rescued HaloTag–fascin levels (Figure 3.20 a). At 1 µM and 10 µM, full rescue of protein levels was observed, indicating excellent cellular permeability of **FSCN-C-VHL-1 (3.60)**.

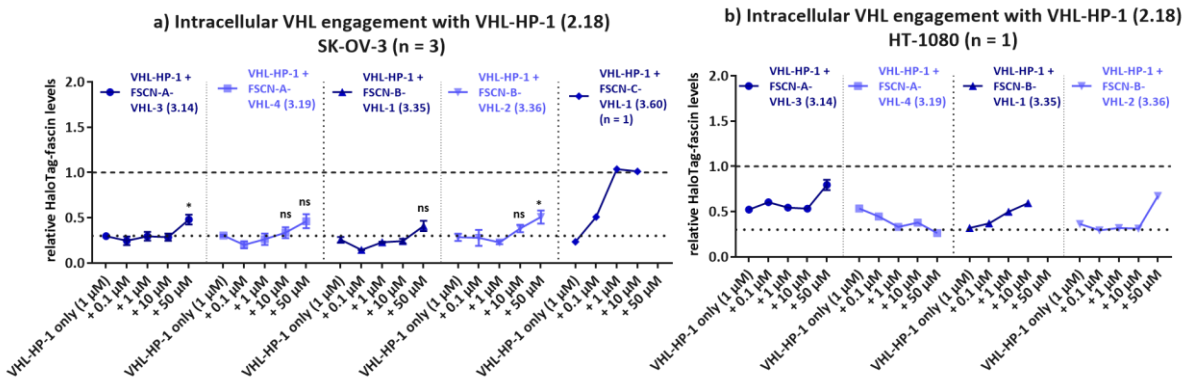

*Figure 3.20: Quantification of western blot analysis – HaloTag–fascin levels for intracellular VHL engagement assay by co-treatment of 1 µM **VHL-HP-1 (2.18)** and increasing concentrations of VHL PROTACs in a) SK-OV-3 and b) HT-1080 cells.*
*Error bars represent SEM, unpaired t-test was applied (ns: $p > 0.05$, *: $p \leq 0.05$, **: $p \leq 0.01$, ***: $p \leq 0.001$)*

The obtained results further confirmed inadequate cell permeability of both the 1st and the 2nd series fascin-targeting PROTACs to represented a major hurdle in assessing their intracellular activity, hence strategies for delivery of compounds into the cells were sought.

3.5.6 Permeabilisation assays

Different methods of delivering non-permeable extracellular agents across cell membranes are known, most of which rely on transiently destabilising the membrane or creating pores in the membrane temporarily, either by physical or by chemical means.[212-214] However, all those methods bear the risk of destabilising the cell membrane to an extent at which membrane resealing cannot be achieved, leading to cell lysis and cell death. Transient permeabilisation of the cell membrane using electroporation and different chemical agents for delivery of the compounds were attempted.

Electroporation

Electroporation, or electropermeabilisation, is a technique for which cells are exposed to short electric pulses in order to transiently destabilise the cell membrane. The temporarily created pores in the lipid bilayer allow otherwise non-permeable agents to enter the cell interior before resealing after several minutes (Figure 3.21).[215] Electroporation is employed for a variety of purposes, such as internalisation of DNA and dyes as well as drug delivery.[216] As electrochemotherapy, it has also found application in the treatment of mostly cutaneous and subcutaneous cancers by delivering otherwise poorly permeable drugs such as bleomycin or cisplatin.[217,218] It was shown to be successful in introducing plasmid DNA for expression of the HaloTag–fascin fusion protein, hence it was hypothesised that it could also be employed to deliver PROTACs into cells.

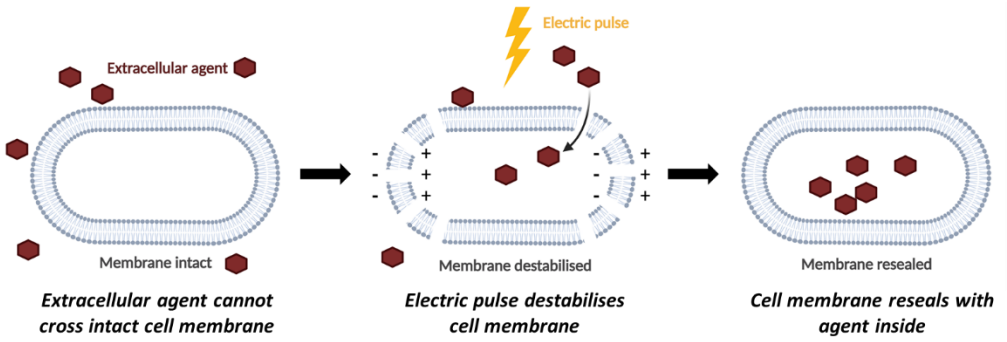

Figure 3.21: Delivery of extracellular agent by cell membrane permeabilisation through application of an electric pulse.

For permeabilisation assays SK-OV-3 cells were electroporated with the 1st series PROTACs at the same concentrations as previously employed in dose-response experiments, and incubated for 24 hours before protein levels were analysed using western blotting. Similar to transient transfection with the HaloTag–fascin plasmid using this technique, some cell death was observed, however, sufficient cells survived for quantification of protein levels. No significant decrease in fascin levels could be detected after electroporation and incubation with any of the compounds (Figure 3.22). Treatment with 10 μM of the VHL-targeting PROTACs **FSCN-A-VHL-1 (3.7)** (Figure 3.22 a), **FSCN-A-VHL-3 (3.14)** and **FSCN-A-VHL-4 (3.19)** (Figure 3.22 b) was tolerated less well compared to electroporation with the remaining PROTACs and treatment with the same PROTACs without electroporation. This could offer some indication for VHL-targeting PROTACs exhibiting intracellular toxicity similar to parent compound **FSCN-A (1.4)**, however, further investigation would be required to confirm this hypothesis.

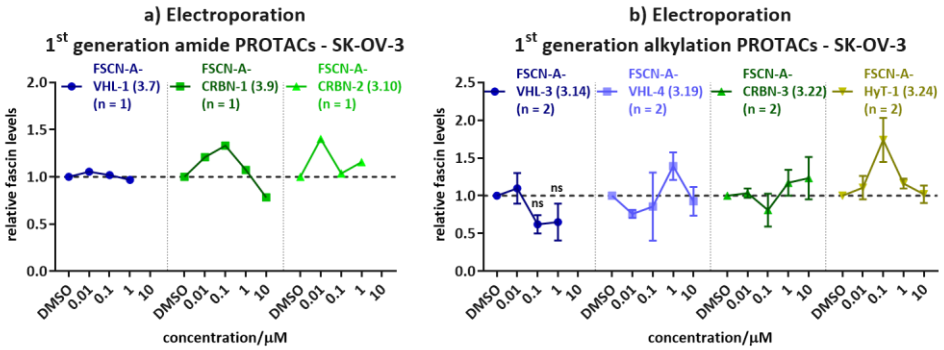

*Figure 3.22: Quantification of western blot analysis – fascin levels 24 hours after electroporation and treatment with increasing concentrations of a) 1st series amide PROTACs and b) 1st series alkylation PROTACs in SK-OV-3 cells. Error bars represent SEM, unpaired t-test was applied (ns: $p > 0.05$, *: $p \leq 0.05$, **: $p \leq 0.01$, ***: $p \leq 0.001$)*

Overall, the results obtained for this assay were inconsistent due to electroporation generally not being tolerated well by the cells hence it was decided to abandon this strategy and shift attention to chemical permeabilisation agents.

Chemical permeabilisation agents

Different chemical agents can be used for a variety of applications to permeabilise cells, such as cellular reprogramming,[219] study of intracellular processes,[212] extraction of membrane components[220] or transport of otherwise cell-impermeable exogeneous factors across the cell membrane.[221] Most chemical agents act by solubilising membrane lipids, usually cholesterol, or by forming pores in the cell membrane. Repair of the membrane is initiated by addition of calcium ions present in cell culture medium and resealing is usually

achieved within minutes to hours.[222] Whereas electroporation produces relatively small pores (~ 2 nm), treatment with chemical permeabilisation agents have been shown to result in larger pores (~ 8 to 15 nm) suitable for transport of larger molecules across the membrane.[212] Three permeabilisers - digitonin, glycodiosgenin (GDN) and streptolysin O (SLO) - were tried for cell permeabilisation.

Digitonin (Figure 3.23 a), a non-ionic detergent, is a steroidal saponin derived from the foxglove plant. It solubilises cholesterol present in the cholesterol-rich cell membrane, however, does not affect the cell's cytoskeleton and the cholesterol-poor nuclear envelope, hence does not impact on cell integrity.[223] Similarly, GDN (Figure 3.23 b), a phytosteroidal sapogenin, is also employed as non-ionic detergent, and was developed for optimised extraction of membrane proteins for further analysis.[224] As detergents, both, digitonin and GDN, are amphiphilic compounds, featuring hydrophilic carbohydrate units and a hydrophobic steroid portion. Streptolysin O (Figure 3.23 c), on the other hand, is a pore-forming bacterial toxin belonging to a family of cholesterol-dependent cytolysins (CDCs). CDCs are secreted proteins which bind to cholesterol in eukaryotic cells and oligomerise forming large transmembrane pores.[225]

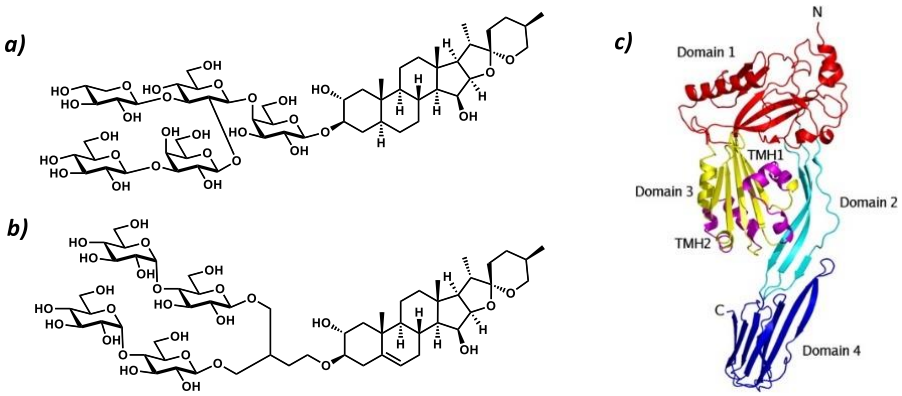

Figure 3.23: Chemical permeabilising agents: a) digitonin, b) GDN and c) streptolysin O.[225]

As for electroporation, a risk of cell lysis is associated with use of high concentrations of chemical permeabilising agents, however, an insufficient concentration would not induce membrane permeabilisation. Since optimal permeabiliser concentrations are dependent on the membrane compositions of the cell lines used, preliminary experiments determining optimal permeabilisation conditions were carried out.[226] To do so, cells were incubated at a range of permeabiliser concentrations for different times before membrane resealing was initiated by addition of cell culture medium along with a cell-impermeable fluorescent dye. Then, fluorescence of the cells was monitored over 24 hours, and any increase of fluorescence beyond fluorescence levels for non-permeabilised control cells would indicate

uptake of the dye through permeabilisation of the cell membrane. However, since the employed dye localises to the nucleus of the cells, any cells with compromised cell membrane, hence also dead cells, would also be stained. Therefore, confluence, a measure of cell growth, was analysed as indicator for survival of the cells after treatment.

Based on permeabilisation procedures reported in literature,[212,219,226] assays with digitonin were carried out at concentrations of 5 µg/mL, 7.5 µg/mL and 10 µg/mL with incubation times of 2, 5 or 10 minutes on ice. Fluorescence of cells treated with digitonin was increased when compared to non-permeabilised control cells treated with the dye only (Figure 3.24 a), indicating membrane permeabilisation was induced for all tested conditions. Expectedly, cell fluorescence also increased with higher digitonin concentration and longer incubation time. However, cell growth of cells treated with higher concentrations was observed to be slowed, especially when incubated for a longer period (Figure 3.24 b), indicating cell growth was impaired for those conditions. Reviewing fluorescence microscope images of the cells, it was noticeable that for 5 µg/mL digitonin concentration with a 5-minute incubation period, cells were partially permeabilised, however, appeared viable (Figure 3.24 c). When increasing the incubation period to 10 minutes, virtually all cells internalised the dye, though some cell death was also observable (Figure 3.24 d).

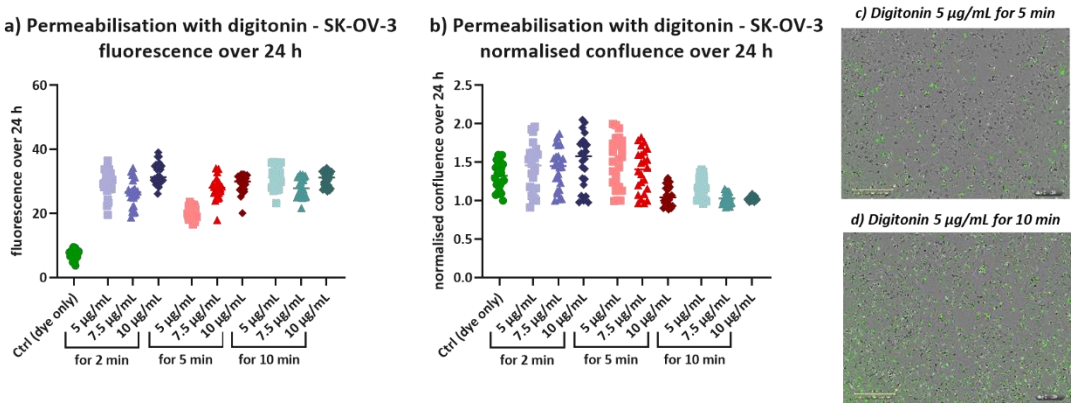

Figure 3.24: Permeabilisation of SK-OV-3 cells with different digitonin concentrations and incubation times: a) fluorescence of cells over 24 hours and b) normalised confluence over 24 hours (1 data point per hour); fluorescence microscope images of cells after treatment with 5 µg/mL of digitonin for c) 5 minutes and d) 10 minutes on ice.

Since both, digitonin and GDN, are non-ionic detergents, the same protocol was employed for permeabilisation assays with GDN. Cells were incubated with 5 µg/mL, 7.5 µg/mL or 10 µg/mL GDN concentration for 2, 5 or 10 minutes on ice, and fluorescence and confluence were then monitored. Although all conditions led to increased fluorescence compared to the untreated control (Figure 3.25 a), this increase was not as pronounced as for

permeabilisation with digitonin, indicating that a lower percentage of the cells were permeabilised. Fluorescence of cells treated at higher concentrations was greater, however, increase in incubation time did not exert any impact on fluorescence. GDN treatment did not impact on cell viability at any of the concentrations and incubation times tested (Figure 3.25 b). Fluorescence microscope images of cells treated with 10 µg/mL of GDN for 5 minutes (Figure 3.25 c) and for 10 minutes (Figure 3.25 d) revealed that only a small number of cells fluoresced, confirming insufficient cell permeabilisation.

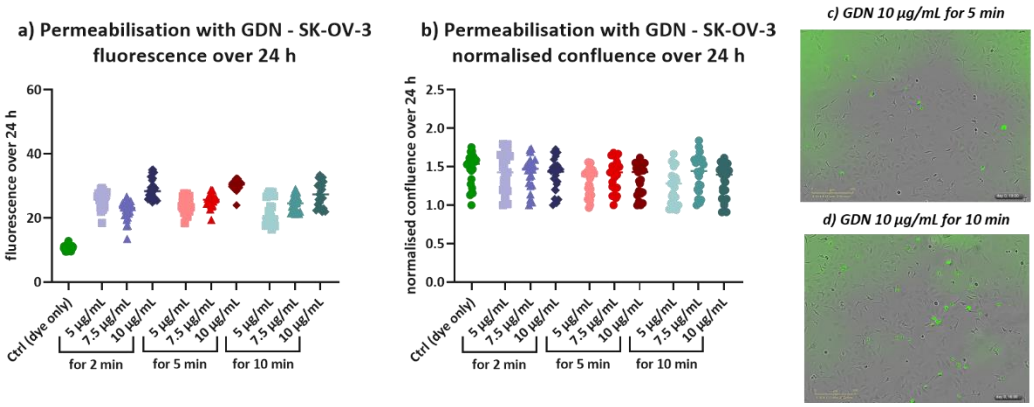

Figure 3.25: Permeabilisation of SK-OV-3 cells with different GDN concentrations and incubation times: a) fluorescence of cells over 24 hours and b) normalised confluence over 24 hours (1 data point per hour); fluorescence microscope images of cells after treatment with 10 µg/mL of GDN for c) 5 minutes and d) 10 minutes on ice.

Assays with streptolysin O (SLO) were carried out at concentrations of 20 ng/mL, 100 ng/mL and 200 ng/mL with incubation times of 5, 10 or 15 minutes at 37 °C, based on procedures reported in literature.[221,225] Whereas no impact on cell growth was detected for any of the tested conditions (Figure 3.26 b), the fluorescence measure did not provide any clear correlation with the tested conditions. Ideally, an increase in fluorescence after treatment would be observed, indicating permeabilisation and uptake of the dye, with fluorescence remaining relatively stable over time. However, a high variability in fluorescence over time was observed and no clear correlation between SLO concentration and incubation times could be established (Figure 3.26 a). Comparing images of cells treated with 200 ng/mL for 5 minutes (Figure 3.26 c) and for 10 minutes at the same concentration (Figure 3.26 d) showed a higher percentage of cells exhibiting fluorescence for the shorter incubation time compared to the longer incubation time. Attempts to reproduce the assay showed a similar lack of pattern and inconsistency between the results, indicating SLO to be an unreliable agent to use for permeabilisation. This was further supported by reports in literature[219,225] observing bacterial toxins to produce an inconsistent degree of cell membrane permeabilisation hence might be difficult to control.

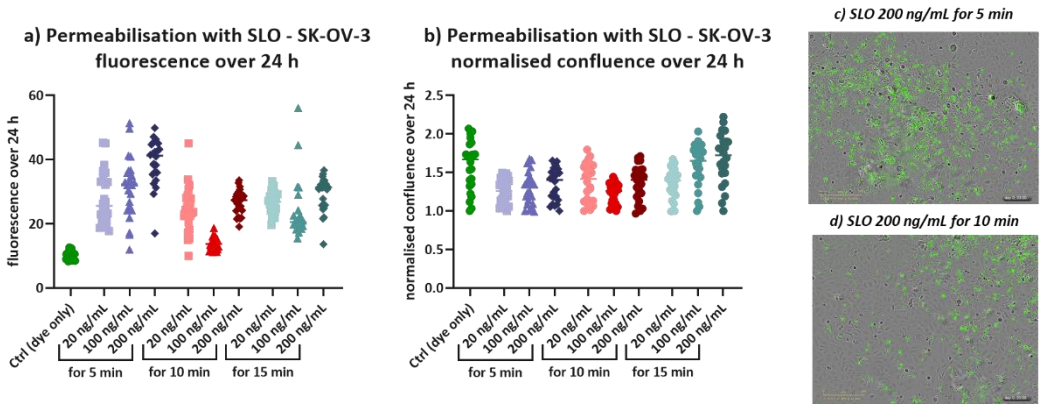

Figure 3.26: Permeabilisation of SK-OV-3 cells with different SLO concentrations and incubation times: a) fluorescence of cells over 24 hours and b) normalised confluence over 24 hours (1 data point per hour); fluorescence microscope images of cells after treatment with 200 ng/mL of SLO for c) 5 minutes and d) 10 minutes at 37 °C.

Taken together, the results supported the decision to employ digitonin as the permeabiliser of choice for further experiments, due to inducing more reliable permeabilisation when compared to SLO, and its increased permeabilisation efficiency when compared to GDN. For the PROTAC dose-response assays, cells were permeabilised with 5 µg/mL of digitonin for 5 or 10 minutes on ice. Then, culture medium with indicated concentrations of the compounds was added, cells were incubated for 24 hours and fascin levels were then analysed using western blotting. Permeabilisation for 5 minutes followed by treatment with 1st series alkylation PROTACs did not induce any decrease of fascin levels (Figure 3.27 a). Increasing the incubation time of digitonin to 10 minutes at the same concentration and subsequent treatment with 1st series alkylation PROTACs resulted in considerable cell death, which complicated western blot analysis of fascin levels (Figure 3.27 b). In the same way, permeabilisation for 5 minutes and treatment with 2nd series long PROTACs was not tolerated well by the cells, rendering analysis of fascin levels difficult (Figure 3.27 c).

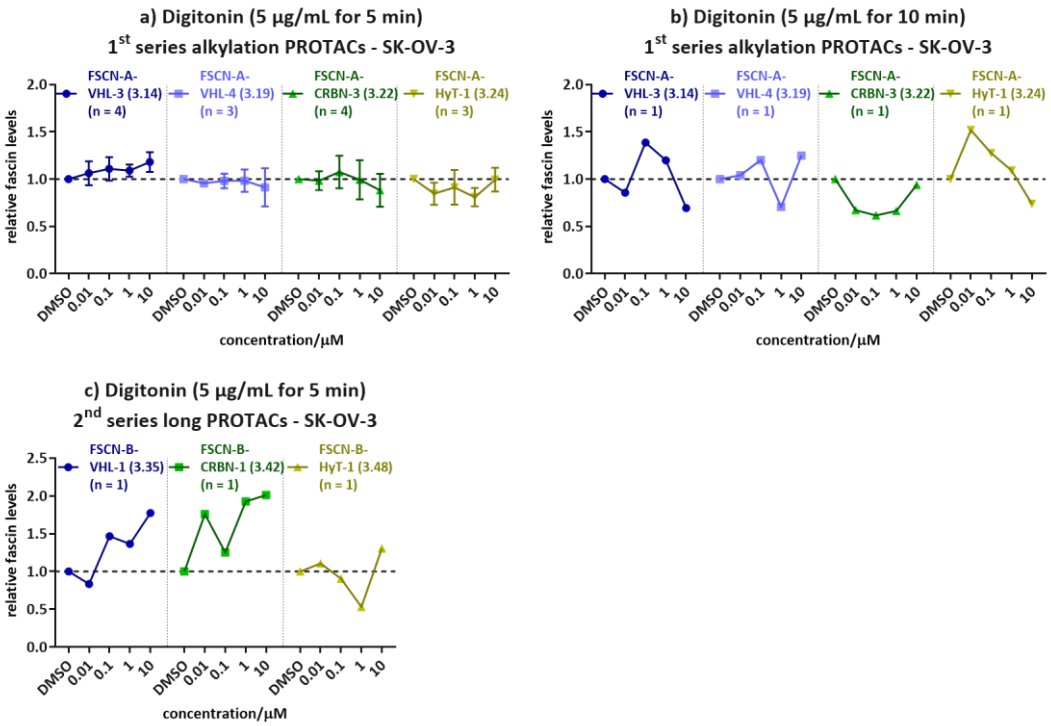

Figure 3.27: Quantification of western blot analysis – fascin levels 24 hours after permeabilisation of SK-OV-3 cells with 5 µg/mL of digitonin for a) 5 minutes on ice and b) 10 minutes on ice, followed by treatment with 1st series alkylation PROTACs, c) 5 minutes, followed by treatment with 2nd series long PROTACs. Error bars represent SEM.

Since the data obtained from the permeabilisation assays using digitonin were inconclusive, a control experiment using the HaloTag system was carried out, aiming at elucidating if penetrance of the compounds could be achieved using digitonin-mediated permeabilisation. It was hypothesised that if permeabilisation with digitonin was successful, degradation of the HaloTag–fascin fusion protein would be observed to occur at lower concentrations of active VHL HaloPROTAC **VHL-HP-1 (2.18)** than for non-permeabilised cells. In addition, degradation mediated by the CRBN HaloPROTAC **CRBN-HP-1 (2.29)**, which was previously determined to be inactive (Chapter 2.3.3), could potentially be observed after membrane permeabilising by increasing intracellular compound concentration.

For the assays, SK-OV-3 cells were transfected with the HaloTag–fascin plasmid, incubated to allow for expression of the fusion protein and then permeabilised with 5 µg/mL of digitonin for 5 minutes prior to HaloPROTAC treatment. Analysis of fusion protein levels revealed no differences in degradation profiles compared to assays with non-permeabilised cells (Figure 3.28 a and b), again not providing evidence for increased delivery of the compounds through permeabilisation. Due to the inconclusive data obtained for the

permeabilisation strategy using chemical agents, this approach was abandoned and attention was turned to other methods which could be used to assess PROTAC activity.

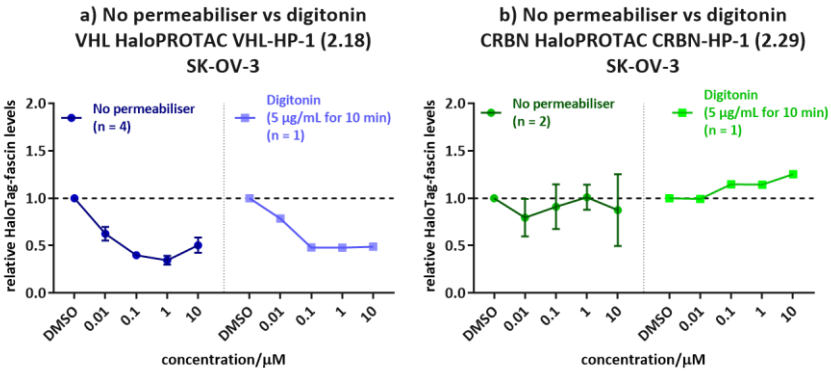

Figure 3.28: Quantification of western blot analysis – HaloTag-fascin levels 24 hours after permeabilisation of SK-OV-3 cells without or with 5 µg/mL of digitonin for 10 minutes on ice, followed by treatment with HaloPROTACs: a) ***VHL-HP-1 (2.18)*** *and b)* ***CRBN-HP-1 (2.29)****.*
Error bars represent SEM.

3.5.7 Assays with whole-cell lysates

In order to bypass the cell membrane barrier entirely, assays using cell lysates instead of whole cells were attempted. This approach can be used to study proteasomal activity[227] as well as protein ubiquitination,[228,229] and has also found application in the PROTAC-context.[230-232] Based on procedures reported in literature,[230,233] degradation assays with lysates were carried out by collecting and lysing SK-OV-3 and HT-1080 cells, incubating whole cell lysates with different concentrations of the PROTACs, followed by analysis of fascin levels using western blotting. Since, for initial experiments, no decrease of fascin levels was observed, different conditions were trialled in an attempt to optimise the procedure. To do so, a range of lysate concentrations from 0.5 to 2 mg/mL, different incubation temperatures (0 °C, room temperature or 37 °C) and incubation times (1, 2 or 4 hours) were tried; however, no fascin degradation was observed for any of the experiments. Literature reports[230,232] suggested that addition of adenosine triphosphate (ATP) to the assay buffer might be necessary for appropriate function of the proteasome and/or omission of protease and phosphatase inhibitor cocktails from the buffer could prove advantageous to the assay. However, the attempts equally failed to show any decrease in fascin levels, as exemplified by dose-response assays carried out with 2nd series long linker PROTACs **FSCN-B-VHL-2 (3.36)** and **FSCN-B-CRBN-2 (3.47)** for which the assay buffer was supplemented with ATP or prepared without phosphatase inhibitors (Figure 3.29).

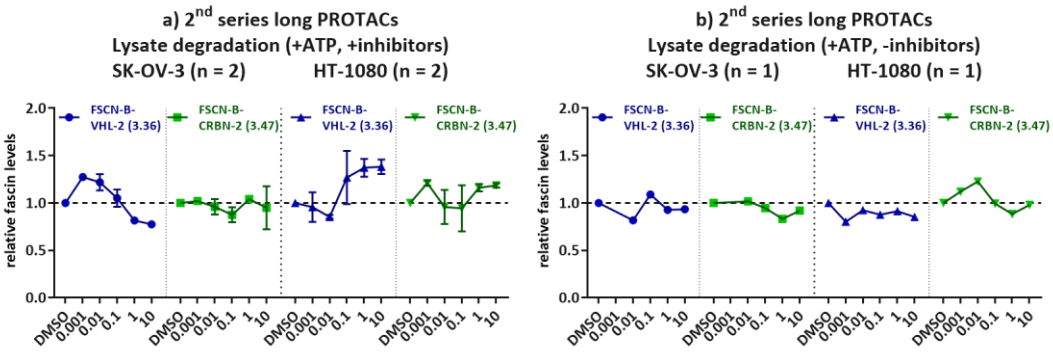

*Figure 3.29: Quantification of western blot analysis – ex vivo degradation assays: fascin levels 24 hours after incubation of SK-OV-3 whole cell lysates with 2nd series long PROTACs **FSCN-B-VHL-2 (3.36)** and **FSCN-B-CRBN-2 (3.47)**, a) using assay buffer supplemented with ATP and protease/phosphatase inhibitor cocktail and b) using assay buffer supplemented with ATP but without protease/phosphatase inhibitor cocktail. Error bars represent SEM.*

Attempts to optimise the conditions of the lysate assays using the HaloTag model system, by transfecting cells with the HaloTag–fascin fusion protein and subsequent treatment with active VHL HaloPROTAC **VHL-HP-1 (2.18)** were equally unfruitful and proved tedious due to insufficient quantities of cells obtained after the transfection step. Further optimisation, for example using lysate of HeLa or HEK293 cells for which degradation in lysate experiments have been shown or addition of purified protein to the cell lysate,[230,231] could be advantageous in future attempts. However, based on issues with reproducibility and inconclusive results indicating extensive optimisation of the conditions would be needed, work on cell lysates was discontinued.

3.5.8 Binary complex formation

To elucidate if the PROTACs bind to fascin, surface plasmon resonance (SPR) experiments were carried out by Katie Pollock at the Beatson Institute for Cancer Research. For SPR, the POI is immobilised on a sensor surface over which the analyte, here the PROTAC, in solution, is flowed. Polarised light is focussed through a prism on the sensor surface. Any binding interaction and dissociation of the analyte causes a small change in the refractive index at the surface which is then detected by a sensor and recorded (Figure 3.30 a).[234] As such, not only can the binding of the analyte to the protein be determined, but also kinetics of the binding interaction and binding affinities. The rate of association (k_{on}) and dissociation (k_{off}) can be measured and the binding affinity, or dissociation constant (K_D), is the ratio of k_{on}/k_{off}. Dissociative half-life ($t_{½}$) is a measure of the life-time of the complex and is dependent on rate of dissociation.[235]

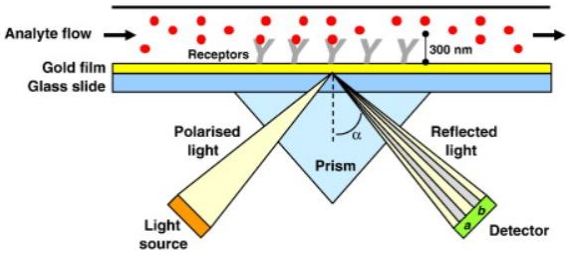

Figure 3.30: Surface plasmon resonance experiment set-up.[234]

Binding affinity of the 1st series of PROTAC parent compound, **FSCN-A (1.4)**, was measured to be 0.97 μM (Table 3.7). Introduction of an amide bond for linker attachment resulted in a two-fold decrease in binding affinity to 2.4 μM for fascin ligand control compound **FSCN-A-ctrl (3.6)**. A further significant drop in K_D to over 6 μM was observed for 1st series amide PROTACs **FSCN-A-VHL-1 (3.7)** and **FSCN-A-CRBN-1 (3.9)**. Binding affinity of shorter linker analogue **FSCN-A-CRBN-2 (3.10)** could not be determined due to precipitation of the compound, indicating poor solubility. Attachment of the linker through alkylation at the piperazine for the 1st series alkylation PROTACs improved binding significantly, however, binding affinity for VHL PROTACs **FSCN-A-VHL-3 (3.14)** and **FSCN-A-VHL-4 (3.19)** was determined to be three-fold lower compared to the parent compound. Interestingly, CRBN PROTAC **FSCN-A-CRBN-3 (3.22)** displayed an improved binding affinity, comparable to the parent compound at around 1 μM. This higher binding affinity compared to the VHL PROTACs could be an indication of additional interactions between the CRBN PROTAC with fascin. HyT PROTAC **FSCN-A-HyT-1 (3.24)** was determined to be non-binding (NB), possibly due to poor solubility of the compound at concentrations needed to assess binding.

	SPR K_D (μM)	***Dissociative half-life $t_{½}$ (s)***
FSCN-A (1.4)	0.97	Not determined
FSCN-A-ctrl (3.6)	2.4	Not determined
1st series amide PROTACs		
FSCN-A-VHL-1 (3.7)	6.2	Not determined
FSCN-A-CRBN-1 (3.9)	6.8	Not determined
FSCN-A-CRBN-2 (3.10)	NB	Not determined
1st series alkylation PROTACs		
FSCN-A-VHL-3 (3.14)	3.5	4.1
FSCN-A-VHL-4 (3.19)	3.8	4.0
FSCN-A-CRBN-3 (3.22)	1.1	4.4
FSCN-A-HyT-1 (3.24)	> 4.4	5.2

Table 3.7: Binary (fascin–PROTAC) complex formation: SPR K_D data for parent compound fascin ligand A, fascin ligand A control and 1st series PROTACs.

With a K_D determined to be 0.05 μM, the parent compound **FSCN-B (1.5)** of the 2nd series PROTACs was shown to bind much more strongly to fascin compared to **FSCN-A (1.4)** (Table 3.8). Although displaying significantly lower affinities compared to the parent ligand, the 2nd series PROTACs still showed improved binding compared to the 1st series PROTACs. CRBN PROTACs **FSCN-B-CRBN-1 (3.42)** and **FSCN-B-CRBN-2 (3.47)** were determined to have a three- to four-fold higher affinity for fascin compared to VHL PROTACs **FSCN-B-VHL-1 (3.35)** and **FSCN-B-VHL-2 (3.36)**. Interestingly, the shorter linker analogues displayed a two-fold improvement of K_D compared to the longer linker PROTACs. The shorter linker length could favour additional interactions of the compounds with fascin, leading to higher affinity binding. HyT PROTACs **FSCN-B-HyT-1 (3.48)** and **FSCN-B-HyT-2 (3.51)** were both determined to have a K_D of 1 μM. Although a literature value for the binding of the parent compound of the 3rd series, **FSCN-C (1.7)**, to fascin was reported using ITC,[63] binding could not be measured for the parent compound or PROTAC **FSCN-C-VHL-1 (3.60)** by SPR.

	SPR K_D (μM)	***Dissociative half-life $t_{½}$ (s)***
FSCN-B (1.5)	0.05	24
2nd series long linker PROTACs		
FSCN-B-VHL-1 (3.35)	2.0	10
FSCN-B-CRBN-1 (3.42)	0.55	12
FSCN-B-HyT-1 (3.48)	1.0	9.1
2nd series short linker PROTACs		
FSCN-B-VHL-2 (3.36)	0.81	11
FSCN-B-CRBN-2 (3.47)	0.26	16
FSCN-B-HyT-2 (3.51)	1.3	15

Table 3.8: Binary (fascin–PROTAC) complex formation: SPR K_D data for parent compound fascin ligand B and 2nd series PROTACs.

3.6 Summary of fascin-targeting PROTACs

Based on three distinct ligands for fascin, a total of 14 PROTACs were synthesised. Six PROTACs were designed to recruit VHL E3 ligase, five would recruit CRBN and three featured an adamantyl moiety to act as HyTs. Activity of the compounds and their ability to bind to fascin were assessed in different biological assays.

3.6.1 Synthetic summary

1st series PROTACs

The initial set of 1st series PROTACs based on **FSCN-A (1.4)** was synthesised using a modular approach by first establishing an E3 ligase–linker library from linkers **3.1a** or **3.1b**. Subsequent coupling to fascin ligand **FSCN-A (1.4)** yielded one VHL PROTAC, **FSCN-A-VHL (3.7)**, and two CRBN PROTACs, **FSCN-A-CRBN (3.9)** and **FSCN-A-CRBN (3.10)**, in 2% to 5% (Figure 2.44). Physicochemical properties of this initial set of 1st series PROTACs were determined to be suboptimal and aqueous solubility was observed to be poor due to the high number of amide bonds present in the molecules.

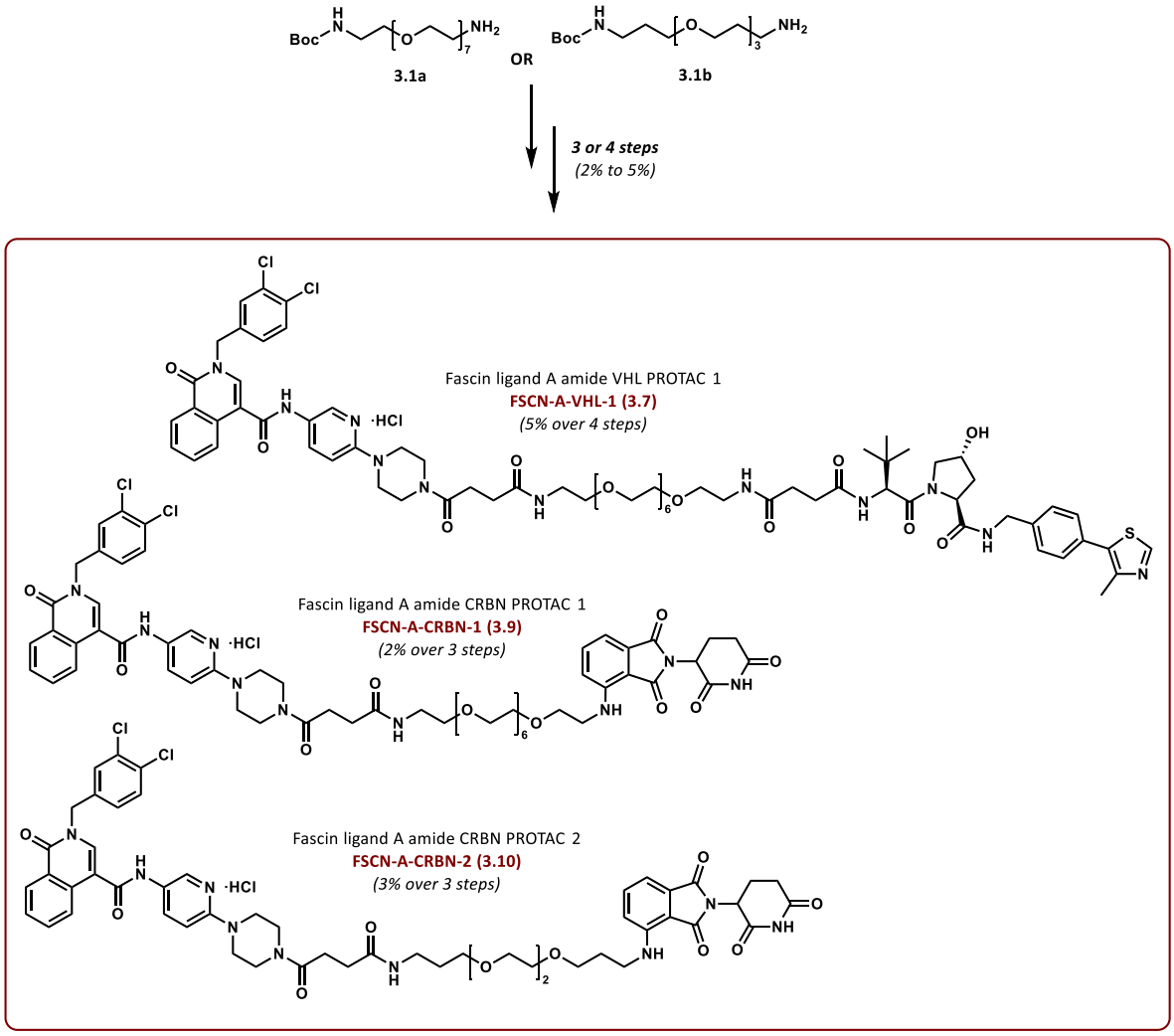

Figure 3.31: Summary of the synthesis of 1st series amide PROTACs.

In an attempt to decrease the number of amide bonds and improve compound properties, a further set of 1st series PROTACs was established by attachment of the linker through alkylation instead of amide bond formation at the piperazine moiety of **FSCN-A (1.4)**. For VHL-recruiting PROTAC **FSCN-A-VHL-3 (3.14),** activated linker **3.12** was synthesised over two steps from pentaethylene glycol (Figure 3.32). *N*-alkylation at the piperazine of **FSCN-**

A (1.4) and coupling to **VHL-1 (2.1)** yielded **FSCN-A-VHL-3 (3.14)** in 11% over five steps. VHL PROTAC **FSCN-A-VHL-4 (3.19)** was synthesised using a CuAAC protocol from azide **3.17** and alkyne **3.18**, affording the final compound in 6% overall yield over three steps for the longest linear sequence (LLS) (Figure 3.32).

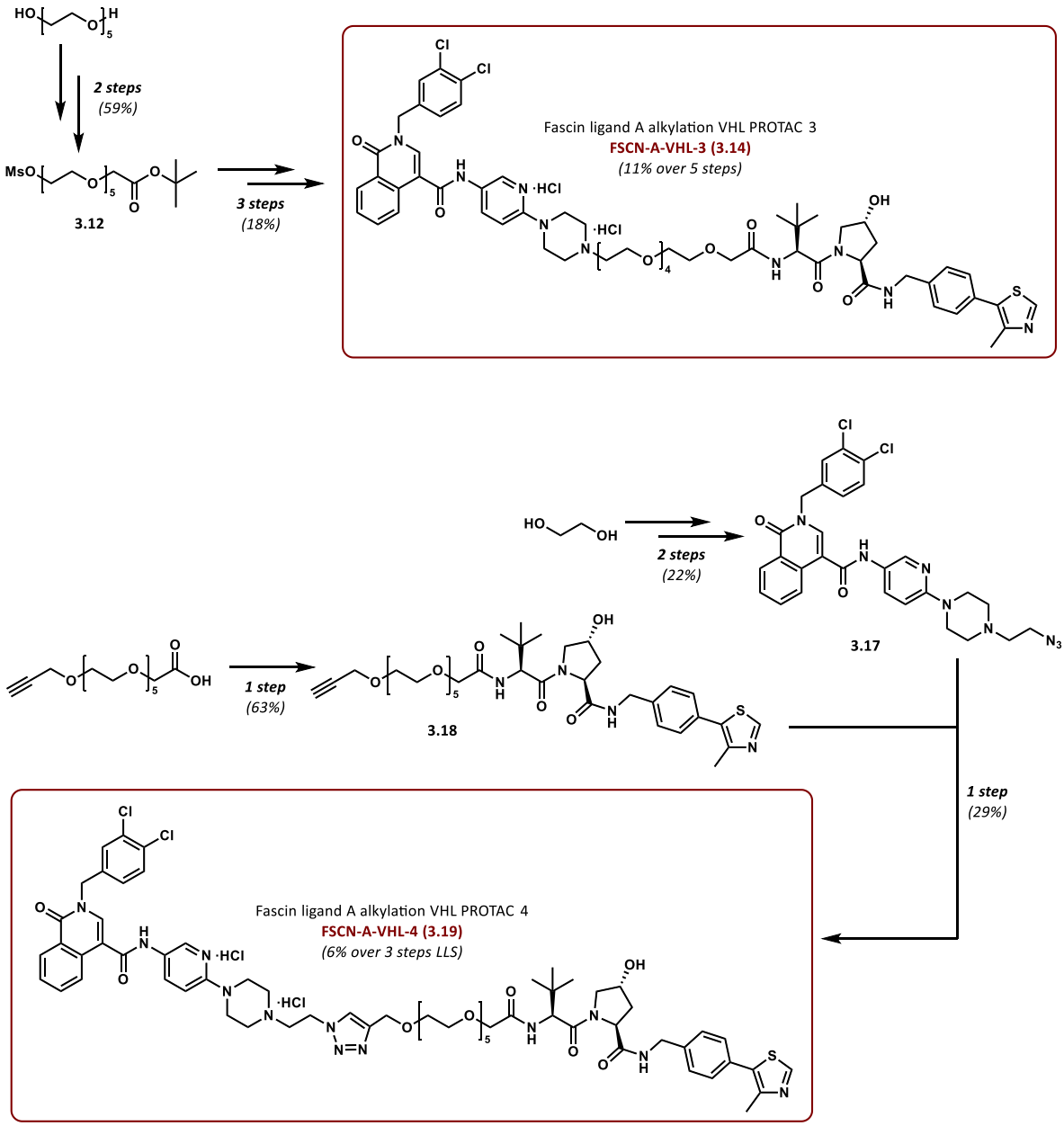

Figure 3.32: Summary of the synthesis of 1st series alkylation VHL PROTACs.

Linker attachment through *N*-alkylation of fascin ligand A **FSCN-A (1.4)** over two steps and subsequent coupling to CRBN ligand **CRBN-2 (2.11)** yielded CRBN PROTAC **FSCN-A-CRBN-3 (3.22)** in 7% yield over five steps (Figure 3.33). The first HyT PROTAC of the series **FSCN-A-HyT-1 (3.24)** was accessed over two steps in 26% yield through previously established HyT–linker fragment **2.35** (Figure 3.33). Calculated physicochemical properties for the alkylation set of 1st series PROTACs showed an overall improvement with fewer HBD/HBA and

therefore a lower tPSA owing to a reduced amide bond count compared to the initial set of compounds.

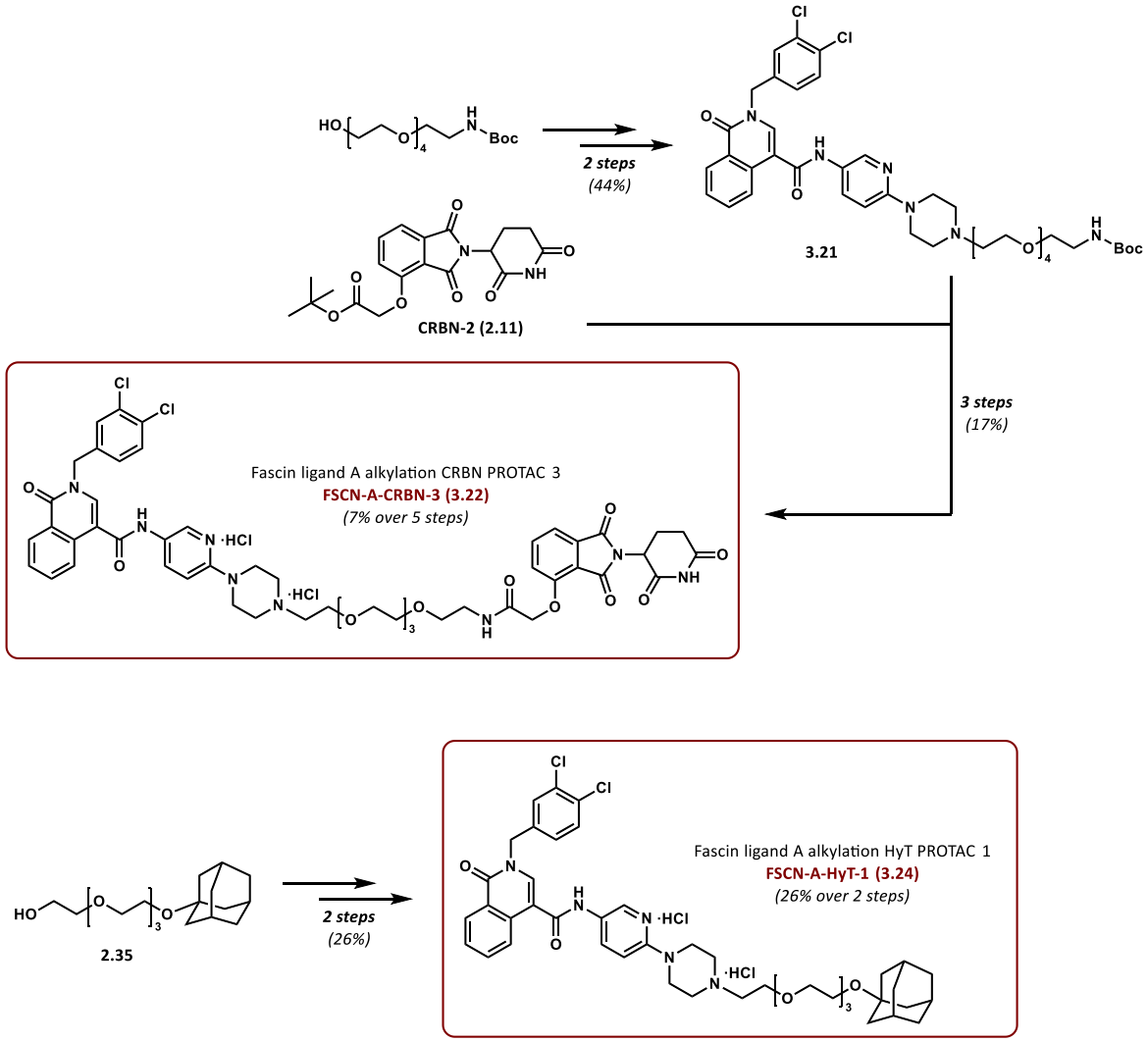

Figure 3.33: Summary of the synthesis of 1st series alkylation CRBN and HyT PROTACs.

2nd series PROTACs

Prior to establishing a library of the 2nd series of PROTACs, parent compound **FSCN-B (1.5)** was synthesised (Figure 3.34). Pyrazole **3.26a** was access over two steps from DMFDMA and *tert*-butyl 4-hydrazinopiperidine-1-carboxylate hydrochloride, however, correct regiochemistry of the obtained pyrazole could not be determined conclusively through NMR analysis. The synthesis was carried forward to obtain **FSCN-B (1.5)** in 38% to 45% overall yield over nine steps, and correct structure of the parent ligand was confirmed through X-ray crystallography.

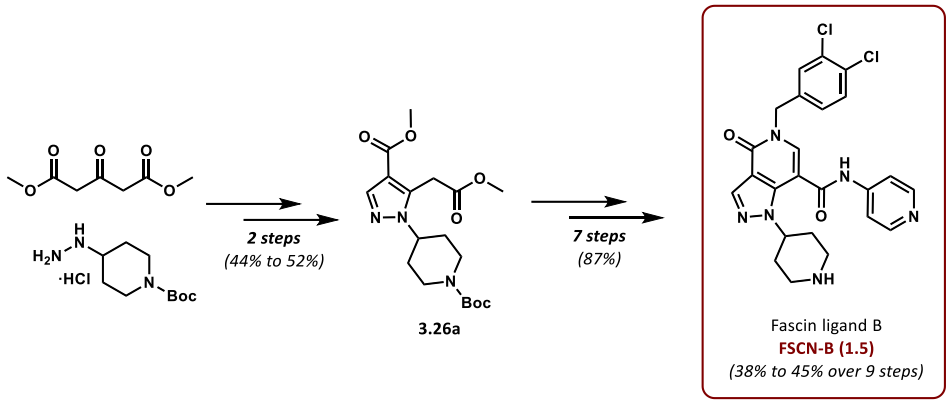

*Figure 3.34: Summary of the synthesis of parent compound **FSCN-B (1.5)**.*

Matched pairs of PROTACs with two different linkers were produced to be able to assess the impact of linker length on degradation efficacy when testing the compounds in biological assays. For VHL PROTACs, first fascin ligand B–longer linker **3.34a** and fascin ligand B–shorter linker **3.34b** were accessed over three steps from tetraethylene glycol and diethylene glycol, respectively (Figure 3.35). Through a further two steps, longer linker VHL PROTAC **FSCN-B-VHL-1 (3.35)** and shorter linker VHL PROTAC **FSCN-B-VHL-2 (3.36)** were afforded in 11% and 9% overall yield, respectively.

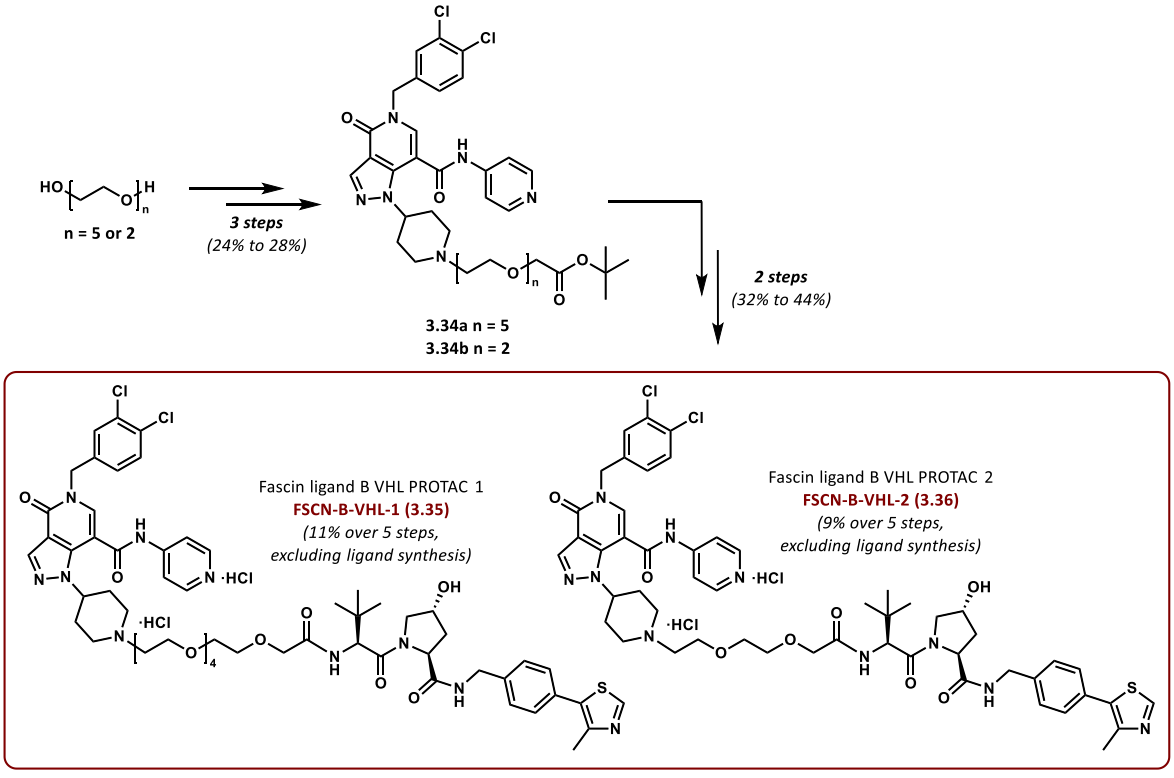

Figure 3.35: Summary of the synthesis of 2nd series VHL PROTACs.

For the CRBN PROTACs, longer linker **3.38** was be synthesised over two steps whereas shorter linker **3.39** was commercially obtained (Figure 3.36). Longer linker PROTAC **FSCN-B-CRBN-1 (3.42)** was accessed in a 2% overall yield *via* an S_NAr reaction at CRBN ligand

CRBN-1 (2.9), however, since the reaction was low-yielding, a different approach was attempted for the longer linker analogue. Amide bond formation between linker **3.39** and CRBN ligand **CRBN-2 (2.11)** generated CRBN ligand–linker fragment **3.45** in acceptable yield. Subsequent activation of the linker and coupling to **FSCN-B (1.5)** afforded shorter linker PROTAC **FSCN-B-CRBN-2 (3.47)** in marginally increased overall yield compared to the longer linker analogue.

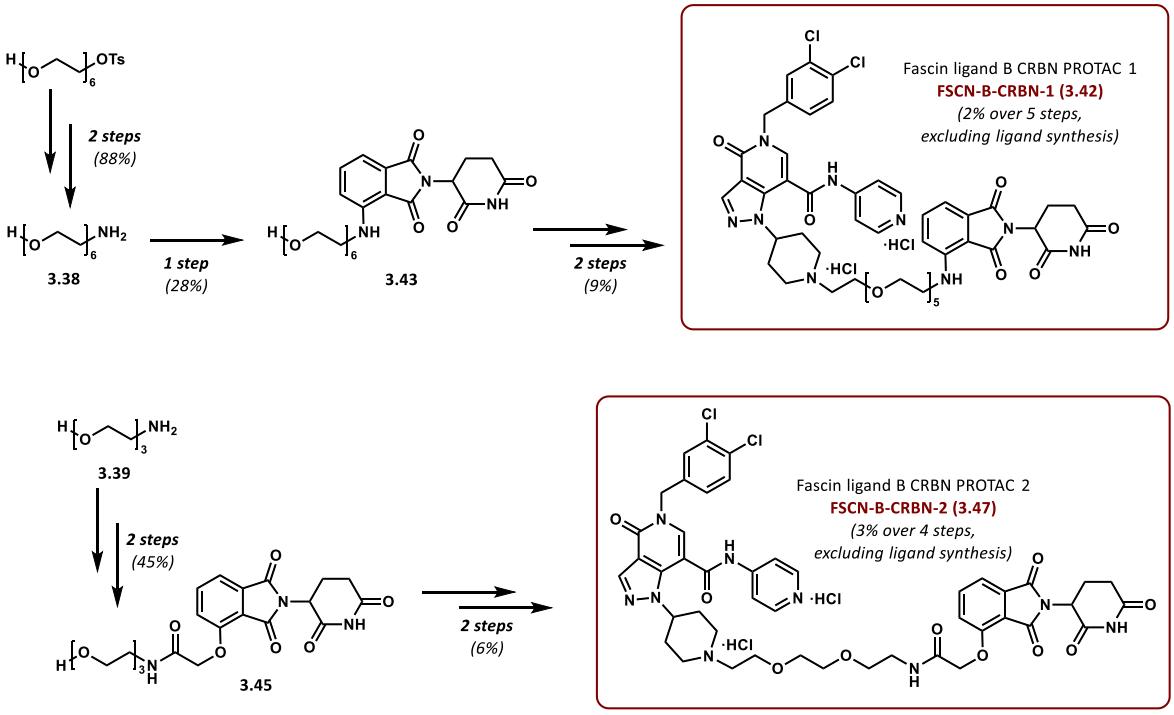

Figure 3.36: Summary of the synthesis of 2nd series CRBN PROTACs.

Longer linker HyT PROTAC **FSCN-B-HyT-1 (3.48)** was afforded over two steps in 29% yield from previously synthesised fascin ligand B–linker fragment **3.41**. Shorter linker analogue **FSCN-B-HyT-2 (3.51)** was generated over three steps in 22% overall yield via HyT–linker intermediate **3.49**. Physicochemical properties of the longer linker PROTACs of the 2nd series were comparable to the 1st series alkylation compounds. The shorter linker analogues expectedly resulted in improved values for HBD/HBA, tPSA and NRotB due to a reduced number of ethylene glycol units.

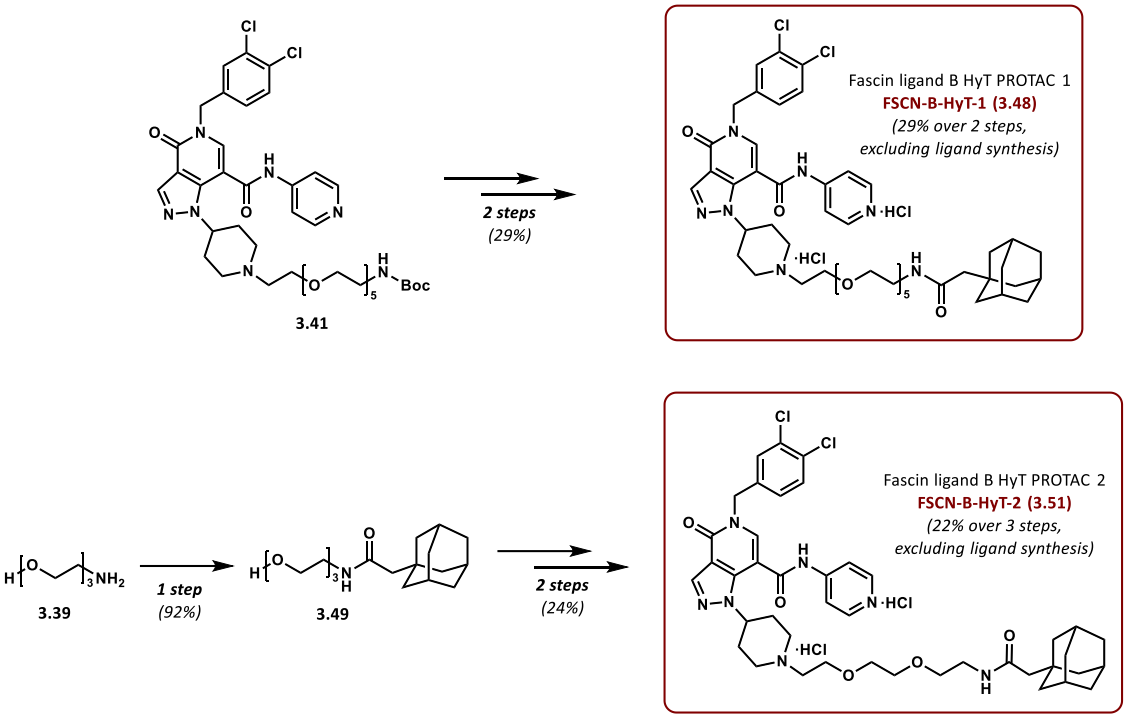

Figure 3.37: Summary of the synthesis of 2nd series HyT PROTACs.

3rd series PROTAC

Initially, different exit vectors for linker attachment at **FSCN-C (1.7)** were envisioned for which the parent compound **FSCN-C (1.7)** and two functionalised analogues, **3.52** and **3.53**, were synthesised (Figure 3.38). Functionalise furoic acid **3.56a** was generated over three steps from methyl 2-methylfuran-3-carboxylate, whereas non-functionalised furoic acid **3.56b** was obtained from the same starting material by saponification of the methyl ester. Alkylation of 1*H*-indazol-3-amine or 5-bromo-1*H*-indazol-3-amine with 4-(trifluoromethyl)benzyl bromide afforded amines **3.57a** and **3.57b**. Through a screen of amidation conditions, a formadinium-based protocol was identified for optimal coupling of deactivated amines **3.57a** and **3.57b** with acids **3.56a** and **3.56b**.

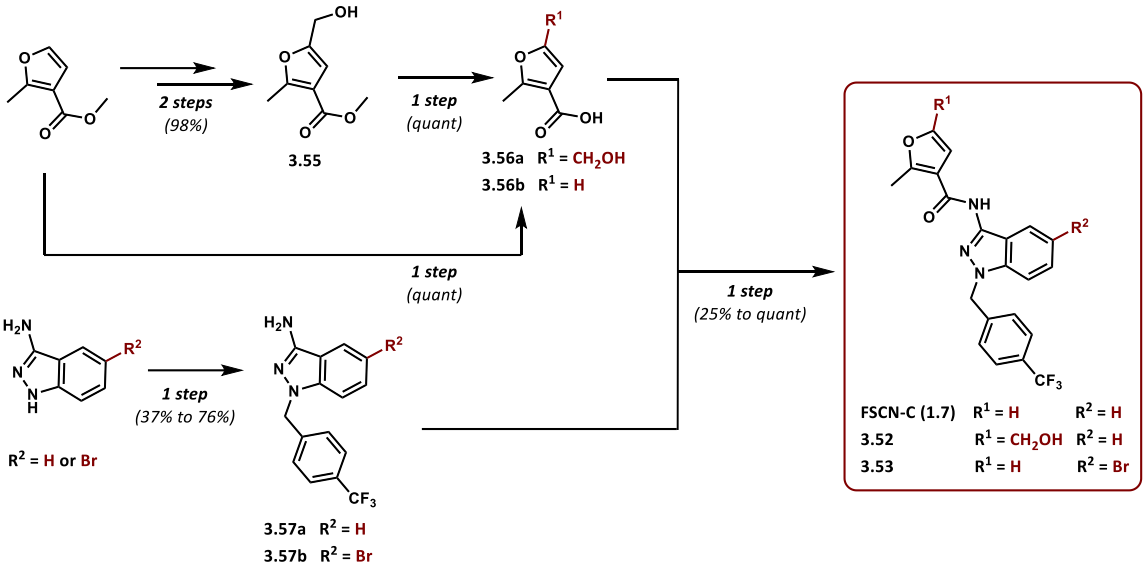

*Figure 3.38: Summary of the synthesis of parent compound **FSCN-C (1.7)** and functionalised analogues.*

For VHL PROTAC **FSCN-C-VHL-1 (3.60)**, a linker was introduced through the alcohol handle of functionalised ligand **3.52**. Subsequent coupling to VHL ligand **VHL-1 (2.1)** yielded the final compound in 9% (Figure 3.39).

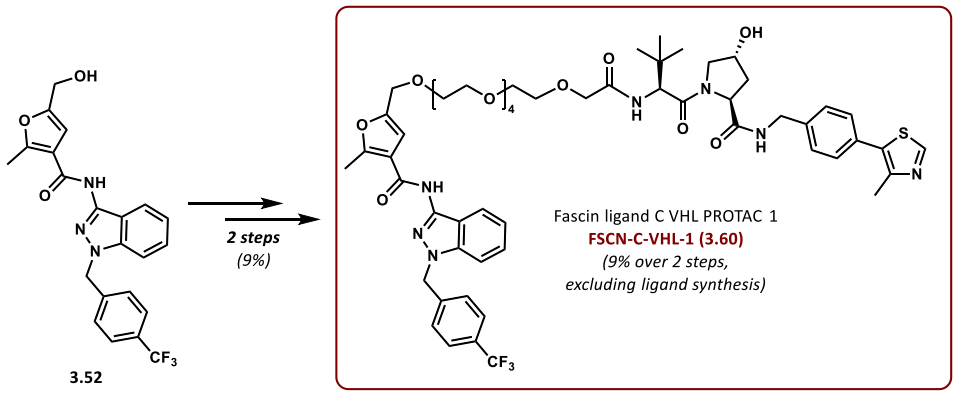

Figure 3.39: Summary of the synthesis of 3rd series PROTAC.

3.6.2 Summary of biological testing

Before the synthesised compounds were tested for their ability to degrade fascin inside cells, fascin's cellular turnover was determined. With an observed cellular half-life of about 24 hours in SK-OV-3 and HT-1080 cells, protein stability was deemed appropriate for PROTAC-mediated degradation. Initial experiments comparing cytotoxicity of the 1st series PROTAC with the parent compound indicated that treatment with compound concentrations up to 10 μM would be tolerated by cells. Subsequently, degradation assays with the compounds were carried out in SK-OV-3 and HT-1080 cells. Incubating different cell lines with increasing concentrations of the PROTACs and analysis of the fascin levels after 24 hours failed to provide any evidence of protein degradation (Figure 3.40).

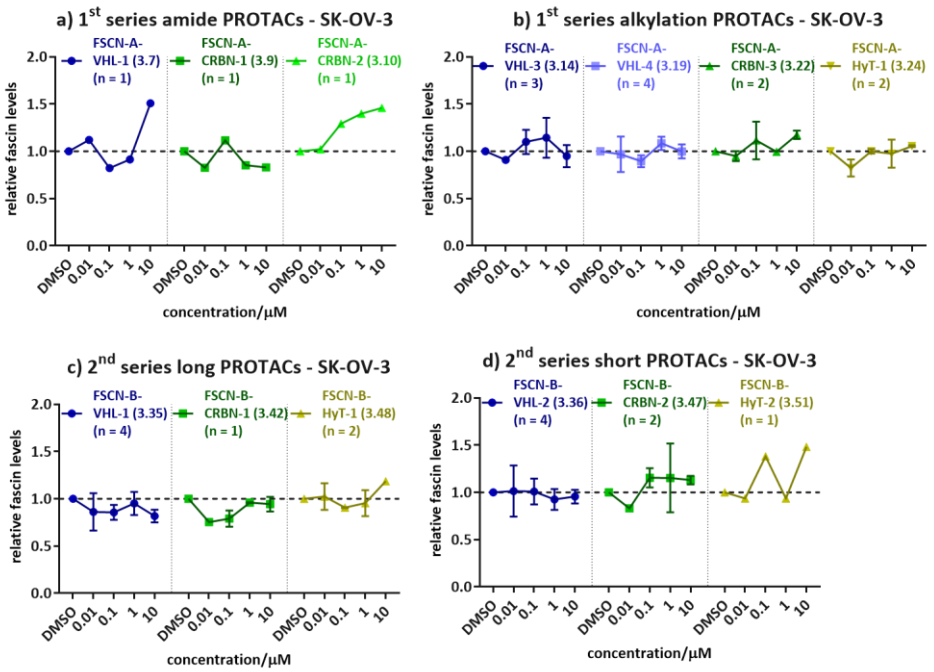

Figure 3.40: Quantification of western blot analysis - fascin levels in SK-OV-3 cells 24 hours after treatment with increasing concentrations of: a) 1st series amide PROTACs, b) 1st series alkylation PROTACs, c) 2nd series longer linker PROTACs and d) 2nd series short linker PROTACs.
Error bars represent SEM.

To determine if poor cell permeability of the compounds due to their suboptimal physicochemical properties could impede entry into the cells, an intracellular VHL engagement assay based on the HaloTag model system was established. 1st and 2nd series VHL-recruiting PROTACs failed to engage VHL intracellularly at tolerable concentrations, whereas the 3rd series PROTAC was shown to bind to VHL even at low concentrations.

Attempting to increase intracellular concentrations of the compounds, different methods for cell permeabilisation were trialled, *via* physical permeablisation through electroporation or by use of chemical agents. Initial permeabilsation assays with digitonin, GDN and SLO using an impermeant fluorescent dye indicated that digitonin would provide sufficient and reproducible cell permeabilisation for delivery of compounds into cells (Figure 3.41). However, dose-response assays with permeabilised cells proved unsuccessful in inducing degradation of fascin, and the approach abandoned due to low cellular tolerability.

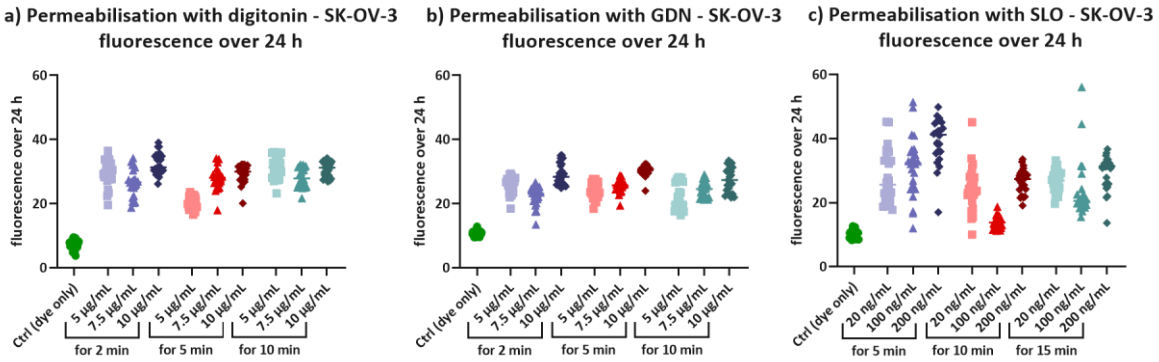

Figure 3.41: Permeabilisation of SK-OV-3 cells - fluorescence of cells over 24 hours at different concentrations and incubation times with: a) digitonin, b) GDN and c) SLO.

Bypassing the cell membrane altogether by conducting degradation assays with whole cell lysates was equally ineffective, despite attempts to optimise the assay. Due to issues with scalability and practicability with the use of lysates, the strategy was deemed unsuitable for further assay development. Finally, binding of the compounds to fascin was assessed by SPR. PROTACs of the 1st and 2nd series were determined to bind to the protein with adequate affinities, however, for the 3rd series PROTAC fascin binding was not observed. Taken together, the results of the different assays indicated that further investigation into the causes for lack of activity of the compounds was required. With additional insights, optimisation of the compounds could be carried out in order to improve their ability to induce intracellular fascin degradation.

4 Conclusions and future work

4.1 HaloTag model system

A HaloTag-based model system was established by synthesis of seven HaloPROTACs recruiting CRBN and VHL as well as HyTs, along with the corresponding mono-functional control compounds (Chapter 2.2.4). A plasmid for transient expression of a HaloTag–fascin fusion protein was cloned and expressed in different cancer cell lines. Degradation assays showed VHL-recruiting HaloPROTACs to induce reproducible and prolonged degradation of the fusion protein *via* the PROTAC mechanism in two cell lines, SK-OV-3 and HT-1080 (Chapter 2.3.3). Then, a SK-OV-3 fascin knock-out cell line was generated using the CRISPR–Cas9 technique for further experiments with the HaloTag model system. Assays assessing the impact of fascin knock-out, expression and subsequent degradation of the fusion protein on cell functionality and morphology were carried out, however, the obtained results were inconclusive, requiring optimisation of the experiments and further investigation (Chapter 2.3.7).

Exploration of linker length

Whereas degradation of the fusion protein was achieved by use of VHL-recruiting HaloPROTACs, only a very limited decrease of protein levels was observed after treatment with CRBN and HyT HaloPROTACs. Moreover, the results obtained from the degradation assays indicated that specificity for a particular target could be modulated by recruiting particular E3 ligases in different cell lines. Literature reports also highlight the importance of linker length for achieving degradation selectivity for a particular POI (Chapter 1.2.4).[91,92] Additional HaloPROTACs with a range of linker lengths or different exit vectors for linker attachment could be synthesised and tested in a variety of cell lines to investigate cell-line dependent target specificity further.

Choice of cell line for functional and phenotype assays

The use of the SK-OV-3 cell line for functional and phenotype assays proved to be suboptimal due to their low invasive ability and limited formation of membrane protrusions, despite adequate expression levels of endogenous fascin. The use of a more invasive cell line, such as HT-1080 cells, and/or cell lines displaying more pronounced

fascin-mediated membrane protrusions should be considered to obtain more meaningful results when assessing cellular function and behaviour with the model system.[155]

Generation of cell line stably expressing fusion protein

Transfection with the HaloTag–fascin plasmid was tolerated adequately by SK-OV-3 and HT-1080 cells, however, not by other cell lines, leading to considerable cell death. The challenge with tolerability of the plasmid also impacted negatively on reproducibility of the data obtained for the degradation assays. In addition, wound-healing assays used for assessment of cell function were carried out over a prolonged period of time, up to 94 hours. However, due to transient expression of the HaloTag–fascin fusion protein through a plasmid, protein levels continuously decreased,[159] reducing the impact of the fusion protein on cell function over time and potentially obscuring the results of the assays. In order to mitigate variations in protein levels, a cell line which stably expresses the fusion protein should be established to obtain reproducible and more indicative results for experiments performed on a longer timescale.[173]

Live-cell imaging of cells in 3D environment

Formation of fascin-mediated actin structures and their interconversion are highly dynamic processes and dependent on the properties of the environment cells are surrounded by (Chapter 1.1.3). Therefore, assessment of any changes in the dynamics of actin structures by either knocking out the endogenous protein or expression and degrading the HaloTag–fusion protein through the PROTAC mechanism should also be carried out. Live-cell imaging of cells moving through different matrices could provide further insights into functionality of the fusion protein as well as the effect of PROTAC treatment (Figure 4.1).[29,236]

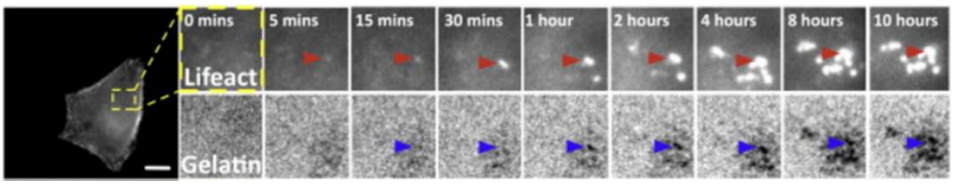

Figure 4.1: Time-lapse microscopy images of A375MM cells expressing GFP–actin. Red arrows indicate invadopodia and blue arrows indicate degradation of gelatin matrix.[29]

Despite potential optimisation required for the functional and phenotype assays, it can be concluded that a successful proof-of-concept was carried out by inducing sustained degradation of the fusion protein *via* the PROTAC mechanism with VHL-recruiting

HaloPROTACs in two cell lines, SK-OV-3 and HT-1080 cells. With the principle of PROTAC-mediated protein degradation confirmed to be effective in the model system, work towards targeted degradation of the endogenous protein was carried out.

4.2 Fascin-targeting PROTACs

A total of 14 PROTACs were synthesised from three fascin binders, **FSCN-A (1.4)**, **FSCN-B (1.5)** and **FSCN-C (1.7)** reported in literature.[59,63,186] The 1st series PROTACs based on **FSCN-A (1.4)** included three VHL-recruiting PROTACs, two CRBN-recruiting PROTACs and one HyT (Chapter 3.2). For the **FSCN-B (1.5)**-based 2nd series PROTACs matched pairs with longer and shorter linkers were synthesised: two VHL-recruiting PROTACs, two CRBN-recruiting PROTACs and two HyTs (Chapter 3.3). In addition, one VHL-recruiting 3rd series PROTAC with **FSCN-C (1.7)** as fascin-recruiting moiety was synthesised (Chapter 3.4).

Degradation assays in different cell lines were carried out to assess the ability of the PROTACs to induce degradation of fascin. However, no decrease in protein levels could be observed, which was hypothesised to be due to poor permeability of the compounds (Chapter 3.5.4). An intracellular engagement assay based on the HaloTag model system was carried out with the VHL-recruiting PROTACs (Chapter 3.5.5). Insufficient intracellular recruitment of VHL by the 1st and 2nd series PROTACs was observed, indicating cell permeability to be the limiting factor to compound activity. Solely, the 3rd series PROTAC showed excellent permeability, despite lack of activity. Different physical and chemical permeabilisation methods were tried in an attempt to increase intracellular compound concentrations, however, this approach was unfruitful (Chapter 3.5.6). To confirm that the PROTACs would in fact bind to fascin, SPR experiments were carried out. All compounds, apart from the 3rd series PROTAC, were shown to bind to the protein with reasonable affinity (Chapter 3.5.8). Additional experiments could be performed in order to elucidate the root cause for the lack of activity of the compounds.

Ternary (fascin–PROTAC–E3 ligase) complex formation

Cooperativity between the POI and the E3 ligase can impact on PROTAC efficacy either positively, by stabilising the interaction between the two proteins, or negatively, through repulsion or clashes of the proteins (Chapter 1.2.4). Therefore, evaluation of ternary POI–PROTAC–E3 ligase complexes can prove useful for assessing PROTAC efficacy. Ternary complex formation can be determined through SPR, similar to binary POI–PROTAC complex

formation, by immobilising on the of the proteins and flowing the analytes, PROTAC and the second protein, over the immobilised protein.[237] The cooperativity factor, which compares binding constants for the binary complex with binding constants for the ternary complex ($K_D^{binary}/K_D^{ternary}$), can give insights if the cooperativity for a given ternary complex is productive or unproductive.[238]

In vitro *assays*

When optimising the trialled assays using cell lysates, use of lysates of cells which have previously been employed for *in vitro* degradation assays, such as HeLa or HEK293 cells, or addition of purified protein to whole cell lysate could provide improved results.[230,231] Cell-free ubiquitination assays could further deliver evidence if lack of compound activity is due to inability of the PROTACs to induce ubiquitination of the target protein.[229] However, cell-free assays require a plethora of components, such as different enzymes involved in the ubiquitination cascade, and might not be physiologically relevant.[239]

Intracellular engagement assays and intracellular compound concentration

PROTAC-specific intracellular engagement assays determining cell permeability as well as recruitment of E3 ligases rely on either competition with known degraders or fluorescent probes. For example, competition experiments with a CRBN-targeting PROTAC known to degrade a FKB12-luciferase fusion protein have been reported.[240] Rescue of protein levels by co-treatment with a known degrader and a test compound would be an indicator of the test compound's cell-permeability and ability to intracellularly engage CRBN, thereby inhibiting the E3 ligase and preventing degradation of the fusion protein. Due to the luciferase portion of the fusion protein, the assay can be easily be read out by monitoring any increase in luminescence as a measure of protein rescue after treatment with the test compounds.[241] However, such assays are E3 ligase-specific and require synthesis of the necessary components. Commercially available assays exploit bioluminescent resonance energy transfer (BRET) to determine intracellular engagement of the compounds with E3 ligases (Figure 4.2). A fluorescent luciferase–E3 ligase fusion protein is expressed and the cells are treated with a cell-permeable fluorescent probe. By binding of the probe to the fusion protein, BRET is achieved through luminescent energy transfer from the fusion protein to the probe. When cells are treated with the test compound, and the compound binds to the E3 ligase portion of the fusion protein, a loss of BRET signal can be detected.[211]

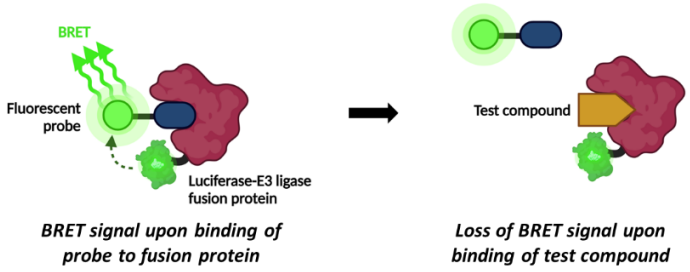

Figure 4.2: BRET target engagement assay - adapted from [211].

A more direct method to measure of intracellular compound concentration is liquid chromatography/tandem mass spectrometry (LC/MS/MS). Samples prepared from cells treated with the compounds to be assessed are separated by liquid chromatography, and components are analysed by tandem mass spectrometry. This double ionisation mass spectrometry technique provides a higher specificity by further fragmentation of the initial ions generated, allowing for analysis of complex mixtures and differentiation of ions with similar mass-to-charge (m/z) ratios (Figure 4.3).[210] However, it is not possible to distinguish between compounds that are associated with the cells, *i.e*. bound to the membrane or trapped in endosomes, and compound concentration in the cytosol necessary for activity. Moreover, lengthy optimisation procedures might be required, especially for compounds of suboptimal permeability which only display low intracellular concentrations.[158]

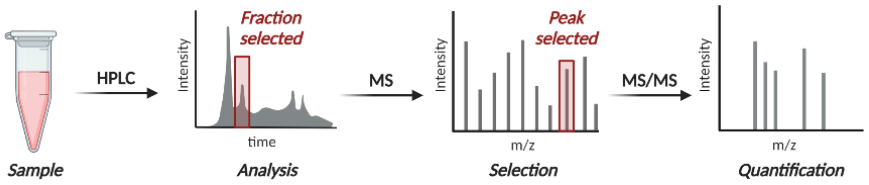

Figure 4.3: Liquid chromatography/tandem mass spectrometry (LC/MS/MS) work-flow - adapted from [210].

Assays assessing permeability and efflux

Permeability of the PROTACs, as well as the mechanisms of compound uptake, such as passive diffusion, active transport into the cell, but also efflux out of the cell can be determined with different permeability assays.[242] The experimental set-up is similar for the assays: A membrane or cell monolayer is used to separate two compartments, and diffusion or transport of drug molecules across this barrier is assessed by measuring and comparing concentrations of the compound in both compartments (Figure 4.4). The simplest type is the cell-free parallel artificial membrane permeability assay (PAMPA) as it uses, as the name suggests, an artificial membrane, usually hexadecane- or lipid-based, as barrier and is a model for passive diffusion (Figure 4.4 a).[243] The compound to be tested is

added to the donor compartment and diffuses through the membrane into the acceptor compartment, then concentrations of the compound in both departments are measured in order to determine the permeability.[244] Cell-based permeability assays commonly rely on Caco-2 cells, an immortalised human colon carcinoma cell line, which can be used as a model for absorption of drugs *in vivo* since the Caco-2 cell monolayer displays properties similar to those of intestinal epithelial cells.[207] As such, movement of drugs across the cell monolayer is mediated by passive diffusion and active transport of compounds in one direction (apical to basolateral, Figure 4.4 b) but also through efflux in the opposing direction (basolateral to apical). Hence permeability of the compounds as well as their susceptibility to efflux can be determined.[208]

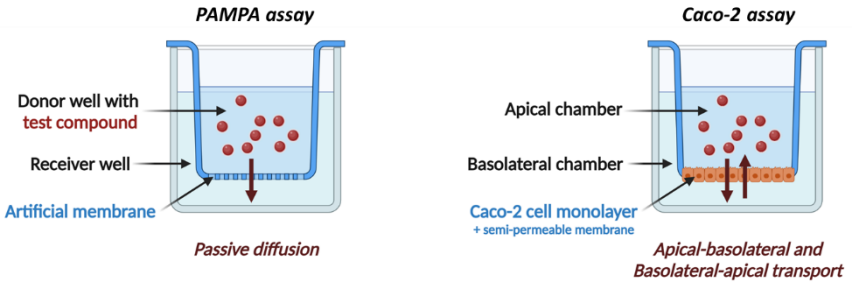

Figure 4.4: Set-up of permeability assays: a) PAMPA assay (adapted from [244]) and b) Caco-2 assay - adapted from [207].

PROTACs are known to be at risk of active efflux,[245] and the efflux rate of fascin ligands **FSCN-A (1.4)** and **FSCN-B (1.5)** was also determined to be high.[186] Since the majority of drug efflux can be attributed to efflux transporter P-glycoprotein (P-gp), it can be crucial to determine if the PROTACs are P-gp substrates using the MDCK-MDR1 permeability assay. Instead of a Caco-2 cell monolayer, it employs canine kidney MDCK cells expressing the *MDR1* gene which encodes for efflux transporter P-gp.[209] Should the PROTACs be determined to be P-gp substrates, employment of an P-gp inhibitor, such as verapamil, could prove beneficial when assessing compound activity in degradation assays. By impeding efflux of the compounds intracellular concentrations could be increased and sustained, impacting positively on activity of the PROTACs.[246]

Next-generation trifunctional PROTACs

A targeted delivery approach could aid in overcoming the challenges encountered with cell permeability of the synthesised PROTACs. Targeted delivery of therapeutic compounds is extensively exploited in the cancer context by conjugation of a targeting group to a drug molecule.[247-249] Due to changes in metabolism, cancer cells display increased uptake of certain cofactors compared to healthy cells, and therefore overexpress the corresponding

membrane receptor and transporters.[248] By conjugating a cofactor, such as glucose or folate, to a drug, the conjugate is taken up selectively by the cancer cells, thereby increasing intracellular concentrations of the drug inside the targeted cell.[247,249] This strategy has recently also found application in the PROTAC context, employing folate as targeting group[250,251] or conjugating the PROTAC to an antibody to mediate selective uptake.[252,253] Attachment of the targeting group through a self-immolating or intracellularly cleavable linker could ensure release of the active PROTAC from the targeting group once the conjugate is delivered across the cell membrane.[252,254] One proposed design features a targeting group attached to the hydroxyproline moiety *via* a reduction sensitive self-immolating linker, which upon linker cleavage inside the cell would release the active PROTAC (Figure 4.5).

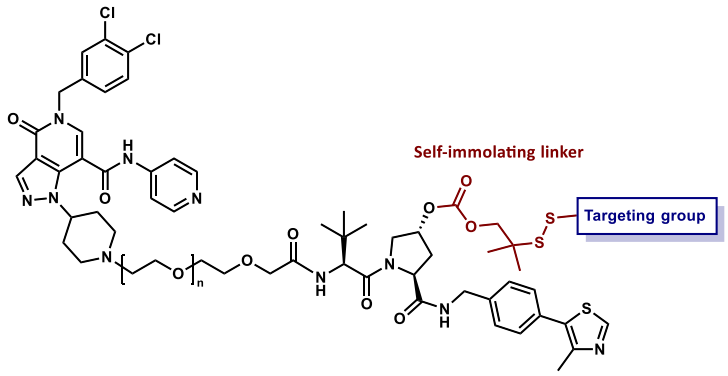

Figure 4.5: Proposed design of PROTAC conjugated through a self-immolating linker to a targeting group.

Based on the information obtained from additional assays, the PROTACs could be further optimised in order to achieve intracellular degradation of fascin. Alternatively, development of PROTACs conjugated to targeting groups could improve cellular uptake of the compounds to then induce fascin degradation. Through functional and phenotype assay similar to the experiments carried out for the HaloTag model system, the effect of fascin degradation on cell function and morphology could be determined, potentially paving the way for the development of a novel anti-metastatic therapeutic.

5 Experimental

Images in this thesis were created with Biorender.com unless referenced.

5.1 Biology materials and methods

5.1.1 Materials and reagents

Cell lines and bacterial strains

Name	Description / application	Source
	Cell lines	
HT-1080	Human fibrosarcoma	Beatson Institute
MIA-PaCa-2	Human pancreatic cancer	ATCC
MEF	Mouse embryonic fibroblasts	Beatson Institute
SK-OV-3	Human ovarian carcinoma	Beatson Institute
SK-OV-3 fascin KO	Human ovarian carcinoma with fascin deletion	This work
	Bacterial strains	
E. Coli *DH5α*	Chemically competent cells for cloning	Beatson Institute

Table 5.1: Cell lines and bacterial strains.

Reagents and solutions

Name	Source / composition
	Cell culture
Complete medium	DMEM with 10% FCS, 2 mM L-glutamine, 100 units/mL PenStrep
Serum-free medium (SFM)	DMEM with 10 units/mL L-glutamine, 10 µg/mL PenStrep
Dulbecco's Modified Eagle Medium (DMEM)	Gibco #21969-035
L-Glutamine	Gibco #253030-032
Penicillin Streptomycin (PenStrep)	LifeTechnologies #15140122
Foetal calf serum (FCS)	Gibco #10270-106
Phosphate buffered saline (PBS)	137 mM NaCl, 3.3 mM KCl, 8 mM Na_2HPO_4, 1.5 mM KH_2PO_4
2.5% Trypsin, no phenol red	Gibco #15090046
PBS-EDTA (PE) buffer	0.037% (w/v) EDTA in PBS
Freezing medium	50% complete medium, 40% FCS, 10% DMSO
DMSO	Fisher Chemical #D/4121/PB08

Protein analysis by immunoblotting (western blotting)	
Radioimmuno-precipitation assay (RIPA) cell lysis buffer	150 mM NaCl, 10 mM Tris-HCl pH 7.5, 1 mM EDTA, 1% Triton X-100, 0.1% SDS
Precision Red Advanced Assay solution	Cytoskeleton #ADV02
Reducing sample buffer (RSB)	10% NuPAGE reducing agent 10× in NuPAGE protein sample buffer 4×
NuPAGE protein sample buffer 4×	Invitrogen #NP0007
NuPAGE reducing agent 10×	Invitrogen #NP0004
4-12% NuPAGE Bis-Tris gels	Invitrogen #NP0321
4-Morpholinepropanesulfonic acid (MOPS) running buffer 20×	Novex #NP0001
PageRuler pre-stained protein ladder	Thermo Scientific #26616
Nitrocellulose blotting membrane (Protran 0.45 µm)	GE Healthcare #10600002
Transfer buffer	20% methanol, 10% SDS blotting buffer 10×, diluted in distilled water
Sodium dodecyl sulfate (SDS) blotting buffer 10×	1% SDS, 250 mM Tris-HCl, 1.92 M glycine
Blocking buffer	5% BSA diluted in TBS-T
Bovine serum albumin (BSA)	SigmaAldrich #10735108001
Tris-buffered saline with Tween20 (TBS-T)	10 mM Tris-HCl pH 7.4, 150 mM NaCl, 2.7 mM KCl, 0.1% polysorbate 20 (Tween20)
Immunofluorescence	
16% Paraformaldehyde (PFA)	Electron Microscopy Sciences #15710
Permeabilisation buffer	20 mM glycine, 0.5% Triton X-100
Matrix	
Matrigel basement membrane matrix	BD Biosciences #354234
Collagen I, rat tail	Corning #10224442
Lysate experiments	
Lysate buffer	50 mM Tris-HCl pH 7.5, 150 mM NaCl, 10% glycerol, 1 % NP40, 1 mM EDTA. Added freshly: 1 mM DTT, 1% protease and phosphatase inhibitor cocktails, 5 mM ATP, 5 mM $MgCl_2$
Surface plasmon resonance (SPR)	
Biacore T200	
NTA chip	GE Healthcare #BR10034
Biacore buffer	PBS, 0.05% P-20, 5% DMSO
Surfactant P-20	GE Healthcare #BR10054
Fascin (His tagged)	Beatson Institute
VHL (His & AVI tagged)	SinoBiological #17359-H40E

Cloning	
Super optimal broth (SOC) medium	2% trypton, 0.5% yeast extract, 10 mM NaCl, 2.5 mM KCl, 10mM $MgCl_2$, 20 mM glucose
LB agar plate	15 g agar/L of LB
Luria broth (LB)	Beatson Institute
Ampicillin	Sigma #A9518
CutSmart buffer	New England BioLabs #B7204S
T4 DNA ligase reaction buffer	New England BioLabs #B0202S
T4 DNA ligase	New England BioLabs #M0202S
Nuclease-free water	Ambion #AM9937
HindIII-HF	New England BioLabs #R3104S
BbsI	New England BioLabs #R0539S
High grade agarose	Melford #MB1200
Tris-acetate-EDTA (TAE) buffer 50×	2 M Tris, 50 mM EDTA, 1 M glacial acetic acid, pH ~8.3
Midori green	Nippon Genetics #MG04
DNA loading buffer 6×	12% glycerol, 60 mM Na_2EDTA, 0.6% SDS, 0.003% bromphenol blue, 0.003% xylene cyanol, H_2O
O'GeneRuler 1 kb	ThermoScientific #SM1163

Table 5.2: Reagents and solutions.

Antibodies and dyes

Target / Type	*Clone / Conjugate*	*Source species*	*Dilution (Application)*	*Source*
Primary antibodies				
VHL		Rabbit	1:1000 (WB)	Cell Signalling #68547
CRBN	D8H3S	Rabbit	1:1000 (WB)	Cell Signalling #71810
Fascin	55K-2	Mouse	1:500 (WB)	DAKO #M3567
Fascin	55K-2	Mouse	1:1000 (WB) 1:100 (IF)	Cell Marque #252M-15
HaloTag		Mouse	1:1000 (WB)	Promega #G921A
GFP		Rabbit	1:1000 (WB)	Cell Signalling #2555S
GAPDH	14C10	Rabbit	1:2000 (WB)	Cell Signalling #2118
GAPDH		Mouse	1:1000 (WB)	EMD Millipore #MAB374
Secondary antibodies				
Mouse IgG	AlexaFluor 680	Donkey	1:5000 (WB)	Invitrogen #A10038
Mouse IgG	DyLight800	Goat	1:5000 (WB)	Invitrogen #SA535521
Rabbit IgG	DyLight800	Goat	1:5000 (WB)	Invitrogen #SA535571
Rabbit IgG	AlexaFluor 680	Goat	1:5000 (WB)	Invitrogen #A21076
Mouse IgG	AlexaFluor 488	Goat	1:500 (IF)	Invitrogen #A12379

Dyes				
Cytox Red			1:10000 (dead cells)	Sartorius #4632
Sytox Green			1:10000 (dead cells)	Sartorius #4633
Nuclight Rapid Red			1:500 (live cells)	Sartorius #4717
Phalloidin 488 nm			1:200 (IF)	Molecular Probe #A12379
Hoechst 33342			1:1000 (IF)	Thermo Scientific #62249

Table 5.3: Primary antibodies, secondary antibodies and dyes.

Inhibitors and permeabilisers

Name	Application	Source
Inhibitors		
Protease inhibitor cocktail	Lysis buffer (WB)	ThermoFisher #1861279
Phosphatase inhibitor cocktail	Lysis buffer (WB)	ThermoFisher #78427
MG132	Proteasome inhibitor	SelleckChem #S2619
Cycloheximide	Protein synthesis inhibitor	Sigma #01810
Permeabilisers		
Digitonin	Cell permeabilisation	Sigma #D141
SLO	Cell permeabilisation	Abcam #126650
GDN	Cell permeabilisation	Avanti #850525P

Table 5.4: Inhibitors and permeabilisers.

Kits

Name	Application	Source
Nucleofection kits		
Amaxa Cell Line Nucleofector Kit V	Transient transfection	Lonza #VCA-1003
Amaxa Cell Line Nucleofector Kit T	Transient transfection	Lonza #VCA-1002
RNAimax	Transient transfection	ThermoFisher #13778150
In-Fusion HD Cloning Plus Kit	Cloning	Takara #638909
Zymoclean Gel DNA Recovery Kit	Cloning	Zymo Research #D4007
Monarch Plasmid Miniprep Kit	Cloning	New England BioLabs #T1010S

Table 5.5: Kits.

DNA constructs, siRNA sequences and CrispR sgRNA

Name	Backbone / sequence (5'-3')	Source
	DNA constructs	
pHaloTag-EGFP	pEGFP-N1	Addgene plasmid #86629
HaloTag-phospholamban	pFN21A	Fuller group
HaloTag-fascin	pFN21A	This work
pSpCas9(BB)-2A-GFP	PX458	Addgene plasmid #48138
Fascin gRNA1-Cas9-GFP	PX458	This work
Fascin gRNA2-Cas9-GFP	PX458	This work
	Silence RNA (siRNA)	
ON-TARGETplus siRNA human fascin-1	CGACUGCCGUUUCCUCAUC	Dharmacon #J-019576-05
ON-TARGETplus siRNA human fascin-1	CAAAGACUCCACAGGCAAA	Dharmacon #J-019576-06
ON-TARGETplus siRNA human fascin-1	GAGCAUGGCUUCAUCGGCU	Dharmacon #J-019576-07
ON-TARGETplus siRNA human fascin-1	GCAAGUUUGUGACCUCCAA	Dharmacon #J-019576-08
AllStars negative control	n/a	Qiagen #SI03650318
	CRISPR guide RNA (gRNA) sequences	
Human fascin (5'-3')	CACCGCCCCATCATCGTGTTCCGCG	Invitrogen, Designed by Heather Spence
Human fascin (3'-5')	AAACCGCGGAACACGATGATGGGGC	Invitrogen, Designed by Heather Spence
Human fascin (5'-3')	CACCGCCCCGCGGAACACGATGATG	Invitrogen, Designed by Heather Spence
Human fascin (3'-5')	AAACCATCATCGTGTTCCGCGGGGC	Invitrogen, Designed by Heather Spence
	Polymerase chain reaction (PCR) primers	
HaloTag destination vector forward	ACGAATTCGGGCTCGGTACC	Designed by Will Fuller
HaloTag destination vector reverse	GGCGATCGCGTTATCGCTC	Designed by Will Fuller
Fascin insert forward	GATAACGCGATCGCCATGACCGCCAACGGCACAGC	Designed by Will Fuller
Fascin insert reverse	CGAGCCCGAATTCGTCTAGTACTCCCAGAGCGAGGC	Designed by Will Fuller
	Sequencing primers	
CMV forward	CGCAAATGGGCGGTAGGCGTG	Invitrogen
HaloTag forward	GATCTGTACTTTCAGAGCGAT	Invitrogen
HaloTag reverse	CCCGGGTACCGAGCCCGAATTCGT	Invitrogen
CRISPR plasmids forward	TTTATGGCGAGGCGGCGG	Invitrogen

Table 5.6: DNA constructs, siRNA sequences, CrispR sgRNA and primers.

Cell culture plastic ware and consumables

Name	*Description / application*	*Source*
Culture flasks	Tissue culture	Falcon #353136
6-well plates	Tissue culture	Falcon #353146
12-well plates	Tissue culture	Falcon #353043
96-well plates	Tissue culture	Falcon #353072
96-well ImageLock plates	Live-cell imaging	Sartorius #4379
10 cm plastic plate	Tissue culture	Corning #430147
25 cm plastic plate	Tissue culture	Falcon #353025
35 mm glass-bottom dish	Live-cell imaging	MatTec #36G-1.5 20-C
2 mL cryovials	Cryopreservation	Greiner bio-one #126263

Table 5.7: Cell culture plastic ware and consumables.

Software and websites

Name	*Provider*	*Version*
Image StudioLite	Li-Cor Biosciences	5.2.5
IncuCyte Zoom	IncuCyte Biosciences	2018A
Fiji	National Health Institute, USA	1.53e
Chemotaxis and Migration Tool	Ibidi GmbH	2.0
Basic Local Alignment Search Tool (BLAST)	U.S. National Library of Medicine	
Prism	GraphPad	9.3.0
PyMOL	Schrödinger	2.4.0
Hermes/GOLD	Cambridge Crystallographic Data Centre	2020.2.0
Mercury	Cambridge Crystallographic Data Centre	2020.2.0
ChemDraw	PerkinElmer Informatics	20.1.0
SwissADME	Swiss Institute of Bioinformatics	
BioRender		

Table 5.8: Softwares and websites.

5.1.2 Cell biology methods

Cell culture

- *Cell growth conditions, maintenance and counting*

All cell lines were cultured in complete medium and maintained in culture flasks at 37 °C in a humidified incubator with 5% CO_2. Once 80% confluency was reached, cells were washed once with 1× PBS. Cells were detached using an appropriate volume of trypsin diluted at 0.25% in PE buffer and incubated at 37 °C. Cell detachment was checked regularly under a light microscope. Once fully detached, cells were resuspended in complete medium, inhibiting trypsin activity.

Cells were counted prior to each experiment or passage. To do so, 10 µL from the cell suspension was carefully added on the cell counter (DeNovix CellDrop FL). The concentration of cells was automatically calculated and the procedure was performed at least two times to reduce any technical errors.

An appropriate amount was taken from the cell suspension, distributed into new culture flasks with fresh complete medium and maintained at 37 °C in a humidified incubator and perfused with 5% CO_2. Cells were passaged at roughly 1:10 and the number of passages was recorded until reaching passage 30.

- *Cryopreservation and cell recovery*

For cryopreservation, cells were grown in culture flasks until optimally confluent and detached as previously described. The cell suspension was collected in a 15 mL falcon tube and centrifuged for 5 minutes at 1000 rpm. The supernatant was discarded and the cell pellet was resuspended in freezing medium. 1 mL of the fresh cell suspension was aliquoted into a 2 mL cryovial and immediately frozen at –80 °C. Once frozen, the cryovials were transferred to a liquid nitrogen tank and stored until recovery when required.

For cell recovery, cryovials were removed from the liquid nitrogen tank and quickly transferred to a water bath at 37 °C. Once thawed, cells were gently resuspended in fresh complete medium which had previously been warmed to 37 °C. For removal of DMSO from the medium, the cell suspension was centrifuged for 5 minutes at 1000 rpm and the supernatant was discarded. Finally, cell pellets were transferred in fresh complete medium in a culture flask and incubated in a humidified incubator at 37 °C supplied with 5% CO_2. Cells were regularly checked to assess attachment. Fresh complete medium was added on the day following thawing, and cells were allowed to recover for at least one week before carrying out experiments.

Transient transfections

- *Transient transfection with plasmid DNA*

Amaxa Cell Line Nucleofector Kit V was used for transfection of SK-OV-3 and MIA-PaCa-2 cells whereas Amaxa Cell Line Nucleofector Kit T was used for transfection of HT-1080 cells. A transfection master mix was prepared by mixing 82 µL Nucleofector solution V or T with 18 µL Supplement 1. Cells were collected and counted as previously described. Approximately 3×10^6 cells were resuspended in the previously prepared master mix and 3 µg DNA was added, and the suspension was gently mixed before transferring it into an electroporation vial. Cells were electroporated with a Nucleofector 2b device, using programme V-005 for SK-OV-3 cells, T-027 for MIA-PaCa-2 cells and L-005 for HT-1080 cells. Cells were resuspended in warm complete medium in a culture flask and incubated in a humidified incubator at 37 °C supplied with 5% CO_2 overnight before carrying out experiments.

- *Transient transfection with siRNA*

The siRNA mixture was prepared for transfection of 2 wells of a 6-well tissue culture plate for each siRNA treatment. To Eppendorf tubes containing 5 µL siRNA or siRNA control, 195 µL of nuclease-free water was added. In a Falcon tube, 38 µL of RNAimax was added to 3.8 mL of SFM and mixed. 600 µL of the RNAimax/SFM mixture was added to each of the Eppendorf tubes containing siRNA or siRNA control, gently mixed and incubated for 15 minutes at room temperature. Cells were collected and counted as previously described, resuspended and plated onto 6-well tissue culture plates at approximately 3×10^5 cells per well in 1.6 mL complete medium. 400 µL of the respective siRNA/RNAimax/SFM mixtures were added dropwise to each well, tissue culture plates were gently swirled and incubated in a humidified incubator at 37 °C supplied with 5% CO_2 for 48 hours before carrying out experiments.

Protein analysis by immunoblotting (western blotting)

- *Preparation of total cell lysates*

Culture medium was aspirated from cultured cells and cells were washed three times with PBS. Plates were then transferred onto ice and ice-cold RIPA cell lysis buffer supplemented with phosphatase and protease inhibitor cocktails was added to the wells. Cells were scraped, cell lysate was transferred into chilled Eppendorf tubes and centrifuged at 13000

rpm for 10 minutes at 4 °C. The supernatant was collected and either directly subjected to sodium dodecyl sulfate–polyacrylamide gel electrophoresis (SDS–PAGE) and immunoblotted or stored at -20 °C until required for analysis.

- *Protein quantification*

Quantification of protein concentration in cell lysates was carried out using Precision Red advanced protein assay. 5 µL of cell lysate was mixed with 995 µL of Precision Red Advanced Assay solution in a cuvette and incubated for 30 seconds at room temperature. The absorbance was measured at OD_{600nm}, protein concentration determined and typically 10 to 20 µg of protein per sample was resolved by SDS–PAGE.

- *Protein electrophoresis by SDS–PAGE*

An appropriate amount of cell lysate was diluted in RSB, samples were boiled for 5 minutes at 100 °C and centrifuged for 5 minutes at 13000 rpm. Typically, 15 to 25 µL protein samples in RSB were loaded onto SDS-PAGE using 4-12% NuPAGE Novex Bis-Tris acrylamide gels, along with 5 µL PageRuler pre-stained protein ladder as molecular weight marker. Gels were resolved in NuPAGE MOPS running buffer using XCell SureLock mini-cells at 180 V for 60 minutes.

- *Electrophoretic transfer*

Proteins resolved by SDS-PAGE were transferred onto Protran 0.45 µm nitrocellulose blotting membrane using XCell II blot modules. Proteins were transferred in transfer buffer at 30 V for 90 minutes.

- *Membrane blocking and antibody probing*

Nitrocellulose membranes were blocked with blocking buffer for 1 hour at room temperature. Membranes were probed with primary antibodies diluted to the appropriate concentration in blocking buffer and incubated overnight at 4 °C. Membranes were washed four times for 10 minutes with TBS-T before incubation with appropriate fluorescent dye-conjugated secondary antibodies diluted in blocking buffer for 1 hour at room temperature, protected from sources of light. Membranes were washed four times for 10 minutes with TBS-T and maintained in water before visualisation. All incubation steps were performed under gentle agitation.

- *Membrane scanning and protein quantification*

Membranes were scanned on the Li-Cor Odyssey CLx InfraRed Imaging System (700 nm and 800 nm channels), using automatic intensity setting mode. Images were processed as grey scale picture and signal intensity was calculated using the Li-Cor Image StudioLite software.

Viability assays with live-cell microscopy

- *Viability assays with compounds*

Cells were collected and counted as previously described, resuspended and plated onto 96-well tissue culture plates at approximately 1×10^3 cells per well in 100 µL complete medium, and allowed to adhere overnight in a humidified incubator at 37 °C supplied with 5% CO_2. Culture medium was aspirated from cultured cells the following day, cells were washed three times with PBS and 100 µL of fresh complete medium with indicated concentrations of compounds, Nuclight Rapid Red and Sytox Green was added. Images were acquired hourly using the IncuCyte Zoom system with automated widefield brightfield and fluorescence with a 10× objective lens for the indicated times and data was analysed using IncuCyte Zoom software.

- *Viability assays with permeabilisers*

Cells were collected and counted as previously described, resuspended and plated onto 12-well tissue culture plates at approximately 1×10^4 cells per well in 1 mL complete medium, and allowed to adhere overnight in a humidified incubator at 37 °C supplied with 5% CO_2. Culture medium was aspirated from cultured cells the following day, cells were washed three times with PBS and 1 mL of fresh PBS with indicated concentrations of permeabilisers or PBS only was added. After incubation for indicated times on ice (digitonin and GDN) or at 37 °C (SLO), cells were washed three times with PBS and 1 mL of complete medium with Sytox Green was added. Images were acquired hourly using the IncuCyte Zoom system with automated widefield brightfield and fluorescence with a 10× objective lens for the indicated times and data was analysed using IncuCyte Zoom software.

Dose-response and time-course assays with compounds

- *Compound stock solutions and dilutions*

Compounds were kept as 10 mM DMSO stock solutions. For treatment of cells, a serial dilution in PBS was carried out prior to experiments. A 400× dilution factor was used for addition of 5 µL of the appropriate concentration to 2 mL of complete medium per well for 6-well tissue culture plates and a 20× dilution factor was used for 100 µL of complete medium per well for 96-well tissue culture plates, respectively.

- *Dose-response and time-course assays*

Cells were collected and counted as previously described, resuspended and plated onto 6-well tissue culture plates at approximately 1×10^5 cells per well in 2 mL complete medium, and allowed to adhere overnight in a humidified incubator at 37 °C supplied with 5% CO_2. Culture medium was aspirated from cultured cells the following day, cells were washed three times with PBS and 2 mL of fresh complete medium was added. Cells were treated with 5 µL of compound in indicated concentrations or DMSO and incubated in a humidified incubator at 37 °C supplied with 5% CO_2 for indicated times before protein analysis by immunoblotting.

- *Permeabilisation with electroporation*

Cells were collected and counted as previously described. Approximately 1×10^5 cells were resuspended in 100 µL complete medium or Nucleofector solution and containing 5 µL of either the compound in indicated concentrations or DMSO. Electroporation was performed using the Nucleofector 2b device according to the manufacturer instructions. Cells were resuspended in 2 mL complete medium and incubated in 6-well tissue culture plates in a humidified incubator at 37 °C supplied with 5% CO_2 for indicated times before protein analysis by immunoblotting.

- *Permeabilisation with permeabilisers*

Cells were collected and counted as previously described, resuspended and plated onto 6-well tissue culture plates at approximately 1×10^5 cells per well in 2 mL complete medium, and allowed to adhere overnight in a humidified incubator at 37 °C supplied with 5% CO_2. Culture medium was aspirated from cultured cells the following day, cells were washed three times with PBS and 2 mL of either PBS alone or PBS containing the indicated concentrations of permeabilisers was added. After incubation for indicated times on ice

(digitonin and GDN) or at 37 °C (SLO), cells were washed three times with PBS and 2 mL of complete medium was added. Cells were treated with 5 µL of compound in indicated concentrations or DMSO and incubated in a humidified incubator at 37 °C supplied with 5% CO_2 for indicated times before protein analysis by immunoblotting.

- *Lysate assay*

After cells were grown to full confluency on 10 cm tissue culture dishes, culture medium was aspirated, cells were washed three times with PBS and 1 mL of ice-cold PBS was added. Through careful scraping with a cell scraper, cells were collected into an Eppendorf tube and centrifuged at 5000 rpm for 5 minutes. The supernatant was discarded and the pellet was either stored at –20 °C until required for experiments or resuspended in 5 volumes of Lysate buffer by careful pipetting. Cells were incubated on ice for 30 minutes and intermittently vortexed before the lysate was centrifuged at 13000 rpm for 10 minutes at 4 °C. The supernatant was collected and protein concentration was measured as previously described. Appropriate amounts of cell lysate (20 µg, 50 µg or 100 µg) were aliquoted into Eppendorf tubes for each reaction and compounds were added at indicated concentrations. After incubation for indicated times, either on ice, at room temperature or at 37 °C, reducing buffer (1 in 4) was added and samples were boiled at 100 °C for 10 minutes, centrifuged and resolved by immunoblotting as previously described.

Proliferation, random migration and wound-healing assay

- *Proliferation and random migration assay*

Cells were collected and counted as previously described, resuspended and plated onto 96-well tissue culture plates at approximately 5×10^2 cells per well in 100 µL complete medium, and allowed to adhere overnight in a humidified incubator at 37 °C supplied with 5% CO_2. Culture medium was aspirated from cultured cells the following day, cells were washed three times with PBS and 100 µL of fresh complete medium with Nuclight Rapid Red was added. Images were acquired hourly using the IncuCyte Zoom system with automated widefield brightfield and fluorescence with a 10× objective lens for the indicated times and data was analysed using IncuCyte Zoom software.

$$\text{Normalised proliferation index} = \frac{\text{cell numbers } (t_n)}{\text{cell numbers } (t_0)}$$

For random migrations assays, cells were individually tracked using the MTrackJ plugin in Fiji. The Chemotaxis and Migration Tool from ibidi was used to plot individual x-y points from each track and to generate a spider plot and calculate velocity.

- *Wound-healing assay*

Cells were collected and counted as previously described, resuspended and plated onto 96-well ImageLock plates (Sartorius) at approximately 4×10^4 cells per well in 100 µL complete medium. For invasion assays, wells were coated with 50 µL of 1% Matrigel in complete medium for 4 hours in a humidified incubator at 37 °C supplied with 5% CO_2 before cell seeding. Cells were allowed to adhere overnight in a humidified incubator at 37 °C supplied with 5% CO_2. The following day, cells were wounded using the IncuCyte WoundMaker according to manufacturer instructions, culture medium was aspirated and cells were washed three times with PBS to remove cell debris. 100 µL complete medium was added to each well. For invasion assays, a 50 µL of Matrigel (4 mg/mL) or a Matrigel/collagen I mixture (2 mg/mL each) in complete medium was added and cells were incubated for 1 hour in a humidified incubator at 37 °C supplied with 5% CO_2 before addition of 100 µL complete medium. Images were acquired hourly using the IncuCyte Zoom system with automated widefield brightfield and fluorescence with a 10× objective lens for the indicated times and data was analysed using IncuCyte Zoom software.

$$\text{Wound closing rate} = \sum \frac{\text{wound width } (t_n) - \text{wound width}(t_{n-1})}{t} \ (\mu m/h)$$

$$\text{Relative wound density} = \frac{\text{density of wound region } (t_n) - \text{density of cell region } (t_n)}{\text{density of wound region } (t_0) - \text{density of cell region } (t_0)} \times 100 \ (\%)$$

Immunofluorescence

- *Phalloidin staining*

Cells were collected and counted as previously described, resuspended and plated onto 35 mm glass-bottom dishes at approximately 5×10^3 cells per dish in 2 mL complete medium, and allowed to adhere overnight in a humidified incubator at 37 °C supplied with 5% CO_2. Culture medium was aspirated, cells were washed three times with PBS and fixed using 1 mL of 4% PFA in PBS for 10 minutes and then washed three times with PBS. For permeabilisation, cells were incubated with 200 µL permeabilisation buffer for 5 minutes and then washed three times with PBS. Cells were stained with 1 mL AlexaFluor488-conjugated-phalloidin dye in PBS for 30 minutes, before cells were washed three times with

PBS and 1 mL of fresh PBS was added. Images were acquired by Nikki Paul using a Zeiss 880 LSM confocal microscope with Airyscan, using a Plan-Apochromat 63×/1.4 Oil DIC M2 objective and 488nm (Argon) laser line. All images were acquired using 2% laser power and 1.8× zoom. Airyscan processing was performed using Zen Black and images were analysed using Fiji (ImageJ) software.

- *Fascin staining*

Cells were collected and counted as previously described, resuspended and plated onto 35 mm glass-bottom dishes at approximately 5×10^3 cells per dish in 2 mL complete medium, and allowed to adhere overnight in a humidified incubator at 37 °C supplied with 5% CO_2. Culture medium was aspirated, cells were washed three times with PBS before fixing and permeabilisation with methanol at –20° C for 15 minutes. Cells were washed three times with PBS and blocked with 1% BSA for 30 minutes, then incubated with 200 µL fascin antibody in 1% BSA for 1 hour. The antibody was washed off with PBS three times and then incubated with 200 µL AlexaFluor488-conjugated-secondary antibody in 1% BSA for 1 hour. The secondary antibody was washed off with PBS three times. Images were acquired by Nikki Paul using a Zeiss 880 LSM confocal microscope with Airyscan, using a Plan-Apochromat 63×/1.4 Oil DIC M2 objective and 488nm (Argon) laser line. All images were acquired using 5% laser power and 1.8× zoom. Airyscan processing was performed using Zen Black and images were analysed using Fiji (ImageJ) Software.

5.1.3 Molecular biology techniques

In-Fusion cloning

Destination vector and insert were amplified with complementary 15 bp extensions by PCR using accordingly designed oligonucleotide primers. The PCR fragments were digested with Dpn1 overnight, purified and the fascin insert was annealed to the linearised HaloTag vector using the In-Fusion cloning method, as per the manufacturers' instructions.

Transformation, inoculation and screening of transformants

50 µL of *E. coli* DH5α was allowed to thaw on ice for 20 minutes. 2.5 µg of HaloTag-fascin DNA was added to the bacteria, gently flicked to mix and incubated on ice for 15 minutes. Bacteria were then heat-shocked in a 42 °C water bath for 45 seconds to allow transient

permeabilisation of the membrane and internalisation of the DNA, followed by recovery on ice for 2 minutes. Then 1 mL of SOC medium was added and bacteria were incubated at 37 °C with constant agitation at 200 rpm for 1 hour. Then, 100 µL of the bacteria suspension was spread on pre-warmed LB agar plates with ampicillin (50 µg/mL) and plates were incubated overnight in a 37 °C incubator. The following day, 8 colonies were selected with a sterile tip and used to inoculate 5 mL of LB containing ampicillin (100 µg/mL) each. Cultures were grown under energetic shaking at 200 rpm at 37 °C overnight. Plasmids were purified using a Monarch Plasmid Miniprep Kit according to the manufacturers' instructions and 2 µL DNA of each culture were used for screening by restriction enzyme digestion.

Restriction enzyme digestion

Reactions were set up using 28 µL of a master mix consisting of 3 µL of Cut Smart Buffer, 24 µL nuclease-free water and 1 µL of restriction enzyme HindIII-HF, and 2 µL DNA. The mixture was left for 1 hour in a 37 °C water bath before resolution by agarose gel electrophoresis.

Agarose gel electrophoresis

DNA gels were prepared with 1% high-grade agarose diluted in TAE buffer, boiled until completely dissolved and 1% Midori green was added before casting the gel. DNA was diluted with 10 µL DNA loading buffer before loading it onto the gel along with a 1 kb DNA ladder. Gels were run in TAE buffer at 100 V for 35 minutes.

Agarose gel purification

DNA fragments were quickly excised under a UV lamp, and DNA was purified using Zymoclean Gel DNA Recovery Kit accordingly to manufacturer instructions. Essentially, agarose fragments were heated to 50 °C in 3 volumes of ADB buffer until completely dissolved. The mixture was then loaded onto a spin column centrifuged at 1000 rpm for 30 seconds. Filters were washed twice with 200 µL washing buffer and DNA was eluted using 15 µL of pre-heated nuclease-free water.

Sequencing and Maxiprep

Clones containing the correct insert were sent for sequencing by Beatson Central Services. DNA sequences were confirmed by sequence alignment using BLAST. DNA was then transformed into new *E. coli* DH5α and 250 mL culture was used for Maxiprep. Purification of the plasmids were performed by Beatson Central Services.

Generation and selection of stable cell line with CRISPR-Cas9 genome editing

- *Generation of gRNA-Cas9-GFP plasmid*

Annealing reactions for each gRNA were set up using 3 µL of T4 DNA ligase reaction buffer, 0.7 µL each of forward and reverse oligonucleotides in 25.6 µL of nuclease-free water. The mixture was added to a 100 °C heat block for 10 minutes and then allowed to slowly cool to room temperature. 1 ug of pSpCas9(BB)-2A-GFP vector was digested using 1 µL of BsbI, 1 µL of Cut Smart Buffer in 7 µL of nuclease-free water at 37 °C for 1 hour. 1 µl of oligonucleotides was ligated to 1 µl of linearised vector with 1 µL of T4 DNA ligase and 1 µL of T4 ligase reaction buffer in 6 µL of nuclease-free water in a thermocycler at 22.5 °C for 1 hour.

- *Transformation, inoculation, Miniprep, sequencing and Maxiprep*

50 µL of *E. coli* DH5α was allowed to warm on ice for 15 minutes. 5 µL of the ligation mixture was added to the bacteria, gently flicked to mix and incubated on ice for 10 minutes. The bacteria were heat shocked in a 42 °C water bath for 30 seconds to allow transient permeabilisation of the membrane and internalisation of the DNA, followed by recovery on ice for 2 minutes. Then 450 µL of SOC medium was added and bacteria were incubated at 37 °C with constant agitation at 200 rpm for 30 minutes. 100 µL of the bacteria suspension was spread on pre-warmed LB agar plates with ampicillin (50 µg/mL) and plates were incubated overnight in a 37 °C incubator. The following day, 10 colonies were selected with a sterile tip and used to inoculate 5 mL of LB containing ampicillin (100 µg/mL) each. Cultures were grown under energetic shaking at 200 rpm at 37 °C overnight. Bacteria were collected by centrifugation and sent for Miniprep and sequencing to Beatson Central Services. DNA sequences were confirmed by sequence alignment using BLAST. DNA was then transformed in new *E. coli* DH5α and 250 mL culture was used for maxiprep. Purification of the plasmids were performed by Beatson Central Services.

- *Transient transfection with plasmid DNA*

Transfections of SK-OV-3 cells with gRNA1-Cas9-GFP plasmid, gRNA2-Cas9-GFP plasmid or empty Cas9-GFP plasmid was carried out as previously described (Chapter 5.1.2). Cells were incubated in a humidified incubator at 37 °C supplied with 5% CO_2 for 36 hours to allow for GFP expression before submission for fluorescence-activated cell sorting (FACS).

- *Fluorescence-activated cell sorting (FACS) and single cell clones*

Cells were collected as previously described, resuspended in SFM and filtered into flow cytometry tubes. FACS was carried out by Beatson Central Services, and individual cells were plated onto 96-well tissue culture plates using serial dilutions. Cells were monitored daily and wells containing single cells were selected for screening for knock-out populations. Once sufficient cells were available, fascin levels were determined using immunoblotting, as previously described, and appropriate cell populations were selected for further experiments or cryopreservation.

5.1.4 Protein biochemistry methods

Surface plasmon resonance (SPR)

SPR analysis was performed by Katie Pollock using Biacore T200 (GE Healthcare). Using GF buffer complemented with 5mM $MgCl_2$ and 0.5% of surfactant P20 as running buffer, His-tagged protein were immobilised at 22 °C onto NTA sensor chip. Immobilisation was done at a flow rate of 10 µL/min. Serial dilution of each analyte was injected across a reference flow cell and the flow cell containing the ligand at a flow rate of 30 µL/min. Data were solvent corrected, reference subtracted, quality controlled and evaluated using the Biacore T200 evaluation software. Affinity was determined by curve fitting a 1:1 binding model.

5.1.5 Statistical analysis

The number of biological repeats is described in the figures. Datasets were analysed using Graph Pad Prism and data are presented as mean with error bars representing standard error of the mean (SEM). Unpaired t-test is are used to compare the mean between 2 samples (ns: $p > 0.05$, *: $p \leq 0.05$, **: $p \leq 0.01$, ***: $p \leq 0.001$).

5.2 Chemistry experimental

5.2.1 Calculations of physicochemical properties

Physicochemical descriptors were calculated using ChemDraw v20.1 for MW, HBD, HBA, NRotB and tPSA based on chemical structures. cLogP was predicted using SwissADME (http://www.swissadme.ch) with molecules submitted in their neutral form.[184]

5.2.2 Protein–ligand docking

Protein crystal structures were obtained from the Protein Data Bank (PDB, https://www.rcsb.org/) and protein–ligand docking was carried out with CCDC CSD Discovery Suite v2020.2.0. Mercury was used for conformer generation of ligand structures prepared in ChemDraw v20.1. Protein–ligand docking was performed using the GOLD module in Hermes. Docking solutions were visualised in PyMOL v2.4.0.

Docking of FSCN-A (1.4) and FSCN-C (1.7) into fascin

Single conformers of **FSCN-A (1.4)** and **FSCN-C (1.7)** were generated in Mercury based on structures drawn in ChemDraw. The fascin co-crystal structure with **FSCN-B (1.5)** obtained from PDB (PDB ID 6i18) was loaded into Hermes and standardised. Water molecules within 6 Å of the ligand binding site were selected for docking (633, 644, 661, 687, 702, 722, 755, 775, 800, 830, 877, 913) and the remaining water molecules were deleted. Using the GOLD wizard, standard protonation rules were applied. The docking site was defined as residues within 6 Å of the ligand binding site, and previously selected water molecules were considered for docking. The generated conformers of **FSCN-A (1.4)** and **FSCN-C (1.7)** and the extracted ligand **FSCN-B (1.5)** were selected as ligands to be docked, using the extracted ligand **FSCN-B (1.5)** as reference. CHEMPLP was used as scoring functions and docking solutions were selected based on docking score as well as visual fit. The selected docking solutions and the protein structure were visualised in PyMOL.

5.2.3 General methods

All reagents were purchased from commercial suppliers and used without further purification unless otherwise stated. Reactions requiring air-sensitive reagents and dry solvents were performed in glassware that had been dried in an oven at 150 °C or flame-dried *in vacuo* prior to use. These reactions were carried out under argon atmosphere

under the exclusion of air. Reactions were monitored by thin-layer chromatography (TLC) on Merck silica gel 60 covered aluminium sheets. TLC plates were visualised under UV light, and, when required, with an acidic ethanolic anisaldehyde solution or a $KMnO_4$ solution. NMR spectra were recorded on a Bruker DPX-400 spectrometer (^{1}H NMR at 400 MHz, ^{13}C NMR at 101 MHz and ^{19}F NMR at 377 MHz) or a Bruker DPX-500 spectrometer (^{1}H NMR at 500 MHz and ^{13}C NMR at 126 MHz). Chemical shifts are reported in ppm. ^{1}H NMR spectra were recorded with chloroform-*d*, methanol-d_4 or DMSO-d_6 as the solvent using residual $CHCl_3$ (δ = 7.26), or CHD_2OD (δ = 3.31) or $(CHD_2)SOCD_3$ (δ = 2.50) as internal standard, and for ^{13}C NMR spectra the chemical shifts are reported relative to the central resonance of $CDCl_3$ (δ = 77.16), CD_3OD (δ = 49.00) or $(CD_3)_2SO$ (δ = 39.52). Signals in the obtained spectra are reported as singlet (s), doublet (d), triplet (t), quartet (q), multiplet (m), broad (br), or a combination of these, to describe the observed spin–spin coupling pattern. Spin–spin coupling constants are reported in Hertz (Hz) and are uncorrected. Two-dimensional NMR spectroscopy (COSY, HSQC, HMBC, NOESY) was employed where appropriate to assist the assignment of signals in the ^{1}H and ^{13}C NMR spectra. The selected assigned resonances were used to confirm connectivity or transformation. IR spectra were obtained on a Shimadzu FTIR-8400 instrument with a Golden Gate™ attachment using a type IIa diamond as a single reflection element for the IR spectra of the solid or liquid compounds to be detected directly (thin layer). High-resolution mass spectra (HRMS) were recorded using ESI or EI conditions by the analytical services at the University of Glasgow. Liquid chromatography–mass spectrometry (LCMS) was recorded on a Thermo Scientific Dionex UltiMate 3000 LC system coupled with a Thermo Scientific LCQ Fleet quadrupole mass spectrometer using positive mode electrospray ionisation (ESI+). A Dr Maisch GmbH Reprosil Gold 120 C18 3 µm 150×4 mm column was used with UV absorption detected at 214 nm. A linear gradient of 5% to 95% HPLC-grade acetonitrile in ultra-pure water with 0.1% trifluoroacetic acid over 10 minutes was utilised with a flow rate of 1 mL min^{-1}. Semi-preparative reverse-phase HPLC was performed on a Gilson HPLC system equipped with Gilson 306 pumps, a Phenomenex Synergi C18 (80 Å, 10 µm, 250×21.2 mm) column at a flow rate of 8 mL min^{-1}. Non-linear gradients between 5% to 100% HPLC grade acetonitrile in ultra-pure water with 0.1% trifluoroacetic acid were utilised. UV absorption was detected at 214 nm and 254 nm using a Gilson 155 UV/VIS detector. Collected fractions were then lyophilised using a Thermo Heto PowerDry LL3000 lyophiliser.

5.2.4 Preparation of compounds

Preparation of E3 ligase ligands

- *VHL ligand* ***VHL-1 (2.3)*** *and epimer control* **cis*VHL-1 (2.4)***:

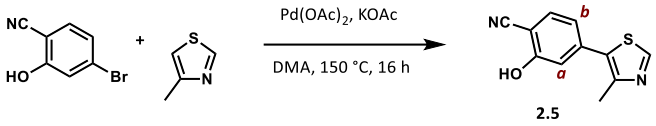

2.5

2.5: To a stirred to solution of 4-bromo-2-hydroxybenzonitrile (9.0 g, 45 mmol, 1 equiv) in *N,N*-dimethylacetamide (153 mL, 0.3 M) was added 4-methylthiazole (8.3 mL, 91 mmol, 2 equiv), palladium(II) acetate (99 mg, 0.45 mmol, 1 mol%) and potassium acetate (9.0 g, 91 mmol, 2 equiv) and the resulting suspension was stirred at 150 °C for 16 hours. The reaction mixture was allowed to cool to room temperature, diluted with water (200 mL) and extracted with ethyl acetate (3 × 200 mL). The combined organic extracts were washed with brine (2 × 200 mL) and 5% aqueous lithium chloride (2 × 200 mL), dried over magnesium sulfate, filtered and concentrated *in vacuo.* Purification by column chromatography on silica gel using an eluent of 30% to 100% ethyl acetate in dichloromethane afforded nitrile **2.5** (4.7 g, 22 mmol, 53%) as a light yellow amorphous solid.

Analytical data observed were in accordance with literature values.[103]

^{1}H NMR (400 MHz, methanol-d_4) δ 8.95 (1H, s, thiazole-CH), 7.64 – 7.57 (1H, m, Ar-CH), 7.12 – 7.02 (2H, m, 2 × Ar-C**H**$^{a/b}$), 2.53 (3H, s, -CH_3). ^{13}C NMR (101 MHz, methanol-d_4) δ 161.7 (Ar-C), 153.9 (thiazole-CH), 150.5 (thiazole-C), 139.3 (Ar-C), 134.9 (Ar-CH), 131.9 (thiazole-C), 121.6 (Ar-**C**^{a}H), 117.4 (nitrile-C), 117.3 (Ar-**C**^{b}H), 100.4 (Ar-C), 16.2 (-CH_3). LCMS (ESI) mass calculated for $C_{11}H_9N_2OS$ $[M+H]^+$ m/z 217.04, found m/z 217.17 with t_R = 5.40 min.

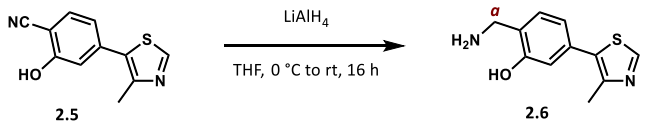

2.5 2.6

2.6: To a dry flask charged with argon was added anhydrous tetrahydrofuran (6 mL, 0.2 M) and nitrile **2.5** (250 mg, 1.16 mmol, 1 equiv) and the reaction mixture was cooled to 0 °C. Lithium aluminium hydride (216 mg, 5.80 mmol, 5 equiv) was added portion-wise and the resulting suspension was stirred at 0 °C for 1 hour, then allowed to warm to room temperature and stirred for a further 16 hours. Once complete consumption of the starting material was confirmed by TLC, the reaction mixture was diluted with anhydrous tetrahydrofuran (10 mL) and cooled to 0 °C. The reaction was quenched by dropwise

addition of water (216 µL), followed by 3 M aqueous sodium hydroxide (216 µL) and water (3 × 216 µL), and the resulting suspension was stirred vigorously at room temperature for 30 minutes. The precipitate was filtered and washed with a copious amount of tetrahydrofuran, and the filtrate was concentrated *in vacuo* to afford amine **2.6** in quantitative yield (255 mg, 1.16 mmol) as a dark yellow oil. The crude material was used in the next step without further purification.

Analytical data observed were in accordance with literature values.[103]

^{1}H NMR (500 MHz, methanol-d_4) δ 8.85 (1H, s, thiazole-CH), 7.31 (1H, d, J = 7.7 Hz, Ar-CH), 6.99 (1H, d, J = 1.7 Hz, Ar-CH), 6.92 (1H, dd, J = 7.7, 1.7 Hz, Ar-CH), 4.06 (2H, s, -C**H$_2$**^{a}), 2.48 (3H, s, -CH$_3$). ^{13}C NMR (101 MHz, methanol-d_4) δ 157.7 (Ar-C), 153.1 (thiazole-CH), 149.4 (thiazole-C), 135.3 (Ar-C), 132.2 (Ar-CH), 121.6 (Ar-CH), 116.9 (Ar-CH), 101.4 (Ar-C), 63.6 (thiazole-C), 53.7 (-C^{a}H$_2$), 16.0 (-CH$_3$). HRMS (ESI) exact mass calculated for $C_{11}H_{13}N_2O_6S$ $[M+H]^+$ m/z 221.0743, found m/z 221.0746. LCMS (ESI) mass calculated for $C_{11}H_{13}N_2O_6S$ $[M+H]^+$ m/z 221.07, found m/z 221.00 with t_R = 4.02 min.

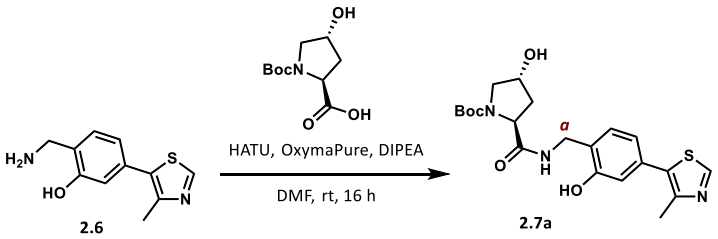

2.7a: To a pre-stirred solution of *N*-Boc-*trans*-4-hydroxy-L-proline (525 mg, 2.27 mmol, 1 equiv), HATU (863 mg, 2.27 mmol, 1 equiv), OxymaPure (323 mg, 2.27 mmol, 1 equiv) and *N,N*-diisopropylethylamine (0.81 mL, 4.5 mmol, 2 equiv) in *N,N*-dimethylformamide (3.8 mL) was added amine **2.6** (500 mg, 2.27 mmol, 1 equiv) in *N,N*-dimethylformamide (3.8 mL, 0.3 M total concentration) and the resulting solution was stirred at room temperature for 16 hours. The reaction mixture was partitioned between dichloromethane (50 mL) and water (50 mL), and the aqueous phase was extracted with dichloromethane (5 × 50 mL). The combined organic phases were washed with 5% aqueous lithium chloride (5 × 100 mL), dried over magnesium sulfate, filtered and concentrated *in vacuo*. Purification by column chromatography on silica gel with an eluent of 5% to 30% ethanol in dichloromethane afforded *trans*-Hyp fragment **2.7a** (533 mg, 1.21 mmol, 53%) as an orange amorphous solid.

Analytical data observed were in accordance with literature values.[103]

^{1}H NMR (400 MHz, methanol-d_4) δ 8.85 (1H, s, thiazole-CH), 7.29 (1H, d, J = 7.8 Hz, Ar-CH), 6.94 – 6.86 (2H, m, 2 × Ar-CH), 4.51 – 4.42 (1H, m, -C*H*OH), 4.41 – 4.36 (2H, m, -C**H$_2$**^{a}), 4.35 – 4.27 (1H, m, -CH), 3.59 – 3.53 (1H, m, -C*H*H), 3.53 – 3.45 (1H, m, -CH*H*), 2.47 (3H, s, -CH$_3$),

2.33 – 2.17 (1H, m, -C*H*H), 2.08 – 1.98 (1H, m, -CH*H*), 1.37 (9H, s, 3 × CH_3). ^{13}C NMR (101 MHz, methanol-d_4) δ 176.1 (-CONH), 157.1 (Ar-C), 156.1 (-NCOOR), 152.7 (thiazole-CH), 148.9 (thiazole-C), 133.4 (Ar-C), 131.7 (Ar-CH), 126.2 (Ar-C), 121.5 (Ar-CH), 117.5 (Ar-CH), 81.7 (-*C*(CH_3)$_3$), 70.1 (-CHOH), 60.7 (thiazole-C), 58.3 (-CH), 56.0 (-CH_2), 40.8 (-CH_2), 39.7 (-**C^a**H_2), 28.4 (3C, -C(*C*H_3)$_3$), 15.9 (-CH_3). HRMS (ESI) exact mass calculated for $C_{21}H_{27}N_3O_5SNa$ $[M+Na]^+$ m/z 456.1564, found m/z 456.1570. LCMS (ESI) mass calculated for $C_{21}H_{28}N_3O_5S$ $[M+H]^+$ m/z 434.17, found m/z 434.17 with t_R = 4.96 min.

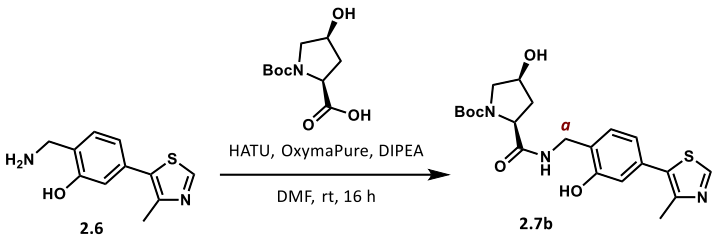

2.7b: To a pre-stirred solution of *N*-Boc-*cis*-4-hydroxy-L-proline (441 mg, 1.91 mmol, 1 equiv), HATU (723 mg, 1.91 mmol, 1 equiv), OxymaPure (271 mg, 1.91 mmol, 1 equiv) and *N,N*-diisopropylethylamine (0.68 mL, 3.8 mmol, 2 equiv) in *N,N*-dimethylformamide (3 mL) was added amine **2.6** (500 mg, 2.27 mmol, 1 equiv) in *N,N*-dimethylformamide (3 mL, 0.3 M total concentration) and the resulting solution was stirred at room temperature for 16 hours. The reaction mixture was partitioned between dichloromethane (50 mL) and water (50 mL), and the aqueous phase was extracted with dichloromethane (5 × 50 mL). The combined organic phases were washed with 5% aqueous lithium chloride (5 × 100 mL), dried over magnesium sulfate, filtered and concentrated *in vacuo*. Purification by column chromatography on silica gel with an eluent of 5% to 30% ethanol in dichloromethane afforded *cis*-Hyp fragment **2.7b** (420 mg, 0.96 mmol, 50%) as an orange amorphous solid. Analytical data observed were in accordance with literature values.[104]

^{1}H NMR (400 MHz, methanol-d_4) δ 8.85 (1H, s, thiazole-CH), 7.33 (1H, d, *J* = 7.6 Hz, Ar-CH), 6.95 – 6.85 (2H, m, 2 × Ar-CH), 4.51 – 4.42 (1H, m, -C*H*OH), 4.41 – 4.29 (2H, m, -**CH$_2^a$**), 4.27 – 4.17 (1H, m, -CH), 3.59 – 3.52 (1H, m, -C*H*H), 3.49 – 3.41 (1H, m, -CH*H*), 2.48 (3H, s, -CH_3), 2.45 – 2.35 (1H, m, -C*H*H), 2.06 – 1.96 (1H, m, -CH*H*), 1.38 (9H, s, 3 × CH_3). ^{13}C NMR (101 MHz, methanol-d_4) δ 176.1 (-CONH), 157.1 (Ar-C), 156.1 (-NCOOR), 152.8 (thiazole-CH), 148.9 (thiazole-C), 133.3 (Ar-C), 131.6 (Ar-CH), 126.1 (Ar-C), 121.4 (Ar-CH), 117.2 (Ar-CH), 81.9 (-*C*(CH_3)$_3$), 70.4 (-CHOH), 61.5 (thiazole-C), 61.1 (-CH), 56.0 (-CH_2), 39.7 (-**C^a**H_2), 28.7 (-CH_2), 28.4 (3C, -C(*C*H_3)$_3$), 15.9 (-CH_3). HRMS (ESI) exact mass calculated for $C_{21}H_{27}N_3O_5S$ $[M-H]^-$ m/z 433.1683, found m/z 433.1612.

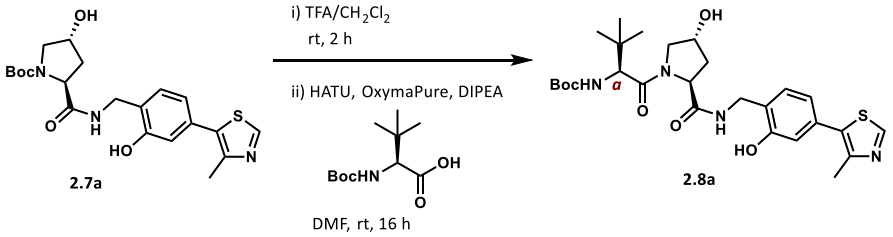

2.8a: Protected *trans*-Hyp fragment **2.7a** (140 mg, 0.32 mmol, 1 equiv) was dissolved in trifluoroacetic acid/dichloromethane (5 mL/5 mL, 0.03 M) and the resulting solution was stirred at room temperature for 2 hours. The reaction was monitored by TLC for complete consumption of the starting material before removal of volatile components *in vacuo*. To the residue was added to a pre-stirred solution of *N*-Boc-L-*tert*-leucine (75 mg, 0.32 mmol, 1 equiv), HATU (120 mg, 0.32 mmol, 1 equiv), OxymaPure (46 mg, 0.32 mmol, 1 equiv) and *N,N*-diisopropylethylamine (0.23 mL, 1.3 mmol, 4 equiv) in *N,N*-dimethylformamide (1 mL, 0.3 M), and the resulting solution was stirred at room temperature for 16 hours. The reaction mixture was partitioned between dichloromethane (20 mL) and water (20 mL), and the aqueous phase was extracted with dichloromethane (3 × 20 mL). The combined organic phases were washed with 5% aqueous lithium chloride (3 × 20 mL), dried over magnesium sulfate, filtered and concentrated *in vacuo*. Purification by column chromatography on silica gel with an eluent of 0% to 20% ethanol in ethyl acetate afforded *tert*-leucine fragment **2.8a** (110 mg, 0.20 mmol, 60%) as a yellow oily solid.

Analytical data observed were in accordance with literature values.[103]

^{1}H NMR (400 MHz, methanol-d_4) δ 8.85 (1H, s, thiazole-CH), 7.98 (1H, s, -NHCOOR), 7.36 (1H, d, J = 8.2 Hz, Ar-CH), 6.94 – 6.85 (2H, m, 2 × Ar-CH), 4.63 – 4.56 (1H, m, -C*H*OH), 4.50 (1H, s, -C**H**^{a}), 4.44 – 4.34 (2H, m, -CH_2), 4.32 – 4.24 (1H, m, -CH), 3.90 – 3.76 (2H, m, -CH_2), 2.48 (3H, s, -CH_3), 2.24 – 2.06 (2H, m, -CH_2), 1.44 (9H, s, 3 × CH_3), 1.00 (9H, s, 3 × CH_3). ^{13}C NMR (101 MHz, methanol-d_4) δ 174.5 (-CONH), 172.9 (-CONH), 167.4 (-NHCOOR), 156.6 (Ar-C), 152.6 (thiazole-CH), 148.8 (thiazole-C), 133.5 (Ar-C), 132.7 (Ar-CH), 126.2 (Ar-C), 121.4 (Ar-CH), 116.8 (Ar-CH), 80.6 (-*C*(CH_3)$_3$), 71.0 (-CHOH), 60.6 (thiazole-C), 60.4 (-**C**^{a}H), 57.9 (-CH), 56.0 (-CH_2), 39.5 (-CH_2), 38.9 (-CH_2), 36.8 (-*C*(CH_3)$_3$), 28.7 (3C, -C(*C*H_3)$_3$), 26.9 (3C, -C(*C*H_3)$_3$), 16.0 (-CH_3). HRMS (ESI) exact mass calculated for $C_{27}H_{39}N_4O_6S$ $[M+H]^+$ m/z 547.2585, found m/z 547.2580. LCMS (ESI) mass calculated for $C_{27}H_{39}N_4O_6S$ $[M+H]^+$ m/z 547.26, found m/z 547.08 with t_R = 5.50 min.

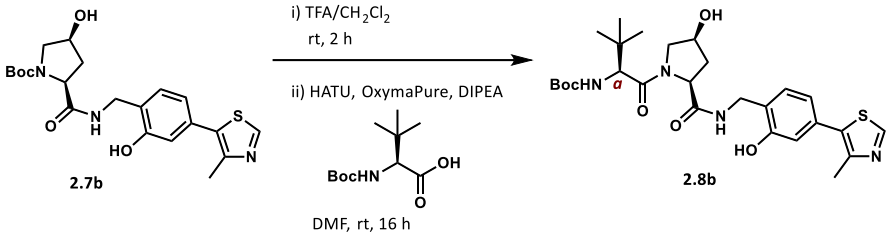

2.8b: Protected *cis*-Hyp fragment **2.7b** (410 mg, 0.95 mmol, 1 equiv) was dissolved in trifluoroacetic acid/dichloromethane (10 mL/10 mL, 0.03 M) and the resulting solution was stirred at room temperature for 2 hours. The reaction was monitored by TLC for complete consumption of the starting material before removal of volatile components *in vacuo*. To the residue was added a pre-stirred solution of *N*-Boc-L-*tert*-leucine (220 mg, 0.95 mmol, 1 equiv), HATU (360 mg, 0.95 mmol, 1 equiv), OxymaPure (130 mg, 0.95 mmol, 1 equiv) and *N,N*-diisopropylethylamine (0.67 mL, 3.8 mmol, 4 equiv) in *N,N*-dimethylformamide (3.2 mL, 0.3 M), and the resulting solution was stirred at room temperature for 16 hours. The reaction mixture was partitioned between dichloromethane (30 mL) and water (30 mL), and the aqueous phase was extracted with dichloromethane (3 × 30 mL). The combined organic phases were washed with 5% aqueous lithium chloride (3 × 40 mL), dried over magnesium sulfate, filtered and concentrated *in vacuo*. Purification by column chromatography on silica gel with an eluent of 0% to 20% ethanol in ethyl acetate afforded the *tert*-leucine fragment **2.8b** (260 mg, 0.47 mmol, 50%) as a yellow oily solid.

Analytical data observed were in accordance with literature values.[104]

^{1}H NMR (400 MHz, MHz, methanol-d_4) δ 8.85 (1H, s, thiazole-CH), 7.98 (1H, s, -NHCOOR), 7.35 (1H, d, *J* = 7.6 Hz, Ar-CH), 6.93 – 6.83 (2H, m, 2 × Ar-CH), 4.58 – 4.51 (1H, m, -C*H*OH), 4.47 – 4.35 (3H, -CH_2 & -C**H**^{a}), 4.25 – 4.18 (1H, m, -CH), 4.03 – 3.95 (1H, m, -C*H*H), 3.73 – 3.66 (1H, m, -CH*H*), 2.48 (3H, s, -CH_3), 2.46 – 2.38 (1H, m, -C*H*H), 2.01 – 1.94 (1H, m, -CH), 1.43 (9H, s, 3 × CH_3), 0.99 (9H, s, 3 × CH_3). ^{13}C NMR (101 MHz, methanol-d_4) δ 175.0 (-CONH), 173.3 (-CONH), 168.6 (-NHCOOR), 156.7 (Ar-C), 152.7 (thiazole-CH), 148.8 (thiazole-C), 133.6 (Ar-C), 132.8 (Ar-CH), 125.9 (Ar-C), 121.4 (Ar-CH), 116.6 (Ar-CH), 80.7 (-*C*(CH_3)$_3$), 71.5 (-CHOH), 61.5 (thiazole-C), 61.0 (-**C**^{a}H), 57.7 (-CH), 54.8 (-CH_2), 39.6 (-CH_2), 38.9 (-CH_2), 36.2 (-*C*(CH_3)$_3$), 28.7 (3C, -C(*C*H_3)$_3$), 26.9 (3C, -C(*C*H_3)$_3$), 15.9 (-CH_3). HRMS (ESI) exact mass calculated for $C_{27}H_{39}N_4O_6S$ $[M+H]^+$ m/z 547.2585, found m/z 547.2579.

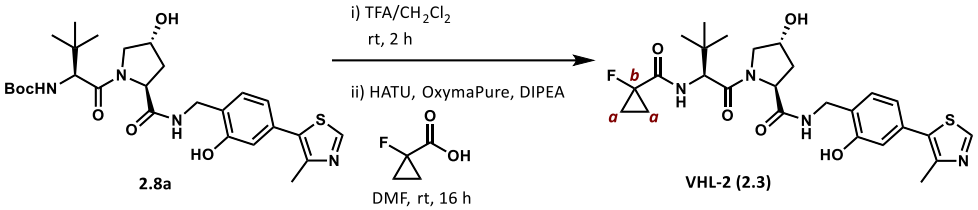

VHL-2 (2.3): Protected *tert*-leucine fragment **2.8a** (100 mg, 0.18 mmol, 1 equiv) was dissolved in trifluoroacetic acid/dichloromethane (3 mL/3 mL, 0.03 M) and the resulting solution was stirred at room temperature for 2 hours. The reaction was monitored by TLC for complete consumption of the starting material before removal of volatile components *in vacuo*. To the residue was added a pre-stirred solution of 1-fluorocyclopropanecarboxylic acid (19 mg, 0.18 mmol, 1 equiv), HATU (70 mg, 0.18 mmol, 1 equiv), OxymaPure (26 mg, 0.18 mmol, 1 equiv) and *N,N*-diisopropylethylamine (0.13 mL, 0.73 mmol, 4 equiv) in *N,N*-dimethylformamide (0.6 mL, 0.3 M), and the resulting solution was stirred at room temperature for 16 hours. The reaction mixture was partitioned between dichloromethane (15 mL) and water (15 mL), and the aqueous phase was extracted with dichloromethane (3 × 15 mL). The combined organic phases were washed with 5% aqueous lithium chloride (3 × 20 mL), dried over magnesium sulfate, filtered and concentrated *in vacuo*. Purification by column chromatography on silica gel with an eluent of 0% to 10% ethanol in ethyl acetate afforded active VHL ligand **VHL-2 (2.3)** (72 mg, 0.14 mmol, 74%) as a pale yellow amorphous solid.

Analytical data observed were in accordance with literature values.[103]

^{1}H NMR (500 MHz, chloroform-*d*) δ 9.30 (1H, s, phenol-OH), 8.64 (1H, s, thiazole-CH), 8.09 – 8.03 (1H, m, -CONH), 7.09 (1H, d, *J* = 7.8 Hz, Ar-CH), 7.05 – 7.00 (1H, m, -CONH), 6.94 (1H, d, *J* = 1.8 Hz, Ar-CH), 6.83 (1H, dd, *J* = 7.8, 1.8 Hz, Ar-CH), 4.67 (1H, t, *J* = 7.9 Hz, -CH), 4.51 – 4.45 (2H, m, -CH & -C*H*OH), 4.42 – 4.35 (1H, m, -C*H*H), 4.20 – 4.14 (1H, m, -CH*H*), 4.02 (1H, br s, hydroxyproline-OH), 3.96 – 3.88 (1H, m, -C*H*H), 3.65 – 3.58 (1H, m, -CH*H*), 2.48 (3H, s, -CH_3), 2.40 – 2.33 (1H, m, -C*H*H), 2.08 – 2.01 (1H, m, -CH*H*), 1.34 – 1.17 (4H, m, 2 × cyclopropyl-C**H**$^{a}_2$), 0.90 (9H, s, 3 × CH_3). ^{13}C NMR (126 MHz, chloroform-*d*) δ 172.9 (-CONH), 171.1 (-CONH), 170.4 (d, $^{2}J_{C\text{-}F}$ = 20.2 Hz, -CONH), 155.8 (Ar-C), 150.5 (thiazole-CH), 148.4 (thiazole-C), 133.3 (thiazole-C), 131.7 (Ar-C), 131.2 (Ar-CH), 124.1 (Ar-C), 120.9 (Ar-CH), 118.2 (Ar-CH), 78.3 (d, $^{1}J_{C\text{-}F}$ = 229.7 Hz, -**C**^{b}F), 70.2 (-CHOH), 58.5 (-CH), 57.8 (-CH), 56.9 (-CH_2), 40.0 (-CH_2), 36.2 (-*C*$(CH_3)_3$), 35.7 (-CH_2), 26.3 (3C, -C(CH_3)$_3$), 16.2 (-CH_3), 13.9 (d, $^{2}J_{C\text{-}F}$ = 10.2 Hz, cyclopropyl-**C**$^{a}H_2$), 13.7 (d, $^{2}J_{C\text{-}F}$ = 10.1 Hz, cyclopropyl-**C**$^{a}H_2$). HRMS (ESI) exact mass calculated for $C_{26}H_{33}FN_4O_5SNa$ $[M+Na]^+$ m/z 555.2053, found m/z 555.2058. LCMS (ESI) mass calculated for $C_{26}H_{34}FN_4O_5S$ $[M+H]^+$ m/z 533.22, found m/z 533.25 with t_R = 5.25 min.

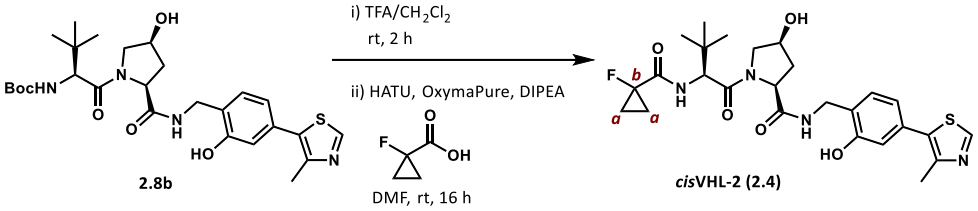

***cis*VHL-2 (2.4)**: Protected *tert*-leucine fragment **2.8b** (120 mg, 0.22 mmol, 1 equiv) was dissolved in trifluoroacetic acid/dichloromethane (3.8 mL/3.8 mL, 0.03 M) and the resulting solution was stirred at room temperature for 2 hours. The reaction was monitored by TLC for complete consumption of the starting material before removal of volatile components *in vacuo*. To the residue was added a pre-stirred solution of 1-fluorocyclopropanecarboxylic acid (23 mg, 0.22 mmol, 1 equiv), HATU (84 mg, 0.22 mmol, 1 equiv), OxymaPure (31 mg, 0.22 mmol, 1 equiv) and *N,N*-diisopropylethylamine (0.16 mL, 0.88 mmol, 4 equiv) in *N,N*-dimethylformamide (0.7 mL, 0.3 M), and the resulting solution was stirred at room temperature for 16 hours. The reaction mixture was partitioned between dichloromethane (15 mL) and water (15 mL), and the aqueous phase was extracted with dichloromethane (3 × 15 mL). The combined organic phases were washed with 5% aqueous lithium chloride (3 × 20 mL), dried over magnesium sulfate, filtered and concentrated *in vacuo*. Purification by column chromatography on silica gel with an eluent of 0% to 10% ethanol in ethyl acetate afforded inactive epimer ***cis*VHL-2 (2.4)** (73 mg, 0.14 mmol, 62%) as a pale yellow amorphous solid.

Analytical data observed were in accordance with literature values.[104]

^{1}H NMR (500 MHz, chloroform-*d*) δ 8.80 – 8.63 (2H, m, phenol-OH & thiazole-CH), 8.11 – 8.04 (1H, m, -CONH), 7.15 (1H, d, *J* = 7.8 Hz, Ar-CH), 6.98 (1H, d, *J* = 1.8 Hz, Ar-CH), 6.90 (1H, dd, *J* = 7.8, 1.8 Hz, Ar-CH), 6.89 – 6.86 (1H, m, -CONH), 5.15 (1H, s, hydroxyproline-OH), 4.77 (1H, d, *J* = 9.0 Hz, -CH), 4.60 – 4.51 (1H, m, -C*H*H), 4.51 – 4.43 (2H, m, -CH & -CHOH), 4.19 (1H, dd, *J* = 14.7, 5.2 Hz, -CH*H*), 3.87 (1H, dd, *J* = 11.0, 4.3 Hz, -C*H*H), 3.78 (1H, dd, *J* = 11.0, 1.3 Hz, -CH*H*), 2.52 (3H, s, -CH_3), 2.35 (1H, d, *J* = 14.3 Hz, -C*H*H), 2.20 (1H, ddd, *J* = 14.3, 9.2, 5.0 Hz, -CH*H*), 1.36 – 1.20 (4H, m, 2 × cyclopropyl-C**H**$^{a}_2$), 0.84 (9H, s, 3 × CH_3). ^{13}C NMR (126 MHz, chloroform-*d*) δ 173.9 (-CONH), 171.9 (-CONH), 170.0 (d, $^{2}J_{C\text{-}F}$ = 20.3 Hz, -CONH), 155.6 (Ar-C), 150.6 (thiazole-CH), 148.6 (thiazole-C), 133.8 (thiazole-C), 131.6 (Ar-C), 131.2 (Ar-CH), 123.3 (Ar-C), 121.3 (Ar-CH), 118.6 (Ar-CH), 78.0 (d, $^{1}J_{C\text{-}F}$ = 241.0 Hz, -**C**^{b}F), 71.2 (-CHOH), 59.6 (-CH), 58.7 (-CH), 57.2 (-CH_2), 40.1 (-CH_2), 35.3 (-*C*(CH_3)$_3$), 34.9 (-CH_2), 26.2 (3C, -C(*C*H_3)$_3$), 16.3 (-CH_3), 13.8 (d, $^{2}J_{C\text{-}F}$ = 10.2 Hz, cyclopropyl-**C**^{a}H_2), 13.7 (d, $^{2}J_{C\text{-}F}$ = 10.2 Hz, cyclopropyl-**C**^{a}H_2). HRMS (ESI) exact mass calculated for $C_{26}H_{33}FN_4O_5SNa$ $[M+Na]^+$ m/z

555.2053, found m/z 555.2052. LCMS (ESI) mass calculated for $C_{26}H_{34}FN_4O_5S$ $[M+H]^+$ m/z 533.22, found m/z 533.17 with t_R = 5.28 min.

- *CRBN ligand **CRBN-1 (2.9)** and methylated control **MeCRBN-1 (2.10)**:*

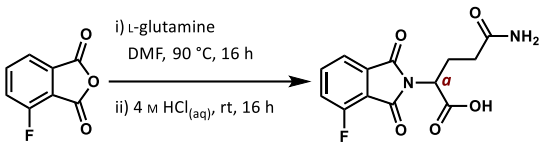

2.13

2.13: To a stirred solution of 3-fluorophthalic anhydride (3.93 g, 23.7 mmol, 1 equiv) in anhydrous *N,N*-dimethylformamide (20 mL, 1.2 M) was added L-glutamine (3.47 g 23.7 mmol, 1 equiv) and the resulting solution was stirred at 90 °C for 16 hours. Complete consumption of starting materials was confirmed by TLC. The reaction mixture was allowed to reach room temperature and volatile components were removed *in vacuo*. The residue was re-dissolved in 4 M aqueous hydrochloric acid (20 mL, 1.2 M) and lithium chloride (1.0 g, 5% w/w) was added. After stirring of the reaction mixture at room temperature for a further 16 hours, the resulting precipitate was collected by filtration, washed with water and dried *in vacuo*, yielding phthalimide **2.13** (5.37 g, 18.3 mmol, 73%) as pale yellow amorphous solid.

Analytical data observed were as in accordance with literature values.[99]

^{1}H NMR (400 MHz, methanol-d_4) δ 7.87 (1H, ddd, J = 8.4, 7.4, 4.4 Hz, Ar-CH), 7.73 (1H, dd, J = 7.4, 0.7 Hz, Ar-CH), 7.55 (1H, ddd, J = 9.2, 8.4, 0.7 Hz, Ar-CH), 4.85 (1H, d, J = 4.8 Hz, -C**H**^{a}), 2.61 – 2.42 (2H, m, -CH_2), 2.31 – 2.25 (2H, m, -CH_2). ^{13}C NMR (101 MHz, methanol-d_4) δ 177.3 (-$CONH_2$), 171.9 (-COOH), 168.0 (-CO), 165.8 (-CO), 159.0 (d, $^1J_{C\text{-}F}$ = 263.8 Hz, Ar-C-F), 138.5 (d, $^3J_{C\text{-}F}$ = 8.0 Hz, Ar-CH), 135.4 (Ar-C), 123.6 (d, $^2J_{C\text{-}F}$ = 20.1 Hz, Ar-CH), 120.7 (d, $^4J_{C\text{-}F}$ = 3.8 Hz, Ar-CH), 118.7 (d, $^2J_{C\text{-}F}$ = 13.3 Hz, Ar-C), 52.9 (-C**H**^{a}), 32.9 (-CH_2), 25.6 (-CH_2). HRMS (ESI) exact mass calculated for $C_{13}H_{11}FN_2O_5Na$ $[M+Na]^+$ m/z 317.0544, found m/z 317.0551. LCMS (ESI) mass calculated for $C_{13}H_{12}FN_2O_5$ $[M+H]^+$ m/z 295.07, found m/z 295.08 with t_R = 4.34 min.

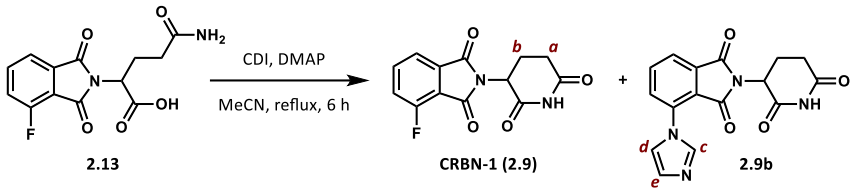

CRBN-1 (2.9): To a stirred solution of phthalimide **2.13** (1.25 g, 4.25 mmol, 1 equiv) in acetonitrile (4 mL, 1 M) was added *N,N'*-carbonyldiimidazole (0.83 g, 5.1 mmol, 1.2 equiv) and 4-dimethylaminopyridine (20 mg, 0.18 mmol, 4 mol%), and the resulting solution was stirred under reflux whilst monitoring the reaction progress by TLC. After 6 hours, when considerable formation of side product **2.9b** was observed to begin, the reaction mixture was allowed to cool to room temperature before removing volatile components *in vacuo*. The residue was re-dissolved in dichloromethane (25 mL) and water (25 mL), and the aqueous phase was extracted with dichloromethane (5 × 25 mL). The combined organic layers were dried over magnesium sulfate, filtered and concentrated *in vacuo*. Purification by column chromatography on silica gel with an eluent of 0% to 50% ethanol in ethyl acetate afforded CRBN ligand **CRBN-1 (2.9)** (647 mg, 2.35 mmol, 55%) as a yellow amorphous solid and imidazole adduct **2.9b** (270 mg, 0.83 mmol, 20%) as a light brown amorphous solid.

CRBN-1 (2.9): Analytical data observed were in accordance with literature values.[99]

^{1}H NMR (400 MHz, chloroform-*d*) δ 8.02 (1H, s, -NH), 7.78 (1H, ddd, *J* = 8.2, 7.4, 4.3 Hz, Ar-CH), 7.72 (1H, dd, *J* = 7.3, 0.7 Hz, Ar-CH), 7.43 (1H, ddd, *J* = 9.2, 8.2, 0.7 Hz, Ar-CH), 5.02 – 4.95 (1H, m, -CH), 2.97 – 2.70 (3H, m, -C***H***^{a}H & -C**H$_2$**$^{b)}$, 2.20 – 2.12 (1H, m, -CH***H***^{a}). ^{13}C NMR (101 MHz, chloroform-*d*) δ 170.8 (-CO), 167.8 (-CO), 166.3 (-CO), 164.1 (-CO), 158.1 (d, $^{1}J_{C\text{-}F}$ = 267.2 Hz, Ar-C-F), 137.4 (d, $^{3}J_{C\text{-}F}$ = 7.6 Hz, Ar-CH), 134.1 (Ar-C), 123.1 (d, $^{2}J_{C\text{-}F}$ = 19.5 Hz, Ar-CH), 120.3 (d, $^{4}J_{C\text{-}F}$ = 3.7 Hz, Ar-CH), 117.8 (Ar-C), 49.7 (-CH), 31.6 (-**C**^{a}H$_2$), 22.8 (-**C**^{b}H$_2$). HRMS (ESI) exact mass calculated for $C_{13}H_9FN_2O_4Na$ $[M+Na]^+$ m/z 299.0439, found m/z 299.0444. LCMS (ESI) mass calculated for $C_{14}H_{14}FN_2O_5$ $[M+CH_3OH+H]^+$ m/z 309.90, found m/z 309.92 with t_R = 5.05 min.

2.9b: ^{1}H NMR (400 MHz, methanol-d_4) δ 8.21 (1H, s, imidazole-C**H**^{c}), 8.01 – 7.95 (2H, m, 2 × Ar-CH), 7.88 (1H, dd, *J* = 6.5, 2.5 Hz, Ar-CH), 7.62 – 7.59 (1H, m, imidazole-C**H**^{d}), 7.18 – 7.15 (1H, m, imidazole-C**H**^{e}), 5.17 (1H, dd, *J* = 12.5, 5.5 Hz, -CH), 2.94 – 2.65 (3H, m, -C*H*H & -CH$_2$), 2.19 – 2.11 (1H, m, -CH*H*'). ^{13}C NMR (101 MHz, methanol-d_4) δ 174.4 (-CO), 171.3 (-CO), 167.6 (-CO), 166.6 (-CO), 139.6 (imidazole-**C**^{c}H), 137.4 (Ar-CH), 135.3 (Ar-C), 135.1 (Ar-C), 131.9 (Ar-CH), 129.6 (imidazole-**C**^{e}H), 124.3 (Ar-C), 123.9 (Ar-CH), 121.7 (imidazole-**C**^{d}H), 50.8 (-CH), 32.1 (-CH$_2$), 23.5 (-CH$_2$). IR (thin film) 1728, 1614, 1491 cm^{-1}. HRMS (ESI) exact

mass calculated for $C_{16}H_{12}N_4O_4Na$ $[M+Na]^+$ m/z 347.0751, found m/z 347.0749. LCMS (ESI) mass calculated for $C_{16}H_{13}N_4O_4$ $[M+H]^+$ m/z 325.09, found m/z 325.08 with t_R = 3.92 min.

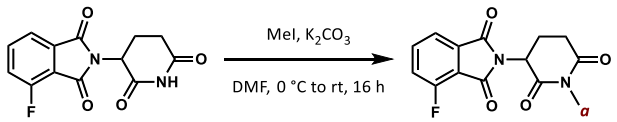

MeCRBN-1 (2.10): CRBN ligand **CRBN-1 (2.9)** (100 mg, 0.36 mmol, 1 equiv) was dissolved in *N,N*-dimethylformamide (2 mL, 0.2 M) and the resulting solution was cooled to 0 °C. Iodomethane (0.14 mL, 2.2 mmol, 6 equiv) and potassium carbonate (75 mg, 0.54 mmol, 3 equiv) were added at 0 °C and the stirred solution was allowed to warm to room temperature. After 16 hours, consumption of **CRBN-1 (2.9)** was confirmed by TLC and the reaction mixture was partitioned between dichloromethane (10 mL) and water (10 mL), and the aqueous phase was extracted with dichloromethane (3 × 10 mL). The combined organic phases were washed with 5% aqueous lithium chloride (3 × 15 mL), dried over magnesium sulfate, filtered and concentrated *in vacuo*. The crude material was filtered through silica gel to afford inactive methylated control ligand **MeCRBN-1 (2.10)** (89 mg, 0.29 mmol, 85%) as an amorphous yellow solid.

Analytical data observed were as in accordance with literature values.[147]

^{1}H NMR (400 MHz, chloroform-*d*) δ 7.77 (1H, ddd, *J* = 8.2, 7.3, 4.3 Hz, Ar-CH), 7.71 (1H, dd, *J* = 7.3, 0.9 Hz, Ar-CH), 7.43 (1H, ddd, *J* = 9.3, 8.3, 0.9 Hz, Ar-CH), 5.02 – 4.94 (1H, m, -CH), 3.22 (3H, s, -C**H$_3$**^{a}), 3.06 – 2.96 (1H, m, -C*H*H), 2.87 – 2.71 (2H, m, -CH_2), 2.18 – 2.09 (1H, m, -CH*H*). ^{13}C NMR (101 MHz, chloroform-*d*) δ 171.0 (-CO), 168.5 (-CO), 166.4 (-CO), 164.2 (-CO), 158.0 (d, $^1J_{C\text{-}F}$ = 266.9 Hz, Ar-C-F), 137.2 (d, $^3J_{C\text{-}F}$ = 7.6 Hz, Ar-CH), 134.1 (Ar-C), 123.0 (d, $^2J_{C\text{-}F}$ = 19.5 Hz, Ar-CH), 120.1 (d, $^4J_{C\text{-}F}$ = 3.8 Hz, Ar-CH), 117.8 (Ar-C), 50.4 (-CH), 32.0 (-CH_2), 27.5 (-**C**^{a}H$_3$), 22.0 (-CH_2). HRMS (ESI) exact mass calculated for $C_{14}H_{11}FN_2O_4Na$ $[M+Na]^+$ m/z 313.0595, found m/z 313.0595. LCMS (ESI) mass calculated for $C_{14}H_{12}FN_2O_4$ $[M+H]^+$ m/z 291.08, found m/z 291.08 with t_R = 5.40 min.

- *CRBN ligand* ***CRBN-2 (2.11)*** *and methylated control* ***MeCRBN-2 (2.12)****:*

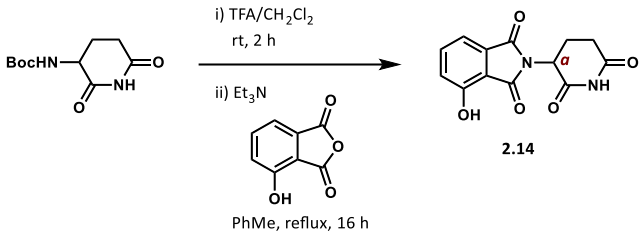

2.14: 3-Boc-amino-2,6-dioxopiperidine (450 mg, 1.97 mmol, 1 equiv) was dissolved in trifluoroacetic acid/dichloromethane (7.5 mL/7.5 mL, 0.03 M) and the resulting solution was stirred at room temperature for 2 hours. The reaction was monitored by TLC for complete consumption of the starting material before removal of volatile components *in vacuo*. The residue was re-dissolved in toluene (20 mL, 0.1 M), and triethylamine (0.55 mL, 3.9 mmol, 2 equiv) was added. The resulting solution was stirred at room temperature for 20 minutes. 3-fluorophthalic anhydride (324 mg, 1.97 mmol, 1 equiv) was added to the reaction mixture and stirred under reflux for 16 hours. The reaction mixture was allowed to reach room temperature before removing volatile components *in vacuo*. Purification by column chromatography on silica gel with an eluent of 50% to 100% ethyl acetate in dichloromethane afforded phenol intermediate **2.14** (502 mg, 1.83 mmol, 93%) as a bright yellow amorphous solid.

Analytical data observed were in accordance with literature values.[114]

^{1}H NMR (400 MHz, methanol-d_4) δ 7.61 (1H, dd, J = 8.4, 7.2 Hz, Ar-H), 7.31 (1H, d, J = 7.2 Hz, Ar-H), 7.16 (1H, d, J = 8.4 Hz, Ar-H), 5.09 (1H, dd, J = 12.5, 5.4 Hz, -C**H**$^{\mathbf{a}}$), 2.92 – 2.81 (1H, m, -C*H*H), 2.79 – 2.67 (2H, m, -CH_2), 2.16 – 2.08 (1H, m, -CH*H*). ^{13}C NMR (126 MHz, methanol-d_4) δ 174.7 (2 × -CO), 171.6 (-CO), 168.9 (-CO), 137.5 (Ar-CH), 134.5 (Ar-C), 125.1 (Ar-CH), 117.0 (Ar-C), 115.9 (Ar-C), 115.5 (Ar-CH), 50.3 (-**C**$^{\mathbf{a}}$H), 32.2 (-CH_2), 23.7 (-CH_2). HRMS (ESI) exact mass calculated for $C_{13}H_{10}N_2O_5Na$ $[M+Na]^+$ m/z 297.0482, found m/z 297.0482. LCMS (ESI) mass calculated for $C_{14}H_{15}N_2O_6$ $[M+CH_3OH+H]^+$ m/z 307.09, found m/z 307.08 with t_R = 4.53 min.

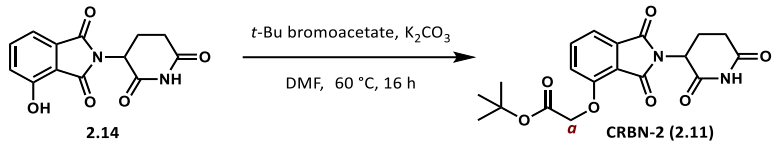

CRBN-2 (2.11): To a stirred solution of phenol **2.14** (566 mg, 2.07 mmol, 1 equiv) in *N,N*-dimethylformamide (20 mL, 0.1 M) was added potassium carbonate (428 mg, 3.10 mmol, 1.5 equiv) and *tert*-butyl bromoacetate (0.31 mL, 2.07 mmol, 1 equiv), and the resulting solution was stirred at 60 °C for 16 hours. The reaction mixture was allowed to cool to room temperature, diluted with ethyl acetate (50 mL) and washed with water (2 × 50 mL) and brine (3 × 50 mL), dried over magnesium sulfate, filtered and concentrated *in vacuo*. Purification by column chromatography on silica gel with an eluent of 50% to 100% ethyl acetate in petroleum ether afforded CRBN ligand **CRBN-2 (2.11)** (470 mg, 1.21 mmol, 59%) as a white amorphous solid.

Analytical data observed were in accordance with literature values.[114]

^{1}H NMR (400 MHz, chloroform-*d*) δ 8.51 (1H, s, -NH), 7.64 (1H, dd, *J* = 8.5, 7.3 Hz, Ar-H), 7.48 (1H, d, *J* = 7.3 Hz, Ar-H), 7.08 (1H, d, *J* = 8.4 Hz, Ar-H), 5.01 – 4.93 (1H, m, -CH), 4.77 (2H, s, -C**H**^{a}), 2.90 – 2.72 (3H, m, -CH_2 & -C*H*H), 2.15 – 2.07 (1H, m, -CH*H*), 1.46 (9H, s, 3 × -CH_3). ^{13}C NMR (101 MHz, chloroform-*d*) δ 171.5 (-CO), 168.3 (-CO), 167.0 (-CO), 166.9 (-CO), 165.6 (-COOR), 155.6 (Ar-C), 136.4 (Ar-CH), 134.0 (Ar-C), 119.9 (Ar-CH), 117.6 (Ar-C), 117.0 (Ar-CH), 83.2 (-*C*$(CH_3)_3$), 66.6 (-**C**$^{a}H_2$), 49.3 (-CH), 31.4 (-CH_2), 28.1 (3C, -C(*C*$H_3)_3$), 22.6 (-CH_2). HRMS (ESI) exact mass calculated for $C_{19}H_{20}N_2O_7Na$ $[M+Na]^+$ m/z 411.1163, found m/z 411.1154.

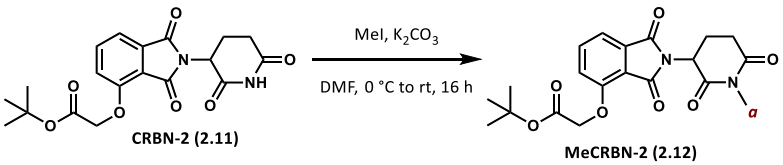

MeCRBN-2 (2.12): CRBN ligand **CRBN-2 (2.11)** (47 mg, 0.12 mmol, 1 equiv) was dissolved in *N,N*-dimethylformamide (1.0 mL, 0.2 M) and the resulting solution was cooled to 0 °C. Iodomethane (0.05 mL, 0.7 mmol, 6 equiv) and potassium carbonate (50 mg, 0.36 mmol, 3 equiv) were added at 0 °C and the stirred solution was allowed to warm to room temperature. After 16 hours complete consumption of **CRBN-2 (2.11)** was confirmed by TLC and the reaction mixture was partitioned between dichloromethane (10 mL) and water (10 mL), and the aqueous phase was extracted with dichloromethane (3 × 10 mL). The combined organic phases were washed with 5% aqueous lithium chloride (3 × 15 mL), dried over magnesium sulfate, filtered and concentrated *in vacuo*. The crude material was

filtered through silica gel to afford inactive methylated control ligand **MeCRBN-2 (2.12)** (47 mg, 0.12 mmol, 96%) as amorphous yellow solid.

Analytical data observed were in accordance with literature values.[115]

^{1}H NMR (400 MHz, chloroform-*d*) δ 7.67 (1H, dd, *J* = 8.5, 7.3 Hz, Ar-CH), 7.51 (1H, dd, *J* = 7.3, 0.7 Hz, Ar-CH), 7.10 (1H, dd, *J* = 8.5, 0.7 Hz, Ar-CH), 5.01 – 4.91 (1H, m, -CH), 4.78 (2H, s, -CH_2), 3.21 (3H, s, -C**H$_3$**^{a}), 3.05 – 2.93 (1H, m, -C*H*H), 2.88 – 2.72 (2H, m, -CH_2), 2.15 – 2.03 (1H, m, -CH*H*), 1.48 (9H, s, 3 × -CH_3). ^{13}C NMR (101 MHz, chloroform-*d*) δ 171.3 (-CO), 168.8 (-CO), 167.1 (-CO), 167.0 (-CO), 165.8 (-COOR), 155.6 (Ar-C), 136.4 (Ar-CH), 134.1 (Ar-C), 119.8 (Ar-CH), 117.8 (Ar-C), 117.0 (Ar-CH), 83.3 (-*C*(CH_3)$_3$), 66.7 (-CH_2), 50.1 (-CH), 32.0 (-CH_2), 28.2 (9H, s, 3 × -CH_3), 27.4 (-**C**^{a}H_3), 22.1 (CH_2). HRMS (ESI) exact mass calculated for $C_{20}H_{23}N_2O_7$ $[M+H]^+$ m/z 403.1500, found m/z 403.1495.

Preparation of HaloPROTACs and mono-functional controls

- *VHL HaloPROTACs and mono-functional controls:*

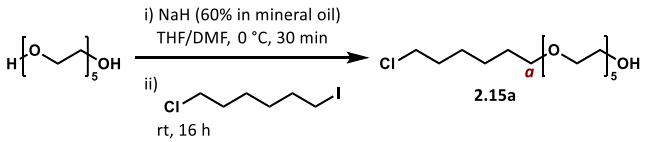

2.15a: To a dry flask charged with argon was added anhydrous tetrahydrofuran/*N,N*-dimethylformamide (1.5 mL/1.5 mL, 1 M), pentaethylene glycol (1.5 mL, 7.0 mmol, 5 equiv) and sodium hydride (60% in mineral oil, 140 mg, 2.5 mmol, 2.5 equiv) at 0 °C. The resulting suspension was stirred for 30 minutes before 1-chloro-6-iodohexane (0.21 mL, 1.7 mmol, 1 equiv) was added slowly at 0 °C. The reaction mixture was allowed to reach room temperature and stirred for further 16 hours. The reaction was quenched by dropwise addition of water (10 mL) before addition of 1 M aqueous hydrochloric acid (10 mL). The aqueous phase was extracted with chloroform (3 × 20 mL) and the combined organic extracts were washed with 5% aqueous lithium chloride (3 × 40 mL), dried over magnesium sulfate, filtered and concentrated *in vacuo*. Purification by column chromatography on silica gel with an eluent of 75% to 100% ethyl acetate in chloroform afforded alcohol **2.15a** (380 mg, 1.06 mmol, 79%) as a clear oil.

Analytical data observed were in accordance with literature values.[103]

^{1}H NMR (400 MHz, chloroform-*d*) δ 3.76 – 3.70 (2H, m, -CH_2), 3.69 – 3.57 (18H, m, 9 × -CH_2), 3.53 (2H, t, *J* = 6.7 Hz, -CH_2), 3.45 (2H, t, *J* = 6.6 Hz, -C**H$_2$**^{a}), 2.55 (1H, t, *J* = 6.3 Hz, -OH), 1.82 – 1.73 (2H, m, -CH_2), 1.63 – 1.54 (2H, m, -CH_2), 1.50 – 1.32 (4H, m, 2 × -CH_2). ^{13}C NMR (101 MHz, chloroform-*d*) δ 72.7 (-CH_2), 71.4 (-**C**^{a}H_2), 70.8 (-CH_2), 70.8 (-CH_2), 70.7 (2 × -CH_2), 70.7

(-CH_2), 70.7 (-CH_2), 70.5 (-CH_2), 70.2 (-CH_2), 61.9 (-CH_2OH), 45.2 (-CH_2Cl), 32.7 (-CH_2), 29.6 (-CH_2), 26.9 (-CH_2), 25.6 (-CH_2). HRMS (ESI) exact mass calculated for $C_{16}H_{33}ClO_6Na$ $[M+Na]^+$ m/z 379.1858, found m/z 379.1847. LCMS (ESI) mass calculated for $C_{16}H_{34}ClO_6$ $[M+H]^+$ m/z 357.20, found m/z 357.17 with t_R = 5.81 min.

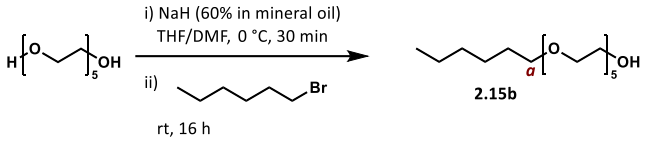

2.15b: To a dry flask charged with argon was added anhydrous tetrahydrofuran/*N,N*-dimethylformamide (1.6 mL/1.6 mL, 1 M), pentaethylene glycol (1.6 mL, 7.8 mmol, 5 equiv) and sodium hydride (60% in mineral oil, 160 mg, 2.5 mmol, 2.5 equiv) at 0 °C. The resulting suspension was stirred for 30 minutes before 1-bromohexane (0.28 mL, 1.8 mmol, 1 equiv) was added slowly at 0 °C. The reaction mixture was allowed to reach room temperature and stirred for further 16 hours. The reaction was quenched by dropwise addition of water (10 mL) before addition of 1 M aqueous hydrochloric acid (10 mL). The aqueous phase was extracted with chloroform (3 × 20 mL) and the combined organic extracts were washed with 5% aqueous lithium chloride (3 × 40 mL), dried over magnesium sulfate, filtered and concentrated *in vacuo*. Purification by column chromatography on silica gel with an eluent of 0% to 25% ethanol in ethyl acetate afforded alcohol **2.15b** in quantitative yield (492 mg, 1.55 mmol) as a light yellow oil.

^{1}H NMR (400 MHz, chloroform-*d*) δ 3.76 – 3.70 (2H, m, -CH_2), 3.69 – 3.50 (18H, m 9 × -CH_2), 3.44 (2H, t, *J* = 6.8 Hz, -C**H$_2$**^{a}), 2.60 (1H, s, -OH), 1.63 – 1.47 (2H, m, -CH_2), 1.40 – 1.18 (6H, m, 3 × -CH_2), 0.92 – 0.84 (3H, m, -CH_3). ^{13}C NMR (101 MHz, chloroform-*d*) δ 72.7 (-CH_2), 71.7 (-**C**^{a}H_2), 70.8 (-CH_2), 70.8 (-CH_2), 70.7 (2 × -CH_2), 70.7 (2 × -CH_2), 70.5 (-CH_2), 70.2 (-CH_2), 61.9 (-CH_2), 31.8 (-CH_2), 29.7 (-CH_2), 25.9 (-CH_2), 22.8 (-CH_2), 14.2 (-CH_3). IR (thin film) 3451, 1247, 1101 cm^{-1}. HRMS (ESI) exact mass calculated for $C_{16}H_{34}O_6Na$ $[M+Na]^+$ m/z 345.2248, found m/z 345.2246.

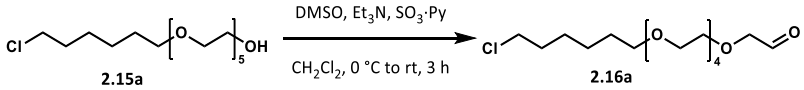

2.16a: To a stirred solution of alcohol **2.15a** (330 mg, 0.93 mmol, 1 equiv) in dichloromethane (9.3 mL, 0.1 M) was added dimethyl sulfoxide (2.2 mL) and triethylamine (0.52 mL, 3.7 mmol, 4 equiv) and reaction mixture was cooled to 0 °C. To anhydrous dimethyl sulfoxide (2.2 mL) was added sulfur trioxide pyridine complex (370 mg, 2.3 mmol,

2.5 equiv) at 0 °C and stirred for 10 minutes before dropwise addition of the pre-stirred solution to the reaction mixture. The resulting solution was stirred for 1 hour at 0 °C and was then allowed to reach room temperature over 2 hours before complete consumption of the starting material was confirmed by LCMS. The reaction mixture was diluted with water (20 mL) and the aqueous phase was extracted with dichloromethane (3 × 20 mL). The combined organic extracts were washed with water (30 mL) and brine (30 mL), dried over magnesium sulfate, filtered and concentrated *in vacuo*. Aldehyde **2.16a** (300 mg, 0.85 mmol, 91%) was afforded as a yellow oil and the crude material was used in the next step without further purification.

LCMS (ESI) mass calculated for $C_{16}H_{32}ClO_6$ $[M+H]^+$ m/z 355.19, found m/z 355.08 with t_R = 5.64 min.

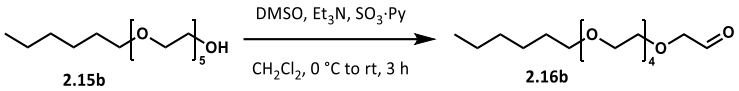

2.16b: To a stirred solution of alcohol **2.15b** (200 mg, 0.64 mmol, 1 equiv) in dichloromethane (6.4 mL, 0.1 M) was added dimethyl sulfoxide (1.5 mL) and triethylamine (0.36 mL, 2.6 mmol, 4 equiv) and reaction mixture was cooled to 0 °C. To anhydrous dimethyl sulfoxide (1.5 mL) was added sulfur trioxide pyridine complex (260 mg, 1.6 mmol, 2.5 equiv) at 0 °C and stirred for 10 minutes before dropwise addition of the pre-stirred solution to the reaction mixture. The resulting solution was stirred for 1 hour at 0 °C and was then allowed to reach room temperature over 2 hours before complete consumption of the starting material was confirmed by LCMS. The reaction mixture was diluted with water (20 mL) and the aqueous phase was extracted with dichloromethane (3 × 20 mL). The combined organic extracts were washed with water (30 mL) and brine (30 mL), dried over magnesium sulfate, filtered and concentrated *in vacuo*. Aldehyde **2.16b** (140 mg, 0.43 mmol, 67%) was afforded as a yellow oil and the crude material was used in the next step without further purification.

LCMS (ESI) mass calculated for $C_{16}H_{33}O_6$ $[M+H]^+$ m/z 321.23, found m/z 321.67 with t_R = 5.79 min.

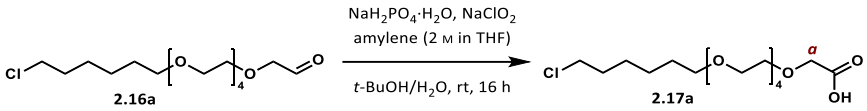

2.17a: To a stirred solution of aldehyde **2.16a** (300 mg, 0.85 mmol, 1 equiv) in *tert*-butanol/water (7.2 mL/1.8 mL, 0.1 M) was added sodium phosphate monobasic monohydrate (224 mg, 1.44 mmol, 1.7 equiv), sodium chlorite (268 mg, 2.98 mmol, 3.5 equiv) and amylene (2 M in THF, 3.2 mL, 6.0 mmol, 7 equiv). The resulting solution was stirred at room temperature for 16 hours. The reaction mixture was diluted with water (10 mL) and brine (10 mL), and the aqueous phase was extracted with ethyl acetate (4 × 20 mL). The combined organic extracts were washed with brine (2 × 40 mL), dried over magnesium sulfate and concentrated *in vacuo*. Purification by column chromatography on silica gel with an eluent of 5% to 20% ethanol in dichloromethane yielded carboxylic acid **2.17a** (260 mg, 0.70 mmol, 82%) as a clear oil.

Analytical data observed were in accordance with literature values.[103]

^{1}H NMR (400 MHz, chloroform-*d*) δ 3.83 (2H, s, -C**H$_2$**^{a}), 3.72 – 3.54 (17H, m, 8 × -CH$_2$ & -COOH), 3.52 (2H, t, *J* = 6.7 Hz, -CH$_2$), 3.43 (2H, t, *J* = 6.7 Hz, -CH$_2$), 1.81 – 1.72 (2H, m, -CH$_2$), 1.62 – 1.53 (2H, m, -CH$_2$), 1.49 – 1.31 (4H, m, 2 × -CH$_2$). ^{13}C NMR (101 MHz, chloroform-*d*) δ 176.1 (-COOH), 71.3 (-**C**^{a}H$_2$), 71.1 (-CH$_2$), 70.5 (-CH$_2$), 70.4 (-CH$_2$), 70.2 (2 × -CH$_2$), 70.1 (-CH$_2$), 70.0 (-CH$_2$), 69.9 (-CH$_2$), 69.2 (-CH$_2$), 45.2 (-CH$_2$Cl), 32.7 (-CH$_2$), 29.5 (-CH$_2$), 26.8 (-CH$_2$), 25.5 (-CH$_2$). HRMS (ESI) exact mass calculated for $C_{16}H_{31}ClO_7Na$ $[M+Na]^+$ m/z 393.1651, found m/z 393.1653. LCMS (ESI) mass calculated for $C_{16}H_{32}ClO_7$ $[M+H]^+$ m/z 371.18, found m/z 371.18 with t_R = 5.80 min.

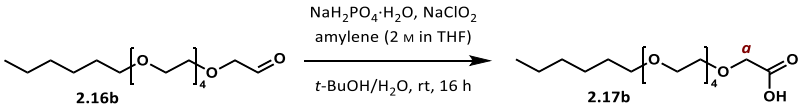

2.17b: To a stirred solution of aldehyde **2.16b** (140 mg, 0.42 mmol, 1 equiv) in *tert*-butanol/water (3.5 mL/0.7 mL, 0.1 M) was added sodium phosphate monobasic monohydrate (110 mg, 0.72 mmol, 1.7 equiv), sodium chlorite (130 mg, 1.5 mmol, 3.5 equiv) and amylene (2 M in THF, 1.6 mL, 3.0 mmol, 7 equiv). The resulting solution was stirred at room temperature for 16 hours. The reaction mixture was diluted with water (10 mL) and brine (10 mL), and the aqueous phase was extracted with ethyl acetate (4 × 20 mL). The combined organic extracts were washed with brine (2 × 40 mL), dried over magnesium sulfate and concentrated *in vacuo*. Purification by column chromatography on

silica gel with an eluent of 5% to 20% ethanol in dichloromethane yielded carboxylic acid **2.17b** (118 mg, 0.35 mmol, 83%) as a clear oil.

^{1}H NMR (400 MHz, chloroform-*d*) δ 6.28 (1H, s, -COOH), 3.90 (2H, s, -C**H$_2$**^{a}), 3.77 – 3.50 (16H, m, 8 × -CH$_2$), 3.41 (2H, t, *J* = 6.7 Hz, -CH$_2$), 1.65 – 1.46 (2H, m, -CH$_2$), 1.44 – 1.16 (6H, m, 3 × -CH$_2$), 0.86 (3H, t, *J* = 6.5 Hz, -CH$_3$). ^{13}C NMR (101 MHz, chloroform-*d*) δ 175.4 (-COOH), 71.6 (-**C**^{a}H$_2$), 70.6 (-CH$_2$), 70.4 (-CH$_2$), 70.3 (-CH$_2$), 70.1 (-CH$_2$), 70.0 (-CH$_2$), 70.0 (-CH$_2$), 69.9 (2 × -CH$_2$), 69.5 (-CH$_2$), 31.8 (-CH$_2$), 29.6 (-CH$_2$), 25.8 (-CH$_2$), 22.7 (-CH$_2$), 14.1 (-CH$_3$). IR (thin film) 2925, 1247, 1099 cm^{-1}. HRMS (ESI) exact mass calculated for $C_{16}H_{32}O_7Na$ $[M+Na]^+$ m/z 359.2040, found m/z 359.2039. LCMS (ESI) mass calculated for $C_{16}H_{33}O_7$ $[M+H]^+$ m/z 337.22, found m/z 337.58 with t_R = 5.95 min.

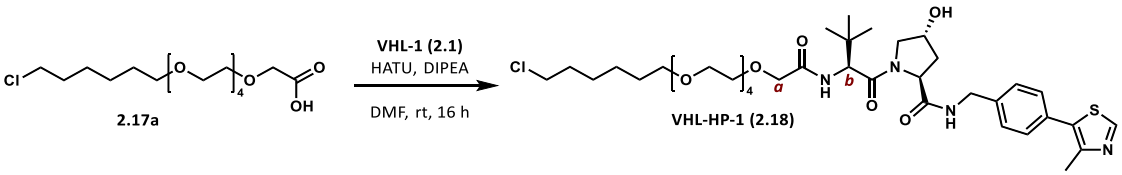

VHL-HP-1 (2.18): To a pre-stirred solution of carboxylic acid **2.17a** (49 mg, 0.13 mmol, 1 equiv), HATU (50 mg, 0.13 mmol, 1 equiv) and *N,N*-diisopropylethylamine (70 µL, 0.39 mmol, 3 equiv) in *N,N*-dimethylformamide (0.5 mL, 0.3 M) was added amine **VHL-1 (2.1)** (57 mg, 0.13 mmol, 1 equiv), and the resulting solution was stirred at room temperature for 16 hours. The reaction mixture was partitioned between dichloromethane (15 mL) and water (15 mL), and the aqueous phase was extracted with dichloromethane (5 × 15 mL). The combined organic phases were washed with 5% aqueous lithium chloride (5 × 20 mL), dried over magnesium sulfate, filtered and concentrated *in vacuo*. Purification by column chromatography on silica gel with an eluent of 5% to 20% ethanol in dichloromethane afforded VHL HaloPROTAC **VHL-HP-1 (2.18)** (80 mg, 0.10 mmol, 77%) as a clear oily solid. Further purification by semi-preparative RP-HPLC using a focussed gradient across 45% and 70% acetonitrile in water over 35 minutes eluted the title compound at t_R = 22 minutes (63% acetonitrile). Lyophilisation of the product fraction generated VHL HaloPROTAC **VHL-HP-1 (2.18)** (36 mg, 0.050 mmol, 35%) as a white fluffy powder.

Analytical data observed were in accordance with literature values.[103]

^{1}H NMR (500 MHz, methanol-*d*$_4$) δ 9.08 (1H, s, thiazole-CH), 7.51 – 7.43 (4H, m, 4 × Ar-CH), 4.70 (1H, s, -C**H**^{b}), 4.60 – 4.47 (3H, m, -CHOH & -CH$_2$), 4.37 (1H, d, *J* = 15.6 Hz, -CH), 4.04 (2H, m, -C**H$_2$**^{a}), 3.88 (1H, dd, *J* = 11.2, 1.7 Hz, -C*H*H), 3.80 (1H, dd, *J* = 11.0, 3.8 Hz, -CH*H*), 3.73 – 3.52 (18H, m, 9 × -CH$_2$), 3.46 (2H, t, *J* = 6.5 Hz, -CH$_2$), 2.50 (3H, s, -CH$_3$), 2.23 (1H, ddd, *J* = 13.2, 7.6, 1.9 Hz, -C*H*H), 2.09 (1H, ddd, *J* = 13.3, 9.1, 4.4 Hz, -CH*H*), 1.79 – 1.72 (2H, m, -

CH_2), 1.61 – 1.53 (2H, m, -CH_2), 1.49 – 1.34 (4H, m, 2 × -CH_3), 1.05 (9H, s, 3 × -CH_3). ^{13}C NMR (126 MHz, methanol-d_4) δ 174.4 (-CONH), 172.1 (-CONH), 171.6 (-CONH), 153.5 (thiazole-CH), 147.9 (thiazole-C), 140.7 (Ar-C), 130.9 (thiazole-C), 130.4 (2 × Ar-CH), 129.6 (Ar-C), 129.0 (2 × Ar-CH), 72.3 (-**C**^{a}H_2), 72.1 (-CH_2), 71.7 (-CH_2), 71.6 (-CH_2), 71.6 (3 × -CH_2), 71.5 (-CH_2), 71.2 (-CH_2), 71.1 (-CH_2), 71.0 (-CHOH), 60.8 (-**C**^{b}H), 58.1 (-CH), 58.1 (-CH_2), 45.7 (-CH_2), 43.7 (-CH_2), 38.9 (-CH_2), 37.1 (-*C*(CH_3)$_3$), 33.7 (-CH_2), 30.6 (-CH_2), 27.7 (-CH_2), 27.0 (3C, -C(*C*H_3)$_3$), 26.5 (-CH_2), 15.4 (-CH_3). HRMS (ESI) exact mass calculated for $C_{38}H_{59}N_4O_9SClNa$ $[M+Na]^+$ m/z 805.3583, found m/z 805.3554. LCMS (ESI) mass calculated for $C_{38}H_{60}N_4O_9SCl$ $[M+H]^+$ m/z 783.38, found m/z 783.08 with t_R = 6.16 min.

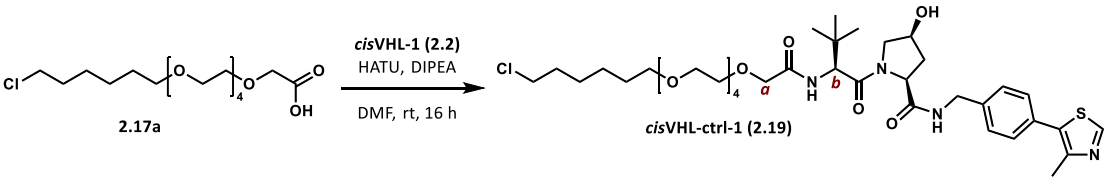

***cis*VHL-ctrl-1 (2.19)**: To a pre-stirred solution of carboxylic acid **2.17a** (22 mg, 0.059 mmol, 1 equiv), HATU (22 mg, 0.059 mmol, 1 equiv) and *N,N*-diisopropylethylamine (30 µL, 0.18 mmol, 3 equiv) in *N,N*-dimethylformamide (0.2 mL, 0.3 M) was added amine ***cis*VHL-1 (2.2)** (26 mg, 0.059 mmol, 1 equiv), and the resulting solution was stirred at room temperature for 16 hours. The reaction mixture was partitioned between dichloromethane (15 mL) and water (15 mL), and the aqueous phase was extracted with dichloromethane (5 × 15 mL). The combined organic phases were washed with 5% aqueous lithium chloride (5 × 20 mL), dried over magnesium sulfate, filtered and concentrated *in vacuo*. Purification by column chromatography on silica gel with an eluent of 5% to 20% ethanol in dichloromethane afforded VHL epimer control ***cis*VHL-ctrl-1 (2.19)** (24 mg, 0.031 mmol, 51%) as a clear oily solid. Further purification by semi-preparative RP-HPLC using a focused gradient across 50% and 80% acetonitrile in water over 30 minutes eluted the title compound at t_R = 21 minutes (71% acetonitrile). Lyophilisation of the product fraction generated VHL epimer control ***cis*VHL-ctrl-1 (2.19)** (14 mg, 0.018 mmol, 30%) as a white fluffy powder.

^{1}H NMR (500 MHz, methanol-d_4) δ 10.08 (1H, s, thiazole-CH), 7.68 – 7.48 (4H, m, 4 × Ar-CH), 4.64 – 4.56 (2H, m, -CHOH & -C**H**^{b}), 4.52 (1H, dd, *J* = 9.0, 4.7 Hz, -CH), 4.46 – 4.37 (2H, m, -CH_2), 4.05 (2H, s, -C**H**$_2^{a}$), 4.03 – 3.99 (1H, m, -C*H*H), 3.74 – 3.53 (19H, m, -CH*H* & 9 × -CH_2), 3.47 (2H, t, *J* = 6.5 Hz, -CH_2), 2.63 (3H, s, -CH_3), 2.50 – 2.41 (1H, m, -C*H*H), 2.00 – 1.93 (1H, m, -CH*H*), 1.79 – 1.71 (2H, m, -CH_2), 1.61 – 1.54 (2H, m, -CH_2), 1.49 – 1.34 (4H, m, 2 × -CH_3), 1.05 (9H, s, 3 × -CH_3). ^{13}C NMR (126 MHz, DMSO-d_6) δ 172.3 (-CONH), 169.3 (-CONH), 168.9 (-CONH), 152.0 (thiazole-CH), 146.9 (thiazole-C), 139.4 (Ar-C), 131.6 (thiazole-C),

129.4 (Ar-C), 128.7 (2 × Ar-CH), 127.5 (2 × Ar-CH), 70.4 (-C[a]H$_2$), 70.2 (-CH$_2$), 69.8 (2 × -CH$_2$), 69.8 (3 × -CH$_2$), 69.6 (-CH$_2$), 69.5 (-CH$_2$), 69.5 (-CH$_2$), 69.0 (-CHOH), 58.6 (-C[b]H), 55.8 (-CH$_2$), 55.6 (-CH), 45.4 (-CH$_2$), 41.8 (-CH$_2$), 39.0 (-CH$_2$), 36.9 (-*C*(CH$_3$)$_3$), 35.2 (-CH$_2$), 32.0 (-CH$_2$), 29.1 (-CH$_2$), 26.2 (3C, -C(*C*H$_3$)$_3$), 24.9 (-CH$_2$), 15.6 (-CH$_3$). IR (thin film) 3304, 1528, 668 cm^{-1}. HRMS (ESI) exact mass calculated for $C_{38}H_{59}N_4O_9SClNa$ $[M+Na]^+$ m/z 805.3583, found m/z 805.3566. LCMS (ESI) mass calculated for $C_{38}H_{60}N_4O_9SCl$ $[M+H]^+$ m/z 783.38, found m/z 783.67 with t_R = 6.27 min.

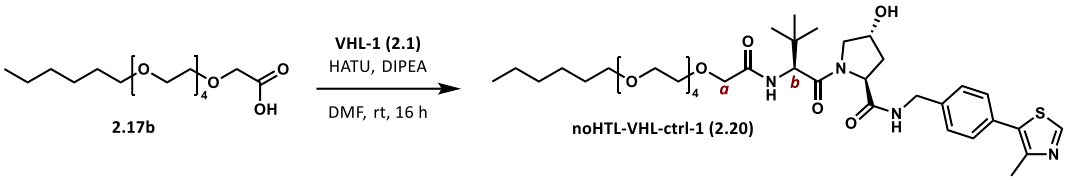

noHTL-VHL-ctrl-1 (2.20): To a pre-stirred solution of carboxylic acid **2.17b** (22 mg, 0.065 mmol, 1 equiv), HATU (25 mg, 0.065 mmol, 1 equiv) and *N,N*-diisopropylethylamine (40 µL, 0.20 mmol, 3 equiv) in *N,N*-dimethylformamide (0.2 mL, 0.3 M) was added amine **VHL-1 (2.1)** (28 mg, 0.065 mmol, 1 equiv), and the resulting solution was stirred at room temperature for 16 hours. Complete consumption of the starting material was confirmed by TLC before removing volatile components *in vacuo*. Purification by column chromatography on silica gel with an eluent of 5% to 20% ethanol in dichloromethane afforded VHL HaloTag control **noHTL-VHL-ctrl-1 (2.20)** (34 mg, 0.045 mmol, 68%) as a clear oily solid. Further purification by semi-preparative RP-HPLC using a focused gradient across 50% and 80% acetonitrile in water over 25 minutes eluted the title compound at t_R = 21 minutes (74% acetonitrile). Lyophilisation of the product fraction generated VHL HaloTag control **noHTL-VHL-ctrl-1 (2.20)** (20 mg, 0.027 mmol, 40%) as a white fluffy powder.

^{1}H NMR (500 MHz, methanol-*d*$_4$) 10.02 (1H, s, thiazole-CH), 7.62 – 7.50 (4H, m, 4 × Ar-CH), 4.70 (1H, s, -C**H**[b]), 4.62 – 4.55 (2H, m, -CH$_2$), 4.54 – 4.48 (1H, m, -CHOH), 4.42 – 4.37 (1H, m, -CH), 4.10 – 4.01 (2H, m, -C**H$_2$**[a]), 3.88 (1H, dd, *J* = 11.0, 1.6 Hz, -C*H*H), 3.81 (1H, dd, J = 11.1, 3.7 Hz, -CH*H*), 3.74 – 3.54 (16H, m, 8 × -CH$_2$), 3.45 (2H, t, *J* = 6.7 Hz, -CH$_2$), 2.62 (3H, s, -CH$_3$), 2.28 – 2.21 (1H, m, -C*H*H), 2.12 – 2.04 (1H, m, -CH*H*), 1.60 – 1.51 (2H, m, -CH$_2$), 1.39 – 1.25 (6H, m, 3 × -CH$_3$), 1.05 (9H, s, 3 × -CH$_3$), 0.90 (3H, t, *J* = 6.8 Hz, CH$_3$). ^{13}C NMR (126 MHz, DMSO-*d*$_6$) δ 171.9 (-CONH), 169.17 (-CONH), 168.7 (-CONH), 153.4 (thiazole-CH), 144.6 (thiazole-C), 140.5 (Ar-C), 133.0 (thiazole-C), 128.8 (2 × Ar-CH), 128.3 (Ar-C), 127.7 (2 × Ar-CH), 70.5 (-C[a]H$_2$), 70.4 (-CH$_2$), 69.9 (2 × -CH$_2$), 69.9 (3 × -CH$_2$), 69.7 (-CH$_2$), 69.5 (-CH$_2$), 68.9 (-CH$_2$), 68.9 (-CHOH), 58.8 (-C[b]H), 56.6 (-CH$_2$), 55.8 (-CH), 41.7 (-CH$_2$), 38.0 (-CH$_2$), 36.2 (-*C*(CH$_3$)$_3$), 35.8 (-CH$_2$), 31.2 (-CH$_2$), 29.2 (-CH$_2$), 26.3 (3C, -C(*C*H$_3$)$_3$), 25.4 (-CH$_2$), 22.2 (-CH$_3$),

14.0 (-CH_3). HRMS (ESI) exact mass calculated for $C_{38}H_{60}N_4O_9SNa$ $[M+Na]^+$ m/z 771.3973, found m/z 771.3955. LCMS (ESI) mass calculated for $C_{38}H_{61}N_4O_9S$ $[M+H]^+$ m/z 749.42, found m/z 749.42 with t_R = 6.32 min.

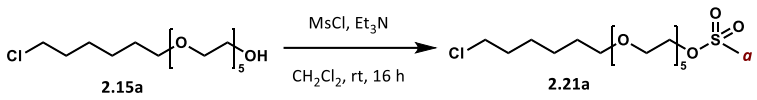

2.15a **2.21a**

2.21a: To a dry flask charged with argon was added anhydrous dichloromethane (19 mL, 0.1 M), alcohol **2.15a** (662 mg, 1.86 mmol, 1 equiv), methanesulfonyl chloride (0.22 mL, 2.8 mmol, 1.5 equiv) and triethylamine (0.76 mL, 5.6 mmol, 3 equiv) and the resulting solution was stirred at room temperature for 16 hours. The reaction mixture was partitioned between 1 M aqueous hydrochloric acid (20 mL) and dichloromethane (20 mL), and the aqueous phase was extracted with dichloromethane (3 × 20 mL). The combined organic extracts were washed with water (2 × 40 mL), dried over magnesium sulfate, filtered and concentrated *in vacuo*. Purification by column chromatography on silica gel with ethyl acetate afforded mesylate **2.21a** (662 mg, 1.40 mmol, 75%) as a light yellow oil.

^{1}H NMR (400 MHz, chloroform-*d*) δ 4.43 – 4.34 (2H, m, -CH_2), 3.80 – 3.73 (2H, m, -CH_2), 3.71 – 3.60 (16H, m, 8 × -CH_2), 3.60 – 3.49 (2H, m, -CH_2), 3.45 (2H, t, *J* = 6.6 Hz, -CH_2), 3.08 (3H, s, -C**H$_3$**^{a}), 1.83 – 1.72 (2H, m, -CH_2), 1.66 – 1.54 (2H, m, -CH_2), 1.52 – 1.30 (4H, m, 2 × -CH_2). ^{13}C NMR (101 MHz, chloroform-*d*) δ 71.4 (-CH_2), 70.8 (-CH_2), 70.8 (-CH_2), 70.8 (2 × -CH_2), 70.8 (2 × -CH_2), 70.7 (-CH_2), 70.3 (-CH_2), 69.4 (-CH_2), 69.2 (-CH_2), 45.2 (-CH_2Cl), 37.9 (-**C**^{a}H_3), 32.7 (-CH_2), 29.6 (-CH_2), 26.9 (-CH_2), 25.6 (-CH_2). IR (thin film) 1349, 1173 cm^{-1}. HRMS (ESI) exact mass calculated for $C_{17}H_{35}O_8SClNa$ $[M+Na]^+$ m/z 457.1633, found m/z 457.1633.

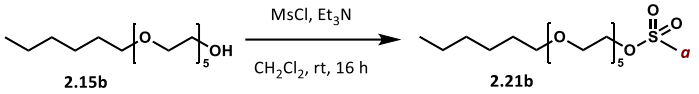

2.15b **2.21b**

2.21b: To a dry flask charged with argon was added anhydrous dichloromethane (13 mL, 0.1 M), alcohol **2.15b** (410 mg, 1.27 mmol, 1 equiv), methanesulfonyl chloride (0.15 mL, 1.9 mmol, 1.5 equiv) and triethylamine (0.52 mL, 3.8 mmol, 3 equiv) and the resulting solution was stirred at room temperature for 16 hours. The reaction mixture was partitioned between 1 M aqueous hydrochloric acid (15 mL) and dichloromethane (15 mL), and the aqueous phase was extracted with dichloromethane (3 × 15 mL). The combined organic extracts were washed with water (2 × 30 mL), dried over magnesium sulfate, filtered and concentrated *in vacuo*. Purification by column chromatography on silica gel with ethyl acetate afforded mesylate **2.21b** (461 mg, 1.15 mmol, 91%) as a light yellow oil.

^{1}H NMR (400 MHz, chloroform-*d*) δ 4.42 – 4.32 (2H, m, -CH$_2$), 3.83 – 3.71 (2H, m, -CH$_2$), 3.72 – 3.54 (16H, m, 8 × -CH$_2$), 3.44 (2H, t, *J* = 6.8 Hz, -CH$_2$), 3.08 (3H, s, -C**H$_3$**^{a}), 1.69 – 1.50 (2H, m, -CH$_2$), 1.41 – 1.20 (6H, m, 3 × -CH$_2$), 0.88 (3H, t, *J* = 7.0 Hz, CH$_2$). ^{13}C NMR (101 MHz, chloroform-*d*) δ 71.7 (-CH$_2$), 70.8 (-CH$_2$), 70.8 (-CH$_2$), 70.8 (2 × -CH$_2$), 70.8 (2 × -CH$_2$), 70.7 (-CH$_2$), 70.2 (-CH$_2$), 69.4 (-CH$_2$), 69.2 (-CH$_2$), 37.9 (-**C**^{a}H$_3$), 31.9 (-CH$_2$), 29.8 (-CH$_2$), 25.9 (-CH$_2$), 22.8 (-CH$_2$), 14.2 (-CH$_3$). IR (thin film) 1349, 1173, 648 cm^{-1}. HRMS (ESI) exact mass calculated for $C_{17}H_{36}O_8SNa$ [M+Na]$^{+}$ m/z 423.2023, found m/z 423.2025.

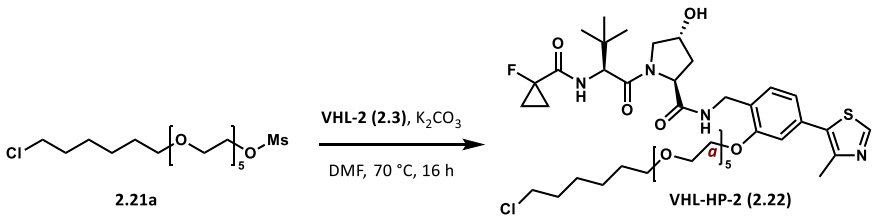

VHL-HP-2 (2.22): To a stirred solution of mesylate **2.21a** (89 mg, 0.21 mmol, 1.5 equiv) in *N,N*-dimethylformamide (0.35 mL, 0.4 M) was added phenol **VHL-2 (2.3)** (73 mg, 0.14 mmol, 1 equiv) and potassium carbonate (48 mg, 0.35 mmol, 2.5 equiv), the resulting solution was heated to 70 °C and stirred for 16 hours. The reaction mixture was diluted with water (15 mL) and the aqueous phase was extracted with dichloromethane (4 × 15 mL). The combined organic extracts were washed with 5% aqueous lithium chloride (3 × 20 mL), dried over magnesium sulfate, filtered and concentrated *in vacuo*. Purification by column chromatography on silica gel with an eluent of 5% to 20% ethanol in dichloromethane afforded VHL HaloPROTAC **VHL-HP-2 (2.22)** (56 mg, 0.064 mmol, 47%) as a clear oily solid. Further purification by semi-preparative RP-HPLC using a focused gradient across 50% and 80% acetonitrile in water over 30 minutes eluted the title compound at t_R = 23 minutes (76% acetonitrile). Lyophilisation of the product fraction generated VHL HaloPROTAC **VHL-HP-2 (2.22)** (30 mg, 0.034 mmol, 25%) as a white fluffy powder.

^{1}H NMR (400 MHz, methanol-*d*$_4$) δ 9.97 (1H, s, thiazole-CH), 7.61 (1H, d, *J* = 7.8 Hz, Ar-CH), 7.17 (1H, d, *J* = 1.6 Hz, Ar-CH), 7.12 (1H, dd, *J* = 7.8, 1.4 Hz, Ar-CH), 4.75 (1H, s, -CH), 4.67 – 4.59 (1H, m, -CH), 4.58 – 4.48 (2H, m, -CH & -C*H*H), 4.45 – 4.35 (2H, m, -CH*H*), 4.33 – 4.23 (2H, m, -C**H$_2$**^{a}), 3.95 – 3.90 (2H, m, -CH$_2$), 3.89 – 3.83 (1H, m, -C*H*H), 3.83 – 3.77 (1H, m, -CH*H*), 3.77 – 3.72 (2H, m, -CH$_2$), 3.71 – 3.66 (2H, m, -CH$_2$), 3.65 – 3.59 (10H, m, 5 × -CH$_2$), 3.58 – 3.52 (4H, m, 2 × -CH$_2$), 3.46 (2H, t, *J* = 6.5 Hz, -CH$_2$), 2.62 (3H, s, -CH$_3$), 2.30 – 2.22 (1H, m, -C*H*H), 2.14 – 2.04 (1H, m, -CH*H*), 1.80 – 1.70 (2H, m, -CH$_2$), 1.61 – 1.52 (2H, m, -CH$_2$), 1.49 – 1.26 (8H, m, 4 × -CH$_2$), 1.03 (9H, s, 3 × CH$_3$). ^{13}C NMR (101 MHz, methanol-*d*$_4$) δ 174.4 (-CONH), 171.7 (-CONH), 171.4 (d, $^{2}J_{C\text{-}F}$ = 20.6 Hz, -CONH), 158.4 (Ar-C), 156.5 (thiazole-CH),

142.5 (thiazole-C), 137.6 (thiazole-C), 130.7 (Ar-C), 130.3 (Ar-CH), 129.1 (Ar-C), 122.8 (Ar-CH), 113.7 (Ar-CH), 79.2 (d, $^{1}J_{C\text{-}F}$ = 231.4 Hz, -CF), 72.1 (-CH_2), 71.8 (-CH_2), 71.6 (2 × -CH_2), 71.6 (2 × -CH_2), 71.5 (2 × -CH_2), 71.2 (-C), 71.1 (-CH_2), 70.8 (-CH_2), 69.6 (-**C**^{a}H_2), 60.8 (-CH), 58.7 (-CH), 58.2 (-CH_2), 45.7 (-CH_2), 39.4 (-CH_2), 39.0 (-CH_2), 37.3 (-*C*(CH_3)$_3$), 33.7 (-CH_2), 30.5 (-CH_2), 27.7 (-CH_2), 26.9 (3 × -CH_3), 26.5 (-CH_2), 14.0 (d, $^{2}J_{C\text{-}F}$ = 11.0 Hz, cyclopropyl-CH_2), 13.9 (d, $^{2}J_{C\text{-}F}$ = 10.9 Hz, cyclopropyl-CH_2), 13.2 (-CH_3). IR (thin film) 3320, 1094, 668 cm^{-1}. HRMS (ESI) exact mass calculated for $C_{42}H_{65}ClFN_4O_{10}S$ $[M+H]^+$ m/z 871.4088, found m/z 871.4101. LCMS (ESI) mass calculated for $C_{42}H_{65}ClFN_4O_{10}S$ $[M+H]^+$ m/z 871.41, found m/z 871.75 with t_R = 6.35 min.

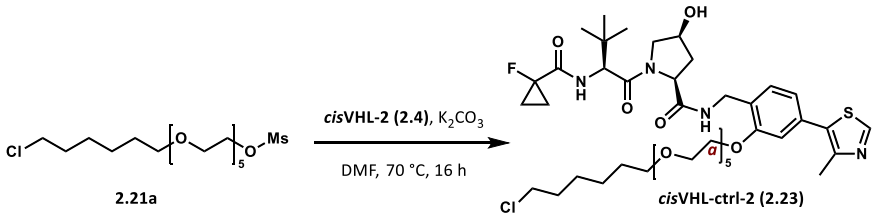

***cis*VHL-ctrl-2 (2.23)**: To a stirred solution of mesylate **2.21a** (27 mg, 0.062 mmol, 1.5 equiv) in *N,N*-dimethylformamide (0.11 mL, 0.4 M) was added phenol **cisVHL-2 (2.4)** (22 mg, 0.041 mmol, 1 equiv) and potassium carbonate (15 mg, 0.10 mmol, 2.5 equiv), the resulting solution was heated to 70 °C and stirred for 16 hours. Complete consumption of the starting material was confirmed by TLC before removing volatile components *in vacuo*. Purification by column chromatography on silica gel with an eluent of 5% to 20% ethanol in dichloromethane afforded VHL epimer control ***cis*VHL-ctrl-2 (2.23)** (32 mg, 0.037 mmol, 89%) as a clear oily solid. Further purification by semi-preparative RP-HPLC using a focused gradient across 60% and 90% acetonitrile in water over 25 minutes eluted the title compound at t_R = 19 minutes (78% acetonitrile). Lyophilisation of the product fraction generated VHL epimer control ***cis*VHL-ctrl-2 (2.23)** (15 mg, 0.017 mmol, 42%) as a white fluffy powder.

^{1}H NMR (400 MHz, methanol-d_4) δ 9.18 (1H, s, thiazole-CH), 7.49 (1H, d, *J* = 7.8 Hz, Ar-CH), 7.09 (1H, d, *J* = 1.6 Hz, Ar-CH), 7.04 (1H, dd, *J* = 7.7, 1.7 Hz, Ar-CH), 4.71 – 4.65 (1H, s, -CH), 4.61 – 4.52 (1H, m, -CH), 4.52 – 4.43 (1H, m, -CH), 4.44 – 4.35 (2H, m, -CH_2), 4.31 – 4.21 (2H, m, -C**H$_2$**^{a}), 3.95 – 3.88 (2H, m, -CH_2), 3.78 – 3.51 (18H, m, 9 × -CH_2), 3.49 – 3.42 (2H, m, -CH_2), 2.53 (3H, s, -CH_3), 2.50 – 2.39 (1H, m, -C*H*H), 2.03 – 1.92 (1H, m, -CH*H*), 1.82 – 1.70 (2H, m, -CH_2), 1.65 – 1.23 (12H, m, 6 × -CH_2), 1.02 (9H, s, 3 × CH_3). ^{13}C NMR (101 MHz, methanol-d_4) δ 174.7 (-CONH), 171.9 (-CONH), 171.6 (d, $^{2}J_{C\text{-}F}$ = 20.7 Hz, -CONH), 158.2 (Ar-C), 153.8 (thiazole-CH), 147.4 (thiazole-C), 134.6 (thiazole-C), 132.0 (Ar-C), 130.3 (Ar-CH),

128.8 (Ar-C), 122.8 (Ar-CH), 113.8 (Ar-CH), 79.1 (d, $^{1}J_{C\text{-}F}$ = 231.7 Hz, -CF), 72.1 (-CH_2), 71.8 (-CH_2), 71.6 (-CH_2), 71.6 (2 × -CH_2), 71.6 (2 × -CH_2), 71.5 (-CH_2), 71.2 (-C), 71.0 (-CH_2), 70.8 (-CH_2), 69.5 (-**C^{a}**H_2), 61.1 (-CH), 58.7 (-CH), 57.8 (-CH_2), 45.7 (-CH_2), 39.6 (-CH_2), 37.8 (-CH_2), 36.8 (-*C*$(CH_3)_3$), 33.8 (-CH_2), 30.6 (-CH_2), 27.7 (-CH_2), 26.9 (3 × -CH_3), 26.5 (-CH_2), 15.2 (-CH_3), 14.1 (d, $^{2}J_{C\text{-}F}$ = 11.0 Hz, cyclopropyl-CH_2), 13.9 (d, $^{2}J_{C\text{-}F}$ = 10.9 Hz, cyclopropyl-CH_2). HRMS (ESI) exact mass calculated for $C_{42}H_{64}ClFN_4O_{10}SNa$ $[M+Na]^+$ m/z 893.3908, found m/z 893.3873. LCMS (ESI) mass calculated for $C_{42}H_{65}ClFN_4O_{10}S$ $[M+H]^+$ m/z 871.41, found m/z 871.67 with t_R = 6.38 min.

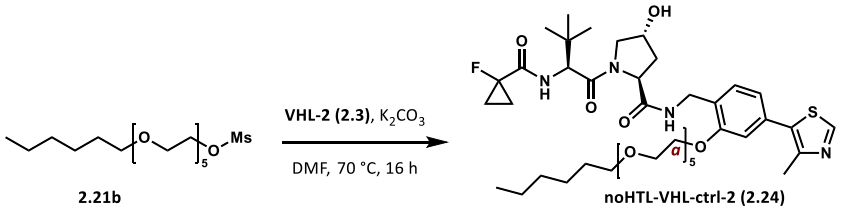

2.21b noHTL-VHL-ctrl-2 (2.24)

noHTL-VHL-ctrl-2 (2.24): To a stirred solution of mesylate **2.21b** (27 mg, 0.068 mmol, 1.5 equiv) in *N,N*-dimethylformamide (0.12 mL, 0.4 M) was added phenol **VHL-2 (2.3)** (22 mg, 0.041 mmol, 1 equiv) and potassium carbonate (16 mg, 0.11 mmol, 2.5 equiv), the resulting solution was heated to 70 °C and stirred for 16 hours. Complete consumption of the starting material was confirmed by TLC before removing volatile components *in vacuo*. Purification by column chromatography on silica gel with an eluent of 5% to 10% ethanol in dichloromethane afforded VHL HaloTag control **noHTL-VHL-ctrl-2 (2.24)** (35 mg, 0.042 mmol, 92%) as a clear oily solid. Further purification by semi-preparative RP-HPLC using a focused gradient across 60% and 90% acetonitrile in water over 25 minutes eluted the title compound at t_R = 18 minutes (77% acetonitrile). Lyophilisation of the product fraction generated VHL HaloTag control **noHTL-VHL-ctrl-2 (2.24)** (14 mg, 0.017 mmol, 37%) as a white fluffy powder.

^{1}H NMR (400 MHz, methanol-d_4) δ 9.27 (1H, s, thiazole-CH), 7.53 (1H, d, *J* = 7.7 Hz, Ar-CH), 7.10 (1H, d, *J* = 1.7 Hz, Ar-CH), 7.06 (1H, dd, *J* = 7.8, 1.6 Hz, Ar-CH), 4.77 – 4.73 (1H, m, -CH), 4.66 – 4.60 (1H, m, -CH), 4.55 – 4.47 (1H, m, -CH & -C*H*H), 4.45 – 4.37 (2H, m, -CH*H*), 4.30 – 4.22 (2H, m, -C**H$_2$^{a}**), 3.95 – 3.90 (2H, m, -CH_2), 3.88 – 3.83 (1H, m, -C*H*H), 3.83 – 3.77 (1H, m, -CH*H*), 3.77 – 3.71 (2H, m, -CH_2), 3.71 – 3.65 (2H, m, -CH_2), 3.65 – 3.58 (10H, m, 5 × -CH_2), 3.58 – 3.52 (2H, m, -CH_2), 3.44 (2H, t, *J* = 6.6 Hz, -CH_2), 2.54 (3H, s, -CH_3), 2.28 – 2.20 (1H, m, -C*H*H), 2.14 – 2.04 (1H, m, -CH*H*), 1.59 – 1.50 (2H, m, -CH_2), 1.42 – 1.23 (10H, m, 5 × -CH_2), 1.03 (9H, s, 3 × CH_3), 0.95 – 0.84 (3H, s, -CH_3). ^{13}C NMR (101 MHz, methanol-d_4) δ 174.3 (-CONH), 171.7 (-CONH), 171.4 (d, $^{2}J_{C\text{-}F}$ = 20.4 Hz, -CONH), 158.2 (Ar-C), 154.0

(thiazole-CH), 147.0 (thiazole-C), 142.8 (thiazole-C), 131.6 (Ar-C), 130.1 (Ar-CH), 129.2 (Ar-C), 122.8 (Ar-CH), 113.8 (Ar-CH), 79.1 (d, $^{1}J_{C\text{-}F}$ = 231.8 Hz, -CF), 72.4 (-CH_2), 71.8 (-CH_2), 71.6 (2 × -CH_2), 71.6 (2 × -CH_2), 71.6 (2 × -CH_2), 71.2 (-C), 71.1 (-CH_2), 70.9 (-CH_2), 69.5 (-**C^{a}**H_2), 60.8 (-CH), 58.7 (-CH), 58.2 (-CH_2), 39.5 (-CH_2), 38.9 (-CH_2), 37.3 (-*C*$(CH_3)_3$), 32.8 (-CH_2), 30.7 (-CH_2), 26.9 (3 × -CH_3), 23.7 (-CH_2), 15.0 (-CH_3), 14.4 (-CH_3), 14.0 (d, $^{2}J_{C\text{-}F}$ = 11.1 Hz, cyclopropyl-CH_2), 13.9 (d, $^{2}J_{C\text{-}F}$ = 11.0 Hz, cyclopropyl-CH_2). IR (thin film) 3416, 1098, 701 cm^{-1}. HRMS (ESI) exact mass calculated for $C_{42}H_{65}FN_4O_{10}SNa$ $[M+Na]^+$ m/z 859.4298, found m/z 859.4291. LCMS (ESI) mass calculated for $C_{42}H_{66}FN_4O_{10}S$ $[M+H]^+$ m/z 837.45, found m/z 837.33 with t_R = 6.44 min.

- *CRBN HaloPROTACs and mono-functional controls:*

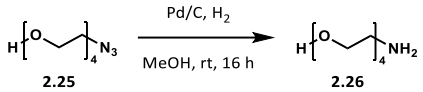

2.26: To a stirred solution of azide **2.25** (1.0 g, 4.6 mmol, 1 equiv) in methanol (46 mL, 0.1 M) under an argon atmosphere was added 10% palladium on carbon (73 mg, 0.46 mmol, 10 mol%). The flask was evacuated and purged with argon three times, before sparging the suspension with hydrogen gas and stirring at room temperature under a hydrogen atmosphere for 16 hours. The hydrogen gas was removed by evacuating the flask and purging it with argon three times. After confirming complete consumption of starting material, the suspension was filtered through a pad of celite in dichloromethane and the celite washed with dichloromethane (250 mL) and methanol (250 mL). The solvents were removed *in vacuo* yielding aminoalcohol **2.26** (754 g, 3.90 mmol, 86%) as a pale yellow oil and the crude material was used in the next step without further purification.

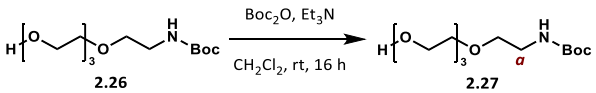

2.27: To a stirred solution of amine **2.26** (697 mg, 3.61 mmol, 1 equiv) in anhydrous dichloromethane (12 mL, 0.3 M) were added di-*tert*-butyl dicarbonate (945 mg, 4.33 mmol, 1.2 equiv) and triethylamine (0.75 mL, 5.4 mmol, 1.5 equiv) and the reaction mixture was stirred at room temperature for 16 hours. Volatile components were removed *in vacuo.* Purification by column chromatography on silica gel with ethyl acetate afforded protected linker **2.27** (876 mg, 2.99 mmol, 83%) as a pale yellow oil.

Analytical data observed were in accordance with literature values.[255]

^{1}H NMR (400 MHz, chloroform-*d*) δ 5.61 (1H, s, -NH), 3.75 – 3.49 (14H, m, 7 × -CH_2), 3.30 (2H, t, *J* = 5.3 Hz, -C**H$_2$**^{a}), 3.07 (1H, s, -OH), 1.42 (9H, s, 3 × -CH_3). ^{13}C NMR (101 MHz, chloroform-*d*) δ 156.3 (-NCOOR), 79.1 (-*C*(CH_3)), 72.8 (-CH_2), 70.8 (-CH_2), 70.6 (2 × -CH_2), 70.4 (-CH_2), 70.2 (-CH_2), 61.8 (-CH_2), 40.5 (-**C**^{a}H_2), 28.6 (3 × -CH_3).

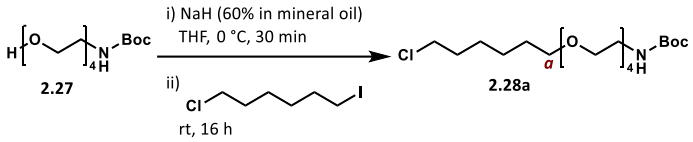

2.28a: To a dry flask charged with argon was added anhydrous tetrahydrofuran (1.4 mL, 0.5 M), protected aminoalcohol **2.27** (200 mg, 0.68 mmol, 1 equiv) and sodium hydride (60% in mineral oil, 68 mg, 1.7 mmol, 2.5 equiv) at 0 °C. The resulting suspension was stirred for 30 minutes before 1-chloro-6-iodohexane (0.10 mL, 0.68 mmol, 1 equiv) was added slowly at 0 °C. The reaction mixture was allowed to reach room temperature and stirred for further 16 hours. The reaction was quenched by dropwise addition of water (10 mL). The aqueous phase was extracted with dichloromethane (3 × 10 mL) and the combined organic extracts were washed with brine (20 mL), dried over magnesium sulfate, filtered and concentrated *in vacuo*. Purification by column chromatography on silica gel with an eluent of 50 % ethyl acetate in petroleum ether afforded linker fragment **2.28a** (92 mg, 0.22 mmol, 33%) as a light yellow oil.

^{1}H NMR (400 MHz, chloroform-*d*) δ 5.04 (1H, s, -NH), 3.69 – 3.48 (16H, m, -C**H$_2$**^{a} & 7 × -CH_2), 3.45 (2H, t, *J* = 6.6 Hz, -CH_2), 3.35 – 3.25 (2H, m, -CH_2), 1.80 – 1.72 (2H, m, -CH_2), 1.63 – 1.55 (2H, m, -CH_2), 1.43 (9H, s, 3 × -CH_3), 1.40 – 1.32 (4H, m, 2 × -CH_2). ^{13}C NMR (101 MHz, chloroform-*d*) δ 156.1 (-NCOOR), 79.3 (-*C*(CH_3)), 71.4 (-**C**^{a}H_2), 70.8 (2 × -CH_2), 70.8 (-CH_2), 70.7 (-CH_2), 70.4 (-CH_2), 70.4 (-CH_2), 70.3 (-CH_2), 45.2 (-CH_2), 40.5 (-CH_2), 32.7 (-CH_2), 29.6 (-CH_2), 28.6 (3 × -CH_3), 26.8 (-CH_2), 25.6 (-CH_2). IR (thin film) 3345, 1711, 864 cm^{-1}. HRMS (ESI) exact mass calculated for $C_{19}H_{38}ClNO_6Na$ $[M+Na]^+$ m/z 434.2280, found m/z 434.2265. LCMS (ESI) mass calculated for $C_{19}H_{39}ClNO_6$ $[M+H]^+$ m/z 412.25, found m/z 412.14 with t_R = 6.70 min.

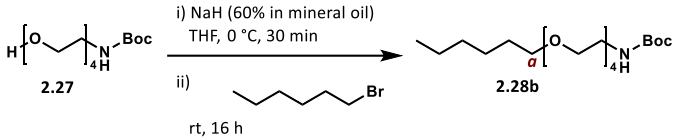

2.28b: To a dry flask charged with argon was added anhydrous tetrahydrofuran (1.4 mL, 0.5 M), protected aminoalcohol **2.27** (200 mg, 0.68 mmol, 1 equiv) and sodium hydride (60% in mineral oil, 68 mg, 1.7 mmol, 2.5 equiv) at 0 °C. The resulting suspension was stirred for 30 minutes before 1-bromohexane (0.10 mL, 0.68 mmol, 1 equiv) was added slowly at 0 °C. The reaction mixture was allowed to reach room temperature and stirred for further 16 hours. The reaction was quenched by dropwise addition of water (10 mL). The aqueous phase was extracted with dichloromethane (3 × 10 mL) and the combined organic extracts were washed with brine (20 mL), dried over magnesium sulfate, filtered and concentrated *in vacuo*. Purification by column chromatography on silica gel with an eluent of 50 % ethyl acetate in petroleum ether afforded linker fragment **2.28b** (73 mg, 0.19 mmol, 28%) as a light yellow oil.

^{1}H NMR (400 MHz, chloroform-*d*) δ 5.03 (1H, s, -NH), 3.74 – 3.50 (14H, m, 7 × -CH_2), 3.44 (2H, t, *J* = 6.8 Hz, -C**H$_2$**^{a}), 3.37 – 3.26 (2H, m, -CH_2), 1.65 – 1.49 (2H, m, -CH_2), 1.43 (9H, s, 3 × -CH_3), 1.38 – 1.16 (6H, m, 3 × -CH_2), 0.88 (3H, t, *J* = 6.9 Hz, -CH_3). ^{13}C NMR (101 MHz, chloroform-*d*) δ 156.1 (-NCOOR), 77.4 (-*C*(CH_3)), 71.7 (-**C**^{a}H_2), 70.8 (-CH_2), 70.8 (2 × -CH_2), 70.7 (-CH_2), 70.4 (-CH_2), 70.4 (-CH_2), 70.2 (-CH_2), 40.6 (-CH_2), 31.8 (-CH_2), 29.8 (-CH_2), 28.6 (3 × -CH_3), 25.9 (-CH_2), 22.8 (-CH_2), 14.2 (-CH_3). IR (thin film) 3351, 1508, 1248 cm^{-1}. HRMS (ESI) exact mass calculated for $C_{19}H_{39}NO_6Na$ $[M+Na]^+$ m/z 400.2669, found m/z 400.2670.

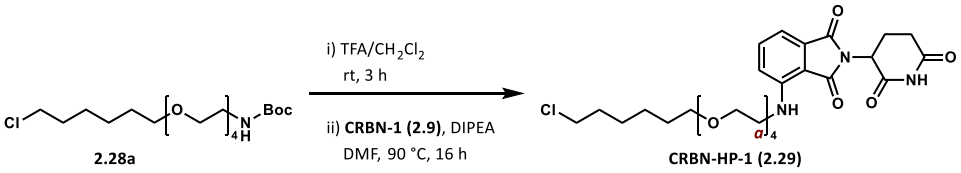

CRBN-HP-1 (2.29): Protected linker fragment **2.28a** (62 mg, 0.15 mmol, 1 equiv) was dissolved in trifluoroacetic acid/dichloromethane (2.5 mL/2.5 mL, 0.03 M) and the resulting solution was stirred at room temperature for 3 hours. The reaction was monitored by TLC for complete consumption of the starting material before removal of volatile components *in vacuo*. The residue was redissolved in *N,N*-dimethylformamide (0.75 mL, 0.2 M), and CRBN ligand **CRBN-1 (2.9)** (42 mg, 0.15 mmol, 1 equiv) and *N,N*-diisopropylethylamine (79 µL, 0.45 mmol, 3 equiv) were added. The resulting solution was heated to 90 °C and stirred for 16 hours. The reaction mixture was partitioned between dichloromethane (20 mL) and water (20 mL), and the aqueous phase was extracted with dichloromethane (3 × 20 mL).

The combined organic phases were washed with 5% aqueous lithium chloride (3 × 20 mL), dried over magnesium sulfate, filtered and concentrated *in vacuo*. Purification by column chromatography on silica gel with an eluent of 25% to 100% ethyl acetate in dichloromethane afforded CRBN HaloPROTAC **CRBN-HP-1 (2.29)** (37 mg, 0.065 mmol, 44%) as a yellow oil. Further purification by semi-preparative RP-HPLC using a focused gradient across 50% and 90% acetonitrile in water over 30 minutes eluted the title compound at t_R = 27 minutes (81% acetonitrile). Lyophilisation of the product fraction generated CRBN HaloPROTAC **CRBN-HP-1 (2.29)** (6 mg, 0.01 mmol, 7%) as a yellow fluffy powder.

^{1}H NMR (400 MHz, methanol-*d*$_4$) δ 7.56 (1H, dd, *J* = 8.6, 7.1 Hz, Ar-CH), 7.13 – 7.04 (2H, m, 2 × Ar-CH), 5.09 – 5.02 (1H, m, -CH), 3.79 – 3.48 (18H, m, -C**H$_2$**^{a} & 8 × -CH$_2$), 3.45 (2H, t, *J* = 6.5 Hz, -CH$_2$), 2.91 – 2.66 (3H, m, -C*H*H & -CH$_2$), 2.16 – 2.07 (1H, m, -CH*H*), 1.79 – 1.70 (2H, m, -CH$_2$), 1.61 – 1.52 (2H, m, -CH$_2$), 1.49 – 1.34 (4H, m, 2 × -CH$_2$). ^{13}C NMR (126 MHz, methanol-*d*$_4$) δ 174.6 (-CO), 171.5 (-CO), 170.6 (-CO), 169.3 (-CO), 148.2 (Ar-C), 137.2 (Ar-C), 133.9 (Ar-CH), 118.3 (Ar-CH), 112.0 (Ar-CH), 111.3 (Ar-C), 72.1 (-CH$_2$), 71.7 (-CH$_2$), 71.7 (-CH$_2$), 71.6 (-CH$_2$), 71.6 (-CH$_2$), 71.5 (-CH$_2$), 71.2 (-CH$_2$), 70.7 (-CH$_2$), 50.2 (-CH), 45.7 (-CH$_2$), 43.3 (-**C^{a}**H$_2$), 33.8 (-CH$_2$), 32.2 (-CH$_2$), 30.5 (-CH$_2$), 27.7 (-CH$_2$), 26.5 (-CH$_2$), 23.8 (-CH$_2$). IR (thin film) 3387, 1697, 748 cm^{-1}. HRMS (ESI) exact mass calculated for $C_{27}H_{38}ClN_3O_8Na$ $[M+Na]^+$ m/z 590.2240, found m/z 590.2220. LCMS (ESI) mass calculated for $C_{27}H_{39}ClN_3O_8$ $[M+H]^+$ m/z 568.24, found m/z 568.67 with t_R = 6.42 min.

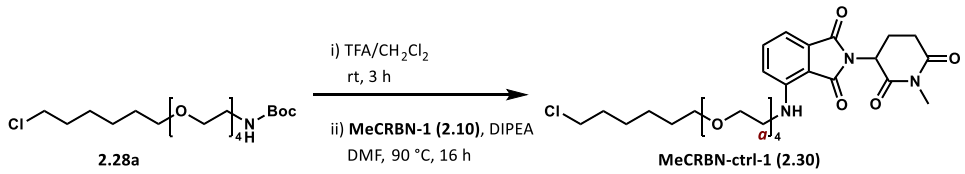

MeCRBN-ctrl-1 (2.30): Protected linker fragment **2.28a** (22 mg, 0.085 mmol, 1 equiv) was dissolved in trifluoroacetic acid/dichloromethane (1 mL/1 mL, 0.03 M) and the resulting solution was stirred at room temperature for 3 hours. The reaction was monitored by TLC for complete consumption of the starting material before removal of volatile components *in vacuo*. The residue was redissolved in *N,N*-dimethylformamide (0.4 mL, 0.2 M), and methylated CRBN ligand **MeCRBN-1 (2.10)** (22 mg, 0.085 mmol, 1 equiv) and *N,N*-diisopropylethylamine (45 µL, 0.25 mmol, 3 equiv) were added. Volatile components were removed *in vacuo*. Purification by column chromatography on silica gel with an eluent of 30% to 100% ethyl acetate in petroleum ether afforded methylated CRBN control **MeCRBN-ctrl-1 (2.30)** (28 mg, 0.048 mmol, 88%) as a yellow oil. Further purification by semi-preparative RP-HPLC using a focused gradient across 50% and 90% acetonitrile in water

over 30 minutes eluted the title compound at t_R = 27 minutes (81% acetonitrile). Lyophilisation of the product fraction generated methylated CRBN control **MeCRBN-ctrl-1 (2.30)** (13 mg, 0.024 mmol, 29%) as a yellow fluffy powder.

^{1}H NMR (400 MHz, methanol-*d*$_4$) δ 7.57 (1H, dd, *J* = 8.6, 7.1 Hz, Ar-CH), 7.13 – 7.05 (2H, m, 2 ×Ar-CH), 5.13 – 5.05 (1H, m, -CH), 3.76 – 3.48 (18H, m, -C**H$_2$**^{a} & 8 × -CH$_2$), 3.45 (2H, t, *J* = 6.5 Hz, -CH$_2$), 3.15 (3H, s, -CH$_3$), 2.92 – 2.85 (2H, m, -CH$_2$), 2.76 – 2.63 (1H, m, -C*H*H), 2.14 – 2.05 (1H, m, -CH*H*), 1.80 – 1.70 (2H, m, -CH$_2$), 1.62 – 1.51 (2H, m, -CH$_2$), 1.50 – 1.28 (4H, m, 2 × -CH$_2$). ^{13}C NMR (101 MHz, methanol-*d*$_4$) δ 173.7 (-CO), 171.4 (-CO), 170.7 (-CO), 169.3 (-CO), 148.3 (Ar-C), 137.2 (Ar-C), 133.9 (Ar-CH), 118.3 (Ar-CH), 112.0 (Ar-CH), 111.3 (Ar-C), 72.1 (-CH$_2$), 71.7 (-CH$_2$), 71.7 (-CH$_2$), 71.6 (-CH$_2$), 71.6 (-CH$_2$), 71.5 (-CH$_2$), 71.2 (-CH$_2$), 70.7 (-CH$_2$), 50.8 (-CH), 45.7 (-CH$_2$), 43.3 (-**C^a**H$_2$), 33.8 (-CH$_2$), 32.5 (-CH$_2$), 30.6 (-CH$_2$), 27.7 (-CH$_2$), 27.3 (-CH$_3$), 26.5 (-CH$_2$), 23.1 (-CH$_2$). IR (thin film) 3390, 1683, 669 cm^{-1}. HRMS (ESI) exact mass calculated for $C_{28}H_{41}ClN_3O_8$ $[M+H]^+$ m/z 582.2577, found m/z 582.2570. LCMS (ESI) mass calculated for $C_{28}H_{41}ClN_3O_8$ $[M+H]^+$ m/z 582.25, found m/z 582.83 with t_R = 6.67 min.

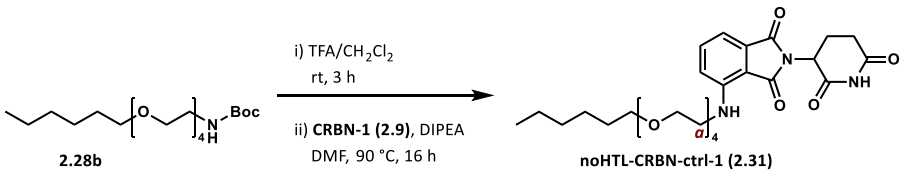

noHTL-CRBN-ctrl-1 (2.31): Protected linker fragment **2.28b** (32 mg, 0.085 mmol, 1 equiv) was dissolved in trifluoroacetic acid/dichloromethane (1.5 mL/1.5 mL, 0.03 M) and the resulting solution was stirred at room temperature for 3 hours. The reaction was monitored by TLC for complete consumption of the starting material before removal of volatile components *in vacuo*. The residue was redissolved in *N,N*-dimethylformamide (0.25 mL, 0.2 M), and CRBN ligand **CRBN-1 (2.9)** (16 mg, 0.055 mmol, 1 equiv) and *N,N*-diisopropylethylamine (29 µL, 0.17 mmol, 3 equiv) were added. The reaction mixture was partitioned between dichloromethane (20 mL) and water (20 mL), and the aqueous phase was extracted with dichloromethane (3 × 20 mL). The combined organic phases were washed with 5% aqueous lithium chloride (3 × 20 mL), dried over magnesium sulfate, filtered and concentrated *in vacuo*. Purification by column chromatography on silica gel with an eluent of 25% to 100% ethyl acetate in petroleum ether afforded HaloTag control **noHTL-CRBN-ctrl-1 (2.31)** (20 mg, 0.036 mmol, 48%) as a yellow oil. Further purification by semi-preparative RP-HPLC using a focused gradient across 50% and 90% acetonitrile in water over 30 minutes eluted the title compound at t_R = 25 minutes (80% acetonitrile).

Lyophilisation of the product fraction generated HaloTag control **noHTL-CRBN-ctrl-1 (2.31)** (3 mg, 0.005 mmol, 10%) as a yellow fluffy powder.

^{1}H NMR (400 MHz, methanol-d_4) δ 7.55 (1H, dd, J = 8.6, 7.1 Hz, Ar-CH), 7.12 – 7.03 (2H, m, 2 × Ar-CH), 5.09 – 5.01 (1H, m, -CH), 3.75 – 3.47 (18H, m, -C**H$_2$**^{a} & 8 × -CH$_2$), 3.44 (2H, t, J = 6.6 Hz, -CH$_2$), 2.92 – 2.65 (3H, m, -C*H*H & -CH$_2$), 2.15 – 2.07 (1H, m, -CH*H*), 1.60 – 1.49 (2H, m, -CH$_2$), 1.39 – 1.23 (4H, m, 2 × -CH$_2$), 0.89 (3H, t, J = 6.8 Hz, -CH$_3$). ^{13}C NMR (101 MHz, methanol-d_4) δ 174.6 (-CO), 171.5 (-CO), 160.6 (-CO), 169.3 (-CO), 148.2 (Ar-C), 137.2 (Ar-C), 133.9 (Ar-CH), 118.2 (Ar-CH), 112.0 (Ar-CH), 72.4 (-CH$_2$), 71.7 (-CH$_2$), 71.6 (-CH$_2$), 71.6 (-CH$_2$), 71.6 (-CH$_2$), 71.5 (-CH$_2$), 71.1 (-CH$_2$), 70.6 (-CH$_2$), 50.2 (CH), 43.3 (-**C^{a}**H$_2$), 32.8 (-CH$_2$), 32.2 (-CH$_2$), 30.7 (-CH$_2$), 26.9 (-CH$_2$), 23.8 (-CH$_2$), 23.7 (-CH$_2$), 14.4 (-CH$_3$). IR (thin film) 3055, 1670, 1179 cm^{-1}. HRMS (ESI) exact mass calculated for $C_{27}H_{40}N_3O_8$ $[M+H]^+$ m/z 534.2810, found m/z 534.2819. LCMS (ESI) mass calculated for $C_{27}H_{40}N_3O_8$ $[M+H]^+$ m/z 534.28, found m/z 534.33 with t_R = 6.61 min.

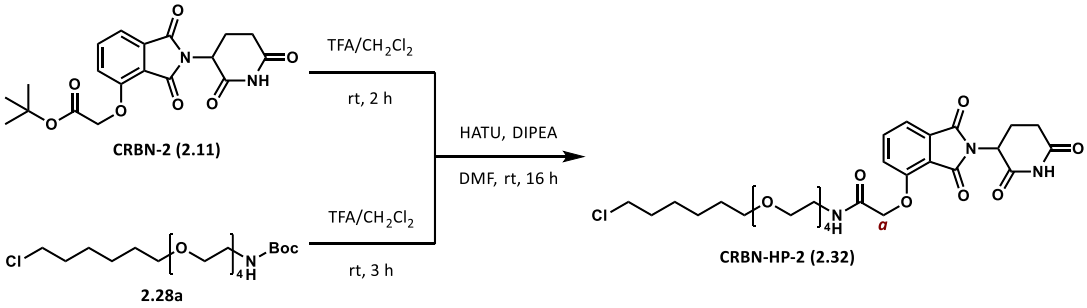

CRBN-HP-2 (2.32): CRBN ligand **CRBN-2 (2.11)** (31 mg, 0.080 mmol, 1 equiv) was dissolved in trifluoroacetic acid/dichloromethane (1.3 mL/1.3 mL, 0.03 M) and the resulting solution was stirred at room temperature for 2 hours. Protected linker fragment **2.28a** (33 mg, 0.080 mmol, 1 equiv) was dissolved in trifluoroacetic acid/dichloromethane (1.3 mL/1.3 mL, 0.03 M) and the resulting solution was stirred at room temperature for 3 hours. The reactions were monitored by TLC for complete consumption of the starting materials before removal of volatile components *in vacuo*. The residues were redissolved in *N,N*-dimethylformamide (0.3 mL, 0.3 M), and HATU (32 mg, 0.080 mmol, 1 equiv) and *N,N*-diisopropylethylamine (42 µL, 0.24 mmol, 3 equiv) were added. The resulting solution was stirred at room temperature for 16 hours before removal of volatile components *in vacuo*. Purification by column chromatography on silica gel with an eluent of 5% to 20% ethanol in dichloromethane afforded CRBN HaloPROTAC **CRBN-HP-2 (2.32)** (43 mg, 0.069 mmol, 86%) as a clear oil. Further purification by semi-preparative RP-HPLC using a focused gradient across 50% and 80% acetonitrile in water over 30 minutes eluted the title compound at t_R

= 21 minutes (72% acetonitrile). Lyophilisation of the product fraction generated CRBN HaloPROTAC **CRBN-HP-2 (2.32)** (17 mg, 0.027 mmol, 34%) as a white fluffy powder. ^{1}H NMR (500 MHz, methanol-d_4) δ 7.83 (1H, dd, *J* = 8.4, 7.3 Hz, Ar-CH), 7.56 (1H, d, *J* = 7.3 Hz, Ar-CH), 7.46 (1H, d, *J* = 8.5 Hz, Ar-CH), 5.18 – 5.12 (1H, m, -CH), 4.80 (2H, s, -C**H$_2$**^{a}), 3.69 – 3.44 (20H, m, 10 × -CH$_2$), 2.95 – 2.70 (3H, m, -C*H*H & -CH$_2$), 2.22 – 2.13 (1H, m, -CH*H*), 1.82 – 1.73 (2H, m, -CH$_2$), 1.63 – 1.54 (2H, m, -CH$_2$), 1.51 – 1.35 (4H, m, 2 × -CH$_2$). ^{13}C NMR (101 MHz, methanol-d_4) δ 173.1 (-CO), 169.9 (-CO), 168.6 (-CO), 166.9 (-CO), 166.1 (-CO), 154.8 (Ar-C), 136.8 (Ar-C), 133.6 (Ar-CH), 120.2 (Ar-CH), 117.8 (Ar-C), 116.5 (Ar-CH), 70.7 (-CH$_2$), 70.2 (-CH$_2$), 70.2 (2 × -CH$_2$), 70.1 (-CH$_2$), 70.0 (-CH$_2$), 69.7 (-CH$_2$), 68.9 (-CH$_2$), 67.8 (-**C**^{a}H$_2$), 49.2 (-CH), 44.3 (-CH$_2$), 38.8 (-CH$_2$), 32.3 (-CH$_2$), 30.8 (-CH$_2$), 29.1 (-CH$_2$), 26.3 (-CH$_2$), 25.1 (-CH$_2$), 22.3 (-CH$_2$). IR (thin film) 3451, 1671, 1178 cm^{-1}. HRMS (ESI) exact mass calculated for $C_{29}H_{41}ClN_3O_{10}$ $[M+H]^+$ m/z 626.2475, found m/z 626.2485. LCMS (ESI) mass calculated for $C_{29}H_{41}ClN_3O_{10}$ $[M+H]^+$ m/z 626.25, found m/z 626.58 with t_R = 5.99 min.

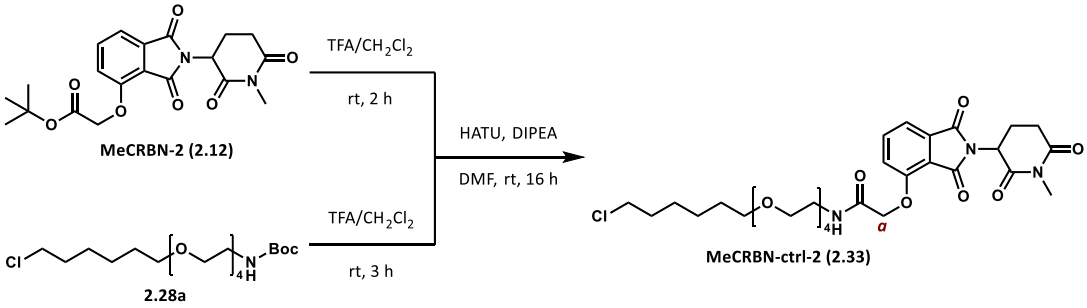

MeCRBN-ctrl-2 (2.33): Methylated CRBN ligand **MeCRBN-2 (2.12)** (32 mg, 0.080 mmol, 1 equiv) was dissolved in trifluoroacetic acid/dichloromethane (1.3 mL/1.3 mL, 0.03 M) and the resulting solution was stirred at room temperature for 2 hours. Protected linker fragment **2.28a** (33 mg, 0.080 mmol, 1 equiv) was dissolved in trifluoroacetic acid/dichloromethane (1.3 mL/1.3 mL, 0.03 M) and the resulting solution was stirred at room temperature for 3 hours. The reactions were monitored by TLC for complete consumption of the starting materials before removal of volatile components *in vacuo*. The residues were redissolved in *N,N*-dimethylformamide (0.3 mL, 0.3 M), and HATU (32 mg, 0.080 mmol, 1 equiv) and *N,N*-diisopropylethylamine (42 µL, 0.24 mmol, 3 equiv) were added. The resulting solution was stirred at room temperature for 16 hours before removal of volatile components *in vacuo*. Purification by column chromatography on silica gel with an eluent of 5% to 20% ethanol in dichloromethane afforded methylated CRBN control **MeCRBN-ctrl-2 (2.33)** (43 mg, 0.067 mmol, 84%) as a clear oil. Further purification by semi-preparative RP-HPLC using a focused gradient across 50% and 80% acetonitrile in water

over 20 minutes eluted the title compound at t_R = 19 minutes (72% acetonitrile). Lyophilisation of the product fraction generated methylated CRBN control **MeCRBN-ctrl-2 (2.33)** (18 mg, 0.028 mmol, 35%) as a white fluffy powder.

^{1}H NMR (400 MHz, methanol-*d*$_4$) δ 7.81 (1H, dd, *J* = 8.4, 7.3 Hz, Ar-CH), 7.54 (1H, d, *J* = 7.3 Hz, Ar-CH), 7.44 (1H, d, *J* = 8.4 Hz, Ar-CH), 5.20 – 5.11 (1H, m, -CH), 4.78 (2H, s, -C**H$_2$**^{a}), 3.70 – 3.57 (12H, m, 6 × -CH$_2$), 3.57 – 3.52 (4H, m, 2 × -CH$_2$), 3.52 – 3.47 (2H, m, -CH$_2$), 3.45 (2H, t, *J* = 6.5 Hz, -CH$_2$), 3.16 (3H, s, -CH$_3$), 2.97 – 2.84 (2H, m, -CH$_2$), 2.79 – 2.64 (1H, m, -C*H*H), 2.19 – 2.08 (1H, m, -CH*H*), 1.81 – 1.68 (2H, m, -CH$_2$), 1.64 – 1.50 (2H, m, -CH$_2$), 1.50 – 1.32 (4H, m, 2 × -CH$_2$). ^{13}C NMR (101 MHz, methanol-*d*$_4$) δ 173.5 (-CO), 171.1 (-CO), 170.0 (-CO), 168.3 (-CO), 167.6 (-CO), 156.3 (Ar-C), 138.2 (Ar-CH), 135.0 (Ar-C), 121.6 (Ar-CH), 119.2 (Ar-C), 117.9 (Ar-CH), 72.1 (-CH$_2$), 71.6 (-CH$_2$), 71.6 (2 × -CH$_2$), 71.5 (-CH$_2$), 71.4 (-CH$_2$), 71.2 (-CH$_2$), 70.3 (-CH$_2$), 69.3 (-**C**^{a}H$_2$), 51.2 (-CH), 45.7 (-CH$_2$), 40.2 (-CH$_2$), 33.7 (-CH$_2$), 32.5 (-CH$_2$), 30.5 (-CH$_2$), 27.7 (-CH$_3$), 27.4 (-CH$_2$), 26.5 (-CH$_2$), 22.9 (-CH$_2$). IR (thin film) 3395, 1676, 1180 cm^{-1}. HRMS (ESI) exact mass calculated for $C_{30}H_{43}ClN_3O_{10}$ $[M+H]^+$ m/z 640.2631, found m/z 640.2640. LCMS (ESI) mass calculated for $C_{30}H_{43}ClN_3O_{10}$ $[M+H]^+$ m/z 640.26, found m/z 640.75 with t_R = 6.25 min.

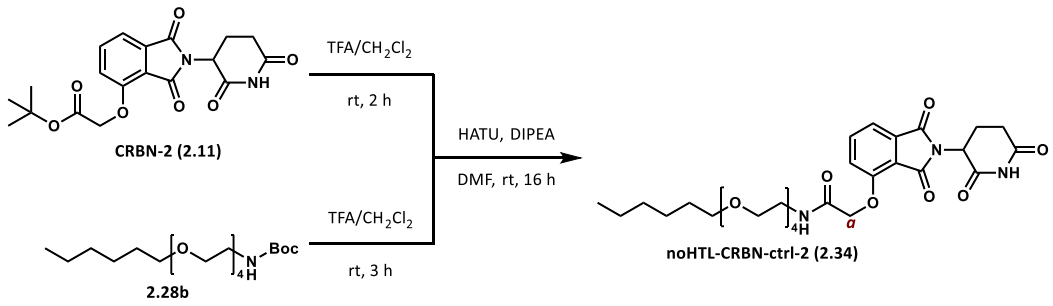

noHTL-CRBN-ctrl-2 (2.34): CRBN ligand **CRBN-2 (2.11)** (33 mg, 0.084 mmol, 1 equiv) was dissolved in trifluoroacetic acid/dichloromethane (1.5 mL/1.5 mL, 0.03 M) and the resulting solution was stirred at room temperature for 2 hours. Protected linker fragment **2.28b** (32 mg, 0.084 mmol, 1 equiv) was dissolved in trifluoroacetic acid/dichloromethane (1.5 mL/1.5 mL, 0.03 M) and the resulting solution was stirred at room temperature for 3 hours. The reactions were monitored by TLC for complete consumption of the starting materials before removal of volatile components *in vacuo*. The residues were redissolved in *N,N*-dimethylformamide (0.3 mL, 0.3 M), and HATU (32 mg, 0.084 mmol, 1 equiv) and *N,N*-diisopropylethylamine (45 µL, 0.25 mmol, 3 equiv) were added. The resulting solution was stirred at room temperature for 16 hours before removal of volatile components *in vacuo*. Purification by column chromatography on silica gel with an eluent of 5% to 10% ethanol

in dichloromethane afforded HaloTag control **noHTL-CRBN-ctrl-2 (2.34)** (44 mg, 0.074 mmol, 88%) as a clear oil. Further purification by semi-preparative RP-HPLC using a focused gradient across 50% and 80% acetonitrile in water over 20 minutes eluted the title compound at t_R = 18 minutes (70% acetonitrile). Lyophilisation of the product fraction generated HaloTag control **noHTL-CRBN-ctrl-2 (2.34)** (31 mg, 0.052 mmol, 62%) as a white fluffy powder.

^{1}H NMR (400 MHz, methanol-*d*$_4$) δ 7.81 (1H, dd, *J* = 8.4, 7.3 Hz, Ar-CH), 7.53 (1H, d, *J* = 7.3 Hz, Ar-CH), 7.43 (1H, d, *J* = 8.4 Hz, Ar-CH), 5.17 – 5.09 (1H, m, -CH), 4.77 (2H, s, -C**H$_2$**^{a}), 3.68 – 3.57 (10H, m, 5 × -CH$_2$), 3.57 – 3.52 (2H, m, -CH$_2$), 3.52 – 3.47 (2H, m, -CH$_2$), 3.44 (2H, t, *J* = 6.7 Hz, -CH$_2$), 2.97 – 2.65 (3H, m, -CH$_2$ & -C*H*H), 2.20 – 2.10 (1H, m, -CH*H*), 1.61 – 1.49 (2H, m, -CH$_2$), 1.41 – 1.23 (6H, m, 3 × -CH$_2$), 0.89 (3H, t, *J* = 6.8 Hz, -CH$_3$). ^{13}C NMR (101 MHz, methanol-*d*$_4$) δ 174.5 (-CO), 171.3 (-CO), 170.0 (-CO), 168.3 (-CO), 167.5 (-CO), 156.2 (Ar-C), 138.2 (Ar-CH), 135.0 (Ar-C), 121.6 (Ar-CH), 119.2 (Ar-C), 117.9 (Ar-CH), 72.4 (-CH$_2$), 71.6 (2 × -CH$_2$), 71.6 (2 × -CH$_2$), 71.5 (-CH$_2$), 71.4 (-CH$_2$), 71.1 (-CH$_2$), 70.3 (-CH$_2$), 69.3 (-**C**^{a}H$_2$), 50.6 (-CH), 40.2 (-CH$_2$), 32.8 (-CH$_2$), 32.2 (-CH$_2$), 30.7 (-CH$_2$), 26.9 (-CH$_2$), 23.7 (-CH$_2$), 14.4 (-CH$_3$). IR (thin film) 1707, 1615, 1197 cm^{-1}. HRMS (ESI) exact mass calculated for $C_{29}H_{42}N_3O_{10}$ [M+H]$^+$ m/z 592.2865, found m/z 592.2874. LCMS (ESI) mass calculated for $C_{29}H_{42}N_3O_{10}$ [M+H]$^+$ m/z 592.29, found m/z 592.42 with t_R = 6.14 min.

- *HyT HaloPROTAC:*

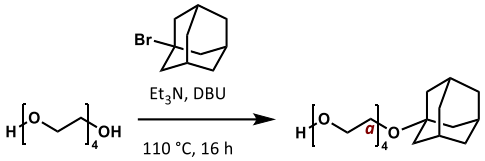

2.35

2.35: To a stirred solution of tetraethylene glycol (3.3 mL, 15 mmol, 5 equiv) and 1-bromoadamantane (640 mg, 3.0 mmol, 1 equiv) in triethylamine (1.2 mL, 9.0 mmol, 3 equiv) was added 1,8-diazabicyclo[5.4.0]undec-7-ene (27 µL, 0.15 mmol, 5 mol%) and the resulting solution was heated to 110 °C and stirred for 16 hours. The reaction mixture was allowed to reach room temperature before addition of 1 M aqueous hydrochloric acid (20 mL). The aqueous phase was extracted with dichloromethane (4 × 20 mL) and the combined organic extracts washed with water (2 × 40 mL), dried over magnesium sulfate, filtered and concentrated *in vacuo*. Purification by column chromatography on silica gel with an eluent

of 0% to 50% ethanol in ethyl acetate afforded alcohol **2.35** (483 mg, 1.47 mmol, 48%) as a brown oil.

Analytical data observed were in accordance with literature values.[148]

^{1}H NMR (400 MHz, chloroform-*d*) δ 3.72 (2H, t, *J* = 4.3 Hz, -CH_2), 3.69 – 3.63 (8H, m, 4 × -CH_2), 3.63 – 3.54 (6H, m, 2 × -CH_2 & -C**H$_2^a$**), 2.67 (1H, s, -OH), 2.20 – 2.07 (3H, m, 3 × -CH), 1.81 – 1.69 (6H, m, 3 × -CH_2), 1.69 – 1.53 (6H, m, 3 × -CH_2). ^{13}C NMR (126 MHz, chloroform-*d*) δ 72.8 (-CH_2), 72.6 (-C), 71.5 (-CH_2), 70.9 (-CH_2), 70.8 (-CH_2), 70.8 (-CH_2), 70.6 (-CH_2), 62.0 (-CH_2), 59.5 (-**C^a**H$_2$), 41.7 (3 × -CH_2), 36.7 (3 × -CH_2), 30.7 (3 × -CH).

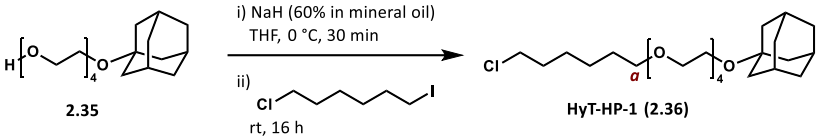

HyT-HP-1 (2.36): To a dry flask charged with argon was added anhydrous tetrahydrofuran (1.0 mL, 0.3 M), alcohol **2.35** (73 mg, 0.22 mmol, 1 equiv) and sodium hydride (60% in mineral oil, 20 mg, 0.44 mmol, 2 equiv) at 0 °C. The resulting suspension was stirred for 30 minutes before 1-chloro-6-iodohexane (0.50 mL, 0.33 mmol, 1.5 equiv) was added slowly at 0 °C. The reaction mixture was allowed to reach room temperature and stirred for a further 16 hours. The reaction was quenched by dropwise addition of water (20 mL). The aqueous phase was extracted with ethyl acetate (4 × 20 mL) and the combined organic extracts were washed with brine (50 mL), dried over magnesium sulfate, filtered and concentrated *in vacuo*. Purification by column chromatography on silica gel with an eluent of 10% to 60% ethyl acetate in petroleum ether afforded HyT HaloPROTAC **HyT-HP-1 (2.36)** (40 mg, 0.090 mmol, 41%) as a clear oil.

^{1}H NMR (400 MHz, chloroform-*d*) δ 3.67 – 3.54 (16H, m, 8 × -CH_2), 3.51 (2H, t, *J* = 6.7 Hz, -CH_2), 3.44 (2H, t, *J* = 6.6 Hz, -C**H$_2^a$**), 2.16 – 2.09 (3H, m, 3 × -CH), 1.80 – 1.70 (8H, m, 4 × -CH_2), 1.66 – 1.53 (8H, m, 4 × -CH_2), 1.48 – 1.30 (4H, m, 2 × -CH_2). ^{13}C NMR (101 MHz, chloroform-*d*) δ 72.4 (-C), 71.5 (-CH_2), 71.4 (-CH_2), 70.8 (3 × -CH_2), 70.8 (-CH_2), 70.3 (-**C^a**H$_2$) 70.3 (-CH_2), 59.5 (-CH_2), 45.2 (-CH_2), 41.7 (3 × -CH_2), 36.7 (3 × -CH_2), 32.8 (-CH_2), 30.7 (3 × -CH), 29.7 (-CH_2), 26.9 (-CH_2), 25.6 (-CH_2). IR (thin film) 2905, 1092, 872 cm^{-1}. HRMS (ESI) exact mass calculated for $C_{24}H_{43}ClO_5Na$ $[M+Na]^+$ m/z 469.2691, found m/z 469.2677.

Preparation of 1st series amide PROTACs

- *E3 ligase ligand–linker fragments:*

3.2a: To a stirred solution of **3.1a** (130 mg, 0.25 mmol, 1 equiv) in dichloromethane (1.2 mL, 0.2 M) was added succinic anhydride (52 mg, 0.52 mmol, 2 equiv) and 4-dimethylaminopyridine (7.0 mg, 0.010 mmol, 0.01 equiv) and the resulting solution was stirred at room temperature for 2 hours. The reaction mixture was partitioned between dichloromethane (10 mL) and 1 M aqueous hydrochloric acid (10 mL), and the aqueous phase was extracted with dichloromethane (3 × 10 mL). The combined organic extracts were dried over magnesium sulfate, filtered and concentrated *in vacuo* yielding **3.2a** (140 mg, 0.25 mmol, 95%) as a clear oil. The crude material was used in the next step without further purification.

^{1}H NMR (400 MHz, chloroform-*d*) δ 6.66 (1H, br s, -NH), 5.10 (1H, br s, -NH), 3.65 – 3.52 (24H, m, 12 × -CH_2), 3.51 – 3.44 (4H, m, 2 × -CH_2), 3.41 – 3.33 (2H, m, -CH_2), 3.27 – 3.19 (2H, m, -CH_2), 2.60 (2H, t, *J* = 6.7 Hz, -C**H**^{a}), 2.46 (2H, t, *J* = 6.7 Hz, -C**H**^{b}), 1.37 (9H, s, -CH_3). ^{13}C NMR (101 MHz, chloroform-*d*) δ 175.0 (-COOH), 172.4 (-CONH), 156.1 (-NCOOR), 79.2 (-*C*(CH_3)$_3$), 70.5 (2 × -CH_2), 70.5 (2 × -CH_2), 70.5 (2 × -CH_2), 70.5 (2 × -CH_2), 70.4 (2 × -CH_2), 70.2 (-CH_2), 70.1 (-CH_2), 69.6 (2 × -CH_2), 40.3 (2 × -CH_2), 39.4 (2 × -CH_2), 30.8 (-**C**^{a}H_2), 29.9 (-**C**^{b}H_2), 28.4 (3 × -CH_3). IR (thin film) 3334, 2829, 1734. HRMS (ESI) exact mass calculated for $C_{25}H_{48}N_2O_{12}Na$ $[M+Na]^+$ m/z 591.31, found m/z 591.31.

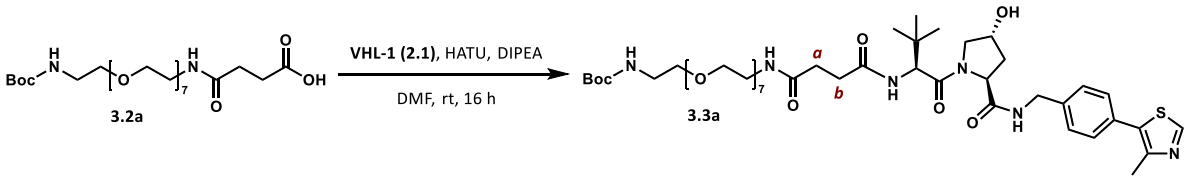

3.3a: To a pre-stirred solution of carboxylic acid **3.2a** (150 mg, 0.26 mmol, 1 equiv), HATU (100 mg, 0.26 mmol, 1 equiv) and *N,N*-diisopropylethylamine (0.20 mL, 1.3 mmol, 5 equiv) in *N,N*-dimethylformamide (0.2 mL, 0.3 M) was added amine **VHL-1 (2.1)** (120 mg, 0.26 mmol, 1 equiv), and the resulting solution was stirred at room temperature for 16 hours. The reaction mixture was partitioned between dichloromethane (20 mL) and water (20 mL), and the aqueous phase was extracted with dichloromethane (5 × 20 mL). The combined organic phases were washed with 5% aqueous lithium chloride (5 × 25 mL), dried over magnesium sulfate, filtered and concentrated *in vacuo*. Purification by column

chromatography on silica gel with an eluent of 10% to 50% ethanol in dichloromethane afforded linker fragment **3.3a** (55 mg, 0.056 mmol, 21%) as a colourless oil.

^{1}H NMR (400 MHz, chloroform-*d*) δ 8.67 (1H, s, thiazole-CH), 7.37 – 7.32 (4H, m, 4 × Ar-CH), 7.00 (1H, br s, -NH), 6.66 (1H, br s, -NH), 5.10 (1H, br s, -NH), 4.77 – 4.72 (1H, m, -CH), 4.57 – 4.29 (4H, m, 2 × -CH & -CH_2), 4.07 (1H, br s, -NH), 3.76 – 3.50 (32H, m, 16 × -CH_2), 3.43 – 3.36 (2H, m, -C**H$_2$**^{a}), 3.33 – 3.26 (2H, m, -C**H$_2$**^{b}), 2.52 – 2.50 (5H, m, -CH_2 & -CH_3), 1.90 – 1.87 (2H, m, -CH_2), 1.43 (9H, s, 3 × CH_3), 0.94 (9H, s, 3 × CH_3). ^{13}C NMR (101 MHz, chloroform-*d*) δ 173.0 (-CONH), 172.6 (-CONH), 171.9 (-CONH), 171.3 (-CONH), 156.2 (-NCOOR), 151.2 (thiazole-CH), 147.4 (thiazole-C), 138.9 (Ar-C), 132.6 (thiazole-C), 130.2 (Ar-C), 129.6 (2 × Ar-CH), 128.3 (2 × Ar-CH), 79.3 (-*C*(CH_3)$_3$), 70.6 (-CH_2), 70.6 (-CH_2), 70.6 (-CH_2), 70.6 (-CH_2), 70.5 (2 × -CH_2), 70.3 (2 × -CH_2), 70.3 (2 × -CH_2), 70.2 (2 × -CH_2), 69.7 (2 × -CH_2), 58.7 (-CH), 58.0 (-CH), 56.9 (-CH_2), 53.5 (-CH), 43.3 (-CH_2), 40.5 (CH_2), 39.5 (-CH_2), 36.5 (-CH_2), 35.2 (-CH), 31.5 (-**C^{a}**H_2), 31.4 (-**C^{b}**H_2), 28.6 (3 × -CH_3), 26.6 (3 × -CH_3), 15.5 (-CH_3). IR (thin film) 3308, 1653, 1096. LRMS (ESI) mass calculated for $C_{47}H_{76}N_6O_{14}SNa$ $[M+Na]^+$ m/z 1003.50, found m/z 1003.48.

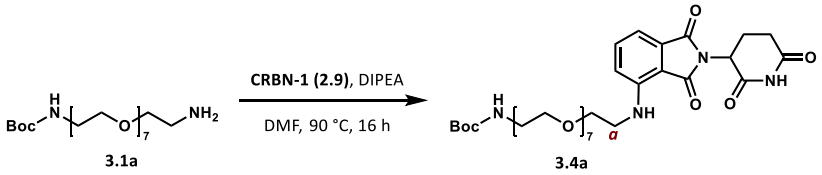

3.4a: To a stirred solution of **3.1a** (150 mg, 0.33 mmol, 1 equiv) in *N,N*-dimethylformamide (1.7 mL, 0.2 M) were added CRBN ligand **CRBN-1 (2.9)** (93 mg, 0.33 mmol, 1 equiv) and *N,N*-diisopropylethylamine (0.12 mL, 0.64 mmol, 2 equiv). The resulting solution was heated to 90 °C and stirred for 16 hours. The reaction mixture was allowed to cool to room temperature, poured into water (30 mL) and extracted with ethyl acetate (4 × 30 mL). The combined organic phases were washed with 5% aqueous lithium chloride (3 × 50 mL), dried over magnesium sulfate, filtered and concentrated *in vacuo*. Purification by column chromatography on silica gel with an eluent of 1% to 10% methanol in dichloromethane afforded linker fragment **3.4a** (100 mg, 0.14 mmol, 42%) as a bright yellow oil.

^{1}H NMR (400 MHz, chloroform-*d*) δ 8.41 (1H, br s, -NH), 7.48 (1H, dd, *J* = 8.5, 7.1 Hz, Ar-H), 7.09 (1H, d, *J* = 7.0 Hz, Ar-H), 6.91 (1H, d, *J* = 8.5 Hz, Ar-H), 6.49 (1H, br s, -NH), 5.05 (1H, br s, -NH), 4.93 – 4.86 (1H, m, -CH), 3.73 – 3.57 (26H, m, 13 × -CH_2), 3.53 (2H, t, *J* = 5.2 Hz, -CH_2), 3.50 – 3.41 (2H, m, -C**H$_2$**^{a}), 3.34 – 3.25 (2H, m, -CH_2), 2.91 – 2.65 (3H, m, -CH_2 & -C*H*H), 2.17 – 2.07 (1H, m, -CH*H*), 1.43 (9H, s, 3 × -CH_3). ^{13}C NMR (101 MHz, chloroform-*d*) δ 171.2 (-CO), 169.4 (-CO), 168.5 (-CO), 167.7 (-CO), 156.1 (-NCOOR), 147.0 (Ar-C), 136.1 (Ar-C),

132.7 (Ar-CH), 116.9 (Ar-CH), 111.8 (Ar-CH), 110.5 (Ar-C), 79.3 (-*C*$(CH_3)_3$), 70.9 (-CH_2), 70.8 (-CH_2), 70.7 (-CH_2), 70.7 (-CH_2), 70.7 (-CH_2), 70.7 (-CH_2), 70.7 (-CH_2), 70.6 (-CH_2), 70.4 (2 × -CH_2), 70.4 (2 × -CH_2), 69.6 (2 × -CH_2), 49.0 (-CH), 42.6 (-**C**$^{a}H_2$), 40.5 (-CH_2), 31.6 (-CH_2), 28.6 (3 × -CH_3), 22.9 (-CH_2). IR (thin film) 1697, 1173, 1109. HRMS (ESI) exact mass calculated for $C_{34}H_{52}N_4O_{13}Na$ $[M+Na]^+$ m/z 747.3423, found m/z 747.3408.

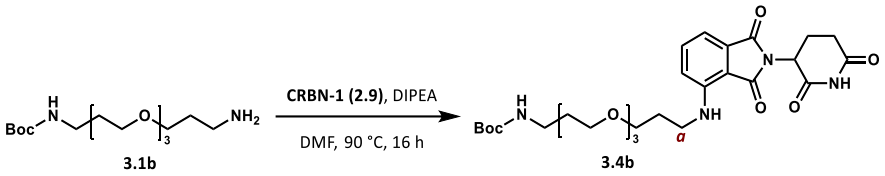

3.4b: To a stirred solution of **3.1b** (290 mg, 0.91 mmol, 1 equiv) in *N,N*-dimethylformamide (3.8 mL, 0.2 M) were added CRBN ligand **CRBN-1 (2.9)** (210 mg, 0.77 mmol, 1 equiv) and *N,N*-diisopropylethylamine (0.27 mL, 1.5 mmol, 2 equiv). The resulting solution was heated to 90 °C and stirred for 16 hours. The reaction mixture was allowed to cool to room temperature, poured into water (40 mL) and extracted with ethyl acetate (4 × 40 mL). The combined organic phases were washed with 5% aqueous lithium chloride (3 × 70 mL), dried over magnesium sulfate, filtered and concentrated *in vacuo*. Purification by column chromatography on silica gel with an eluent of 30% ethyl acetate in dichloromethane afforded linker fragment **3.4b** (230 mg, 0.40 mmol, 53%) as a bright yellow oil.

^{1}H NMR (400 MHz, chloroform-*d*) δ 8.18 (1H, br s, -NH), 7.49 (1H, dd, *J* = 8.6, 7.1 Hz, Ar-H), 7.08 (1H, d, *J* = 7.0 Hz, Ar-H), 6.93 (1H, d, *J* = 8.5 Hz, Ar-H), 4.97 (1H, br s, -NH), 4.94 – 4.87 (1H, m, -CH), 3.73 – 3.56 (10H, m, 5 × -CH_2), 3.53 (2H, t, *J* = 6.0 Hz, -CH_2), 3.40 (2H, t, *J* = 6.6 Hz, -C**H**$_2^{a}$), 3.26 – 3.17 (2H, m, -CH_2), 2.92 – 2.67 (3H, m, -CH_2 & -C*H*H), 2.16 – 2.09 (1H, m, -CH*H*), 1.98 – 1.87 (2H, m, -CH_2), 1.80 – 1.69 (2H, m, -CH_2), 1.43 (9H, s, 3 × -CH_3). ^{13}C NMR (101 MHz, chloroform-*d*) δ 171.1 (-CO), 169.5 (-CO), 168.5 (-CO), 167.8 (-CO), 147.2 (-NCOOR), 136.3 (Ar-C), 132.7 (Ar-C), 116.8 (Ar-CH), 111.5 (2 × Ar-CH), 110.1 (Ar-C), 77.4 (-*C*$(CH_3)_3$), 70.7 (2 × -CH_2), 70.6 (2 × -CH_2), 70.3 (2× -CH_2), 69.0 (-CH_2), 49.0 (-CH), 40.4 (-**C**$^{a}H_2$), 31.6 (CH_2), 29.8 (-CH_2), 29.5 (-CH_2), 28.6 (3 × -CH_3), 23.0 (-CH_2). IR (thin film) 3401, 1695, 1601. HRMS (ESI) exact mass calculated for $C_{28}H_{40}N_4O_9Na$ $[M+Na]^+$ m/z 599.2687, found m/z 599.2675.

- *Fascin ligand A fragment and control:*

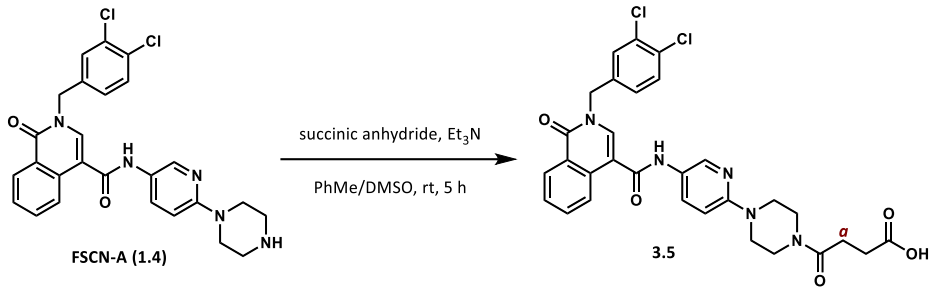

3.5: To a stirred solution of fascin ligand A **FSCN-A (1.4)** (250 mg, 0.50 mmol, 1 equiv) in toluene/ dimethyl sulfoxide (12 mL/7.0 mL, 0.03 M) were added succinic anhydride (100 mg, 0.99 mmol, 2 equiv) and triethylamine (0.14 mL, 0.99 mmol, 2 equiv) and the resulting solution was stirred at room temperature for 5 hours. To the reaction mixture was added water (100 mL) and washed with dichloromethane (2 × 100 mL) to remove organic impurities. The aqueous phase was acidified with 1 M aqueous hydrochloric acid and the resulting precipitate was collected by filtration, washed with water and dried *in vacuo* to yield fascin ligand A fragment **3.5** (290 mg, 0.47 mmol, 96%) as a light purple amorphous solid.

^{1}H NMR (400 MHz, DMSO-d_6) δ 12.05 (1H, br s, -OH), 10.29 (1H, s, -NH), 8.45 (1H, d, *J* = 2.6 Hz, Ar-H), 8.29 (1H, dd, *J* = 8.1, 1.4 Hz, Ar-H), 8.25 (1H, s, -CH), 8.14 (1H, d, *J* = 8.2 Hz, Ar-H), 7.92 (1H, dd, *J* = 9.2, 2.6 Hz, Ar-H), 7.79 (1H, ddd, *J* = 8.5, 7.1, 1.5 Hz, Ar-H), 7.71 (1H, d, *J* = 2.0 Hz, Ar-H), 7.65 – 7.55 (2H, m, 2 × Ar-H), 7.41 (1H, dd, *J* = 8.4, 2.1 Hz, Ar-H), 6.92 (1H, d, *J* = 9.1 Hz, Ar-H), 5.22 (2H, s, -CH_2), 3.62 – 3.40 (8H, m, 4 × -CH_2), 2.59 (2H, t, *J* = 6.5 Hz, -C**H$_2$**^{a}), 2.45 (2H, t, *J* = 6.5 Hz, -CH_2). ^{13}C NMR (101 MHz, DMSO-d_6) δ 173.9 (-COOH), 169.7 (-CONR), 164.0 (-CONR), 160.8 (-CONH), 155.5 (Ar-C), 139.7 (Ar-C), 138.2 (Ar-CH), 135.2 (-CH), 134.2 (Ar-C), 132.9 (Ar-CH), 131.0 (Ar-CH), 130.9 (Ar-CH), 130.7 (Ar-CH), 130.2 (Ar-C), 130.0 (Ar-C), 128.3 (Ar-CH), 127.4 (Ar-CH), 127.3 (Ar-CH), 126.8 (Ar-C), 124.9 (Ar-CH), 124.8 (Ar-C), 113.0 (-C), 107.1 (Ar-CH), 51.0 (-CH_2), 45.4 (-CH_2), 45.2 (-CH_2), 44.9 (-CH_2), 44.2 (-CH_2), 28.9 (-**C**^{a}H_2), 27.5 (-CH_2). IR (thin film) 1728, 1616, 694. HRMS (ESI) exact mass calculated for $C_{30}H_{27}Cl_2N_5O_5Na$ $[M+Na]^+$ m/z 630.1281, found m/z 630.1271.

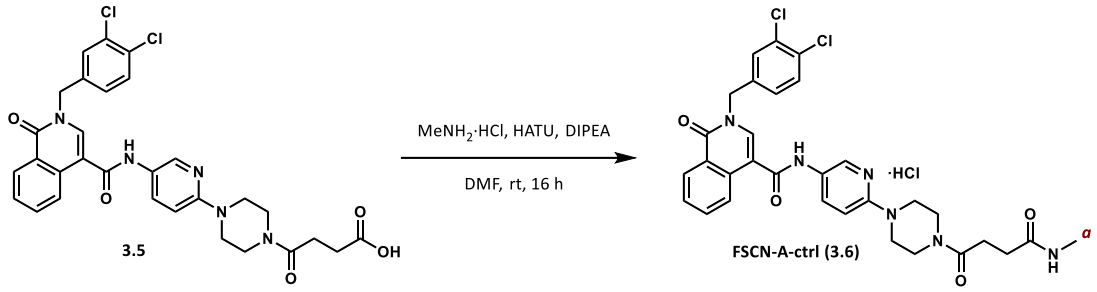

FSCN-A-ctrl (3.6): To a pre-stirred solution of carboxylic acid **3.5** (50 mg, 0.08 mmol, 1 equiv), HATU (30 mg, 0.08 mmol, 1 equiv) and *N,N*-diisopropylethylamine (70 µL, 0.4 mmol, 5 equiv) in *N,N*-dimethylformamide (0.3 mL, 0.3 M) was added methylamine hydrochloride (6 mg, 0.08 mmol, 1 equiv), and the resulting solution was stirred at room temperature for 16 hours. The reaction mixture was partitioned between dichloromethane (10 mL) and water (10 mL), and the aqueous phase was extracted with dichloromethane (5 × 10 mL). The combined organic phases were washed with 5% aqueous lithium chloride (5 × 20 mL), dried over magnesium sulfate, filtered and concentrated *in vacuo*. Purification by column chromatography on silica gel with an eluent of 5% to 20% ethanol in dichloromethane afforded the product (30 mg, 0.05 mmol, 66%) as a white amorphous solid. Further purification by semi-preparative RP-HPLC using a focused gradient across 40% and 60% acetonitrile in water over 30 minutes eluted the title compound at t_R = 27 minutes (58% acetonitrile) and the product fraction was lyophilised. Redissolving the resulting trifluoroacetate salt in 1 M aqueous hydrochloric acid and acetonitrile, followed by lyophilisation, yielded fascin ligand A amide control **FSCN-A-ctrl (3.6)** (10 mg, 0.02 mmol, 24%) as a white fluffy powder.

^{1}H NMR (400 MHz, chloroform-*d*) δ 8.68 (1H, s, -NH), 8.43 (1H, dd, *J* = 8.2, 1.4 Hz, Ar-H), 8.30 (1H, s, -CH), 8.17 (1H, d, *J* = 8.2 Hz, Ar-H), 8.08 (1H, d, *J* = 8.9 Hz, Ar-H), 7.74 – 7.66 (2H, m, 2 × Ar-H), 7.54 (1H, ddd, *J* = 8.3, 7.2, 1.2 Hz, Ar-H), 7.46 (1H, d, *J* = 2.1 Hz, Ar-H), 7.36 (1H, d, *J* = 8.3 Hz, Ar-H), 7.18 (1H, dd, *J* = 8.3, 2.1 Hz, Ar-H), 6.62 (1H, d, *J* = 9.1 Hz, Ar-H), 5.96 (1H, br s, -NH), 5.10 (2H, s, -CH_2), 3.69 – 3.64 (2H, m, -CH_2), 3.56 – 3.47 (4H, m, 2 × -CH_2), 3.37 – 3.30 (2H, m, -CH_2), 2.67 (2H, t, *J* = 6.3 Hz, -CH_2), 2.62 (3H, d, *J* = 4.4 Hz, -C**H$_3$**^{a}), 2.48 (2H, t, *J* = 6.3 Hz, -CH_2). ^{13}C NMR (101 MHz, chloroform-*d*) δ 173.1 (-CONH), 170.6 (-CONR), 164.6 (-CONR), 162.0 (-CONR), 156.4 (Ar-C), 140.4 (-CH), 136.6 (Ar-CH), 134.1 (Ar-C), 133.4 (Ar-CH), 133.3 (Ar-CH), 133.1 (Ar-C), 132.5 (Ar-C), 131.3 (Ar-C), 131.0 (Ar-CH), 130.1 (Ar-CH), 128.5 (Ar-CH), 128.0 (Ar-CH), 127.6 (Ar-CH), 126.7 (Ar-C), 125.7 (Ar-CH), 124.9 (Ar-C), 115.0 (Ar-CH), 107.1 (-C), 51.3 (-CH_2), 45.5 (-CH_2), 45.3 (-CH_2), 45.0 (-CH_2), 41.4 (-CH_2), 31.1 (-CH_2), 29.8 (-CH_2), 26.4 (-**C^a**H$_3$). IR (thin film) 2924, 1645, 694. HRMS (ESI) exact mass calculated for $C_{31}H_{31}Cl_2N_6O_4$ $[M+H]^+$ m/z 621.1778, found m/z 621.1756.

- *1st series amide PROTACs:*

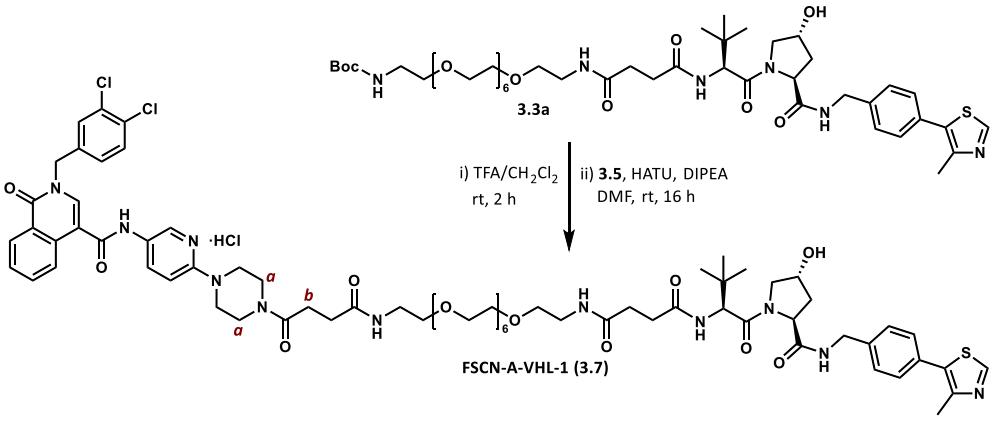

FSCN-A-VHL-1 (3.7): Protected linker fragment **3.3a** (34 mg, 0.034 mmol, 1 equiv) was dissolved in trifluoroacetic acid/dichloromethane (0.5 mL/0.5 mL, 0.03 M) and the resulting solution was stirred at room temperature for 2 hours. The reaction was monitored by TLC for complete consumption of the starting material before removal of volatile components *in vacuo*. The residue was redissolved in *N,N*-dimethylformamide (0.2 mL, 0.3 M), and fascin ligand A fragment **3.5** (21 mg, 0.034 mmol, 1 equiv), HATU (13 mg, 0.024 mmol, 1 equiv) and *N,N*-diisopropylethylamine (30 µL, 0.17 mmol, 5 equiv) were added. The resulting solution was stirred at room temperature for 16 hours before partitioning the reaction mixture between dichloromethane (10 mL) and water (10 mL). The aqueous phase was extracted with dichloromethane (5 × 10 mL) and the combined organic phases were washed with 5% aqueous lithium chloride (5 × 20 mL), dried over magnesium sulfate, filtered and concentrated *in vacuo*. Purification by column chromatography on silica gel with an eluent of 5% to 30% ethanol in dichloromethane afforded the product (18 mg, 0.012 mmol, 41%) as a colourless oil. Further purification by semi-preparative RP-HPLC using a focused gradient across 40% and 70% acetonitrile in water over 35 minutes eluted the title compound at t_R = 28 minutes (60% acetonitrile) and the product fraction was lyophilised. Redissolving the resulting trifluoroacetate salt in 1 M aqueous hydrochloric acid and acetonitrile, followed by lyophilisation, yielded fascin ligand A amide VHL PROTAC **FSCN-A-VHL-1 (3.7)** (10 mg, 0.007 mmol, 23%) as a white fluffy powder.

^{1}H NMR (400 MHz, methanol-*d*$_4$) δ 8.90 (1H, br s, -NH), 8.65 (1H, d, *J* = 2.7 Hz, Ar-H), 8.42 – 8.37 (1H, m, Ar-H), 8.20 (1H, d, *J* = 8.3 Hz, Ar-H), 8.10 (1H, s, -CH), 8.06 (1H, dd, *J* = 9.5, 2.5 Hz, Ar-H), 7.80 (1H, ddd, *J* = 8.4, 7.0, 1.4 Hz, Ar-H), 7.65 – 7.58 (2H, m, 2 × Ar-H), 7.50 (1H, dd, *J* = 8.4, 1.1 Hz, Ar-H), 7.48 – 7.37 (4H, m, 4 × Ar-H), 7.34 (1H, dd, *J* = 8.4, 1.9 Hz, Ar-H), 7.27 (1H, d, *J* = 9.6 Hz, Ar-H), 5.26 (2H, s, -CH$_2$), 4.62 – 4.30 (5H, m, 3 × -CH & -CH$_2$), 3.91 – 3.57 (32H, m, 16 × -CH$_2$), 3.57 – 3.47 (4H, m, 2 × -CH$_2$), 3.39 – 3.32 (4H, m, 2 × -C**H$_2^a$**), 2.73

(2H, t, *J* = 6.8 Hz, -CH_2), 2.61 – 2.48 (4H, m, 2 × -CH_2), 2.48 – 2.45 (3H, s, -CH_3m), 2.24 – 2.03 (2H, m, -CH_2), 1.33 – 1.27 (2H, m, -CH_2), 1.18 (2H, t, *J* = 7.0 Hz, -C**H$_2$**^{b}), 1.03 (9H, s, 3 × -CH_3). ^{13}C NMR (101 MHz, methanol-d_4) δ 174.8 (-CONH), 174.6 (-CONH), 174.5 (-CONH), 174.4 (-CONH), 173.1 (-CONR), 172.2 (-CONR), 166.9 (-CONH), 163.5 (-CONR), 152.9 (Ar-C), 148.9 (thiazole-CH), 140.3 (thiazole-C), 138.8 (Ar-CH), 135.8 (-CH), 135.6 (thiazole-C), 134.4 (Ar-C), 133.6 (Ar-C), 133.5 (Ar-C), 132.9 (Ar-C), 131.9 (Ar-CH), 131.4 (2 × Ar-C), 131.1 (Ar-CH), 130.4 (Ar-C & Ar-CH), 129.0 (3 × Ar-CH), 128.9 (3 × Ar-CH), 128.4 (Ar-CH), 126.7 (Ar-C), 126.0 (2 × Ar-CH), 115.3 (-C), 112.4 (Ar-CH), 71.6 (4 × -CH_2), 71.5 (2 × -CH_2), 71.3 (2 × -CH_2), 71.1 (2 × -CH_2), 70.6 (2 × -CH_2), 70.5 (2 × -CH_2), 60.8 (-CH), 59.1 (-CH), 58.3 (-CH_2), 57.9 (-CH_2), 52.8 (-CH), 46.7 (-CH_2), 46.6 (-CH_2), 45.4 (-C^{a}H_2), 43.7 (-C^{a}H_2), 41.9 (-CH_2), 40.5 (2 × -CH_2), 39.0 (-CH_2), 36.6 (-*C*(CH_3)$_3$), 32.2 (-CH_2), 32.0 (-CH_2), 31.7 (-C^{a}H_2), 29.1 (-CH_2), 27.0 (3 × -CH_3), 15.8 (-CH_3). IR (thin film) 3364, 1636, 1105. HRMS (ESI) exact mass calculated for $C_{72}H_{93}Cl_2N_{11}O_{16}Na$ $[M+Na]^+$ m/z 1469.5900, found m/z 1469.5891. LCMS (ESI) mass calculated for $C_{72}H_{94}Cl_2N_{11}O_{16}$ $[M+H]^+$ m/z 1470.60, found m/z 1470.00 with t_R = 5.71 min.

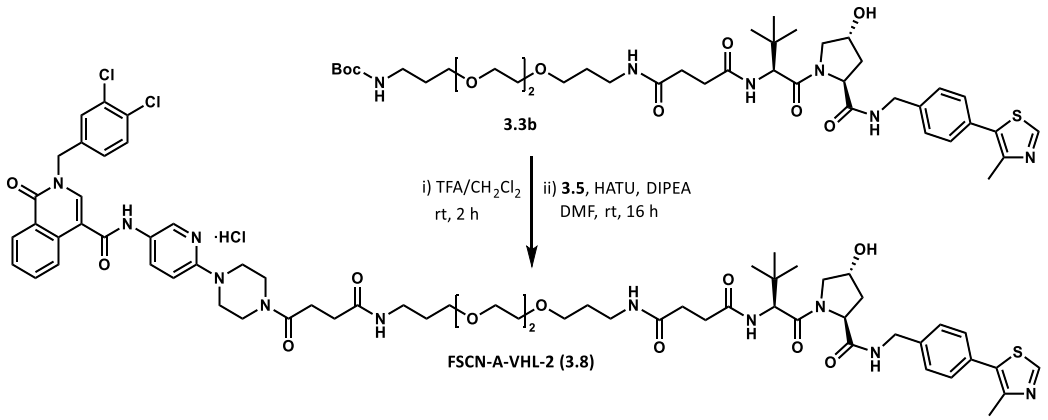

FSCN-A-VHL-2 (3.8): Protected linker fragment **3.4b** (17 mg, 0.020 mmol, 1 equiv) was dissolved in trifluoroacetic acid/dichloromethane (0.3 mL/0.3 mL, 0.03 M) and the resulting solution was stirred at room temperature for 2 hours. The reaction was monitored by TLC for complete consumption of the starting material before removal of volatile components *in vacuo*. The residue was redissolved in *N,N*-dimethylformamide (0.1 mL, 0.3 M), and fascin ligand A fragment **3.5** (12 mg, 0.020 mmol, 1 equiv), HATU (7.8 mg, 0.020 mmol, 1 equiv) and *N,N*-diisopropylethylamine (17 µL, 0.10 mmol, 5 equiv) were added. The resulting solution was stirred at room temperature for 16 hours before partitioning the reaction mixture between dichloromethane (10 mL) and water (10 mL). The aqueous phase was extracted with dichloromethane (5 × 10 mL) and the combined organic phases were washed with 5% aqueous lithium chloride (5 × 20 mL), dried over magnesium sulfate, filtered and concentrated *in vacuo*. Purification by column chromatography on silica gel

with an eluent of 10% to 30% ethanol in dichloromethane afforded the product (10 mg, 0.008 mmol, 42%) as a colourless oil. Further purification by semi-preparative RP-HPLC using a focused gradient across 40% and 70% acetonitrile in water over 35 minutes eluted the title compound at t_R = 30 minutes (62% acetonitrile) and the product fraction was lyophilised. Redissolving the resulting trifluoroacetate salt in 1 M aqueous hydrochloric acid and acetonitrile, followed by lyophilisation, yielded fascin ligand A amide VHL PROTAC **FSCN-A-VHL-2 (3.8)** (1 mg, 0.001 mmol, 4%) as a clear oil.

Insufficient material for full characterisation was obtained.

LCMS (ESI) mass calculated for $C_{66}H_{82}Cl_2N_{11}O_{12}$ $[M+H]^+$ m/z 1322.52, found m/z 1322.00 with t_R = 5.75 min.

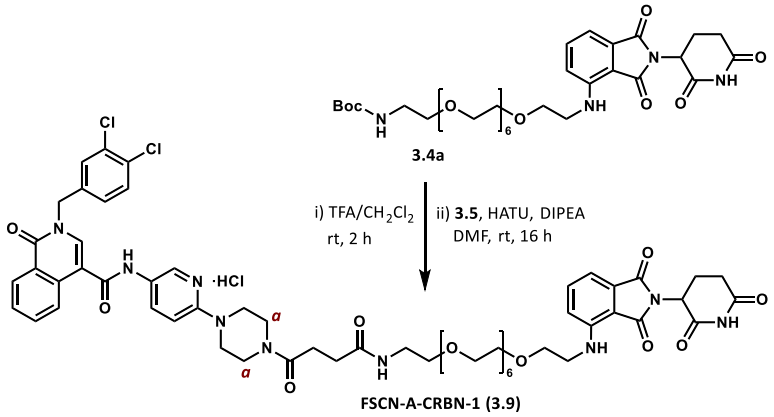

FSCN-A-CRBN-1 (3.9): Protected linker fragment **3.4a** (45 mg, 0.062 mmol, 1 equiv) was dissolved in trifluoroacetic acid/dichloromethane (1 mL/1 mL, 0.03 M) and the resulting solution was stirred at room temperature for 2 hours. The reaction was monitored by TLC for complete consumption of the starting material before removal of volatile components *in vacuo*. The residue was redissolved in *N,N*-dimethylformamide (0.3 mL, 0.3 M), and fascin ligand A fragment **3.5** (38 mg, 0.062 mmol, 1 equiv), HATU (24 mg, 0.062 mmol, 1 equiv) and *N,N*-diisopropylethylamine (54 µL, 0.31 mmol, 5 equiv) were added. The resulting solution was stirred at room temperature for 16 hours before partitioning the reaction mixture between dichloromethane (10 mL) and water (10 mL). The aqueous phase was extracted with dichloromethane (5 × 10 mL) and the combined organic phases were washed with 5% aqueous lithium chloride (5 × 20 mL), dried over magnesium sulfate, filtered and concentrated *in vacuo*. Purification by column chromatography on silica gel with an eluent of 10% to 50% ethanol in dichloromethane afforded the product (19 mg, 0.015 mmol, 24%) as a bright yellow oil. Further purification by semi-preparative RP-HPLC using a focused gradient across 30% and 70% acetonitrile in water over 35 minutes eluted the title compound at t_R = 29 minutes (65% acetonitrile) and the product fraction was

lyophilised. Redissolving the resulting trifluoroacetate salt in 1 M aqueous hydrochloric acid and acetonitrile, followed by lyophilisation, yielded fascin ligand A amide CRBN PROTAC **FSCN-A-CRBN-1 (3.9)** (8 mg, 0.007 mmol, 11%) as a bright yellow fluffy powder.

^{1}H NMR (400 MHz, chloroform-*d*) δ 10.16 (1H, br, -NH), 9.22 (1H, br, -NH), 8.69 (1H, d, *J* = 2.5 Hz, Ar-H), 8.38 – 8.31 (2H, m, 2 × Ar-H), 8.22 (1H, d, *J* = 8.2 Hz, Ar-H), 8.06 (1H, s, -CH), 7.67 (1H, ddd, *J* = 8.4, 7.1, 1.4 Hz, Ar-H), 7.54 – 7.43 (3H, m, 3 × Ar-H), 7.33 (1H, d, *J* = 8.3 Hz, Ar-H), 7.21 (1H, dd, *J* = 8.3, 2.1 Hz, Ar-H), 7.06 (1H, d, *J* = 7.1 Hz, Ar-H), 6.91 – 6.78 (4H, m, 2 × Ar-H & 2 × -NH), 5.15 (2H, s, -CH_2), 4.94 – 4.88 (1H, m, -CH), 3.81 – 3.50 (36H, m, 18 × 2H, s, -CH_2), 3.43 – 3.36 (4H, m, 2 × -**CH_2^a**), 2.87 – 2.64 (5H, m, 2 × -CH_2 & -C*H*H), 2.61 – 2.54 (2H, m, -CH_2), 2.15 – 2.07 (1H, m, -CH*H*). ^{13}C NMR (101 MHz, chloroform-*d*) δ 172.8 (-CONH), 171.7 (-CONH), 171.2 (-CONH), 169.4 (-CONH), 169.2 (2 × -CONR), 167.8 (-CONH), 165.0 (-CONR), 161.9 (Ar-C), 146.9 (Ar-C), 136.8 (Ar-CH), 136.3 (-CH), 136.3 (Ar-CH), 135.3 (Ar-C), 134.1 (Ar-C), 133.3 (Ar-CH), 132.8 (2 × Ar-C), 132.6 (Ar-CH), 132.2 (Ar-CH), 130.9 (Ar-C), 130.3 (Ar-CH), 128.1 (Ar-CH), 127.8 (Ar-CH), 127.8 (Ar-CH), 127.7 (Ar-CH), 125.6 (Ar-CH), 125.1 (Ar-C), 117.0 (Ar-CH), 116.9 (Ar-CH), 112.8 (Ar-C), 111.8 (Ar-CH), 110.3 (-C), 70.8 (2 × -CH_2), 70.6 (-CH_2), 70.5 (-CH_2), 70.4 (4 × -CH_2), 70.1 (-CH_2), 70.0 (-CH_2), 69.5 (2 × CH_2), 51.6 (-CH_2), 49.1 (-CH), 45.9 (2 × -**C^aH_2**), 44.3 (2 × -CH_2), 42.5 (-CH_2), 40.8 (-CH_2), 32.1 (-CH_2), 31.6 (-CH_2), 31.1 (-CH_2), 29.5 (-CH_2), 28.5 (-CH_2), 22.9 (-CH_2). IR (thin film) 3362, 1697, 748. HRMS (ESI) exact mass calculated for $C_{59}H_{69}Cl_2N_9O_{15}Na$ $[M+Na]^+$ m/z 1236.4182, found m/z 1236.4134. LCMS (ESI) mass calculated for $C_{59}H_{70}Cl_2N_9O_{15}$ $[M+H]^+$ m/z 1215.44, found m/z 1216.06 with t_R = 6.07 min.

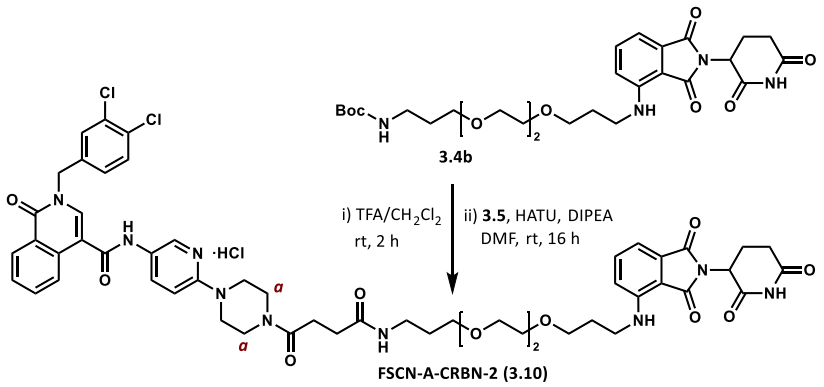

FSCN-A-CRBN-2 (3.10): Protected linker fragment **3.4b** (50 mg, 0.087 mmol, 1 equiv) was dissolved in trifluoroacetic acid/dichloromethane (1.5 mL/1.5 mL, 0.03 M) and the resulting solution was stirred at room temperature for 2 hours. The reaction was monitored by TLC for complete consumption of the starting material before removal of volatile components

in vacuo. The residue was redissolved in *N,N*-dimethylformamide (0.3 mL, 0.3 M), and fascin ligand A fragment **3.5** (53 mg, 0.087 mmol, 1 equiv), HATU (33 mg, 0.087 mmol, 1 equiv) and *N,N*-diisopropylethylamine (76 µL, 0.43 mmol, 5 equiv) were added. The resulting solution was stirred at room temperature for 16 hours before partitioning the reaction mixture between dichloromethane (10 mL) and water (10 mL). The aqueous phase was extracted with dichloromethane (5 × 10 mL) and the combined organic phases were washed with 5% aqueous lithium chloride (5 × 20 mL), dried over magnesium sulfate, filtered and concentrated *in vacuo*. Purification by column chromatography on silica gel with an eluent of 20% to 50% ethanol in dichloromethane afforded the product (21 mg, 0.020 mmol, 23%) as a bright yellow oil. Further purification by semi-preparative RP-HPLC using a focused gradient across 30% and 70% acetonitrile in water over 35 minutes eluted the title compound at t_R = 30 minutes (67% acetonitrile) and the product fraction was lyophilised. Redissolving the resulting trifluoroacetate salt in 1 M aqueous hydrochloric acid and acetonitrile, followed by lyophilisation, yielded fascin ligand A amide CRBN PROTAC **FSCN-A-CRBN-2 (3.10)** (5 mg, 0.005 mmol, 6%) as a bright yellow fluffy powder.

^{1}H NMR (400 MHz, chloroform-*d*) δ 9.10 (1H, br s, -NH), 8.46 (1H, s, -CH), 8.41 (1H, d, *J* = 8.2 Hz, Ar-H), 8.25 – 8.12 (2H, m, 2 × Ar-H), 7.94 – 7.88 (1H, m, Ar-H), 7.74 – 7.65 (1H, m, Ar-H), 7.57 – 7.42 (3H, m, 3 × Ar-H), 7.38 – 7.31 (2H, m, 2 × Ar-H), 7.04 (1H, d, *J* = 7.1 Hz, Ar-H), 6.89 (1H, d, *J* = 8.6 Hz, Ar-H), 6.72 – 6.57 (2H, m, Ar-H & -NH), 6.49 (1H, br s, -NH), 5.17 (2H, s, -CH_2), 4.93 – 4.85 (1H, m, -CH), 3.77 – 3.41 (24H, m, 12 × -CH_2), 3.41 – 3.21 (4H, m, 2 × -C**H$_2$**^{a}), 2.87 – 2.63 (5H, m, 2 × -CH_2 & -C*H*H), 2.55 – 2.47 (2H, m, -CH_2), 2.15 – 2.06 (1H, m, -CH*H*). ^{13}C NMR (101 MHz, chloroform-*d*) δ 172.5 (-CONH), 171.7 (-CONH), 170.8 (-CONR), 169.5 (-CONH), 169.0 (-CONR), 167.8 (-CONR), 165.9 (-CONR), 164.8 (-CONH), 162.0 (Ar-C), 147.1 (-CH), 136.7 (Ar-CH), 136.4 (Ar-C), 136.3 (Ar-C), 134.1 (Ar-CH), 134.0 (Ar-CH), 133.3 (Ar-C), 132.9 (2 × Ar-C), 132.6 (Ar-C), 132.4 (Ar-CH), 130.9 (Ar-CH), 130.2 (Ar-CH), 128.4 (Ar-CH), 127.9 (Ar-CH), 127.8 (Ar-C), 126.9 (Ar-CH), 125.7 (Ar-C), 125.0 (Ar-CH), 123.3 (2 × Ar-CH), 116.8 (Ar-C), 111.4 (Ar-CH), 109.9 (-C), 70.6 (2 × -CH_2), 70.2 (2 × -CH_2), 69.9 (-CH_2), 69.2 (-CH_2), 51.4 (-CH_2), 51.0 (-CH), 49.8 (-CH_2), 49.0 (-CH_2), 45.7 (-CH_2), 44.9 (-CH_2), 41.3 (-**C^a**H_2), 40.6 (-**C^a**H_2), 31.6 (-CH_2), 31.2 (-CH_2), 29.8 (-CH_2), 29.3 (-CH_2), 28.9 (-CH_2), 22.6 (-CH_2). IR (thin film) 2957, 1606, 764. HRMS (ESI) exact mass calculated for $C_{53}H_{57}Cl_2N_9O_{11}Na$ $[M+Na]^+$ m/z 1088.3447, found m/z 1088.3468. LCMS (ESI) mass calculated for $C_{53}H_{58}Cl_2N_9O_{11}$ $[M+H]^+$ m/z 1066.36, found m/z 1066.25 with t_R = 6.03 min.

Preparation of 1st series alkylation PROTACs

- *Fascin ligand A alkylation VHL PROTACs:*

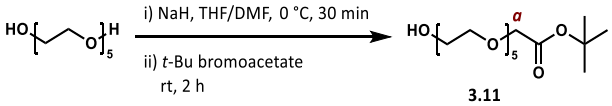

3.11: To a dry flask charged with argon was added anhydrous tetrahydrofuran/*N,N*-dimethylformamide (0.7 mL/0.7 mL, 1 M), pentaethylene glycol (1.2 mL, 5.7 mmol, 4 equiv) and sodium hydride (60% in mineral oil, 110 mg, 2.8 mmol, 2 equiv) at 0 °C. The resulting suspension was stirred for 30 minutes before *tert*-butyl bromoacetate (0.21 mL, 1.4 mmol, 1 equiv) was added dropwise at 0 °C. The reaction mixture was allowed to reach room temperature and stirred for further 2 hours. The reaction was quenched by dropwise addition of water (20 mL). The aqueous phase was extracted with dichloromethane (3 × 20 mL) and the combined organic extracts were washed with brine (3 × 60 mL), dried over magnesium sulfate, filtered and concentrated *in vacuo*. Purification by column chromatography on silica gel with an eluent of 2% to 20% ethanol in dichloromethane afforded protected linker **3.11** (340 mg, 0.97 mmol, 68%) as a clear oil.

Analytical data observed were in accordance with literature values.[98]

^{1}H NMR (500 MHz, chloroform-*d*) δ 3.93 (2H, s, -C**H$_2$**^{a}), 3.71 – 3.39 (20H, m, 10 × -CH$_2$), 2.84 (1H, br, -OH), 1.39 (9H, s, 3 × -CH$_3$). ^{13}C NMR (126 MHz, chloroform-*d*) δ 169.6 (-COOR), 81.4 (-*C*(CH$_3$)$_3$), 72.5 (-CH$_2$), 70.6 (-CH$_2$), 70.5 (-CH$_2$), 70.5 (2 × -CH$_2$), 70.5 (2 × -CH$_2$), 70.3 (2 × -CH$_2$), 68.9 (-**C**^{a}H$_2$), 61.6 (-CH$_2$), 28.0 (3 × -CH$_3$).

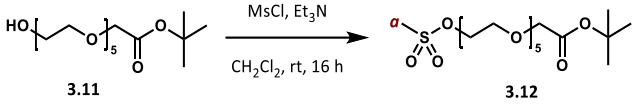

3.12: To a dry flask charged with argon was added anhydrous dichloromethane (12 mL, 0.1 M), alcohol **3.11** (380 mg, 1.1 mmol, 1 equiv), methanesulfonyl chloride (0.13 mL, 1.6 mmol, 1.5 equiv) and triethylamine (0.45 mL, 3.3 mmol, 3 equiv) and the resulting solution was stirred at room temperature for 16 hours. The reaction mixture was partitioned between 1 M aqueous hydrochloric acid (15 mL) and dichloromethane (15 mL), and the aqueous phase was extracted with dichloromethane (4 × 15 mL). The combined organic extracts were washed with water (2 × 30 mL), dried over magnesium sulfate, filtered and concentrated *in vacuo*. Purification by column chromatography on silica gel with an eluent of 5% to 30% acetone in dichloromethane afforded mesylate **3.12** (430 mg, 0.99 mmol, 87%) as a clear oil.

^{1}H NMR (400 MHz, chloroform-*d*) δ 4.33 (2H, s, -CH_2), 4.02 – 3.91 (2H, m, -CH_2), 3.81 – 3.48 (18H, m, 9 × -CH_2), 3.04 (3H, s, -C**H$_3$**^{a}), 1.43 (9H, s, 3 × -CH_3). ^{13}C NMR (101 MHz, chloroform-*d*) δ 169.7 (-COOR), 81.5 (-*C*(CH_3)$_3$), 70.7 (-CH_2), 70.7 (2 × -CH_2), 70.6 (-CH_2), 70.6 (2 × -CH_2), 70.6 (2 × -CH_2), 69.4 (-CH_2), 69.1 (-CH_2), 69.1 (-CH_2), 37.8 (-**C**^{a}H_3), 28.2 (3 × -CH_3). IR (thin film) 1744, 1350, 1126 cm^{-1}. HRMS (ESI) exact mass calculated for $C_{17}H_{34}O_{10}SNa$ [M+Na]$^{+}$ m/z 453.1765, found m/z 453.1766.

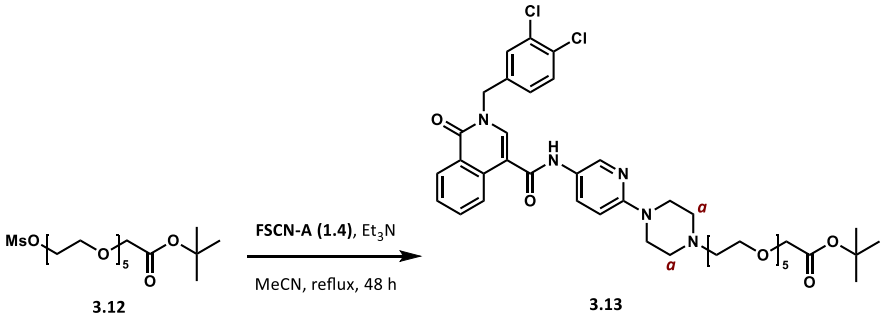

3.12 3.13

3.13: To a dry flask charged with argon was added anhydrous acetonitrile (1.2 mL, 0.1 M), mesylated linker **3.12** (51 mg, 0.12 mmol, 1 equiv), fascin ligand A **FSCN-A (1.4)** (72 mg, 0.14 mmol, 1.2 equiv) and triethylamine (60 µL, 0.48 mmol, 4 equiv) and the resulting solution was stirred under reflux for 48 hours. After consumption of starting materials was confirmed by TLC, volatile components were removed *in vacuo.* Purification by column chromatography on silica gel with an eluent of 5% to 100% ethanol in dichloromethane afforded fascin ligand fragment **3.13** (71 mg, 0.084 mmol, 71%) as a light brown amorphous solid.

^{1}H NMR (400 MHz, chloroform-*d*) δ 8.41 (1H, dd, *J* = 8.3, 1.2 Hz, Ar-H), 8.36 (1H, br s, -NH), 8.30 (1H, s, -CH), 8.13 (1H, d, *J* = 8.2 Hz, Ar-H), 7.94 (1H, d, *J* = 9.2 Hz, Ar-H), 7.72 – 7.62 (2H, m, 2 × Ar-H), 7.52 (1H, ddd, *J* = 8.3, 7.2, 1.2 Hz, Ar-H), 7.39 (1H, d, *J* = 2.1 Hz, Ar-H), 7.35 (1H, d, *J* = 8.3 Hz, Ar-H), 7.14 (1H, dd, *J* = 8.3, 2.1 Hz, Ar-H), 6.64 (1H, d, *J* = 9.2 Hz, Ar-H), 5.04 (2H, s, -CH_2), 3.98 (2H, s, -CH_2), 3.69 – 3.57 (18H, m, 9 × -CH_2), 3.57 – 3.47 (4H, m, 2 × -CH_2), 2.69 – 2.57 (6H, m, -CH_2 & 2 × -C**H$_2$**^{a}), 1.44 (9H, s, 3 × -CH_3). ^{13}C NMR (101 MHz, chloroform-*d*) δ 162.0 (-COOR), 157.1 (-CONR), 140.6 (-CONH), 136.5 (Ar-C), 134.0 (Ar-C), 133.4 (Ar-C), 133.2 (Ar-C), 133.1 (Ar-C), 132.5 (Ar-C), 131.0 (Ar-C), 130.0 (Ar-C), 128.5 (Ar-C), 128.0 (Ar-C), 127.5 (Ar-C), 125.8 (2 × Ar-C), 125.7 (2 Ar-C), 124.9 (2 × Ar-C), 107.1 (Ar-C), 100.1 (-C), 77.4 (-*C*(CH_3)$_3$), 70.7 (-CH_2), 70.6 (3 × -CH_2), 70.6 (2 × -CH_2), 70.4 (-CH_2), 69.1 (2 × -CH_2), 68.7 (2 × -CH_2), 57.9 (-CH_2), 53.3 (2 × -**C**^{a}H_2), 51.4 (-CH_2), 45.5 (-CH_2), 28.2 (3 × -CH_3). IR (thin film) 1659, 1141, 779 cm^{-1}. HRMS (ESI) exact mass calculated for $C_{42}H_{53}N_5O_9Cl_2Na$ [M+Na]$^{+}$ m/z 846.3113, found m/z 846.3071.

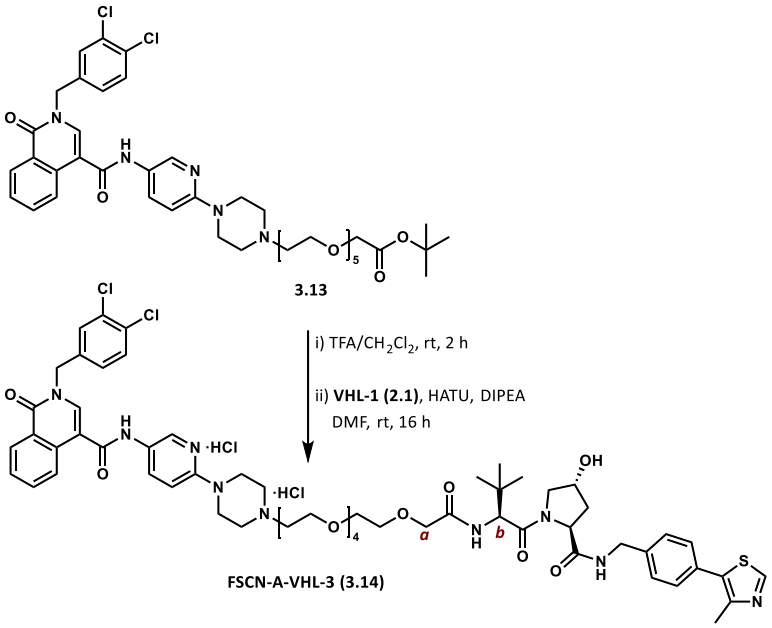

FSCN-A-VHL-3 (3.14): Protected fragment **3.13** (42 mg, 0.050 mmol, 1 equiv) was dissolved in trifluoroacetic acid/dichloromethane (0.8 mL/0.8 mL, 0.03 M) and the resulting solution was stirred at room temperature for 2 hours. The reaction was monitored by TLC for complete consumption of the starting material before removal of volatile components *in vacuo*. The residue was redissolved in *N,N*-dimethylformamide (0.16 mL, 0.3 M) and VHL ligand **VHL-1 (2.1)** (21 mg, 0.050 mmol, 1 equiv), HATU (19 mg, 0.050 mmol, 1 equiv) and *N,N*-diisopropylethylamine (44 µL, 0.25 mmol, 5 equiv) were added. The resulting solution was stirred at room temperature for 16 hours before partitioning the reaction mixture between dichloromethane (15 mL) and water (15 mL). The aqueous phase was extracted with dichloromethane (5 × 15 mL) and the combined organic phases were washed with 5% aqueous lithium chloride (5 × 30 mL), dried over magnesium sulfate, filtered and concentrated *in vacuo*. Purification by column chromatography on silica gel with an eluent of 20% to 50% ethanol in dichloromethane afforded the product (38 mg, 0.032 mmol, 63%) as pale yellow oil. Further purification by semi-preparative RP-HPLC using a focused gradient across 45% and 75% acetonitrile in water over 20 minutes eluted the title compound at t_R = 14 minutes (58% acetonitrile) and the product fraction was lyophilised. Redissolving the resulting trifluoroacetate salt in 1 M aqueous hydrochloric acid and acetonitrile, followed by lyophilisation, yielded fascin ligand A alkylation VHL PROTAC **FSCN-A-VHL-3 (3.14)** (15 mg, 0.013 mmol, 25%) as a white fluffy powder.

^{1}H NMR (400 MHz, methanol-d_4) δ 9.91 (1H, s, thiazole-H), 8.84 (1H, s, Ar-H), 8.37 (1H, d, *J* = 7.9 Hz, Ar-H), 8.31 (1H, s, -CH), 8.28 – 8.19 (2H, m, 2 × Ar-H), 7.84 – 7.75 (1H, m, Ar-H), 7.67 – 7.57 (2H, m, 2 × Ar-H), 7.57 – 7.43 (6H, m, 6 × Ar-H), 7.38 (1H, d, *J* = 8.1 Hz, Ar-H), 5.28 (2H, s, -CH_2), 4.71 – 4.28 (7H, m, -C**H$_2$**^{a} & -C**H**^{b} & 2 × -CH & -CH_2), 4.18 – 3.38 (30H, m,

15 × -CH_2), 2.58 (3H, s, -CH_3), 2.33 – 2.00 (2H, m, -CH_2), 1.04 (9H, s, 3 × -CH_3). ^{13}C NMR (126 MHz, methanol-d_4) δ 174.4 (-CONH), 172.1 (-CONH), 171.8 (-CONR), 166.8 (-CONH), 163.4 (-CONR), 156.2 (Ar-C), 150.9 (thiazole-C), 143.2 (thiazole-C), 142.3 (Ar-C), 139.3 (-CH), 138.7 (Ar-C), 137.0 (Ar-C), 136.8 (Ar-C), 135.5 (Ar-C), 134.4 (Ar-C), 133.5 (Ar-C), 132.8 (Ar-C), 131.9 (Ar-C), 131.3 (Ar-C), 130.5 (Ar-C), 129.8 (Ar-C), 129.8 (Ar-C), 129.3 (2 × Ar-C), 129.1 (2 × Ar-C), 129.0 (Ar-C), 128.8 (Ar-C), 128.4 (Ar-C), 126.6 (Ar-C), 126.1 (Ar-C), 114.9 (Ar-C), 114.3 (Ar-C), 72.2 (-CH), 71.7 (2 × -CH_2), 71.6 (2 × -CH_2), 71.5 (-CH_2), 71.5 (-**C^a**H_2), 71.5 (-CH_2), 71.4 (-CH_2), 71.3 (-CH_2), 71.1 (-CH_2), 65.4 (-CH_2), 60.9 (-**C^b**H), 58.5 (-CH), 58.2 (-CH_2), 57.6 (-CH_2), 52.9 (-CH_2), 52.4 (2 -CH_2), 44.9 (2 -CH_2), 43.6 (-CH_2), 39.2 (-CH_2), 36.9 (-*C*(CH_3)$_3$), 27.0 (3 × -CH_3), 13.6 (-CH_3). IR (thin film) 1659, 1489, 826 cm^{-1}. HRMS (ESI) exact mass calculated for $C_{60}H_{74}N_9O_{11}Cl_2S$ $[M+H]^+$ m/z 1198.4600, found m/z 1198.4541. LCMS (ESI) mass calculated for $C_{60}H_{74}N_9O_{11}Cl_2S$ $[M+H]^+$ m/z 1198.46, found m/z 1199.03 with t_R = 5.88 min.

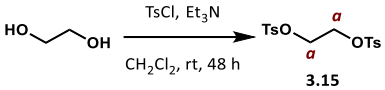

3.15

3.15: To a stirred solution of ethylene glycol (0.30 mL, 5.4 mmol, 1 equiv) and triethylamine (2.2 mL, 16 mmol, 3 equiv) in dichloromethane (36 mL, 0.15 M) was added a solution of *p*-toluenesulfonyl chloride (3.1 g, 16 mmol, 3 equiv) in dichloromethane (18 mL, 0.3 M) dropwise at 0 °C. The resulting solution was allowed to reach room temperature and stirred for 48 hours. Complete consumption of the starting material was confirmed by TLC after and volatile components were removed *in vacuo*. The residue was dissolved in water (100 mL) and the aqueous phase was extracted with dichloromethane (3 × 100 mL). The combined organic extracts were dried over magnesium sulfate, filtered and concentrated *in vacuo.* Purification by column chromatography on silica gel with an eluent of 10% to 100% ethyl acetate in petroleum ether afforded di-tosylate **3.15** (1.9 g, 5.0 mmol, 93%) as a white amorphous solid.

Analytical data observed were in accordance with literature values.[256]

^{1}H NMR (400 MHz, chloroform-*d*) δ 7.76 – 7.71 (4H, m, 4 × Ar-H), 7.37 – 7.32 (4H, m, 4 × Ar-H), 4.18 (4H, s, 2 -C**H$_2$^{a}**), 2.46 (6H, s, 2 × -CH_3). ^{13}C NMR (101 MHz, chloroform-*d*) δ 145.5 (2 × Ar-C), 132.6 (2 × Ar-C), 130.2 (4 × Ar-CH), 128.2 (4 × Ar-CH), 77.5, 66.9 (2 × -**C^a**H_2), 21.9 (2 × -CH_3).

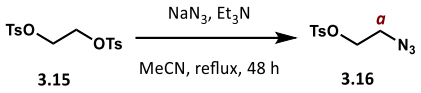

3.16: To a dry flask charged with argon was added anhydrous acetonitrile (6 mL, 0.2 M), ditosylate **3.15** (450 mg, 1.2 mmol, 1 equiv) and sodium azide (79 mg, 1.2 mmol, 1 equiv), and the resulting solution was stirred for 48 hours under reflux. Volatile components were removed *in vacuo* and the residue was redissolved in water (50 mL) and dichloromethane (50 mL). The aqueous phase was extracted with dichloromethane (5 × 50 mL), and the combined organic extracts were dried over magnesium sulfate, filtered and concentrated *in vacuo.* Purification by column chromatography on silica gel with an eluent of 5% to 15% ethyl acetate in petroleum ether afforded tosylazide **3.16** (69 mg, 0.29 mmol, 24%) as a white amorphous solid.

Analytical data observed were in accordance with literature values.[257]

^{1}H NMR (400 MHz, chloroform-*d*) δ 7.84 – 7.78 (2H, m, 2 × Ar-H), 7.39 – 7.33 (2H, m, 2 × Ar-H), 4.15 (2H, t, *J* = 5.2 Hz, -CH_2), 3.48 (2H, t, *J* = 5.1 Hz, -C**H$_2$**^{a}), 2.45 (3H, s, -CH_3). ^{13}C NMR (101 MHz, chloroform-*d*) δ 145.4 (Ar-C), 132.7 (Ar-C), 130.1 (2 × Ar-CH), 128.1 (2 × Ar-CH), 68.2 (-CH_2), 49.7 (-**C**^{a}H$_2$), 21.8 (-CH_3).

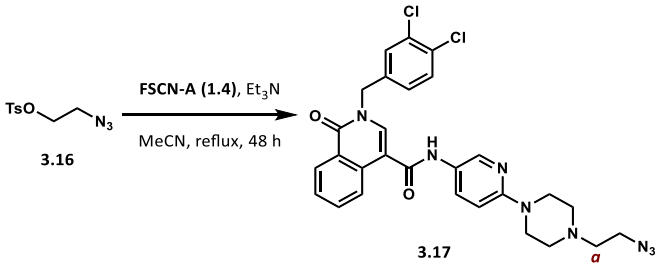

3.17: To a dry flask charged with argon was added anhydrous acetonitrile (0.6 mL, 0.4 M), tosylazide **3.16** (61 mg, 0.26 mmol, 1 equiv), fascin ligand A **FSCN-A (1.4)** (130 mg, 0.26 mmol, 1 equiv) and triethylamine (70 µL, 0.52 mmol, 2 equiv) and the resulting solution was stirred under reflux for 48 hours. Consumption of starting materials was confirmed by TLC and volatile components were removed *in vacuo.* Purification by column chromatography on silica gel with an eluent of 10% to 50% ethanol in dichloromethane azide fragment **3.17** (140 mg, 0.24 mmol, 97%) as a light purple amorphous solid.

^{1}H NMR (400 MHz, chloroform-*d*) δ 8.46 (1H, dd, *J* = 8.1, 1.4 Hz, Ar-H), 8.26 (1H, s, -CH), 8.09 (1H, d, *J* = 8.1 Hz, Ar-H), 7.95 (1H, d, *J* = 9.2 Hz, Ar-H), 7.77 – 7.69 (2H, m, 2 × Ar-H), 7.60 – 7.51 (2H, m, Ar-H & -NH), 7.42 – 7.36 (2H, m, 2 × Ar-H), 7.15 (1H, d, *J* = 8.4 Hz, Ar-H), 6.69 (1H, d, *J* = 9.2 Hz, Ar-H), 5.06 (2H, s, -CH_2), 3.61 – 3.52 (4H, m, 2 × -CH_2), 3.40 (2H, t, *J* = 6.0 Hz, -C**H$_2$**^{a}), 2.69 – 2.60 (6H, m, 2 × -CH_2 & -CH_2). ^{13}C NMR (101 MHz, chloroform-*d*) δ

161.9 (-CONR), 157.3 (-CONH), 156.8 (Ar-C), 142.0 (Ar-CH), 140.6 (-CH), 136.3 (Ar-C), 133.8 (Ar-C), 133.5 (Ar-CH), 133.3 (Ar-C), 132.8 (Ar-CH), 132.7 (Ar-CH), 131.1 (2 Ar-C), 130.0 (Ar-C), 128.8 (Ar-CH), 128.2 (Ar-C), 127.5 (Ar-CH), 125.8 (Ar-CH), 125.3 (Ar-CH), 124.6 (Ar-CH), 118.6 (-C), 107.1 (-CH_2), 57.4 (-**C**^{a}H_2), 53.1 (2 × -CH_2), 51.5 (-CH_2), 48.4 (-CH_2), 45.7 (2 × -CH_2). IR (thin film) 1616, 1489, 814 cm^{-1}. HRMS (ESI) exact mass calculated for $C_{28}H_{27}N_8O_2Cl_2$ $[M+H]^+$ m/z 577.1629, found m/z 577.1614.

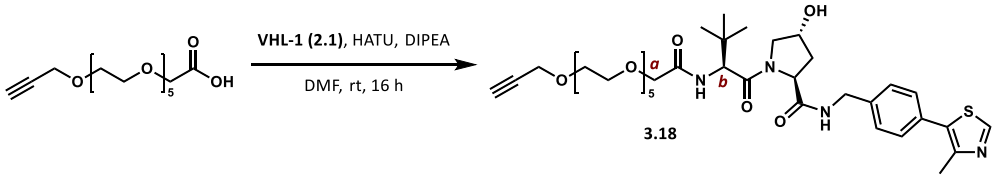

3.18: To a pre-stirred solution of alkyne carboxylic acid (25 mg, 0.081 mmol, 1 equiv), HATU (31 mg, 0.081 mmol, 1 equiv) and *N,N*-diisopropylethylamine (50 µL, 0.33 mmol, 4 equiv) in *N,N*-dimethylformamide (0.3 mL, 0.3 M) was added amine **VHL-1 (2.1)** (35 mg, 0.081 mmol, 1 equiv), and the resulting solution was stirred at room temperature for 16 hours. The reaction mixture was partitioned between dichloromethane (20 mL) and water (20 mL), and the aqueous phase was extracted with dichloromethane (5 × 20 mL). The combined organic phases were washed with 5% aqueous lithium chloride (5 × 40 mL), dried over magnesium sulfate, filtered and concentrated *in vacuo*. Purification by column chromatography on silica gel with an eluent of % to 50% ethanol in dichloromethane afforded alkyne fragment **3.18** (37 mg, 0.051 mmol, 63%) as clear oil.

Analytical data observed were in accordance with literature values.[188]

^{1}H NMR (500 MHz, chloroform-*d*) δ 8.67 (1H, s, thiazole-H), 7.44 (1H, br s, -NH), 7.38 – 7.31 (4H, m, 4 × Ar-H), 7.03 (1H, br s, -NH), 4.74 – 4.68 (1H, m, -CH), 4.58 – 4.30 (3H, m, -CH & -CH_2), 4.21 – 4.16 (2H, m, -CH_2), 4.11 – 4.07 (1H, m, -C**H**^{a}), 3.78 – 3.53 (20H, m, 10 × -CH_2), 3.09 (1H, s, alkyne-H), 2.50 (3H, s, -CH_3), 2.49 – 2.41 (2H, m, -CH_2), 2.18 – 2.05 (2H, m, -C**H**$_2$^{a}), 0.93 (9H, s, 3 × -CH_3). ^{13}C NMR (125 MHz, chloroform-*d*) δ 172.3 (-CONH), 171.8 (-CONH), 171.0 (-CONR), 150.4 (thiazole-CH), 148.6 (thiazole-C), 138.3 (thiazole-C), 131.7 (Ar-C), 131.0 (Ar-C), 129.6 (2 × Ar-CH), 128.2 (2 × Ar-CH), 79.7 (alkyne-C), 74.8 (alkyne-CH), 70.7 (-CH_2), 70.6 (-CH_2), 70.6 (2 × -CH_2), 70.6 (-CH_2), 70.5 (-CH_2), 70.5 (-CH_2), 70.2 (-CH), 69.2 (-CH_2), 67.2 (-CH_2), 58.5 (-CH_2), 57.9 (-CH), 56.8 (-**C**^{b}H), 53.9 (-CH_2), 43.3 (-CH_2), 36.8 (-**C**^{a}H_2), 36.1 (-CH_2), 29.8 (-C), 26.5 (3 × -CH_3), 16.2 (-CH_3).

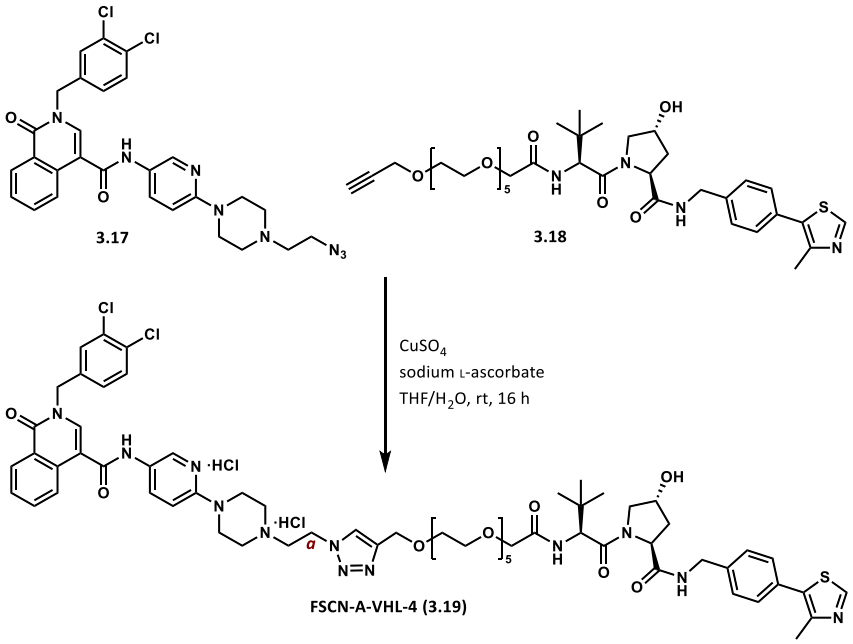

FSCN-A-VHL-4 (3.19): To a stirred solution of alkyne **3.18** (17 mg, 0.024 mmol, 1 equiv) in tetrahydrofuran (0.2 mL, 0.1 M) was added sodium L-ascorbate (1.4 mg, 0.0071 mmol, 0.3 equiv), copper(II) sulfate powder (1.1 mg, 0.0071 mmol, 0.3 equiv), azide **3.17** (14 mg, 0.024 mmol, 1 equiv) and a few drops of water. The resulting solution was stirred at room temperature for 16 hours before removing volatile components *in vacuo.* The crude product was purified column chromatography on silica gel with an eluent of 10% to 50% ethanol in dichloromethane afforded the product (23 mg, 0.018 mmol, 74%) as clear oil. Further purification by semi-preparative RP-HPLC using a focused gradient across 45% and 75% acetonitrile in water over 20 minutes eluted the title compound at t_R = 14 minutes (52% acetonitrile) and the product fraction was lyophilised. Redissolving the resulting trifluoroacetate salt in 1 M aqueous hydrochloric acid and acetonitrile, followed by lyophilisation, yielded fascin ligand A alkylation VHL PROTAC **FSCN-A-VHL-4 (3.19)** (9 mg, 0.007 mmol, 29%) as a white fluffy powder.

^{1}H NMR (500 MHz, methanol-*d*$_4$) δ 9.89 (1H, s, thiazole-H), 8.84 (1H, s, Ar-H), 8.38 (1H, d, *J* = 8.0 Hz, Ar-H), 8.28 (1H, s, -CH), 8.26 – 8.13 (3H, m, triazole-H & 2 × Ar-H), 7.83 – 7.75 (1H, m, Ar-H), 7.66 – 7.59 (2H, m, 2 × Ar-H), 7.59 – 7.43 (6H, m, 6 × Ar-H), 7.37 (1H, d, *J* = 8.2 Hz, Ar-H), 5.28 (2H, s, -CH_2), 5.04 (2H, s, -C**H$_2$**^{a}), 4.71 – 4.34 (7H, m, 2 × -CH_2 & 3 × -CH), 4.00 – 3.52 (32 H, m, 16 × -CH_2), 2.59 (3H, s, -CH_3), 2.51 – 2.42 (2H, m, -CH_2), 2.27 – 2.03 (2H, m, -CH_2), 1.04 (9H, s, 3 × -CH_3). ^{13}C NMR (126 MHz, methanol-*d*$_4$) δ 174.6 (-CONH), 173.8 (-CONH), 172.1 (-CONR), 166.8 (-CONH), 163.5 (-CONR), 156.1 (Ar-C), 151.3 (thiazole-C), 144.4 (triazole-C), 143.4 (thiazole-C), 142.3 (Ar-C), 138.9 (thiazole-C), 138.8 (Ar-C), 138.8 (-CH), 136.5 (Ar-C), 136.5 (Ar-C), 135.5 (Ar-C), 134.4 (Ar-C), 133.5 (Ar-C), 132.9 (Ar-C), 131.9 (Ar-C), 131.2 (Ar-C), 130.4 (Ar-C), 129.9 (Ar-C), 129.5 (Ar-C), 129.4 (4 × Ar-C), 129.0 (Ar-C),

128.9 (Ar-C), 128.4 (Ar-C), 126.6 (Ar-C), 126.3 (triazole-C), 126.0 (Ar-C), 114.6 (-C), 114.6 (Ar-C), 71.6 (2 × -CH_2), 71.5 (-CH), 71.5 (2 × -CH_2), 71.4 (-CH_2), 71.1 (-CH_2), 71.0 (-CH_2), 68.3 (-CH_2), 65.0 (-CH), 60.9 (-CH), 59.1 (-CH), 58.0 (-CH_2), 56.6 (-CH_2), 52.9 (-CH_2), 52.6 (2 × -CH_2), 45.6 (-**C**$^{a}H_2$), 44.8 (2 × -CH_2), 43.6 (-CH), 39.0 (-CH_2), 37.3 (-CH_2), 37.3 (-CH_2), 36.7 (-*C*$(CH_3)_3$), 27.1 (3 × -CH_3), 13.6 (-CH_3). IR (thin film) 1659, 1126, 802 cm^{-1}. HRMS (ESI) exact mass calculated for $C_{65}H_{81}N_{12}O_{12}Cl_2S$ $[M+H]^+$ m/z 1323.5189, found m/z 1323.5192. LCMS (ESI) mass calculated for $C_{65}H_{81}N_{12}O_{12}Cl_2S$ $[M+H]^+$ m/z 1323.52, found m/z 1323.00 with t_R = 5.83 min.

- *Fascin ligand A alkylation CRBN PROTAC:*

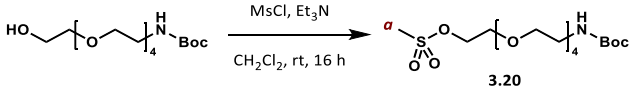

3.20

3.20: To a stirred solution of mono-protected linker (80 mg, 0.24 mmol, 1 equiv) in dichloromethane (3 mL, 0.1 M), was added methanesulfonyl chloride (55 µL, 0.71 mmol, 3 equiv) and triethylamine (99 µL, 0.71 mmol, 3 equiv) and the resulting solution was stirred at room temperature for 16 hours. The reaction mixture was partitioned between 1 M aqueous hydrochloric acid (10 mL) and dichloromethane (10 mL), and the aqueous phase was extracted with dichloromethane (4 × 10 mL). The combined organic extracts were washed with water (2 × 20 mL), dried over magnesium sulfate, filtered and concentrated *in vacuo*. Purification by column chromatography on silica gel with an eluent of 100% ethyl acetate afforded mesylate **3.20** (76 mg, 0.19 mmol, 77%) as a clear oil.

^{1}H NMR (400 MHz, chloroform-*d*) δ 4.94 (1H, br s, -NH), 4.31 – 4.23 (2H, m, -CH_2), 3.73 – 3.59 (2H, m, -CH_2), 3.60 – 3.47 (12H, m, 6 × -CH_2), 3.43 (2H, t, *J* = 5.1 Hz, -CH_2), 3.26 – 3.16 (2H, m, -CH_2), 2.97 (3H, s, -C**H**$_3^{a}$), 1.33 (9H, s, 3 × -CH_3). ^{13}C NMR (101 MHz, chloroform-*d*) δ 156.1 (-NCOOR), 79.3 (-*C*$(CH_3)_3$), 70.8 (-CH_2), 70.7 (3 × -CH_2), 70.7 (2 × -CH_2), 70.4 (-CH_2), 69.4 (-CH_2), 69.2 (-CH_2), 40.5 (-CH_2), 37.9 (-**C**$^{a}H_3$), 28.6 (3 × -CH_3). IR (thin film) 3348, 1705, 1173 cm^{-1}. HRMS (ESI) exact mass calculated for $C_{16}H_{33}NO_9SNa$ $[M+Na]^+$ m/z 438.1768, found m/z 438.1768.

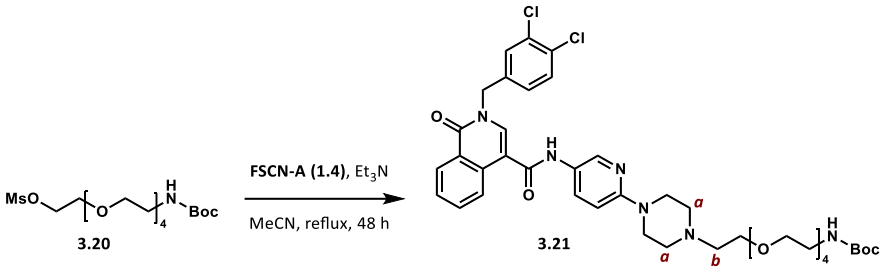

3.21: To a dry flask charged with argon was added anhydrous acetonitrile (1 mL, 0.1 M), mesylated linker **3.20** (36 mg, 0.087 mmol, 1 equiv), fascin ligand A **FSCN-A (1.4)** (53 mg, 0.10 mmol, 1.2 equiv) and triethylamine (24 µL, 0.17 mmol, 2 equiv) and the resulting solution was stirred under reflux for 48 hours. After consumption of starting materials was confirmed by TLC, volatile components were removed *in vacuo.* Purification by column chromatography on silica gel with an eluent of 20% to 100% ethanol in dichloromethane afforded fascin ligand fragment **3.21** (41 mg, 0.050 mmol, 57%) as a light brown oil.

^{1}H NMR (400 MHz, chloroform-*d*) δ 8.40 (1H, dd, *J* = 8.2, 1.4 Hz, Ar-H), 8.33 (1H, br s, -NH), 8.29 (1H, s, -CH), 8.11 (1H, d, *J* = 8.2 Hz, Ar-H), 7.93 (1H, d, *J* = 9.1 Hz, Ar-H), 7.69 (1H, ddd, *J* = 8.2, 7.1, 1.4 Hz, Ar-H), 7.58 (1H, s, Ar-H), 7.51 (1H, ddd, *J* = 8.2, 7.1, 1.2 Hz, Ar-H), 7.40 – 7.31 (2H, m, 2 × Ar-H), 7.12 (1H, dd, *J* = 8.2, 2.1 Hz, Ar-H), 6.64 (1H, d, *J* = 9.1 Hz, Ar-H), 5.09 (1H, br s, -NH), 5.00 (2H, s, -CH_2), 3.68 – 3.54 (14H, m, 7 × -CH_2), 3.55 – 3.43 (6H, m, 3 × -CH_2), 3.30 – 3.21 (2H, m, -CH_2), 2.68 – 2.56 (6H, m, 2 × -CH_2^a & -CH_2^b), 1.41 (9H, s, 3 × -CH_3).

^{13}C NMR (101 MHz, chloroform-*d*) δ 162.0 (-CONR), 157.1 (-CONH), 156.3 (-NCOOR), 140.6 (-CH), 136.4 (Ar-C), 134.0 (Ar-C), 133.4 (2 Ar-C), 133.1 (Ar-C), 133.1 (Ar-C), 132.5 (Ar-C), 131.4 (Ar-C), 131.0 (Ar-C), 130.0 (Ar-C), 128.5 (Ar-C), 128.0 (Ar-C), 127.4 (Ar-C), 125.7 (Ar-C), 125.7 (Ar-C), 124.8 (Ar-C), 115.1 (Ar-C), 107.1 (Ar-C), 79.4 (-*C*(CH_3)$_3$), 70.7 (2 × -CH_2), 70.6 (2 × -CH_2), 70.5 (2 × -CH_2), 70.3 (-CH_2), 68.7 (-CH_2), 57.8 (-C^bH_2), 53.3 (2 × -C^aH_2), 51.4 (-CH_2), 45.5 (2 × -CH_2), 40.5 (-CH_2), 28.5 (3 × -CH_3). IR (thin film) 1651, 1489, 733 cm^{-1}. HRMS (ESI) exact mass calculated for $C_{41}H_{52}N_6O_8Cl_2Na$ $[M+Na]^+$ m/z 849.3116, found m/z 849.3085.

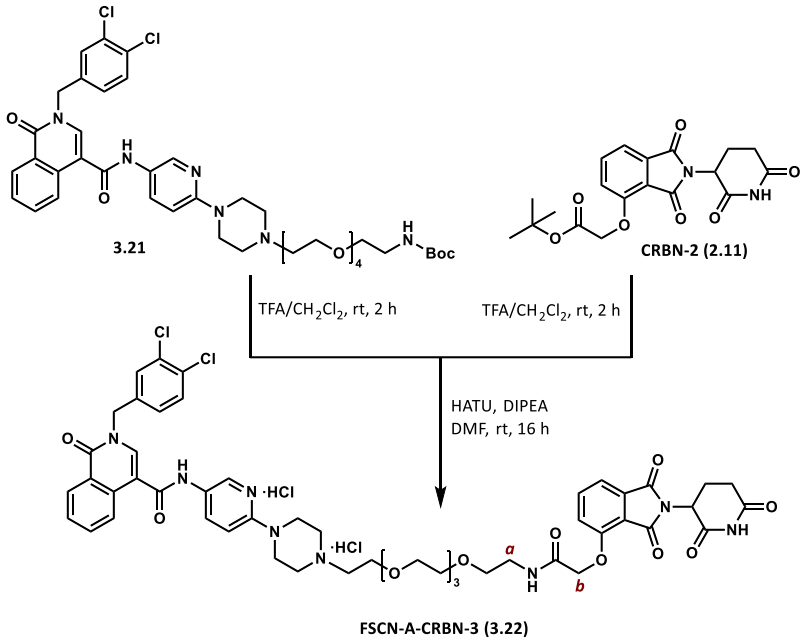

FSCN-A-CRBN-3 (3.22): Protected linker fragment **3.21** (40 mg, 0.047 mmol, 1 equiv) was dissolved in trifluoroacetic acid/dichloromethane (0.75 mL/0.75 mL, 0.03 M) and the resulting solution was stirred at room temperature for 2 hours. CRBN ligand **CRBN-2 (2.11)** (18 mg, 0.047 mmol, 1 equiv) was dissolved in trifluoroacetic acid/dichloromethane (0.75 mL/0.75 mL, 0.03 M) and the resulting solution was stirred at room temperature for 2 hours. The reactions were monitored by TLC for complete consumption of the starting materials before removal of volatile components *in vacuo*. The residues were redissolved in *N,N*-dimethylformamide (0.15 mL, 0.3 M), and HATU (18 mg, 0.047 mmol, 1 equiv) and *N,N*-diisopropylethylamine (50 µL, 0.28 mmol, 6 equiv) were added. The resulting solution was stirred at room temperature for 16 hours before partitioning it between dichloromethane (10 mL) and water (10 mL). The aqueous phase was extracted with dichloromethane (5 × 10 mL) and the combined organic phases were washed with 5% aqueous lithium chloride (3 × 20 mL), dried over magnesium sulfate, filtered and concentrated *in vacuo*. Purification by column chromatography on silica gel with an eluent of 10% to 50% ethanol in dichloromethane afforded the product (27 mg, 0.026 mmol, 56%) as a clear oil. Further purification by semi-preparative RP-HPLC using a focused gradient across 45% and 75% acetonitrile in water over 20 minutes eluted the title compound at t_R = 14 minutes (61% acetonitrile) and the product fraction was lyophilised. Redissolving the resulting trifluoroacetate salt in 1 M aqueous hydrochloric acid and acetonitrile, followed by lyophilisation, yielded fascin ligand A alkylation CRBN PROTAC **FSCN-A-CRBN-3 (3.22)** (8 mg, 0.008 mmol, 17%) as a pale yellow oil.

^{1}H NMR (400 MHz, methanol-d_4) δ 8.67 (1H, s, -cH), 8.38 (1H, dd, *J* = 8.2, 1.2 Hz, Ar-H), 8.21 (1H, d, *J* = 8.2 Hz, Ar-H), 8.18 – 8.11 (2H, m, 2 × Ar-H), 7.82 – 7.77 (1H, m, Ar-H), 7.77 – 7.72

(1H, m, Ar-H), 7.65 – 7.58 (2H, m, 2 × Ar-H), 7.52 – 7.44 (2H, m, 2 × Ar-H), 7.40 – 7.31 (3H, m, 3 × Ar-H), 5.27 (2H, s, -CH_2), 5.15 – 5.07 (1H, m, -CH), 4.75 (2H, s, -C**H_2^b**), 4.49 – 4.34 (2H, m, -C**H_2^a**), 3.92 (2H, t, *J* = 4.1 Hz, -CH_2), 3.89 – 3.78 (2H, m, -CH_2), 3.74 – 3.59 (16H, m, 8 × -CH_2), 3.54 – 3.47 (4H, m, 2 × -CH_2), 3.47 – 3.36 (2H, m, -CH_2), 2.94 – 2.63 (3H, m, -CH_2 & -C*H*H), 2.19 – 2.09 (1H, m, -CH*H*). ^{13}C NMR (101 MHz, methanol-d_4) δ 174.5 (-CONH), 171.5 (-CONH), 170.0 (-CONH), 168.2 (-CONR), 167.6 (-CONR), 166.7 (-CONR), 163.5 (-CONH), 156.1 (Ar-C), 156.1 (Ar-C), 138.8 (-CH), 138.3 (Ar-C), 136.3 (Ar-C), 135.5 (Ar-C), 134.8 (Ar-C), 134.4 (2 × Ar-C) 133.5 (Ar-C), 132.9 (Ar-C), 131.9 (Ar-C), 131.2 (Ar-C), 129.6 (Ar-C), 129.0 (2 × Ar-C), 128.9 (2 × Ar-C), 126.6 (Ar-C), 126.0 (Ar-C), 121.5 (2 × Ar-C), 119.0 (Ar-C), 117.9 (Ar-C), 114.8 (-C), 71.5 (-CH_2), 71.5 (-CH_2), 71.4 (-CH_2), 71.3 (-CH_2), 71.3 (-CH_2), 70.2 (2 × -CH_2), 69.1 (-**C^b**H_2), 65.2 (-CH_2), 57.4 (-CH_2), 52.8 (-CH_2), 52.4 (2 × -CH_2), 50.6 (-CH), 44.6 (2 × -CH_2), 40.2 (-**C^a**H_2), 32.2 (-CH_2), 23.7 (-CH_2). IR (thin film) 1674, 1134, 802 cm^{-1}. HRMS (ESI) exact mass calculated for $C_{51}H_{55}N_8O_{12}Cl_2$ $[M+H]^+$ m/z 1041.3311, found m/z 1041.3273. LCMS (ESI) mass calculated for $C_{51}H_{55}N_8O_{12}Cl_2$ $[M+H]^+$ m/z 1041.33, found m/z 1041.50 with t_R = 5.87 min.

- *Fascin ligand A alkylation HyT PROTAC:*

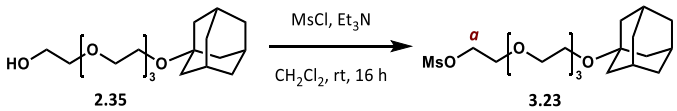

3.23: To a stirred solution of alcohol **2.35** (400 mg, 1.2mmol, 1 equiv) in dichloromethane (8 mL, 0.3 M) was added methanesulfonyl chloride (0.14 mL, 1.8 mmol, 1.5 equiv) and triethylamine (0.50 mL, 3.6 mmol, 3 equiv) and the resulting solution was stirred at room temperature for 16 hours. The reaction mixture was partitioned between 1 M aqueous hydrochloric acid (10 mL) and dichloromethane (10 mL), and the aqueous phase was extracted with dichloromethane (4 × 10 mL). The combined organic extracts were washed with water (2 × 20 mL), dried over magnesium sulfate, filtered and concentrated *in vacuo*. Purification by column chromatography on silica gel with an eluent of 50% ethyl acetate in dichloromethane afforded mesylate **3.23** (390 mg, 0.98 mmol, 80%) as a light brown oil. ^{1}H NMR (400 MHz, chloroform-*d*) δ 4.37 (2H, t, *J* = 4.1 Hz, -C**H_2^a**), 3.76 (2H, t, *J* = 4.1 Hz, -CH_2), 3.69 – 3.59 (8H, m, 4 × -CH_2), 3.60 – 3.52 (4H, m, 2 × -CH_2), 3.07 (3H, s, -CH_3), 2.18 – 2.07 (3H, m, 3 × -CH), 1.80 – 1.67 (6H, m, 3 × -CH_2), 1.68 – 1.52 (6H, m, 3 × -CH_2). ^{13}C NMR (101 MHz, chloroform-*d*) δ 72.3 (-C), 71.5 (-CH_2), 70.8 (-CH_2), 70.7 (2 × -CH_2), 70.7 (-CH_2), 69.4 (-CH_2), 69.1 (-**C^a**H_2), 59.4 (-CH_2), 41.6 (3 × -CH_2), 37.9 (-CH_3), 36.6 (3 × -CH_2), 30.6 (3 × -

CH). IR (thin film) 2905, 1350, 1088 cm^{-1}. HRMS (ESI) exact mass calculated for $C_{19}H_{34}O_7SNa$ $[M+Na]^+$ m/z 429.1917, found m/z 429.1901.

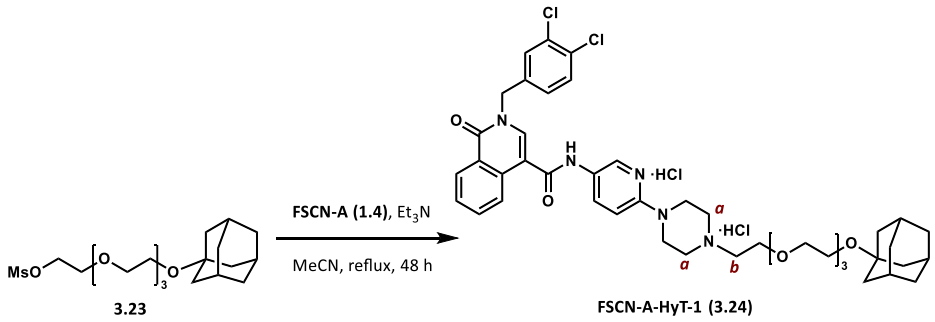

FSCN-A-HyT-1 (3.24): To a dry flask charged with argon was added anhydrous acetonitrile (4.2 mL, 0.1 M), mesylated linker **3.23** (170 mg, 0.42 mmol, 1 equiv), fascin ligand A **FSCN-A (1.4)** (250 mg, 0.50 mmol, 1.2 equiv) and triethylamine (0.15 mL, 0.84 mmol, 2 equiv) and the resulting solution was stirred under reflux for 48 hours. After consumption of starting materials was confirmed by TLC, volatile components were removed *in vacuo.* Purification by column chromatography on silica gel with an eluent of 10% to 20% ethanol in dichloromethane afforded the product (250 mg, 0.31 mmol, 74%) as a light purple amorphous solid oil. Further purification by semi-preparative RP-HPLC using a focused gradient across 55% and 80% acetonitrile in water over 35 minutes eluted the title compound at t_R = 17 minutes (66% acetonitrile) and the product fraction was lyophilised. Redissolving the resulting trifluoroacetate salt in 1 M aqueous hydrochloric acid and acetonitrile, followed by lyophilisation, yielded fascin ligand A alkylation CRBN PROTAC **FSCN-A-HyT-1 (3.24)** (110 mg, 0.13 mmol, 32%) as a light brown oil.

^{1}H NMR (500 MHz, methanol-d_4) δ 8.50 (1H, s, -CH), 8.40 (1H, dd, *J* = 8.4, 1.4 Hz, Ar-H), 8.16 (1H, d, *J* = 8.2 Hz, Ar-H), 8.05 – 7.98 (2H, m, 2 × Ar-H), 7.79 (1H, ddd, *J* = 8.2, 7.1, 1.4 Hz, Ar-H), 7.64 – 7.58 (2H, m, 2 × Ar-H), 7.50 (1H, d, *J* = 8.3 Hz, Ar-H), 7.35 (1H, dd, *J* = 8.3, 2.1 Hz, Ar-H), 7.01 (1H, d, *J* = 9.1 Hz, Ar-H), 5.26 (2H, s, -CH_2), 3.92 – 3.87 (2H, m, -CH_2), 3.75 – 3.53 (16H, m, 8 × -CH_2), 3.48 – 3.42 (2H, m, -C**H$_2^b$**), 2.68 – 2.64 (4H, m, 2 -C**H$_2^a$**), 2.12 – 2.06 (3H, m, 3 × -CH), 1.75 – 1.70 (6H, m, 3 × -CH_2), 1.69 – 1.55 (6H, m, 3 × -CH_2). ^{13}C NMR (126 MHz, methanol-d_4) δ 166.8 (-CONH), 163.5 (-CONR), 138.7 (Ar-C), 136.5 (Ar-CH), 135.5 (Ar-C), 135.5 (-CH), 134.4 (Ar-C), 133.5 (Ar-C), 132.9 (Ar-C), 131.9 (2 × Ar-C), 131.2 (Ar-C), 129.9 (Ar-C), 129.0 (2 × Ar-C), 129.0 (2 × Ar-C), 128.8 (Ar-C), 126.6 (Ar-C), 126.1 (Ar-C), 114.6 (Ar-C), 73.7 (-C), 72.4 (-CH_2), 71.6 (-CH_2), 71.5 (-CH_2), 71.4 (2 × -CH_2), 65.3 (-CH_2), 60.4 (-CH_2), 57.6 (-**C^b**H$_2$), 52.9 (-CH_2), 52.5 (2 × -**C^a**H$_2$), 44.8 (2 × -CH_2), 42.6 (3 × -CH_2), 37.5 (3 × -CH_2), 32.0 (3 × -CH). IR (thin film) 1659, 1489, 1134 cm^{-1}. HRMS (ESI) exact mass calculated for

$C_{44}H_{53}Cl_2N_5O_6Na$ $[M+Na]^+$ m/z 840.3265, found m/z 840.3226. LCMS (ESI) mass calculated for $C_{44}H_{54}N_5O_6Cl_2$ $[M+H]^+$ m/z 818.34, found m/z 818.50 with t_R = 6.44 min.

Preparation of fascin ligand B FSCN-B (1.5)

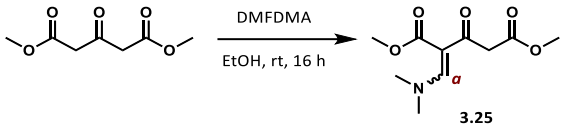

3.25

3.25: To a stirred solution of dimethyl 3-oxoglutarate (5.0 mL, 35 mmol, 1 equiv) in ethanol (10 mL, 3.5 M) was added *N,N*-dimethylformamide dimethyl acetal (4.6 mL, 35 mmol, 1 equiv) and the resulting solution was stirred at room temperature for 16 hours. Volatile components were removed *in vacuo* and purification by column chromatography on silica gel with an eluent of 10% to 100% ethyl acetate in dichloromethane afforded a 1:1 mixture of *E* and *Z* isomers of enaminone **3.25** (5.3 g, 22 mmol, 64%) as dark yellow oil.

Analytical data were in accordance with literature values.[258]

^{1}H NMR (400 MHz, chloroform-*d*) δ 7.81 (1H, s, enaminone-**H**[a]), 3.76 (2H, s, -CH_2), 3.69 (3H, s, -CH_3), 3.67 (3H, s, -CH_3), 3.26 (3H, s, -CH_3), 2.88 (3H, s, -CH_3). ^{13}C NMR (101 MHz, chloroform-*d*) δ 189.3 (-CO), 169.8 (-COOR), 167.8 (-COOR), 159.7 (enaminone-**C**[a]), 100.6 (-C), 52.0 (-OCH_3), 51.1 (-OCH_3), 48.4 (-CH_2), 48.0 (-NCH_3), 42.8 (-NCH_3).

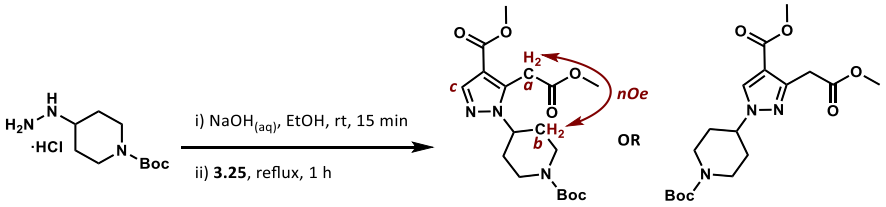

3.26a 3.26b

3.26a or **3.26b**: To a stirred solution of *tert*-butyl 4-hydrazinopiperidine-1-carboxylate hydrochloride (2.0 g, 12 mmol, 1 equiv) in ethanol (40 mL, 0.3 M) was added 1 M aqueous sodium hydroxide (1 equiv) and the resulting solution was stirred at room temperature for 15 minutes. Enaminone **3.25** (2.7 g, 12 mmol, 1 equiv) was added and the reaction mixture was stirred under reflux for 1 hour. Volatile components were removed *in vacuo* and purification by column chromatography on silica gel with an eluent of 30% to 100% ethyl acetate in petroleum ether afforded pyrazole **3.26a** or **3.26b** (3.7 g, 9.8 mmol, 82%) as a light yellow oil.

Analytical data were in accordance with literature values.[258]

^{1}H NMR (400 MHz, chloroform-*d*) δ 7.89 (1H, s, pyrazole-**H^{c}**), 4.26 (2H, br s, -CH_2), 4.15 (2H, s, -**CH_2^{a}**), 4.13 – 4.08 (1H, m, -CH), 3.80 (3H, s, -OCH_3), 3.72 (3H, s, -OCH_3), 2.92 – 2.72 (2H, m, -CH_2), 2.22 – 2.08 (2H, m, -CH_2), 1.89 – 1.80 (2H, m, -**CH_2^{b}**), 1.45 (9H, s, 3 × -CH_3). 2D NOESY indicated cross-peak between -**CH_2^{a}** and -**CH_2^{b}**. ^{13}C NMR (101 MHz, chloroform-*d*) δ 169.1 (-COOR), 163.9 (-COOR), 154.4 (-NCOOR), 140.8 (pyrazole-**C^{c}**H), 138.1 (pyrazole-C), 112.1 (pyrazole-C), 79.9 (-*C*$(CH_3)_3$), 56.5 (2 × -CH_2), 52.6 (-CH), 51.2 (2 × -CH_3), 31.8 (-**C^{b}**H_2 & -CH_2), 29.9 (-**C^{a}**H_2), 28.4 (3 × -CH_3). HRMS (ESI) exact mass calculated for $C_{18}H_{27}N_3O_6Na$ $[M+Na]^+$ m/z 404.1798, found m/z 404.1886. LCMS (ESI) mass calculated for $C_{18}H_{28}N_3O_6$ $[M+H]^+$ m/z 381.19, found m/z 381.83 with t_R = 6.41 min.

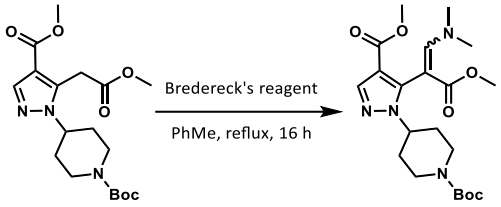

3.26 **3.27**

3.27: To a stirred solution of pyrazole **3.26a** (300 mg, 0.78 mmol, 1 equiv) in anhydrous toluene (2.6 mL, 0.3 M) was added Bredereck's reagent (0.24 mL, 1.2 mmol, 1.5 equiv) and the resulting solution was stirred under reflux for 16 hours. Complete consumption of pyrazole **3.26a** was confirmed by TLC and volatile components were removed *in vacuo*. Enaminone **3.27** was afforded in quantitative yield as a mixture of *E* and *Z* isomers and used in the next step without further purification.

LCMS (ESI) mass calculated for $C_{21}H_{33}N_4O_6$ $[M+H]^+$ m/z 437.24, found m/z 437.42 with t_R = 6.20 min and m/z 437.33 with t_R = 6.33.

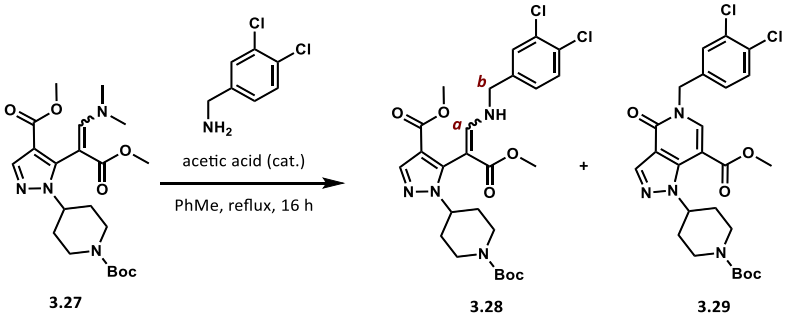

3.27 **3.28** **3.29**

3.28: To a stirred solution of enaminone **3.27** (2.9 g, 6.6 mmol, 1 equiv) in anhydrous toluene (30 mL, 0.2 M) were added 3,4-dichlorobenzylamine (3.5 mL, 26 mmol, 4 equiv) and glacial acetic acid (0.04 mL, 0.1 equiv) and the resulting solution was stirred under reflux for 16 hours. Volatile components were removed *in vacuo* and the residue was redissolved in ethyl acetate (30 mL) and washed with saturated aqueous sodium hydrogen

bicarbonate solution until pH 8. The organic phase was washed with brine (3 × 10 mL), dried over magnesium sulfate, filtered and concentrated *in vacuo.* The crude product was purified by column chromatography on silica gel with an eluent of 30% to 100% ethyl acetate in petroleum ether to afford substitution product **3.28** (2.3 g, 4.0 mmol, 61%) as a light yellow amorphous solid and annulation product **3.29** (1.0 g, 1.9 mmol, 28%) an off white amorphous solid.

Analytical data were in accordance with literature values.[258]

3.28: ^{1}H NMR (400 MHz, chloroform-*d*) δ 8.88 (1H, br, -NH), 7.92 (1H, s, pyrazole-H), 7.49 – 7.42 (2H, m, 2 × Ar-H), 7.18 (1H, dd, *J* = 8.2, 2.1 Hz, Ar-H), 6.92 (1H, d, *J* = 13.3 Hz, alkene-**H**^{a}), 4.43 (2H, d, *J* = 6.1 Hz, -C**H**$_2$^{b}), 4.38 – 4.11 (2H, m, -CH_2), 4.11 – 4.00 (1H, m, -CH), 3.75 (3H, s, -OCH_3), 3.64 (3H, s, -OCH_3), 2.88 – 2.64 (2H, m, -CH_2), 2.26 – 1.80 (4H, m, 2 × -CH_2), 1.47 (9H, s, 3 × -CH_3). ^{13}C NMR (101 MHz, chloroform-*d*) δ 168.5 (-COOR), 163.8 (-COOR), 156.0 (alkene-**C**^{a}H), 154.4 (-NCOOR), 141.6 (pyrazole-CH), 141.1 (pyrazole-C), 137.9 (Ar-C), 133.0 (Ar-C), 132.1 (Ar-C), 130.8 (Ar-CH), 129.2 (Ar-CH), 126.5 (Ar-CH), 111.8 (pyrazole-C), 83.4 (alkene-C), 79.7 (-*C*(CH_3)$_3$), 56.0 (-**C**^{b}H_2), 51.4 (-OCH_3), 51.0 (-CH_2), 50.8 (-OCH_3), 32.3 (2 × -CH_2), 30.9 (2 × -CH_2), 28.4 (3 × -CH_3). HRMS (ESI) exact mass calculated for $C_{26}H_{32}N_4Cl_2O_6Na$ $[M+Na]^+$ m/z 589.1597, found m/z 589.1577. LCMS (ESI) mass calculated for $C_{26}H_{33}N_4Cl_2O_6$ $[M+H]^+$ m/z 567.18, found m/z 567.33 with t_R = 7.40 min.

Data for **3.29** matched data reported below.

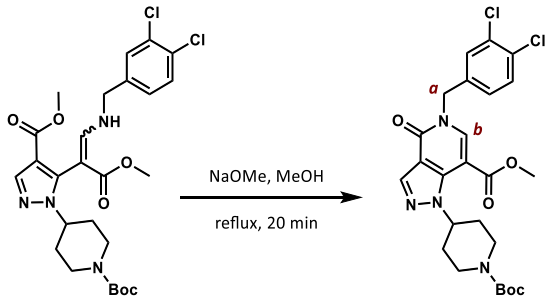

3.28 3.29

3.29: To a stirred solution of substitution product **3.28** (2.3 g, 4.1 mmol, 1 equiv) in anhydrous methanol (41 mL, 0.1 M) was added 0.01 M sodium methoxide solution (4 mL, 0.4 mmol, 0.1 equiv) and the resulting solution was stirred under reflux for 20 minutes until full consumption of the starting material was confirmed by TLC. The reaction mixture was partitioned between dichloromethane (200 mL) and water (200 mL). The aqueous phase was extracted with dichloromethane (3 × 200 mL). The combined organic extracts were washed with brine (2 × 200 mL), dried over magnesium sulfate, filtered and concentrated *in vacuo.* The crude product was purified by column chromatography on silica gel with an

eluent of 30% to 100% ethyl acetate in petroleum ether to afford annulation product **3.29** (2.1 g, 4.1 mmol) in quantitative yield as an off white amorphous solid.

Analytical data were in accordance with literature values.[258]

^{1}H NMR (400 MHz, chloroform-*d*) δ 8.25 (1H, s, -C**H**^{b}), 8.02 (1H, s, pyrazole-H), 7.45 – 7.39 (2H, m, 2 × Ar-H), 7.18 (1H, dd, *J* = 8.3, 2.1 Hz, Ar-H), 5.42 – 5.29 (1H, m, -CH), 5.15 (2H, s, -C**H$_2$**^{a}), 4.41 – 4.13 (2H, m, -CH_2), 3.90 (3H, s, -CH_3), 3.01 – 2.77 (2H, m, -CH_2), 2.26 – 1.91 (4H, m, 2 × -CH_2), 1.47 (9H, s, 3 × -CH_3). ^{13}C NMR (101 MHz, chloroform-*d*) δ 163.8 (-COOR), 158.2 (-CONH), 154.6 (-NCOOR), 141.3 (-**C**^{b}H), 138.9 (Ar-C), 137.5 (pyrazole-CH), 136.2 (pyrazole-C), 133.1 (Ar-C), 132.6 (Ar-C), 131.0 (Ar-CH), 129.8 (Ar-CH), 127.3 (Ar-CH), 113.7 (pyrazole-C), 101.1 (-C), 79.7 (-*C*(CH_3)$_3$), 59.0 (-CH), 52.5 (-OCH_3), 50.5 (-**C**^{a}H_2), 43.5 (2 × -CH_2), 32.5 (2 × -CH_2), 28.4 (3 × -CH_3). HRMS (ESI) exact mass calculated for $C_{25}H_{28}N_4Cl_2O_5Na$ $[M+Na]^+$ m/z 557.1329, found m/z 557.1315. LCMS (ESI) mass calculated for $C_{25}H_{29}N_4Cl_2O_5$ $[M+H]^+$ m/z 534.15, found m/z 534.35 with t_R = 6.60 min.

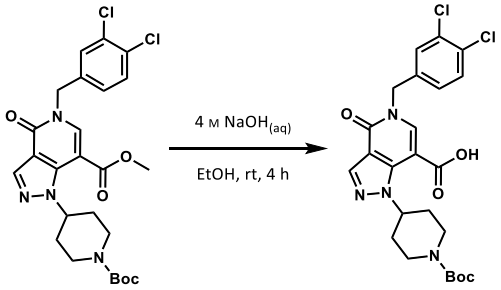

3.29 **3.30**

3.30: To a stirred solution of **3.29** (500 mg, 0.94 mmol, 1 equiv) in ethanol (3 mL, 0.3 M) was added 4 M aqueous sodium hydroxide (0.16 mL, 4.7 mmol, 4 equiv) and the resulting solution was stirred at room temperature for 4 hours. After complete consumption of the starting material was confirmed by TLC, volatile components were removed *in vacuo*. The residue was redissolved in water (20 mL) and 1 M aqueous hydrochloric acid was added until pH 3. The acidified aqueous phase was extracted with dichloromethane (3 × 20 mL), and the combined organic extracts were dried over magnesium sulfate, filtered and concentrated *in vacuo*. Carboxylic acid **3.30** (490 mg, 0.94 mmol) was afforded in quantitative yield as a light yellow amorphous solid and used in the next step without further purification.

LCMS (ESI) mass calculated for $C_{24}H_{27}N_4Cl_2O_5$ $[M+H]^+$ m/z 520.14, found m/z 520.14 with t_R = 6.77 min.

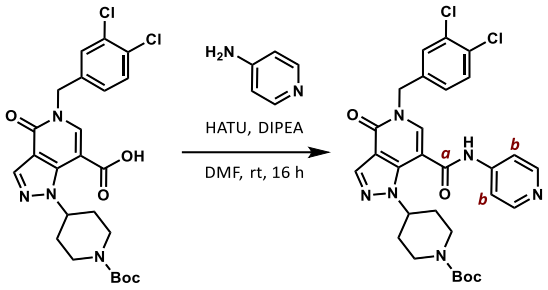

3.30 3.31

3.31: To a pre-stirred solution of carboxylic acid **3.30** (37 mg, 0.071 mmol, 1 equiv), HATU (27 mg, 0.071 mmol, 1 equiv) and *N,N*-diisopropylethylamine (37 µL, 0.21 mmol, 3 equiv) in *N,N*-dimethylformamide (0.2 mL, 0.3 M) was added amine 4-aminopyridine (6.7 mg, 0.071 mmol, 1 equiv), and the resulting solution was stirred at room temperature for 16 hours. The reaction mixture was partitioned between dichloromethane (20 mL) and water (20 mL), and the aqueous phase was extracted with dichloromethane (5 × 20 mL). The combined organic phases were washed with 5% aqueous lithium chloride (5 × 40 mL), dried over magnesium sulfate, filtered and concentrated *in vacuo*. Purification by column chromatography on silica gel with an eluent of 5% to 20% ethanol in dichloromethane afforded protected fascin ligand B **3.31** (41 mg, 0.069 mmol, 98%) as a colourless oily solid. Analytical data were in accordance with literature values.[258]

^{1}H NMR (500 MHz, chloroform-*d*) δ 9.43 (1H, s, -NH), 8.56 – 8.45 (2H, m, 2 × Ar-H), 8.12 (1H, s, -CH), 7.66 – 7.59 (1H, m, 2 × Ar-**H^{b}**), 7.47 (1H, s, pyrazole-H), 7.37 (1H, d, *J* = 8.3 Hz, Ar-H), 7.31 (1H, d, *J* = 2.1 Hz, Ar-H), 7.07 (1H, dd, *J* = 8.3, 2.1 Hz, Ar-H), 4.92 (2H, s, -CH_2), 4.67 – 4.56 (1H, m, -CH), 4.26 – 4.09 (2H, m, -CH_2), 2.84 – 2.55 (2H, m, -CH_2), 2.20 – 1.91 (4H, m, 2 × -CH_2), 1.44 (9H, s, 3 × -CH_3). ^{13}C NMR (126 MHz, chloroform-*d*) δ 163.8 (-**C^{a}**ONH), 158.3 (-CONR), 154.7 (-NCOOR), 150.9 (2 × Ar-CH), 145.2 (pyrazole-C), 138.7 (Ar-C), 137.1 (-CH), 135.9 (pyrazole-CH), 135.6 (Ar-C), 133.3 (Ar-C), 133.0 (Ar-C), 131.2 (Ar-CH), 130.0 (Ar-CH), 127.4 (Ar-CH), 113.9 (2 × Ar-**C^{b}**H), 113.6 (pyrazole-C), 106.7 (-C), 80.2 (-*C*(CH_3)$_3$), 58.8 (-CH), 50.3 (-CH_2), 32.2 (2 × -CH_2), 29.8 (2 × -CH_2), 28.5 (3 × -CH_3). HRMS (ESI) exact mass calculated for $C_{29}H_{30}N_6Cl_2O_4Na$ $[M+Na]^+$ m/z 619.1598, found m/z 619.1587.

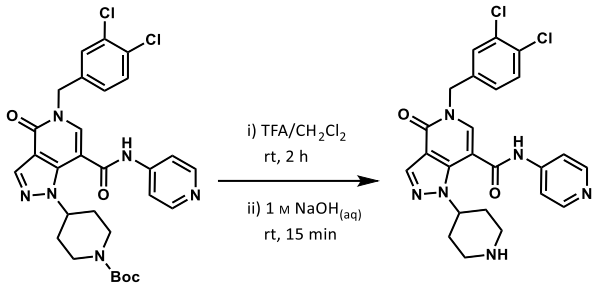

3.31 FSCN-B (1.5)

FSCN-B (1.5): Protected ligand **3.31** (240 mg, 0.40 mmol, 1 equiv) was dissolved in trifluoroacetic acid/dichloromethane (7 mL/7 mL, 0.03 M) and the resulting solution was stirred at room temperature for 2 hours. The reaction was monitored by TLC for complete consumption of the starting material before removal of volatile components *in vacuo*. The residue was redissolved in 1 M aqueous sodium hydroxide (5 mL) and stirred for a further 15 minutes. The aqueous phase was extracted with dichloromethane (2 × 5 mL) and the combined organic phases were dried over magnesium sulfate, filtered and concentrated *in vacuo*. Filtration through a silica gel afforded fascin ligand B **FSCN-B (1.5)** (199 mg, 0.40 mmol) in quantitative yield as a white amorphous solid. Further purification by semi-preparative RP-HPLC of some material using a focused gradient across 40% and 70% acetonitrile in water over 30 minutes eluted the title compound at t_R = 22 minutes (58% acetonitrile) and the product fraction was lyophilised. Redissolving the resulting trifluoroacetate salt in 1 M aqueous hydrochloric acid and acetonitrile, followed by lyophilisation, yielded fascin ligand B **FSCN-B (1.5)** as a white fluffy powder. Single crystals were obtained using two-solvent recrystallisation with methanol as primary solvent and hexane as co-solvent.

Analytical data were in accordance with literature values.[258]

^{1}H NMR (500 MHz, methanol-d_4) δ 8.73 – 8.66 (2H, m, 2 × Ar-H), 8.43 (1H, s, -CH), 8.30 – 8.27 (2H, m, 2 × Ar-H), 8.26 (1H, s, pyrazole-H), 7.56 (1H, d, *J* = 2.1 Hz, Ar-H), 7.49 (1H, d, *J* = 8.3 Hz, Ar-H), 7.32 (1H, dd, *J* = 8.3, 2.2 Hz, Ar-H), 5.26 (2H, s, -CH_2), 5.10 – 5.00 (1H, m, -CH), 3.62 – 3.54 (2H, m, -CH_2), 3.24 – 3.09 (2H, m, -CH_2), 2.53 – 2.29 (4H, m, 2 × -CH_2). ^{13}C NMR (126 MHz, methanol-d_4) δ 166.1 (-CONH), 160.0 (-CONR), 155.7 (pyrazole-C), 143.2 (2 × Ar-CH), 141.9 (-CH), 140.7 (Ar-C), 138.5 (Ar-C), 138.4 (pyrazole-CH), 133.6 (Ar-C), 133.0 (Ar-C), 131.9 (Ar-CH), 131.0 (Ar-CH), 128.8 (Ar-CH), 116.7 (2 × Ar-CH), 114.9 (pyrazole-C), 105.9 (-C), 56.6 (-CH), 52.2 (-CH_2), 44.4 (2 × -CH_2), 30.1 (2 × -CH_2). HRMS (ESI) exact mass calculated for $C_{24}H_{22}N_6Cl_2O_2Na$ $[M+Na]^+$ m/z 519.1079, found m/z 519.1072.

Preparation of 2nd series PROTACs

- *Fascin ligand B VHL PROTACs:*

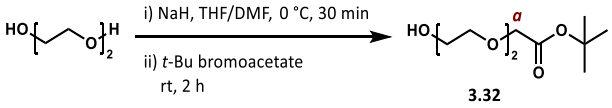

3.32: To a dry flask charged with argon was added anhydrous tetrahydrofuran/*N,N*-dimethylformamide (1.9 mL/1.9 mL, 1 M), diethylene glycol (1.44 mL, 15.2 mmol, 4 equiv) and sodium hydride (60% in mineral oil, 303 mg, 7.58 mmol, 2 equiv) at 0 °C. The resulting suspension was stirred for 30 minutes before *tert*-butyl bromoacetate (0.56 mL, 3.8 mmol, 1 equiv) was added dropwise at 0 °C. The reaction mixture was allowed to reach room temperature and stirred for a further 2 hours. The reaction was quenched by dropwise addition of water (50 mL). The aqueous phase was extracted with dichloromethane (3 × 50 mL) and the combined organic extracts were washed with brine (3 × 150 mL), dried over magnesium sulfate, filtered and concentrated *in vacuo*. Purification by column chromatography on silica gel with an eluent of 30% to 70% ethyl acetate in petroleum ether afforded protected linker **3.32** (532 mg, 2.42 mmol, 64%) as a clear oil.

Analytical data observed were in accordance with literature values.[98]

^{1}H NMR (500 MHz, chloroform-*d*) δ 3.97 (2H, s, -C**H$_2$**^{a}), 3.72 – 3.61 (6H, m, 3 × -CH$_2$), 3.60 – 3.54 (2H, m, -CH$_2$), 3.03 (1H, br s, -OH), 1.42 (9H, s, 3 × -CH$_3$). ^{13}C NMR (126 MHz, chloroform-*d*) δ 169.7 (-COOR), 81.8 (-*C*(CH$_3$)$_3$), 72.6 (-CH$_2$), 70.8 (-CH$_2$), 70.3 (-CH$_2$), 69.0 (-CH$_2$), 61.6 (-**C**^{a}H$_2$), 28.1 (3 × -CH$_3$).

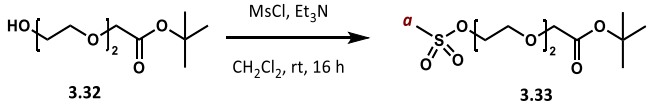

3.33: To a dry flask charged with argon was added anhydrous dichloromethane (4.5 mL, 0.1 M), alcohol **3.32** (100 mg, 0.45 mmol, 1 equiv), methanesulfonyl chloride (53 µL, 0.68 mmol, 1.5 equiv) and triethylamine (0.19 mL, 1.4 mmol, 3 equiv) and the resulting solution was stirred at room temperature for 16 hours. The reaction mixture was partitioned between 1 M aqueous hydrochloric acid (10 mL) and dichloromethane (10 mL), and the aqueous phase was extracted with dichloromethane (4 × 10 mL). The combined organic extracts were washed with water (2 × 20 mL), dried over magnesium sulfate, filtered and concentrated *in vacuo*. Purification by column chromatography on silica gel with an eluent of 50% to 100% ethyl acetate in petroleum ether afforded mesylate **3.33** (130 mg, 0.44 mmol, 96%) as a clear oil.

^{1}H NMR (500 MHz, chloroform-*d*) δ 4.38 (2H, t, *J* = 4.5 Hz, -CH_2), 3.99 (2H, s, -CH_2), 3.78 (2H, t, *J* = 4.6 Hz, -CH_2), 3.74 – 3.68 (4H, m, 2 × -CH_2), 3.07 (3H, s, -C**H$_3$**^{a}), 1.47 (9H, s, 3 × -CH_3). ^{13}C NMR (126 MHz, chloroform-*d*) δ 169.6 (-COOR), 81.8 (-*C*(CH_3)$_3$), 70.8 (2 × -CH_2), 69.3 (-CH_2), 69.2 (-CH_2), 69.1 (-CH_2), 37.9 (-**C**^{a}H_3), 28.2 (3 × -CH_3). IR (thin film) 1742, 1395, 1171 cm^{-1}. HRMS (ESI) exact mass calculated for $C_{11}H_{22}O_7SNa$ [M+Na]$^+$ m/z 321.0978, found m/z 321.0979.

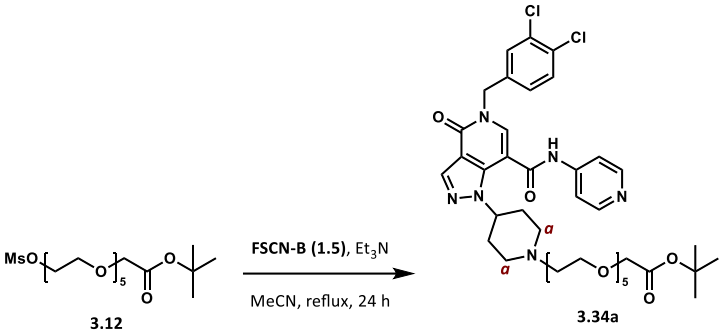

3.34a: To a dry flask charged with argon was added anhydrous acetonitrile (2.8 mL, 0.1 M), mesylated linker **3.12** (120 mg, 0.28 mmol, 1 equiv), fascin ligand B **FSCN-B (1.5)** (140 mg, 0.28 mmol, 1 equiv) and triethylamine (0.15 mL, 0.85 mmol, 3 equiv) and the resulting solution was stirred under reflux for 24 hours. After consumption of starting materials was confirmed by TLC, volatile components were removed *in vacuo.* Purification by column chromatography on silica gel with an eluent of 10% to 50% ethanol in dichloromethane afforded fascin ligand fragment **3.34a** (95 mg, 0.11 mmol, 41%) as a clear oil.

^{1}H NMR (400 MHz, methanol-*d4*) δ 8.54 – 8.44 (2H, m, 2 × Ar-H), 8.20 (1H, s, -CH), 8.19 (1H, s, pyrazole-H), 7.83 – 7.76 (2H, m, 2 × Ar-H), 7.58 (1H, d, *J* = 2.1 Hz, Ar-H), 7.50 (1H, dd, *J* = 8.4, 1.9 Hz, Ar-H), 7.34 (1H, dd, *J* = 8.4, 2.1 Hz, Ar-H), 5.25 (2H, s, -CH_2), 4.74 – 4.60 (1H, m, -CH), 4.06 (2H, s, -CH_2), 3.75 – 3.55 (18H, m, 9 × -CH_2), 3.17 – 3.07 (2H, m, -CH_2), 2.68 – 2.60 (2H, m, -CH_2), 2.40 – 2.25 (2H, m, -CH_2), 2.25 – 1.99 (4H, m, 2 × -C**H$_2$**^{a}), 1.48 (9H, s, 3 × -CH_3). ^{13}C NMR (101 MHz, methanol-*d4*) δ 172.2 (-COOR), 165.7 (-CONH), 160.2 (-CONR), 151.0 (2 × Ar-CH), 148.0 (pyrazole-C), 140.6 (Ar-C), 139.2 (Ar-C), 138.9 (pyrazole-CH), 137.7 (-CH), 133.5 (Ar-C), 132.8 (Ar-C), 131.9 (Ar-CH), 131.1 (Ar-CH), 128.9 (Ar-CH), 115.6 (2 × Ar-CH), 114.8 (pyrazole-C), 107.3 (-C), 83.6 (-*C*(CH_3)$_3$), 71.2 (2 × -CH_2), 71.1 (2 × -CH_2), 71.0 (-CH_2), 70.9 (2 × -CH_2), 70.6 (-CH_2), 69.4 (-CH_2), 69.2 (-CH_2), 59.2 (-CH), 58.2 (2 × -CH_2), 54.1 (-CH_2), 51.8 (-CH_2), 32.5 (2 × -**C**^{a}H_2), 28.4 (3 × -CH_3). IR (thin film) 1744, 1672, 1591 cm^{-1}. HRMS (ESI) exact mass calculated for $C_{40}H_{52}N_6Cl_2O_9Na$ [M+Na]$^+$ m/z 853.3065, found m/z 853.3056. LCMS (ESI) mass calculated for $C_{40}H_{53}N_6Cl_2O_9$ [M+H]$^+$ m/z 831.32, found m/z 831.58 with t_R = 6.21 min.

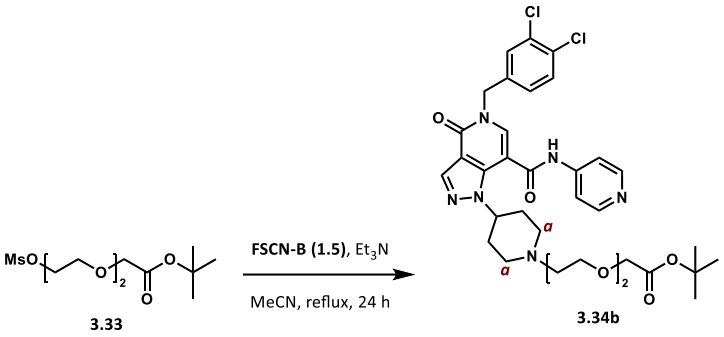

3.34b: To a dry flask charged with argon was added anhydrous acetonitrile (2 mL, 0.1 M), mesylated linker **3.33** (60 mg, 0.20 mmol, 1 equiv), fascin ligand B **FSCN-B (1.5)** (100 mg, 0.20 mmol, 1 equiv) and triethylamine (0.11 mL, 0.60 mmol, 3 equiv) and the resulting solution was stirred under reflux for 24 hours. After consumption of starting materials was confirmed by TLC, volatile components were removed *in vacuo.* Purification by column chromatography on silica gel with an eluent of 5% to 50% ethanol in dichloromethane afforded fascin ligand fragment **3.34b** (63 mg, 0.090 mmol, 45%) as a clear oil.

^{1}H NMR (400 MHz, chloroform-*d*) δ 11.01 (1H, s, -NH), 8.44 – 8.31 (2H, m, 2 × Ar-H), 8.11 – 8.01 (2H, m, pyrazole-H & -CH), 7.77 – 7.65 (2H, m, 2 × Ar-H), 7.44 (1H, d, *J* = 2.0 Hz, Ar-H), 7.34 (1H, d, *J* = 8.3 Hz, Ar-H), 7.21 (1H, dd, *J* = 8.3, 2.1 Hz, Ar-H), 5.18 (2H, s, -CH_2), 5.00 (1H, s, -CH), 3.97 (2H, s, -CH_2), 3.84 (2H, t, *J* = 4.9 Hz, -CH_2), 3.66 (6H, s, 3 × -CH_2), 3.56 – 3.42 (2H, m, -CH_2), 3.04 – 2.89 (2H, m, -CH_2), 2.46 – 2.13 (4H, m, 2 × -C**H$_2$**^{a}), 1.42 (9H, s, 3 × -CH_2). ^{13}C NMR (101 MHz, chloroform-*d*) δ 169.7 (-COOR), 164.3 (-CONH), 158.3 (-CONR), 149.7 (2 × Ar-CH), 146.7 (Ar-C), 139.6 (-CH), 139.1 (Ar-C), 137.2 (pyrazole-C), 136.8 (pyrazole-CH), 132.9 (Ar-C), 132.3 (Ar-C), 130.9 (Ar-CH), 130.2 (Ar-CH), 127.8 (Ar-CH), 118.4 (pyrazole-C), 114.5 (Ar-CH), 114.0 (Ar-CH), 105.1 (-C), 82.1 (-*C*(CH_3)$_3$), 70.7 (-CH_2), 70.5 (-CH_2), 68.9 (-CH_2), 66.1 (-CH_2), 56.7 (-CH_2), 50.3 (-CH), 46.0 (2 × -**C^{a}**H_2), 39.8 (2 × -CH_2), 28.2 (3 × -CH_3). IR (thin film) 1742, 1668, 1591 cm^{-1}. HRMS (ESI) exact mass calculated for $C_{34}H_{41}N_6Cl_2O_6$ $[M+H]^+$ m/z 699.2459, found m/z 699.2463.

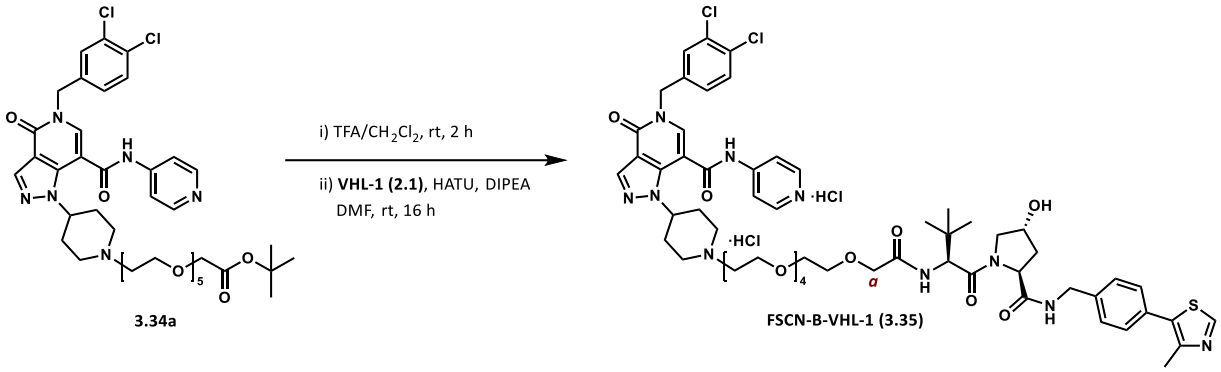

FSCN-B-VHL-1 (3.35): Protected fragment **3.34a** (91 mg, 0.11 mmol, 1 equiv) was dissolved in trifluoroacetic acid/dichloromethane (1.8 mL/1.8 mL, 0.03 M) and the resulting solution was stirred at room temperature for 2 hours. The reaction was monitored by TLC for complete consumption of the starting material before removal of volatile components *in vacuo*. The residue was redissolved in *N,N*-dimethylformamide (0.4 mL, 0.3 M) and VHL ligand **VHL-1 (2.1)** (47 mg, 0.11 mmol, 1 equiv), HATU (42 mg, 0.11 mmol, 1 equiv) and *N,N*-diisopropylethylamine (58 µL, 0.33 mmol, 3 equiv) were added. The resulting solution was stirred at room temperature for 16 hours before partitioning the reaction mixture between dichloromethane (50 mL) and water (50 mL). The aqueous phase was extracted with dichloromethane (5 × 50 mL) and the combined organic phases were washed with 5% aqueous lithium chloride (5 × 100 mL), dried over magnesium sulfate, filtered and concentrated *in vacuo*. Purification by column chromatography on silica gel with an eluent of 20% to 50% ethanol in dichloromethane afforded the product (74 mg, 0.062 mmol, 57%) as clear oil. Further purification by semi-preparative RP-HPLC using a focused gradient across 40% and 70% acetonitrile in water over 30 minutes eluted the title compound at t_R = 18 minutes (50% acetonitrile) and the product fraction was lyophilised. Redissolving the resulting trifluoroacetate salt in 1 M aqueous hydrochloric acid and acetonitrile, followed by lyophilisation, yielded fascin ligand B VHL PROTAC **FSCN-B-VHL-1 (3.35)** (57 mg, 0.048 mmol, 44%) as a white fluffy powder.

^{1}H NMR (500 MHz, methanol-d_4) δ 9.54 (1H, s, thiazole-CH), 8.75 – 8.68 (2H, m, 2 × Ar-CH), 8.49 (1H, s, pyrazole-CH), 8.38 – 8.30 (2H, m, 2 × Ar-CH), 8.27 (1H, s, -CH), 7.60 (1H, d, *J* = 2.0 Hz, Ar-CH), 7.54 – 7.44 (5H, m, 5 × Ar-CH), 7.37 (1H, dd, *J* = 8.3, 2.1 Hz, Ar-CH), 5.27 (2H, s, -CH_2), 5.11 – 5.00 (1H, m, -CH), 4.79 – 4.33 (7H, m, 3 × -CH & -CH_2 & -C**H$_2$**^{a}), 4.08 – 3.43 (20H, m, 10 × CH_2), 3.43 – 3.36 (2H, m, -CH_2), 3.27 – 3.15 (2H, m, -CH_2), 2.68 – 2.57 (2H, m, -CH_2), 2.55 (3H, s, -CH_3), 2.46 – 2.19 (4H, m, 2 × -CH_2), 2.11 – 2.00 (2H, m, -CH_2), 1.01 (9H, s, 3 × -CH_3). ^{13}C NMR (126 MHz, methanol-d_4) δ 174.4 (-CONH), 172.1 (-CONR), 171.7 (-CONH), 166.0 (-CONH), 160.0 (-CONR), 156.6 (pyrazole-C), 155.7 (pyrazole-C), 143.0 (2 × Ar-CH),

142.5 (thiazole-C), 142.3 (-CH), 140.9 (Ar-C), 138.6 (pyrazole-CH), 138.3 (Ar-C), 138.2 (thiazole-C), 133.4 (Ar-CH), 132.8 (Ar-CH), 131.8 (Ar-C), 131.3 (Ar-C), 130.5 (Ar-CH), 129.4 (2 × Ar-CH), 129.3 (Ar-C), 128.0 (2 × Ar-CH), 117.0 (2 × Ar-CH), 114.9 (Ar-C), 105.7 (pyrazole-C), 101.3 (-C), 73.6 (2 × -CH_2), 73.5 (-CH_2), 73.4 (-C^aH_2), 72.5 (-CH_2), 72.4 (2 × -CH_2), 72.3 (-CHOH), 71.4 (2 × -CH_2), 62.1 (-CH_2), 62.0 (-CH_2), 60.9 (-CH), 52.2 (-CH), 51.6 (-CH_2), 51.4 (-CH_2), 51.2 (-CH), 49.8 (-CH_2), 43.9 (-CH_2), 39.1 (2 × -CH_2), 36.9 (-$C(CH_3)_3$), 27.0 (2 × -CH_2), 21.7 (3 × -CH_3), 20.6 (-CH_3). IR (thin film) 1660, 1198, 1045 cm^{-1}. HRMS (ESI) exact mass calculated for $C_{58}H_{72}N_{10}Cl_2O_{11}SNa$ $[M+Na]^+$ m/z 1209.4372, found m/z 1209.4395. LCMS (ESI) mass calculated for $C_{58}H_{73}N_{10}Cl_2O_{11}S$ $[M+H]^+$ m/z 1187.46, found m/z 1187.58 with t_R = 5.43 min.

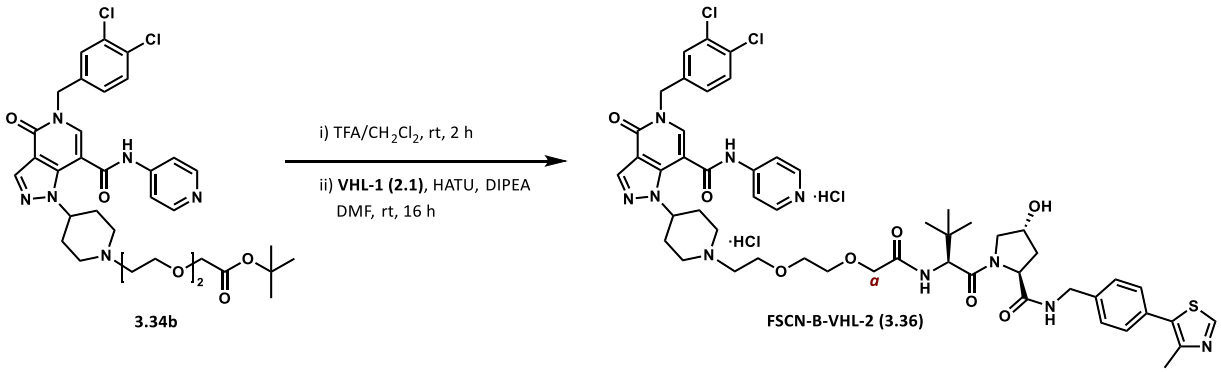

FSCN-B-VHL-2 (3.36): Protected fragment **3.34b** (33 mg, 0.047 mmol, 1 equiv) was dissolved in trifluoroacetic acid/dichloromethane (0.8 mL/0.8 mL, 0.03 M) and the resulting solution was stirred at room temperature for 2 hours. The reaction was monitored by TLC for complete consumption of the starting material before removal of volatile components *in vacuo*. The residue was redissolved in *N,N*-dimethylformamide (0.16 mL, 0.3 M) and VHL ligand **VHL-1 (2.1)** (20 mg, 0.047 mmol, 1 equiv), HATU (18 mg, 0.047 mmol, 1 equiv) and *N,N*-diisopropylethylamine (25 µL, 0.14 mmol, 3 equiv) were added. The resulting solution was stirred at room temperature for 16 hours before partitioning the reaction mixture between dichloromethane (20 mL) and water (20 mL). The aqueous phase was extracted with dichloromethane (5 × 20 mL) and the combined organic phases were washed with 5% aqueous lithium chloride (5 × 40 mL), dried over magnesium sulfate, filtered and concentrated *in vacuo*. Purification by column chromatography on silica gel with an eluent of 30% to 50% ethanol in dichloromethane afforded the product (21 mg, 0.020 mmol, 42%) as clear oil. Further purification by semi-preparative RP-HPLC using a focused gradient across 30% and 80% acetonitrile in water over 30 minutes eluted the title compound at t_R = 24 minutes (57% acetonitrile) and the product fraction was lyophilised. Redissolving the

resulting trifluoroacetate salt in 1 M aqueous hydrochloric acid and acetonitrile, followed by lyophilisation, yielded fascin ligand B VHL PROTAC **FSCN-B-VHL-2 (3.36)** (16 mg, 0.015 mmol, 32%) as a white fluffy powder.

^{1}H NMR (400 MHz, methanol-*d*$_4$) δ 9.98 (1H, s, thiazole-CH), 8.85 – 8.57 (2H, m, 2 × Ar-H), 8.56 – 8.29 (3H, m, 2 × Ar-H & pyrazole-H), 8.21 (1H, s, -CH), 7.68 – 7.58 (1H, m, Ar-H), 7.57 – 7.44 (5H, m, 5 × Ar-H), 7.46 – 7.33 (1H, m, Ar-H), 5.35 – 5.00 (3H, m, -CH$_2$ & -CH), 4.72 (2H, s, -C**H$_2$**^{a}), 4.63 – 4.28 (5H, m, 3 × -CH & -CH$_2$), 4.21 – 3.99 (2H, m, -CH$_2$), 4.01 – 3.67 (8H, m, 4 × -CH$_2$), 3.64 – 3.38 (2H, m, -CH$_2$), 2.79 – 2.64 (2H, m, -CH$_2$), 2.60 (3H, s, -CH$_3$), 2.52 – 2.13 (4H, m, 2 × -CH$_2$), 1.41 – 1.23 (2H, m, -CH$_2$), 1.03 (9H, m, 3 × -CH$_3$). ^{1}H NMR (500 MHz, methanol-*d*$_4$) δ 172.1 (-CONH), 170.5 (-CONH), 170.2 (-CONR), 162.9 (-CONH), 161.3 (-CONR), 155.4 (pyrazole-C), 151.6 (pyrazole-C), 142.7 (2 × Ar-CH), 142.6 (-CH), 142.4 (thiazole-C), 141.7 (Ar-C), 138.6 (pyrazole-CH), 138.5 (Ar-C), 138.3 (pyrazole-CH), 137.9 (thiazole-C), 133.8 (Ar-CH), 132.6 (Ar-CH), 131.7 (Ar-C), 131.0 (Ar-C), 130.8 (Ar-CH), 128.4 (2 × Ar-CH), 127.8 (Ar-C), 126.7 (2 × Ar-CH), 118.1 (2 × Ar-CH), 116.9 (Ar-C), 113.7 (pyrazole-C), 105.4 (-C), 73.6 (-CH$_2$), 73.6 (-CH$_2$), 73.2 (-**C**^{a}H$_2$), 72.6 (-CHOH), 68.1 (-CH$_2$), 61.5 (-CH), 54.3 (-CH), 52.8 (-CH), 52.4 (-CH$_2$), 51.4 (-CH$_2$), 49.8 (-CH$_2$), 43.9 (-CH$_2$), 40.3 (2 × -CH$_2$), 35.9 (-*C*(CH$_3$)$_3$), 28.5 (2 × -CH$_2$), 23.2 (3 × -CH$_3$), 18.2 (-CH$_3$). IR (thin film) 1672, 1189, 1061 cm^{-1}. HRMS (ESI) exact mass calculated for $C_{52}H_{61}N_{10}Cl_2O_8S$ $[M+H]^+$ m/z 1055.3766, found m/z 1055.3800. LCMS (ESI) mass calculated for $C_{52}H_{61}N_{10}Cl_2O_8S$ $[M+H]^+$ m/z 1055.38, found m/z 1055.42 with t_R = 5.43 min.

- *Fascin ligand B CRBN PROTACs:*

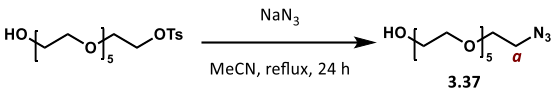

3.37

3.37: To a stirred solution of hexaethylene glycol monotosylate (950 mg, 2.18 mmol, 1 equiv) in acetonitrile (8 mL, 0.3 M) was added sodium azide (566 mg, 8.70 mmol, 4 equiv), and the resulting solution was stirred for 24 hours under reflux. The reaction was quenched by addition of water before removing volatile components *in vacuo*. The residue was redissolved in water (50 mL) and dichloromethane (50 mL). The aqueous phase was extracted with dichloromethane (3 × 50 mL), and the combined organic extracts were dried over magnesium sulfate, filtered and concentrated *in vacuo.* Azide **3.37** (589 mg, 1.92 mmol, 88%) was afforded as a clear oil and used in the next step without further purification.

Analytical data observed were in accordance with literature values.[259]

^{1}H NMR (400 MHz, chloroform-*d*) δ 3.78 – 3.64 (20H, m, 10 × -CH_2), 3.64 – 3.56 (2H, m, -CH_2), 3.38 (2H, t, *J* = 5.1 Hz, -C**H$_2$**^{a}), 2.58 (1H, t, *J* = 6.2 Hz, -OH). ^{13}C NMR (101 MHz, chloroform-*d*) δ 72.7 (-CH_2), 70.8 (-CH_2), 70.8 (-CH_2), 70.8 (2 × -CH_2), 70.7 (2 × -CH_2), 70.7 (-CH_2), 70.5 (-CH_2), 70.2 (-CH_2), 61.9 (-CH_2), 50.8 (-**C**^{a}H_2).

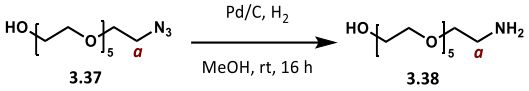

3.37 **3.38**

3.38: To a stirred solution of azide **3.37** (456 mg, 1.48 mmol, 1 equiv) in methanol (15 mL, 0.1 M) under an argon atmosphere was added 10% palladium on carbon (16 mg, 0.15 mmol, 10 mol%). The flask was evacuated and purged with argon three times, before sparging the suspension with hydrogen gas and stirring at room temperature under a hydrogen atmosphere for 16 hours. The hydrogen gas was removed by evacuating the flask and purging it with argon three times. After confirming complete consumption of starting material with TLC, the suspension was filtered through a pad of celite in dichloromethane and the celite washed with dichloromethane (150 mL) and methanol (150 mL). The solvents were removed *in vacuo* affording aminoalcohol **3.38** (417 mg, 1.58 mmol) as a pale yellow oil in quantitative yield. The crude material was used in the next step without further purification.

^{1}H NMR (400 MHz, chloroform-*d*) δ 3.73 – 3.55 (20H, m, 10 × -CH_2), 3.53 – 3.46 (2H, m, -CH_2), 2.88 – 2.82 (2H, t, *J* = 5.1 Hz, -C**H$_2$**^{a}), 2.39 (2H, t, *J* = 6.2 Hz, -NH_2). ^{13}C NMR (101 MHz, chloroform-*d*) δ 73.4 (-CH_2), 73.0 (-CH_2), 70.7 (-CH_2), 70.7 (2 × -CH_2), 70.7 (2 × -CH_2), 70.4 (-CH_2), 70.4 (-CH_2), 70.3 (-CH_2), 61.6 (-CH_2), 41.7 (-**C**^{a}H_2). HRMS (ESI) exact mass calculated for $C_{12}H_{27}NO_6Na$ $[M+Na]^+$ m/z 304.1731, found m/z 304.1728.

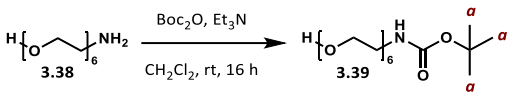

3.38 **3.39**

3.39: To a stirred solution of amine **3.38** (400 mg, 1.42 mmol, 1 equiv) in anhydrous dichloromethane (4.7 mL, 0.3 M) were added di-*tert*-butyl dicarbonate (373 mg, 1.71 mmol, 1.2 equiv) and triethylamine (0.30 mL, 5.4 mmol, 1.5 equiv) and the reaction mixture was stirred at room temperature for 16 hours. Volatile components were removed *in vacuo.* Purification by column chromatography on silica gel with an eluent of 0% to 20% ethanol in dichloromethane afforded protected linker **3.39** (250 mg, 0.66 mmol, 47%) as a pale yellow oil.

Analytical data observed were in accordance with literature values.[260]

^{1}H NMR (400 MHz, chloroform-*d*) δ 5.15 (1H, br s, -NH), 3.78 – 3.70 (2H, m, -CH_2), 3.70 – 3.58 (18H, m, 9 × -CH_2), 3.53 (2H, t, *J* = 5.1 Hz, -CH_2), 3.37 – 3.25 (2H, m, -CH_2), 2.71 (1H, br s, -OH), 1.44 (9H, s, 3 × -C**H$_3$**^{a}). ^{13}C NMR (101 MHz, chloroform-*d*) δ 156.2 (-NCOOR), 79.3 (-*C*$(CH_3)_3$), 72.6 (-CH_2), 70.7 (-CH_2), 70.7 (2 × -CH_2), 70.7 (-CH_2), 70.7 (-CH_2), 70.7 (2 × -CH_2), 70.5 (-CH_2), 70.4 (-CH_2), 61.9 (-CH_2), 40.5 (-CH_2), 28.6 (3 × -**C**^{a}H_3).

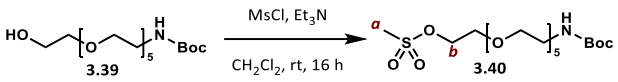

3.40: To a dry flask charged with argon was added anhydrous dichloromethane (1.8 mL, 0.1 M), alcohol **3.39** (200 mg, 0.52 mmol, 1 equiv), methanesulfonyl chloride (61 µL, 0.79 mmol, 1.5 equiv) and triethylamine (0.11 mL, 1.6 mmol, 3 equiv) and the resulting solution was stirred at room temperature for 16 hours. The reaction mixture was partitioned between 1 M aqueous hydrochloric acid (5 mL) and dichloromethane (5 mL), and the aqueous phase was extracted with dichloromethane (3 × 5 mL). The combined organic extracts were washed with water (2 × 10 mL), dried over magnesium sulfate, filtered and concentrated *in vacuo*. Purification by column chromatography on silica gel with an eluent of 0% to 10% ethanol in ethyl acetate afforded mesylate **3.40** (190 mg, 0.42 mmol, 81%) as a clear oil. Analytical data observed were in accordance with literature values.[261]

^{1}H NMR (400 MHz, chloroform-*d*) δ 5.17 (1H, br s, -NH), 4.37 – 4.28 (2H, m, -C**H$_2$**^{b}), 3.74 – 3.68 (2H, m, -CH_2), 3.67 – 3.53 (16H, m, 8 × -CH_2), 3.49 (2H, t, *J* = 5.1 Hz, -CH_2), 3.31 – 3.21 (2H, m, -CH_2), 3.04 (3H, s, -C**H$_3$**^{a}), 1.39 (9H, s, 3 × -CH_3). ^{13}C NMR (101 MHz, chloroform-*d*) δ 156.1 (-NCOOR), 79.1 (-*C*$(CH_3)_3$), 70.6 (-CH_2), 70.6 (2 × -CH_2), 70.5 (2 × -CH_2), 70.5 (2 × -CH_2), 70.3 (-CH_2), 70.2 (-CH_2), 69.3 (-CH_2), 69.0 (-**C**^{b}H_2), 40.4 (-CH_2), 37.7 (-**C**^{a}H_3), 28.5 (3 × -CH_3).

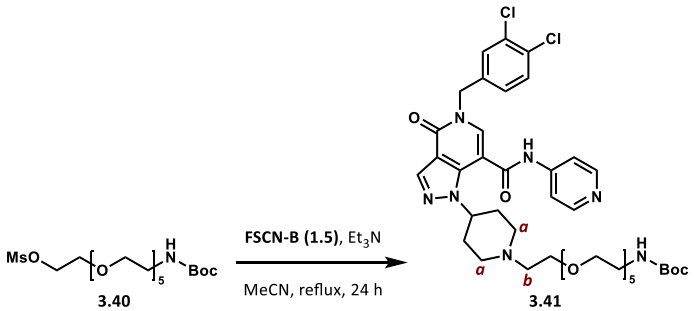

3.41: To a dry flask charged with argon was added anhydrous acetonitrile (1.3 mL, 0.1 M), mesylated linker **3.40** (51 mg, 0.11 mmol, 1 equiv), fascin ligand B **FSCN-B (1.5)** (66 mg, 0.13 mmol, 1.2 equiv) and triethylamine (59 µL, 0.33 mmol, 3 equiv) and the resulting solution was stirred under reflux for 24 hours. After consumption of starting materials was confirmed by TLC, volatile components were removed *in vacuo.* Purification by column

chromatography on silica gel with an eluent of 10% to 50% ethanol in dichloromethane afforded fascin ligand fragment **3.41** (59 mg, 0.069 mmol, 61%) as a clear oil.

^{1}H NMR (400 MHz, chloroform-*d*) δ 10.38 (1H, br s, -NH), 8.56 – 8.32 (2H, m, 2 × Ar-H), 8.06 (1H, s, -CH), 7.86 (1H, s, pyrazole-H), 7.81 – 7.71 (2H, m, 2 × Ar-H), 7.38 (1H, d, *J* = 2.0 Hz, Ar-H), 7.33 (1H, d, *J* = 8.2 Hz, Ar-H), 7.15 (1H, dd, J = 8.4, 2.1 Hz, Ar-H), 5.16 (1H, br s, -NH), 5.06 (2H, s, -CH_2), 4.76 – 4.57 (1H, m, -CH), 3.67 – 3.50 (18H, m, 9 × -CH_2), 3.46 (2H, t, *J* = 5.2 Hz, -CH_2), 3.28 – 3.13 (4H, m, 2 × -C**H$_2$**^{a}), 3.12 – 3.01 (2H, m, -CH_2), 2.69 – 2.59 (2H, m, -C**H$_2$**^{b}), 2.36 – 2.15 (2H, m, -CH_2), 2.07 – 1.90 (2H, m, -CH_2), 1.40 (9H, s, 3 × -CH_3). ^{13}C NMR (101 MHz, chloroform-*d*) δ 163.9 (-CONH), 158.4 (-CONR), 156.3 (-NCOOR), 150.6 (2 × Ar-CH), 145.9 (pyrazole-C), 139.2 (Ar-C), 137.4 (Ar-C), 136.9 (-CH), 136.6 (pyrazole-CH), 133.0 (Ar-C), 132.4 (Ar-C), 131.0 (Ar-CH), 130.1 (Ar-CH), 127.6 (Ar-CH), 114.3 (2 × Ar-CH), 113.7 (pyrazole-C), 105.9 (-C), 79.4 (-*C*(CH_3)$_3$), 70.6 (2 × -CH_2), 70.6 (3 × -CH_2), 70.5 (3 × -CH_2), 70.3 (2 × -CH_2), 57.6 (-CH), 57.3 (-**C**^{b}H_2), 52.9 (-CH_2), 50.3 (-CH_2), 40.5 (2 × -**C**^{a}H_2), 31.4 (2 × -CH_2), 28.5 (3 × -CH_3). IR (thin film) 1670, 1591, 1099 cm^{-1}. HRMS (ESI) exact mass calculated for $C_{41}H_{55}N_7Cl_2O_9Na$ $[M+Na]^+$ m/z 882.3331, found m/z 882.3316. LCMS (ESI) mass calculated for $C_{41}H_{55}N_7Cl_2O_9$ $[M+H]^+$ m/z 860.35, found m/z 860.75 with t_R = 5.69 min.

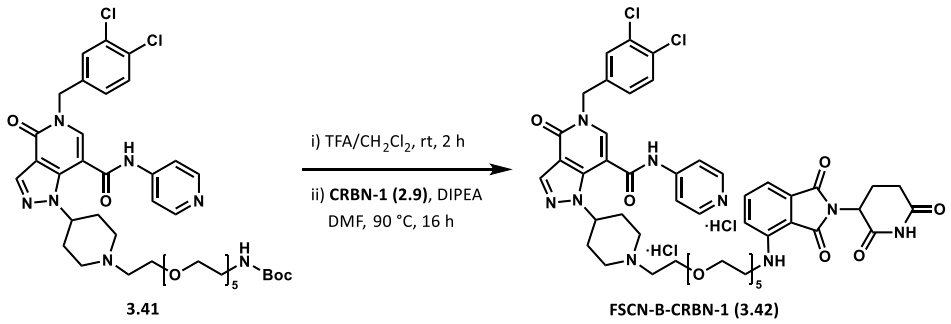

3.41 FSCN-B-CRBN-1 (3.42)

FSCN-B-CRBN-1 (3.42) ***via*** **Route A**: Fragment **3.41** (25 mg, 0.029 mmol, 1 equiv) was dissolved in trifluoroacetic acid/dichloromethane (0.5 mL/0.5 mL, 0.03 M) and the resulting solution was stirred at room temperature for 2 hours. The reaction was monitored by TLC for complete consumption of the starting material before removal of volatile components *in vacuo*. The residue was redissolved in *N,N*-dimethylformamide (0.15 mL, 0.2 M) and CRBN ligand **CRBN-1 (2.9)** (8 mg, 0.03 mmol, 1 equiv) and *N,N*-diisopropylethylamine (15 µL, 0.087 mmol, 3 equiv) were added. The resulting solution was heated to 90 °C and stirred for 16 hours. The reaction mixture was allowed to cool to room temperature, poured into water (20 mL) and extracted with ethyl acetate (5 × 20 mL). The combined organic phases were washed with 5% aqueous lithium chloride (3 × 50 mL), dried over magnesium sulfate, filtered and concentrated *in vacuo*. Purification by column chromatography on silica gel

with an eluent of 10% to 30% ethanol in dichloromethane afforded the product (13 mg, 0.013 mmol, 41%) as a bright yellow oil. Further purification by semi-preparative RP-HPLC using a focused gradient across 40% and 75% acetonitrile in water over 60 minutes eluted the title compound at t_R = 12 minutes (45% acetonitrile) and the product fraction was lyophilised. Redissolving the resulting trifluoroacetate salt in 1 M aqueous hydrochloric acid and acetonitrile, followed by lyophilisation, yielded fascin ligand B CRBN PROTAC **FSCN-B-CRBN-1 (3.42)** (2 mg, 0.002 mmol, 6%) as a yellow fluffy powder. Insufficient material for full characterisation was obtained – see **FSCN-B-CRBN-1 (3.42)** ***via*** **Route B** for full characterisation data.

HRMS (ESI) exact mass calculated for $C_{49}H_{56}N_9Cl_2O_{11}$ $[M+H]^+$ m/z 1016.3471, found m/z 1016.3430. LCMS (ESI) mass calculated for $C_{49}H_{56}N_9Cl_2O_{11}$ $[M+H]^+$ m/z 1016.35, found m/z 1016.92 with t_R = 5.60 min.

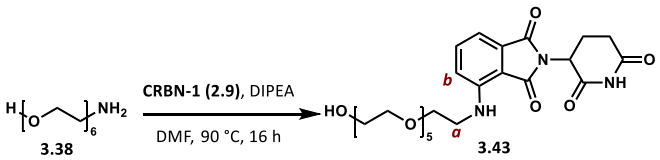

3.43: To a stirred solution of aminoalcohol **3.38** (220 mg, 0.78 mmol, 1 equiv) in *N,N*-dimethylformamide (3.9 mL, 0.2 M) were added CRBN ligand **CRBN-1 (2.9)** (210 mg, 0.78 mmol, 1 equiv) and *N,N*-diisopropylethylamine (0.28 mL, 1.6 mmol, 2 equiv). The resulting solution was heated to 90 °C and stirred for 16 hours. The reaction mixture was allowed to cool to room temperature, poured into water (20 mL) and extracted with dichloromethane (5 × 20 mL). The combined organic phases were washed with 5% aqueous lithium chloride (3 × 50 mL), dried over magnesium sulfate, filtered and concentrated *in vacuo*. Purification by column chromatography on silica gel with an eluent of 0% to 50% ethanol in ethyl acetate afforded linker fragment **3.43** (120 mg, 0.21 mmol, 28%) as a bright yellow oil.

^{1}H NMR (400 MHz, chloroform-*d*) δ 8.53 (1H, s, -NH), 7.49 (1H, dd, *J* = 8.5, 7.1 Hz, Ar-H), 7.10 (1H, d, *J* = 7.1 Hz, Ar-H), 6.92 (1H, d, *J* = 8.5 Hz, Ar-**H^b**), 6.50 (1H, t, *J* = 5.7 Hz, -NH), 5.01 – 4.84 (1H, m, -CH), 3.80 – 3.52 (22H, m, 11 × -CH_2), 3.53 – 3.43 (2H, m, -C**H$_2^a$**), 2.91 – 2.63 (3H, m, -C*H*H & -CH_2), 2.18 – 2.04 (1H, m, -CH*H*). ^{13}C NMR (101 MHz, chloroform-*d*) δ 171.3 (-CO), 169.4 (-CO), 168.6 (-CO), 167.8 (-CO), 147.0 (Ar-C), 136.2 (Ar-CH), 132.7 (Ar-C), 116.9 (Ar-**C^b**H), 111.8 (Ar-CH), 110.5 (Ar-C), 72.8 (-CH_2), 70.9 (-CH_2), 70.8 (-CH_2), 70.7 (2 × -CH_2), 70.7 (2 × -CH_2), 70.6 (-CH_2), 70.4 (-CH_2), 69.6 (-CH_2), 61.8 (-CH_2), 49.0 (-CH), 42.5 (-**C^a**H_2), 31.6 (-CH_2), 23.0 (-CH_2). IR (thin film) 3393, 1756, 1110 cm^{-1}. HRMS (ESI) exact mass calculated for $C_{25}H_{35}N_3O_{10}Na$ $[M+Na]^+$ m/z 560.2215, found m/z 560.2220.

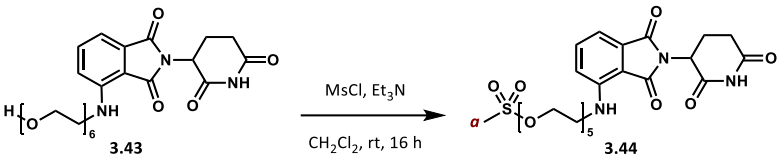

3.44: To a dry flask charged with argon was added anhydrous dichloromethane (2.2 mL, 0.1 M), alcohol **3.43** (117 mg, 0.22 mmol, 1 equiv), methanesulfonyl chloride (25 µL, 0.33 mmol, 1.5 equiv) and triethylamine (91 µL, 0.65 mmol, 3 equiv) and the resulting solution was stirred at room temperature for 16 hours. The reaction mixture was partitioned between 1 M aqueous hydrochloric acid (5 mL) and dichloromethane (5 mL), and the aqueous phase was extracted with dichloromethane (3 × 5 mL). The combined organic extracts were washed with water (2 × 10 mL), dried over magnesium sulfate, filtered and concentrated *in vacuo*. Purification by column chromatography on silica gel with an eluent of 5% to 20% ethanol in ethyl acetate afforded mesylate **3.44** (72 mg, 0.12 mmol, 54%) as a yellow oil. ^{1}H NMR (400 MHz, chloroform-*d*) δ 8.53 (1H, s, -NH), 7.52 – 7.43 (1H, m, Ar-H), 7.08 (1H, d, *J* = 7.1 Hz, Ar-H), 6.91 (1H, d, *J* = 8.5 Hz, Ar-H), 6.48 (1H, t, J = 5.6 Hz, -NH), 4.96 – 4.87 (1H, m, -CH), 4.39 – 4.31 (2H, m, -CH_2), 3.78 – 3.53 (20H, m, 10 × -CH_2), 3.51 – 3.39 (2H, m, -CH_2), 3.06 (3H, s, -C**H$_3$**^{a}), 2.90 – 2.69 (3H, m, -C*H*H & -CH_2), 2.16 – 2.06 (1H, m, -CH*H*). ^{13}C NMR (101 MHz, chloroform-*d*) δ 171.4 (-CO), 169.4 (-CO), 168.6 (-CO), 167.7 (-CO), 146.9 (Ar-C), 136.1 (Ar-CH), 132.6 (Ar-C), 116.9 (Ar-CH), 111.7 (Ar-CH), 110.4 (Ar-C), 70.9 (-CH_2), 70.8 (-CH_2), 70.7 (2 × -CH_2), 70.7 (2 × -CH_2), 70.6 (-CH_2), 70.6 (-CH_2), 69.6 (-CH_2), 69.4 (-CH_2), 69.1 (-CH_2), 49.0 (-CH), 42.5 (-CH_2), 37.8 (-**C**^{a}H$_3$), 31.5 (-CH_2), 22.9 (-CH_2). IR (thin film) 1756, 1408, 1111 cm^{-1}. HRMS (ESI) exact mass calculated for $C_{26}H_{37}N_3O_{12}SNa$ $[M+Na]^+$ m/z 638.1990, found m/z 638.1987.

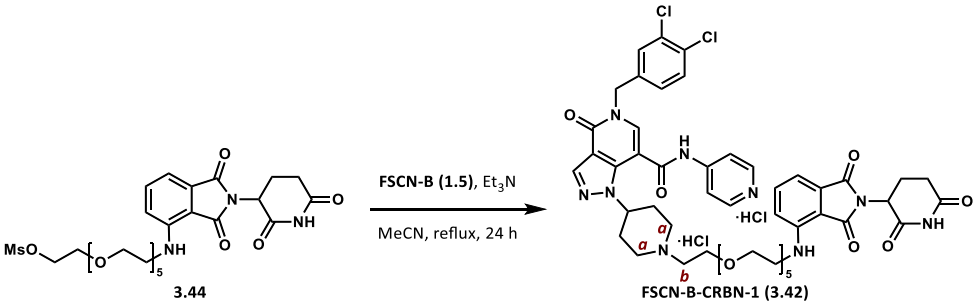

FSCN-B-CRBN-1 (3.42) ***via*** **Route B**: To a dry flask charged with argon was added anhydrous acetonitrile (1 mL, 0.1 M), mesylated fragment **3.44** (65 mg, 0.11 mmol, 1 equiv), fascin ligand B **FSCN-B (1.5)** (63 mg, 0.13 mmol, 1.2 equiv) and triethylamine (44 µL, 0.32 mmol, 3 equiv) and the resulting solution was stirred under reflux for 24 hours. After consumption of starting materials was confirmed by TLC, volatile components were removed *in vacuo.*

Purification by column chromatography on silica gel with an eluent of 10% to 30% ethanol in dichloromethane afforded the product (48 mg, 0.047 mmol, 47%) as a bright yellow oil. Further purification by semi-preparative RP-HPLC using a focused gradient across 30% and 80% acetonitrile in water over 40 minutes eluted the title compound at t_R = 23 minutes (55% acetonitrile) and the product fraction was lyophilised. Redissolving the resulting trifluoroacetate salt in 1 M aqueous hydrochloric acid and acetonitrile, followed by lyophilisation, yielded fascin ligand B CRBN PROTAC **FSCN-B-CRBN-1 (3.42)** (16 mg, 0.016 mmol, 16%) as a yellow fluffy powder.

^{1}H NMR (500 MHz, methanol-d_4) δ 8.75 – 8.63 (2H, m, 2 × Ar-H), 8.45 (1H, s, pyrazole-H), 8.36 – 8.22 (3H, m, -CH & 2 × Ar-H), 7.60 (1H, d, J = 1.9 Hz, Ar-H), 7.54 – 7.44 (2H, m, 2 × Ar-H), 7.37 (1H, dd, J = 8.4, 2.1 Hz, Ar-H), 7.06 – 6.94 (2H, m, 2 × Ar-H), 5.27 (2H, s, -CH_2), 5.08 – 4.98 (2H, m, 2 × -CH), 3.91 – 3.40 (22H, m, 11 × -CH_2), 3.40 – 3.35 (2H, m, -C**H$_2$**^{b}), 3.27 – 3.15 (2H, m, -CH_2), 2.91 – 2.53 (6H, m, -CH_2 & 2 × -C**H$_2$**^{a}), 2.53 – 2.31 (3H, m, -C*H*H & -CH_2), 2.13 – 2.05 (1H, m, -CH*H*). ^{13}C NMR (101 MHz, methanol-d_4) δ 174.5 (-CO), 171.6 (-CO), 170.6 (-CO), 169.1 (-CO), 165.9 (-CONH), 160.0 (-CONH), 155.7 (pyrazole-C), 147.8 (Ar-C), 143.4 (2 × Ar-CH), 142.5 (-CH), 140.9 (Ar-C), 138.6 (Ar-C), 138.4 (pyrazole-CH), 137.3 (Ar-CH), 133.7 (Ar-C), 133.4 (Ar-C), 132.9 (Ar-C), 131.9 (Ar-CH), 131.3 (Ar-CH), 129.3 (Ar-CH), 118.6 (Ar-CH), 117.3 (2 × Ar-CH), 114.9 (pyrazole-C), 112.3 (Ar-CH), 111.3 (Ar-C), 105.8 (-C), 71.7 (-CH_2), 71.7 (2 × -CH_2), 71.6 (2 × -CH_2), 71.5 (-CH_2), 71.4 (-CH_2), 71.3 (-CH_2), 70.6 (-CH_2), 65.7 (-CH_2), 57.5 (-**C^b**H$_2$), 54.1 (-CH), 52.3 (-CH_2), 50.3 (-CH), 43.5 (-CH_2), 39.5 (2 × -CH_2), 32.4 (2 × -**C^a**H$_2$), 30.9 (-CH_2), 23.9 (-CH_2). IR (thin film) 1703, 1670, 1067 cm^{-1}. HRMS (ESI) exact mass calculated for $C_{49}H_{56}N_9Cl_2O_{11}$ $[M+H]^+$ m/z 1016.3471, found m/z 1016.3473. LCMS (ESI) mass calculated for $C_{49}H_{56}N_9Cl_2O_{11}$ $[M+H]^+$ m/z 1016.35, found m/z 1016.92 with t_R = 5.65 min.

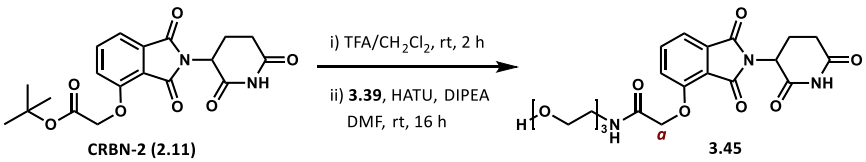

3.45: CRBN ligand **CRBN-2 (2.11)** (200 mg, 0.52 mmol, 1 equiv) was dissolved in trifluoroacetic acid/dichloromethane (8.5 mL/8.5 mL, 0.03 M) and the resulting solution was stirred at room temperature for 2 hours. The reaction was monitored by TLC for complete consumption of the starting material before removal of volatile components *in vacuo*. The residue was redissolved in *N,N*-dimethylformamide (1.7 mL, 0.3 M), and **3.39** (72 µL, 0.52 mmol, 1 equiv), HATU (200 mg, 0.52 mmol, 1 equiv) and *N,N*-

diisopropylethylamine (0.28 mL, 1.6 mmol, 3 equiv) were added. The resulting solution was stirred at room temperature for 16 hours before partitioning the reaction mixture between dichloromethane (10 mL) and water (10 mL). The aqueous phase was extracted with dichloromethane (5 × 10 mL) and the combined organic phases were washed with 5% aqueous lithium chloride (3 × 20 mL), dried over magnesium sulfate, filtered and concentrated *in vacuo*. Purification by column chromatography on silica gel with an eluent of 5% to 20% ethanol in dichloromethane afforded fragment **3.45** (96 mg, 0.21 mmol, 45%) as clear oil.

^{1}H NMR (500 MHz, chloroform-*d*) δ 8.76 (1H, br s, -OH), 7.77 – 7.72 (1H, m, Ar-H), 7.70 (1H, br s, -NH), 7.55 (1H, d, *J* = 7.3 Hz, Ar-H), 7.20 (1H, d, *J* = 8.4 Hz, Ar-H), 6.16 (1H, br s, -NH), 5.02 – 4.94 (1H, m, -CH), 4.66 (2H, s, -C**H$_2$**^{a}), 3.79 – 3.61 (10H, m, 5 × -CH$_2$), 3.23 – 3.13 (2H, m, -CH$_2$), 2.93 – 2.70 (3H, m, -C*H*H & -CH$_2$), 2.23 – 2.12 (1H, m, -CH*H*). ^{13}C NMR (126 MHz, chloroform-*d*) δ 171.4 (-CO), 168.4 (-CO), 167.1 (-CO), 166.7 (-CO), 166.1 (-CONH), 154.6 (Ar-C), 137.2 (Ar-CH), 133.8 (Ar-C), 119.6 (Ar-CH), 118.2 (Ar-C), 117.5 (Ar-C), 72.6 (-CH$_2$), 70.3 (-CH$_2$), 69.7 (-CH$_2$), 68.1 (-CH$_2$), 61.9 (-**C**^{a}H$_2$), 55.9 (-CH$_2$), 49.4 (-CH), 39.2 (-CH$_2$), 31.4 (-CH$_2$), 22.9 (-CH$_2$). IR (thin film) 1709, 1665, 1198 cm^{-1}. HRMS (ESI) exact mass calculated for $C_{21}H_{25}N_3O_9Na$ [M+Na]$^{+}$ m/z 486.1483, found m/z 486.1480.

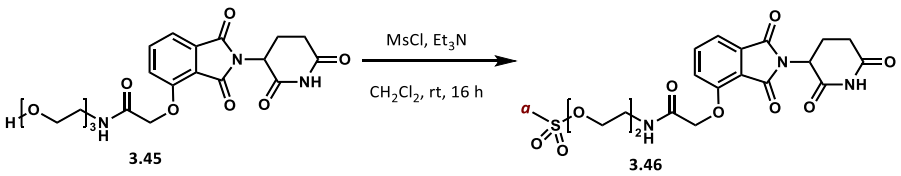

3.46: To a dry flask charged with argon was added anhydrous dichloromethane (2 mL, 0.1 M), alcohol **3.45** (90 mg, 0.19 mmol, 1 equiv), methanesulfonyl chloride (23 µL, 0.29 mmol, 1.5 equiv) and triethylamine (81 µL, 0.58 mmol, 3 equiv) and the resulting solution was stirred at room temperature for 16 hours. The reaction mixture was partitioned between 1 M aqueous hydrochloric acid (10 mL) and dichloromethane (10 mL), and the aqueous phase was extracted with dichloromethane (3 × 10 mL). The combined organic extracts were washed with water (2 × 20 mL), dried over magnesium sulfate, filtered and concentrated *in vacuo*. Purification by column chromatography on silica gel with an eluent of 5% to 20% ethanol in dichloromethane afforded mesylate **3.46** (66 mg, 0.12 mmol, 64%) as a clear oil.

^{1}H NMR (400 MHz, chloroform-*d*) δ 8.59 (1H, br s, -NH), 7.73 (1H, dd, *J* = 8.4, 7.4 Hz, Ar-H), 7.59 (1H, br s,-NH), 7.54 (1H, d, *J* = 7.3 Hz, Ar-H), 7.20 (1H, d, *J* = 8.3 Hz, Ar-H), 5.04 – 4.91 (1H, m, -CH), 4.66 (2H, s, -CH$_2$), 4.40 – 4.29 (2H, m, -CH$_2$), 3.81 – 3.72 (2H, m, -CH$_2$), 3.72 –

3.52 (8H, m, 4 × -CH_2), 3.07 (3H, s, -C**H_3**[a]), 2.93 – 2.70 (3H, m, -C*H*H & -CH_2), 2.21 – 2.09 (1H, m, -CH*H*). ^{13}C NMR (101 MHz, chloroform-*d*) 171.4 (-CO), 168.5 (-CO), 167.2 (-CO), 166.9 (-CO), 166.1 (-CONH), 154.7 (Ar-C), 137.2 (Ar-CH), 133.9 (Ar-C), 119.6 (Ar-CH), 118.2 (Ar-C), 117.6 (Ar-CH), 77.5, 70.7 (-CH_2), 70.6 (-CH_2), 69.8 (-CH_2), 69.6 (-CH_2), 69.3 (-CH_2), 68.2 (-CH_2), 49.5 (-CH), 39.3 (-CH_2), 37.9 (-**C**[a]H_3), 31.8 (-CH_2), 22.8 (-CH_2). IR (thin film) 1707, 1682, 1393 cm^{-1}. HRMS (ESI) exact mass calculated for $C_{22}H_{27}N_3O_{11}Na$ $[M+Na]^+$ m/z 564.1259, found m/z 564.1251.

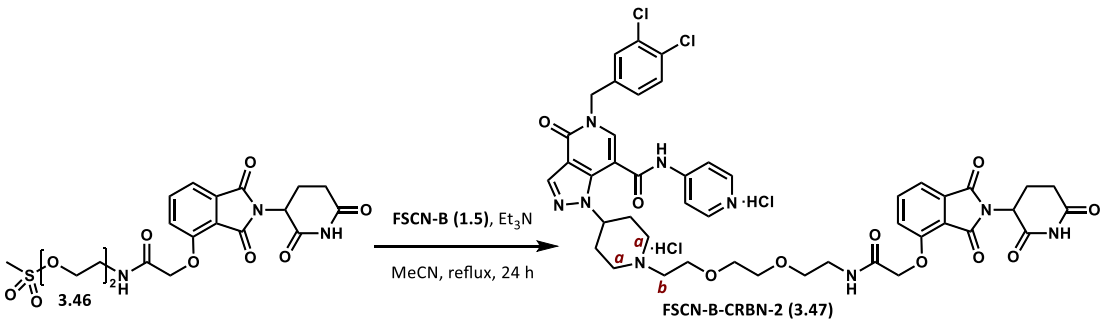

FSCN-B-CRBN-2 (3.47): To a dry flask charged with argon was added anhydrous acetonitrile (1 mL, 0.1 M), mesylated fragment **3.46** (54 mg, 0.10 mmol, 1 equiv), fascin ligand B **FSCN-B (1.5)** (60 mg, 0.12 mmol, 1.2 equiv) and triethylamine (42 µL, 0.30 mmol, 3 equiv) and the resulting solution was stirred under reflux for 24 hours. After consumption of starting materials was confirmed by TLC, volatile components were removed *in vacuo.* Purification by column chromatography on silica gel with an eluent of 5% to 30% ethanol in dichloromethane afforded the product (20 mg, 0.021 mmol, 21%) as a clear oil. Further purification by semi-preparative RP-HPLC using a focused gradient across 30% and 70% acetonitrile in water over 30 minutes eluted the title compound at t_R = 22 minutes (55% acetonitrile) and the product fraction was lyophilised. Redissolving the resulting trifluoroacetate salt in 1 M aqueous hydrochloric acid and acetonitrile, followed by lyophilisation, yielded fascin ligand B CRBN PROTAC **FSCN-B-CRBN-2 (3.47)** (8 mg, 0.009 mmol, 9%) as a white fluffy powder.

^{1}H NMR (400 MHz, methanol-*d*$_4$) δ 8.75 – 8.62 (2H, m, 2 × Ar-H), 8.48 (1H, s, pyrazole-H), 8.41 – 8.28 (2H, m, 2 × Ar-H), 8.20 (1H, s, -CH), 7.68 – 7.63 (1H, m, Ar-H), 7.62 – 7.46 (2H, m, 2 × Ar-H), 7.47 – 7.27 (3H, m, 3 × Ar-H), 5.28 (2H, s, -CH_2), 5.18 – 4.97 (2H, m, 2 × -CH), 4.72 (2H, s, -CH_2), 3.93 – 3.59 (10H, m, 5 × -CH_2), 3.58 – 3.46 (2H, m, -C**H_2**[b]), 3.42 – 3.34 (2H, m, -CH_2), 3.27 – 3.11 (2H, m, -CH_2), 2.94 – 2.44 (4H, m, 2 × -C**H_2**[a]), 2.44 – 2.27 (3H, m, -C*H*H & -CH_2), 2.21 – 2.10 (1H, m, -CH*H*). ^{13}C NMR (101 MHz, methanol-*d*$_4$) δ 174.5 (-CO), 171.5 (-CO), 170.0 (-CONH), 168.2 (-CO), 167.8 (-CO), 165.9 (-CONH), 160.0 (-CONR), 156.0

(pyrazole-C), 143.2 (Ar-C), 142.1 (2 × Ar-C), 140.7 (-CH), 138.6 (Ar-C), 138.4 (pyrazole-CH), 138.2 (Ar-C), 138.1 (Ar-CH), 134.8 (Ar-C), 133.6 (Ar-C), 133.0 (Ar-C), 131.9 (Ar-CH), 131.3 (Ar-CH), 129.2 (Ar-CH), 121.5 (Ar-CH), 119.0 (Ar-CH), 117.9 (Ar-C), 117.0 (2 × Ar-CH), 114.9 (pyrazole-C), 105.7 (-C), 71.5 ($-CH_2$), 71.4 ($-CH_2$), 70.5 ($-CH_2$), 69.2 ($-CH_2$), 65.6 ($-CH_2$), 56.9 (-**C**$^{b}H_2$), 53.6 (-CH), 52.2 ($-CH_2$), 50.6 (-CH), 40.4 ($-CH_2$), 32.2 (2 × $-CH_2$), 30.7 (2 × -**C**$^{a}H_2$), 23.7 ($-CH_2$), 21.6 ($-CH_2$). IR (thin film) 1708, 1665, 1033 cm^{-1}. HRMS (ESI) exact mass calculated for $C_{45}H_{46}N_9Cl_2O_{10}$ $[M+H]^+$ m/z 942.2739, found m/z 942.2763.

- *Fascin ligand B HyT PROTACs:*

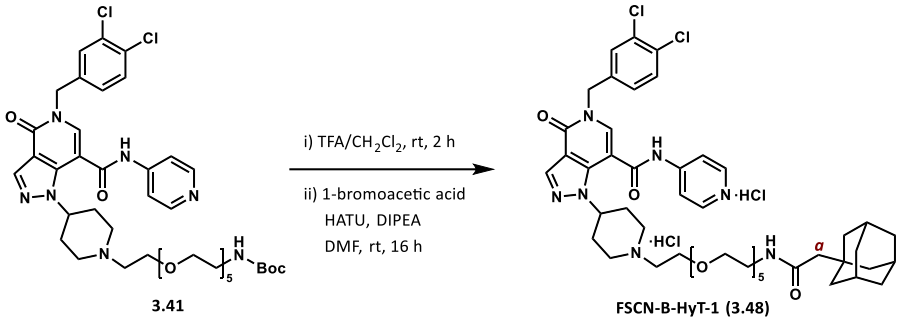

FSCN-B-HyT-1 (3.48): Fragment **3.41** (25 mg, 0.029 mmol, 1 equiv) was dissolved in trifluoroacetic acid/dichloromethane (0.5 mL/0.5 mL, 0.03 M) and the resulting solution was stirred at room temperature for 2 hours. The reaction was monitored by TLC for complete consumption of the starting material before removal of volatile components *in vacuo*. The residue was redissolved in *N,N*-dimethylformamide (0.1 mL, 0.3 M), and 1-adamantylacetic acid (6 mg 0.03 mmol, 1 equiv), HATU (12 mg, 0.029 mmol, 1 equiv) and *N,N*-diisopropylethylamine (15 µL, 0.087 mmol, 3 equiv) were added. The resulting solution was stirred at room temperature for 16 hours before partitioning the reaction mixture between dichloromethane (10 mL) and water (10 mL). The aqueous phase was extracted with dichloromethane (5 × 10 mL) and the combined organic phases were washed with 5% aqueous lithium chloride (4 × 20 mL), dried over magnesium sulfate, filtered and concentrated *in vacuo*. Purification by column chromatography on silica gel with an eluent of 10% to 30% ethanol in dichloromethane afforded the product (18 mg, 0.019 mmol, 64%) as a clear oil. Further purification by semi-preparative RP-HPLC using a focused gradient across 40% and 70% acetonitrile in water over 30 minutes eluted the title compound at t_R = 24 minutes (58% acetonitrile) and the product fraction was lyophilised. Redissolving the resulting trifluoroacetate salt in 1 M aqueous hydrochloric acid and acetonitrile, followed by lyophilisation, yielded fascin ligand B HyT PROTAC **FSCN-B-HyT-1 (3.48)** (8 mg, 0.009 mmol, 29%) as a white fluffy powder.

^{1}H NMR (500 MHz, methanol-*d*$_4$) δ 8.76 – 8.66 (2H, m, 2 × Ar-H), 8.52 (1H, s, pyrazole-H), 8.43 – 8.33 (2H, m, 2 × Ar-H), 8.28 (1H, s, -CH), 7.62 (1H, d, *J* = 1.8 Hz, Ar-H), 7.51 (1H, d, *J* = 8.2 Hz, Ar-H), 7.39 (1H, dd, *J* = 8.4, 1.9 Hz, Ar-H), 5.28 (2H, s, -CH$_2$), 5.13 – 5.01 (1H, m, -CH), 3.92 – 3.48 (22H, m, 11 × -CH$_2$), 3.47 – 3.36 (2H, m, -CH$_2$), 2.71 – 2.56 (6H, m, 3 × -CH$_2$), 2.47 – 2.35 (2H, m, -CH$_2$), 1.93 (2H, s, -C**H$_2$**^{a}), 1.92 – 1.89 (3H, m, 3 × -CH), 1.76 – 1.56 (12H, m, 6 × -CH$_2$). ^{13}C NMR (126 MHz, methanol-*d*$_4$) δ 174.0 (-CONH), 166.1 (-CONH), 160.0 (-CONR), 155.8 (pyrazole-C) 143.2 (2 × Ar-CH), 142.2 (-CH), 140.9 (Ar-C), 138.6 (Ar-C), 138.4 (pyrazole-CH), 133.6 (Ar-C), 133.0 (Ar-C), 131.9 (Ar-CH), 131.2 (Ar-CH), 129.1 (Ar-CH), 116.9 (2 × Ar-CH), 115.0 (pyrazole-C), 105.8 (-C), 71.6 (2 × -CH$_2$), 71.5 (2 × -CH$_2$), 71.5 (2 × -CH$_2$), 71.4 (-CH$_2$), 71.3 (-CH$_2$), 70.6 (-CH$_2$), 65.4 (-CH$_2$), 57.7 (-CH$_2$), 56.9 (-CH$_2$), 53.5 (-CH), 52.2 (-CH$_2$), 51.8 (-**C**^{a}H$_2$), 43.7 (3 × -CH$_2$), 40.3 (2 × -CH$_2$), 37.9 (3 × -CH$_2$), 33.8 (-C), 30.7 (2 × -CH$_2$), 30.2 (3 × -CH). IR (thin film) 1670, 1508, 1103 cm^{-1}. HRMS (ESI) exact mass calculated for $C_{48}H_{63}N_7Cl_2O_8Na$ [M+Na]$^+$ m/z 958.4007, found m/z 958.3975. LCMS (ESI) mass calculated for $C_{48}H_{64}N_7Cl_2O_8$ [M+H]$^+$ m/z 937.42, found m/z 937.67 with t_R = 6.11 min.

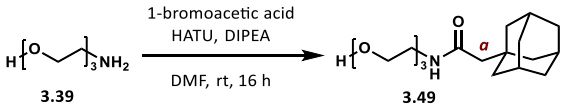

3.49: To a pre-stirred solution of 1-adamantylacetic acid (360 mg, 1.8 mmol, 1 equiv), HATU (700 mg, 1.8 mmol, 1 equiv) and *N,N*-diisopropylethylamine (0.98 mL, 1.8 mmol, 3 equiv) in *N,N*-dimethylformamide (6 mL, 0.3 M) was added aminoalcohol **3.39** (0.25 mL, 1.8 mmol, 1 equiv), and the resulting solution was stirred at room temperature for 16 hours. The reaction mixture was partitioned between dichloromethane (30 mL) and water (30 mL), and the aqueous phase was extracted with dichloromethane (5 × 30 mL). The combined organic phases were washed with 5% aqueous lithium chloride (3 × 100 mL), dried over magnesium sulfate, filtered and concentrated *in vacuo*. Purification by column chromatography on silica gel with an eluent of 10% to 30% ethanol in dichloromethane afforded HyT fragment **3.49** (550 mg, 1.7 mmol, 92%) as clear oil.

^{1}H NMR (400 MHz, chloroform-*d*) δ 6.01 (1H, br s, -NH), 3.85 – 3.52 (8H, m, 4 × -CH$_2$), 3.52 – 3.42 (2H, m, -CH$_2$), 2.65 (1H, br s, -OH), 2.02 – 1.95 (3H, m, 3 × -CH), 1.94 (2H, s, -C**H$_2$**^{a}), 1.74 – 1.56 (12H, m, 6 × -CH$_2$), 1.52 – 1.40 (2H, m, -CH$_2$). ^{13}C NMR (101 MHz, chloroform-*d*) δ 70.4 (3 × -CH$_2$), 61.8 (-CH$_2$), 51.9 (-**C**^{a}H$_2$), 42.8 (3 × -CH$_2$), 39.2 (-CH$_2$), 36.9 (3 × -CH$_2$), 32.9 (-C), 28.8 (3 × -CH). IR (thin film) 3300, 1639, 1101 cm^{-1}. HRMS (ESI) exact mass calculated for $C_{18}H_{31}NO_4Na$ [M+Na]$^+$ m/z 348.2145, found m/z 348.2136.

3.50: To a dry flask charged with argon was added anhydrous dichloromethane (8 mL, 0.1 M), alcohol **3.49** (250 mg, 0.77 mmol, 1 equiv), methanesulfonyl chloride (0.10 mL, 1.2 mmol, 1.5 equiv) and triethylamine (0.32 mL, 2.3 mmol, 3 equiv) and the resulting solution was stirred at room temperature for 16 hours. The reaction mixture was partitioned between 1 M aqueous hydrochloric acid (10 mL) and dichloromethane (10 mL), and the aqueous phase was extracted with dichloromethane (3 × 10 mL). The combined organic extracts were washed with water (2 × 20 mL), dried over magnesium sulfate, filtered and concentrated *in vacuo*. Purification by column chromatography on silica gel with ethyl acetate afforded mesylate **3.50** (190 mg, 0.47 mmol, 62%) as a clear oil.

^{1}H NMR (500 MHz, chloroform-*d*) δ 5.89 (1H, br s, -NH), 4.38 – 4.31 (2H, m, -CH_2), 3.77 – 3.72 (2H, m, -CH_2), 3.66 – 3.57 (4H, m, 2× -CH_2), 3.51 (2H, t, *J* = 5.2 Hz, -CH_2), 3.43 – 3.38 (2H, m, 2× -CH_2), 3.04 (3H, s, -C**H$_3$**^{a}), 1.97 – 1.92 (3H, m, 3 × -CH), 1.91 (2H, s, -CH_2), 1.70 – 1.55 (12H, m, 6 × -CH_2). ^{13}C NMR (101 MHz, chloroform-*d*) δ 171.2 (-CONH), 70.8 (-CH_2), 70.3 (-CH_2), 70.3 (-CH_2), 69.2 (-CH_2), 69.2 (-CH_2), 51.8 (-CH_2), 42.7 (3 × -CH_2), 39.2 (-CH_2), 37.9 (-C**H$_3$**^{a}), 36.8 (3 × -CH_2), 32.9 (-C), 28.8 (3 × CH). ^{13}C NMR (101 MHz, chloroform-*d*) δ 70.4 (3 × -CH_2), 61.8 (-CH_2), 51.9 (-**C**^{a}H_2), 42.8 (3 × -CH_2), 39.2 (-CH_2), 36.9 (3 × -CH_2), 32.9 (-C), 28.8 (3 × -CH). IR (thin film) 1643, 1348, 1103 cm^{-1}. HRMS (ESI) exact mass calculated for $C_{19}H_{33}NO_6SNa$ $[M+Na]^+$ m/z 426.1926, found m/z 426.1793.

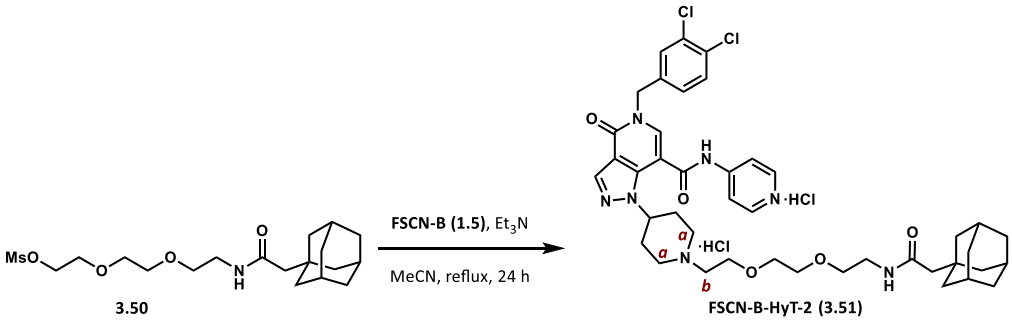

FSCN-B-HyT-2 (3.51): To a dry flask charged with argon was added anhydrous acetonitrile (1 mL, 0.1 M), mesylated fragment **3.50** (41 mg, 0.10 mmol, 1 equiv), fascin ligand B **FSCN-B (1.5)** (61 mg, 0.12 mmol, 1.2 equiv) and triethylamine (42 µL, 0.30 mmol, 3 equiv) and the resulting solution was stirred under reflux for 24 hours. After consumption of starting materials was confirmed by TLC, volatile components were removed *in vacuo.* Purification by column chromatography on silica gel with an eluent of 5% to 50% ethanol in dichloromethane afforded the product (61 mg, 0.076 mmol, 75%) as a clear oil. Further

purification by semi-preparative RP-HPLC using a focused gradient across 40% and 80% acetonitrile in water over 30 minutes eluted the title compound at t_R = 21 minutes (58% acetonitrile) and the product fraction was lyophilised. Redissolving the resulting trifluoroacetate salt in 1 M aqueous hydrochloric acid and acetonitrile, followed by lyophilisation, yielded fascin ligand B HyT PROTAC **FSCN-B-HyT-2 (3.51)** (31 mg, 0.039 mmol, 38%) as a white fluffy powder.

^{1}H NMR (500 MHz, methanol-*d*$_4$) δ 8.75 – 8.68 (2H, m, 2 × Ar-H), 8.51 (1H, s, pyrazole-H), 8.40 – 8.33 (2H, m, 2 × Ar-H), 8.26 (1H, s, -CH), 7.62 (1H, d, *J* = 2.0 Hz, Ar-H), 7.51 (1H, d, *J* = 8.3 Hz, Ar-H), 7.39 (1H, dd, *J* = 8.4, 2.1 Hz, Ar-H), 5.28 (2H, s, -CH$_2$), 5.13 – 5.01 (1H, m, -CH), 3.91 – 3.49 (10H, m, 5 × -CH$_2$), 3.40 (2H, d, *J* = 4.7 Hz, -C**H$_2^b$**), 3.39 – 3.33 (2H, m, -CH$_2$), 3.29 – 3.20 (2H, m, -CH$_2$), 2.69 – 2.37 (4H, m, 2 × -C**H$_2^a$**), 1.93 (2H, s, -CH$_2$), 1.92 – 1.85 (3H, m, 3 × -CH), 1.73 – 1.55 (12H, m, 6 × -CH$_2$). ^{13}C NMR (126 MHz, methanol-*d*$_4$) δ 174.1 (-CONH), 166.1 (-CONH), 160.0 (-CONR), 155.8 (pyrazole-C), 143.2 (2 × Ar-CH), 142.1 (-CH), 140.9 (Ar-C), 138.6 (Ar-C), 138.4 (pyrazole-CH), 133.6 (Ar-C), 133.0 (Ar-C), 131.9 (Ar-CH), 131.3 (Ar-CH), 129.1 (Ar-CH), 117.0 (2 × Ar-CH), 114.9 (pyrazole-C), 105.8 (-C), 71.4 (-CH$_2$), 71.2 (-CH$_2$), 70.6 (-CH$_2$), 65.7 (-CH$_2$), 57.7 (-**C^b**H$_2$), 57.0 (-CH), 53.6 (-CH$_2$), 52.2 (-CH$_2$), 51.8 (-CH$_2$), 43.7 (3 × -CH$_2$), 40.2 (2 × -**C^a**H$_2$), 37.9 (3 × -CH$_2$), 33.8 (-C), 30.8 (2 × -CH$_2$), 30.1 (3 × -CH). IR (thin film) 1169, 1507, 1103 cm^{-1}. HRMS (ESI) exact mass calculated for $C_{42}H_{51}N_7Cl_2O_4Na$ [M+Na]$^+$ m/z 826.3221, found m/z 826.3224.

Preparation of fascin ligand C FSCN-C (1.7) and analogues

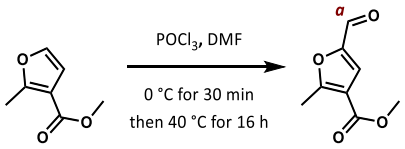

3.54

3.54: To a dry flask charged with argon was added anhydrous *N,N*-dimethylformamide (0.3 mL, 2.4 M) and methyl 2-methylfuran-3-carboxylate (90 µL, 0.71 mmol, 1 equiv) and the reaction mixture was cooled to 0 °C. Phosphorous(V) oxychloride (0.14 mL, 1.4 mmol, 2 equiv) was added dropwise at 0 °C and the solution was stirred at 0 °C for 30 minutes and then heated to 40 °C and stirred for a further 16 hours. The reaction mixture was poured into ice water and 5 M aqueous sodium hydroxide was added until pH 8. The aqueous phase was extracted with diethyl ether (2 × 10 mL) and the combined organic extracts were washed with water (20 mL) and saturated aqueous sodium hydrogen bicarbonate solution (20 mL), dried over magnesium sulfate, filtered and concentrated *in vacuo* to afford furfural

3.54 in quantitative yield (120 mg, 0.71 mmol) as a white amorphous solid. The crude material was used in the next step without further purification.

Analytical data observed were as in accordance with literature values.[191]

^{1}H NMR (400 MHz, chloroform-*d*) δ 9.56 (1H, s, aldehyde-**H**^{a}), 7.47 (1H, s, furan-H), 3.87 (3H, s, -OCH_3), 2.70 (3H, s, -CH_3). ^{13}C NMR (101 MHz, chloroform-*d*) δ 177.2 (aldehyde-**C**^{a}H), 165.0 (-COOR), 163.2 (furan-C), 150.6 (furan-C), 122.4 (furan-CH), 116.4 (furan-C), 52.0 (-OCH_3), 14.5 (-CH_3).

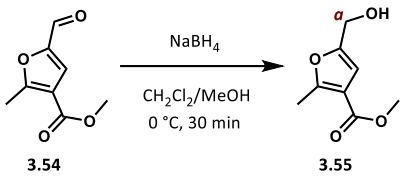

3.54 **3.55**

3.55: Aldehyde **3.54** (300 mg, 1.8 mmol, 1 equiv) was dissolved in dichloromethane/methanol (1.6 mL/3.2 mL, 0.4 M) and the resulting solution was cooled to 0 °C. Sodium borohydride (150 mg, 3.9 mmol, 2 equiv) was added portion-wise, and the reaction mixture was stirred for 30 minutes at 0 °C. The reaction was monitored by TLC for complete consumption of the starting material before it was quenched with saturated aqueous sodium hydrogen bicarbonate solution (20 mL). The aqueous phase was extracted with dichloromethane (3 × 10 mL) and the combined organic extracts were washed with brine (30 mL), dried over magnesium sulfate, filtered and concentrated *in vacuo* to afford alcohol **3.55** (300 mg, 1.8 mmol, 98%) as a white amorphous solid. The crude material was used in the next step without further purification.

Analytical data observed were as in accordance with literature values.[191]

^{1}H NMR (400 MHz, chloroform-*d*) δ 6.52 (1H, s, furan-H), 4.55 (2H, d, *J* = 4.9 Hz, -C***H***$_2^{a}$OH), 3.81 (3H, s, -OCH_3), 2.57 (3H, s, -CH_3), 1.81 (1H, br s, -OH). ^{13}C NMR (101 MHz, chloroform-*d*) δ 164.5 (-COOR), 159.6 (furan-C), 152.0 (furan-C), 114.0 (furan-C), 108.8 (furan-CH), 57.3 (-**C**^{a}HOH), 51.5 (-OCH_3), 13.9 (-CH_3).

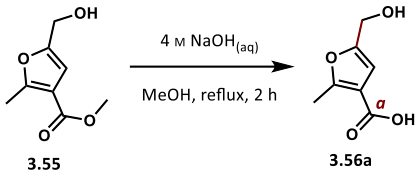

3.56a: To a stirred solution of **3.55** (150 mg, 0.89 mmol, 1 equiv) in methanol (3 mL, 0.3 M) was added 4 M aqueous sodium hydroxide (0.12 mL, 3.6 mmol, 4 equiv) and the resulting solution was stirred at reflux for 2 hours. After complete consumption of the starting material was confirmed by TLC, volatile components were removed *in vacuo*. The residue was redissolved in water (20 mL) and 1 M aqueous hydrochloric acid was added until pH 3. The acidified aqueous phase was extracted with dichloromethane (3 × 20 mL), and the combined organic extracts were dried over magnesium sulfate, filtered and concentrated *in vacuo*. Carboxylic acid **3.56a** (110 mg, 0.71 mmol, 79%) was afforded as a white amorphous solid and used in the next step without further purification.

Analytical data observed were as in accordance with literature values.[191]

^{1}H NMR (400 MHz, methanol-d_4) δ 6.50 (1H, s, furan-H), 4.45 (2H, s, -CH_2), 2.54 (3H, s, -CH_3). ^{13}C NMR (101 MHz, methanol-d_4) δ 167.3 (-**C**^{a}OOH), 160.3 (furan-C), 154.2 (furan-C), 115.5 (furan-C), 109.4 (furan-CH), 57.1 (-CH_2), 13.7 (-CH_3).

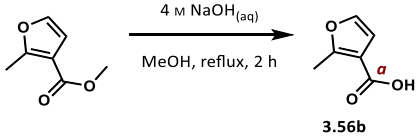

3.56b: To a stirred solution of methyl 2-methylfuran-3-carboxylate (0.10 mL, 0.80 mmol, 1 equiv) in methanol (2.7 mL, 0.3 M) was added 4 M aqueous sodium hydroxide (0.14 mL, 4.0 mmol, 4 equiv) and the resulting solution was stirred at reflux for 2 hours. After complete consumption of the starting material was confirmed by TLC, volatile components were removed *in vacuo*. The residue was redissolved in water (20 mL) and 1 M aqueous hydrochloric acid was added until pH 3. The acidified aqueous phase was extracted with dichloromethane (3 × 20 mL), and the combined organic extracts were dried over magnesium sulfate, filtered and concentrated *in vacuo*. Carboxylic acid **3.56b** (100 mg, 0.80 mmol) was afforded in quantitative yield as a light brown amorphous solid and used in the next step without further purification.

Analytical data observed were as in accordance with literature values.[191]

^{1}H NMR (400 MHz, chloroform-*d*) δ 12.00 (1H, br s, -COOH), 7.26 (1H, d, *J* = 2.0 Hz, furan-H), 6.69 (1H, d, *J* = 2.0 Hz, furan-H), 2.61 (3H, s, -CH_3). ^{13}C NMR (101 MHz, chloroform-*d*) δ

169.9 (-C[a]OOH), 161.4 (furan-C), 141.1 (furan-CH), 113.3 (furan-C), 111.4 (furan-CH), 77.7, 14.4 (-CH_3).

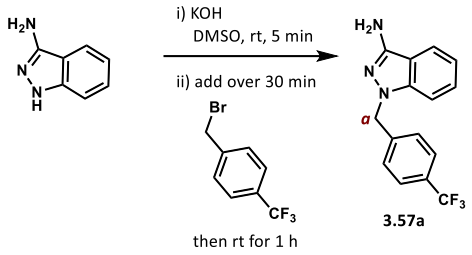

3.57a: To a stirred solution of potassium hydroxide (210 mg, 3.8 mmol, 2 equiv) in dimethylsulfoxide (5 mL, 0.4 M) was 1*H*-indazol-3-amine (250 mg, 1.9 mmol, 1 equiv) and the resulting solution was stirred at room temperature for 5 minutes. 4-(trifluoromethyl)benzyl bromide (450 mg, 1.9 mmol, 1 equiv) in dimethylsulfoxide (2.5 mL, 0.25 M total concentration) was added dropwise over 30 min, and the resulting solution was stirred for 1 hour. The reaction mixture was poured into ice water (20 mL) and the aqueous phase was extracted with dichloromethane (3 × 20 mL). The combined organic extracts were washed with water (2 × 40 mL) and brine (40 mL), dried over magnesium sulfate, filtered and concentrated *in vacuo*. Purification by column chromatography on silica gel with an eluent of 50% to 100% ethyl acetate in petroleum ether afforded alkylated indazole **3.57a** (380 mg, 1.3 mmol, 69%) as a brown oily solid.

Analytical data observed were as in accordance with literature values.[64]

^{1}H NMR (400 MHz, chloroform-*d*) δ 7.60 – 7.56 (1H, m, indazole-H), 7.56 – 7.51 (2H, m, 2 × Ar-H), 7.34 (1H, ddd, *J* = 8.5, 6.9, 1.1 Hz, indazole-H), 7.30 – 7.25 (2H, m, 2 × Ar-H), 7.21 – 7.15 (1H, m, indazole-H), 7.06 (1H, ddd, *J* = 7.9, 6.9, 0.8 Hz, indazole-H), 5.41 (2H, s, -C**H$_2$**[a]), 4.09 (2H, br s, -NH_2). ^{13}C NMR (101 MHz, chloroform-*d*) δ 147.9 (indazole-C), 141.6 (indazole-C), 141.3 (Ar-C), 130.1 (d, $^2J_{C\text{-}F}$ = 32.4 Hz, Ar-C), 128.0 (indazole-CH), 127.5 (2 × Ar-CH), 125.8 (d, $^3J_{C\text{-}F}$ = 3.8 Hz, 2 × Ar-CH), 124.1 (d, $^1J_{C\text{-}F}$ = 272.0 Hz, -CF_3), 120.1 (indazole-CH), 119.5 (indazole-CH), 115.0 (indazole-C), 108.9 (indazole-CH), 77.4, 51.7 (-C**H$_2$**[a]).

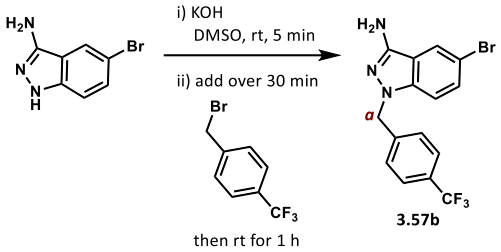

3.57b: To a stirred solution of potassium hydroxide (400 mg, 7.1 mmol, 2 equiv) in dimethylsulfoxide (9 mL) was 5-bromo-1*H*-indazol-3-amine (750 mg, 3.5 mmol, 1 equiv) and the resulting solution was stirred at room temperature for 5 minutes. 4-(trifluoromethyl)benzyl bromide (850 mg, 3.5 mmol, 1 equiv) in dimethylsulfoxide (5 mL, 0.25 M total concentration) was added dropwise over 30 min, and the resulting solution was stirred for 1 hour. The reaction mixture was poured into ice water (40 mL) and the aqueous phase was extracted with dichloromethane (3 × 40 mL). The combined organic extracts were washed with water (2 × 80 mL) and brine (80 mL), dried over magnesium sulfate, filtered and concentrated *in vacuo*. Purification by column chromatography on silica gel with an eluent of 20% to 50% ethyl acetate in petroleum ether afforded alkylated indazole **3.57b** (1.0 g, 2.7 mmol, 76%) as an orange oily solid.

^{1}H NMR (400 MHz, chloroform-*d*) δ 7.71 (1H, dd, *J* = 1.8, 0.7 Hz, indazole-H), 7.59 – 7.51 (2H, m, 2 × Ar-H), 7.39 (1H, dd, *J* = 8.8, 1.8 Hz, indazole-H), 7.26 – 7.21 (2H, m, 2 × Ar-H), 7.06 (1H, dd, *J* = 8.9, 0.7 Hz, indazole-H), 5.38 (2H, s, -C**H$_2$**^{a}), 4.06 (2H, br s, -NH$_2$). ^{13}C NMR (101 MHz, chloroform-*d*) δ 147.1 (indazole-C), 141.2 (Ar-C), 140.2 (indazole-C), 130.5 (indazole-CH), 130.1 (d, $^{2}J_{C\text{-}F}$ = 32.4 Hz, Ar-C), 127.4 (2 × Ar-CH), 125.9 (d, $^{3}J_{C\text{-}F}$ = 3.9 Hz, 2 × Ar-CH), 124.1 (d, $^{1}J_{C\text{-}F}$ = 272.1 Hz, -CF$_3$), 122.5 (indazole-CH), 116.7 (indazole-C-Br), 111.8 (indazole-C), 110.3 (indazole-CH), 51.9 (-C**H$_2$**^{a}). HRMS (ESI) exact mass calculated for $C_{15}H_{12}N_3F_3Br$ $[M+H]^+$ m/z 370.0161, found m/z 370.0157. LCMS (ESI) mass calculated for $C_{15}H_{12}N_3F_3Br$ $[M+H]^+$ m/z 370.02, found m/z 369.78 with t_R = 6.54 min.

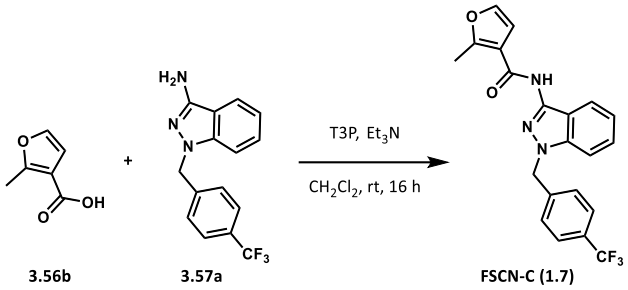

FSCN-C (1.7): To a stirred solution of acid **3.56a** (24 mg, 0.19 mmol, 1.1 equiv), amine **3.57a** (50 mg, 0.17 mmol, 1 equiv) and triethylamine (71 µL, 0.51 mmol, 3 equiv) in dichloromethane (3.4 mL, 0.05 M) was added propanephosphonic acid anhydride (50% in ethyl acetate, 0.21 ml, 0.34 mmol, 2 equiv). The resulting solution was stirred at room temperature for 16 hours before removing volatile components *in vacuo*. Purification by column chromatography on silica gel with an eluent of 30% to 50% ethyl acetate in petroleum ether afforded the product (21 mg, 0.053 mmol, 30%) as a yellow oil. Further purification by semi-preparative RP-HPLC using a focused gradient across 50% and 90% acetonitrile in water over 30 minutes eluted the title compound at t_R = 25 minutes (85% acetonitrile) and the product fraction was lyophilised, yielding fascin ligand C **FSCN-C (1.7)** (8 mg, 0.02 mmol, 12%) as a white fluffy powder.

Analytical data observed were as in accordance with literature values.[64]

^{1}H NMR (500 MHz, methanol-d_4) δ 7.84 – 7.77 (1H, m, indazole-H), 7.63 – 7.56 (2H, m, 2 × Ar-H), 7.54 – 7.48 (1H, m, indazole-H), 7.45 (1H, d, J = 2.1 Hz, furan-H), 7.44 – 7.37 (3H, m, 2 × Ar-H & indazole-H), 7.17 (1H, ddd, J = 7.9, 6.8, 0.8 Hz, indazole-H), 6.94 (1H, s, furan-H), 5.68 (2H, s, -CH_2), 2.61 (3H, s, -CH_3). ^{13}C NMR (126 MHz, methanol-d_4) δ 165.4 (-CONH), 159.7 (furan-C), 143.2 (indazole-C), 142.4 (indazole-C), 142.0 (furan-CH), 140.8 (Ar-C), 130.9 (d, $^2J_{C\text{-}F}$ = 32.2 Hz, Ar-C), 128.9 (2 × Ar-CH), 128.5 (indazole-CH), 126.7 (indazole-C), 126.6 (d, $^3J_{C\text{-}F}$ = 3.8 Hz, 2 × Ar-CH), 124.5 (indazole-CH), 123.0 (indazole-CH), 121.8 (indazole-CH), 118.1 (d, $^1J_{C\text{-}F}$ = 410.0 Hz, -CF_3), 110.5 (furan-CH), 110.1 (furan-C), 52.7 (-CH_2), 13.7 (-CH_3). HRMS (ESI) exact mass calculated for $C_{21}H_{16}N_3F_3O_2Na$ $[M+Na]^+$ m/z 422.1087, found m/z 422.1088. LCMS (ESI) mass calculated for $C_{21}H_{17}N_3F_3O_2$ $[M+H]^+$ m/z 400.13, found m/z 400.08 with t_R = 6.65 min.

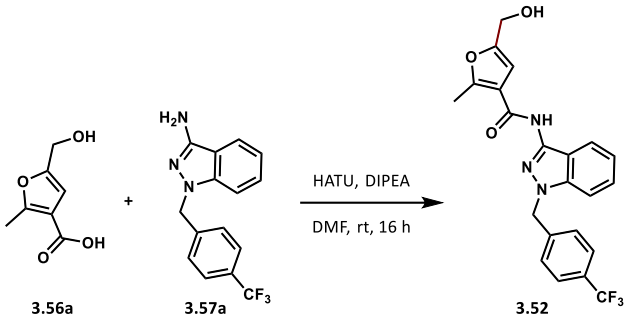

3.52: To a pre-stirred solution of carboxylic acid **3.56a** (30 mg, 0.17 mmol, 1 equiv), HATU (65 mg, 0.17 mmol, 1 equiv) and *N,N*-diisopropylethylamine (91 µL, 0.17 mmol, 3 equiv) in *N,N*-dimethylformamide (0.6 mL, 0.3 M) was added amine **3.57a** (50 mg, 0.17 mmol, 1 equiv), and the resulting solution was stirred at room temperature for 16 hours. The reaction mixture was partitioned between dichloromethane (20 mL) and water (20 mL), and the aqueous phase was extracted with dichloromethane (5 × 20 mL). The combined organic phases were washed with 5% aqueous lithium chloride (3 × 40 mL), dried over magnesium sulfate, filtered and concentrated *in vacuo*. Purification by column chromatography on silica gel with an eluent of 50% to 100% ethyl acetate in petroleum ether afforded functionalised fascin ligand C **3.52** (32 mg, 0.074 mmol, 43%) as a light brown amorphous solid.

^{1}H NMR (400 MHz, chloroform-*d*) δ 8.51 (1H, br s, -NH), 8.11 – 8.02 (1H, m, indazole-H), 7.52 – 7.45 (2H, m, 2 × Ar-H), 7.39 (1H, ddd, *J* = 8.1, 6.9, 1.1 Hz, indazole-H), 7.29 – 7.23 (1H, m, indazole-H), 7.22 – 7.18 (2H, m, 2 × Ar-H), 7.18 – 7.14 (1H, m, indazole-H), 6.46 (1H, s, furan-H), 5.49 (2H, s, -CH_2), 4.50 (2H, s, -CH_2), 2.76 (1H, br s, 1H), 2.60 (3H, s, -CH_3). ^{13}C NMR (101 MHz, chloroform-*d*) δ 171.36 (-CONH), 162.0 (indazole-C), 158.8 (furan-C), 152.4 (furan-C), 141.4 (indazole-C), 140.3 (Ar-C), 130.3 (d, $^{2}J_{C\text{-}F}$ = 32.7 Hz, Ar-C), 127.9 (indazole-CH), 127.4 (indazole-CH), 125.9 (d, $^{3}J_{C\text{-}F}$ = 3.8 Hz, 2 × Ar-CH), 124.0 (d, $^{1}J_{C\text{-}F}$ = 278.0 Hz, -CF_3), 123.9 (indazole-CH), 121.0 (indazole-CH), 117.3 (indazole-C), 115.7 (furan-C), 108.9 (2 × Ar-CH), 106.4 (furan-CH), 57.2 (-CH_2), 52.0 (-CH_2), 13.9 (-CH_3). HRMS (ESI) exact mass calculated for $C_{22}H_{18}N_3F_3O_3Na$ $[M+Na]^+$ m/z 452.1192, found m/z 452.1197. LCMS (ESI) mass calculated for $C_{22}H_{19}N_3F_3O_3$ $[M+H]^+$ m/z 430.14, found m/z 430.14 with t_R = 6.21 min.

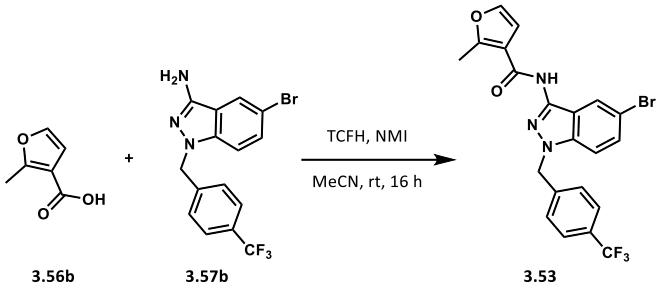

3.56b 3.57b 3.53

3.53: To a stirred solution of carboxylic acid **3.56b** (26 mg, 0.21 mmol, 1 equiv), amine **3.57a** (100 mg, 0.27 mmol, 1 equiv) and *N*-methylimidazole (58 µL, 0.72 mmol, 3.5 equiv) in acetonitrile (0.7 mL, 0.4 M) was added chloro-*N,N,N′,N′*-tetramethylformamidinium hexafluorophosphate (69 mg, 0.25 mmol, 1.2 equiv). The resulting solution was stirred at room temperature for 16 hours before removing volatile components *in vacuo*. Purification by column chromatography on silica gel with an eluent of 20% to 100% ethyl acetate in petroleum ether afforded functionalised fascin ligand C **3.53** (21 mg, 0.21 mmol) in quantitative yield as an orange amorphous solid.

^{1}H NMR (400 MHz, chloroform-*d*) δ 8.31 (1H, d, *J* = 1.8 Hz, indazole-H), 8.23 (1H, br s, -NH), 7.58 – 7.47 (2H, m, 2 × Ar-H), 7.44 (1H, dd, *J* = 8.9, 1.9 Hz, indazole-H), 7.29 (1H, d, *J* = 2.1 Hz, furan-H), 7.25 – 7.18 (2H, m, 2 × Ar-H), 7.14 (1H, dd, *J* = 8.9, 0.7 Hz, indazole-H), 6.59 (1H, d, *J* = 2.1 Hz, furan-H), 5.47 (2H, s, -CH_2), 2.67 (3H, s, -CH_3). ^{13}C NMR (101 MHz, chloroform-*d*) δ 161.9 (-CONH), 159.0 (furan-C), 140.9 (furan-CH), 140.3 (indazole-C), 140.1 (indazole-C), 139.7 (Ar-C), 131.0 (indazole-CH), 130.5 (d, $^{2}J_{C\text{-}F}$ = 32.6 Hz, Ar-C), 127.4 (2 × Ar-CH), 126.6 (indazole-CH), 126.0 (d, $^{3}J_{C\text{-}F}$ = 3.8 Hz, 2 × Ar-CH), 124.0 (d, $^{1}J_{C\text{-}F}$ = 272.2 Hz, -CF_3), 118.6 (indazole-C), 114.9 (indazole-C), 113.9 (indazole-CH), 110.3 (furan-C), 108.5 (furan-CH), 52.3 (-CH_2), 13.9 (-CH_3). HRMS (ESI) exact mass calculated for $C_{21}H_{15}N_3F_3O_2BrNa$ $[M+Na]^+$ m/z 500.0192, found m/z 500.0195. LCMS (ESI) mass calculated for $C_{21}H_{16}N_3F_3O_2BrNa$ $[M+H]^+$ m/z 479.04, found m/z 479.92 with t_R = 7.08 min.

Preparation of 3rd series PROTAC

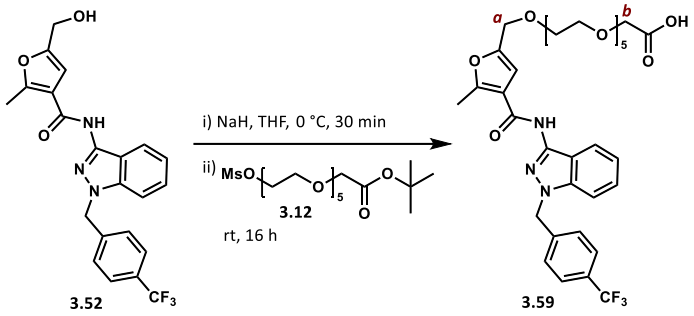

3.59: To a dry flask charged with argon was added anhydrous tetrahydrofuran (0.3 mL, 0.4 M), functionalised fascin ligand C **3.52** (50 mg, 0.12 mmol, 1 equiv) and sodium hydride (60% in mineral oil, 28 mg, 0.70 mmol, 6 equiv) at 0 °C. The resulting suspension was stirred for 30 minutes before mesylated linker **3.12** (50 mg, 0.12 mmol, 1 equiv) was added slowly at 0 °C. The reaction mixture was allowed to reach room temperature and stirred for further 16 hours. The reaction was quenched by dropwise addition of water (10 mL). The aqueous phase was extracted with dichloromethane (3 × 10 mL) and the combined organic extracts were washed with brine (20 mL), dried over magnesium sulfate, filtered and concentrated *in vacuo*. Purification by column chromatography on silica gel with an eluent of 50% to 100% ethanol in ethyl acetate afforded fragment **3.59** (23 mg, 0.033 mmol, 28%) as a light yellow oil.

^{1}H NMR (400 MHz, chloroform-*d*) δ 9.63 (1H, s, -NH), 8.07 (1H, d, *J* = 8.2 Hz, indazole-H), 7.56 – 7.46 (2H, m, 2 × Ar-H), 7.33 (1H, ddd, *J* = 8.2, 6.9, 1.1 Hz, indazole-H), 7.26 – 7.23 (2H, m, 2× Ar-H), 7.20 (1H, d, *J* = 8.5 Hz, indazole-H), 7.16 – 7.08 (1H, m, indazole-H), 6.95 (1H, s, furan-H), 5.53 (2H, s, -CH_2), 4.47 (2H, s, -C**H$_2$**^{a}), 3.88 (2H, s, -C**H$_2$**^{b}), 3.69 – 3.51 (20H, m, 10 × -CH_2), 2.63 (3H, s, -CH_3). ^{13}C NMR (101 MHz, chloroform-*d*) δ 175.1 (-COOH), 170.1 (-CONH), 162.4 (indazole-C), 158.7 (furan-C), 149.4 (furan-C), 141.2 (indazole-C), 140.6 (Ar-C), 130.1 (d, $^{2}J_{C\text{-}F}$ = 32.5 Hz, Ar-C), 127.5 (2 × indazole-CH), 125.8 (d, $^{3}J_{C\text{-}F}$ = 3.9 Hz, 2 × Ar-CH), 124.6 (d, $^{1}J_{C\text{-}F}$ = 271.5 Hz, -CF_3), 123.7 (indazole-CH), 120.6 (indazole-CH), 117.8 (indazole-C), 116.4 (furan-C), 109.2 (furan-C), 108.8 (2 × Ar-CH), 71.0 (-**C^{b}**H_2), 70.0 (-CH_2), 69.8 (-CH_2), 69.6 (2 × -CH_2), 69.5 (2 × -CH_2), 69.4 (-CH_2), 69.3 (-CH_2), 69.2 (-CH_2), 68.9 (-CH_2), 64.9 (-**C^{a}**H_2), 52.1 (-CH_2), 13.9 (-CH_3). HRMS (ESI) exact mass calculated for $C_{34}H_{41}N_3F_3O_{10}$ $[M+H]^+$ m/z 708.2739, found m/z 708.2730. LCMS (ESI) mass calculated for $C_{34}H_{41}N_3F_3O_{10}$ $[M+H]^+$ m/z 708.27, found m/z 708.75 with t_R = 6.27 min.

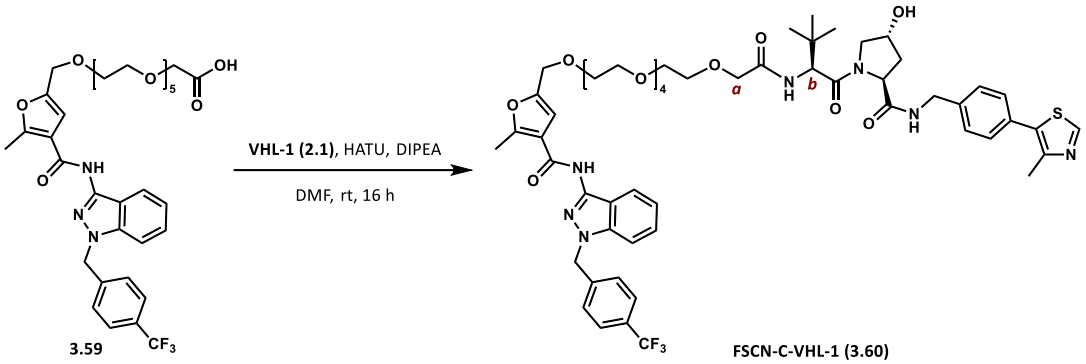

FSCN-C-VHL-1 (3.60): To a pre-stirred solution of carboxylic acid **3.59** (18 mg, 0.025 mmol, 1 equiv), HATU (10 mg, 0.025 mmol, 1 equiv) and *N,N*-diisopropylethylamine (14 µL, 0.070 mmol, 3 equiv) in *N,N*-dimethylformamide (0.1 mL, 0.3 M) was added amine **VHL-1 (2.1)** (11 mg, 0.025 mmol, 1 equiv), and the resulting solution was stirred at room temperature for 16 hours. The reaction mixture was partitioned between dichloromethane (20 mL) and water (20 mL), and the aqueous phase was extracted with dichloromethane (5 × 20 mL). The combined organic phases were washed with 5% aqueous lithium chloride (5 × 40 mL), dried over magnesium sulfate, filtered and concentrated *in vacuo*. Purification by column chromatography on silica gel with an eluent of 5% to 50% ethanol in dichloromethane afforded the product (17 mg, 0.015 mmol, 61%) as a clear oil. Further purification by semi-preparative RP-HPLC using a focused gradient across 50% and 90% acetonitrile in water over 30 minutes eluted the title compound at t_R = 17 minutes (74% acetonitrile) and the product fraction was lyophilised, yielding fascin ligand C VHL PROTAC **FSCN-C-VHL-1 (3.60)** (9 mg, 0.008 mmol, 32%) as a white fluffy powder.

^{1}H NMR (500 MHz, methanol-d_4) δ 9.08 (1H, s, thiazole-H), 7.83 – 7.78 (1H, m, indazole-H), 7.62 – 7.56 (2H, m, 2 × Ar-H), 7.53 – 7.36 (8H, 6 × Ar-CH & 2 × indazole-CH), 7.16 (1H, ddd, *J* = 8.3, 6.9, 0.9 Hz, indazole-H), 6.89 (1H, s, furan-H), 5.68 (2H, s, -CH_2), 4.69 (1H, m, -C**H**$^{\mathbf{b}}$), 4.61 – 4.50 (2H, m, -CH_2), 4.51 – 4.45 (3H, m, -C*H*OH & -CH_2), 4.37 – 4.30 (1H, m, -CH), 4.08 – 3.96 (2H, m, -C**H**$_2^{\mathbf{a}}$), 3.89 – 3.75 (2H, m, -CH_2), 3.71 – 3.56 (20H, m, 10 × -CH_2), 2.60 (3H, s, -CH_3), 2.48 (3H, s, -CH_3), 2.25 – 2.18 (1H, m, -C*H*H), 2.12 – 2.02 (1H, m, -CH*H*), 1.03 (9H, s, 3 × -CH_3). ^{13}C NMR (101 MHz, methanol-d_4) δ 174.4 (-CONH), 172.1 (-CONR), 171.6 (-CONH), 165.1 (-CONH), 159.9 (indazole-C), 153.0 (thiazole-CH), 151.4 (furan-C), 148.8 (furan-C), 143.2 (thiazole-C), 142.5 (indazole-C), 140.8 (Ar-C), 140.3 (Ar-C), 131.4 (thiazole-C), 130.9 (d, $^2J_{C\text{-}F}$ = 32.0 Hz, Ar-C), 130.7 (Ar-C), 130.4 (indazole-CH), 129.5 (d, $^1J_{C\text{-}F}$ = 261.5 Hz, -CF_3), 129.0 (2 × Ar-CH), 128.9 (2 × Ar-CH), 128.5 (indazole-C), 126.6 (d, $^3J_{C\text{-}F}$ = 3.8 Hz, 2 × Ar-CH), 123.1 (indazole-CH), 121.8 (indazole-CH), 119.6 (indazole-C), 117.1 (furan-C), 110.5 (furan-CH), 109.8 (2 × Ar-CH), 72.3 (-C$^{\mathbf{a}}$H$_2$), 71.6 (-CH_2), 71.6 (-CH_2), 71.6 (2 × -CH_2), 71.5 (2 × -CH_2),

71.5 (2 × -CH_2), 71.1 (-CHOH), 71.1 (-CH_2), 70.5 (-CH_2), 65.6 (-CH_2), 60.8 (-**C[b]**H), 58.1 (-CH_2), 52.7 (-CH), 43.7 (-CH_2), 40.4 (-*C*(CH_3)$_3$), 38.9 (-CH_2), 37.1 (-CH_2), 27.0 (3 × -CH_3), 15.7 (-CH_3), 13.9 (-CH_3). HRMS (ESI) exact mass calculated for $C_{56}H_{69}N_7F_3O_{12}$ $[M+H]^+$ m/z 1120.4672, found m/z 1120.4669. LCMS (ESI) mass calculated for $C_{56}H_{69}N_7F_3O_{12}$ $[M+H]^+$ m/z 1120.47, found m/z 1120.89 with t_R = 6.46 min.

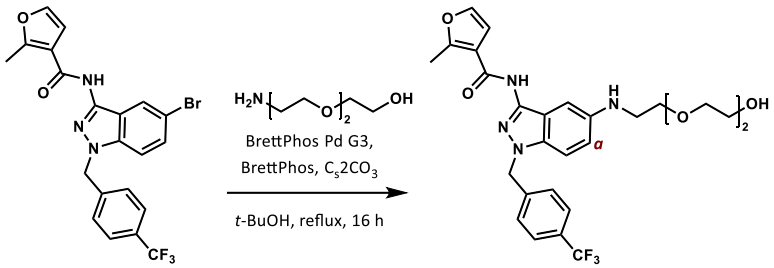

3.53 3.61c

3.61c: To a dry flask charged with argon was added *tert*-butanol (0.6 mL, 0.2 M), functionalised fascin ligand B **3.53** (60 mg, 0.13 mmol, 1 equiv), 2-[2-(2-aminoethoxy)ethoxy]-ethanol (21 µL, 0.16 mmol, 1.2 equiv), BrettPhos Pd G3 (6 mg, 0.007 mmol, 5 mol%), BrettPhos (4 mg, 0.007 mmol, 5 mol%) and caesium carbonate (110 mg, 0.31 mmol, 2.4 equiv), and flask was evacuated and filled with argon three times. The reaction was stirred for 24 hours under reflux before allowing it to reach room temperature. The reaction mixture was partitioned between water (10 mL) and dichloromethane (10 mL), and the aqueous phase was extracted with dichloromethane (3 × 10 mL). The combined organic extracts were washed with brine (20 mL), dried over magnesium sulfate, filtered and concentrated *in vacuo*. Purification by column chromatography on silica gel with an eluent of 0% to 5% ethanol in dichloromethane afforded fragment **3.61c** (14 mg, 0.026 mmol, 21%) as a light yellow oil.

^{1}H NMR (400 MHz, chloroform-*d*) δ 8.86 (1H, s, -NH), 8.19 (1H, s, -NH), 8.06 (1H, dd, *J* = 9.0, 1.6 Hz, indazole-C**H[a]**), 7.62 – 7.49 (2H, m, 2 × Ar-CH), 7.38 – 7.27 (5H, m, 2 × Ar-CH & 2 × indazole-CH & furan-CH), 6.63 (1H, d, *J* = 2.1 Hz, furan-CH), 5.54 (2H, s, -CH_2), 3.85 – 3.60 (12H, m, 6 × -CH_2), 2.67 (3H, s, -CH_3). ^{13}C NMR (101 MHz, chloroform-*d*) δ 173.7 (-CONH), 158.4 (furan-C), 142.9 (Ar-C), 141.1 (indazole-C), 140.7 (furan-CH), 138.7 (Ar-C), 136.7 (Ar-**C[a]**H), 130.1 (d, $^2J_{C\text{-}F}$ = 32.5 Hz, Ar-C), 127.4 (2 × Ar-CH), 125.8 (d, $^3J_{C\text{-}F}$ = 3.8 Hz, 2 × Ar-CH), 125.5 (d, $^1J_{C\text{-}F}$ = 279.2 Hz, -CF_3), 120.0 (indazole-CH), 118.5 (furan-C), 115.4 (indazole-C), 109.8 (furan-CH), 108.7 (indazole-CH), 101.9 (indazole-C), 72.8 (-CH_2), 70.7 (-CH_2), 70.6 (-CH_2), 70.4 (-CH_2), 69.6 (-CH_2), 61.8 (-CH_2), 52.2 (-CH_2), 13.8 (-CH_3). HRMS (ESI) exact mass calculated for $C_{27}H_{30}N_3F_3N_4O_5$ $[M+H]^+$ m/z 547.2163, found m/z 547.2171. LCMS (ESI) mass calculated for $C_{27}H_{30}N_3F_3N_4O_5$ $[M+H]^+$ m/z 547.22, found m/z 547.08 with t_R = 6.09 min.

References

1 Roser, M. *Causes of death globally: What do people die from?*, <https://ourworldindata.org/causes-of-death-treemap> (2021).

2 World Health Organisation. *Global Health Estimates 2020: Deaths by Cause, Age, Sex, by Country and by Region*, <https://www.who.int/data/gho/data/themes/mortality-and-global-health-estimates/ghe-leading-causes-of-death> (2020).

3 Hanahan, D. & Weinberg, R. A. Hallmarks of Cancer: The Next Generation. *Cell* **144**, 646-674 (2011).

4 GLOBOCAN. *Leading Cancer Types in 2020*, <https://infogram.com/globocan-2020-1h9j6qg7xdp8v4g?live> (2022).

5 Sasieni, P. D., Shelton, J., Ormiston-Smith, N., Thomson, C. S. & Silcocks, P. B. What is the lifetime risk of developing cancer?: the effect of adjusting for multiple primaries. *Br J Cancer* **105** (2011).

6 Cancer Research UK. *Cancer survival statistics for all cancers combined*, <https://www.cancerresearchuk.org/health-professional/cancer-statistics/survival/all-cancers-combined> (2015).

7 Seyfried, T. N. & Huysentruyt, L. C. On the origin of cancer metastasis. *Crit Rev Oncog* **18**, 43-73 (2013).

8 Eccles, S. A. & Welch, D. R. Metastasis: recent discoveries and novel treatment strategies. *The Lancet* **369**, 1742-1757 (2007).

9 Guan, X. Cancer metastases: challenges and opportunities. *Acta Pharm Sin B* **5**, 402-418 (2015).

10 Lambert, A. W., Pattabiraman, D. R. & Weinberg, R. A. Emerging Biological Principles of Metastasis. *Cell* **168**, 670-691 (2017).

11 Ganesh, K. & Massagué, J. Targeting metastatic cancer. *Nat Med* **27**, 34-44 (2021).

12 Meirson, T., Gil-Henn, H. & Samson, A. O. Invasion and metastasis: the elusive hallmark of cancer. *Oncogene* **39**, 2024-2026 (2020).

13 Anderson, R. L. *et al.* A framework for the development of effective anti-metastatic agents. *Nat Rev Clin Oncol* **16**, 185-204 (2019).

14 Fernandes, M., Rosel, D. & Brábek, J. Translation in solid cancer: are size-based response criteria an anachronism? *Clin Transl Oncol* **17** (2015).

15 Gandalovicova, A. *et al.* Migrastatics-Anti-metastatic and Anti-invasion Drugs: Promises and Challenges. *Trends Cancer* **3**, 391-406 (2017).

16 Tarin, D. Cell and tissue interactions in carcinogenesis and metastasis and their clinical significance. *Semin Cancer Biol* **21**, 72-82 (2011).

17 Fidler, I. J. The pathogenesis of cancer metastasis: the 'seed and soil' hypothesis revisited. *Nat Rev Cancer* **3**, 453-458 (2003).

18 Fontebasso, Y. & Dubinett, S. M. Drug Development for Metastasis Prevention. *Crit Rev Oncog* **20**, 449-473 (2015).

19 Alizadeh, A. M., Shiri, S. & Farsinejad, S. Metastasis review: from bench to bedside. *Tumour Biol* **35**, 8483-8523 (2014).

20 Kuriyama, S. & Mayor, R. Molecular analysis of neural crest migration. *Philos Trans R Soc Lond B Biol Sci* **363**, 1349-1362 (2008).

21 Madri, J. A. & Graesser, D. Cell migration in the immune system: the evolving inter-related roles of adhesion molecules and proteinases. *Dev Immunol* **7**, 103-116 (2000).

22 Chang, H. Y. *et al.* Gene Expression Signature of Fibroblast Serum Response Predicts Human Cancer Progression: Similarities between Tumors and Wounds. *PLOS Biol* **2**, e7 (2004).

23 Olson, M. F. & Sahai, E. The actin cytoskeleton in cancer cell motility. *Clin Exp Metastas* **26**, 273-287 (2008).

24 Ridley, Anne J. Life at the Leading Edge. *Cell* **145**, 1012-1022 (2011).

25 Machesky, L. M. Lamellipodia and filopodia in metastasis and invasion. *FEBS Letters* **582**, 2102-2111 (2008).

26 Mattila, P. K. & Lappalainen, P. Filopodia: molecular architecture and cellular functions. *Nat Rev Mol Cell Biol* **9**, 446-454 (2008).

27 Vignjevic, D. *et al.* Role of fascin in filopodial protrusion. *J Cell Biol* **174**, 863-875 (2006).

28 Alblazi, K. M. & Siar, C. H. Cellular protrusions--lamellipodia, filopodia, invadopodia and podosomes--and their roles in progression of orofacial tumours: current understanding. *Asian Pac J Cancer Prev* **16**, 2187-2191 (2015).

29 Li, A. *et al.* The Actin-Bundling Protein Fascin Stabilizes Actin in Invadopodia and Potentiates Protrusive Invasion. *Curr Biol* **20**, 339-345 (2010).

30 Deryugina, E. I. & Quigley, J. P. in *Extracellular Matrix Degradation* (eds William C. Parks & Robert P. Mecham), 145-191 (2011).

31 Wu, J.-S. *et al.* Plasticity of cancer cell invasion: Patterns and mechanisms. *Transl Onc* **14**, 100899 (2021).

32 Friedl, P. & Wolf, K. Tumour-cell invasion and migration: diversity and escape mechanisms. *Nat Rev Cancer* **3**, 362-374 (2003).

33 Wyckoff, J. B., Pinner, S. E., Gschmeissner, S., Condeelis, J. S. & Sahai, E. ROCK- and Myosin-Dependent Matrix Deformation Enables Protease-Independent Tumor-Cell Invasion In Vivo. *Curr Biol* **16**, 1515-1523 (2006).

34 Wolf, K. *et al.* Compensation mechanism in tumor cell migration: mesenchymal-amoeboid transition after blocking of pericellular proteolysis. *J Cell Biol* **160**, 267-277 (2003).

35 Eddy, R. J., Weidmann, M. D., Sharma, V. P. & Condeelis, J. S. Tumor Cell Invadopodia: Invasive Protrusions that Orchestrate Metastasis. *Trends Cell Biol* **27**, 595-607 (2017).

36 Paz, H., Pathak, N. & Yang, J. Invading one step at a time: the role of invadopodia in tumor metastasis. *Oncogene* **33**, 4193-4202 (2014).

37 Meirson, T. & Gil-Henn, H. Targeting invadopodia for blocking breast cancer metastasis. *Drug Resist Updat* **39**, 1-17 (2018).

38 Ramos-García, P. *et al.* An update of knowledge on cortactin as a metastatic driver and potential therapeutic target in oral squamous cell carcinoma. *Oral Dis* **25**, 949-971 (2019).

39 Revach, O. Y. & Geiger, B. The interplay between the proteolytic, invasive, and adhesive domains of invadopodia and their roles in cancer invasion. *Cell Adh Migr* **8**, 215-225 (2014).

40 Luo, Y. *et al.* Invadopodia: A potential target for pancreatic cancer therapy. *Crit Rev Oncol Hematol* **159**, 103236 (2021).

41 Vandenbroucke, R. E. & Libert, C. Is there new hope for therapeutic matrix metalloproteinase inhibition? *Nat Rev Drug Discov* **13**, 904-927 (2014).

42 Li, A. *et al.* Fascin is regulated by slug, promotes progression of pancreatic cancer in mice, and is associated with patient outcomes. *Gastroenterology* **146**, 1386-1396 (2014).

43 Yamashiro, S., Yamakita, Y., Ono, S. & Matsumura, F. Fascin, an actin-bundling protein, induces membrane protrusions and increases cell motility of epithelial cells. *Mol Biol Cell* **9**, 993-1006 (1998).

44 Hashimoto, Y., Kim, D. J. & Adams, J. C. The roles of fascins in health and disease. *J Pathol* **224**, 289-300 (2011).

45 Tan, V. Y., Lewis, S. J., Adams, J. C. & Martin, R. M. Association of fascin-1 with mortality, disease progression and metastasis in carcinomas: a systematic review and meta-analysis. *BMC Medicine* **11**, 52 (2013).

46 Villari, G. *et al.* A direct interaction between fascin and microtubules contributes to adhesion dynamics and cell migration. *J Cell Sci* **128**, 4601-4614 (2015).

47 Yang, S. *et al.* Molecular Mechanism of Fascin Function in Filopodial Formation. *J Biol Chem* **288**, 274-284 (2013).

48 Lin, S. *et al.* Monoubiquitination Inhibits the Actin Bundling Activity of Fascin. *J Biol Chem* **291**, 27323-27333 (2016).

49 Mattila, P. K. & Lappalainen, P. Filopodia: molecular architecture and cellular functions. *Nat Rev Mol Cell Biol* **9**, 446-454 (2008).

50 Jayo, A. & Parsons, M. Fascin: a key regulator of cytoskeletal dynamics. *Int J Biochem Cell Biol* **42**, 1614-1617 (2010).

51 Machesky, L. M. & Li, A. Fascin. *Commun Integr Biol* **3**, 263-270 (2010).

52 Zou, J. *et al.* Prognostic significance of fascin-1 and E-cadherin expression in laryngeal squamous cell carcinoma. *Eur J Cancer Prev* **19**, 11-17 (2010).

53 Shan, D. *et al.* Synthetic analogues of migrastatin that inhibit mammary tumor metastasis in mice. *PNAS* **102**, 3772 (2005).

54 Chen, L., Yang, S., Jakoncic, J., Zhang, J. J. & Huang, X.-Y. Migrastatin analogues target fascin to block tumour metastasis. *Nature* **464**, 1062-1066 (2010).

55 Nagorny, P. *et al.* Confirmation of the structures of synthetic derivatives of migrastatin in the light of recently disclosed crystallographically based claims. *Tetrahedron Lett* **51**, 3873-3875 (2010).

56 Lo Re, D. *et al.* Synthesis of Migrastatin Analogues as Inhibitors of Tumour Cell Migration: Exploring Structural Change in and on the Macrocyclic Ring. *Chem Eur J* **21**, 18109-18121 (2015).

57 Majchrzak, K. *et al.* Migrastatin Analogues Inhibit Canine Mammary Cancer Cell Migration and Invasion. *PLOS ONE* **8**, e76789 (2013).

58 Croft, D. *et al.* Abstract A113: A fragment-based approach towards the identification of small molecule inhibitors of fascin 1. *Mol Cancer Ther* **14**, A113 (2015).

59 Francis, S. *et al.* Structure-based design, synthesis and biological evaluation of a novel series of isoquinolone and pyrazolo[4,3-c]pyridine inhibitors of fascin 1 as potential anti-metastatic agents. *Bioorg Med Chem Lett* **29**, 1023-1029 (2019).

60 Huang, X.-Y. & Shue, C. Y. Methods for Inhibiting Fascin. (2014).

61 Croft, D. *et al. Unpublished work* (Drug Discovery Unit, Beatson Institute of Cancer Research, 2019).

62 Huang, F. K. *et al.* Targeted inhibition of fascin function blocks tumour invasion and metastatic colonization. *Nat Commun* **6**, 7465 (2015).

63 Han, S. *et al.* Improving fascin inhibitors to block tumor cell migration and metastasis. *Mol Oncol* **10**, 966-980 (2016).

64 Huang, J. *et al.* Structural Insights into the Induced-fit Inhibition of Fascin by a Small-Molecule Inhibitor. *J Mol Biol* **430**, 1324-1335 (2018).

65 Wang, Y., Zhang, J. J. & Huang, X.-Y. Anti-Metastasis Fascin Inhibitors Decrease the Growth of Specific Subtypes of Cancers. *Cancers* **12** (2020).

66 Wang, Y. *et al.* Fascin inhibitor increases intratumoral dendritic cell activation and anti-cancer immunity. *Cell Rep* **35**, 108948 (2021).

67 Alburquerque-González, B. *et al.* The FDA-Approved Antiviral Raltegravir Inhibits Fascin1-Dependent Invasion of Colorectal Tumor Cells In Vitro and In Vivo. *Cancers* **13** (2021).

68 Alburquerque-González, B. *et al.* New role of the antidepressant imipramine as a Fascin1 inhibitor in colorectal cancer cells. *Exp Mol Med* **52**, 281-292 (2020).

69 Scott, D. E., Bayly, A. R., Abell, C. & Skidmore, J. Small molecules, big targets: drug discovery faces the protein–protein interaction challenge. *Nat Rev Drug Discov* **15** (2016).

70 Ivanov, A. A., Khuri, F. R. & Fu, H. Targeting protein-protein interactions as an anticancer strategy. *Trends Pharmacol Sci* **34**, 393-400 (2013).

71 Nevola, L. & Giralt, E. Modulating protein–protein interactions: the potential of peptides. *Chem Commun* **51**, 3302-3315 (2015).

72 Lu, H. *et al.* Recent advances in the development of protein–protein interactions modulators: mechanisms and clinical trials. *Sig Transduc Target Ther* **5**, 213 (2020).

73 Neklesa, T. K., Winkler, J. D. & Crews, C. M. Targeted protein degradation by PROTACs. *Pharmacol Ther* **174**, 138-144 (2017).

74 He, Y. *et al.* Proteolysis targeting chimeras (PROTACs) are emerging therapeutics for hematologic malignancies. *J Hematol Oncol* **13**, 103 (2020).

75 Ocaña, A. & Pandiella, A. Proteolysis targeting chimeras (PROTACs) in cancer therapy. *J Exp Clin Cancer Res* **39**, 189 (2020).

76 Arvinas. The Discovery of ARV-110, a first in class androgen receptor degrading PROTAC for the treatment of men with metastatic castration resistant prostate cancer. *American Association for Cancer Research Annual Meeting* (2021).

77 Arvinas. The Discovery of ARV-471, an Orally Bioavailable Estrogen Receptor Degrading PROTAC for the Treatment of Patients with Breast Cancer. *American Association for Cancer Research Annual Meeting* (2021).

78 Hines, J., Gough, J. D., Corson, T. W. & Crews, C. M. Posttranslational protein knockdown coupled to receptor tyrosine kinase activation with phosphoPROTACs. *PNAS* **110**, 8942 (2013).

79 Dölle, A. *et al.* Design, Synthesis, and Evaluation of WD-Repeat-Containing Protein 5 (WDR5) Degraders. *J Med Chem* **64**, 10682-10710 (2021).

80 Pohl, C. & Dikic, I. Cellular quality control by the ubiquitin-proteasome system and autophagy. *Science* **366**, 818-822 (2019).

81 Ballabio, A. & Bonifacino, J. S. Lysosomes as dynamic regulators of cell and organismal homeostasis. *Nat Rev Mol Cell Biol* **21**, 101-118 (2020).

82 Pagan, J., Seto, T., Pagano, M. & Cittadini, A. Role of the Ubiquitin Proteasome System in the Heart. *Circ Res* **112**, 1046-1058 (2013).

83 Schrader, E. K., Harstad, K. G. & Matouschek, A. Targeting proteins for degradation. *Nat Chem Biol* **5**, 815-822 (2009).

84 Zheng, N. & Shabek, N. Ubiquitin Ligases: Structure, Function, and Regulation. *Annu Rev Biochem* **86**, 129-157 (2017).

85 Bondeson, D. P. & Crews, C. M. Targeted Protein Degradation by Small Molecules. *Ann Rev Pharmacol* **57**, 107-123 (2017).

86 Dong, G., Ding, Y., He, S. & Sheng, C. Molecular Glues for Targeted Protein Degradation: From Serendipity to Rational Discovery. *J Med Chem* **64**, 10606-10620 (2021).

87 Toure, M. & Crews, C. M. Small-Molecule PROTACS: New Approaches to Protein Degradation. *Angew Chem Int Ed Engl* **55**, 1966-1973 (2016).

88 Lai, A. C. & Crews, C. M. Induced protein degradation: an emerging drug discovery paradigm. *Nat Rev Drug Discov* **16**, 101-114 (2017).

89 An, S. & Fu, L. Small-molecule PROTACs: An emerging and promising approach for the development of targeted therapy drugs. *EBioMedicine* **36**, 553-562 (2018).

90 Cromm, P. M. & Crews, C. M. Targeted Protein Degradation: from Chemical Biology to Drug Discovery. *Cell Chem Biol* **24**, 1181-1190 (2017).

91 Smith, B. E. *et al.* Differential PROTAC substrate specificity dictated by orientation of recruited E3 ligase. *Nat Commun* **10**, 131 (2019).

92 Jaime-Figueroa, S., Buhimschi, A. D., Toure, M., Hines, J. & Crews, C. M. Design, synthesis and biological evaluation of Proteolysis Targeting Chimeras (PROTACs) as a BTK degraders with improved pharmacokinetic properties. *Bioorg Med Chem Lett* **30**, 126877 (2020).

93 Clague, M. J., Heride, C. & Urbe, S. The demographics of the ubiquitin system. *Trends Cell Biol* **25**, 417-426 (2015).

94 Edmondson, S. D., Yang, B. & Fallan, C. Proteolysis targeting chimeras (PROTACs) in 'beyond rule-of-five' chemical space: Recent progress and future challenges. *Bioorg Med Chem Lett* **29**, 1555-1564 (2019).

95 Bricelj, A., Steinebach, C., Kuchta, R., Gütschow, M. & Sosič, I. E3 Ligase Ligands in Successful PROTACs: An Overview of Syntheses and Linker Attachment Points. *Front Chem* **9** (2021).

96 Ishida, T. & Ciulli, A. E3 Ligase Ligands for PROTACs: How They Were Found and How to Discover New Ones. *SLAS discov* **26**, 484-502 (2021).

97 Lai, A. C. *et al.* Modular PROTAC Design for the Degradation of Oncogenic BCR-ABL. *Angew Chem Int Ed Engl* **55**, 807-810 (2016).

98 Crew, A. P. *et al.* Identification and Characterization of Von Hippel-Lindau-Recruiting Proteolysis Targeting Chimeras (PROTACs) of TANK-Binding Kinase 1. *J Med Chem* **61**, 583-598 (2018).

99 Lu, J. *et al.* Hijacking the E3 Ubiquitin Ligase Cereblon to Efficiently Target BRD4. *Chem Biol* **22**, 755-763 (2015).

100 Maple, H. J., Clayden, N., Baron, A., Stacey, C. & Felix, R. Developing degraders: principles and perspectives on design and chemical space. *Med Chem Comm* **10**, 1755-1764 (2019).

101 Buckley, D. L. *et al.* Targeting the von Hippel–Lindau E3 Ubiquitin Ligase Using Small Molecules To Disrupt the VHL/HIF-1α Interaction. *J Am Chem Soc* **134**, 4465-4468 (2012).

102 Galdeano, C. *et al.* Structure-guided design and optimization of small molecules targeting the protein-protein interaction between the von Hippel-Lindau (VHL) E3 ubiquitin ligase and the hypoxia inducible factor (HIF) alpha subunit with in vitro nanomolar affinities. *J Med Chem* **57**, 8657-8663 (2014).

103 Buckley, D. L. *et al.* HaloPROTACS: Use of Small Molecule PROTACs to Induce Degradation of HaloTag Fusion Proteins. *ACS Chem Biol* **10**, 1831-1837 (2015).

104 Zoppi, V. *et al.* Iterative Design and Optimization of Initially Inactive Proteolysis Targeting Chimeras (PROTACs) Identify VZ185 as a Potent, Fast, and Selective von Hippel–Lindau (VHL) Based Dual Degrader Probe of BRD9 and BRD7. *J Med Chem* **62**, 699-726 (2019).

105 Farnaby, W. *et al.* BAF complex vulnerabilities in cancer demonstrated via structure-based PROTAC design. *Nat Chem Biol* **15**, 672-680 (2019).

106 Frost, J. *et al.* Potent and selective chemical probe of hypoxic signalling downstream of HIF-α hydroxylation via VHL inhibition. *Nat Commun* **7**, 13312 (2016).

107 Soares, P. *et al.* Group-Based Optimization of Potent and Cell-Active Inhibitors of the von Hippel–Lindau (VHL) E3 Ubiquitin Ligase: Structure–Activity Relationships Leading to the Chemical Probe (2S,4R)-1-((S)-2-(1-Cyanocyclopropanecarboxamido)-3,3-dimethylbutanoyl)-4-hydroxy-N-(4-(4-methylthiazol-5-yl)benzyl)pyrrolidine-2-carboxamide (VH298). *J Med Chem* **61**, 599-618 (2018).

108 Ito, T. *et al.* Identification of a Primary Target of Thalidomide Teratogenicity. *Science* **327**, 1345-1350 (2010).

109 Tokunaga, E., Yamamoto, T., Ito, E. & Shibata, N. Understanding the Thalidomide Chirality in Biological Processes by the Self-disproportionation of Enantiomers. *Sci Rep* **8**, 17131 (2018).

110 Knoche, B. & Blaschke, G. Investigations on the in vitro racemization of thalidomide by high-performance liquid chromatography. *J Chromatogr A* **666**, 235-240 (1994).

111 Fischer, E. S. *et al.* Structure of the DDB1-CRBN E3 ubiquitin ligase in complex with thalidomide. *Nature* **512**, 49-53 (2014).

112 Mori, T. *et al.* Structural basis of thalidomide enantiomer binding to cereblon. *Sci Rep* **8**, 1294 (2018).

113 Min, J. *et al.* Phenyl-Glutarimides: Alternative Cereblon Binders for the Design of PROTACs. *Angew Chem Int Ed* **60**, 26663-26670 (2021).

114 Zhou, B. *et al.* Discovery of a Small-Molecule Degrader of Bromodomain and Extra-Terminal (BET) Proteins with Picomolar Cellular Potencies and Capable of Achieving Tumor Regression. *J Med Chem* **61**, 462-481 (2018).

115 Brand, M. *et al.* Homolog-Selective Degradation as a Strategy to Probe the Function of CDK6 in AML. *Cell Chem Biol* **26**, 300-306.e309 (2019).

116 Fischer, E. S. *et al.* The molecular basis of CRL4DDB2/CSA ubiquitin ligase architecture, targeting, and activation. *Cell* **147**, 1024-1039 (2011).

117 Tae, H. S. *et al.* Identification of hydrophobic tags for the degradation of stabilized proteins. *Chembiochem* **13**, 538-541 (2012).

118 Gustafson, J. L. *et al.* Small-Molecule-Mediated Degradation of the Androgen Receptor through Hydrophobic Tagging. *Angew Chem Int Ed Engl* **54**, 9659-9662 (2015).

119 Zengerle, M., Chan, K.-H. & Ciulli, A. Selective Small Molecule Induced Degradation of the BET Bromodomain Protein BRD4. *ACS Chem Biol* **10**, 1770-1777 (2015).

120 Bondeson, D. P. *et al.* Lessons in PROTAC Design from Selective Degradation with a Promiscuous Warhead. *Cell Chem Biol* **25**, 78-87.e75 (2018).

121 Roy, R. D., Rosenmund, C. & Stefan, M. I. Cooperative binding mitigates the high-dose hook effect. *BMC Syst Biol* **11**, 74 (2017).

122 Hughes, Scott J. & Ciulli, A. Molecular recognition of ternary complexes: a new dimension in the structure-guided design of chemical degraders. *Essays Biochem* **61** (2017).

123 Troup, R. I., Fallan, C. & Baud, M. G. J. Current strategies for the design of PROTAC linkers: a critical review. *Explor Target Antitumor Ther* **1**, 273-312 (2020).

124 Zorba, A. *et al.* Delineating the role of cooperativity in the design of potent PROTACs for BTK. *PNAS* **115**, E7285 (2018).

125 Cyrus, K. *et al.* Impact of linker length on the activity of PROTACs. *Mol Biosyst* **7**, 359-364 (2011).

126 Han, X. *et al.* Discovery of Highly Potent and Efficient PROTAC Degraders of Androgen Receptor (AR) by Employing Weak Binding Affinity VHL E3 Ligase Ligands. *J Med Chem* **62**, 11218-11231 (2019).

127 Webster, R. *et al.* PEGylated Proteins: Evaluation of Their Safety in the Absence of Definitive Metabolism Studies. *Drug Metabo Dispos* **35**, 9 (2007).

128 Chessum, N. E. A. *et al.* Demonstrating In-Cell Target Engagement Using a Pirin Protein Degradation Probe (CCT367766). *J Med Chem* **61**, 918-933 (2018).

129 Mares, A. *et al.* Extended pharmacodynamic responses observed upon PROTAC-mediated degradation of RIPK2. *Commun Biol* **3**, 140 (2020).

130 Veber, D. F. *et al.* Molecular Properties That Influence the Oral Bioavailability of Drug Candidates. *J Med Chem* **45**, 2615-2623 (2002).

131 Rossi Sebastiano, M. *et al.* Impact of Dynamically Exposed Polarity on Permeability and Solubility of Chameleonic Drugs Beyond the Rule of 5. *J Med Chem* **61**, 4189-4202 (2018).

132 Whitty, A., Viarengo, L. A. & Zhong, M. Progress towards the broad use of non-peptide synthetic macrocycles in drug discovery. *Org Biomol Chem* **15**, 7729-7735 (2017).

133 Lipinski, C. A., Lombardo, F., Dominy, B. W. & Feeney, P. J. Experimental and computational approaches to estimate solubility and permeability in drug discovery and development settings. *Adv Drug Deliv Rev* **23**, 3-25 (1997).

134 Poongavanam, V., Doak, B. C. & Kihlberg, J. Opportunities and guidelines for discovery of orally absorbed drugs in beyond rule of 5 space. *Curr Opin Chem Biol* **44**, 23-29 (2018).

135 Doak, Bradley C., Over, B., Giordanetto, F. & Kihlberg, J. Oral Druggable Space beyond the Rule of 5: Insights from Drugs and Clinical Candidates. *Chem Biol* **21**, 1115-1142 (2014).

136 Mullard, A. Targeted protein degraders crowd into the clinic. *Nat Rev Drug Discov* **20**, 247-250 (2021).

137 Tovell, H. *et al.* Rapid and Reversible Knockdown of Endogenously Tagged Endosomal Proteins via an Optimized HaloPROTAC Degrader. *ACS Chem Biol* **14**, 882-892 (2019).

138 Neklesa, T. K. *et al.* Small-molecule hydrophobic tagging–induced degradation of HaloTag fusion proteins. *Nat Chem Biol* **7**, 538-543 (2011).

139 Yesbolatova, A., Tominari, Y. & Kanemaki, M. T. Ligand-induced genetic degradation as a tool for target validation. *Drug Discov Today Technol* **31**, 91-98 (2019).

140 Janssen, D. B. Evolving haloalkane dehalogenases. *Curr Opin Chem Biol* **8**, 150-159 (2004).

141 Los, G. V. *et al.* HaloTag: A Novel Protein Labeling Technology for Cell Imaging and Protein Analysis. *ACS Chem Biol* **3**, 373-382 (2008).

142 England, C. G., Luo, H. & Cai, W. HaloTag Technology: A Versatile Platform for Biomedical Applications. *Bioconjugate Chem* **26**, 975-986 (2015).

143 Bond, M. J., Chu, L., Nalawansha, D. A., Li, K. & Crews, C. M. Targeted Degradation of Oncogenic KRASG12C by VHL-Recruiting PROTACs. *ACS Cent Sci* **6**, 1367-1375 (2020).

144 Micovic, V. & Mihailovic, M. The Reduction of Acid Amides with Lithium Aluminum Hydride. *J Org Chem* **18**, 1190-1200 (1953).

145 Cangi, A. S. *Improving HaloPROTAC efficacy through enhanced VHL binding* (BSc thesis) University of Glasgow (2020).

146 Subirós-Funosas, R., Prohens, R., Barbas, R., El-Faham, A. & Albericio, F. Oxyma: An Efficient Additive for Peptide Synthesis to Replace the Benzotriazole-Based HOBt and HOAt with a Lower Risk of Explosion. *Chem Eur J* **15**, 9394-9403 (2009).

147 Cheng, J., Li, Y., Wang, X., Dong, G. & Sheng, C. Discovery of Novel PDEδ Degraders for the Treatment of KRAS Mutant Colorectal Cancer. *J Med Chem* **63**, 7892-7905 (2020).

148 Galstyan, A., Kauscher, U., Block, D., Ravoo, B. J. & Strassert, C. A. Silicon(IV) Phthalocyanine-Decorated Cyclodextrin Vesicles as a Self-Assembled Phototherapeutic Agent against MRSA. *ACS Appl Mater Interfaces* **8**, 12631-12637 (2016).

149 Brodie, G. *Bactacs: A Chemical Tool for Targeted Protein Degradation within Bacteria* (PhD thesis) University of Glasgow (2020).

150 Fuller, W. & Gallen, E. *Unpublished work* (University of Glasgow).

151 Ohana, R. F. *et al.* HaloTag7: A genetically engineered tag that enhances bacterial expression of soluble proteins and improves protein purification. *Protein Expr Purif* **68**, 110-120 (2009).

152 Berrow, N. S. *et al.* A versatile ligation-independent cloning method suitable for high-throughput expression screening applications. *Nucleic Acids Res* **35**, e45-e45 (2007).

153 Noblejas-López, M. d. M. *et al.* Activity of BET-proteolysis targeting chimeric (PROTAC) compounds in triple negative breast cancer. *J Exp Clin Cancer Res* **38**, 383 (2019).

154 Sun Joo, P., and You Jin, J., lt, Sup & gt. Dieckol from Ecklonia cava Suppresses the Migration and Invasion of HT1080 Cells by Inhibiting the Focal Adhesion Kinase Pathway Downstream of Rac1-ROS Signaling. *Mol Cells* **33**, 141-149 (2012).

155 Fisher, K. E. *et al.* Tumor cell invasion of collagen matrices requires coordinate lipid agonist-induced G-protein and membrane-type matrix metalloproteinase-1-dependent signaling. *Mol Cancer* **5**, 69 (2006).

156 Khan, S. *et al.* A selective BCL-XL PROTAC degrader achieves safe and potent antitumor activity. *Nat Med* **25**, 1938-1947 (2019).

157 Schapira, M., Calabrese, M. F., Bullock, A. N. & Crews, C. M. Targeted protein degradation: expanding the toolbox. *Nat Rev Drug Discov* **18**, 949-963 (2019).

158 Peraro, L. *et al.* Cell Penetration Profiling Using the Chloroalkane Penetration Assay. *J Am Chem Soc* **140**, 11360-11369 (2018).

159 Gill, D. R., Pringle, I. A. & Hyde, S. C. Progress and Prospects: The design and production of plasmid vectors. *Gene Ther* **16**, 165-171 (2009).

160 Collins, I., Wang, H., Caldwell, J. J. & Chopra, R. Chemical approaches to targeted protein degradation through modulation of the ubiquitin–proteasome pathway. *Biochem J* **474**, 1127-1147 (2017).

161 Harer, S. L., Bhatia, M. S. & Bhatia, N. M. Proteasome inhibitors mechanism; source for design of newer therapeutic agents. *J Antibiot* **65**, 279-288 (2012).

162 Kisselev, A. F. & Goldberg, A. L. Proteasome inhibitors: from research tools to drug candidates. *Chem Biol* **8**, 739-758 (2001).

163 Adams, J. The proteasome: structure, function, and role in the cell. *Cancer Treat Rev* **29**, 3-9 (2003).

164 Laganà, A. *et al.* in *RNA Bioinformatics* (ed Ernesto Picardi), 393-412 (Springer New York, 2015).

165 Morita, E., Arii, J., Christensen, D., Votteler, J. & Sundquist, W. I. Attenuated protein expression vectors for use in siRNA rescue experiments. *Biotechniques* **0**, 1-5 (2012).

166 Jonkman, J. E. N. *et al.* An introduction to the wound healing assay using live-cell microscopy. *Cell Adh Migr* **8**, 440-451 (2014).

167 Grada, A., Otero-Vinas, M., Prieto-Castrillo, F., Obagi, Z. & Falanga, V. Research Techniques Made Simple: Analysis of Collective Cell Migration Using the Wound Healing Assay. *J Invest Dermatol* **137**, e11-e16 (2017).

168 Unbekandt, M. *et al.* A novel small-molecule MRCK inhibitor blocks cancer cell invasion. *Cell Commun Signal* **12**, 54 (2014).

169 Kleinman, H. K., Kim, K. & Kang, H. Matrigel uses in cell biology and for the identification of thymosin β4, a mediator of tissue regeneration. *Appl Biol Chem* **61**, 703-708 (2018).

170 Westermann, L., Neubauer, B. & Köttgen, M. Nobel Prize 2020 in Chemistry honors CRISPR: a tool for rewriting the code of life. *Eur J Physiol* **473**, 1-2 (2021).

171 Jinek, M. *et al.* A Programmable Dual-RNA–Guided DNA Endonuclease in Adaptive Bacterial Immunity. *Science* **337**, 816-821 (2012).

172 Listgarten, J. *et al.* Prediction of off-target activities for the end-to-end design of CRISPR guide RNAs. *Nat Biomed Eng* **2**, 38-47 (2018).

173 Adli, M. The CRISPR tool kit for genome editing and beyond. *Nat Commun* **9**, 1911 (2018).

174 Mohr, S. E. *et al.* CRISPR guide RNA design for research applications. *FEBS J* **283**, 3232-3238 (2016).

175 Lino, C. A., Harper, J. C., Carney, J. P. & Timlin, J. A. Delivering CRISPR: a review of the challenges and approaches. *Drug deliv* **25**, 1234-1257 (2018).

176 Ran, F. A. *et al.* Genome engineering using the CRISPR-Cas9 system. *Nat Protoc* **8**, 2281-2308 (2013).

177 Blayney, J. *et al.* Unexpectedly High Levels of Inverted Re-Insertions Using Paired sgRNAs for Genomic Deletions. *Methods and Protocols* **3** (2020).

178 Single, A., Beetham, H., Telford, B., Guilford, P. & Chen, A. A Comparison of Real-Time and Endpoint Cell Viability Assays for Improved Synthetic Lethal Drug Validation. *J Biomol Screen* **20** (2015).

179 Petrie, R. J., Doyle, A. D. & Yamada, K. M. Random versus directionally persistent cell migration. *Nat Rev Mol Cell Biol* **10**, 538-549 (2009).

180 Fishman, D. A. *et al.* Metastatic Dissemination of Human Ovarian Epithelial Carcinoma Is Promoted by α2β1-Integrin-Mediated Interaction with Type I Collagen. *Invasion Metastasis* **18**, 15-26 (1998).

181 Burleson, K. M., Hansen, L. K. & Skubitz, A. P. N. Ovarian carcinoma spheroids disaggregate on type I collagen and invade live human mesothelial cell monolayers. *Clin Exp Metastasis* **21**, 685-697 (2005).

182 Hallas-Potts, A., Dawson, J. C. & Herrington, C. S. Ovarian cancer cell lines derived from non-serous carcinomas migrate and invade more aggressively than those derived from high-grade serous carcinomas. *Sci Rep* **9**, 5515 (2019).

183 Sodek, K. L., Brown, T. J. & Ringuette, M. J. Collagen I but not Matrigel matrices provide an MMP-dependent barrier to ovarian cancer cell penetration. *BMC Cancer* **8**, 223 (2008).

184 Daina, A., Michielin, O. & Zoete, V. SwissADME: a free web tool to evaluate pharmacokinetics, drug-likeness and medicinal chemistry friendliness of small molecules. *Sci Rep* **7**, 42717 (2017).

185 Fisher, S. L. & Phillips, A. J. Targeted protein degradation and the enzymology of degraders. *Curr Opin Chem Biol* **44**, 47-55 (2018).

186 Croft, D. *et al. Unpublished work* (Drug Discovery Unit, Beatson Institute of Cancer Research, 2019).

187 Bolin, D. R. *et al.* Diacylglycerol Acyltransferase Inhibitors. United States patent (2012).

188 Wurz, R. P. *et al.* A "Click Chemistry Platform" for the Rapid Synthesis of Bispecific Molecules for Inducing Protein Degradation. *J Med Chem* **61**, 453-461 (2018).

189 Grošelj, U. *et al.* Synthesis of 1,5-disubstituted-4-oxo-4,5-dihydro-1H-pyrazolo[4,3-c]pyridine-7-carboxamides. *Tetrahedron* **71**, 109-123 (2015).

190 Fandrick, D. R. *et al.* A Michael Equilibration Model To Control Site Selectivity in the Condensation toward Aminopyrazoles. *Org Lett* **17**, 2964-2967 (2015).

191 Hashmi, A. S. K. *et al.* Gold Catalysis: Dihydroisobenzofurans and Isochromanes by the Intramolecular Furan/Alkyne Reaction. *Adv Synth Catal* **348**, 2501-2508 (2006).

192 Ghosh, A. K. & Shahabi, D. Synthesis of amide derivatives for electron deficient amines and functionalized carboxylic acids using EDC and DMAP and a catalytic amount of HOBt as the coupling reagents. *Tetrahedron Lett* **63**, 152719 (2021).

193 Sabatini Marco, T., Boulton Lee, T. & Sheppard Tom, D. Borate esters: Simple catalysts for the sustainable synthesis of complex amides. *Sci Adv* **3**, e1701028 (2017).

194 Lanigan, R. M., Starkov, P. & Sheppard, T. D. Direct Synthesis of Amides from Carboxylic Acids and Amines Using $B(OCH_2CF_3)_3$. *J Org Chem* **78**, 4512-4523 (2013).

195 Beutner, G. L. *et al.* TCFH–NMI: Direct Access to N-Acyl Imidazoliums for Challenging Amide Bond Formations. *Org Lett* **20**, 4218-4222 (2018).

196 Kwong, F. Y., Klapars, A. & Buchwald, S. L. Copper-Catalyzed Coupling of Alkylamines and Aryl Iodides: An Efficient System Even in an Air Atmosphere. *Org Lett* **4**, 581-584 (2002).

197 Lang, F., Zewge, D., Houpis, I. N. & Volante, R. P. Amination of aryl halides using copper catalysis. *Tetrahedron Lett* **42**, 3251-3254 (2001).

198 Surry, D. S. & Buchwald, S. L. Dialkylbiaryl phosphines in Pd-catalyzed amination: a user's guide. *Chem Sci* **2**, 27-50 (2011).

199 Fors, B. P., Davis, N. R. & Buchwald, S. L. An Efficient Process for Pd-Catalyzed C–N Cross-Coupling Reactions of Aryl Iodides: Insight Into Controlling Factors. *J Am Chem Soc* **131**, 5766-5768 (2009).

200 Maiti, D., Fors, B. P., Henderson, J. L., Nakamura, Y. & Buchwald, S. L. Palladium-catalyzed coupling of functionalized primary and secondary amines with aryl and heteroaryl halides: two ligands suffice in most cases. *Chem Sci* **2**, 57-68 (2011).

201 Stauffer, S. R. & Steinbeiser, M. A. Pd-catalyzed amination in a polar medium: rate enhancement, convenient product isolation, and tandem Suzuki cross-coupling. *Tetrahedron Lett* **46**, 2571-2575 (2005).

202 Moreau, K. *et al.* Proteolysis-targeting chimeras in drug development: A safety perspective. *Br J Pharmacol* **177**, 1709-1718 (2020).

203 Dai, C.-L. *et al.* Inhibition of Protein Synthesis Alters Protein Degradation through Activation of Protein Kinase B (AKT). *J Biol Chem* **288**, 23875-23883 (2013).

204 Schneider-Poetsch, T. *et al.* Inhibition of eukaryotic translation elongation by cycloheximide and lactimidomycin. *Nat Chem Biol* **6**, 209-217 (2010).

205 Zhou, P. in *Signal Transduction Protocols Methods in Molecular Biology* (eds Robert C. Dickson & Michael D. Mendenhall) 67-77 (Humana Press, 2004).

206 Park, Y. *et al.* Versatile Synthetic Route to Cycloheximide and Analogues That Potently Inhibit Translation Elongation. *Angew Chem Int Ed* **58**, 5387-5391 (2019).

207 Hubatsch, I., Ragnarsson, E. G. E. & Artursson, P. Determination of drug permeability and prediction of drug absorption in Caco-2 monolayers. *Nat Protoc* **2**, 2111-2119 (2007).

208 Wang, Z., Hop, C. E. C. A., Leung, K. H. & Pang, J. Determination of in vitro permeability of drug candidates through a Caco-2 cell monolayer by liquid chromatography/tandem mass spectrometry. *J Mass Spectrom* **35**, 71-76 (2000).

209 Jin, X. *et al.* Comparison of MDCK-MDR1 and Caco-2 cell based permeability assays for anti-malarial drug screening and drug investigations. *J Pharmacol Toxicol Methods* **70**, 188-194 (2014).

210 Colletti, L. M. *et al.* Methods to measure the intracellular concentration of unlabeled compounds within cultured cells using liquid chromatography/tandem mass spectrometry. *Anal Biochem* **383**, 186-193 (2008).

211 Riching, K. M. *et al.* Quantitative Live-Cell Kinetic Degradation and Mechanistic Profiling of PROTAC Mode of Action. *ACS Chem Biol* **13**, 2758-2770 (2018).

212 Schulz, I. in *Meth Enzymol* Vol. 192, 280-300 (Academic Press, 1990).

213 Gomperts, B. D. & Fernandez, J. M. Techniques for membrane permeabilization. *Trends Biochem Sci* **10**, 414-417 (1985).

214 Stewart, M. P. *et al.* In vitro and ex vivo strategies for intracellular delivery. *Nature* **538**, 183-192 (2016).

215 Jaroszeski, M. J. *et al.* Toxicity of anticancer agents mediated by electroporation in vitro. *Anticancer Drugs* **11**, 201-208 (2000).

216 Gehl, J. Electroporation: theory and methods, perspectives for drug delivery, gene therapy and research. *Acta Physiol Scand* **177**, 437-447 (2003).

217 Esmaeili, N. & Friebe, M. Electrochemotherapy: A Review of Current Status, Alternative IGP Approaches, and Future Perspectives. *J Healthc Eng* **2019**, 2784516 (2019).

218 Michie, J., Janssens, D., Cilliers, J., Smit, B. J. & Böhm, L. Assessment of electroporation by flow cytometry. *Cytometry* **41**, 96-101 (2000).

219 Chênais, N. *et al.* Nuclear import of Xenopus egg extract components into cultured cells for reprogramming purposes: a case study on goldfish fin cells. *Sci Rep* **9**, 2861 (2019).

220 Chae, P. S. *et al.* A New Class of Amphiphiles Bearing Rigid Hydrophobic Groups for Solubilization and Stabilization of Membrane Proteins. *Chem Eur J* **18**, 9485-9490 (2012).

221 Walev, I. *et al.* Delivery of proteins into living cells by reversible membrane permeabilization with streptolysin-O. *Proc Natl Acad Sci U.S.A* **98**, 3185-3190 (2001).

222 Babiychuk, E. B., Monastyrskaya, K., Potez, S. & Draeger, A. Intracellular Ca2+ operates a switch between repair and lysis of streptolysin O-perforated cells. *Cell Death Differ* **16**, 1126-1134 (2009).

223 Geelen, M. J. H. The use of digitonin-permeabilized mammalian cells for measuring enzyme activities in the course of studies on lipid metabolism. *Anal Biochem* **347**, 1-9 (2005).

224 Ehsan, M. *et al.* Steroid-Based Amphiphiles for Membrane Protein Study: The Importance of Alkyl Spacers for Protein Stability. *ChemBioChem* **19**, 1433-1443 (2018).

225 Wesche, J. & Olsnes, S. in *Cell Biology* (ed Julio E. Celis) Ch. 3, 19-22 (Academic Press, 2006).

226 Miyamoto, K. *et al.* Reversible Membrane Permeabilization of Mammalian Cells Treated with Digitonin and Its Use for Inducing Nuclear Reprogramming by Xenopus Egg Extracts. *Cloning Stem Cells* **10**, 535-542 (2008).

227 Valera, E., Dargusch, R., Maher, P. A. & Schubert, D. Modulation of 5-Lipoxygenase in Proteotoxicity and Alzheimer's Disease. *Journal Neurosci* **33**, 10512 (2013).

228 Zhao, Q., Liu, L. & Xie, Q. in *Plant Signalling Networks: Methods and Protocols* (eds Zhi-Yong Wang & Zhenbiao Yang), 163-172 (Humana Press, 2012).

229 Zeng, M. *et al.* Exploring Targeted Degradation Strategy for Oncogenic $KRAS^{G12C}$. *Cell Chem Biol* **27**, 19-31.e16 (2020).

230 Wang, X. *et al.* New strategy for renal fibrosis: Targeting Smad3 proteins for ubiquitination and degradation. *Biochem Pharmacol* **116**, 200-209 (2016).

231 Sakamoto, K. M. *et al.* Protacs: Chimeric molecules that target proteins to the Skp1–Cullin–F box complex for ubiquitination and degradation. *Proc Natl Acad Sci U S A* **98**, 8554 (2001).

232 Long, Marcus J. C., Gollapalli, Deviprasad R. & Hedstrom, L. Inhibitor Mediated Protein Degradation. *Cell Chem Biol* **19**, 629-637 (2012).

233 Maher, P. Proteasome Assay in Cell Lysates. *Bio Protoc* **4**, e1028 (2014).

234 Patching, S. G. Surface plasmon resonance spectroscopy for characterisation of membrane protein–ligand interactions and its potential for drug discovery. *BBA-Biomembranes* **1838**, 43-55 (2014).

235 Corzo, J. Time, the forgotten dimension of ligand binding teaching. *Biochem Mol Biol Educ* **34**, 413-416 (2006).

236 Yu, X. & Machesky, L. M. Cells Assemble Invadopodia-Like Structures and Invade into Matrigel in a Matrix Metalloprotease Dependent Manner in the Circular Invasion Assay. *PLOS ONE* **7**, e30605 (2012).

237 Roy, M. J. *et al.* SPR-Measured Dissociation Kinetics of PROTAC Ternary Complexes Influence Target Degradation Rate. *ACS Chem Biol* **14**, 361-368 (2019).

238 Law, R. P. *et al.* Discovery and Characterisation of Highly Cooperative FAK-Degrading PROTACs. *Angew Chem Int Ed* **60**, 23327-23334 (2021).

239 Liu, X. *et al.* Assays and technologies for developing proteolysis targeting chimera degraders. *Future Med Chem* **12**, 1155-1179 (2020).

240 Erb, M. A. *et al.* Transcription control by the ENL YEATS domain in acute leukaemia. *Nature* **543**, 270-274 (2017).

241 Huang, H. T. *et al.* A Chemoproteomic Approach to Query the Degradable Kinome Using a Multi-kinase Degrader. *Cell Chem Biol* **25**, 88-99 (2018).

242 Di, L. & Kerns, E. H. Profiling drug-like properties in discovery research. *Curr Opin Chem Biol* **7**, 402-408 (2003).

243 Kansy, M., Avdeef, A. & Fischer, H. Advances in screening for membrane permeability: high-resolution PAMPA for medicinal chemists. *Drug Discov Today Technol* **1**, 349-355 (2004).

244 Berben, P. *et al.* Drug permeability profiling using cell-free permeation tools: Overview and applications. *Eur J Pharm Sci* **119**, 219-233 (2018).

245 Cecchini, C., Pannilunghi, S., Tardy, S. & Scapozza, L. From Conception to Development: Investigating PROTACs Features for Improved Cell Permeability and Successful Protein Degradation. *Front Chem* **9** (2021).

246 Zhang, X. *et al.* Protein targeting chimeric molecules specific for bromodomain and extra-terminal motif family proteins are active against pre-clinical models of multiple myeloma. *Leukemia* **32**, 2224-2239 (2018).

247 Vlahov, I. R. & Leamon, C. P. Engineering Folate–Drug Conjugates to Target Cancer: From Chemistry to Clinic. *Bioconjugate Chem* **23**, 1357-1369 (2012).

248 Zhang, R., Qin, X., Kong, F., Chen, P. & Pan, G. Improving cellular uptake of therapeutic entities through interaction with components of cell membrane. *Drug Deliv* **26**, 328-342 (2019).

249 Calvaresi, E. C. & Hergenrother, P. J. Glucose conjugation for the specific targeting and treatment of cancer. *Chem Sci* **4**, 2319-2333 (2013).

250 Liu, J. *et al.* Cancer Selective Target Degradation by Folate-Caged PROTACs. *J Am Chem Soc* **143**, 7380-7387 (2021).

251 Chen, H., Liu, J., Kaniskan, H. Ü., Wei, W. & Jin, J. Folate-Guided Protein Degradation by Immunomodulatory Imide Drug-Based Molecular Glues and Proteolysis Targeting Chimeras. *J Med Chem* **64**, 12273-12285 (2021).

252 Pillow, T. H. *et al.* Antibody Conjugation of a Chimeric BET Degrader Enables in vivo Activity. *ChemMedChem* **15**, 17-25 (2020).

253 Dragovich, P. S. *et al.* Antibody-mediated delivery of chimeric protein degraders which target estrogen receptor alpha (ERα). *Bioorg Med Chem Lett* **30**, 126907 (2020).

254 He, M. *et al.* A traceless linker for aliphatic amines that rapidly and quantitatively fragments after reduction. *Chem Sci* **11**, 8973-8980 (2020).

255 Yang, K. S., Budin, G., Tassa, C., Kister, O. & Weissleder, R. Bioorthogonal Approach to Identify Unsuspected Drug Targets in Live Cells. *Angew Chem Int Edit* **52**, 10593-10597 (2013).

256 Danjou, P.-E., Wallyn, D., Cazier-Dennin, F. & Delattre, F. Ultrasound-promoted tosylation of oligo(ethylene glycols). *Ultrason Sonochem* **19**, 1201-1204 (2012).

257 Choi, H., Shirley, H. J., Hume, P. A., Brimble, M. A. & Furkert, D. P. Unexpected Direct Synthesis of N-Vinyl Amides through Vinyl Azide–Enolate [3+2] Cycloaddition. *Angew Chem Int Edit* **56**, 7420-7424 (2017).

258 Baškovč, J., Bevk, D., Stanovnik, B. & Svete, J. Bis-enaminone Based Parallel Solution-Phase Synthesis of 1,4-Dihydropyridine Derivatives. *J Comb Chem* **11**, 500-507 (2009).

259 Bonnet, M., Flanagan, J. U., Chan, D. A., Giaccia, A. J. & Hay, M. P. Identifying novel targets in renal cell carcinoma: Design and synthesis of affinity chromatography reagents. *Bioorg Med Chem* **22**, 711-720 (2014).

260 Rublack, N. & Müller, S. Synthesis of a bifunctional cytidine derivative and its conjugation to RNA for in vitro selection of a cytidine deaminase ribozyme. *Beilstein J Org Chem* **10**, 1906-1913 (2014).

261 Walton, J. G. A. *et al.* Synthesis and biological evaluation of functionalised tetrahydro-β-carboline analogues as inhibitors of Toxoplasma gondii invasion. *Org Biomol Chem* **7**, 3049-3060 (2009).

Appendix 1 – additional biology data

CRISPR-Cas9 gene editing

Fascin gRNA-Cas9-GFP plasmid sequencing

Fluorescence activated cell sorting (FACS)

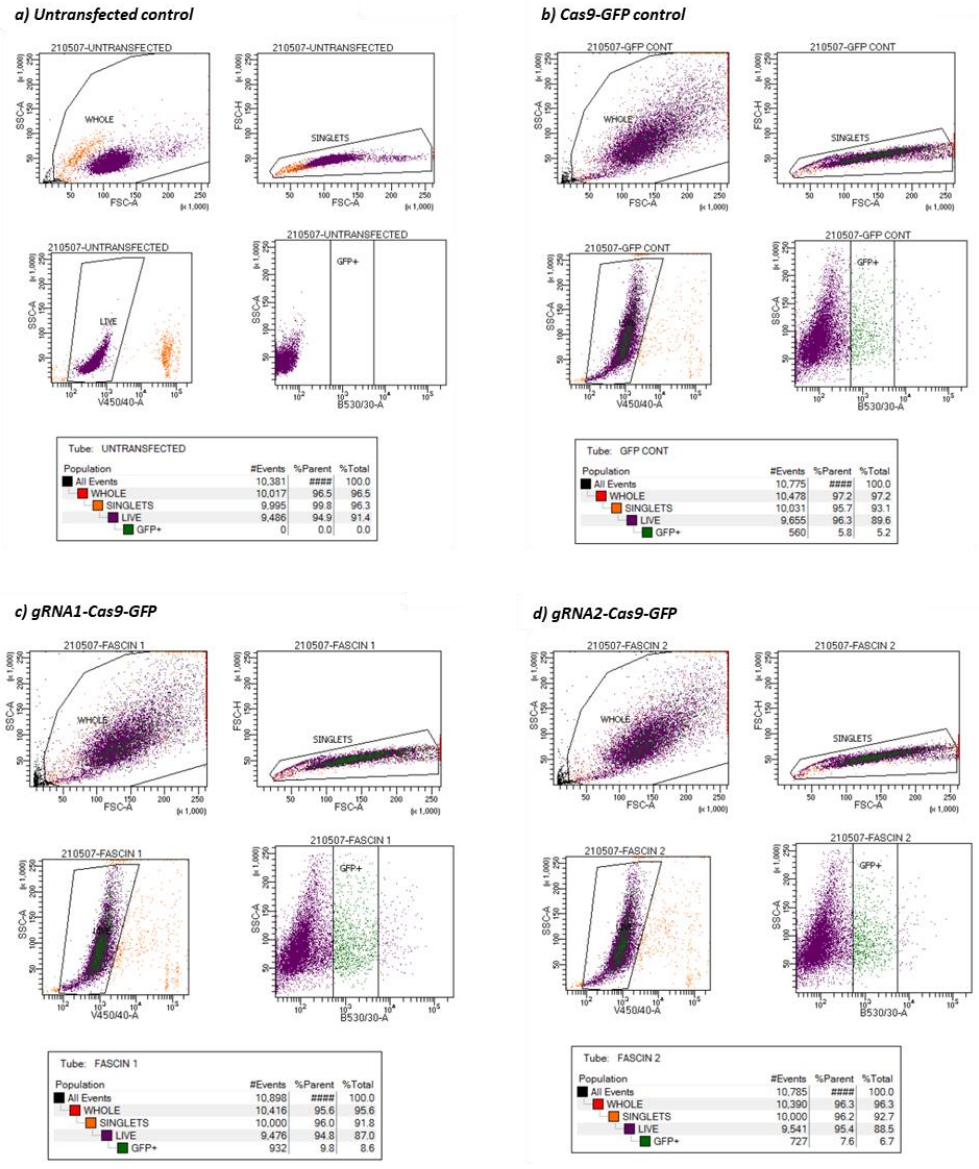

Proliferation and wound healing assays

Fascin knock-down trials

Normalised proliferation index (mean ± SEM)	**SK-OV-3 (at t = 70 h)**	**HT-1080 (at t = 70 h)**
Untreated ctrl	3.4 ± 0.35	8.2 ± 0.41
siRNA ctrl	3.9 ± 0.61	5.7 ± 0.70
siRNA07	3.6 ± 0.15	5.1 ± 0.31
siRNA08	1.3 ± 0.085	2.2 ± 0.44
FSCN-B (10 µM)	4.2 ± 0.29	7.2 ± 1.3
FSCN-B (30 µM)	3.5 ± 0.52	6.7 ± 0.21

Migration – wound closing rate (mean ± SEM)	**SK-OV-3 (at t = 6 h)**	**HT-1080 (at t = 4 h)**
Untreated ctrl	52 ± 0.67 µm/h	110 ± 6.6 µm/h
siRNA ctrl	50 ± 4.5 µm/h	130 ± 2.6 µm/h
siRNA07	51 ± 0.90 µm/h	109 ± 1.8 µm/h
siRNA08	38 ± 1.1 µm/h	89 ± 2.4 µm/h
FSCN-B (10 µM)	59 ± 2.3 µm/h	120 ± 1.7 µm/h
FSCN-B (30 µM)	46 ± 1.8 µm/h	95 ± 2.3 µm/h

Invasion – wound closing rate (mean ± SEM)	**SK-OV-3 (at t = 36 h)**	**HT-1080 (at t = 12 h)**
Untreated ctrl	14 ± 3.9 µm/h	44 ± 5.6 µm/h
siRNA ctrl	10 ± 1.7 µm/h	46 ± 5.2 µm/h
siRNA07	7.6 ± 2.1 µm/h	45 ± 2.4 µm/h
siRNA08	9.9 ± 4.4 µm/h	24 ± 2.5 µm/h
FSCN-B (10 µM)	5.7 ± 1.8 µm/h	38 ± 4.4 µm/h
FSCN-B (30 µM)	7.6 ± 3.9 µm/h	40 ± 1.9 µm/h

Fascin knock-out cell line

Normalised proliferation index (mean ± SEM)	**SK-OV-3 (at t = 94 h)**
WT ctrl	4.4 ± 0.40
200% fascin	6.2 ± 0.52
Fascin KO + VHL-HP-1	3.8 ± 0.43
Fascin KO	4.2 ± 0.31
Fascin KO + HaloTag–fascin	3.0 ± 0.35
Fascin KO + HaloTag–fascin + VHL-HP-1	3.2 ± 0.28

Random migration – velocity (mean ± SEM)	**SK-OV-3**
WT ctrl	0.20 ± 0.013 µm/h
200% fascin	0.21 ± 0.013 µm/h
Fascin KO + VHL-HP-1	0.14 ± 0.011 µm/h
Fascin KO	0.27 ± 0.018 µm/h
Fascin KO + HaloTag–fascin	0.32 ± 0.013 µm/h
Fascin KO + HaloTag–fascin + VHL-HP-1	0.27 ± 0.024 µm/h

Migration – wound closing rate (mean ± SEM)	**SK-OV-3 (at t = 6 h)**
WT ctrl	53 ± 3.9 µm/h
200% fascin	68 ± 4.4 µm/h
Fascin KO + VHL-HP-1	37 ± 1.6 µm/h
Fascin KO	32 ± 1.7 µm/h
Fascin KO + HaloTag–fascin	43 ± 3.7 µm/h
Fascin KO + HaloTag–fascin + VHL-HP-1	42 ± 1.9 µm/h

Invasion (matrigel) – wound closing rate (mean ± SEM)	**SK-OV-3 (at t = 48 h)**
WT ctrl	2.1 ± 0.30 µm/h
200% fascin	7.3 ± 0.62 µm/h
Fascin KO + VHL-HP-1	3.3 ± 0.28 µm/h
Fascin KO	3.3 ± 0.30 µm/h
Fascin KO + HaloTag–fascin	5.6 ± 1.1 µm/h
Fascin KO + HaloTag–fascin + VHL-HP-1	4.1 ± 0.48 µm/h

Invasion (matrigel/collagen I) – wound closing rate (mean ± SEM)	**SK-OV-3 (at t = 48 h)**
WT ctrl	1.3 ± 0.43 µm/h
200% fascin	5.2 ± 0.39 µm/h
Fascin KO + VHL-HP-1	3.9 ± 0.99 µm/h
Fascin KO	2.2 ± 0.24 µm/h
Fascin KO + HaloTag–fascin	5.2 ± 0.53 µm/h
Fascin KO + HaloTag–fascin + VHL-HP-1	4.1 ± 0.45 µm/h

Surface plasmon resonance (SPR) data

FSCN-A-VHL-1 (3.7)

	Steady state K_D (μM)	Kinetic K_D (μM)	k_a ($M^{-1}s^{-1}$)	k_d (s^{-1})	$t_{½}$ (s)
n = 1	6.30	Not measured			
n = 2	6.15	Not measured			

Sensorgram	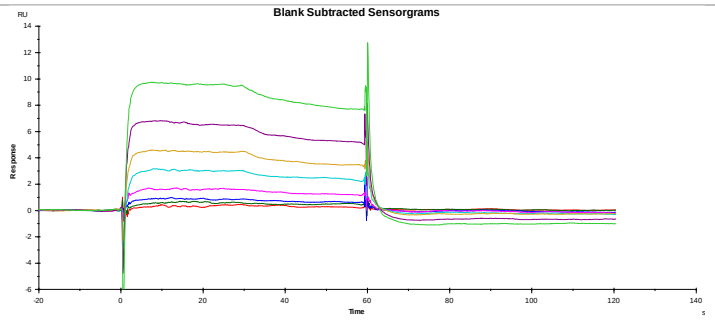
Steady state fit	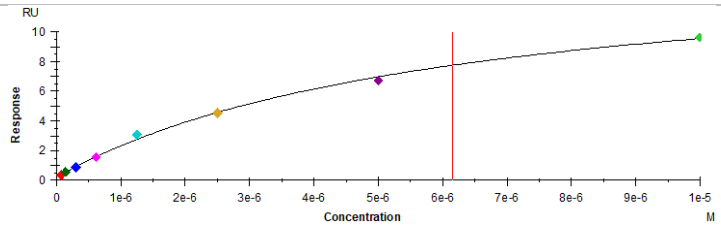

FSCN-A-CRBN-1 (3.9)

	Steady state K_D (μM)	Kinetic K_D (μM)	k_a ($M^{-1}s^{-1}$)	k_d (s^{-1})	$t_{½}$ (s)
n = 1	7.00	Not measured			
n = 2	6.60	Not measured			

Sensorgram	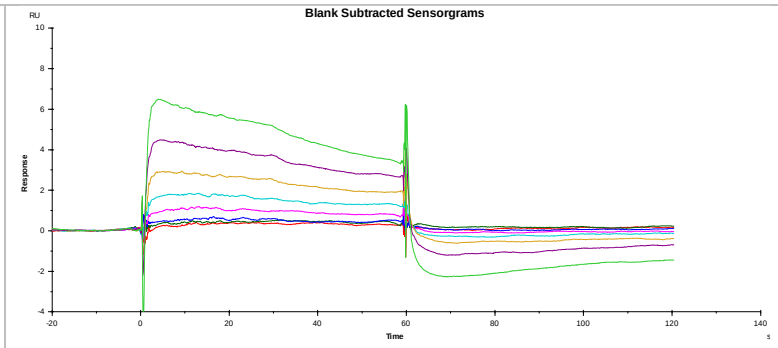
Steady state fit	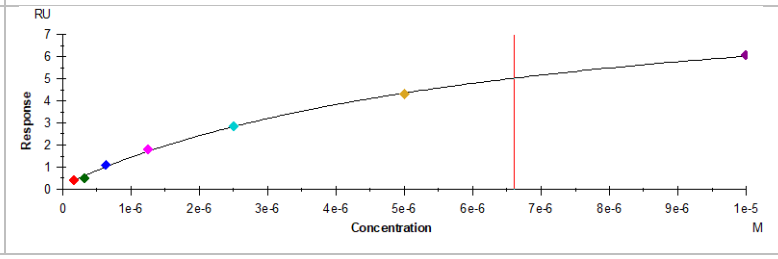

FSCN-A-CRBN-2 (3.10)

	Steady state K_D (μM)	Kinetic K_D (μM)	k_a ($M^{-1}s^{-1}$)	k_d (s^{-1})	$t_{½}$ (s)
n = 1	Not binding	Not measured			
n = 2	Not binding	Not measured			

Sensorgram	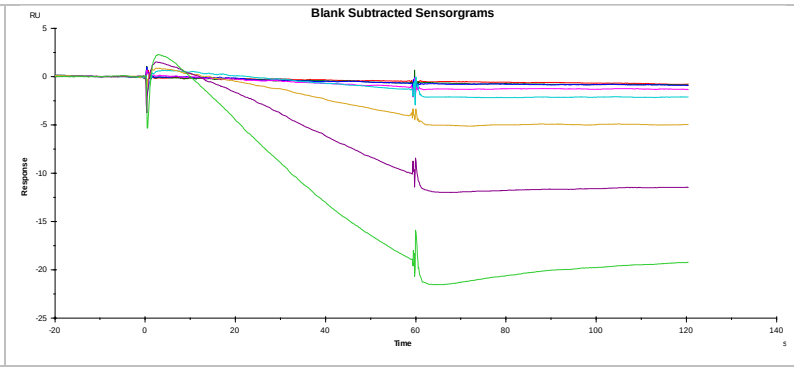

FSCN-A-VHL-3 (3.14)

	Steady state K_D (µM)	Kinetic K_D (µM)	k_a ($M^{-1}s^{-1}$)	k_d (s^{-1})	$t_{½}$ (s)
n = 1	2.38	2.34	68100	0.16	4.35
n = 2	4.71	4.12	43700	0.18	3.86

Sensorgram	Steady state fit	Kinetic fit
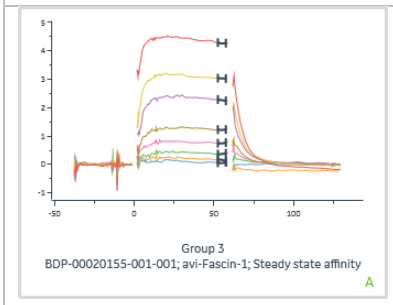	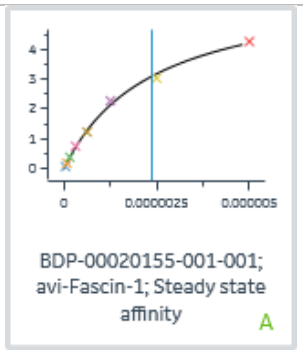	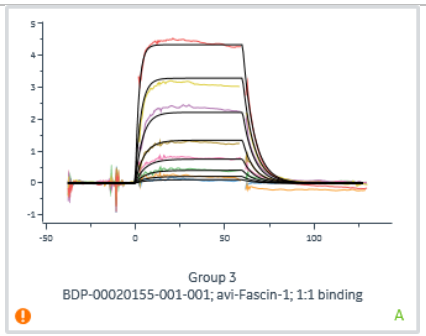

FSCN-A-VHL-4 (3.19)

	Steady state K_D (µM)	Kinetic K_D (µM)	k_a ($M^{-1}s^{-1}$)	k_d (s^{-1})	$t_{½}$ (s)
n = 1	4.19	4.12	43100	0.18	3.9
n = 2	3.44	3.34	51500	0.17	4.03

Sensorgram	Steady state fit	Kinetic fit
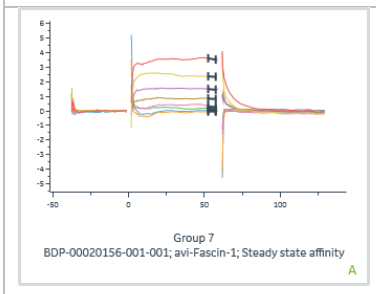	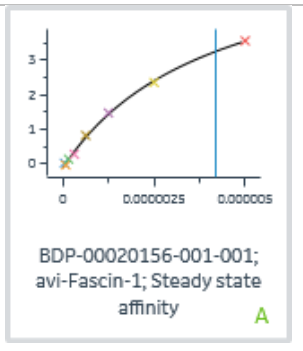	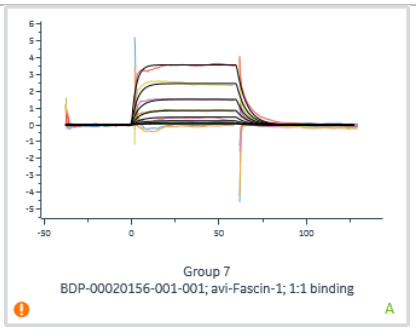

FSCN-A-CRBN-3 (3.22)

	Steady state K_D (µM)	Kinetic K_D (µM)	k_a ($M^{-1}s^{-1}$)	k_d (s^{-1})	$t_{½}$ (s)
n = 1	0.804	0.737	204000	0.15	4.61
n = 2	1.35	1.22	134000	0.16	4.24

Sensorgram	Steady state fit	Kinetic fit
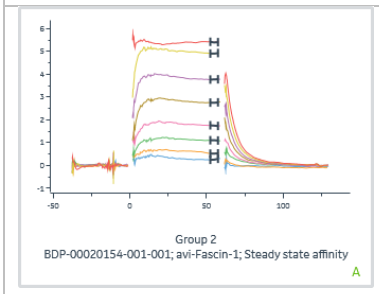	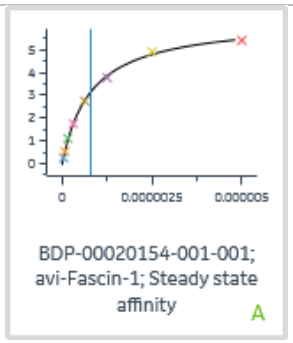	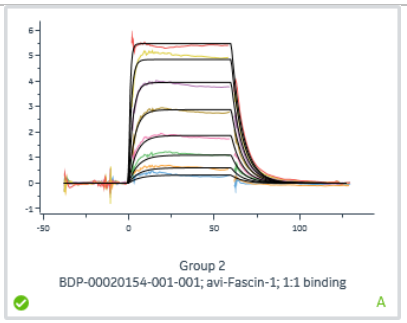

FSCN-A-HyT-1 (3.24)

	Steady state K_D (µM)	Kinetic K_D (µM)	k_a ($M^{-1}s^{-1}$)	k_d (s^{-1})	$t_{½}$ (s)
n = 1	K_D > 5 µM Binds but not soluble enough to determine accurate KD with steady state analysis				
n = 2	3.72	3.07	43500	0.13	5.19

Sensorgram	Steady state fit	Kinetic fit
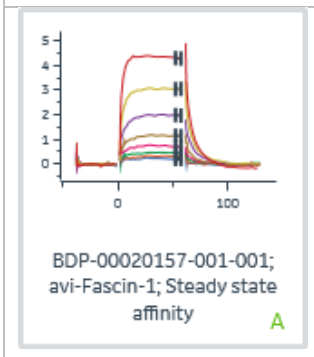	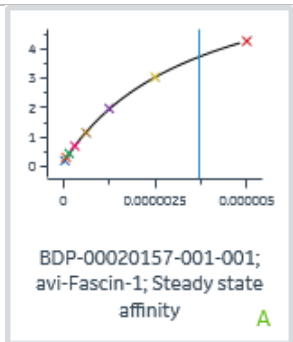	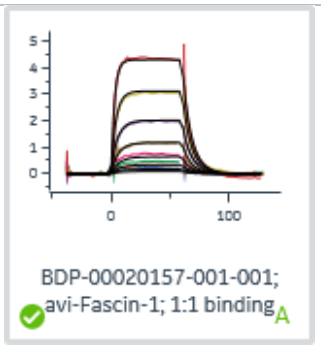

FSCN-B (1.5)

	Steady state K_D (µM)	Kinetic K_D (µM)	k_a ($M^{-1}s^{-1}$)	k_d (s^{-1})	$t_{½}$ (s)
n = 1	0.0528	0.0446	681000	0.03	22.8
n = 2	0.0426	0.0358	752000	0.03	25.7

Sensorgram	Steady state fit	Kinetic fit
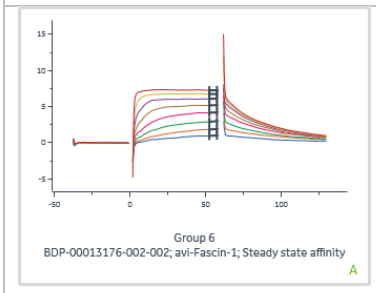	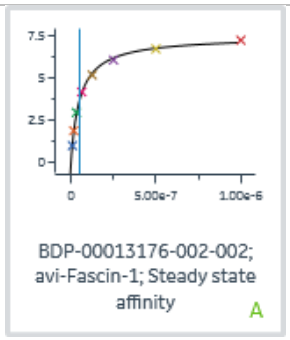	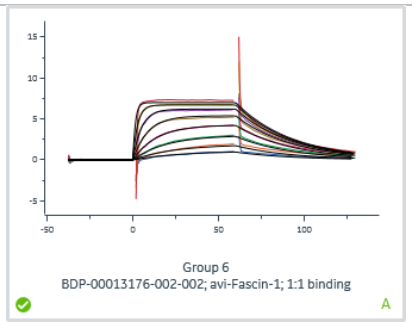

FSCN-B-VHL-1 (3.35)

	Steady state K_D (µM)	Kinetic K_D (µM)	k_a ($M^{-1}s^{-1}$)	k_d (s^{-1})	$t_{½}$ (s)
n = 1	2.04	1.73	38900	0.07	10.3
n = 2	2.04	1.8	38600	0.07	9.98

Sensorgram	Steady state fit	Kinetic fit
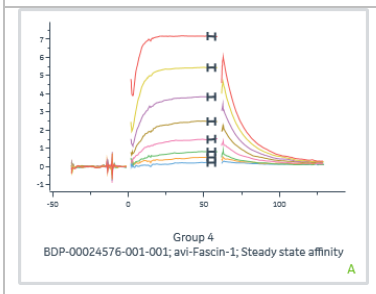	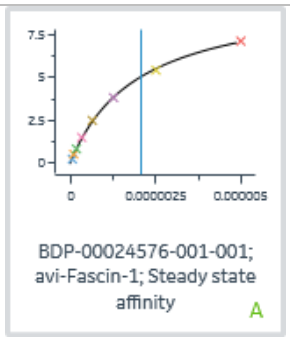	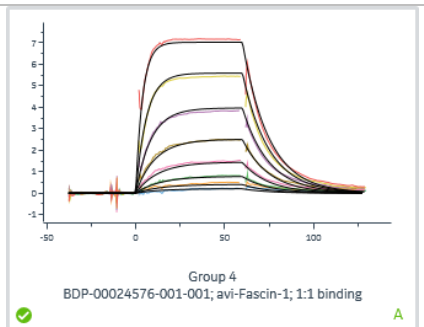

FSCN-B-VHL-2 (3.36)

	Steady state K_D (μM)	Kinetic K_D (μM)	k_a ($M^{-1}s^{-1}$)	k_d (s^{-1})	$t_{½}$ (s)
n = 1	0.765	0.726	104000	0.08	9.16
n = 2	0.856	0.741	70900	0.05	13.2

Sensorgram	Steady state fit	Kinetic fit
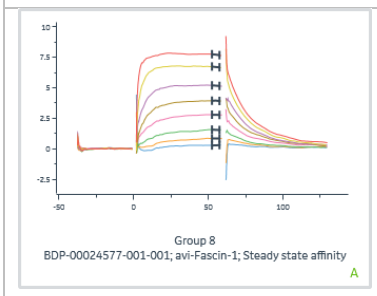	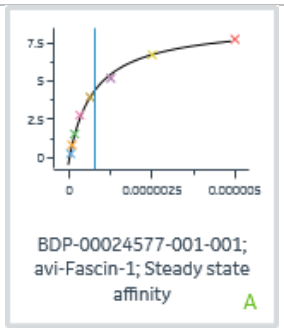	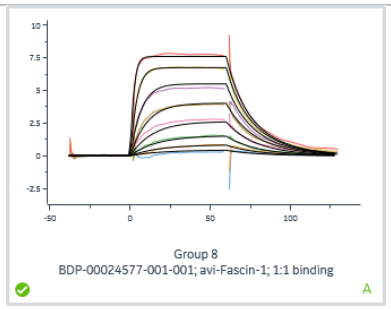

FSCN-B-CRBN-1 (3.42)

	Steady state K_D (μM)	Kinetic K_D (μM)	k_a ($M^{-1}s^{-1}$)	k_d (s^{-1})	$t_{½}$ (s)
n = 1	0.565	0.473	130000	0.06	11.3
n = 2	0.531	0.464	126000	0.06	11.9

Sensorgram	Steady state fit	Kinetic fit
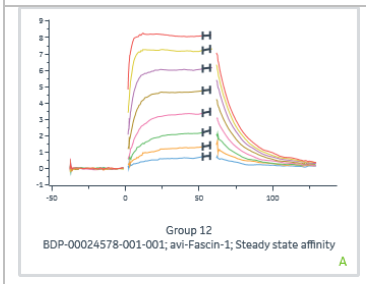	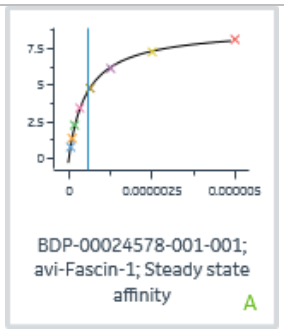	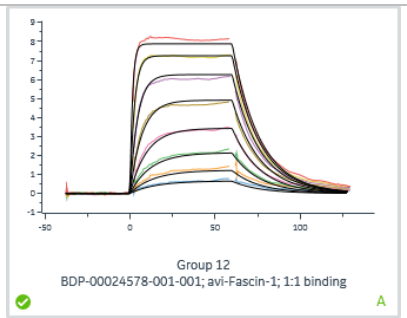

FSCN-B-CRBN-2 (3.47)

	Steady state K_D (μM)	Kinetic K_D (μM)	k_a ($M^{-1}s^{-1}$)	k_d (s^{-1})	$t_{½}$ (s)
n = 1	0.216	0.196	220000	0.04	16
n = 2	0.294	0.249	181000	0.05	15.3

Sensorgram	Steady state fit	Kinetic fit
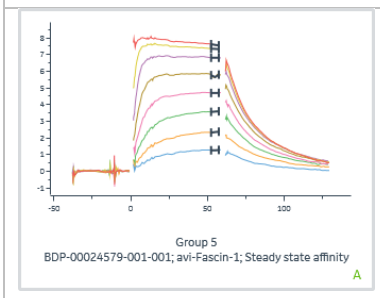	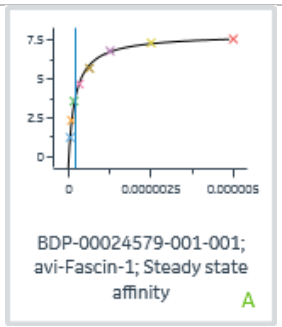	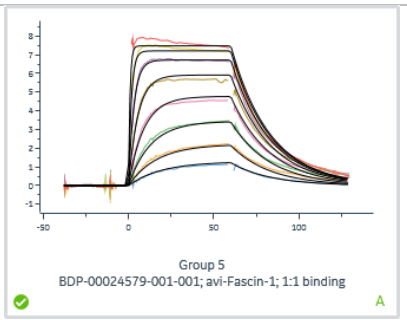

FSCN-B-HyT-1 (3.48)

	Steady state K_D (μM)	Kinetic K_D (μM)	k_a ($M^{-1}s^{-1}$)	k_d (s^{-1})	$t_{½}$ (s)
n = 1	1.08	1.08	71700	0.08	8.97
n = 2	0.925	0.875	84900	0.07	9.32

Sensorgram	Steady state fit	Kinetic fit
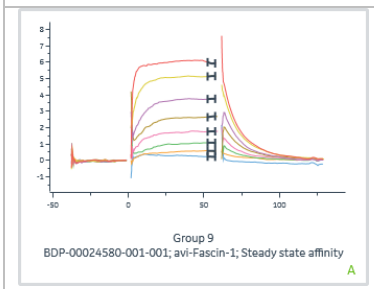	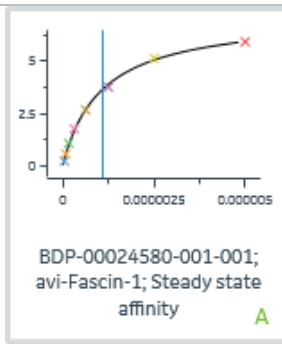	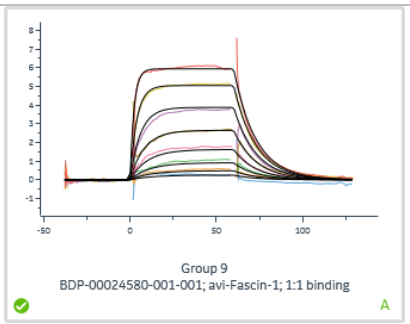

FSCN-B-HyT-2 (3.51)

	Steady state K_D (µM)	Kinetic K_D (µM)	k_a ($M^{-1}s^{-1}$)	k_d (s^{-1})	$t_{½}$ (s)
n = 1	1.16	1.15	43700	0.05	13.8
n = 2	1.38	1.15	35600	0.04	17

Sensorgram	Steady state fit	Kinetic fit
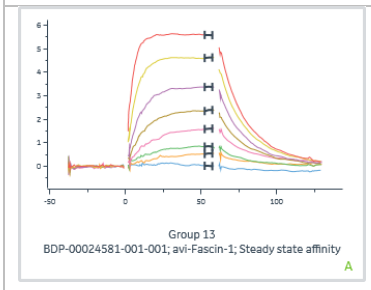	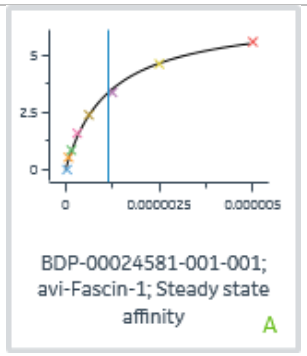	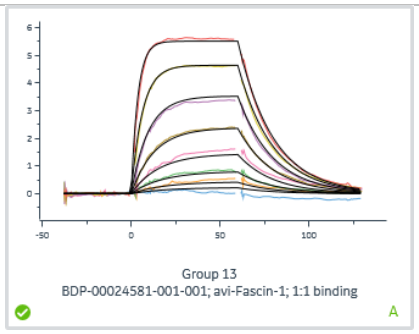

FSCN-C (1.7)

	Steady state K_D (µM)	Kinetic K_D (µM)	k_a ($M^{-1}s^{-1}$)	k_d (s^{-1})	$t_{½}$ (s)
n = 1	Not binding				
n = 2	Not binding				

Sensorgram

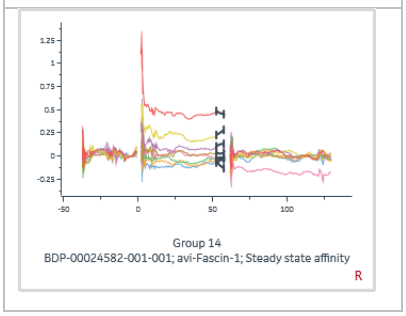

FSCN-C-VHL-1 (3.60)

	Steady state K_D (µM)	Kinetic K_D (µM)	k_a ($M^{-1}s^{-1}$)	k_d (s^{-1})	$t_{½}$ (s)
n = 1	Not binding				
n = 2	Not binding				

Sensorgram

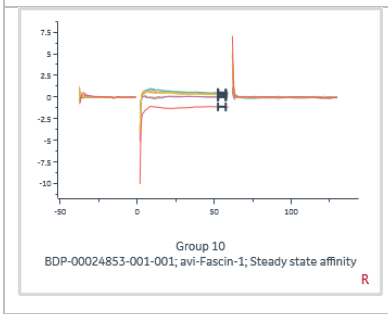

Appendix 2 - additional chemistry data

Compound characterisation data

E3 ligase ligands

- *VHL ligand VHL-2 (2.3) and epimer control* cis*VHL-2 (2.4):*

2.5:

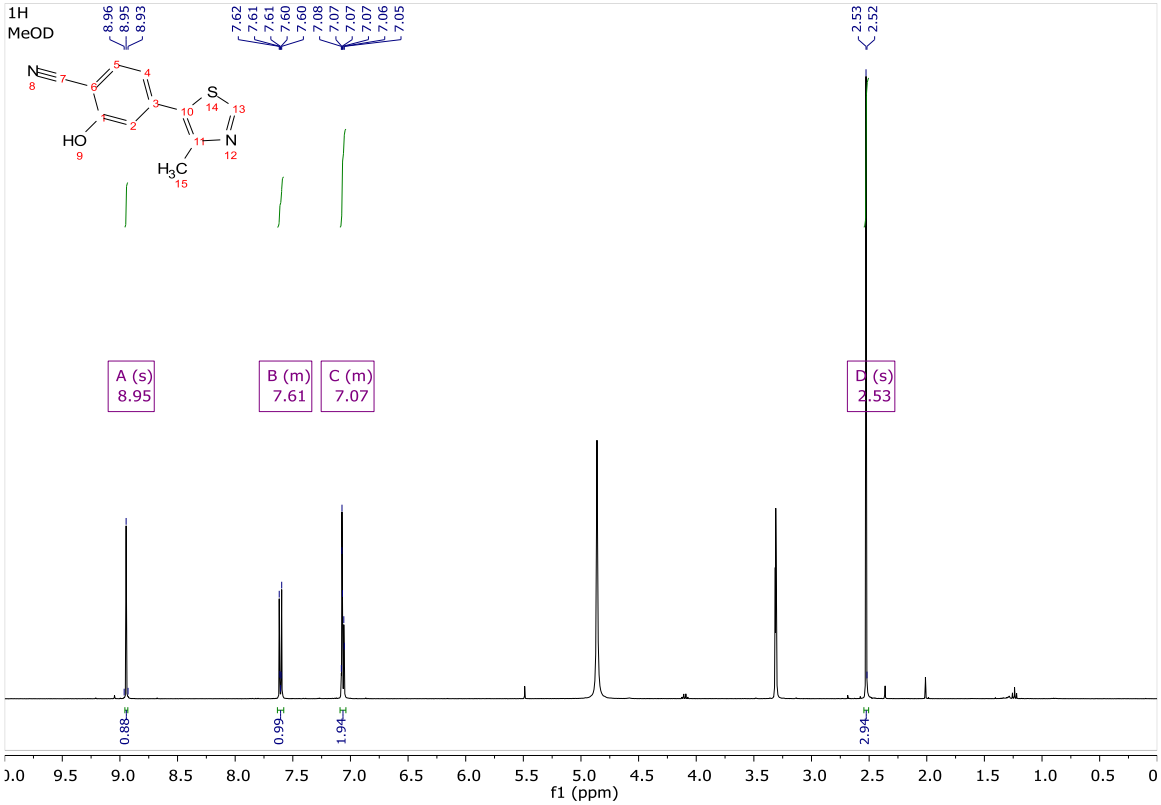

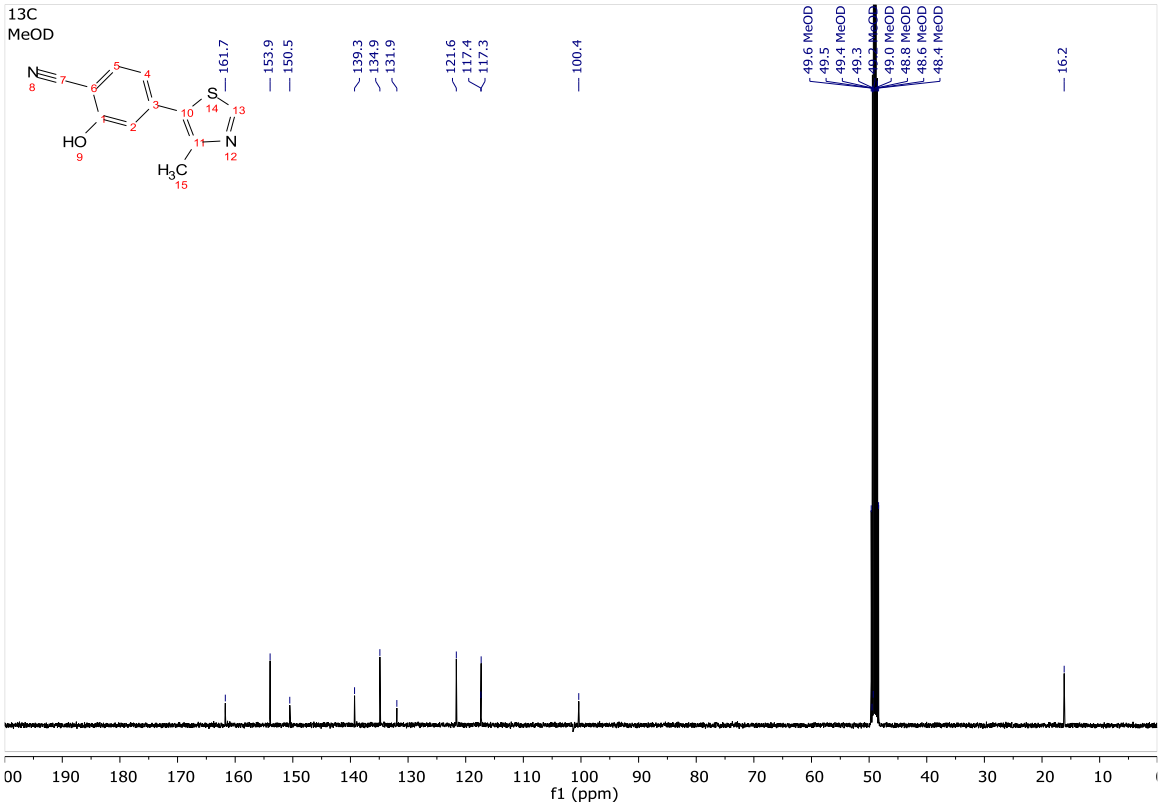

2.6:

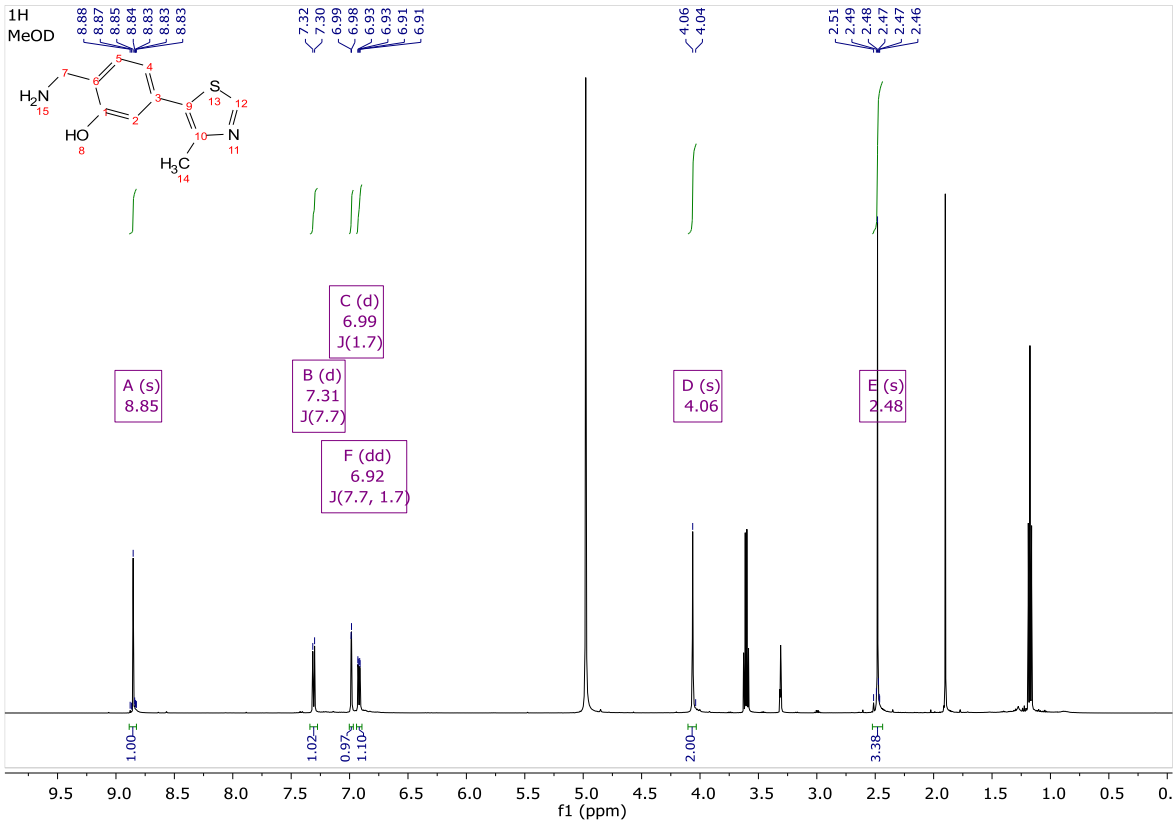
1H
MeOD
A (s)
8.85
B (d)
7.31
J(7.7)
C (d)
6.99
J(1.7)
F (dd)
6.92
J(7.7, 1.7)
D (s)
4.06
E (s)
2.48
f1 (ppm)

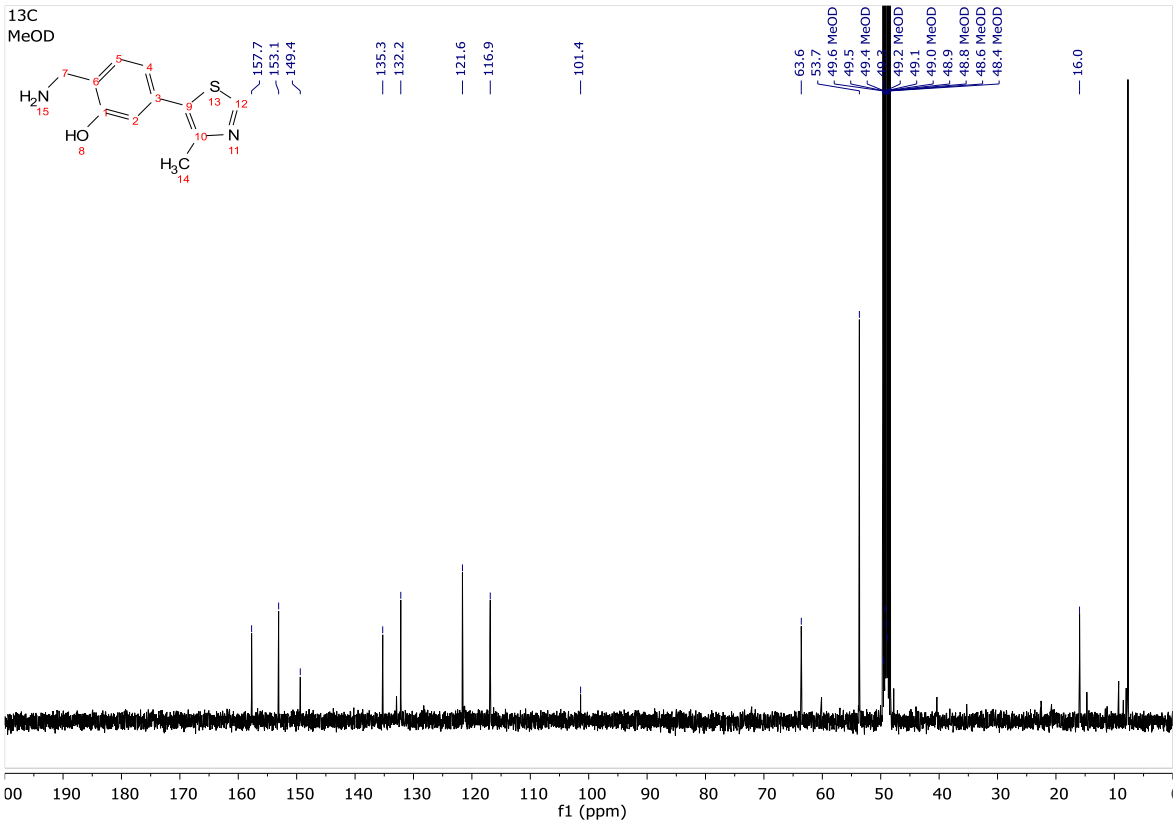
13C
MeOD
f1 (ppm)

2.7a:

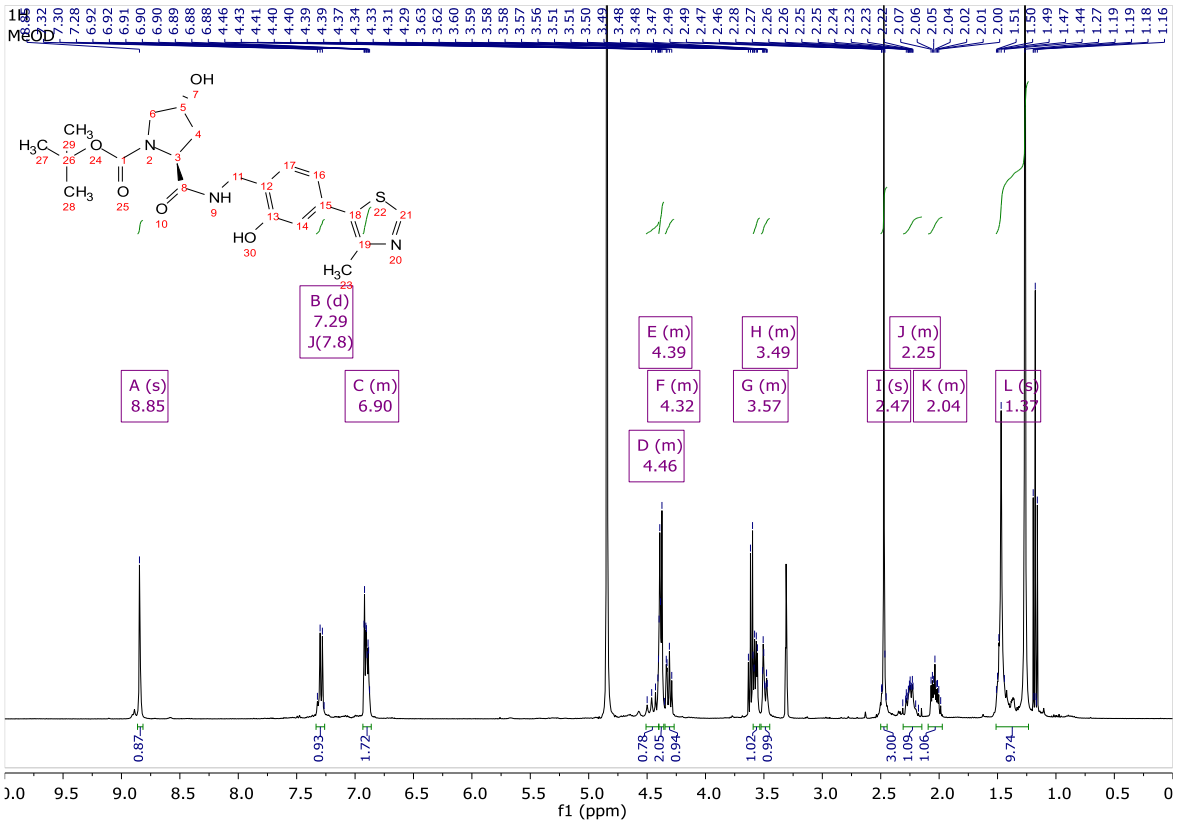
1H
MeOD
A (s) 8.85
B (d) 7.29 J(7.8)
C (m) 6.90
D (m) 4.46
E (m) 4.39
F (m) 4.32
G (m) 3.57
H (m) 3.49
I (s) 2.47
J (m) 2.25
K (m) 2.04
L (s) 1.37
f1 (ppm)

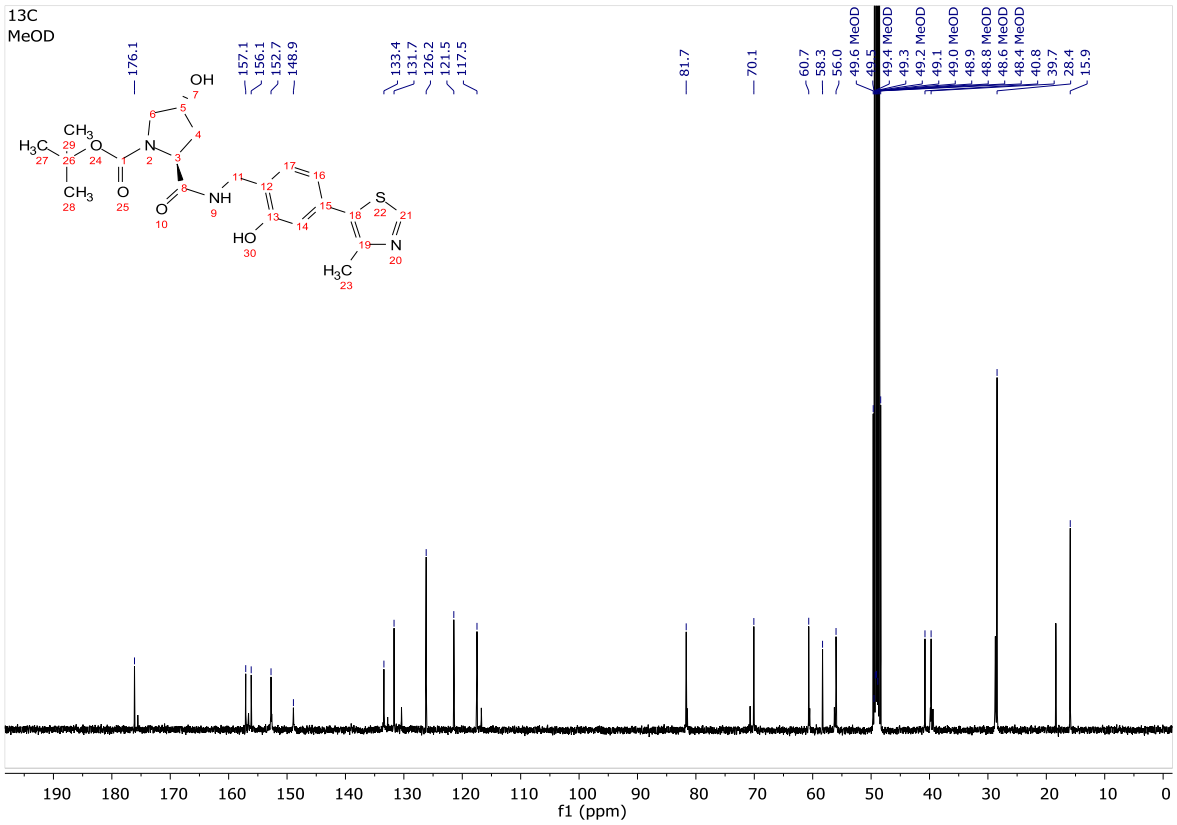
13C
MeOD
f1 (ppm)

2.7b:

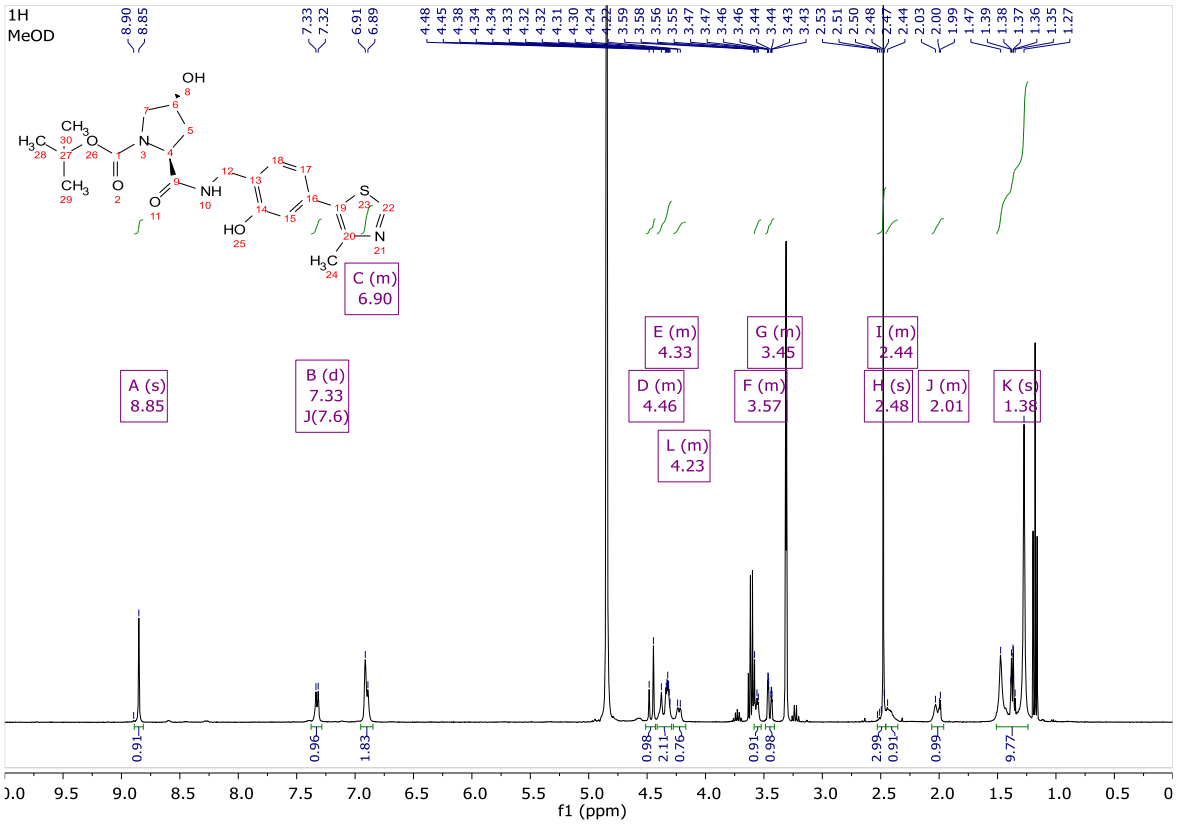
1H
MeOD
A (s) 8.85
B (d) 7.33 J(7.6)
C (m) 6.90
D (m) 4.46
E (m) 4.33
F (m) 3.57
G (m) 3.45
H (s) 2.48
I (m) 2.44
J (m) 2.01
K (s) 1.38
L (m) 4.23
f1 (ppm)

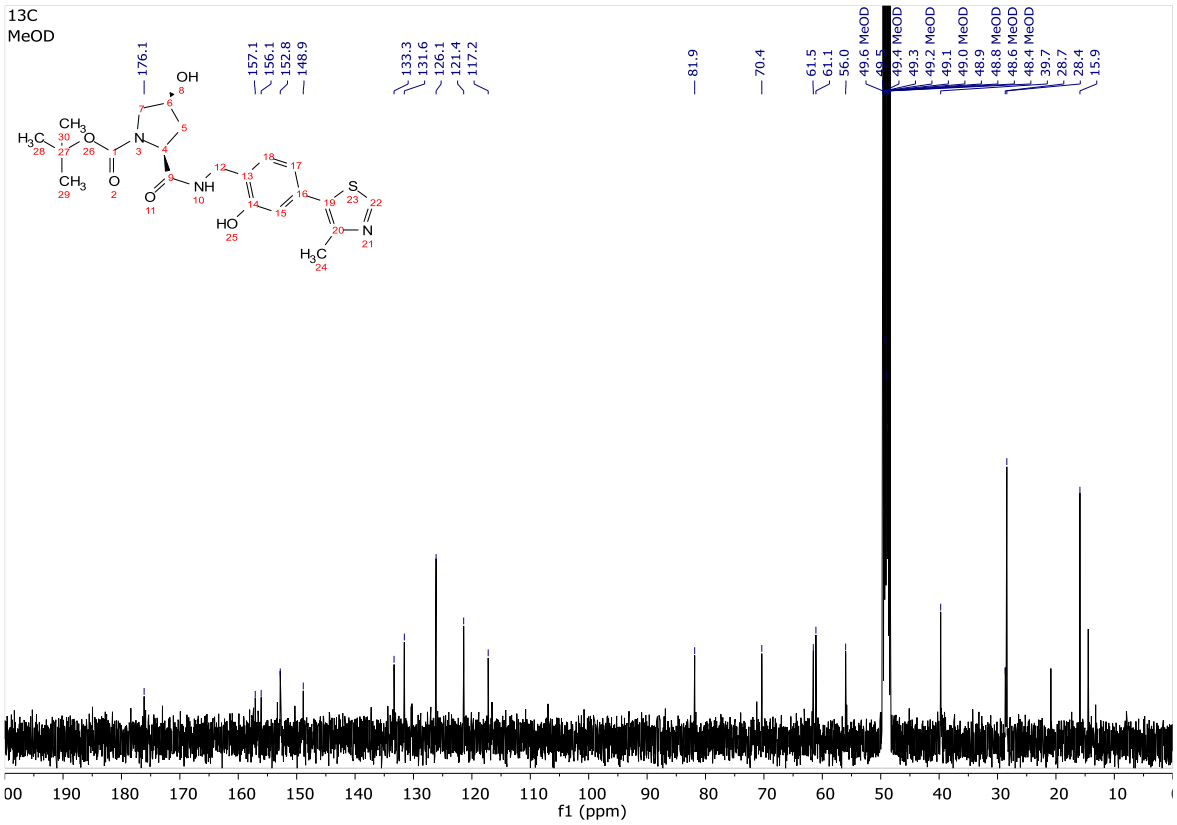
13C
MeOD
f1 (ppm)

2.8a:

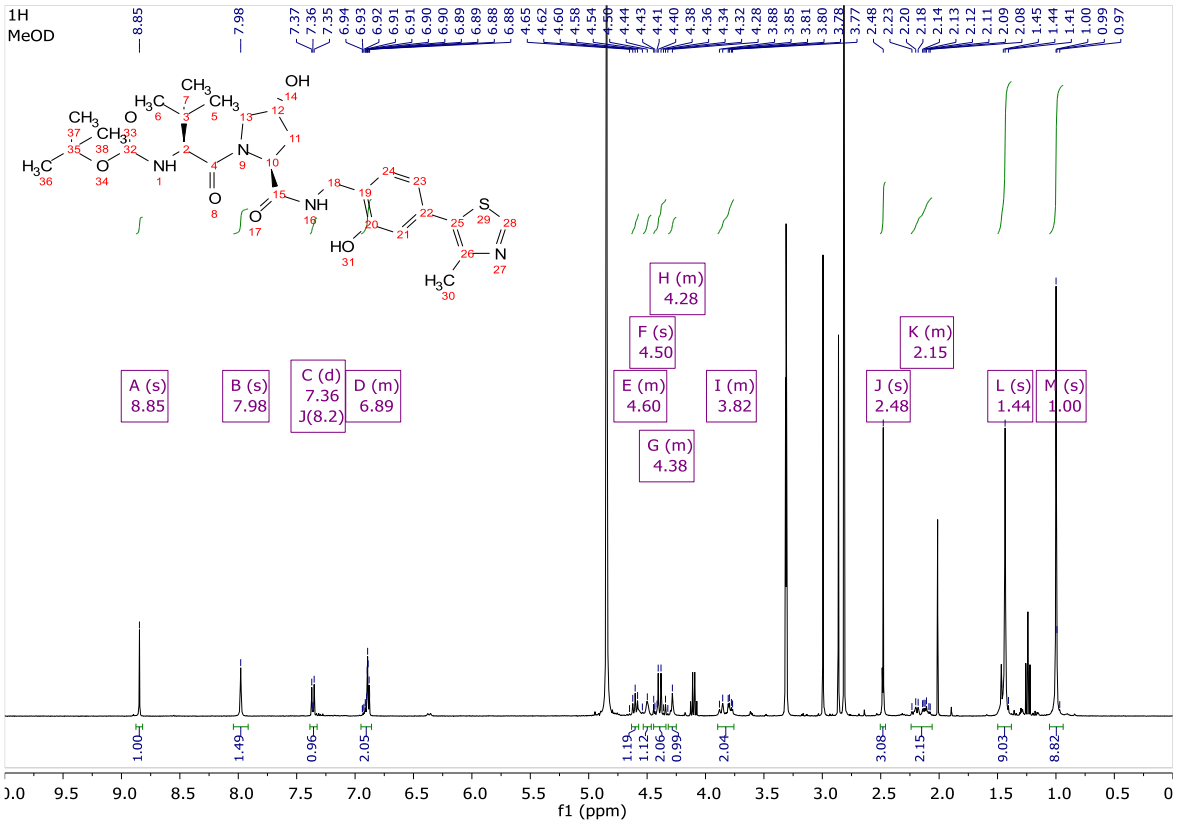
1H
MeOD
A (s) 8.85
B (s) 7.98
C (d) 7.36 J(8.2)
D (m) 6.89
E (m) 4.60
F (s) 4.50
G (m) 4.38
H (m) 4.28
I (m) 3.82
J (s) 2.48
K (m) 2.15
L (s) 1.44
M (s) 1.00
f1 (ppm)

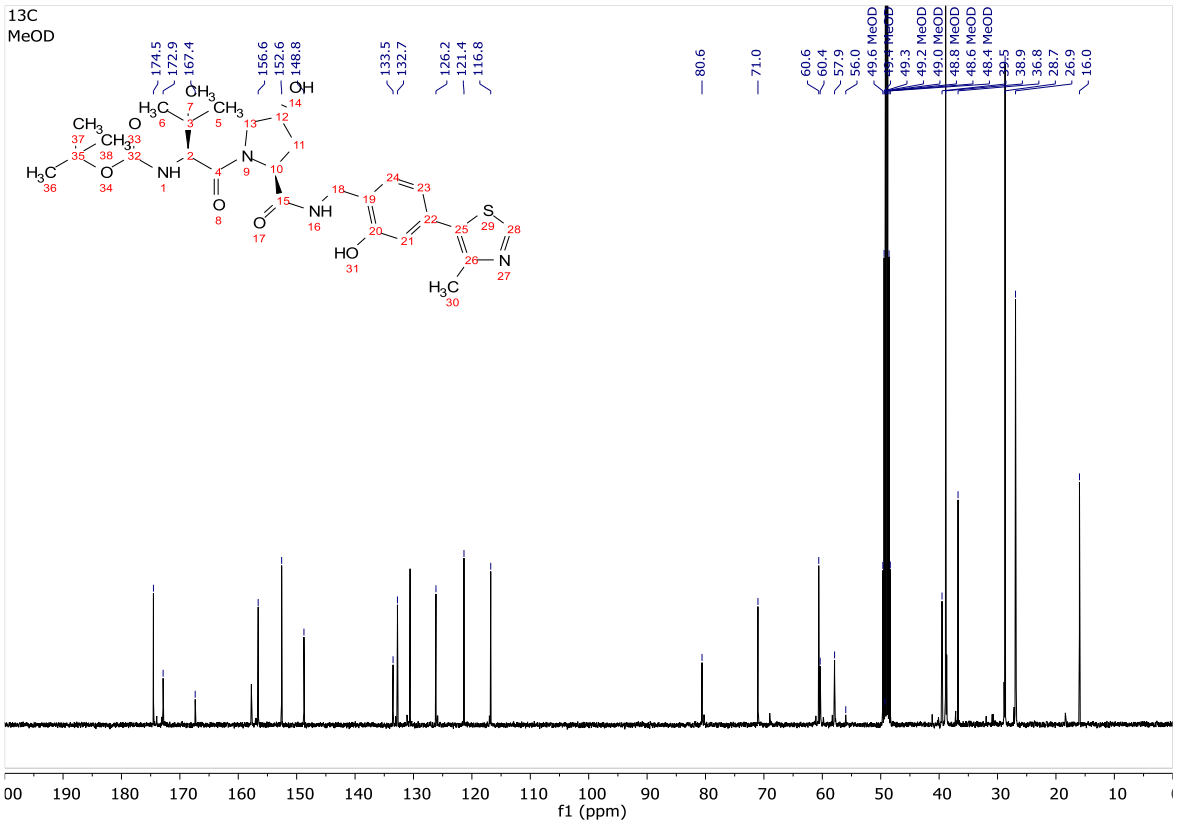
13C
MeOD
f1 (ppm)

2.8b:

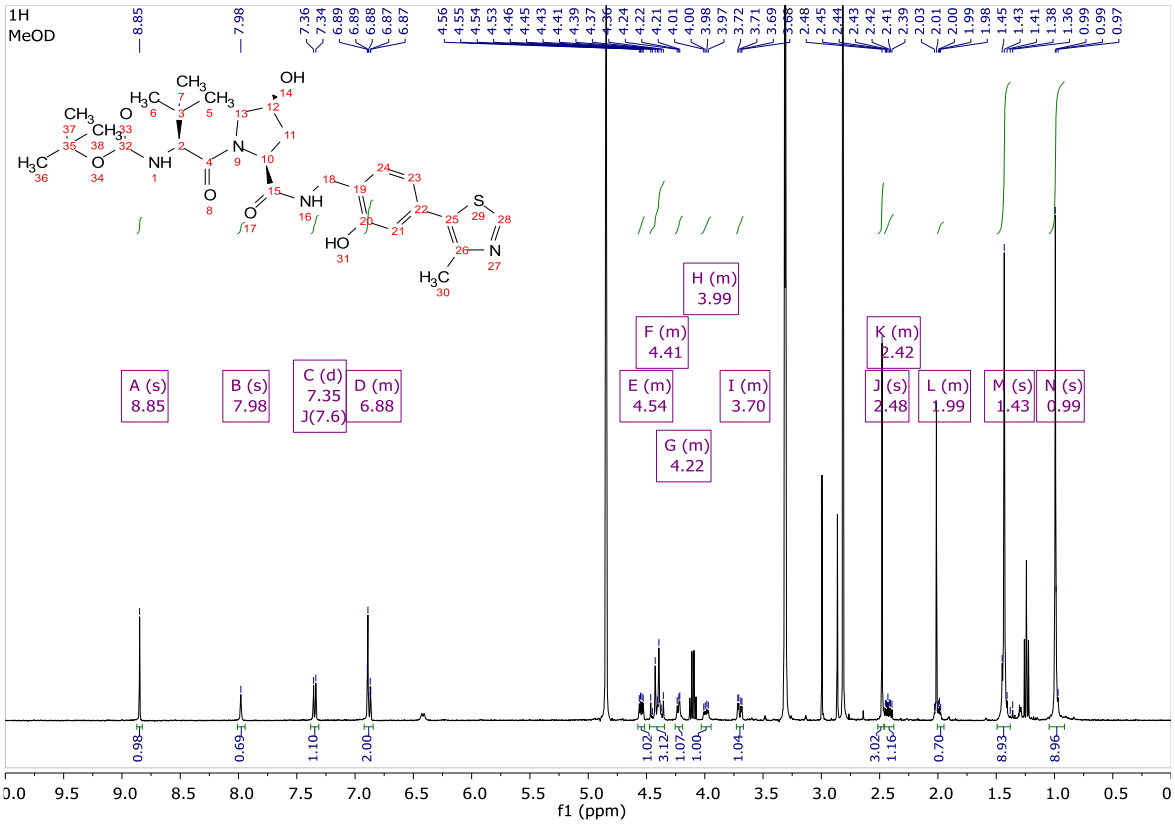
1H
MeOD
A (s) 8.85
B (s) 7.98
C (d) 7.35 J(7.6)
D (m) 6.88
E (m) 4.54
F (m) 4.41
G (m) 4.22
H (m) 3.99
I (m) 3.70
J (s) 2.48
K (m) 2.42
L (m) 1.99
M (s) 1.43
N (s) 0.99
f1 (ppm)

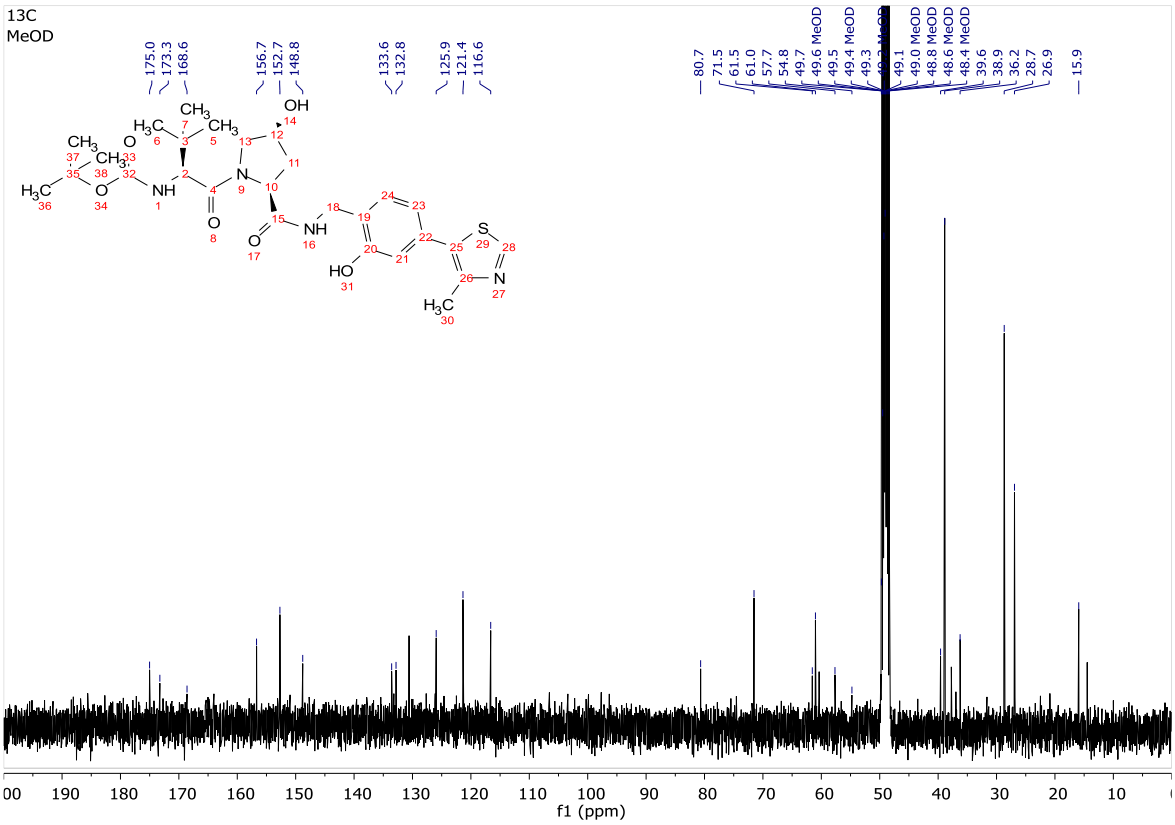
13C
MeOD
f1 (ppm)

VHL-2 (2.3):

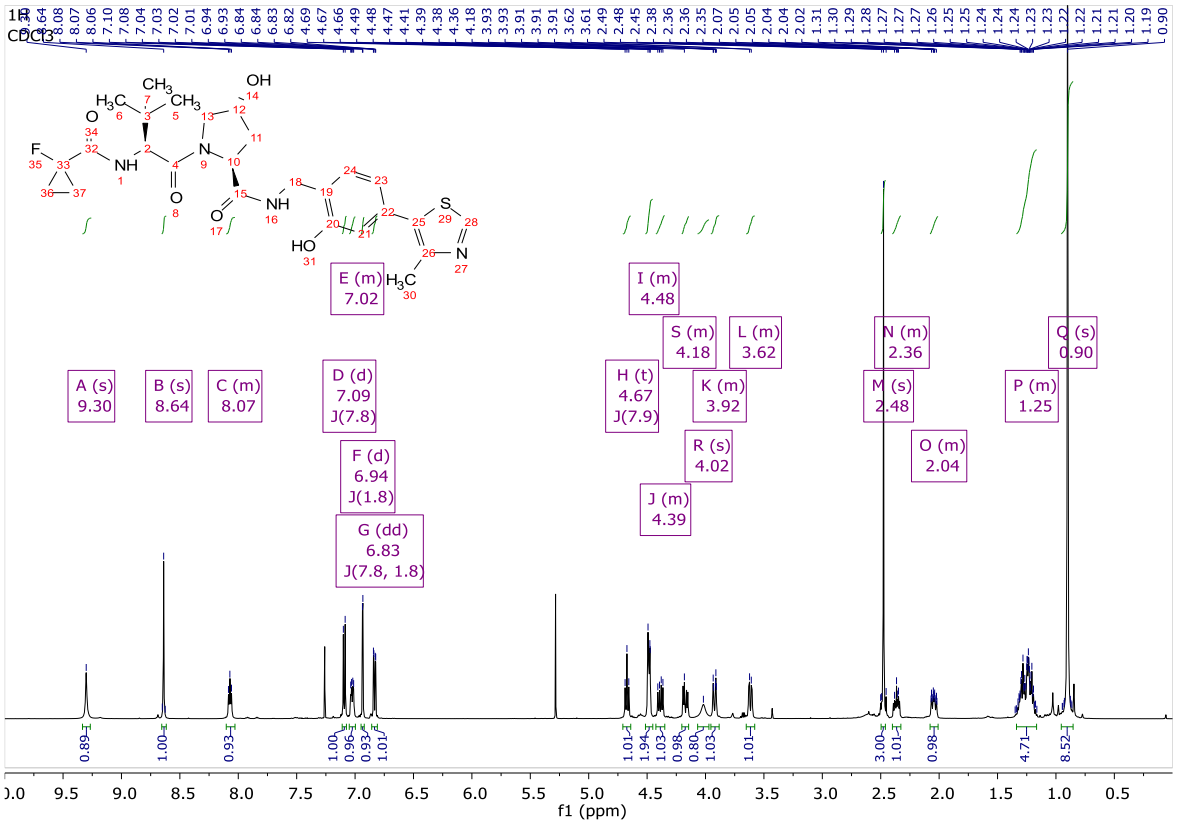
1H
CDCl3
A (s) 9.30
B (s) 8.64
C (m) 8.07
D (d) 7.09 J(7.8)
E (m) 7.02
F (d) 6.94 J(1.8)
G (dd) 6.83 J(7.8, 1.8)
H (t) 4.67 J(7.9)
I (m) 4.48
J (m) 4.39
K (m) 3.92
L (m) 3.62
M (s) 2.48
N (m) 2.36
O (m) 2.04
P (m) 1.25
Q (s) 0.90
R (s) 4.02
S (m) 4.18
f1 (ppm)

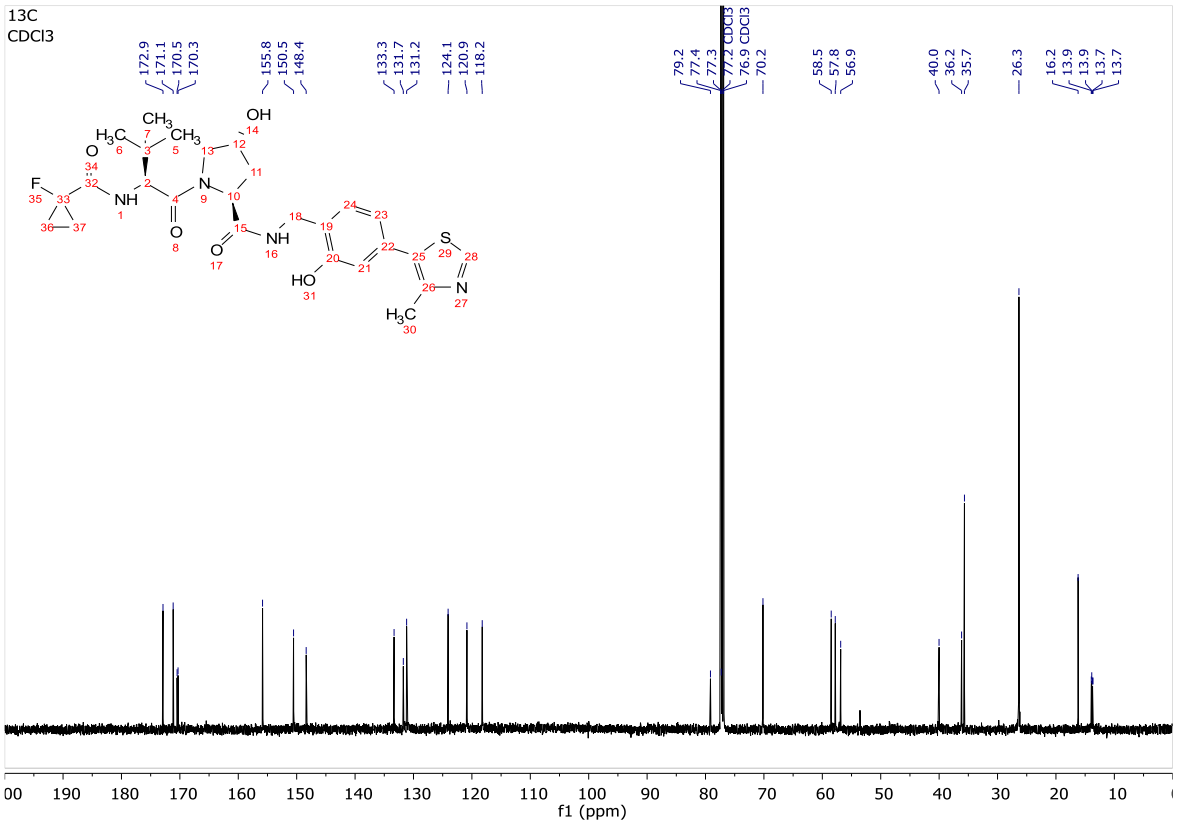
13C
CDCl3
f1 (ppm)

***cis*VHL-2 (2.4)**:

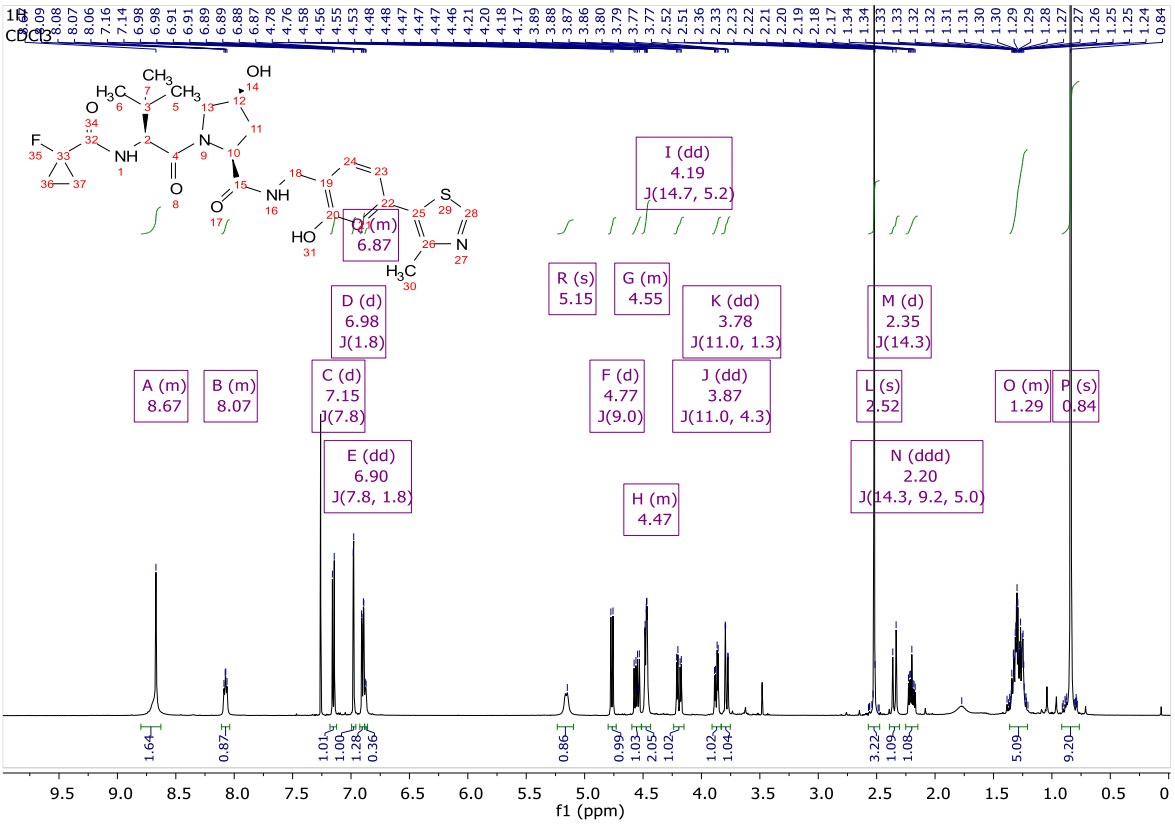
1H
CDCl3
A (m)
8.67
B (m)
8.07
C (d)
7.15
J(7.8)
D (d)
6.98
J(1.8)
E (dd)
6.90
J(7.8, 1.8)
Q (m)
6.87
R (s)
5.15
G (m)
4.55
H (m)
4.47
F (d)
4.77
J(9.0)
I (dd)
4.19
J(14.7, 5.2)
J (dd)
3.87
J(11.0, 4.3)
K (dd)
3.78
J(11.0, 1.3)
N (ddd)
2.20
J(14.3, 9.2, 5.0)
M (d)
2.35
J(14.3)
L (s)
2.52
O (m)
1.29
P (s)
0.84
f1 (ppm)

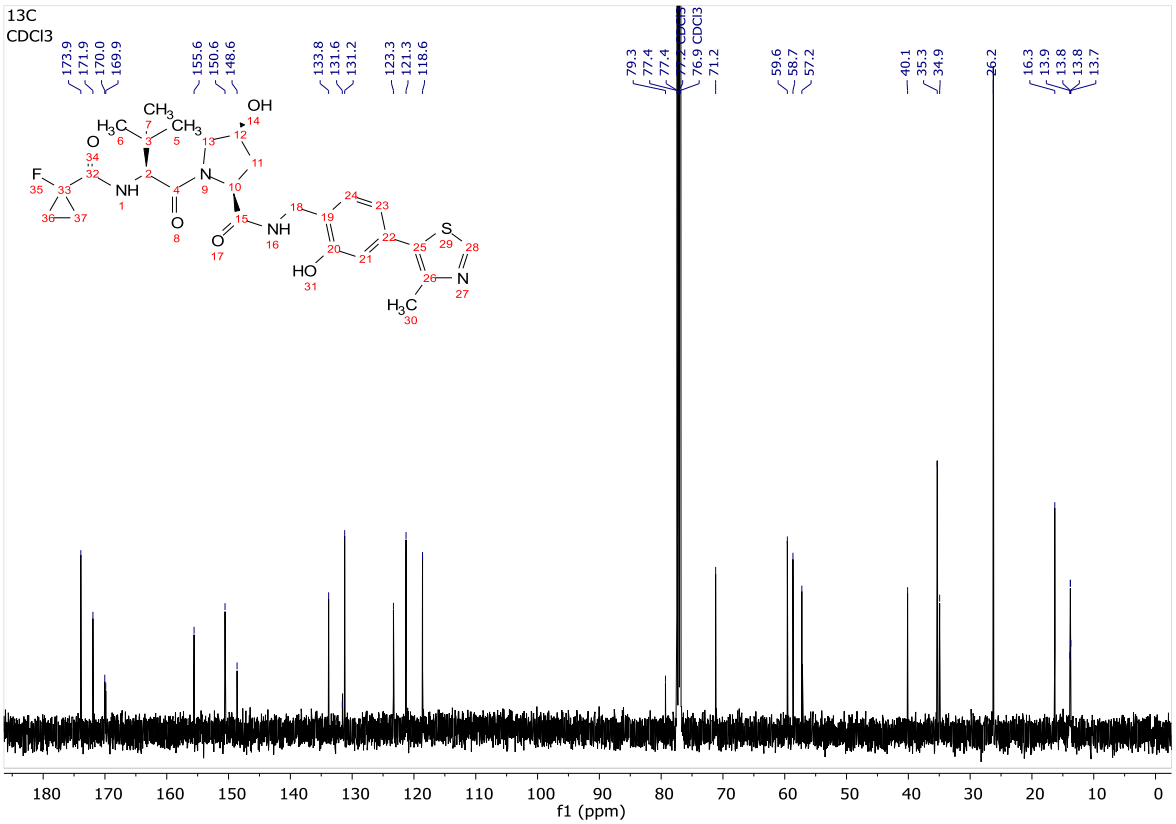
13C
CDCl3
f1 (ppm)

- *CRBN ligand CRBN-1 (2.9) and methylated control MeCRBN-1 (2.10):*

2.13:

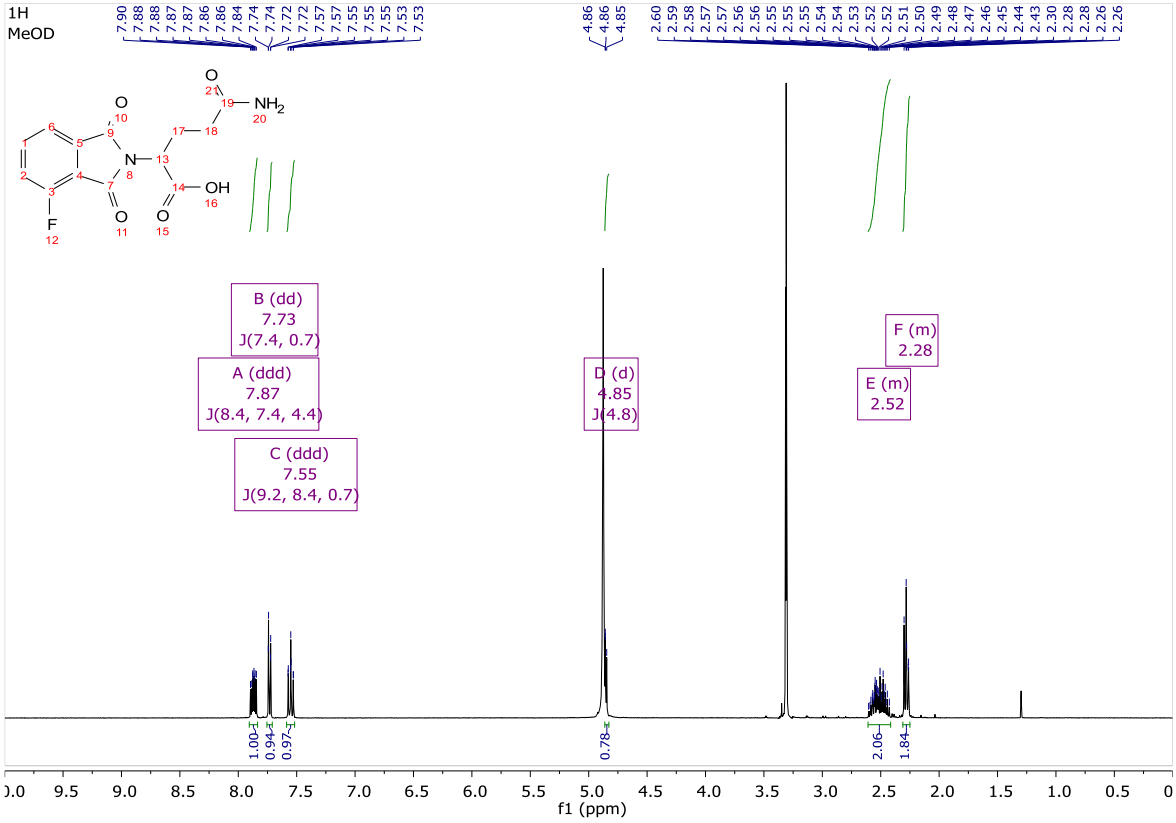

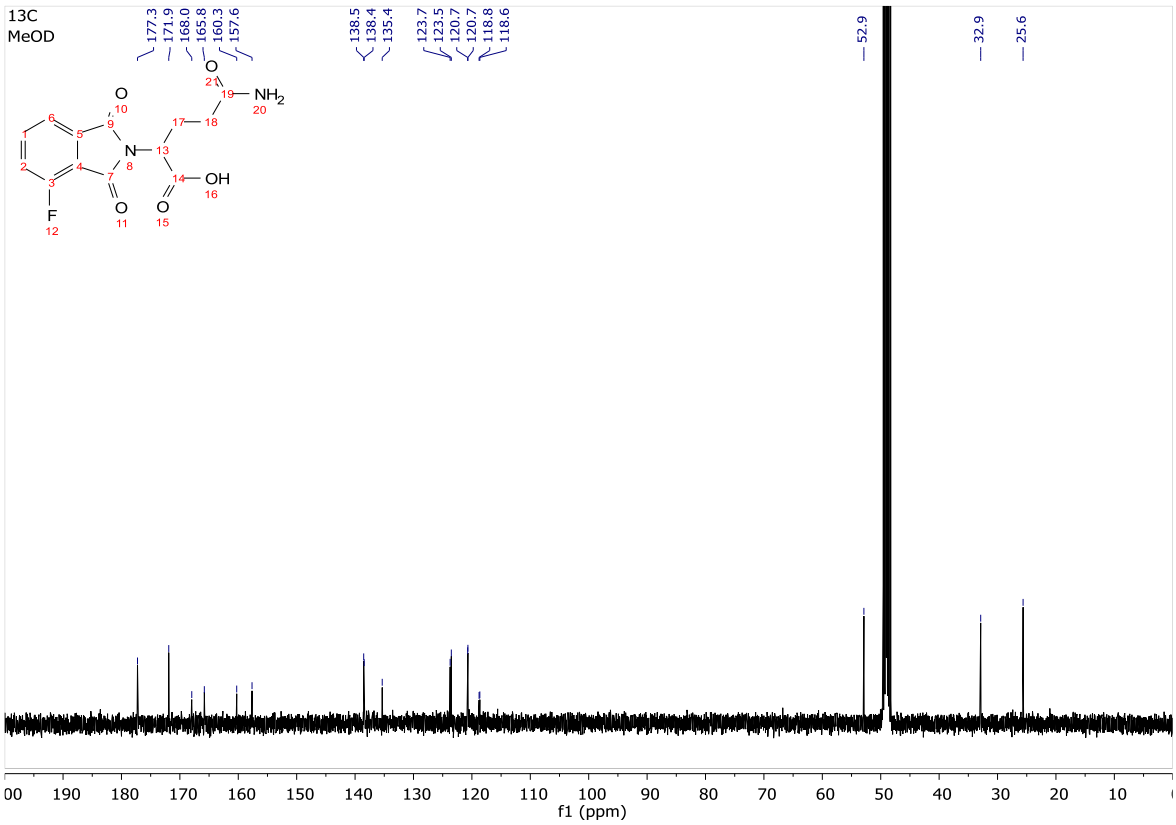

CRBN-1 (2.9):

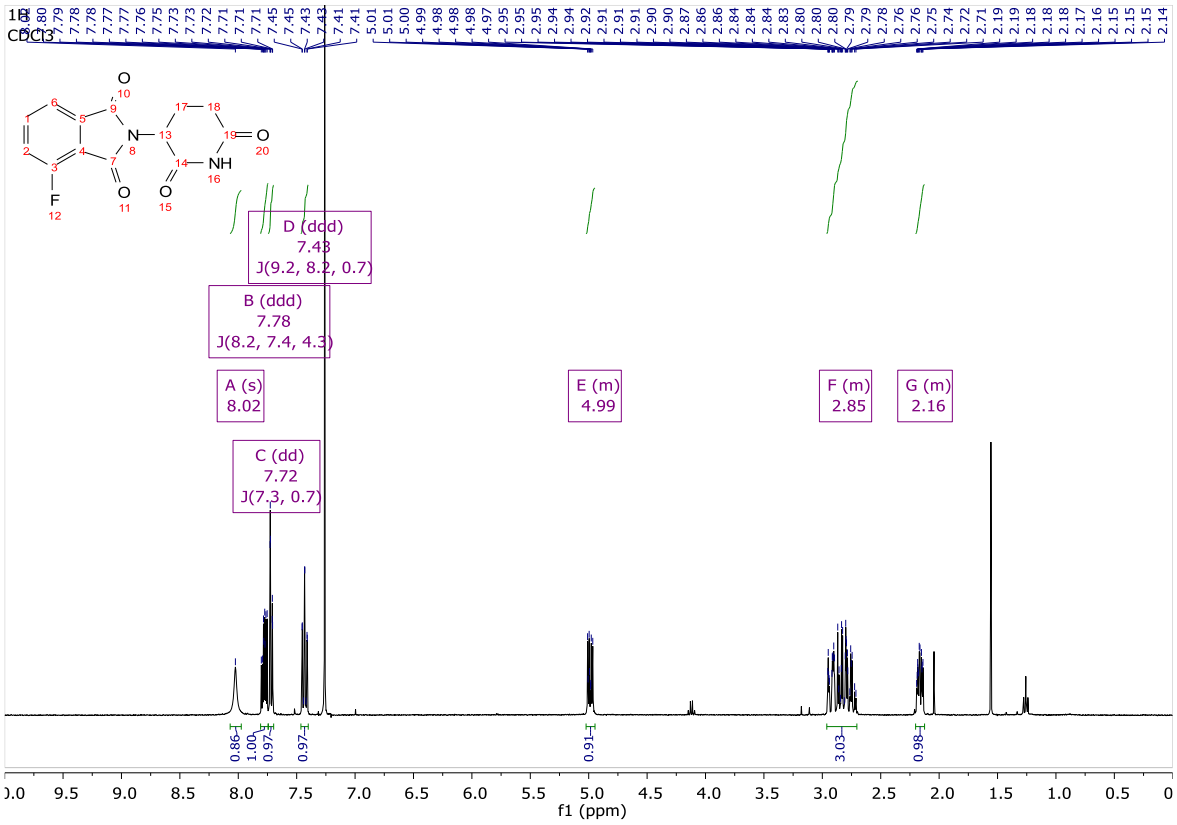
1H
CDCl3
D (ddd)
7.43
J(9.2, 8.2, 0.7)
B (ddd)
7.78
J(8.2, 7.4, 4.3)
A (s)
8.02
E (m)
4.99
F (m)
2.85
G (m)
2.16
C (dd)
7.72
J(7.3, 0.7)
0.86
1.00
0.97
0.97
0.91
3.03
0.98
f1 (ppm)

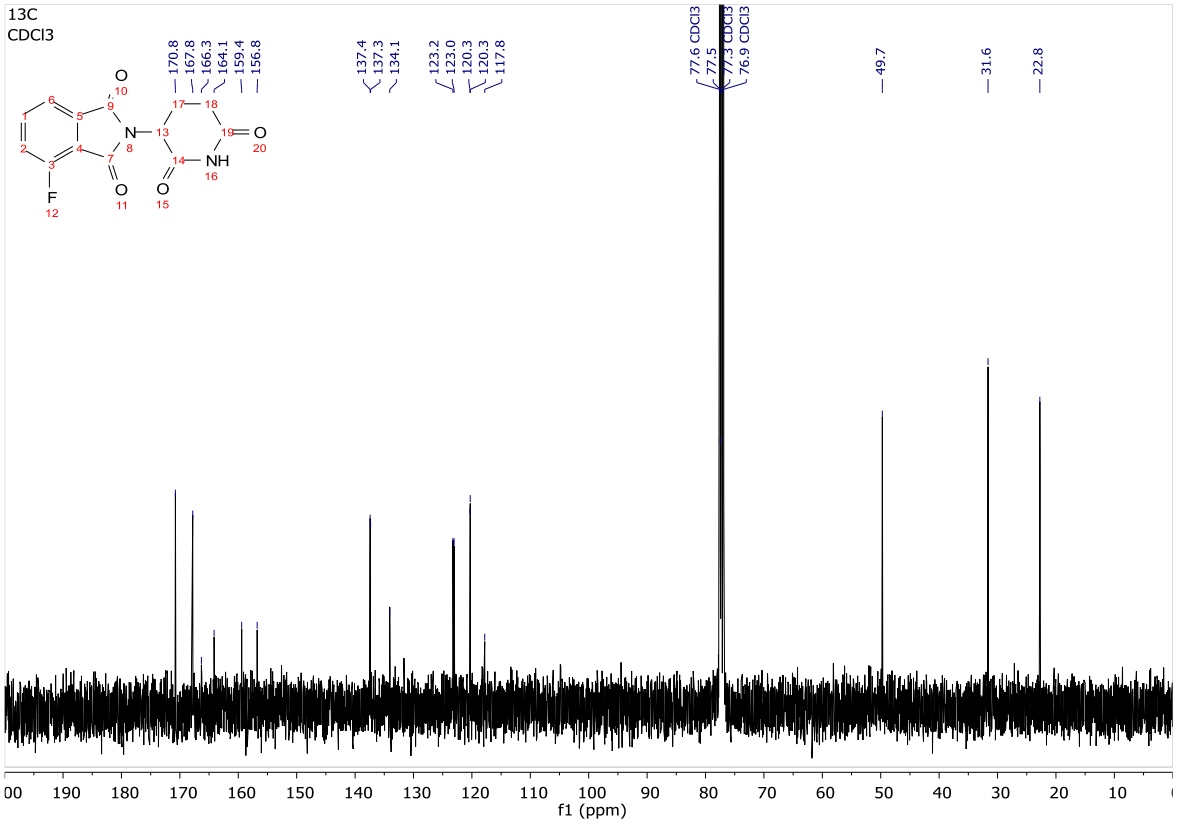
13C
CDCl3
170.8
167.8
166.3
164.1
159.4
156.8
137.4
137.3
134.1
123.2
123.0
120.3
120.3
117.8
77.6 CDCl3
77.5
77.3 CDCl3
76.9 CDCl3
49.7
31.6
22.8
f1 (ppm)

2.9b:

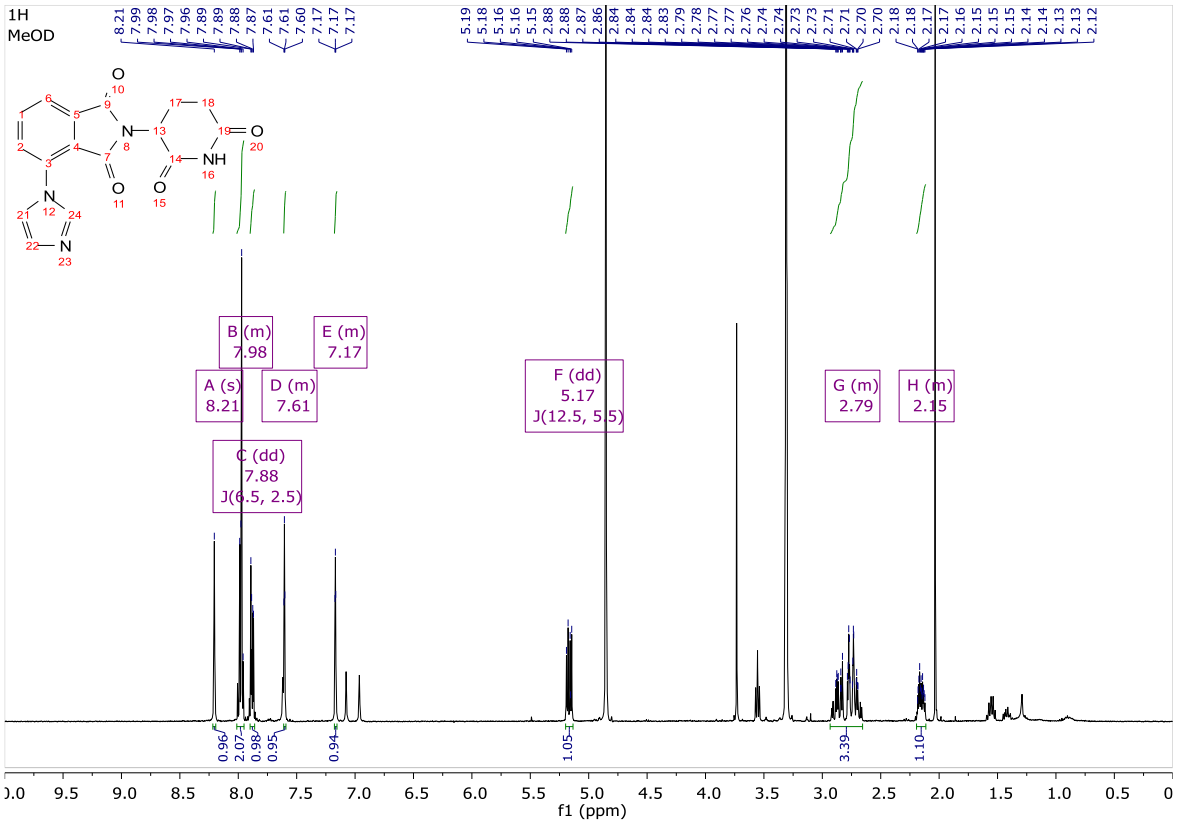
1H
MeOD
B (m)
7.98
E (m)
7.17
A (s)
8.21
D (m)
7.61
C (dd)
7.88
J(6.5, 2.5)
F (dd)
5.17
J(12.5, 5.5)
G (m)
2.79
H (m)
2.15
f1 (ppm)

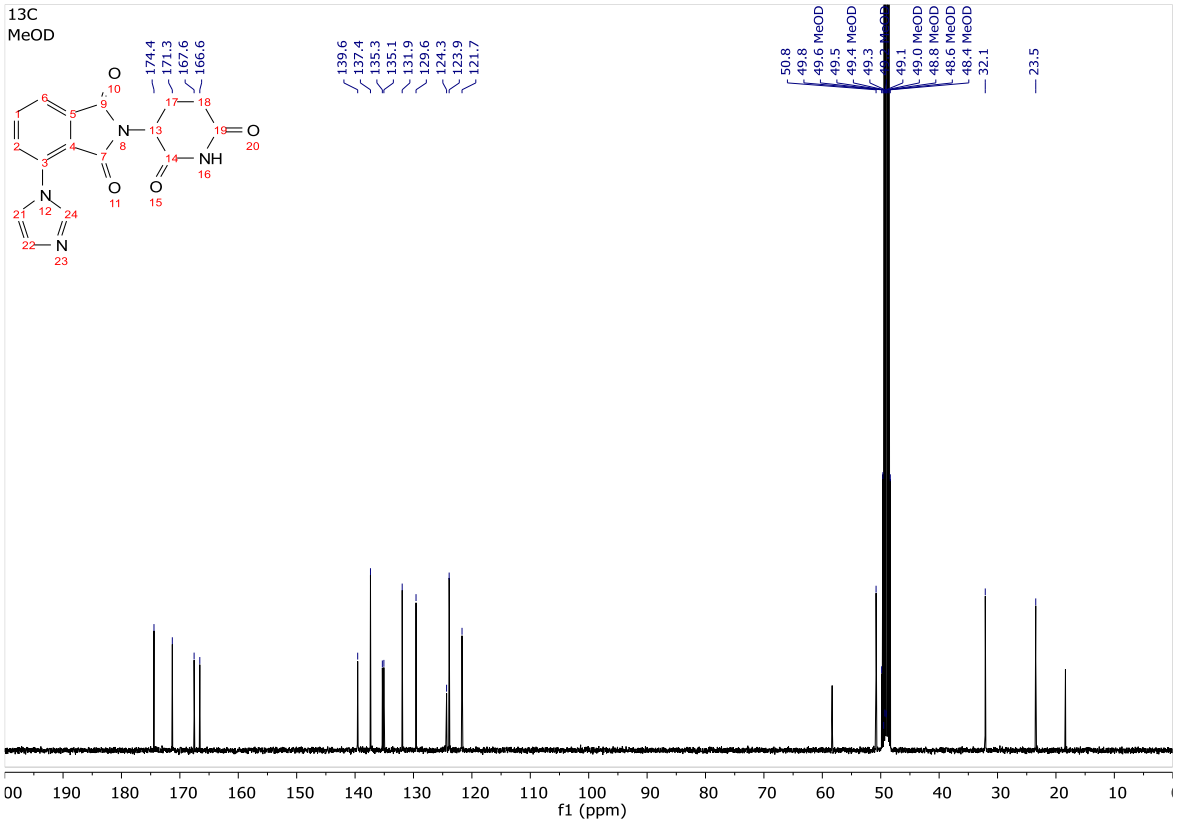
13C
MeOD
f1 (ppm)

MeCRBN-1 (2.10):

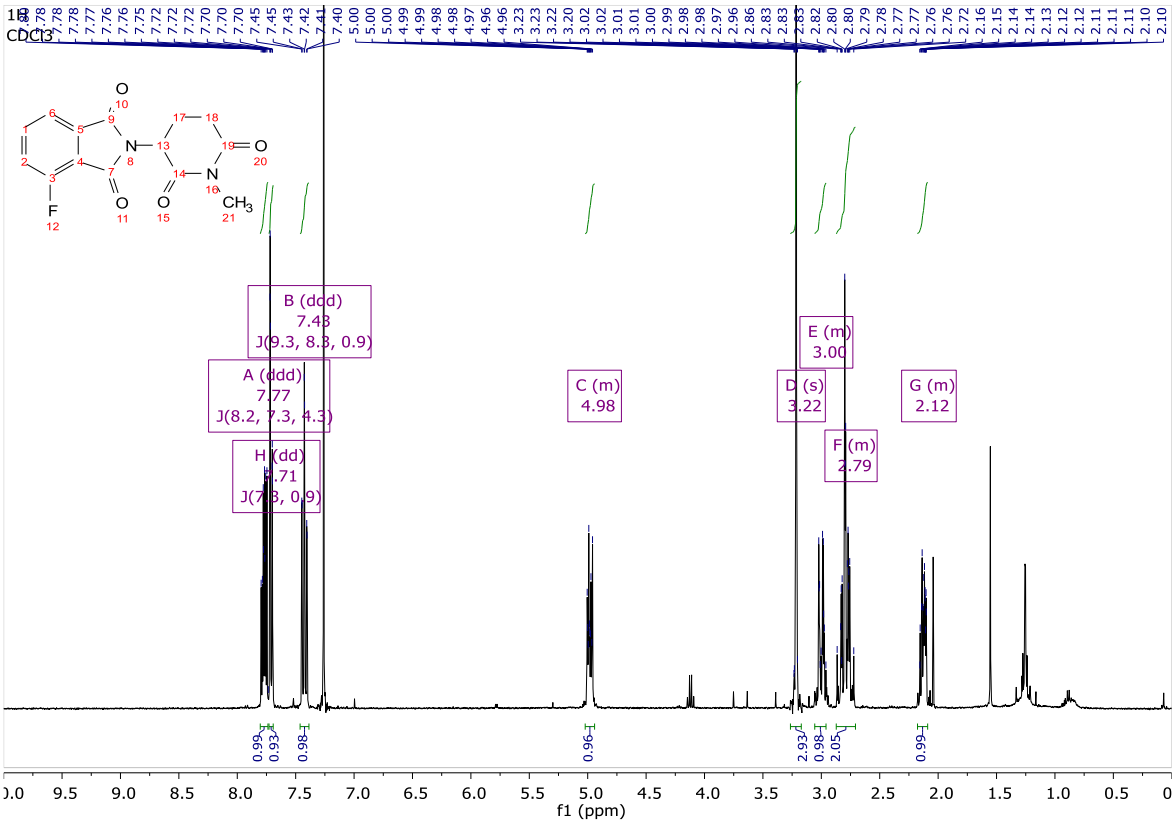
1H
CDCl3
B (ddd)
7.43
J(9.3, 8.3, 0.9)
A (ddd)
7.77
J(8.2, 7.3, 4.3)
H (dd)
7.71
J(7.3, 0.9)
C (m)
4.98
E (m)
3.00
D (s)
3.22
F (m)
2.79
G (m)
2.12
0.99
0.93
0.98
0.96
2.93
0.98
2.05
0.99
f1 (ppm)

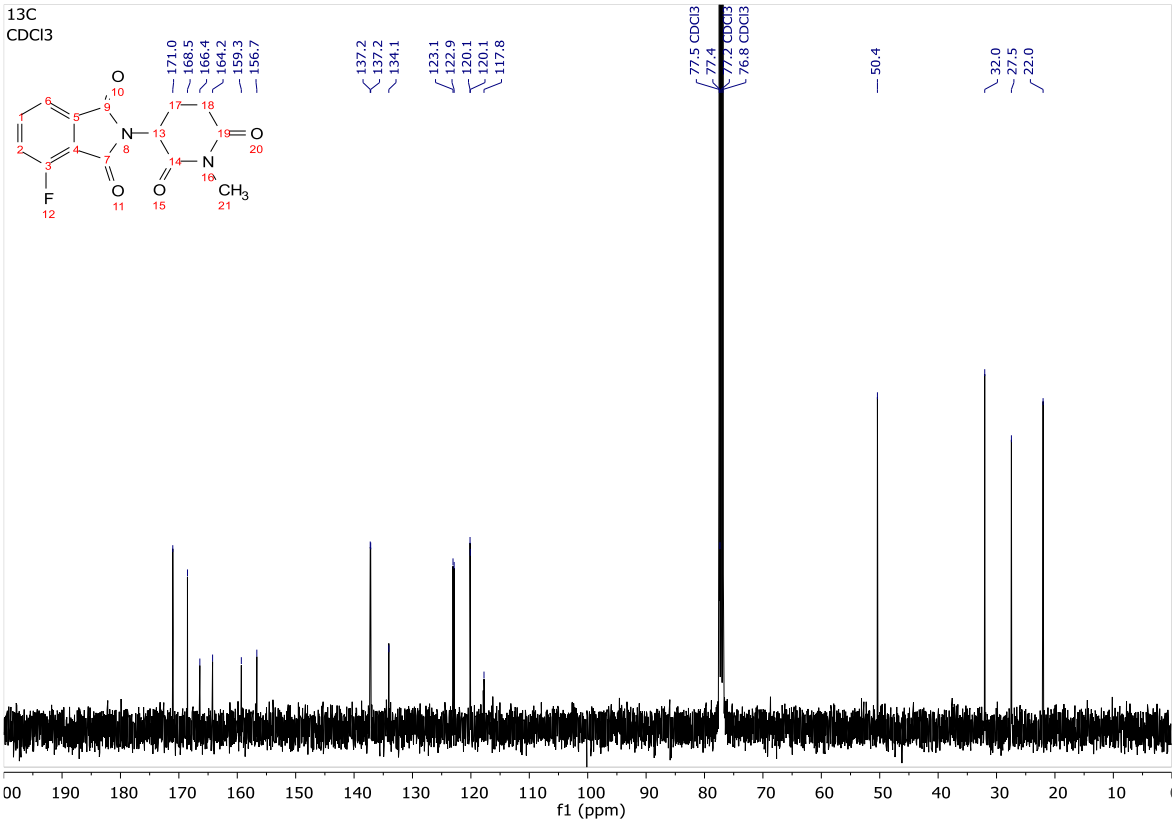
13C
CDCl3
171.0
168.5
166.4
164.2
159.3
156.7
137.2
137.2
134.1
123.1
122.9
120.1
120.1
117.8
77.5 CDCl3
77.4
77.2 CDCl3
76.8 CDCl3
50.4
32.0
27.5
22.0
f1 (ppm)

2.14:

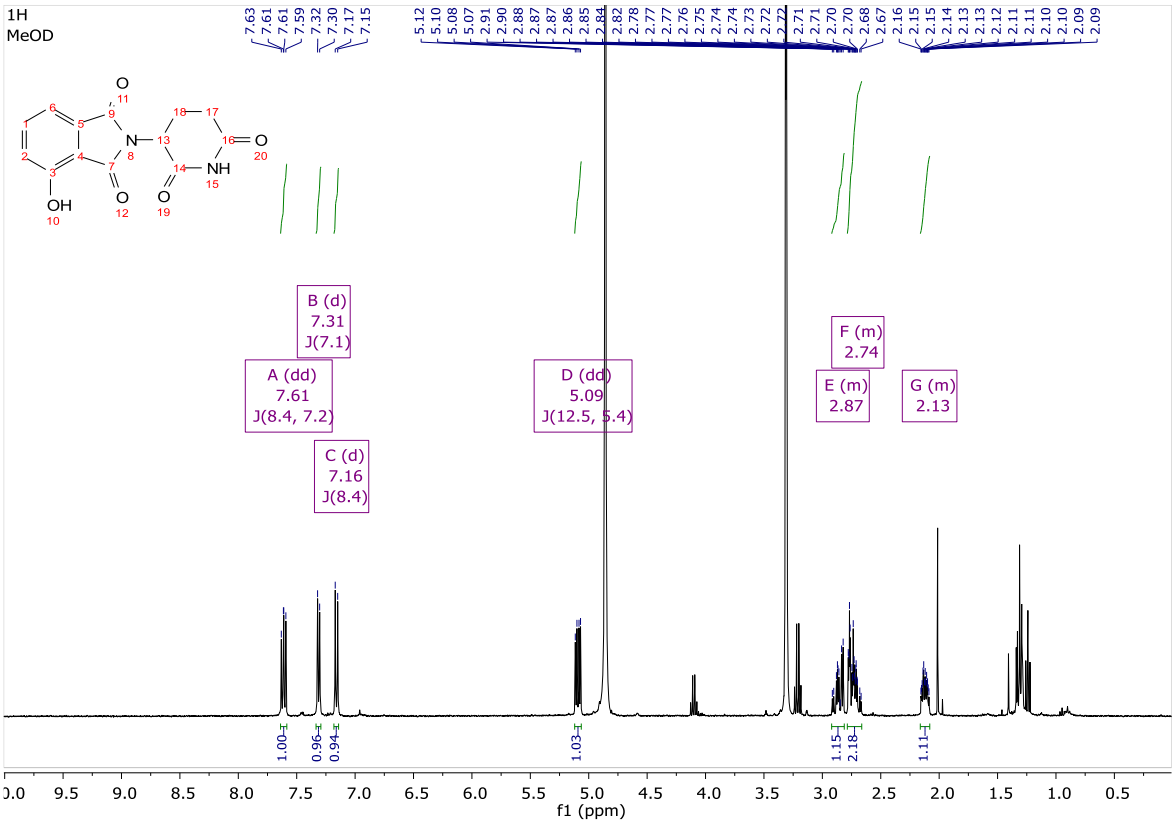
1H
MeOD
B (d)
7.31
J(7.1)
A (dd)
7.61
J(8.4, 7.2)
C (d)
7.16
J(8.4)
D (dd)
5.09
J(12.5, 5.4)
F (m)
2.74
E (m)
2.87
G (m)
2.13
f1 (ppm)

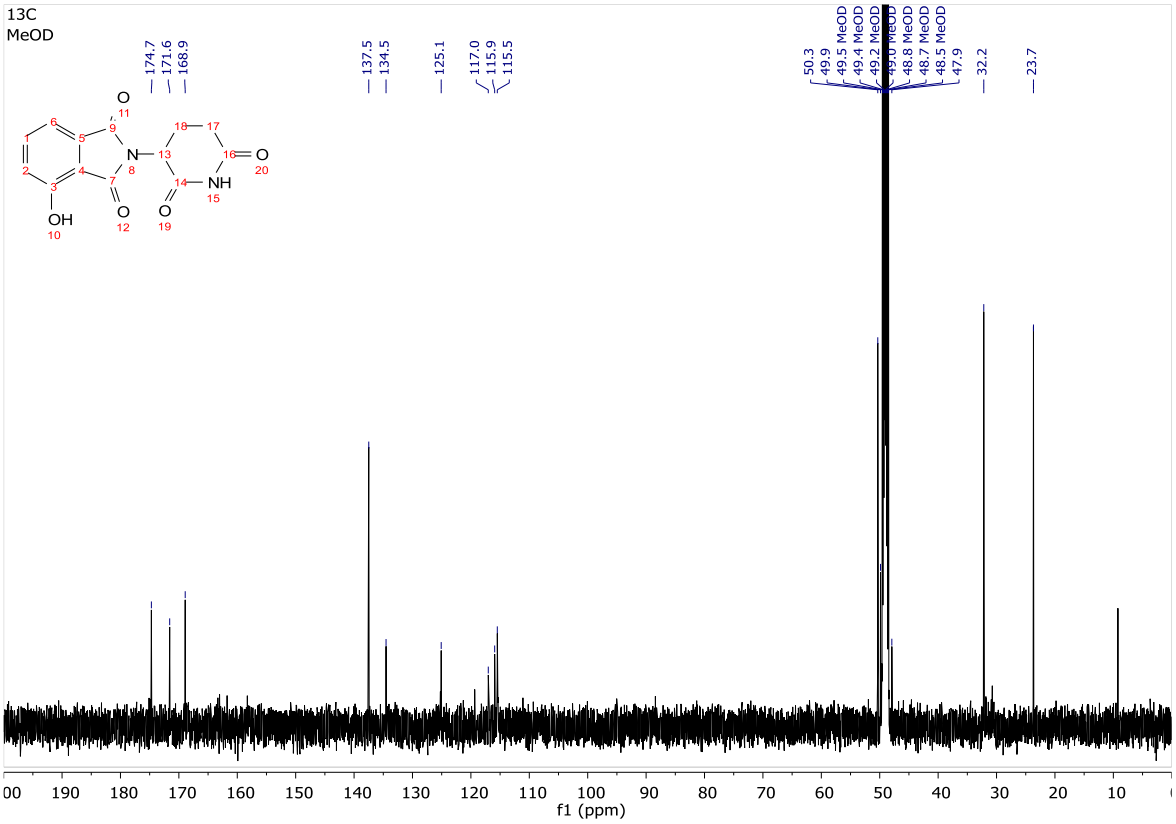
13C
MeOD
f1 (ppm)

CRBN-2 (2.11):

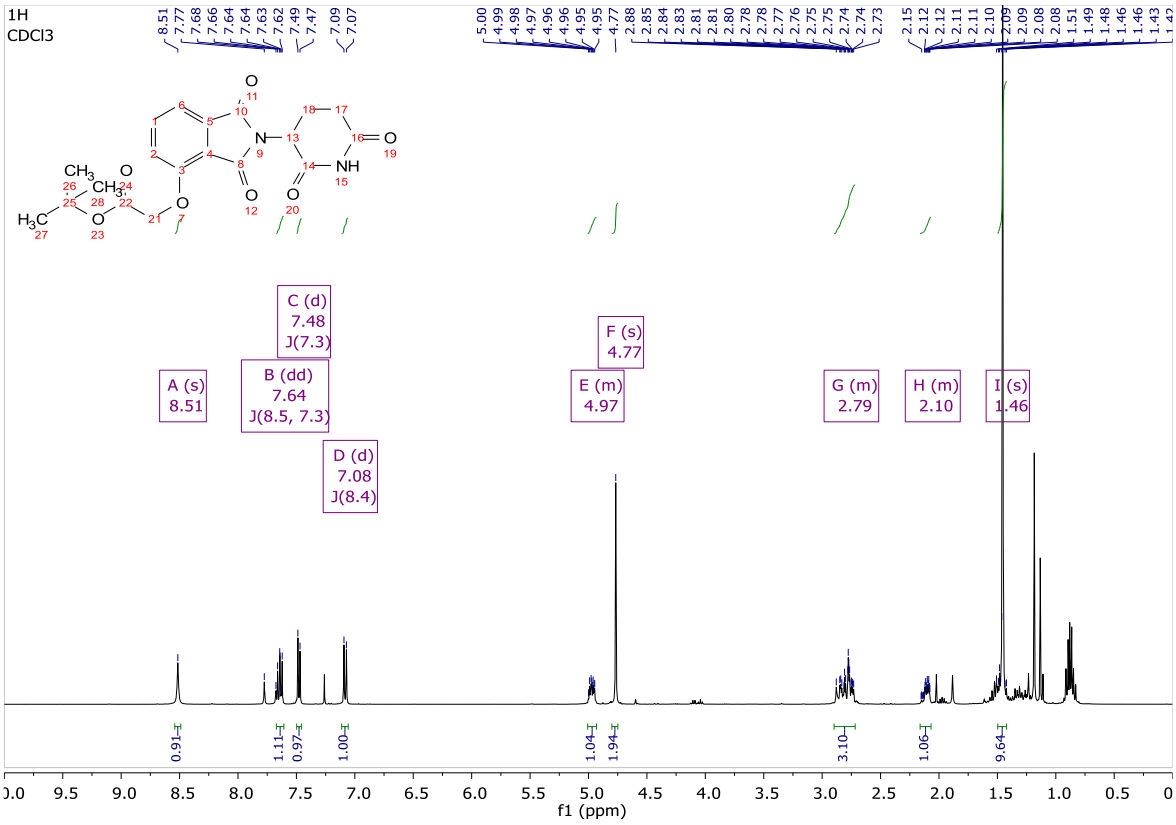
1H
CDCl3
A (s)
8.51
B (dd)
7.64
J(8.5, 7.3)
C (d)
7.48
J(7.3)
D (d)
7.08
J(8.4)
E (m)
4.97
F (s)
4.77
G (m)
2.79
H (m)
2.10
I (s)
1.46
f1 (ppm)

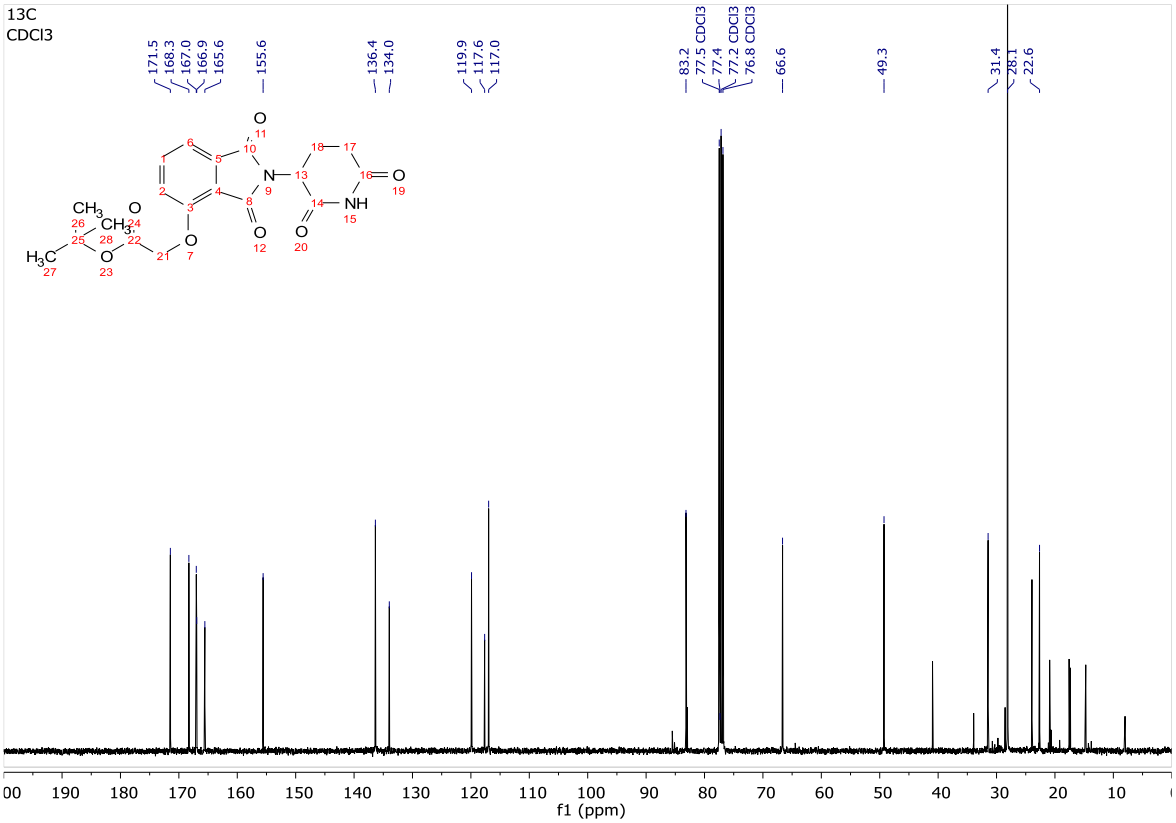
13C
CDCl3
f1 (ppm)

MeCRBN-2 (2.12):

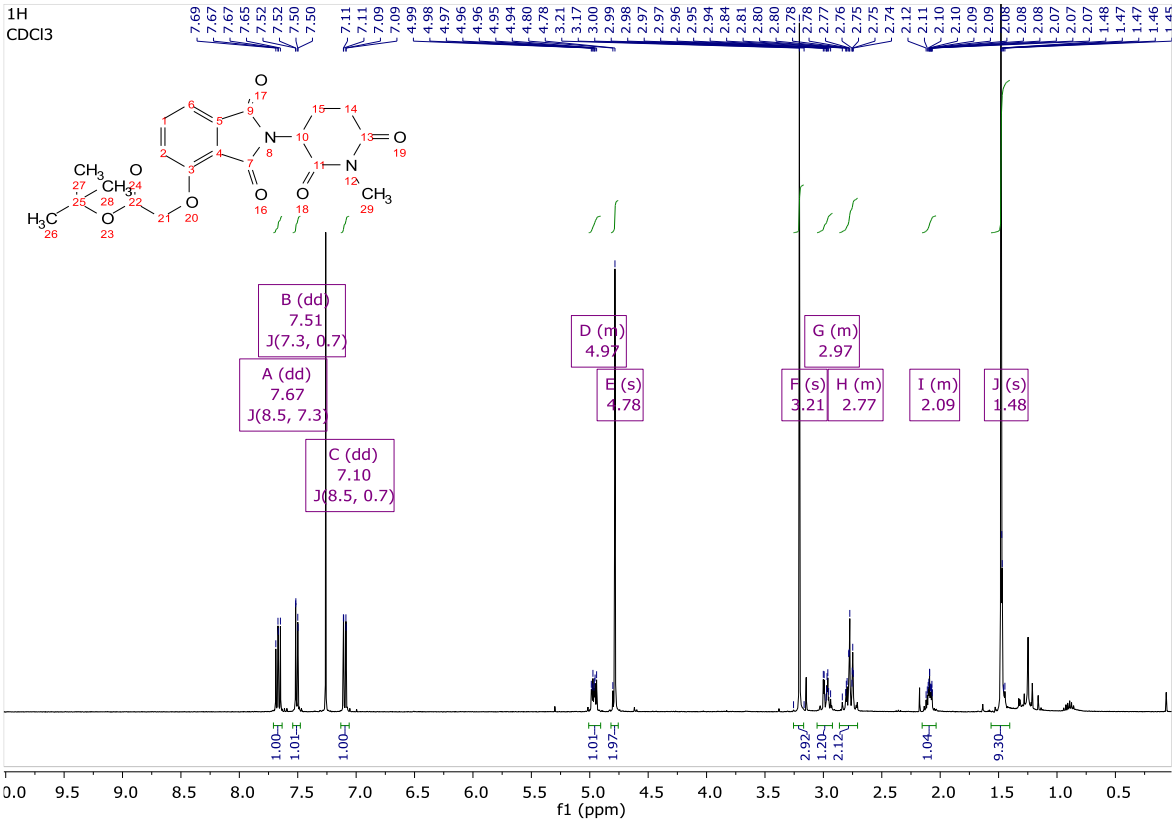
1H
CDCl3
B (dd)
7.51
J(7.3, 0.7)
A (dd)
7.67
J(8.5, 7.3)
C (dd)
7.10
J(8.5, 0.7)
D (m)
4.97
E (s)
4.78
G (m)
2.97
F (s)
3.21
H (m)
2.77
I (m)
2.09
J (s)
1.48
f1 (ppm)

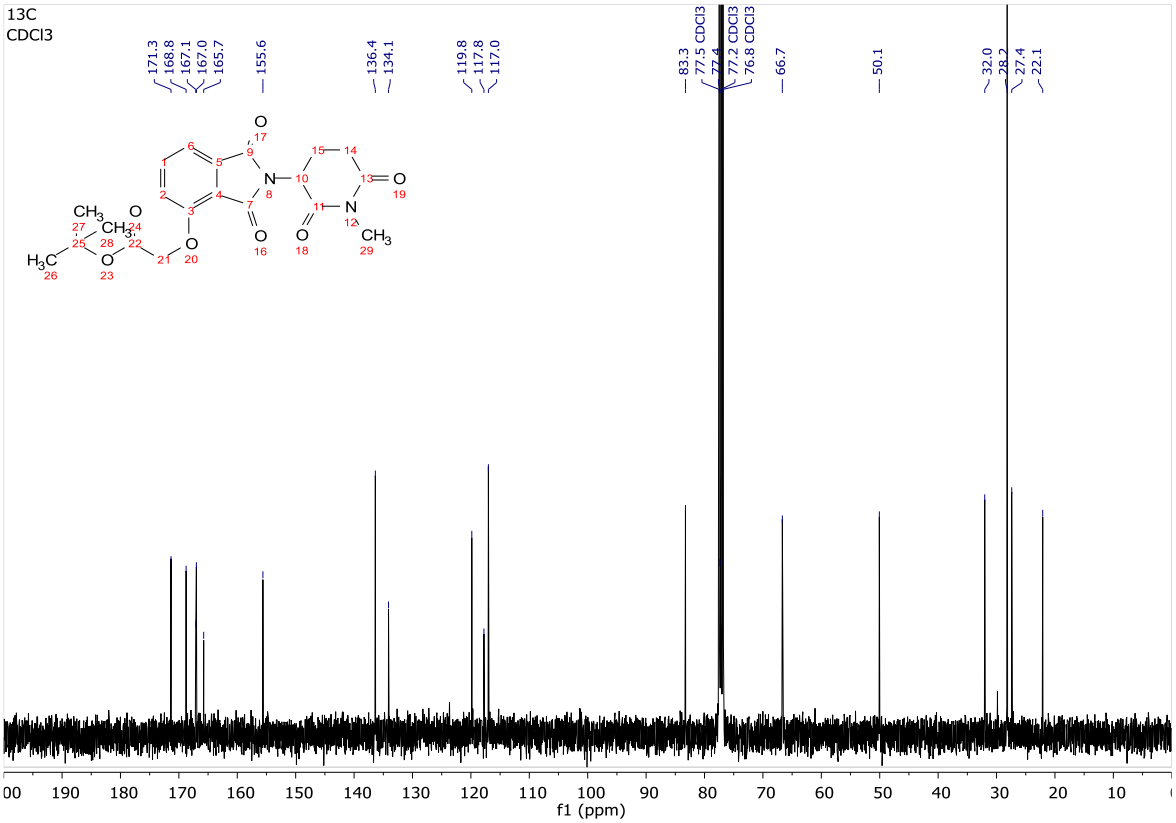
13C
CDCl3
f1 (ppm)

HaloPROTACs and mono-functional controls

- *VHL HaloPROTACs and mono-functional controls*

2.15a:

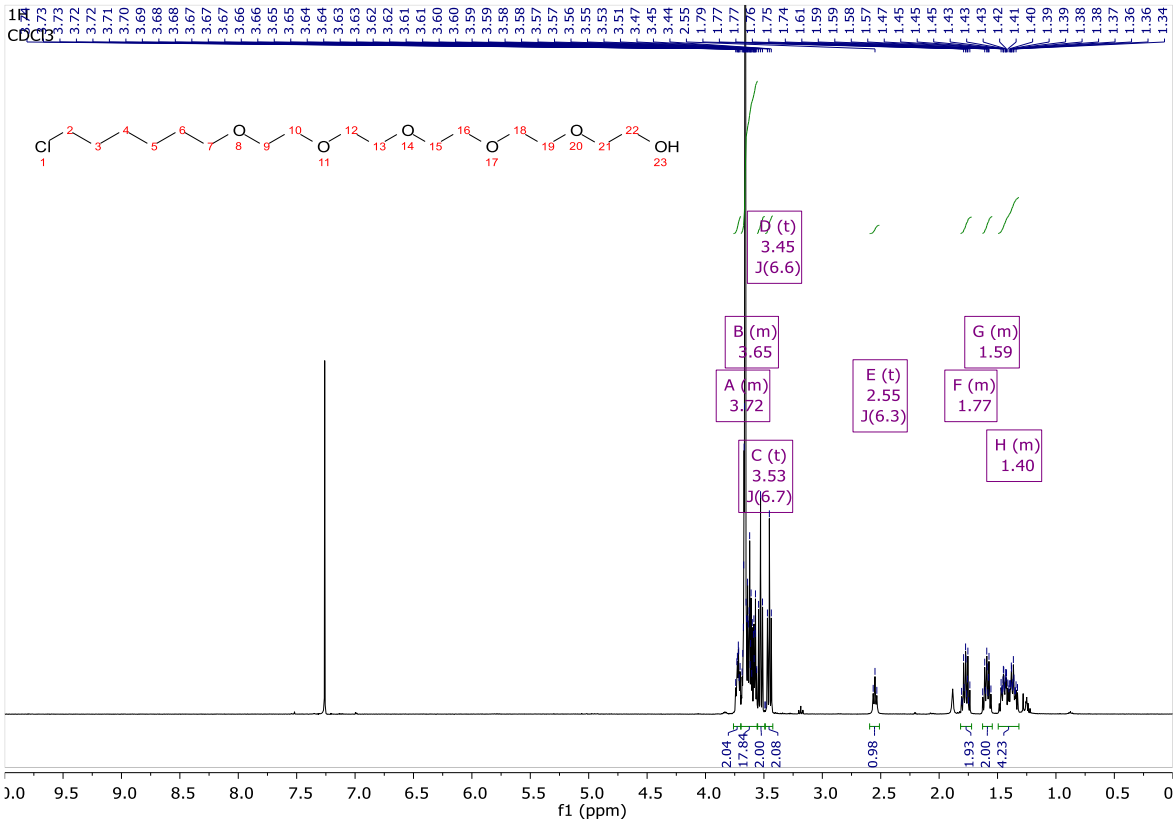

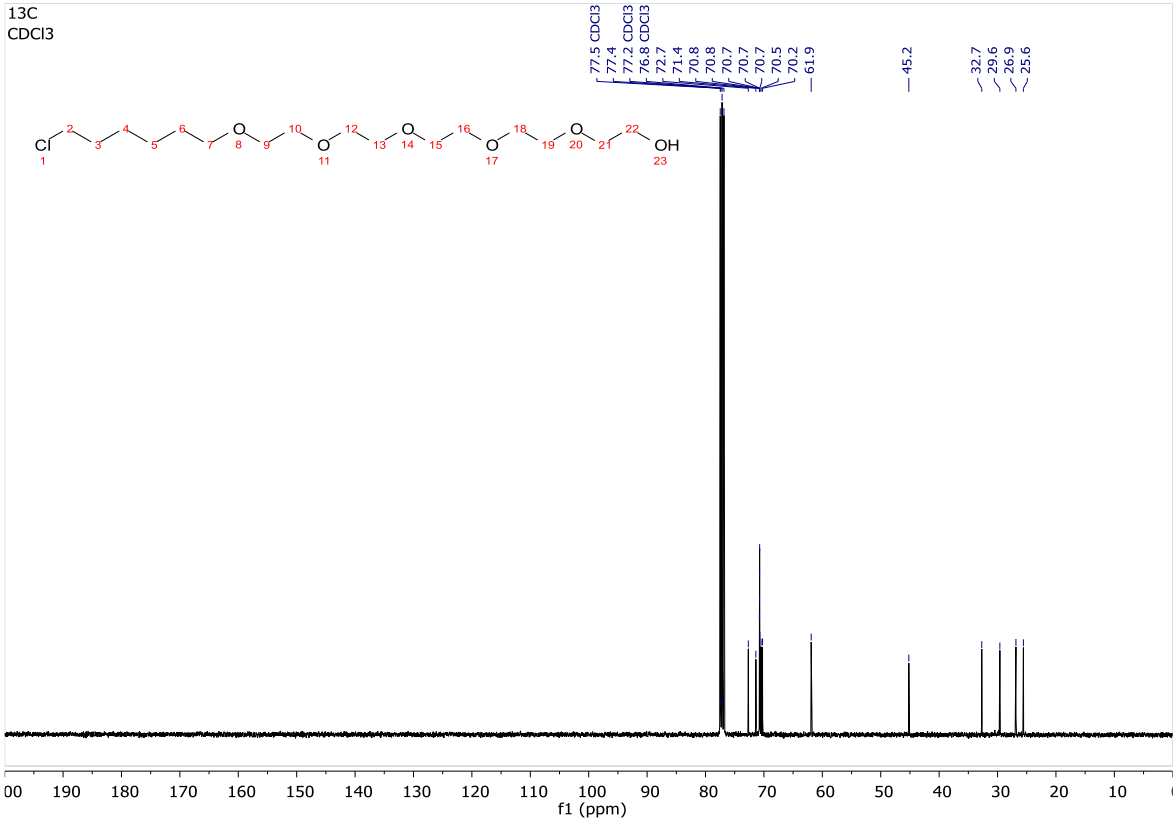

2.15b:

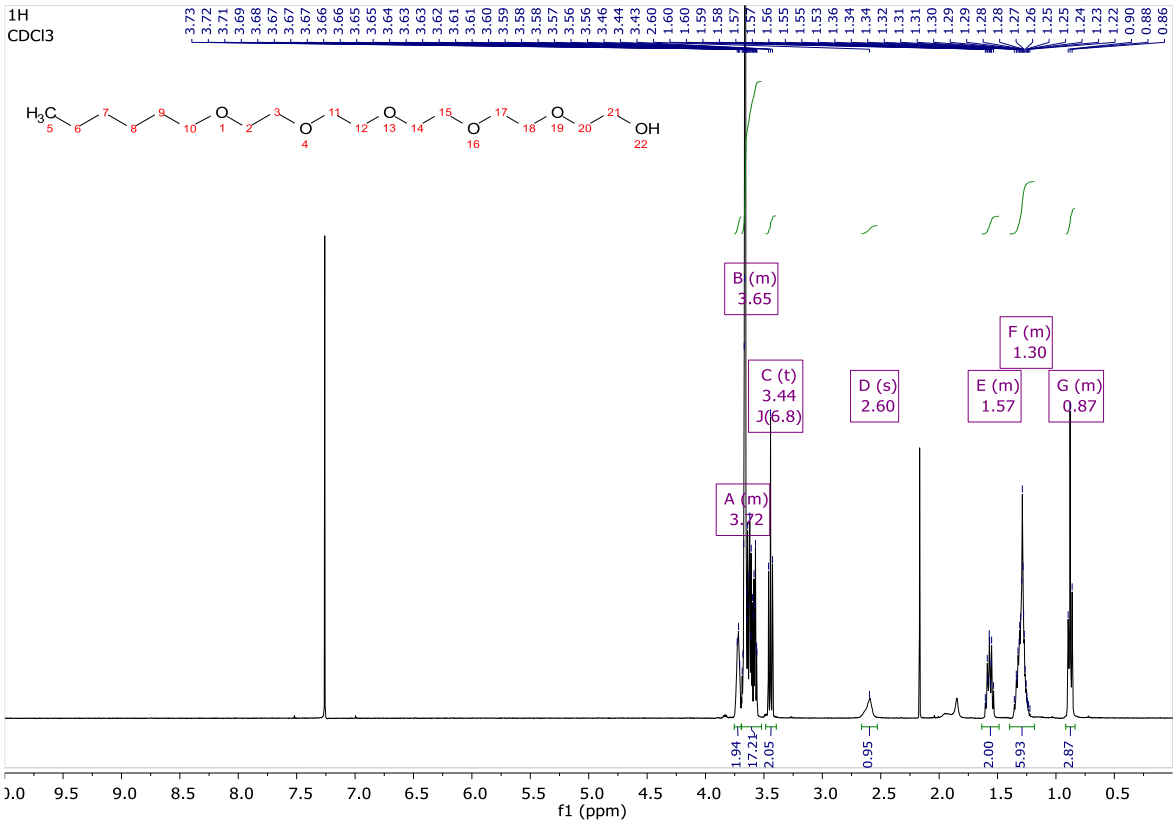
1H
CDCl3
B (m)
3.65
C (t)
3.44
J(6.8)
D (s)
2.60
F (m)
1.30
E (m)
1.57
G (m)
0.87
A (m)
3.72
f1 (ppm)

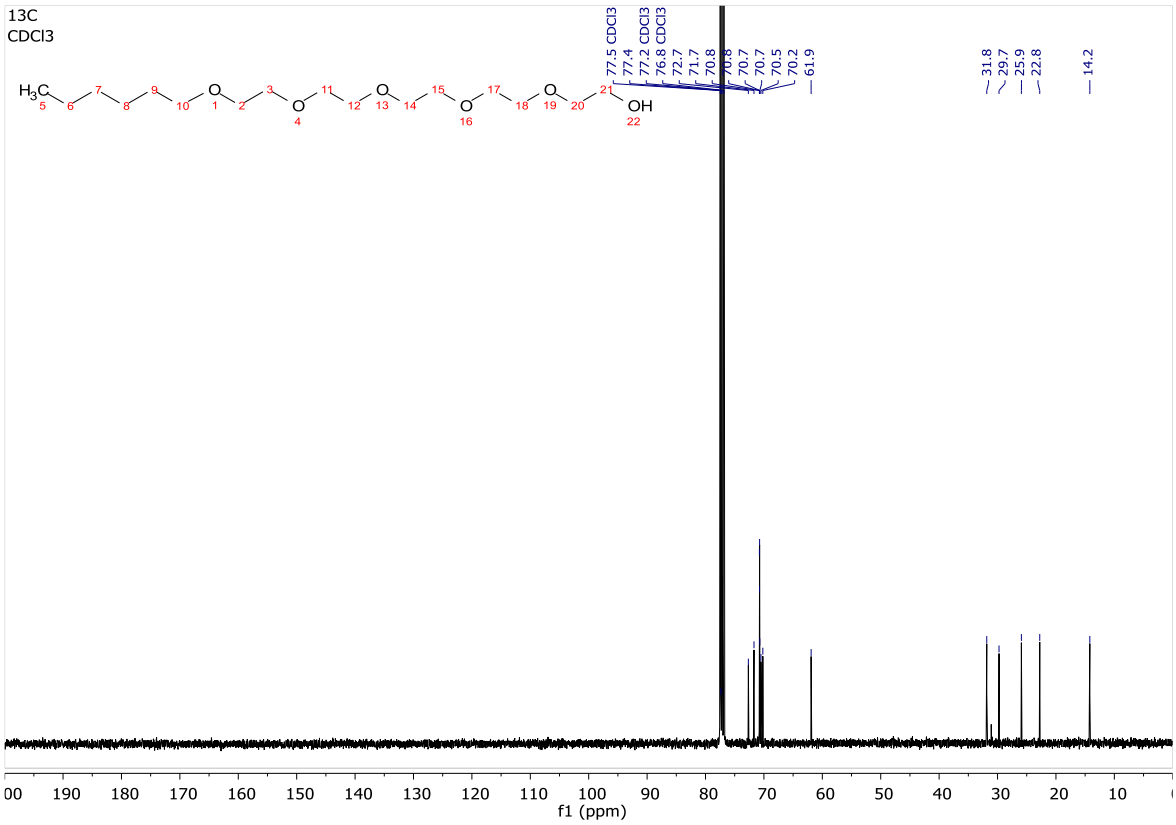
13C
CDCl3
77.5 CDCl3
77.4
77.2 CDCl3
76.8 CDCl3
72.7
71.7
70.8
70.8
70.7
70.7
70.5
70.2
61.9
31.8
29.7
25.9
22.8
14.2
f1 (ppm)

2.17a:

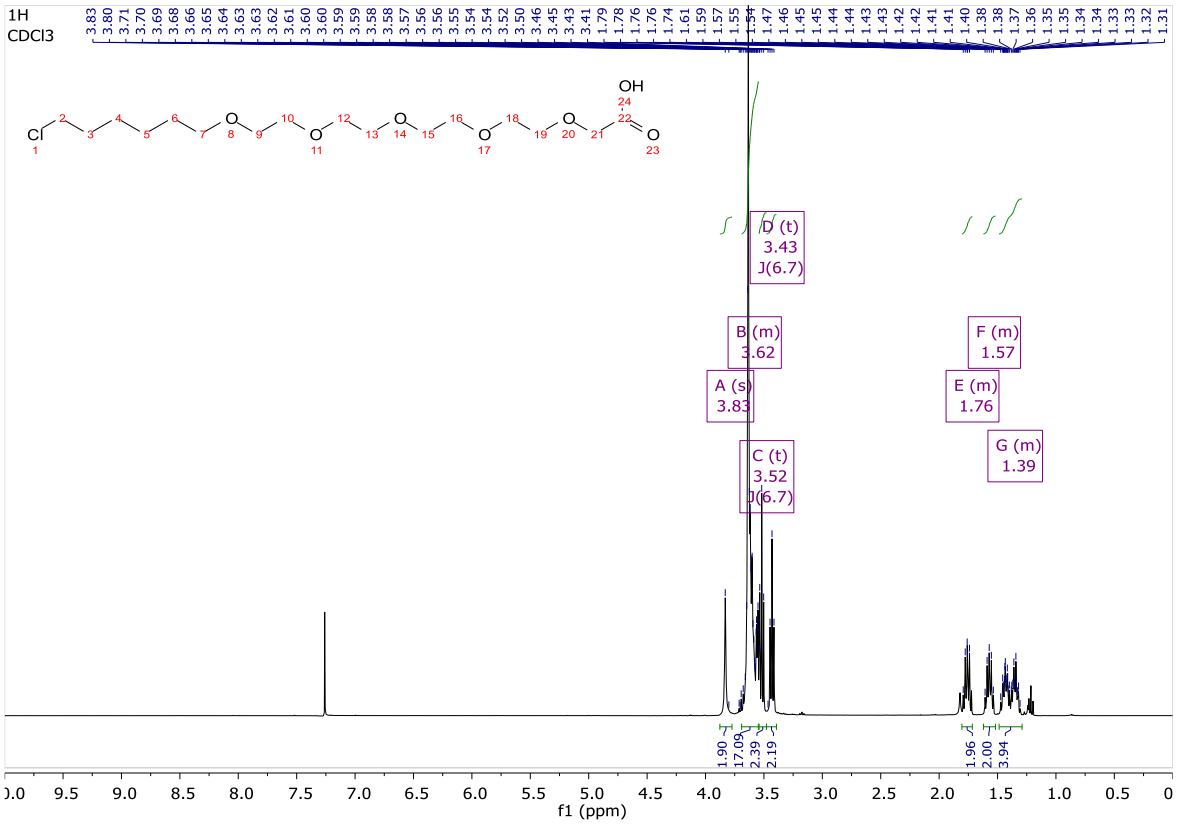
1H
CDCl3
D (t)
3.43
J(6.7)
B (m)
3.62
A (s)
3.83
C (t)
3.52
J(6.7)
F (m)
1.57
E (m)
1.76
G (m)
1.39
1.90
17.09
2.39
2.19
1.96
2.00
3.94
f1 (ppm)

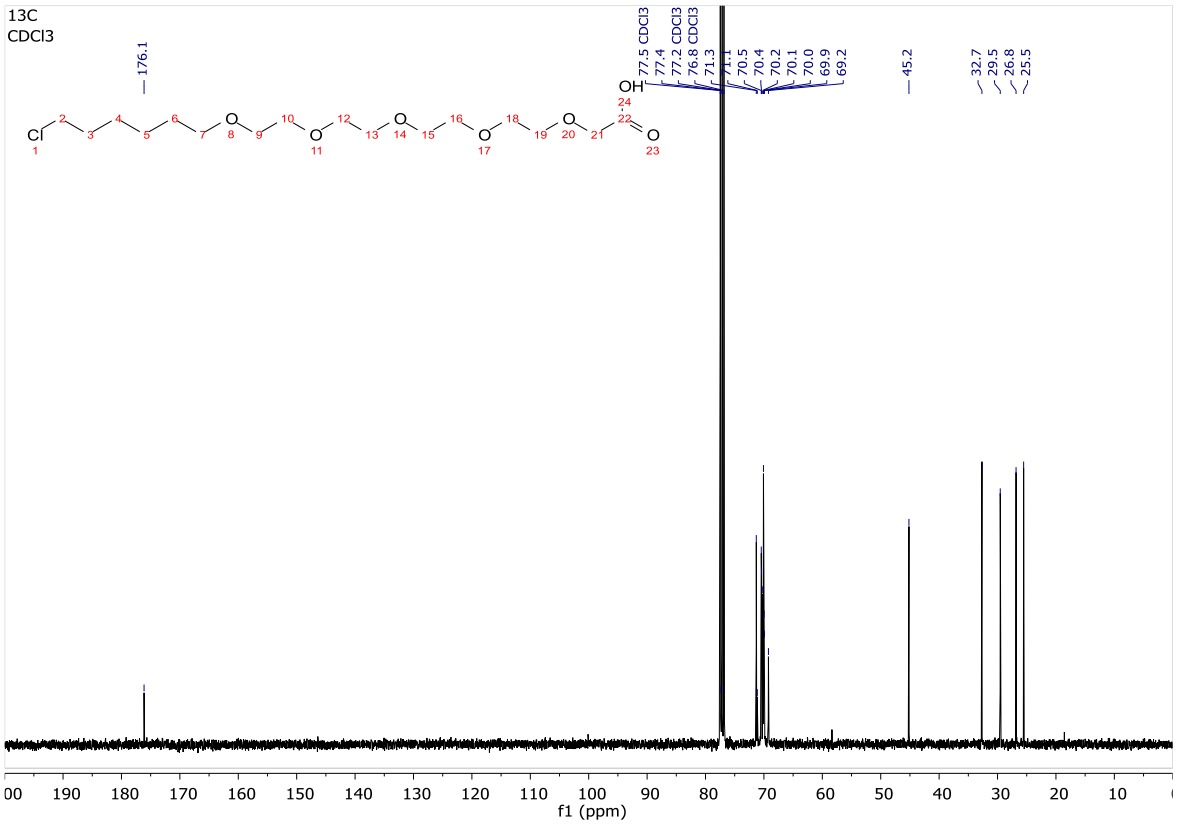
13C
CDCl3
176.1
77.5 CDCl3
77.4
77.2 CDCl3
76.8 CDCl3
71.3
70.5
70.4
70.2
70.1
70.0
69.9
69.2
45.2
32.7
29.5
26.8
25.5
f1 (ppm)

2.17b:

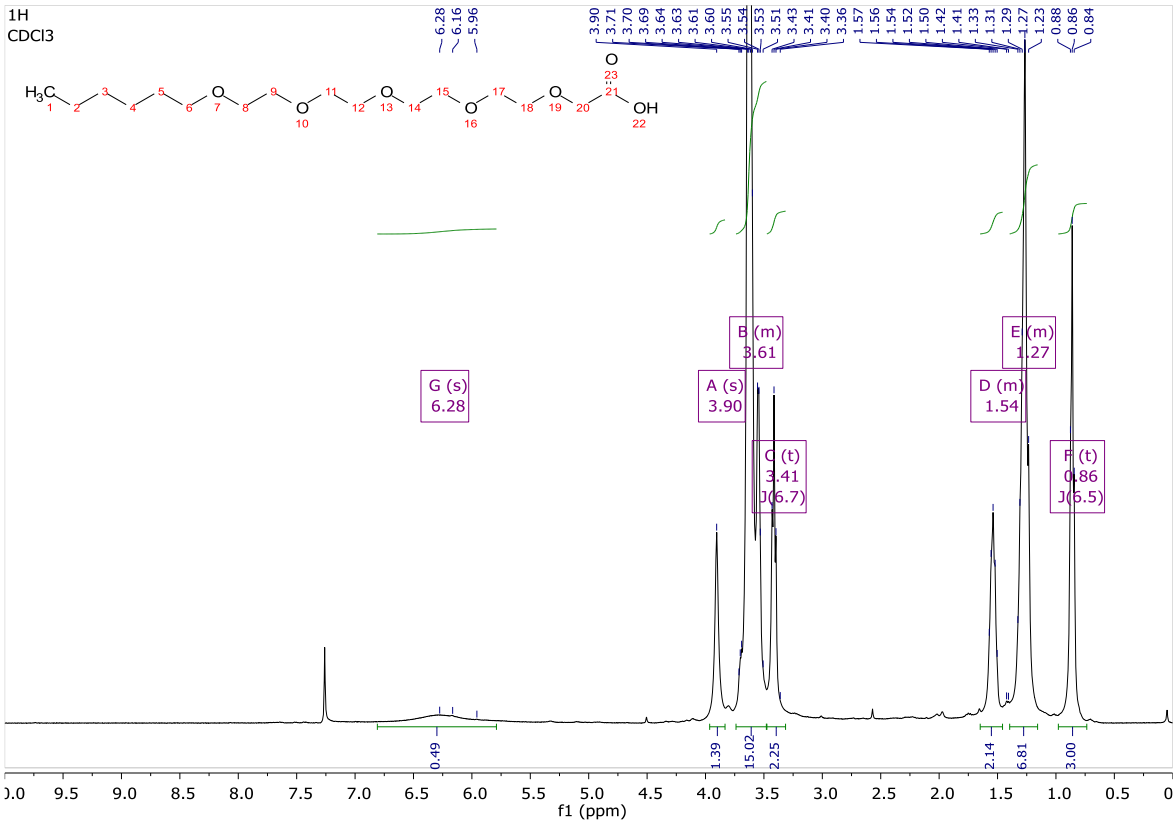
1H
CDCl3
G (s)
6.28
A (s)
3.90
B (m)
3.61
C (t)
3.41
J(6.7)
D (m)
1.54
E (m)
1.27
F (t)
0.86
J(6.5)
f1 (ppm)

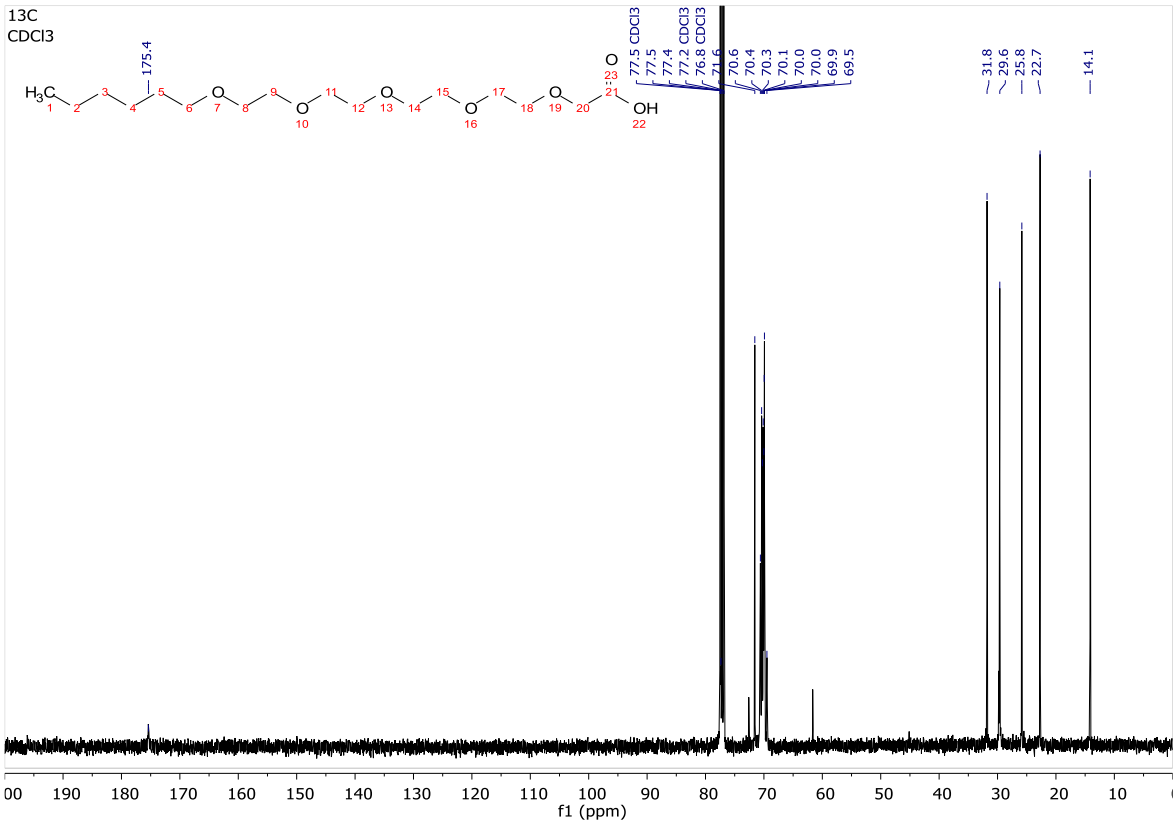
13C
CDCl3
f1 (ppm)

VHL-HP-1 (2.18):

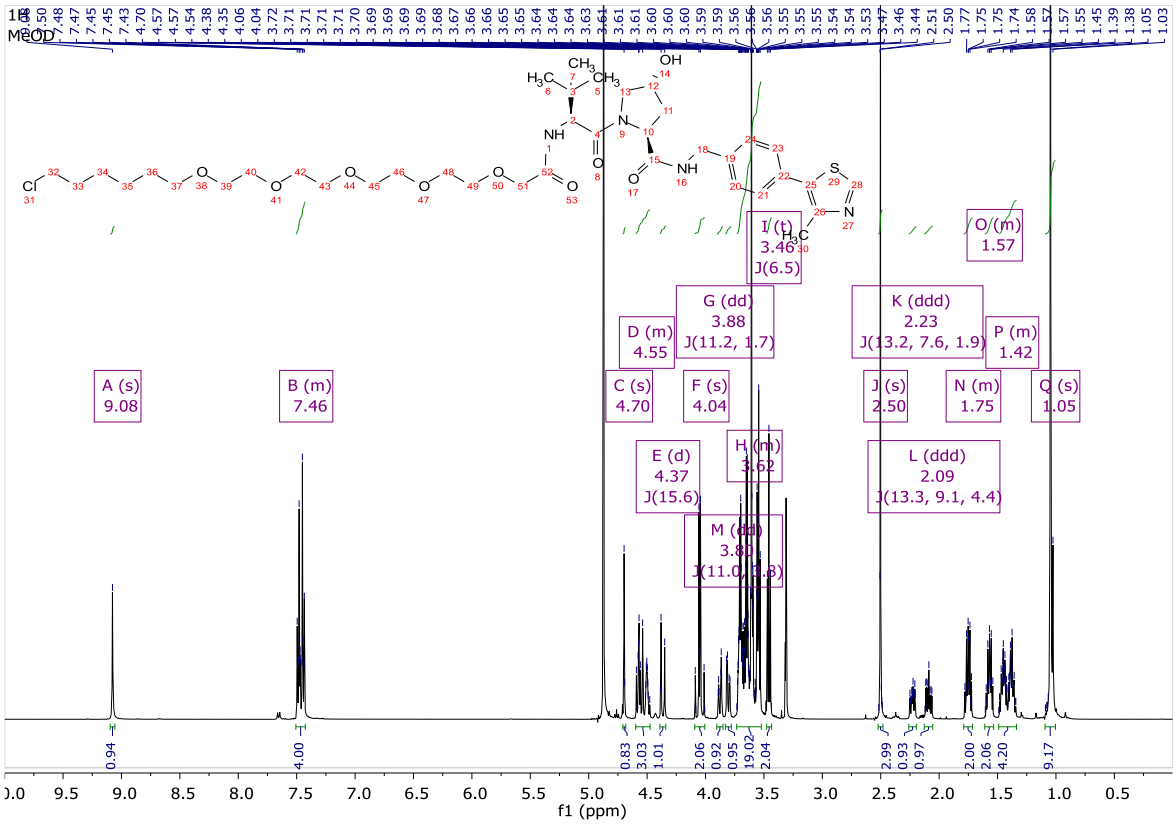
1H
MeOD
A (s)
9.08
B (m)
7.46
C (s)
4.70
D (m)
4.55
E (d)
4.37
J(15.6)
F (s)
4.04
G (dd)
3.88
J(11.2, 1.7)
H (m)
3.62
I (t)
3.46
J(6.5)
J (s)
2.50
K (ddd)
2.23
J(13.2, 7.6, 1.9)
L (ddd)
2.09
J(13.3, 9.1, 4.4)
N (m)
1.75
O (m)
1.57
P (m)
1.42
Q (s)
1.05
f1 (ppm)

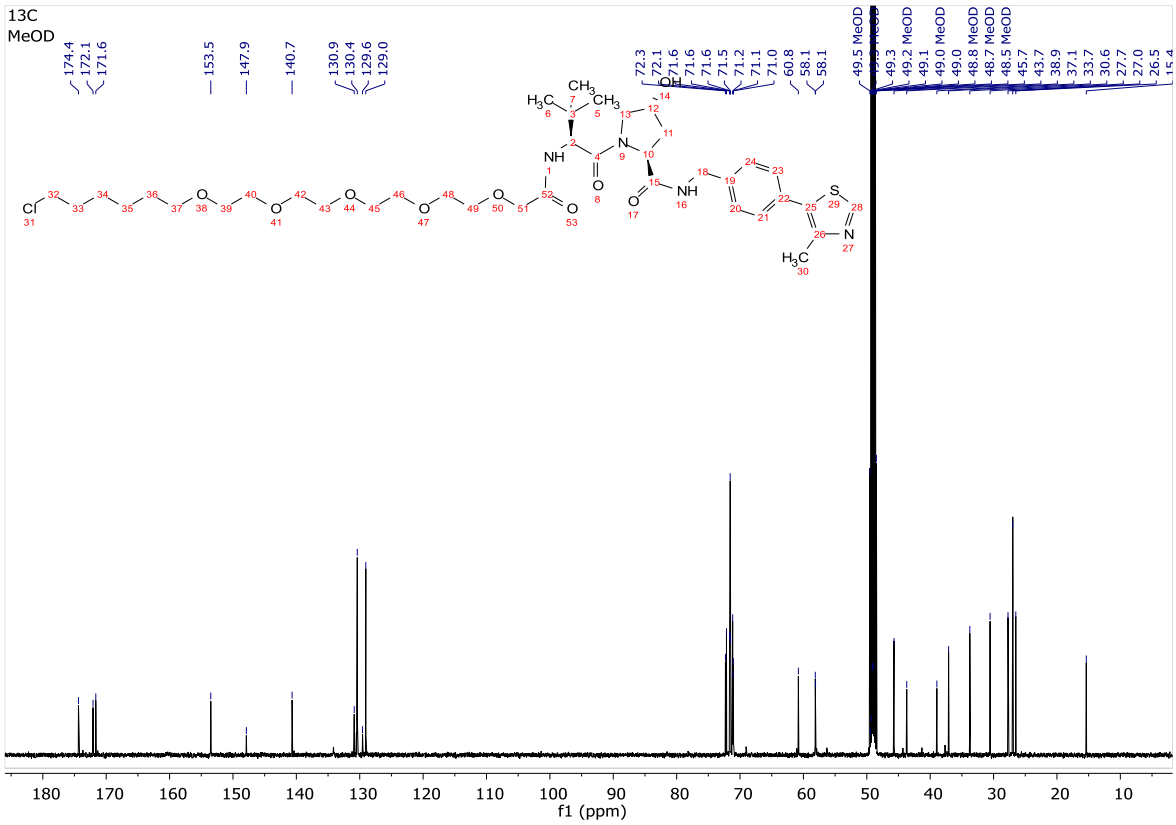
13C
MeOD
f1 (ppm)

***cis*VHL-ctrl-1 (2.19)**:

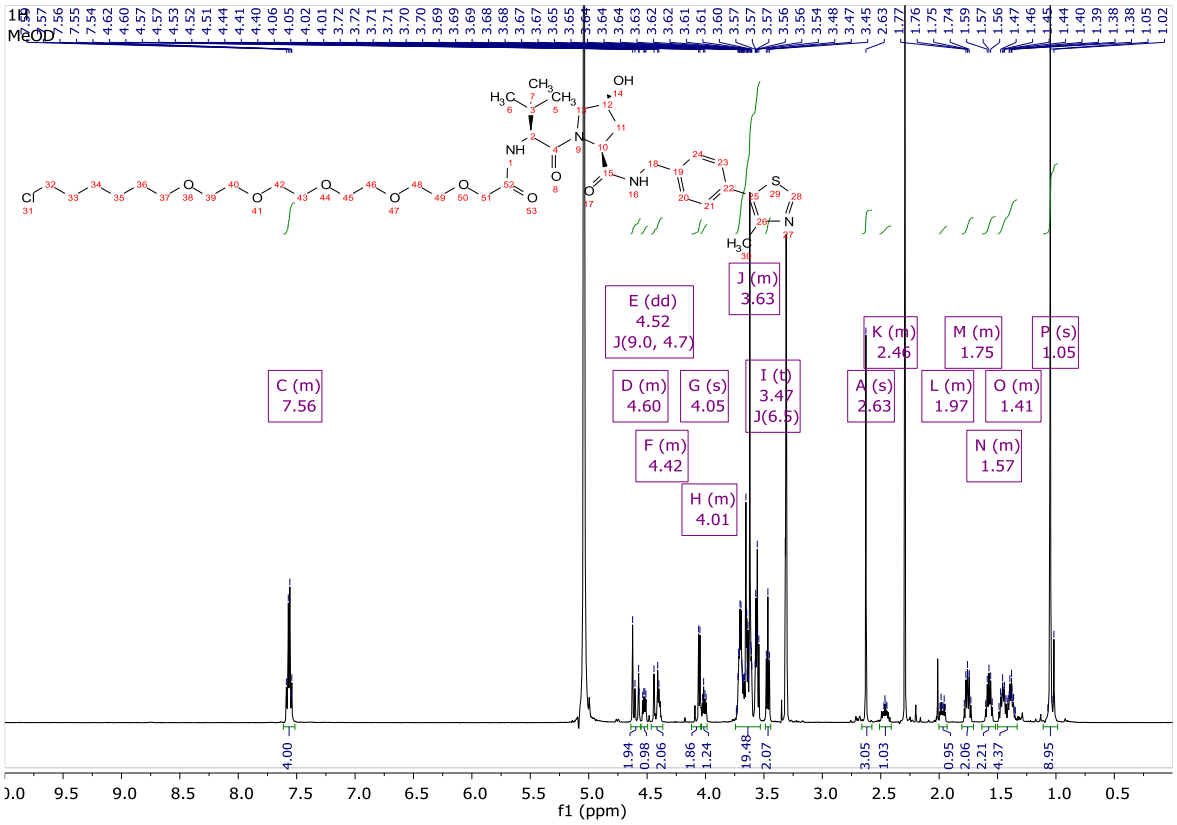

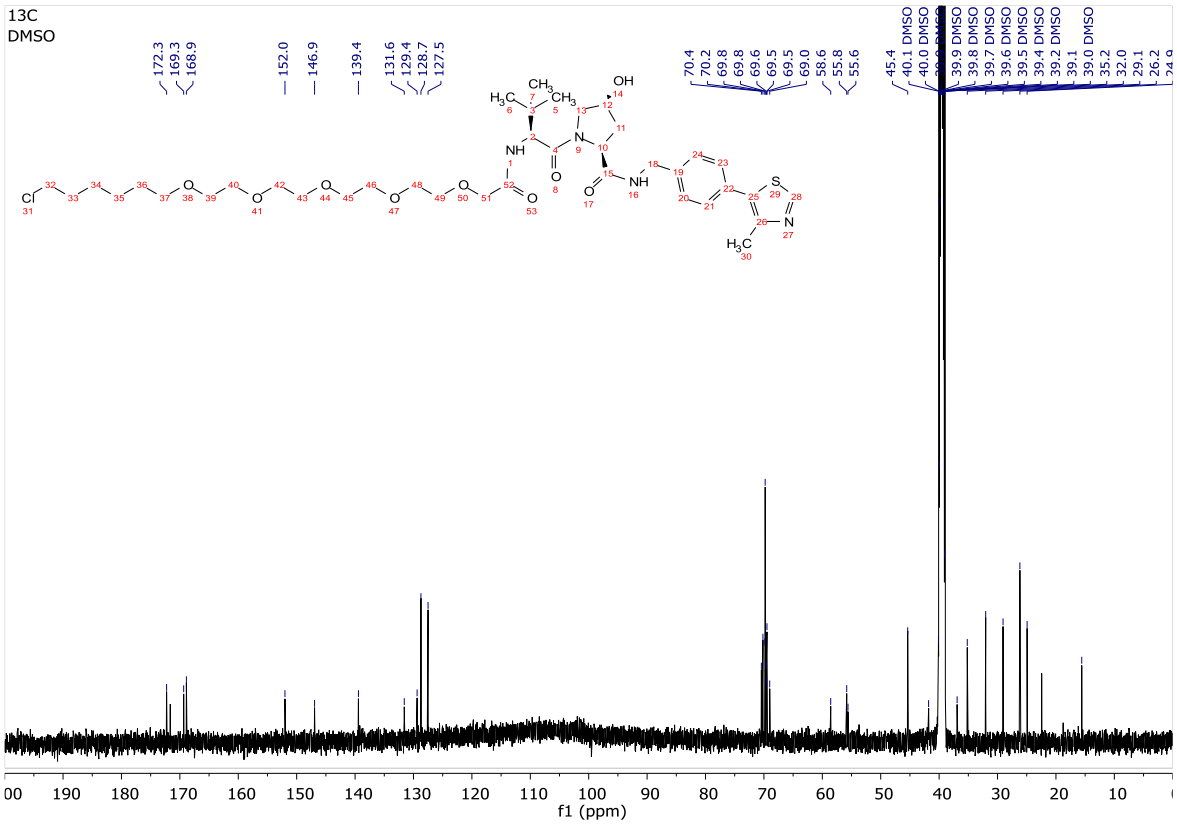

noHTL-VHL-ctrl-1 (2.20):

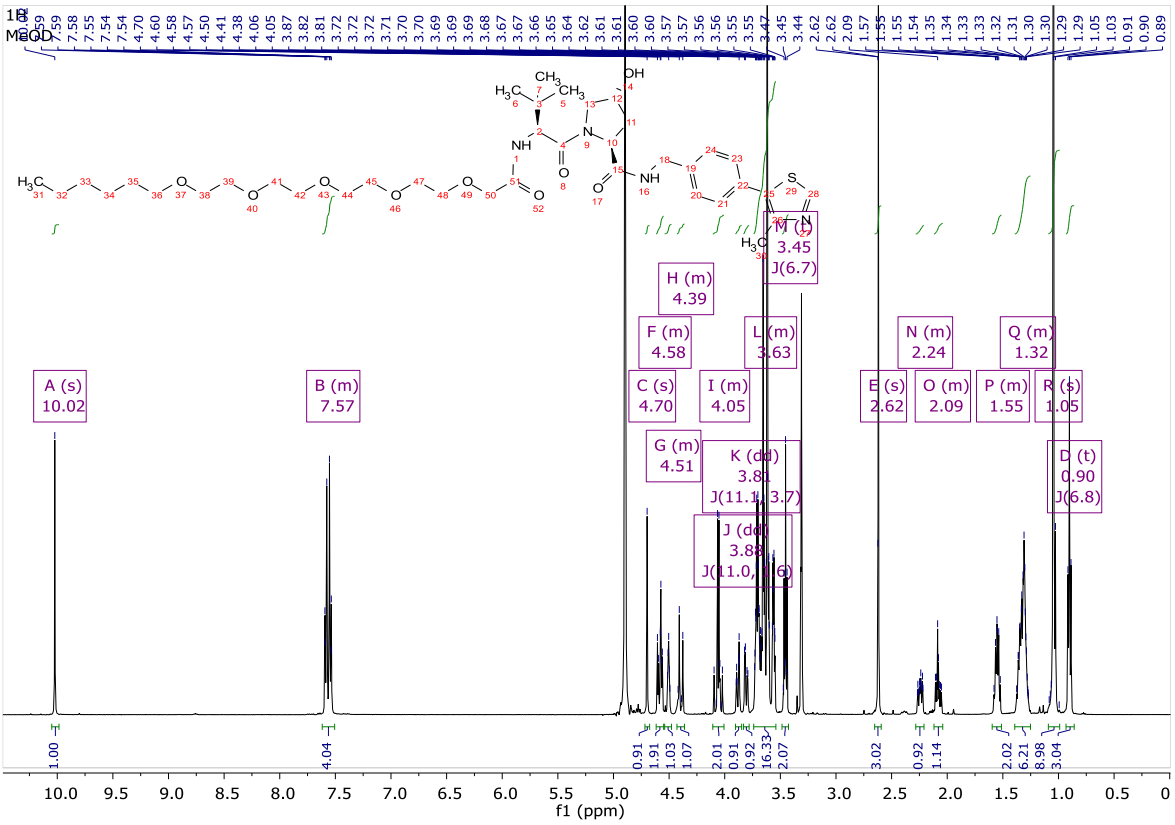

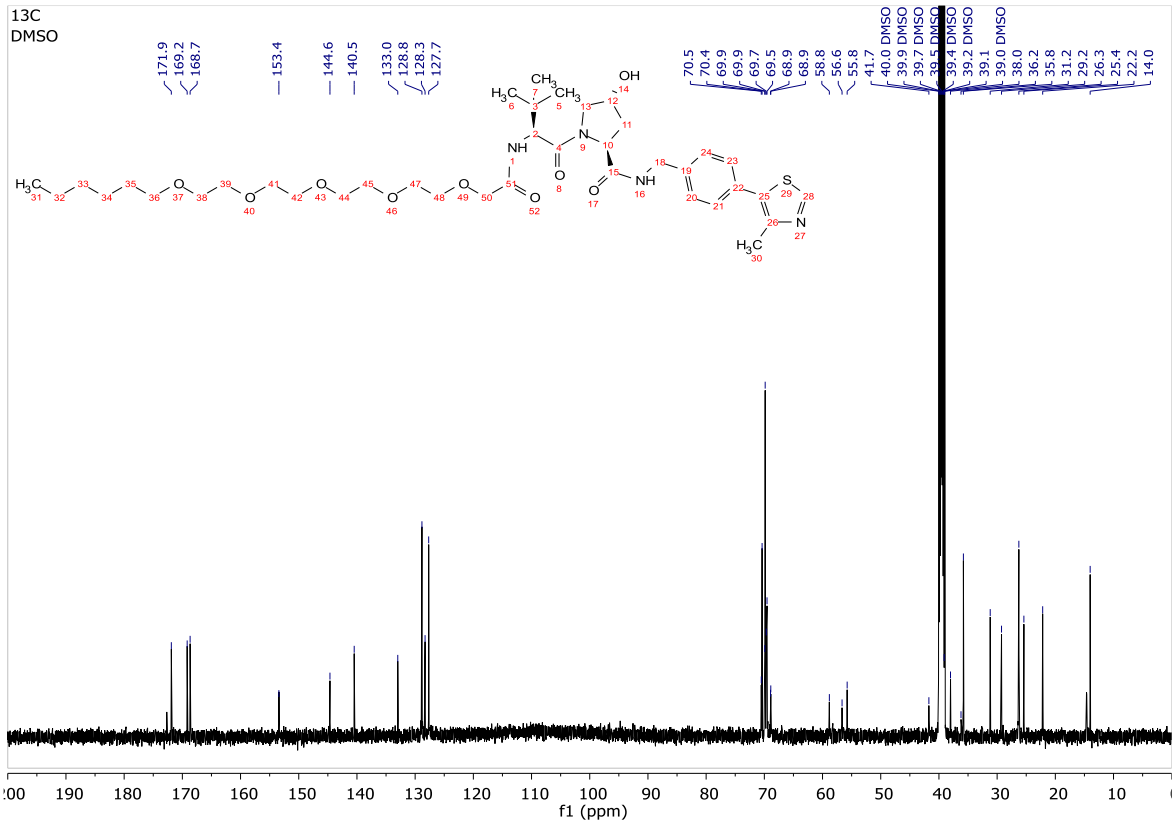

2.21a:

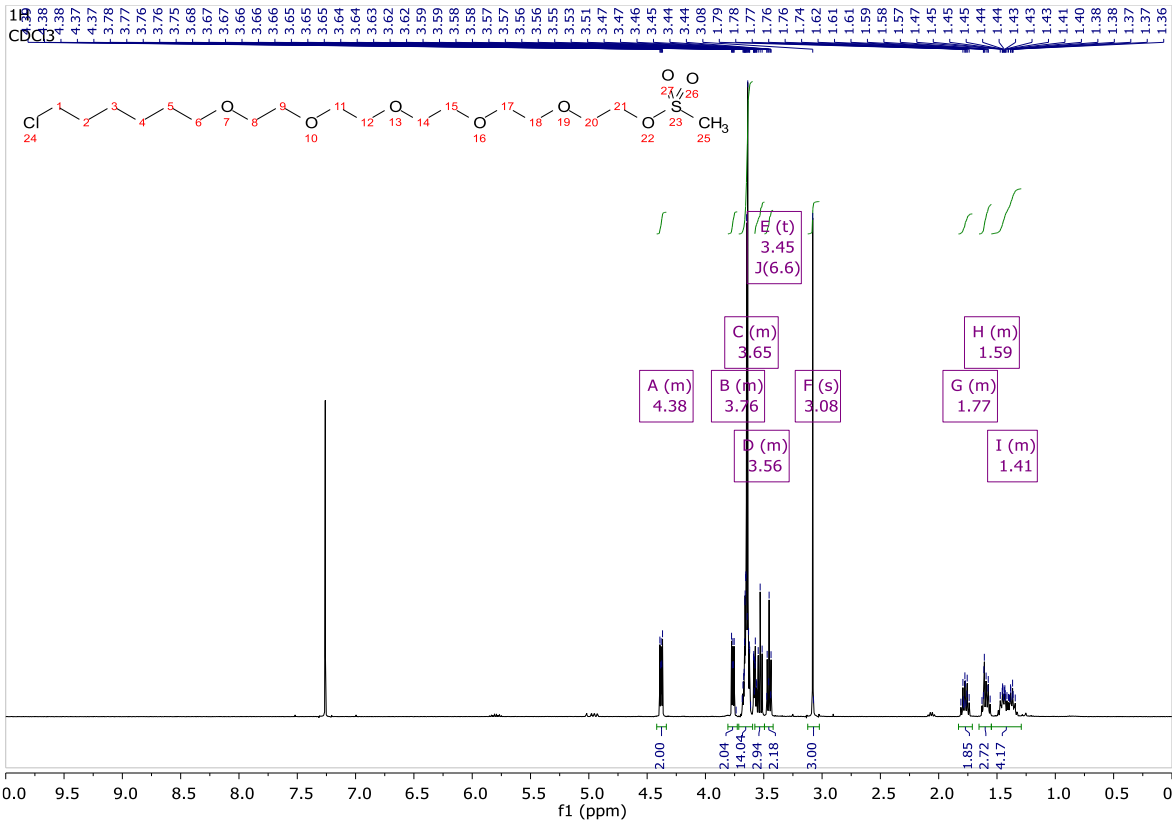
1H
CDCl3
E (t)
3.45
J(6.6)
C (m)
3.65
H (m)
1.59
A (m)
4.38
B (m)
3.76
F (s)
3.08
G (m)
1.77
D (m)
3.56
I (m)
1.41
2.00
2.04
14.04
2.94
2.18
3.00
1.85
2.72
4.17
f1 (ppm)

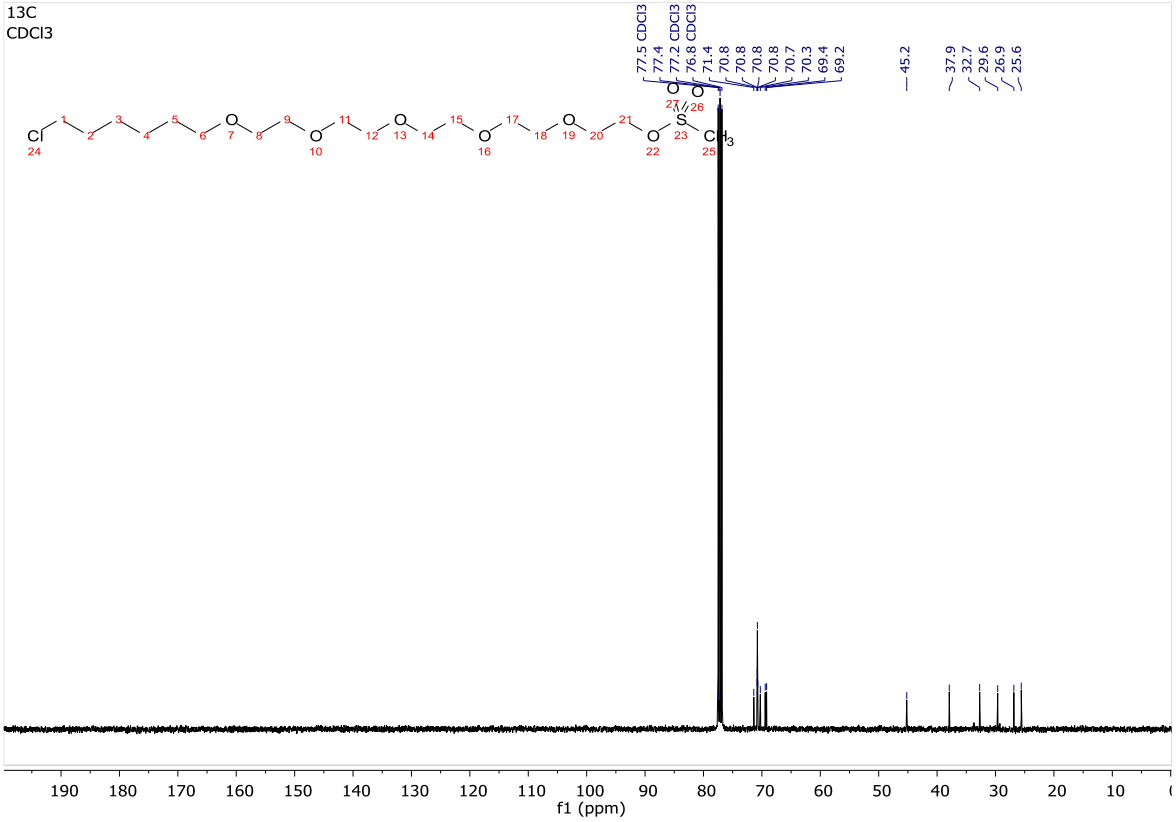
13C
CDCl3
77.5 CDCl3
77.4
77.2 CDCl3
76.8 CDCl3
71.4
70.8
70.8
70.8
70.7
70.3
69.4
69.2
45.2
37.9
32.7
29.6
26.9
25.6
f1 (ppm)

2.21b:

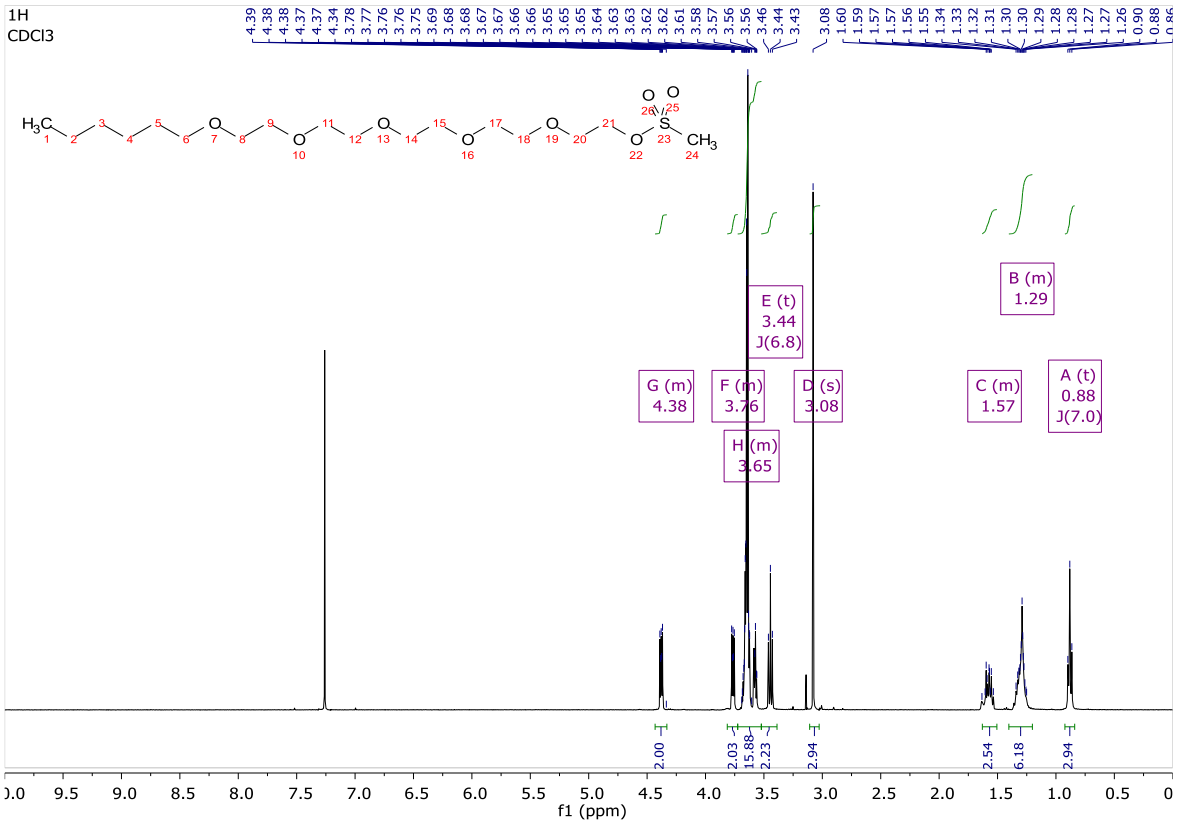
1H
CDCl3
E (t)
3.44
J(6.8)
B (m)
1.29
G (m)
4.38
F (m)
3.76
D (s)
3.08
C (m)
1.57
A (t)
0.88
J(7.0)
H (m)
3.65
f1 (ppm)

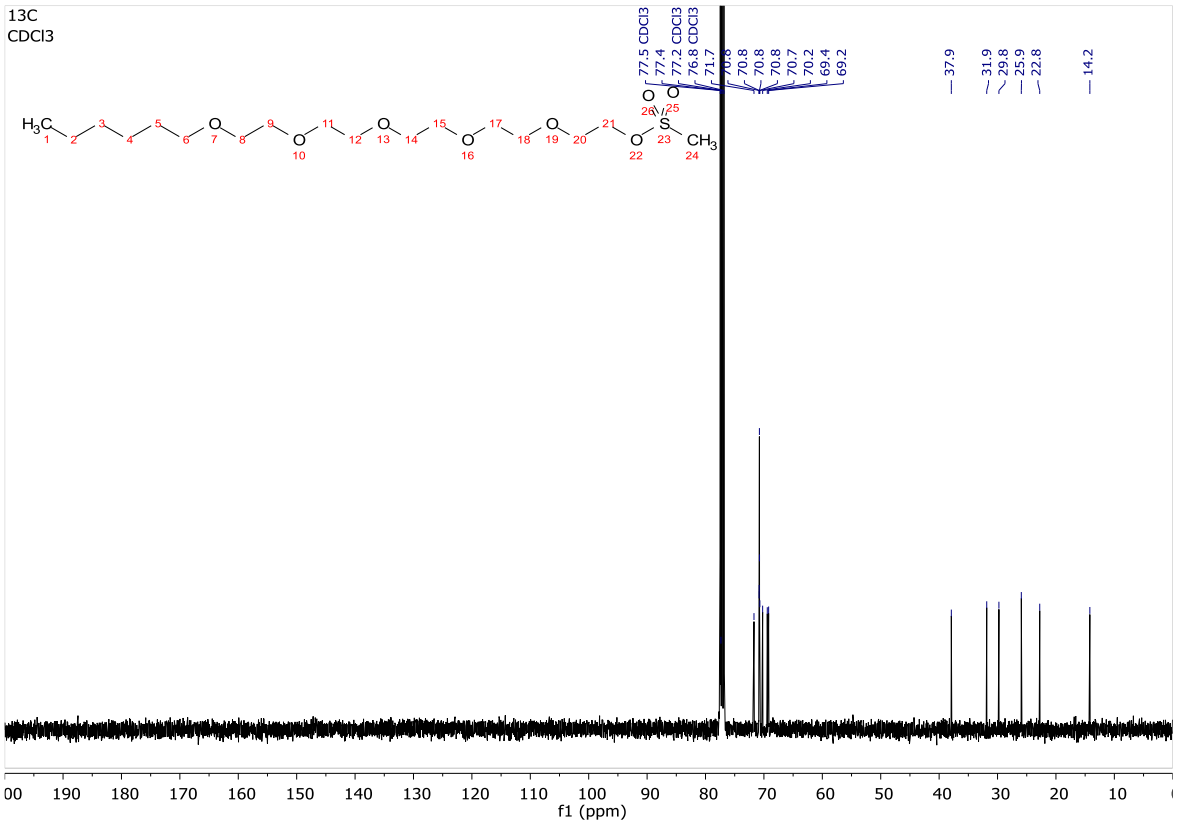
13C
CDCl3
77.5 CDCl3
77.4
77.2 CDCl3
76.8 CDCl3
f1 (ppm)

VHL-HP-2 (2.22):

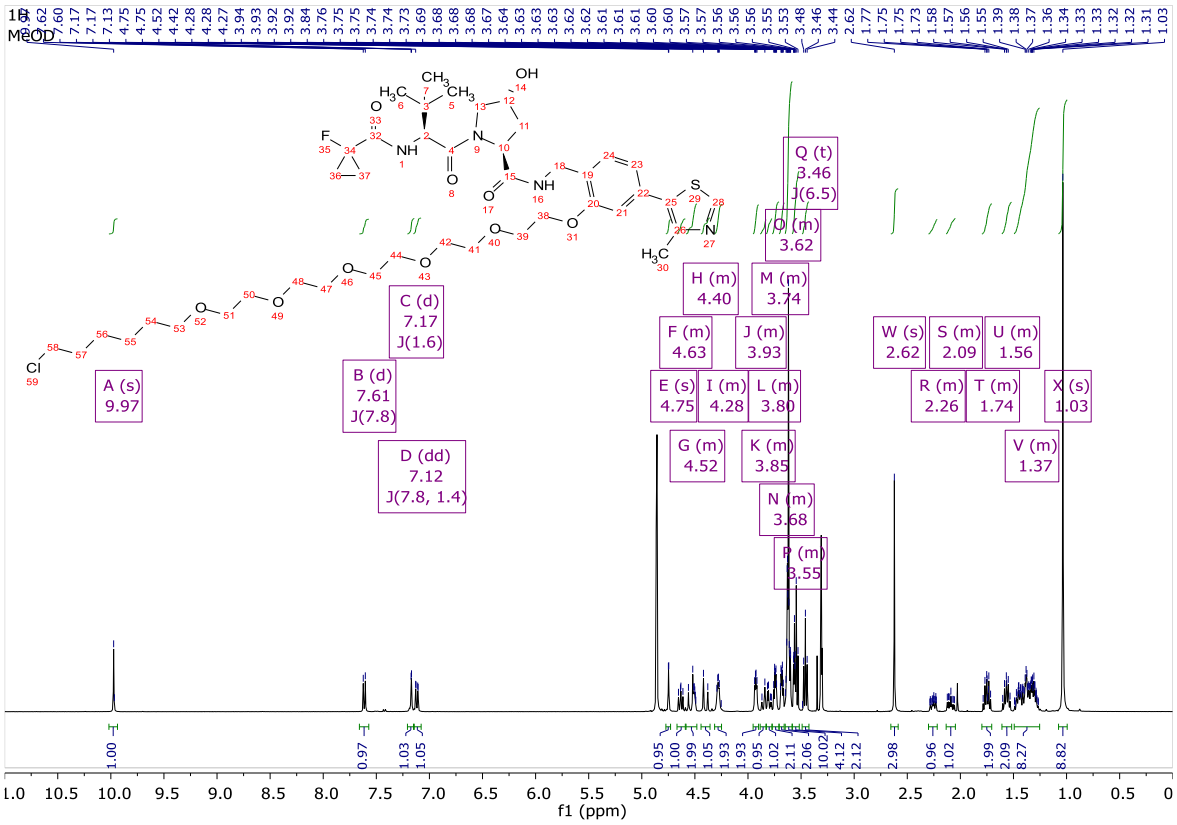
1H
MeOD
A (s) 9.97
B (d) 7.61 J(7.8)
C (d) 7.17 J(1.6)
D (dd) 7.12 J(7.8, 1.4)
E (s) 4.75
F (m) 4.63
G (m) 4.52
H (m) 4.40
I (m) 4.28
J (m) 3.93
K (m) 3.85
L (m) 3.80
M (m) 3.74
N (m) 3.68
O (m) 3.62
P (m) 3.55
Q (t) 3.46 J(6.5)
R (m) 2.26
S (m) 2.09
T (m) 1.74
U (m) 1.56
V (m) 1.37
W (s) 2.62
X (s) 1.03
f1 (ppm)

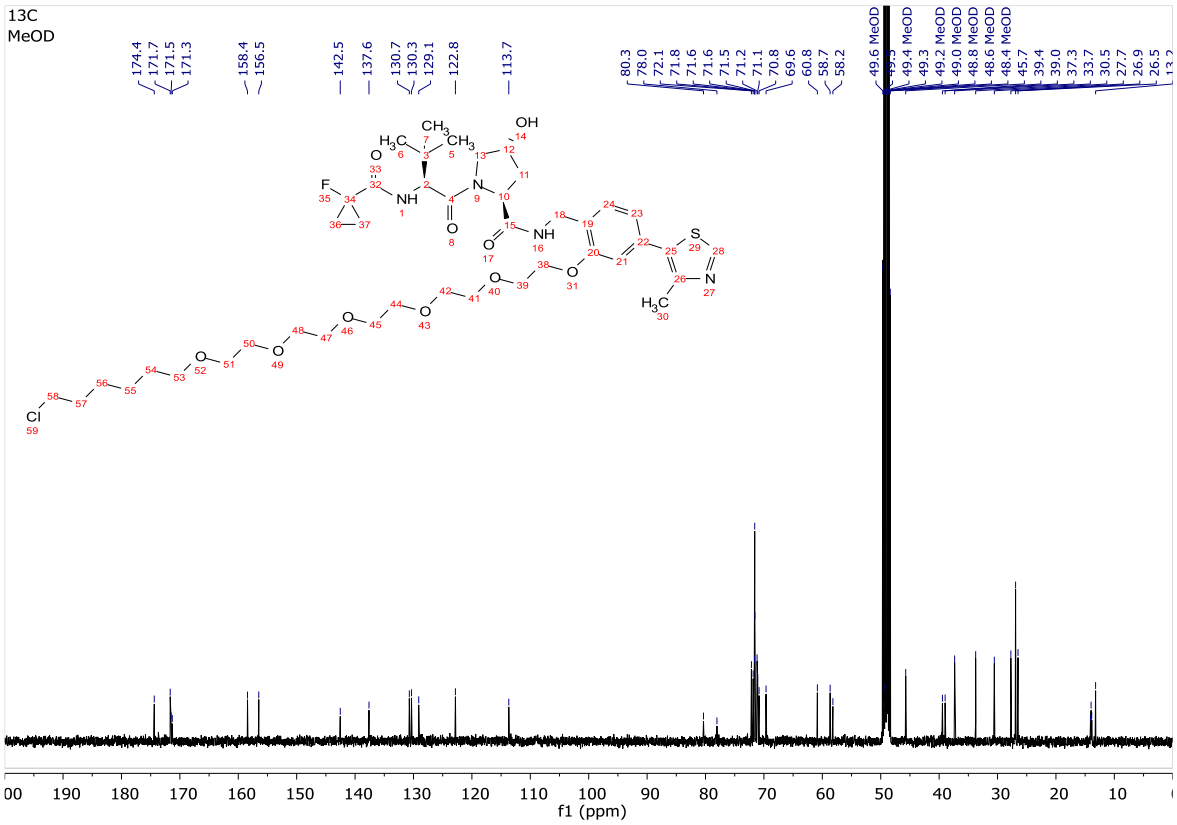
13C
MeOD
f1 (ppm)

***cis*VHL-ctrl-2 (2.23)**:

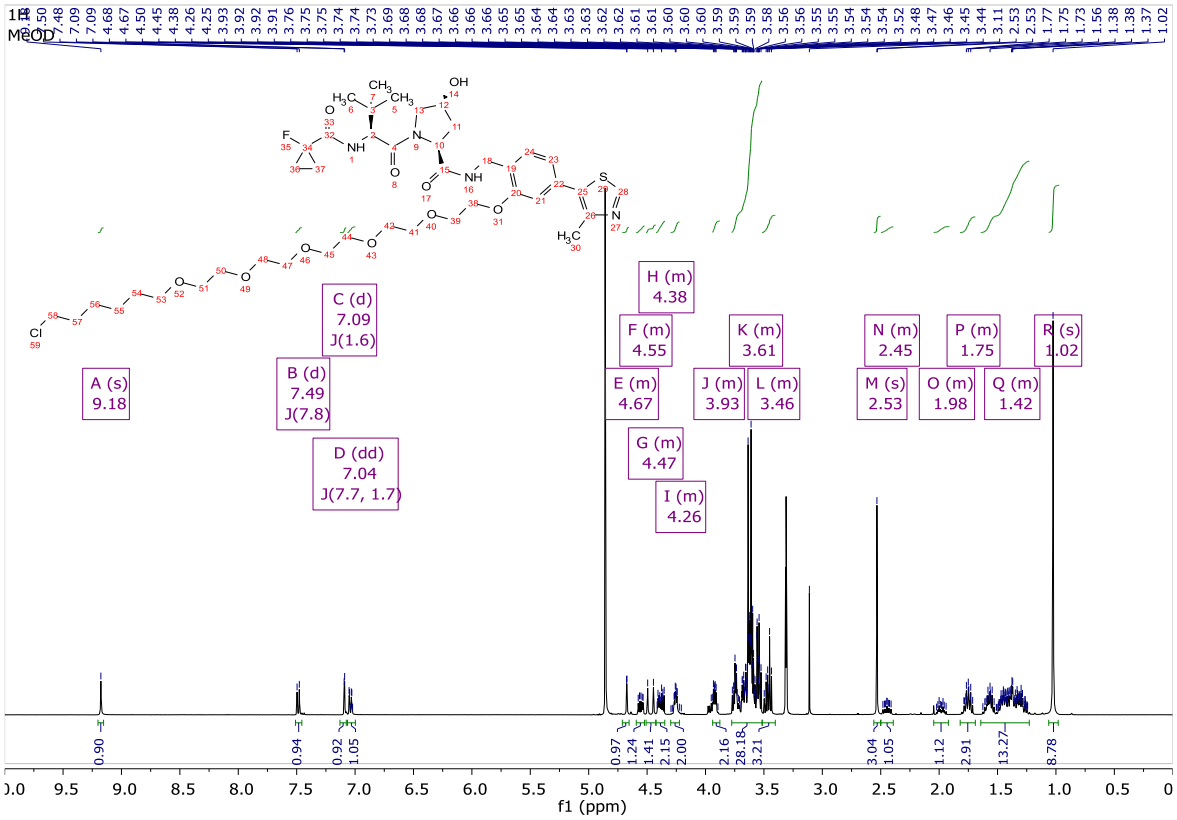

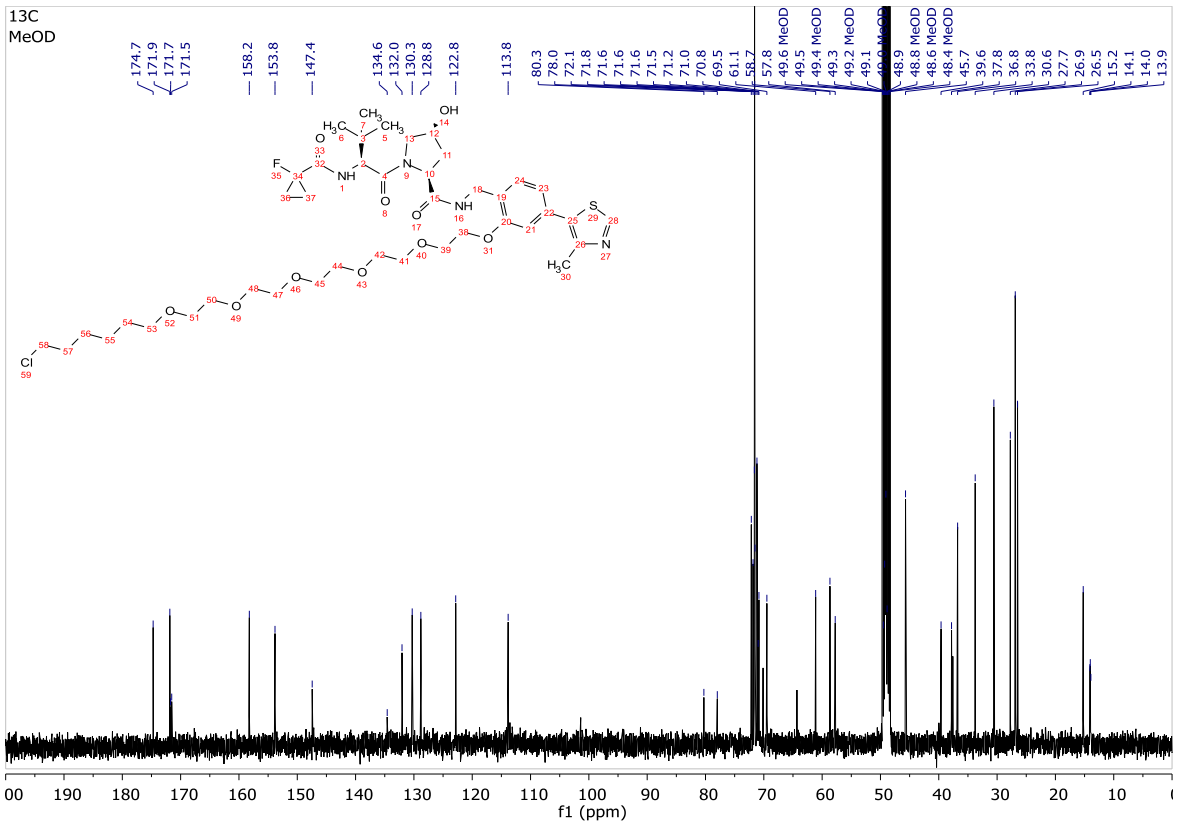

noHTL-VHL-ctrl-2 (2.24):

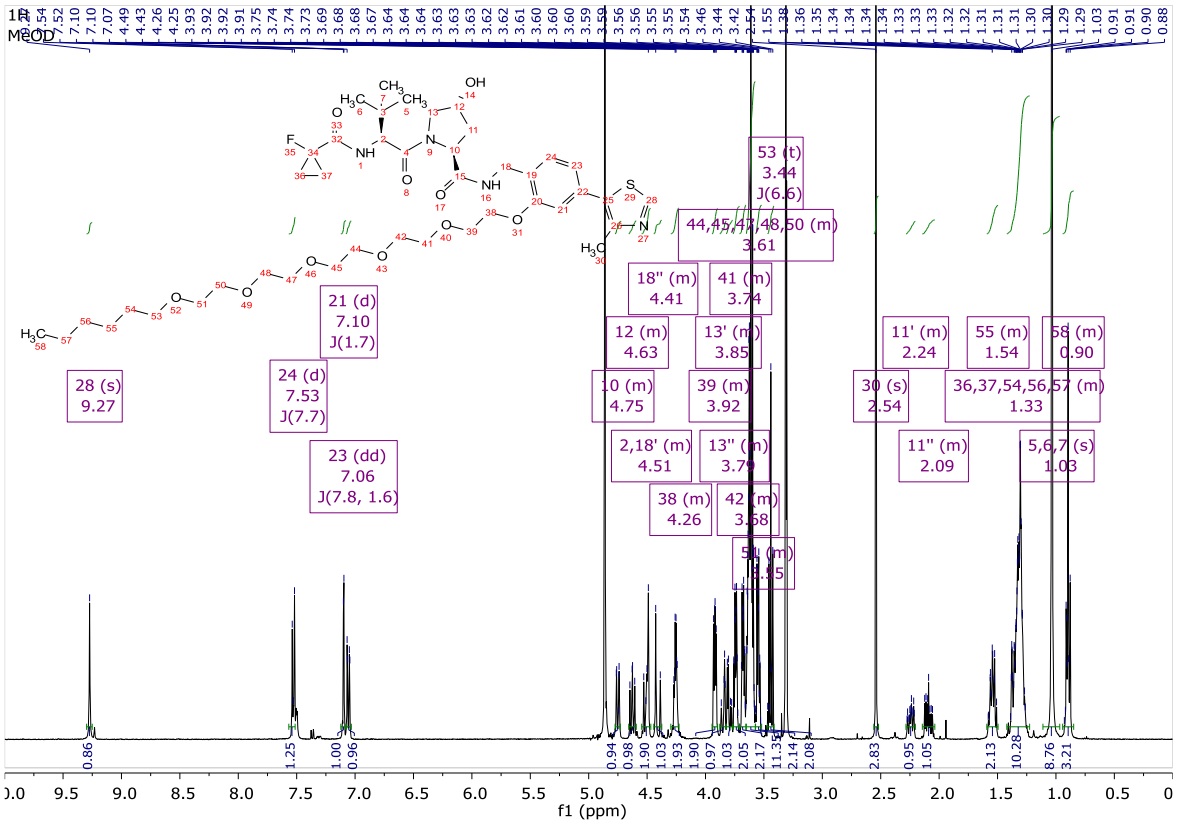

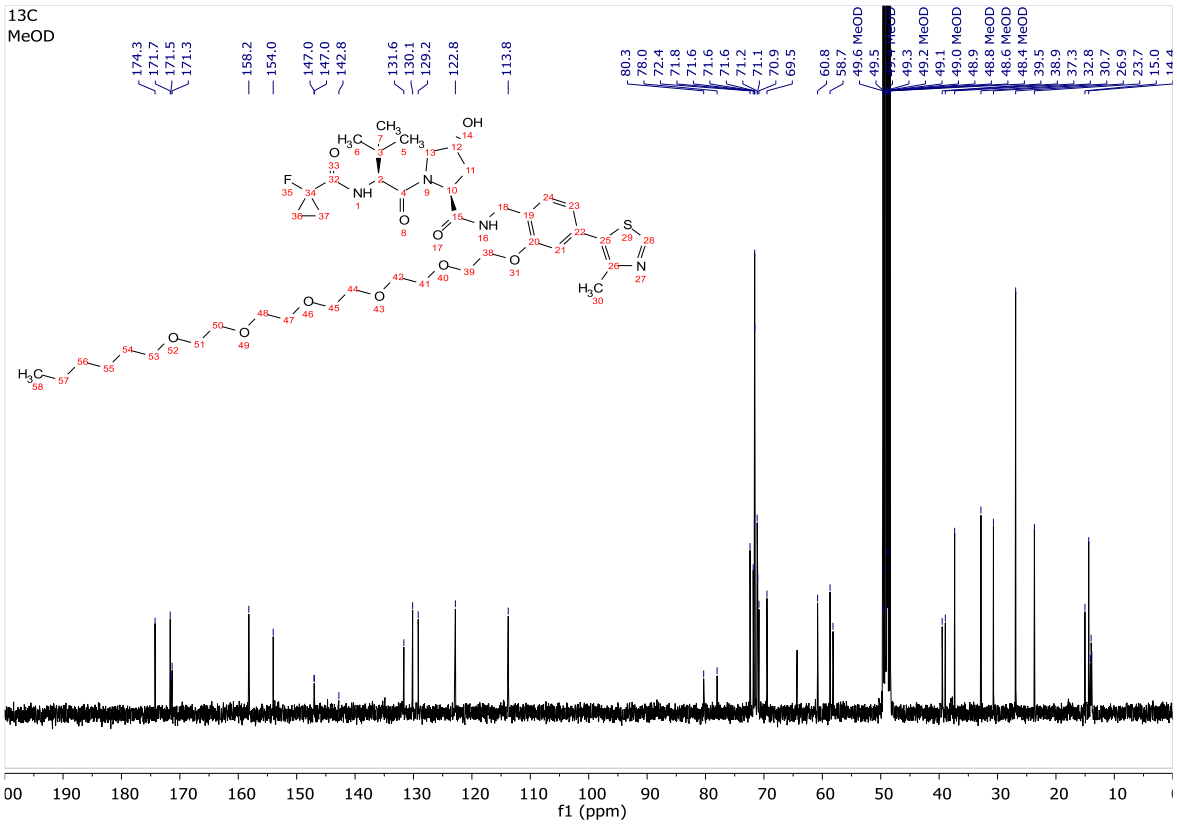

- *CRBN HaloPROTACs and mono-functional controls:*

2.27:

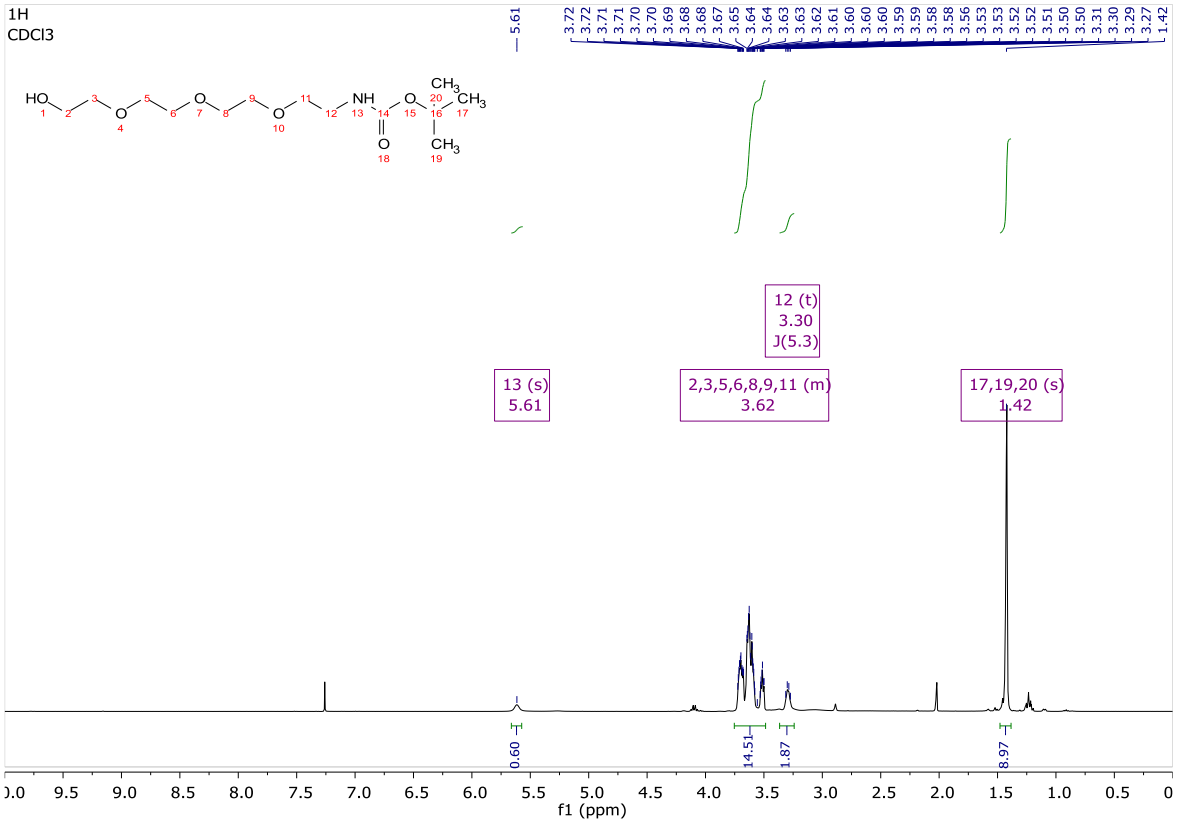

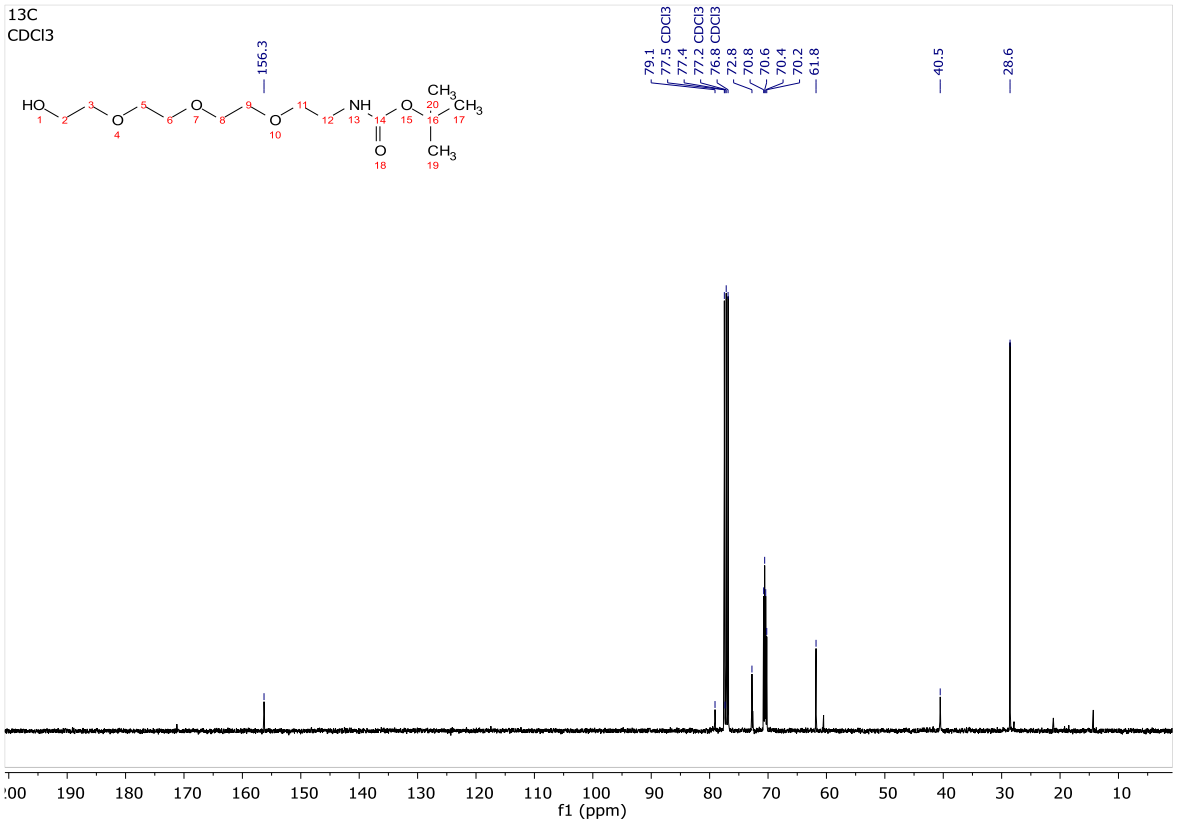

2.28a:

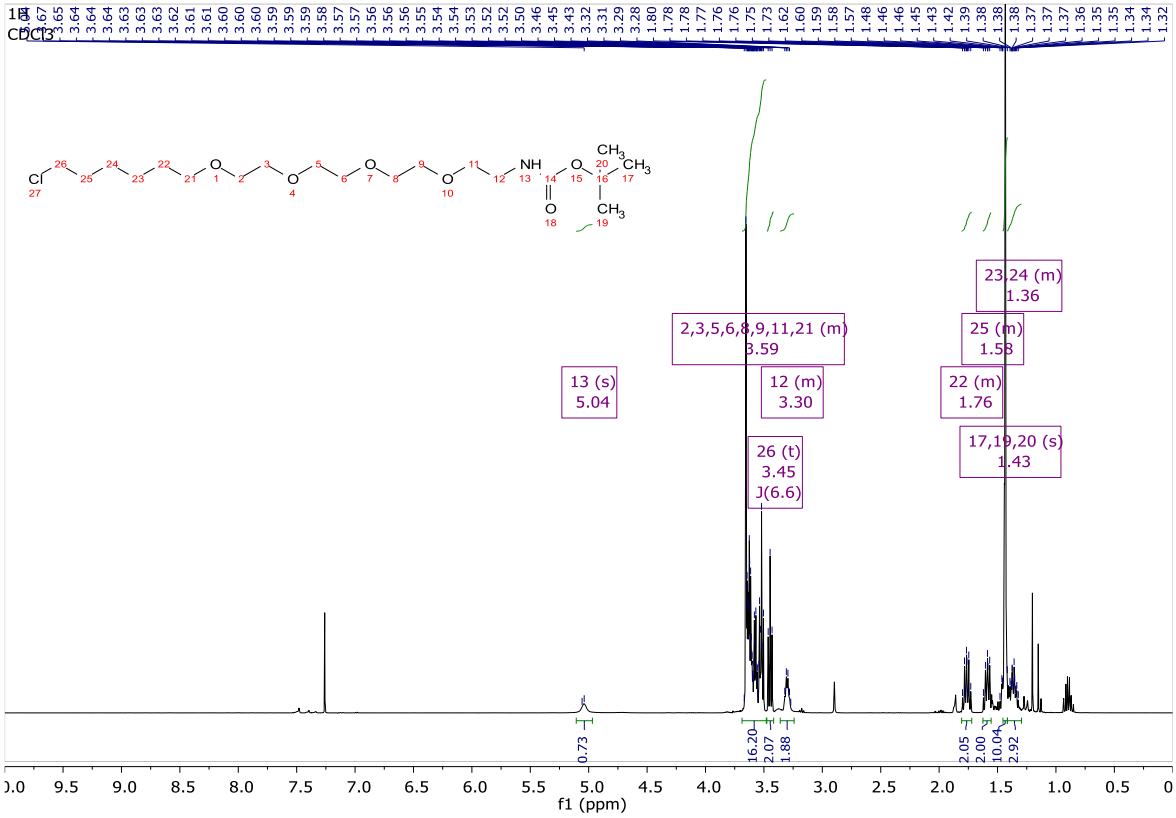
1H
CDCl3
23,24 (m)
1.36
2,3,5,6,8,9,11,21 (m)
3.59
25 (m)
1.58
13 (s)
5.04
12 (m)
3.30
22 (m)
1.76
26 (t)
3.45
J(6.6)
17,19,20 (s)
1.43
f1 (ppm)

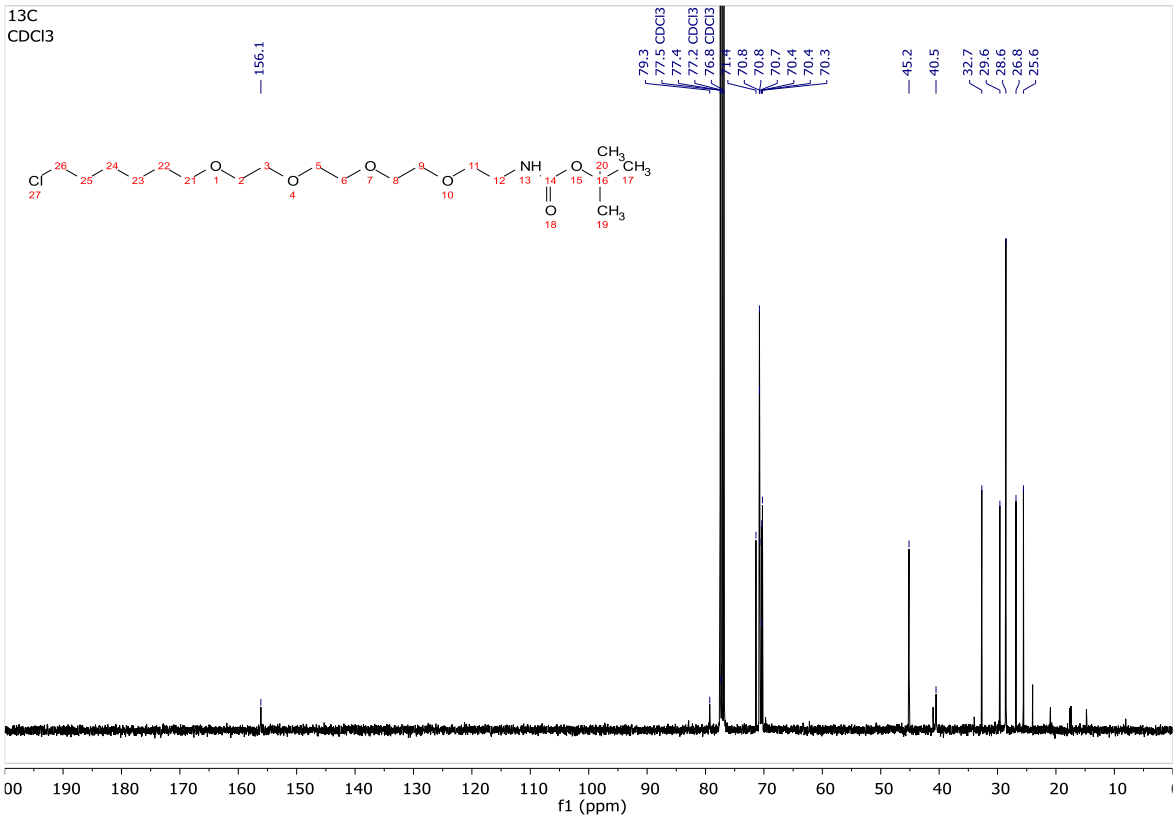
13C
CDCl3
f1 (ppm)

2.28b:

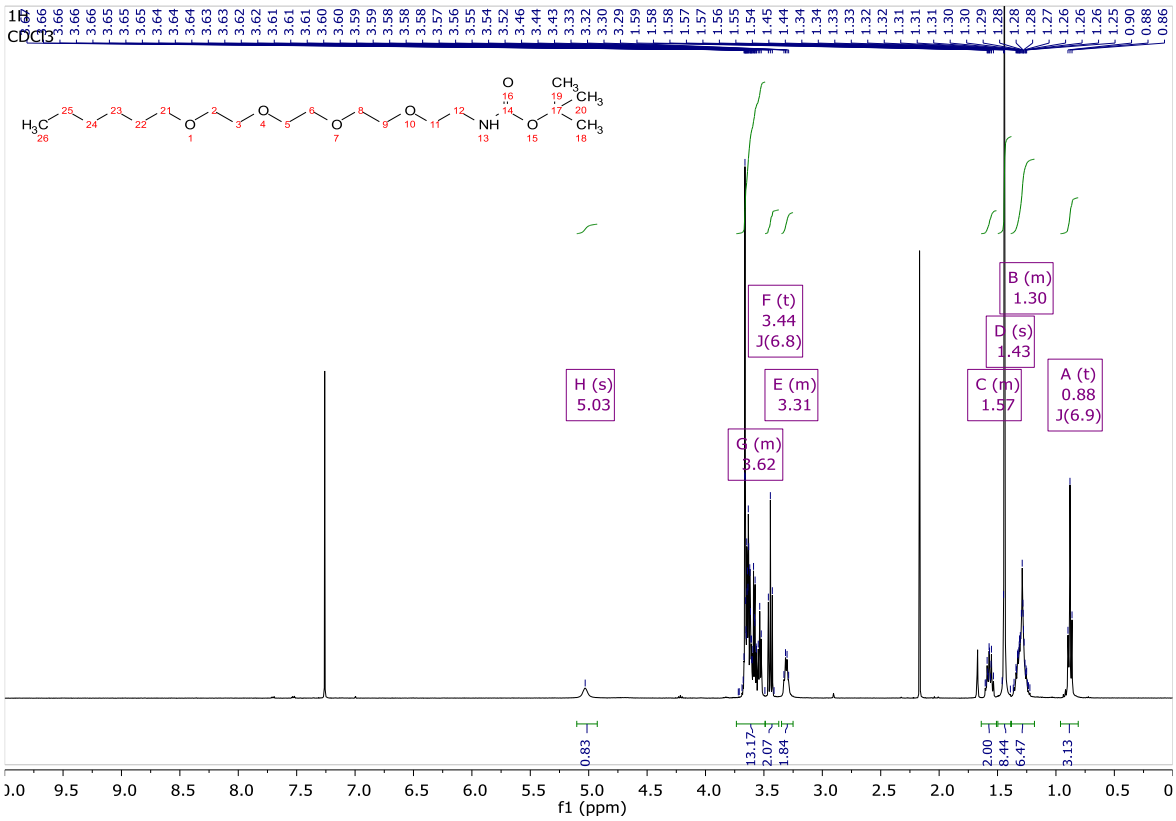
1H
CDCl3
H (s)
5.03
G (m)
3.62
F (t)
3.44
J(6.8)
E (m)
3.31
B (m)
1.30
D (s)
1.43
C (m)
1.57
A (t)
0.88
J(6.9)
f1 (ppm)

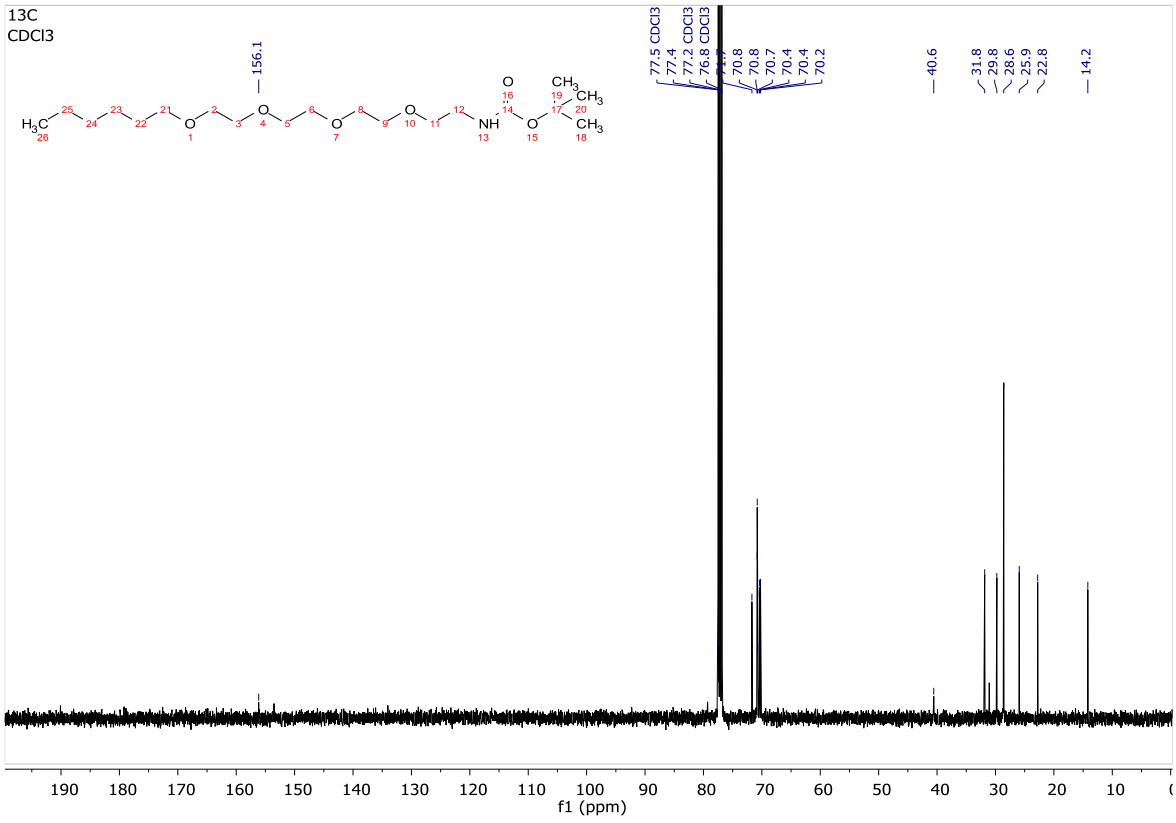
13C
CDCl3
156.1
77.5 CDCl3
77.4
77.2 CDCl3
76.8 CDCl3
70.8
70.8
70.7
70.4
70.4
70.2
40.6
31.8
29.8
28.6
25.9
22.8
14.2
f1 (ppm)

CRBN-HP-1 (2.29):

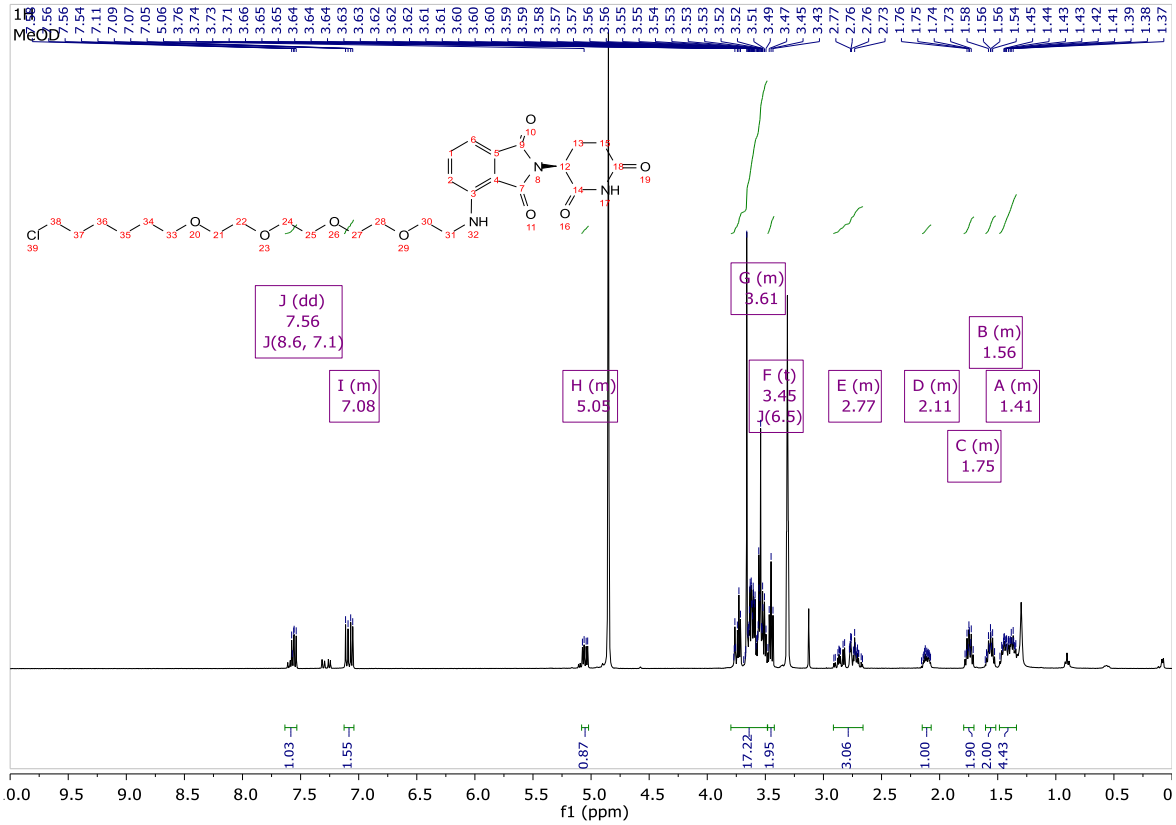
1H
MeOD
J (dd)
7.56
J(8.6, 7.1)
I (m)
7.08
H (m)
5.05
G (m)
3.61
F (t)
3.45
J(6.5)
E (m)
2.77
D (m)
2.11
C (m)
1.75
B (m)
1.56
A (m)
1.41
1.03
1.55
0.87
17.22
1.95
3.06
1.00
1.90
2.00
4.43
f1 (ppm)

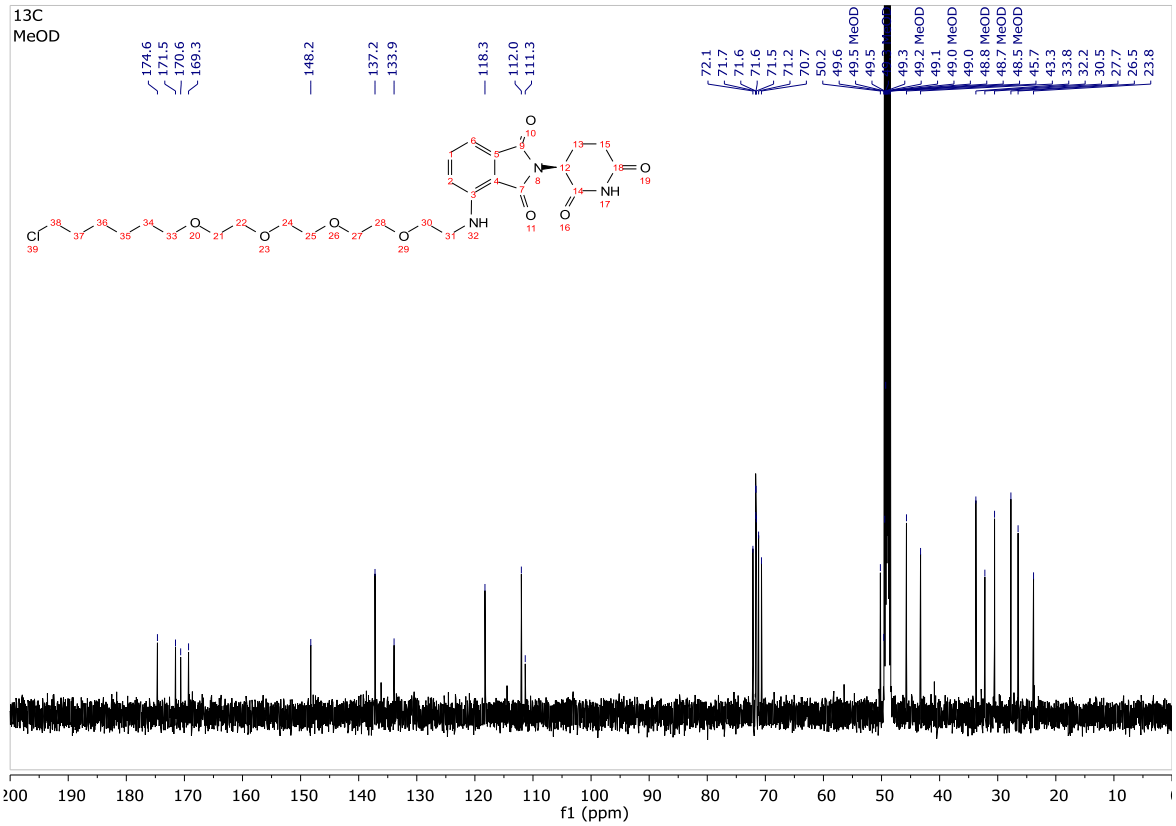
13C
MeOD
174.6
171.5
170.6
169.3
148.2
137.2
133.9
118.3
112.0
111.3
72.1
71.7
71.6
71.6
71.5
71.2
70.7
50.2
49.6
49.5 MeOD
49.5
49.3
49.2 MeOD
49.1
49.0 MeOD
49.0
48.8 MeOD
48.7 MeOD
48.5 MeOD
45.7
43.3
33.8
32.2
30.5
27.7
26.5
23.8
f1 (ppm)

MeCRBN-ctrl-1 (2.30):

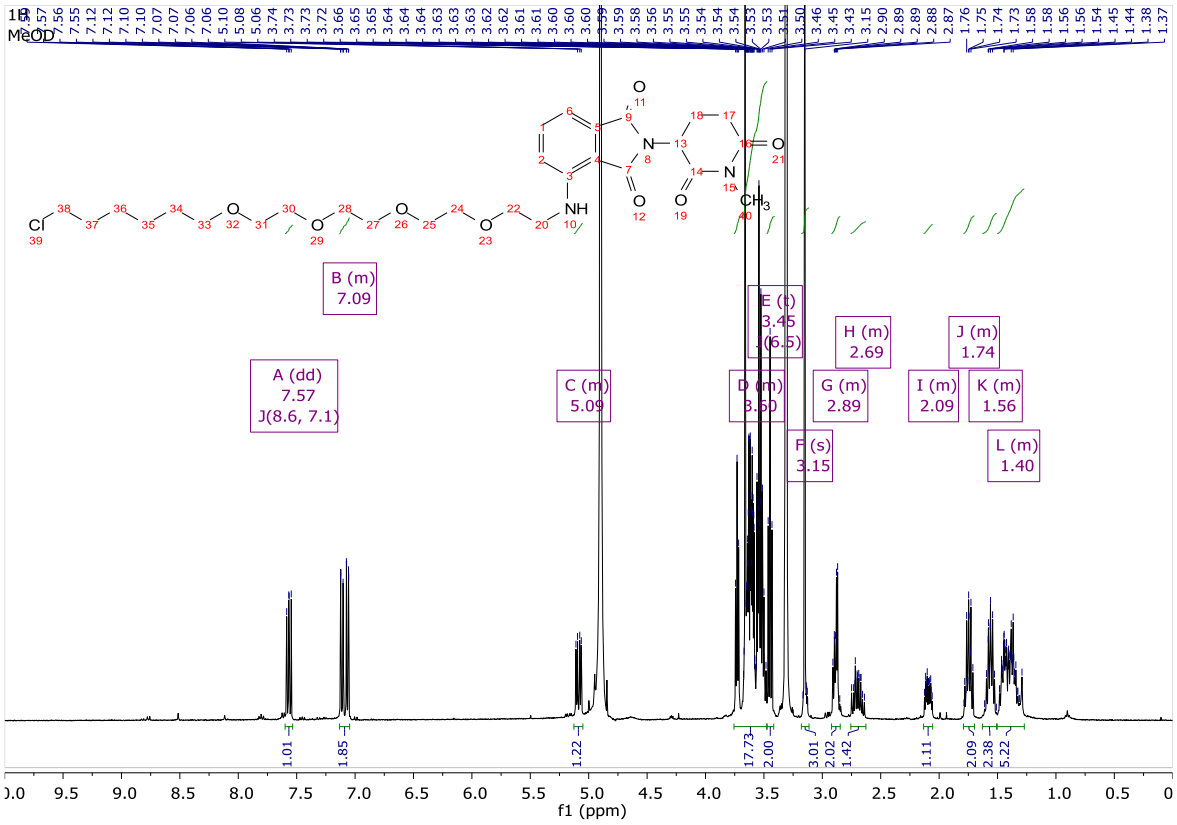

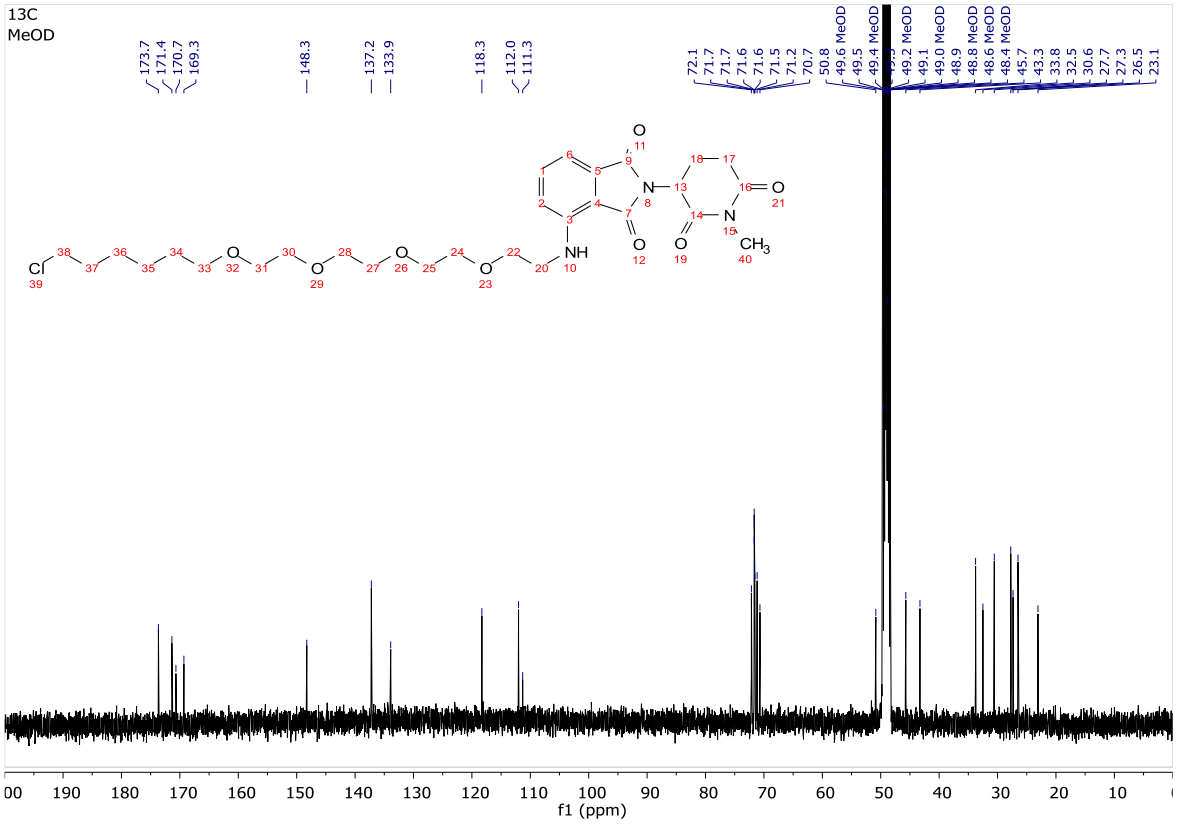

noHTL-CRBN-ctrl-1 (2.31):

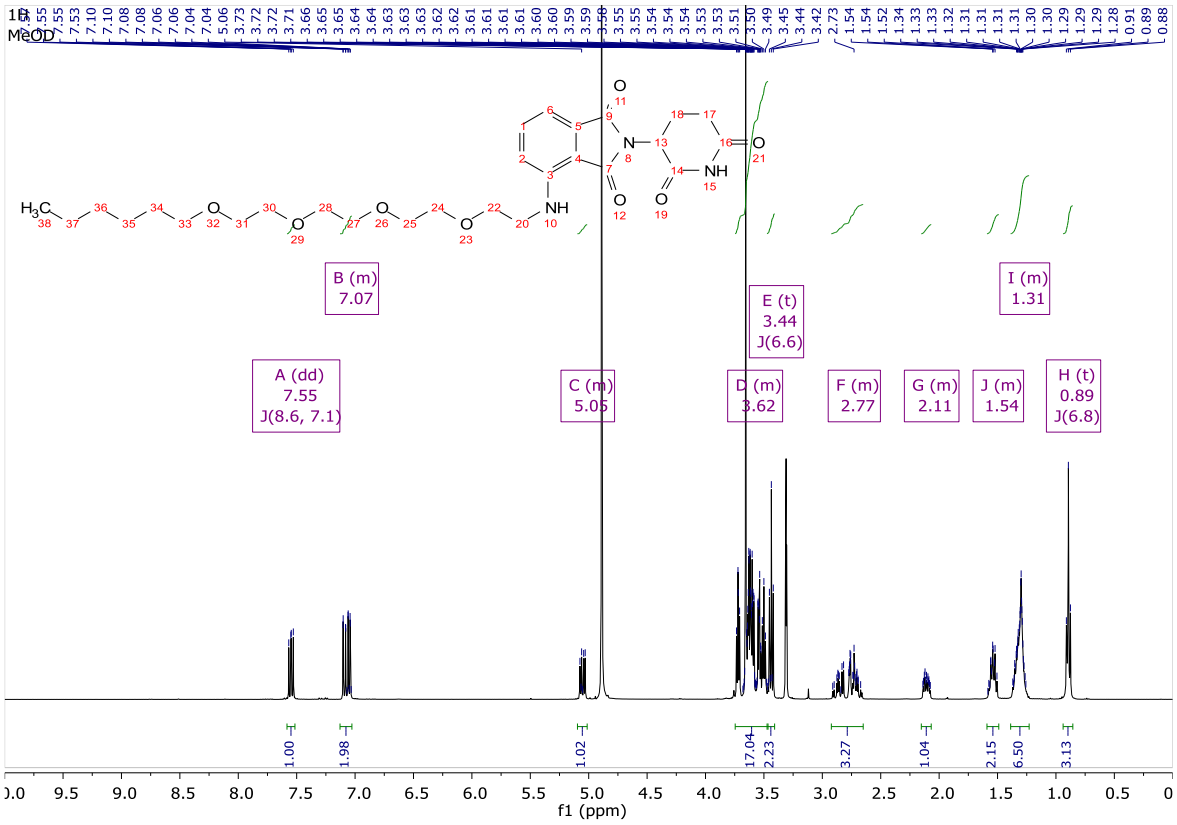

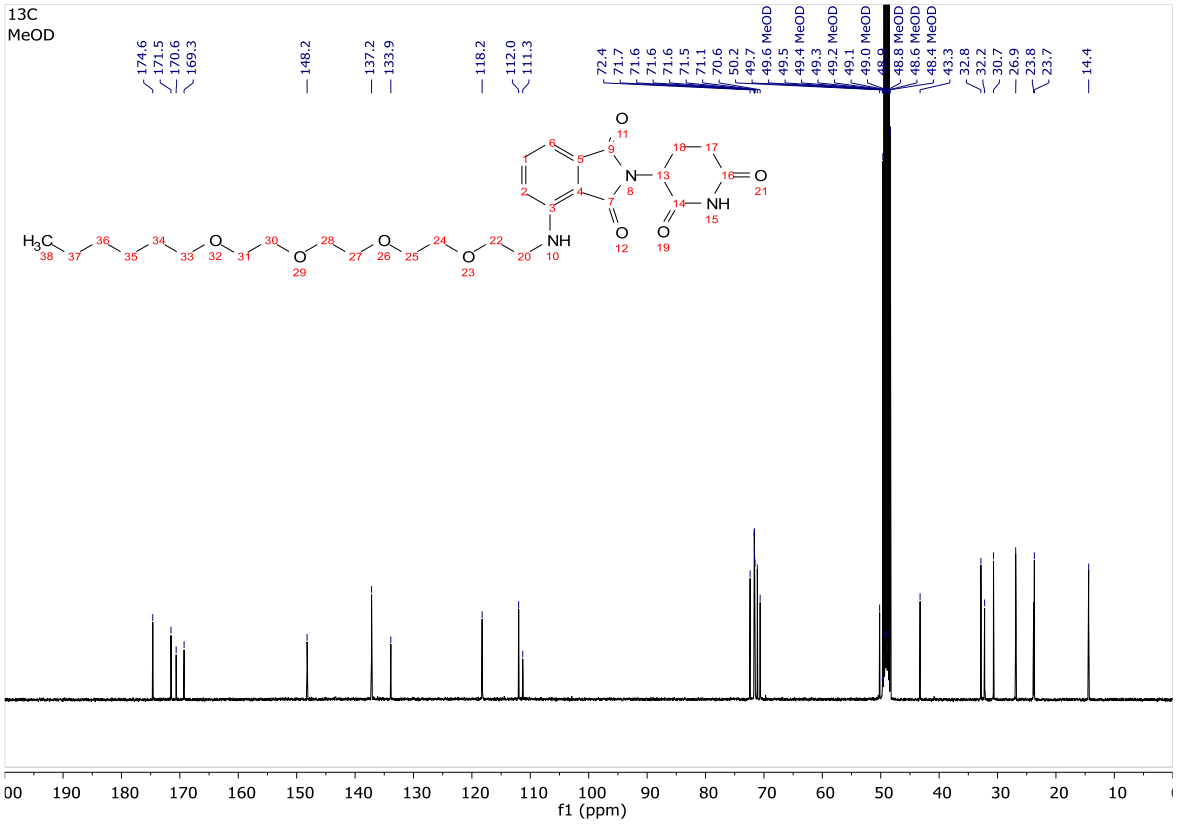

CRBN-HP-2 (2.32):

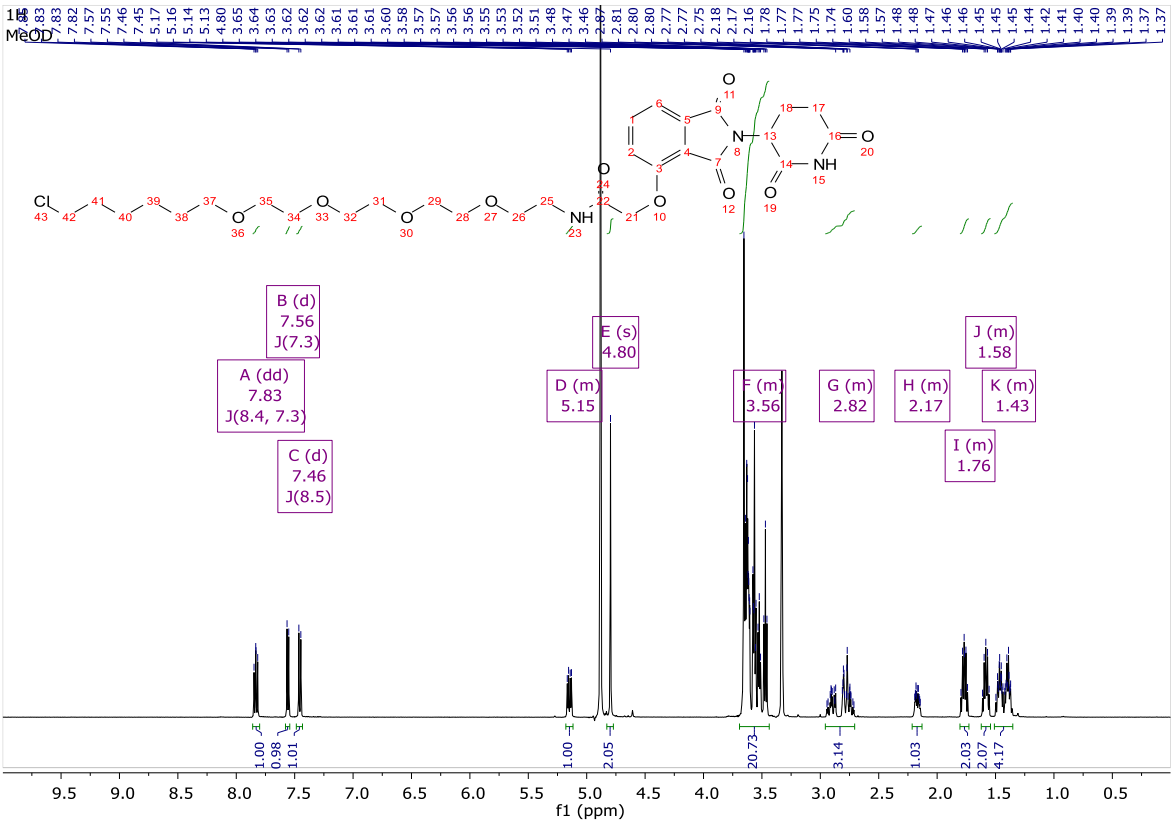
1H
MeOD
B (d)
7.56
J(7.3)
A (dd)
7.83
J(8.4, 7.3)
C (d)
7.46
J(8.5)
E (s)
4.80
D (m)
5.15
F (m)
3.56
G (m)
2.82
H (m)
2.17
J (m)
1.58
K (m)
1.43
I (m)
1.76
1.00
0.98
1.01
1.00
2.05
20.73
3.14
1.03
2.03
2.07
4.17
f1 (ppm)

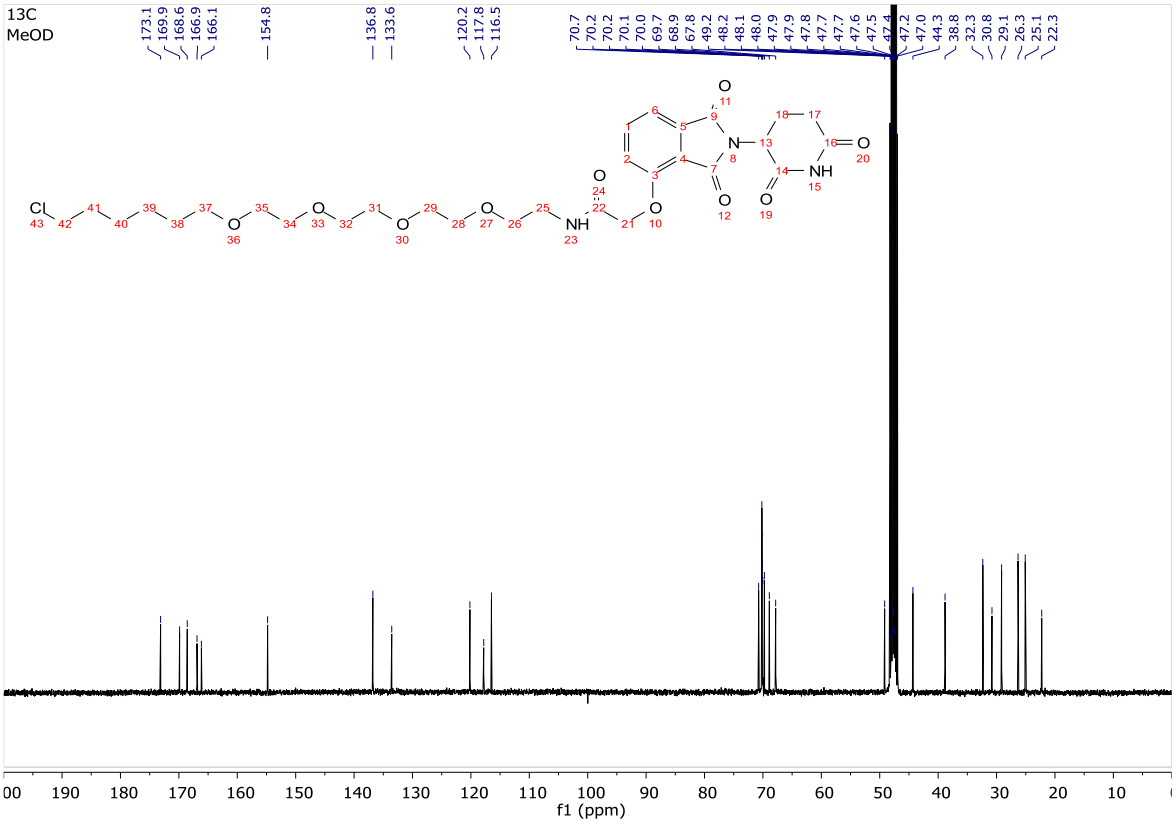
13C
MeOD
f1 (ppm)

MeCRBN-ctrl-2 (2.33):

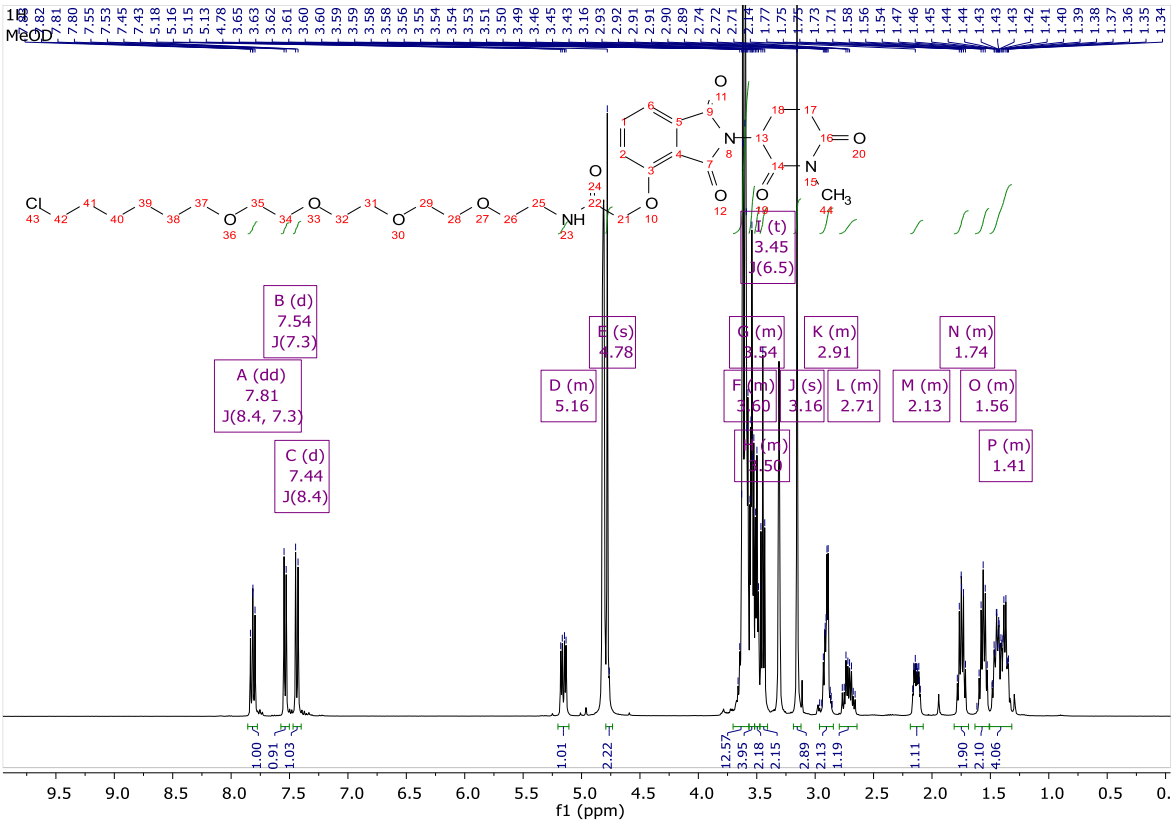

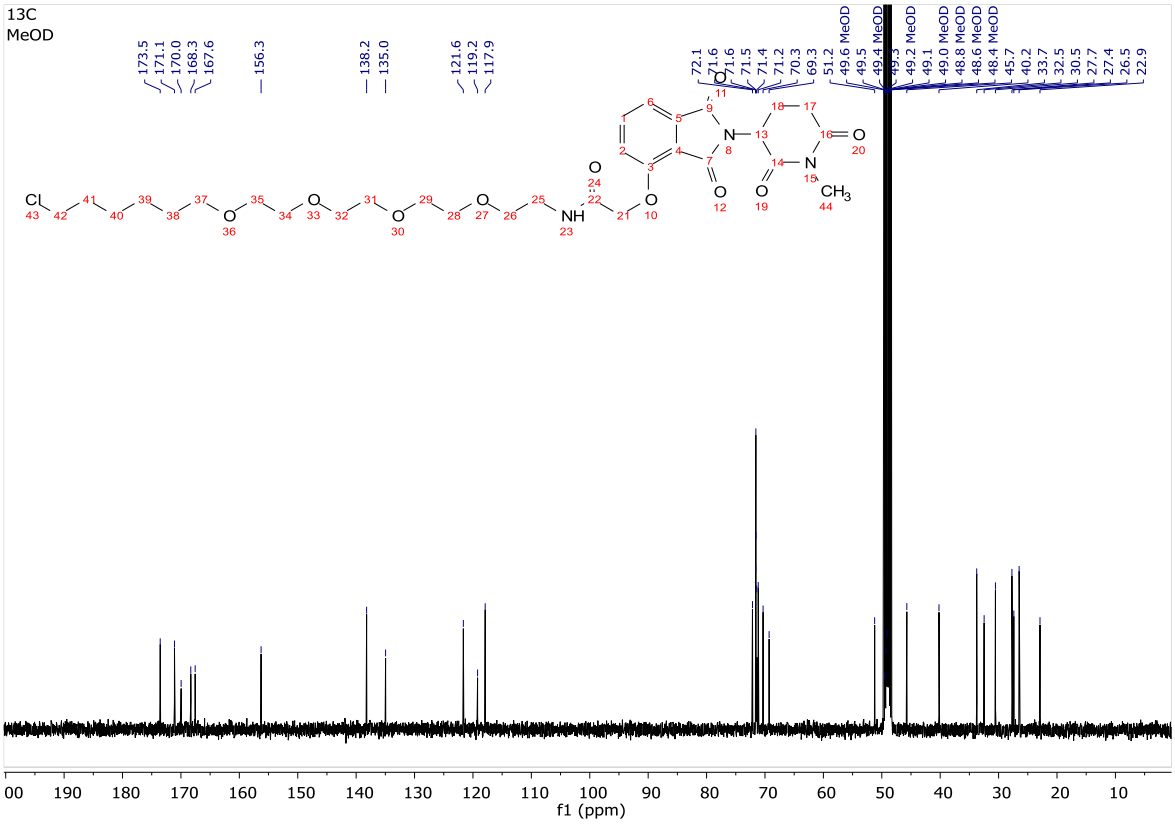

noHTL-CRBN-ctrl-2 (2.34):

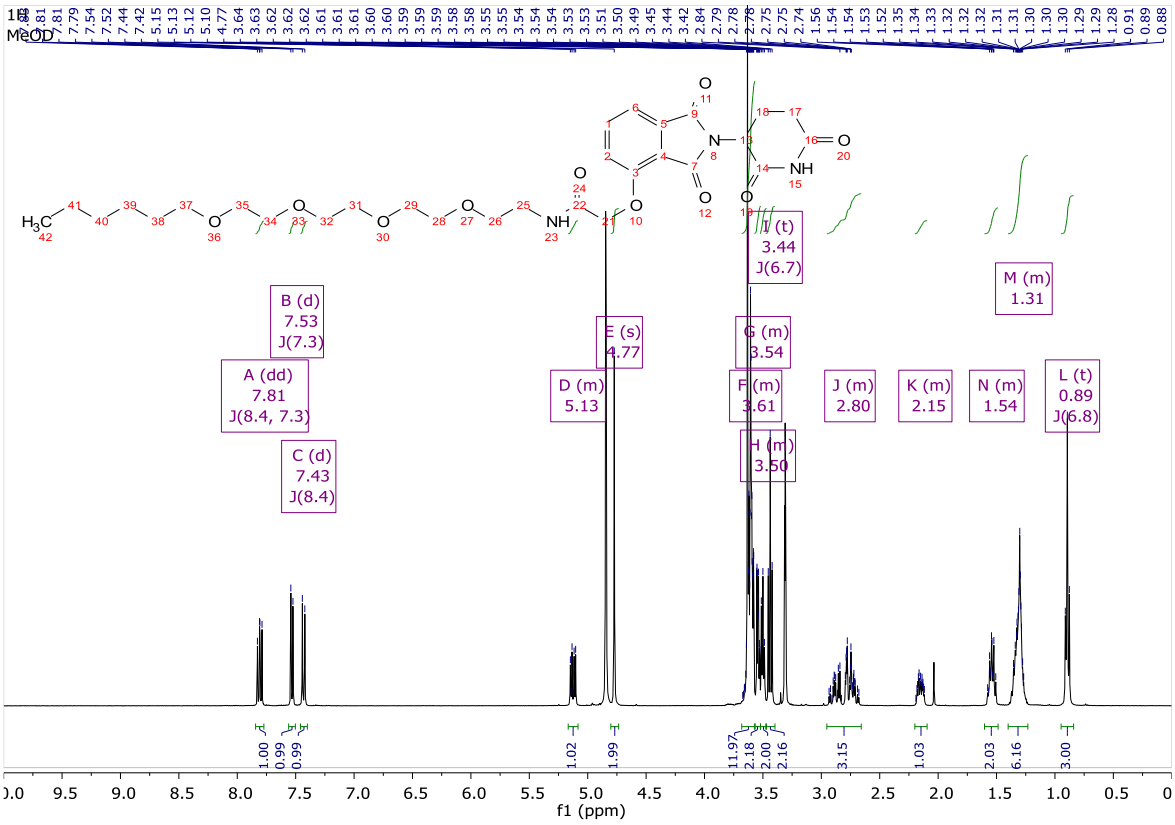

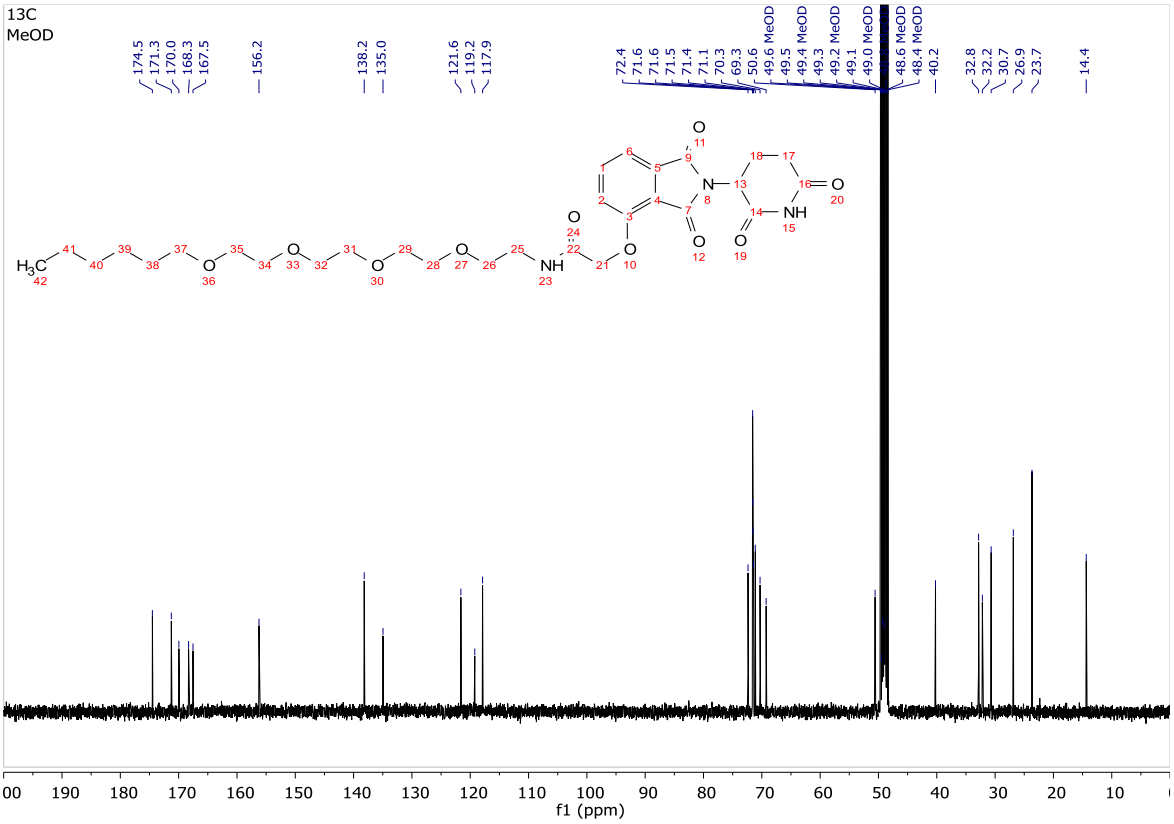

- *HyT HaloPROTAC:*

2.35:

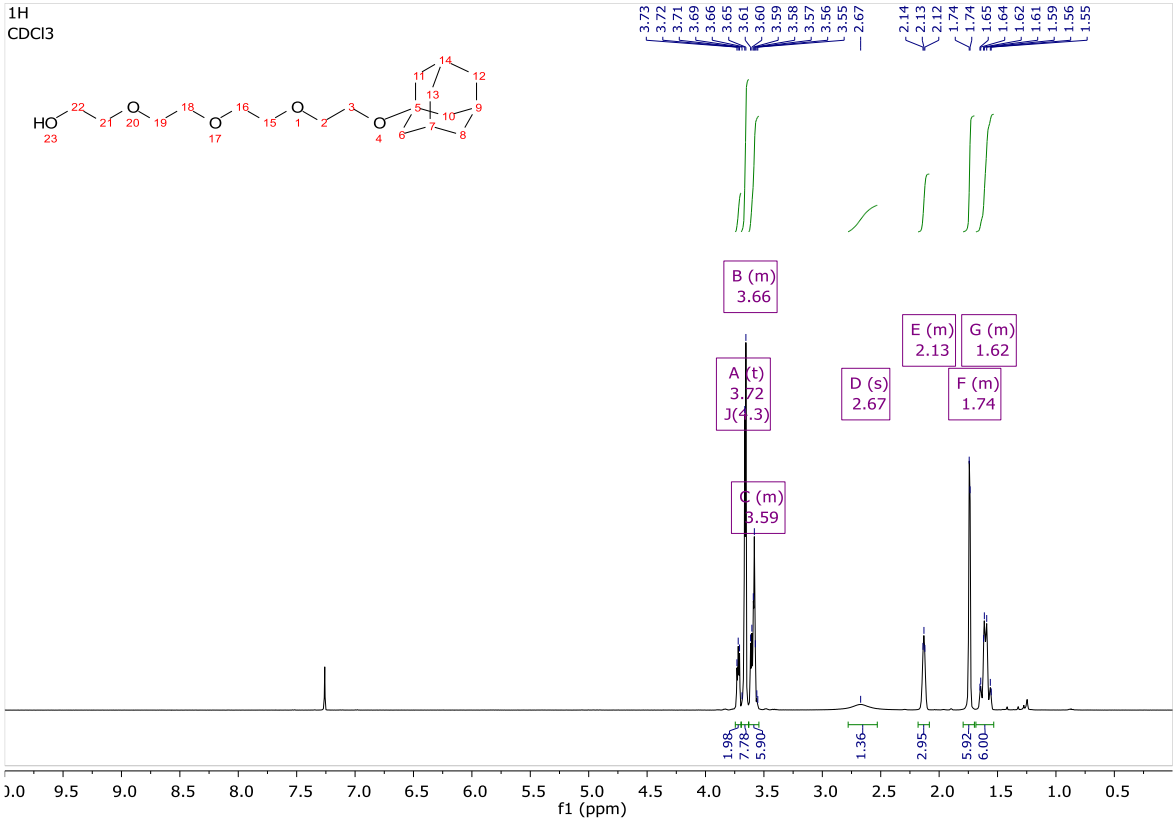

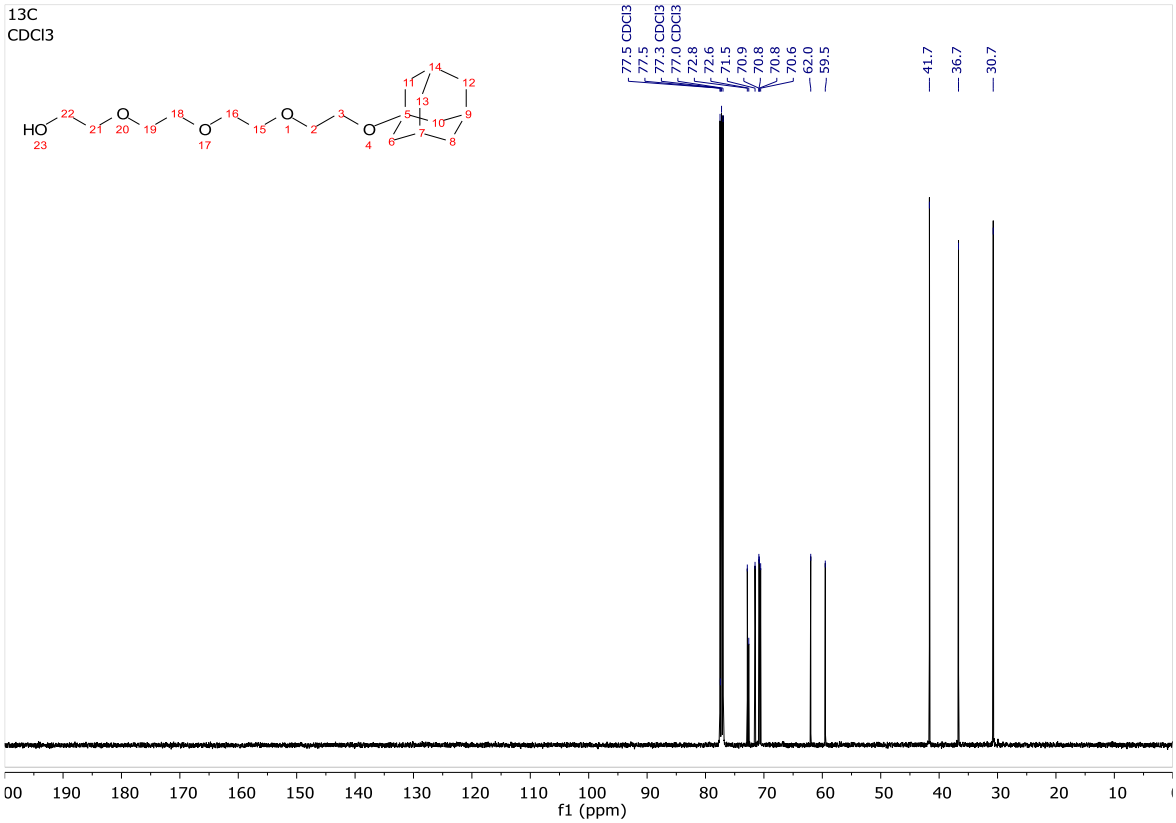

HyT-HP-1 (2.36):

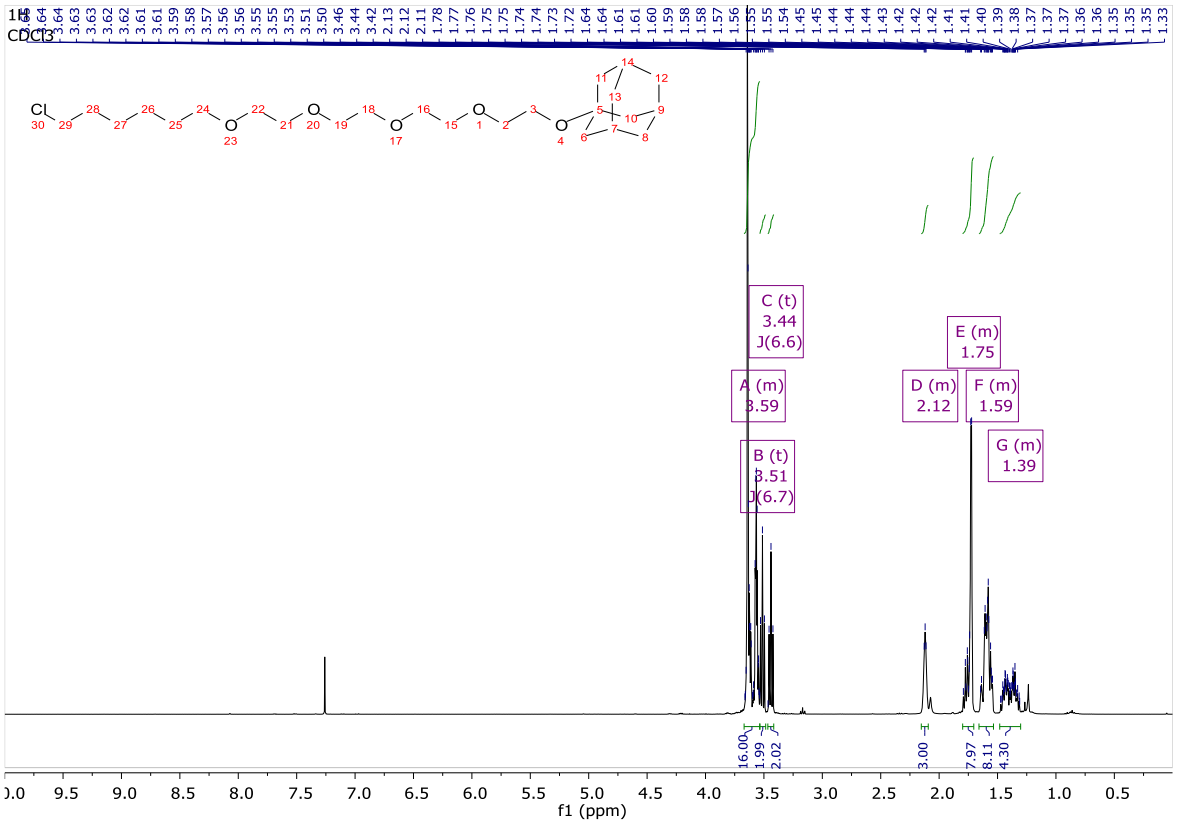
1H
CDCl3
C (t)
3.44
J(6.6)
E (m)
1.75
A (m)
3.59
D (m)
2.12
F (m)
1.59
B (t)
3.51
J(6.7)
G (m)
1.39
16.00
1.99
2.02
3.00
7.97
8.11
4.30
f1 (ppm)

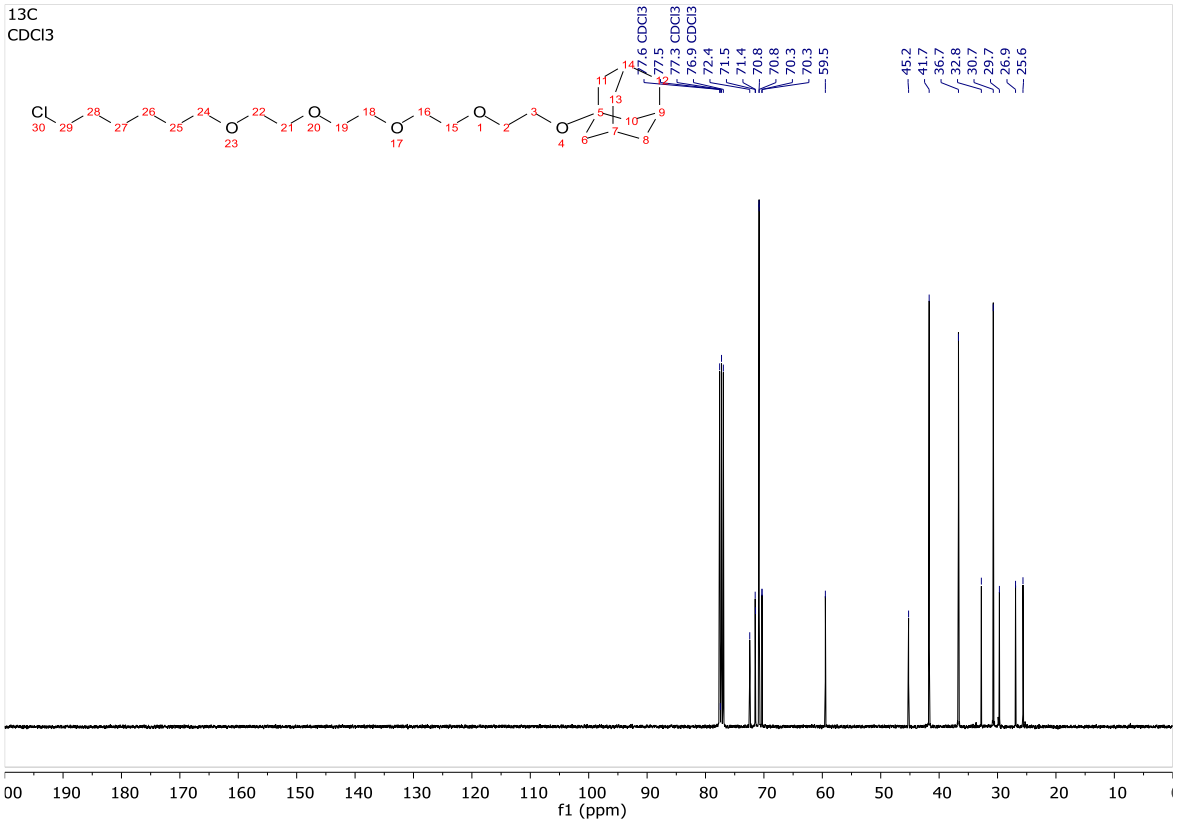
13C
CDCl3
77.6 CDCl3
77.5
77.3 CDCl3
76.9 CDCl3
72.4
71.5
71.4
70.8
70.8
70.3
70.3
59.5
45.2
41.7
36.7
32.8
30.7
29.7
26.9
25.6
f1 (ppm)

1st series amide PROTACs

- *E3 ligase ligand–linker fragments:*

3.2a:

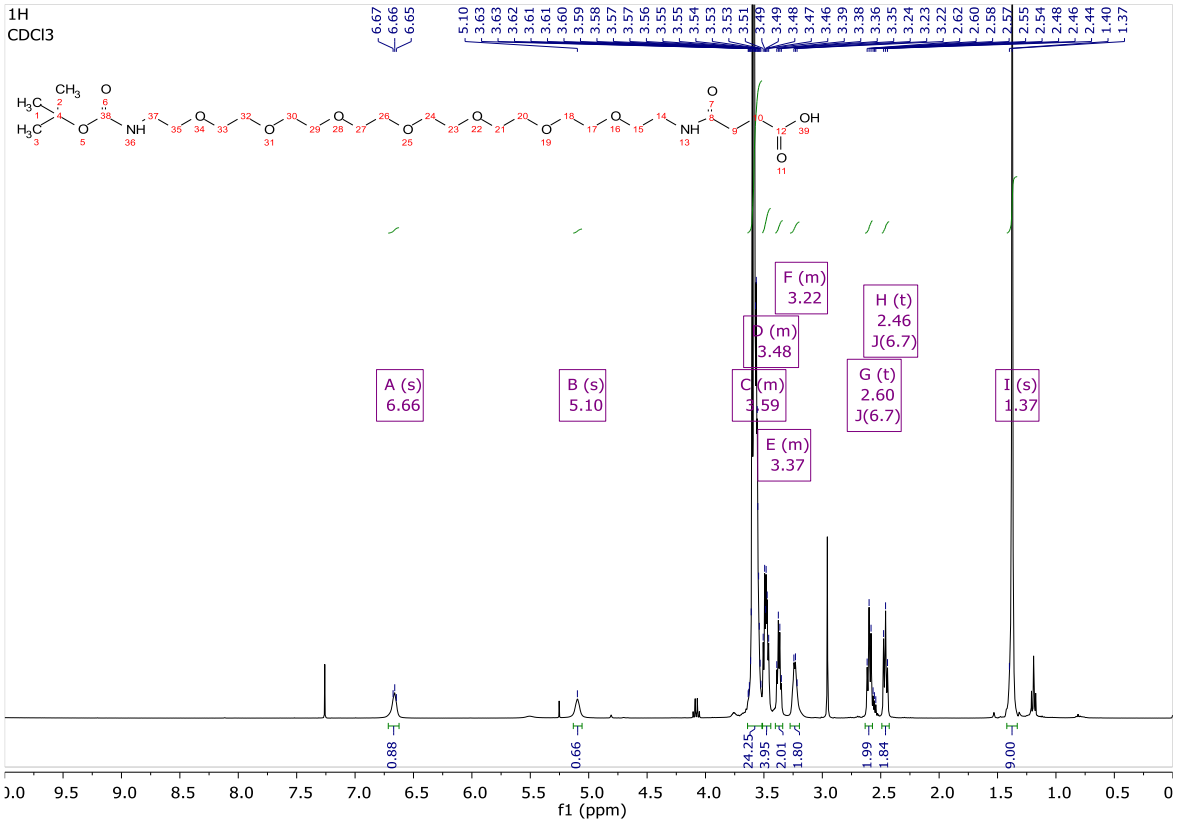

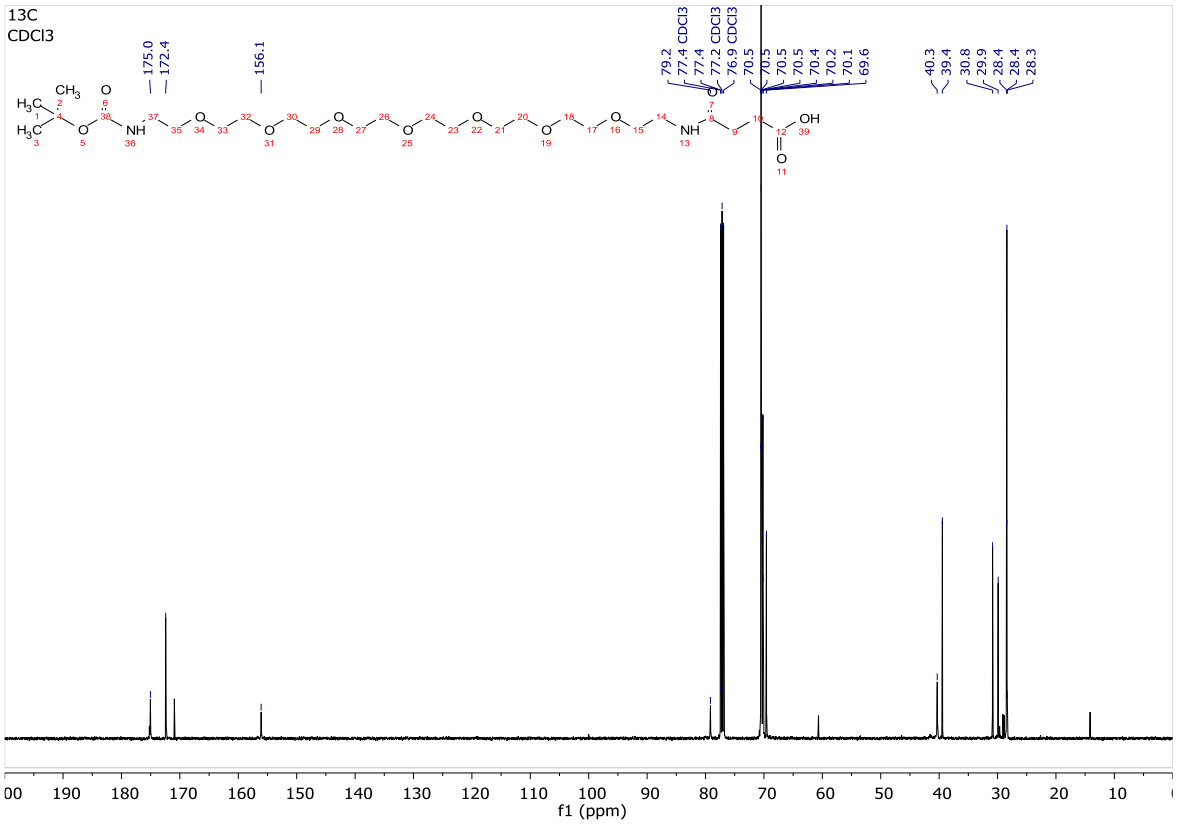

3.3a:

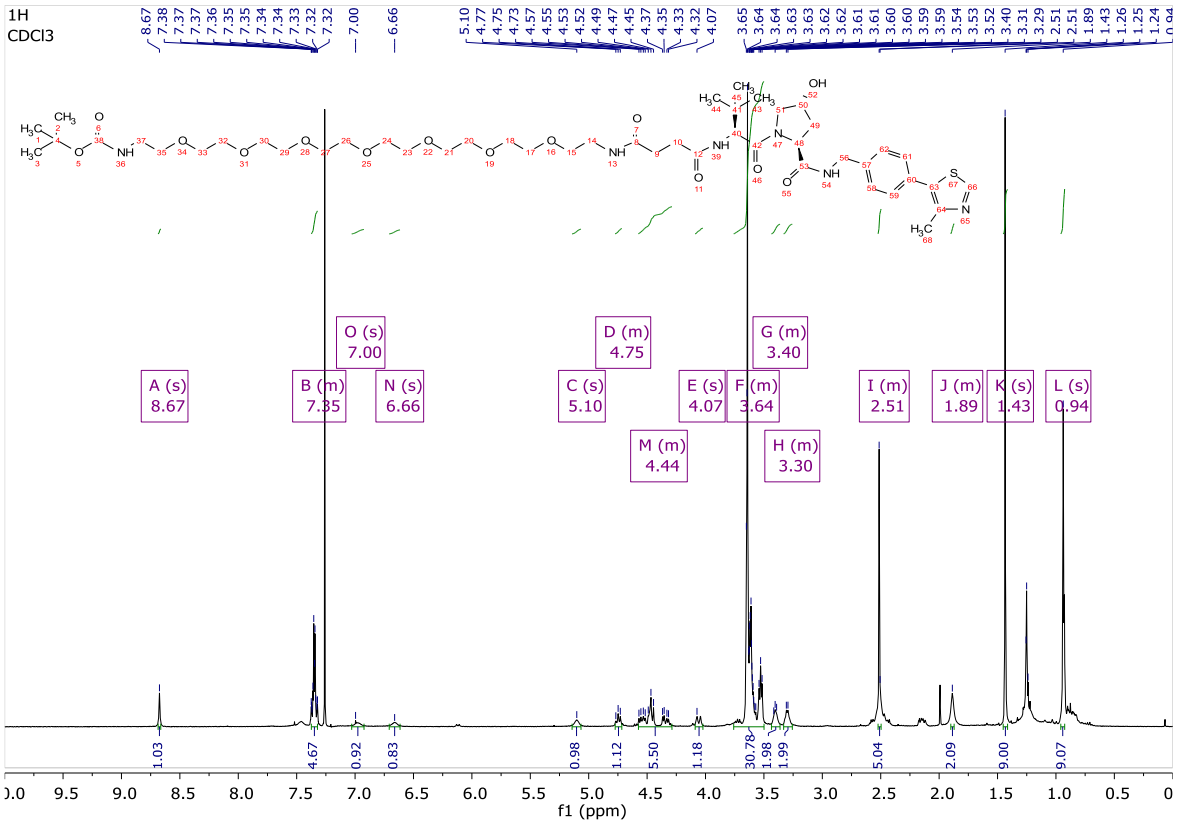
1H
CDCl3
A (s) 8.67
B (m) 7.35
O (s) 7.00
N (s) 6.66
C (s) 5.10
D (m) 4.75
M (m) 4.44
E (s) 4.07
F (m) 3.64
G (m) 3.40
H (m) 3.30
I (m) 2.51
J (m) 1.89
K (s) 1.43
L (s) 0.94
f1 (ppm)

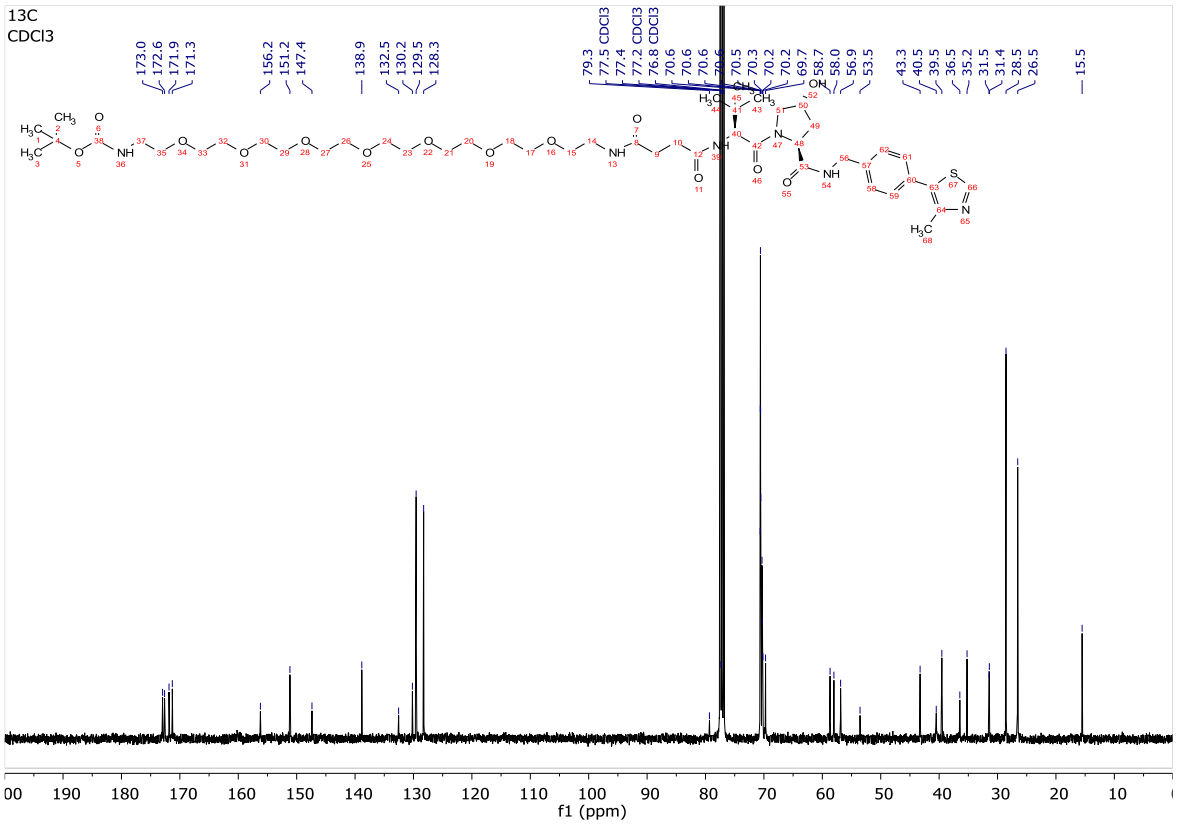
13C
CDCl3
f1 (ppm)

3.4a:

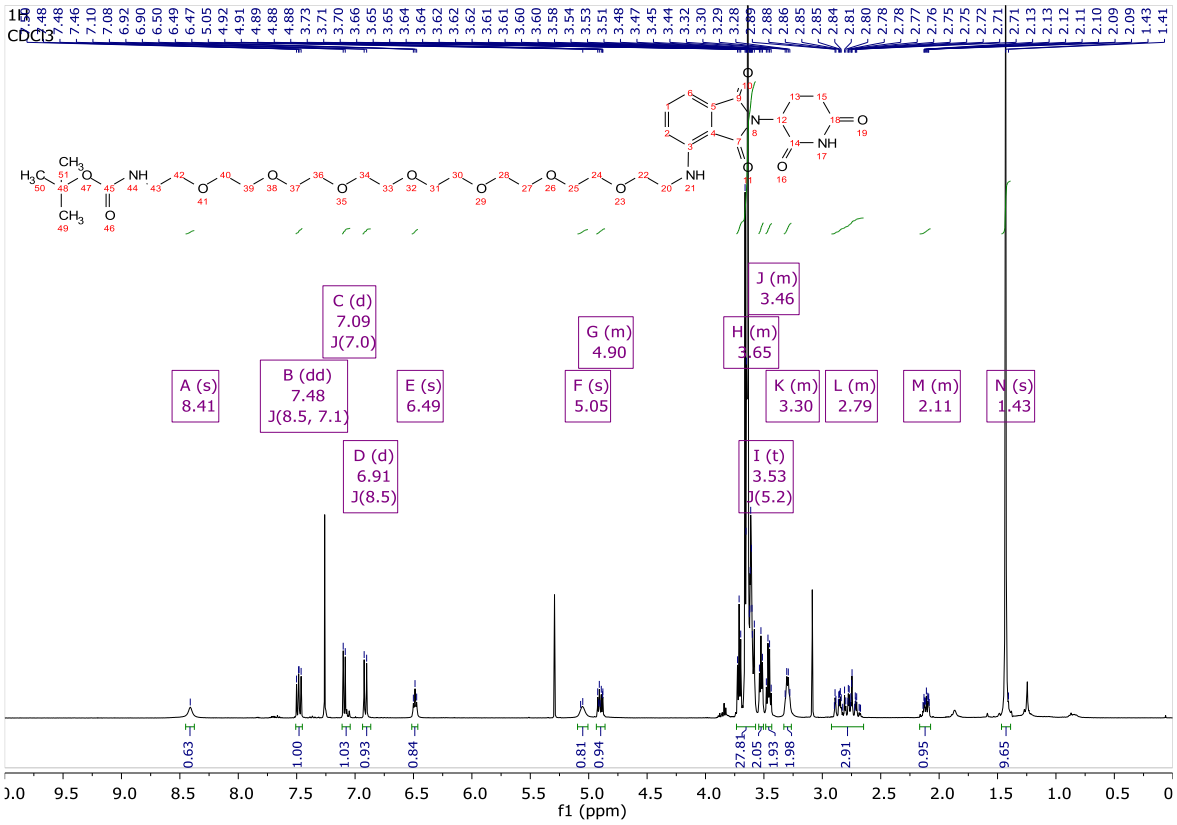
1H
CDCl3
A (s)
8.41
B (dd)
7.48
J(8.5, 7.1)
C (d)
7.09
J(7.0)
D (d)
6.91
J(8.5)
E (s)
6.49
F (s)
5.05
G (m)
4.90
H (m)
3.65
I (t)
3.53
J(5.2)
J (m)
3.46
K (m)
3.30
L (m)
2.79
M (m)
2.11
N (s)
1.43
f1 (ppm)

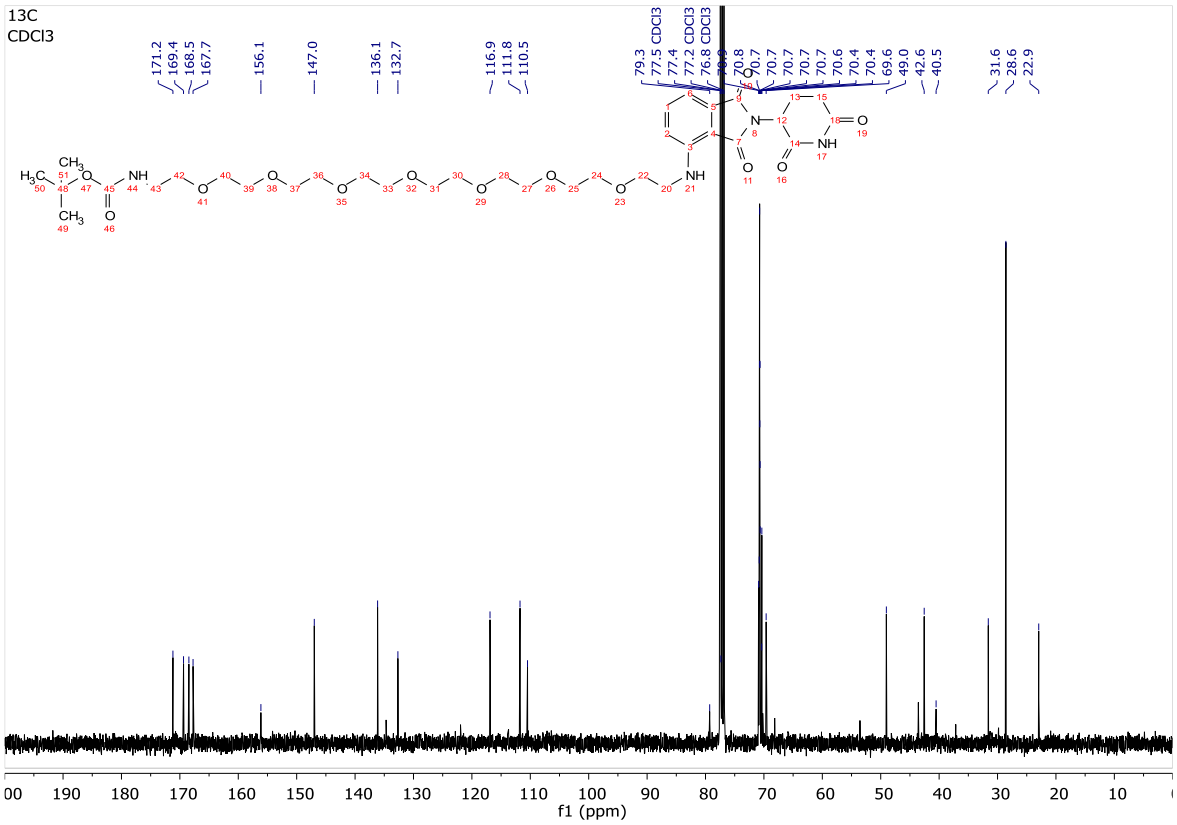
13C
CDCl3
f1 (ppm)

3.4b:

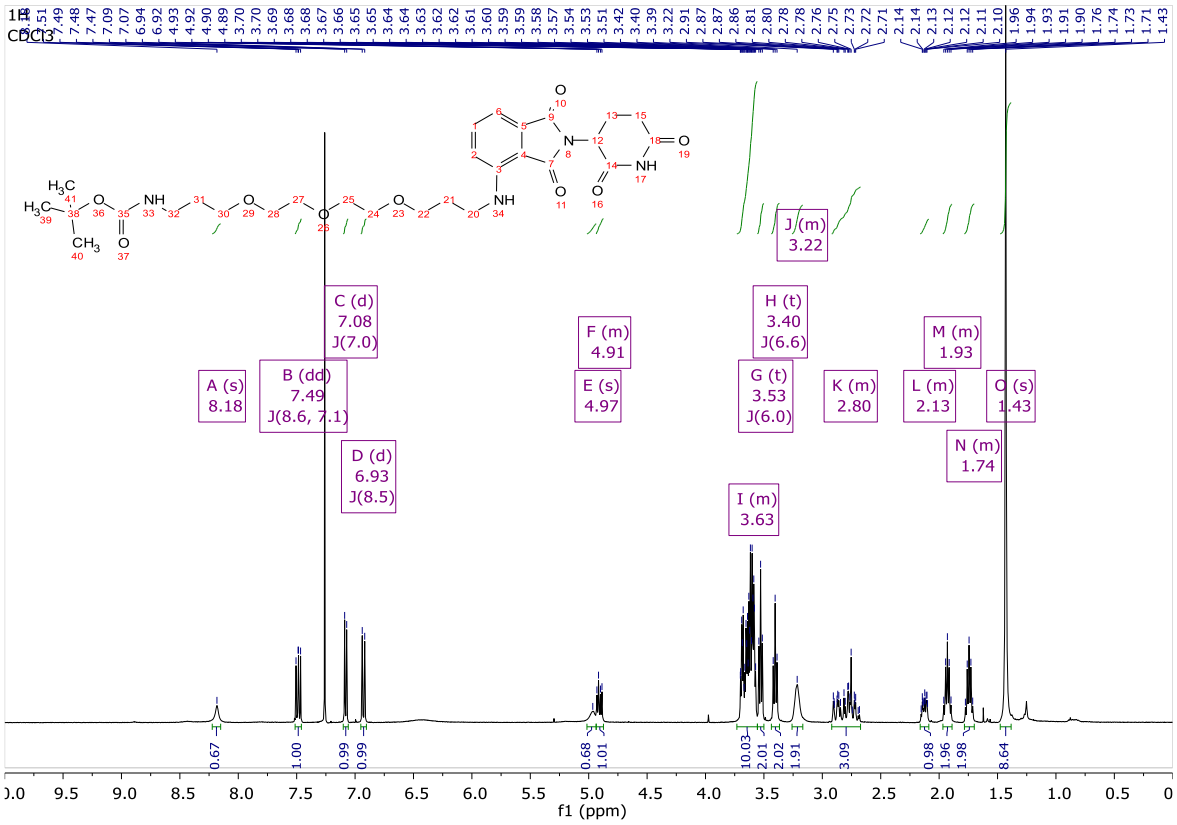
1H
CDCl3
A (s) 8.18
B (dd) 7.49 J(8.6, 7.1)
C (d) 7.08 J(7.0)
D (d) 6.93 J(8.5)
E (s) 4.97
F (m) 4.91
G (t) 3.53 J(6.0)
H (t) 3.40 J(6.6)
I (m) 3.63
J (m) 3.22
K (m) 2.80
L (m) 2.13
M (m) 1.93
N (m) 1.74
O (s) 1.43
f1 (ppm)

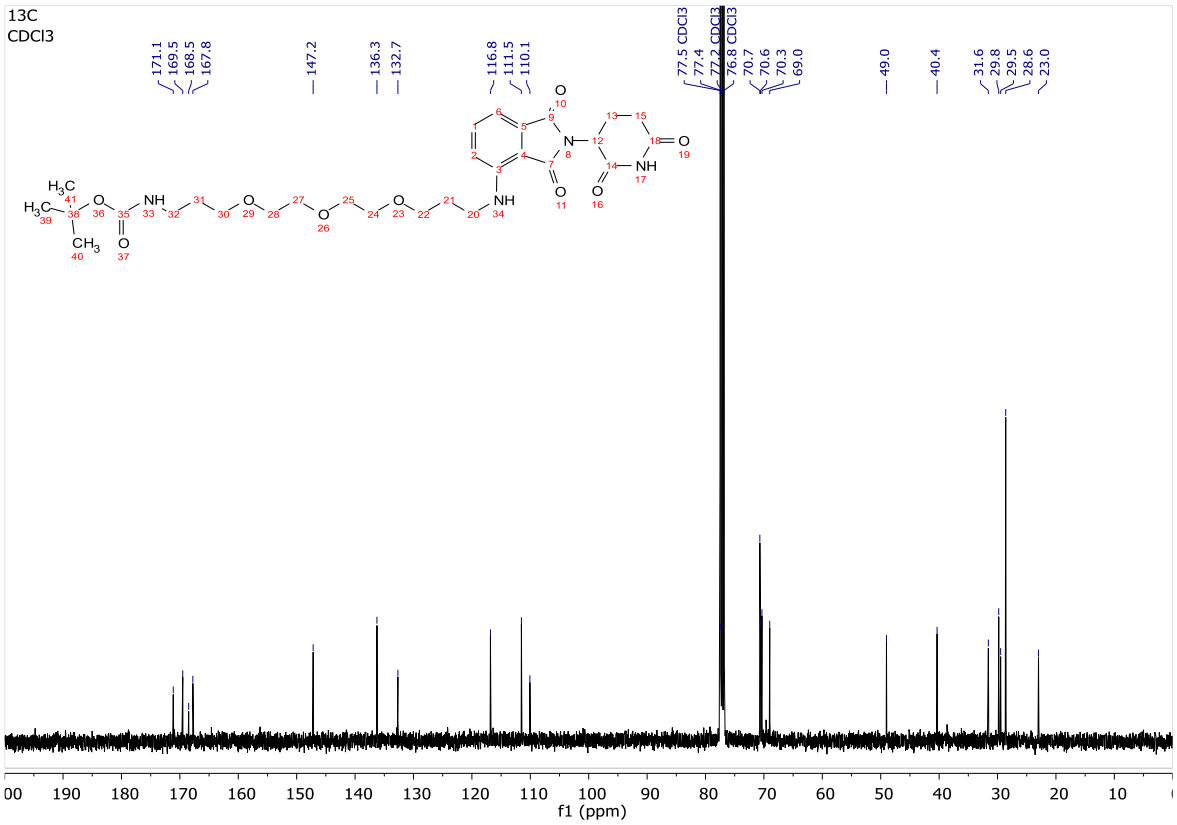
13C
CDCl3
171.1
169.5
168.5
167.8
147.2
136.3
132.7
116.8
111.5
110.1
77.5 CDCl3
77.4
77.2 CDCl3
76.8 CDCl3
70.7
70.6
70.3
69.0
49.0
40.4
31.6
29.8
29.5
28.6
23.0
f1 (ppm)

3.5:

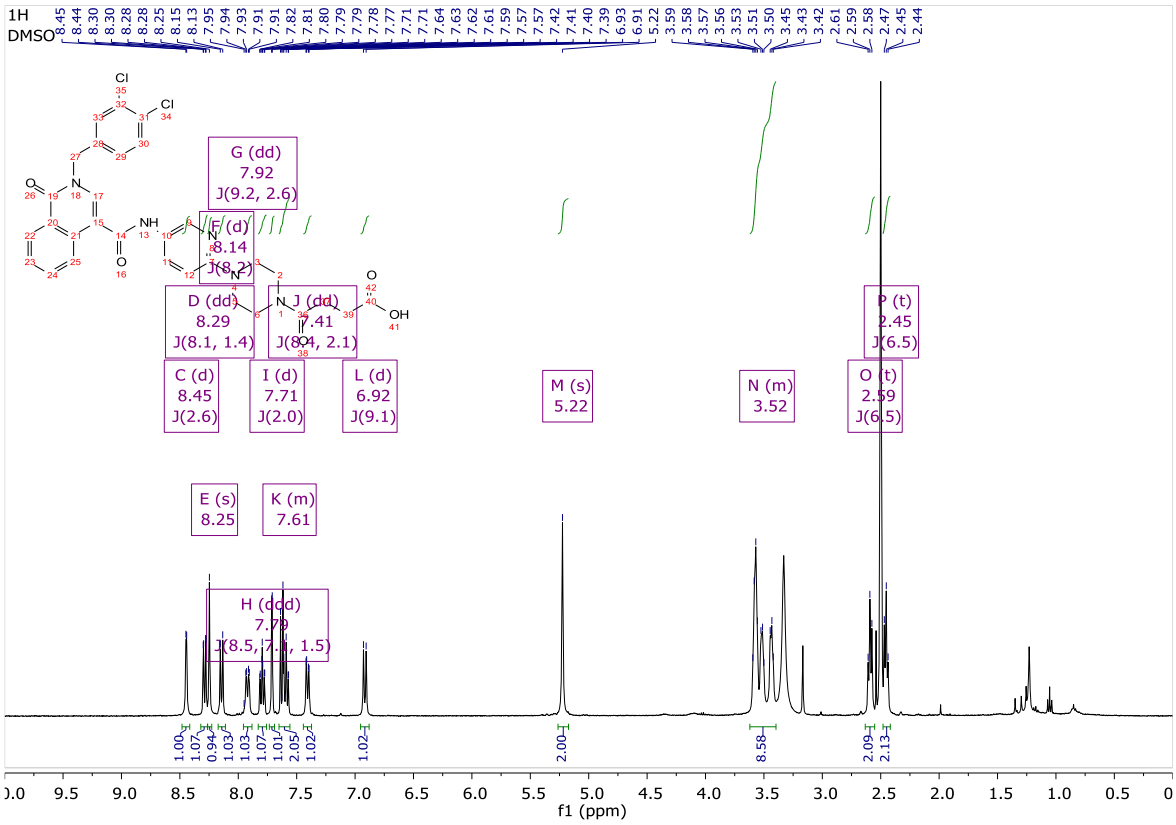
1H
DMSO
G (dd)
7.92
J(9.2, 2.6)
F (d)
8.14
J(8.2)
D (dd)
8.29
J(8.1, 1.4)
J (dd)
7.41
J(8.1, 2.1)
P (t)
2.45
J(6.5)
C (d)
8.45
J(2.6)
I (d)
7.71
J(2.0)
L (d)
6.92
J(9.1)
M (s)
5.22
N (m)
3.52
O (t)
2.59
J(6.5)
E (s)
8.25
K (m)
7.61
H (ddd)
7.79
J(8.5, 7.1, 1.5)
f1 (ppm)

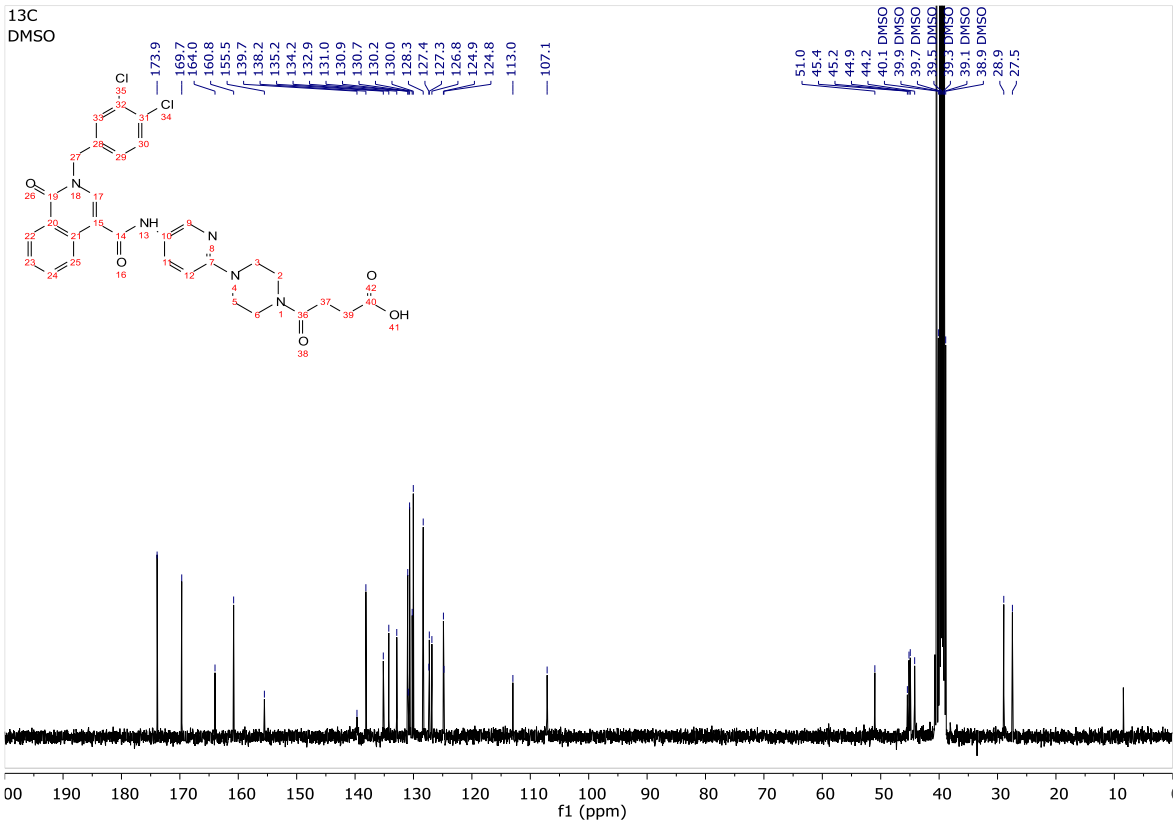
13C
DMSO
f1 (ppm)

FSCN-A-ctrl (3.6):

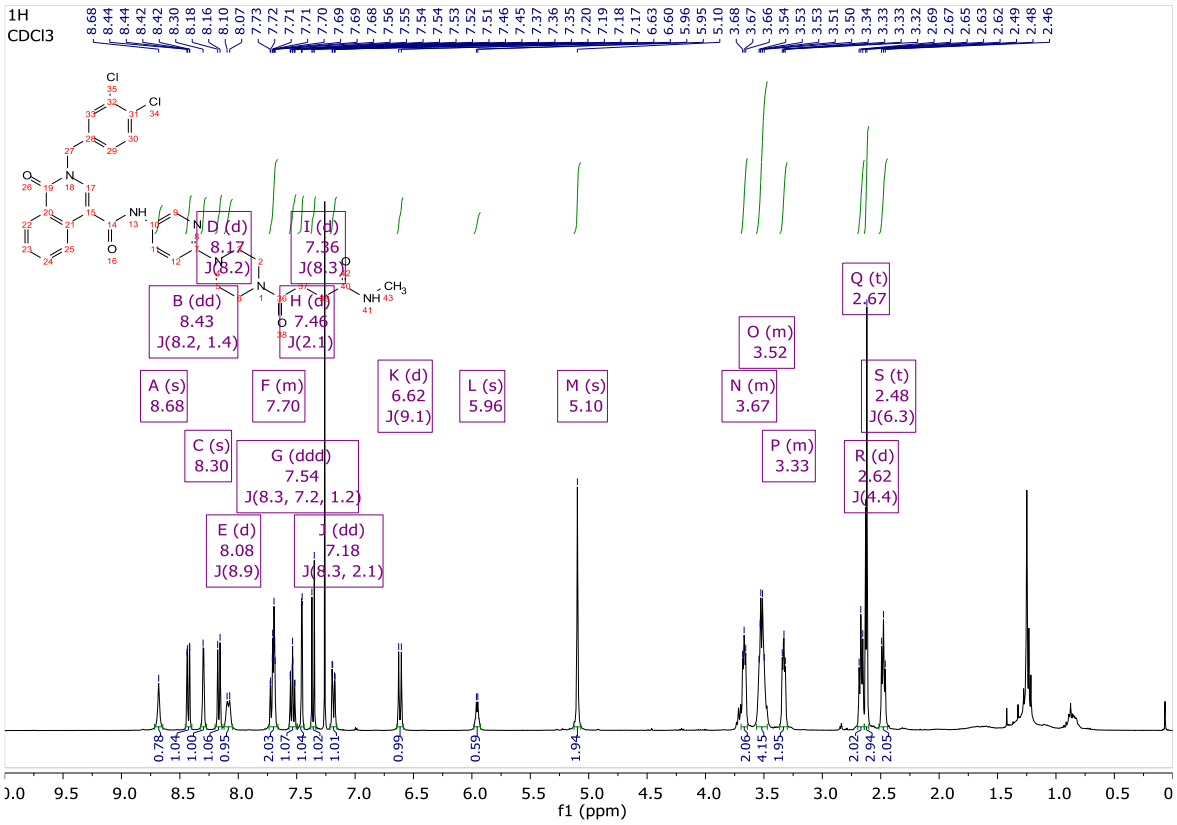

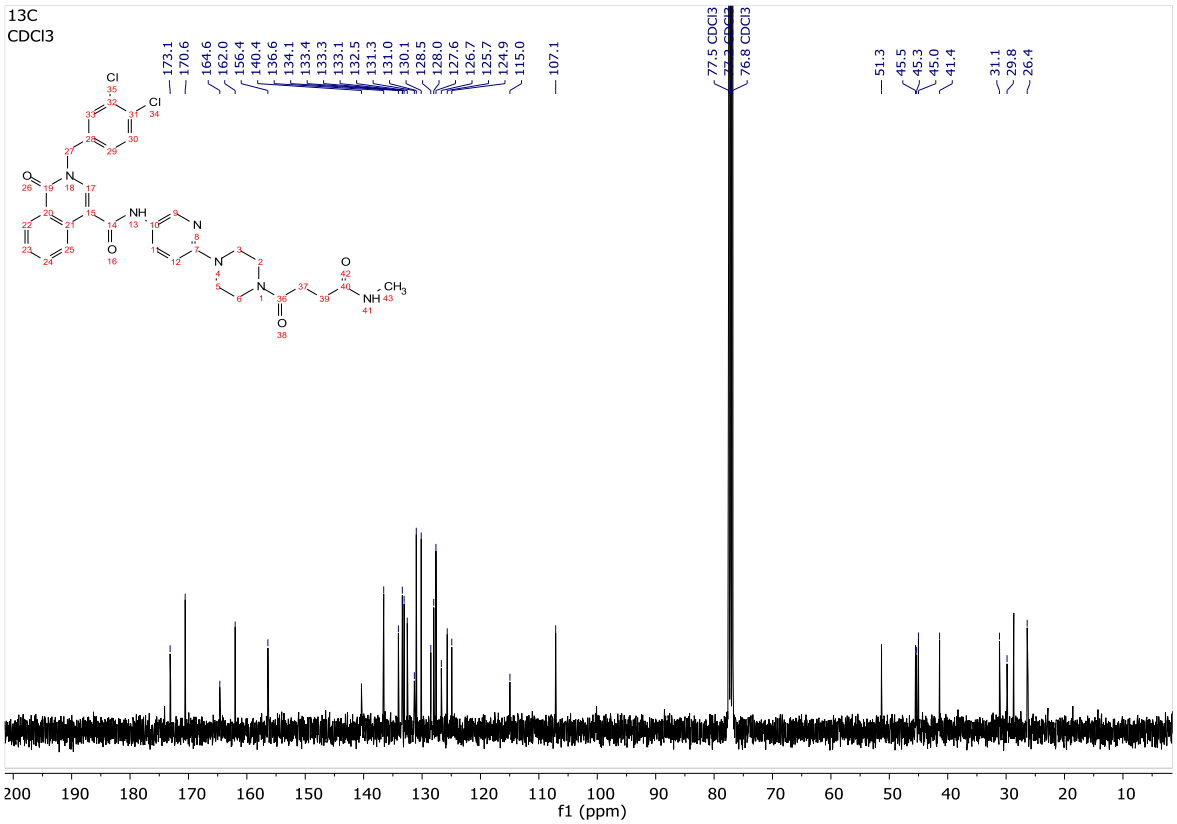

- *1st series amide PROTACs:*

FSCN-A-VHL-1 (3.7):

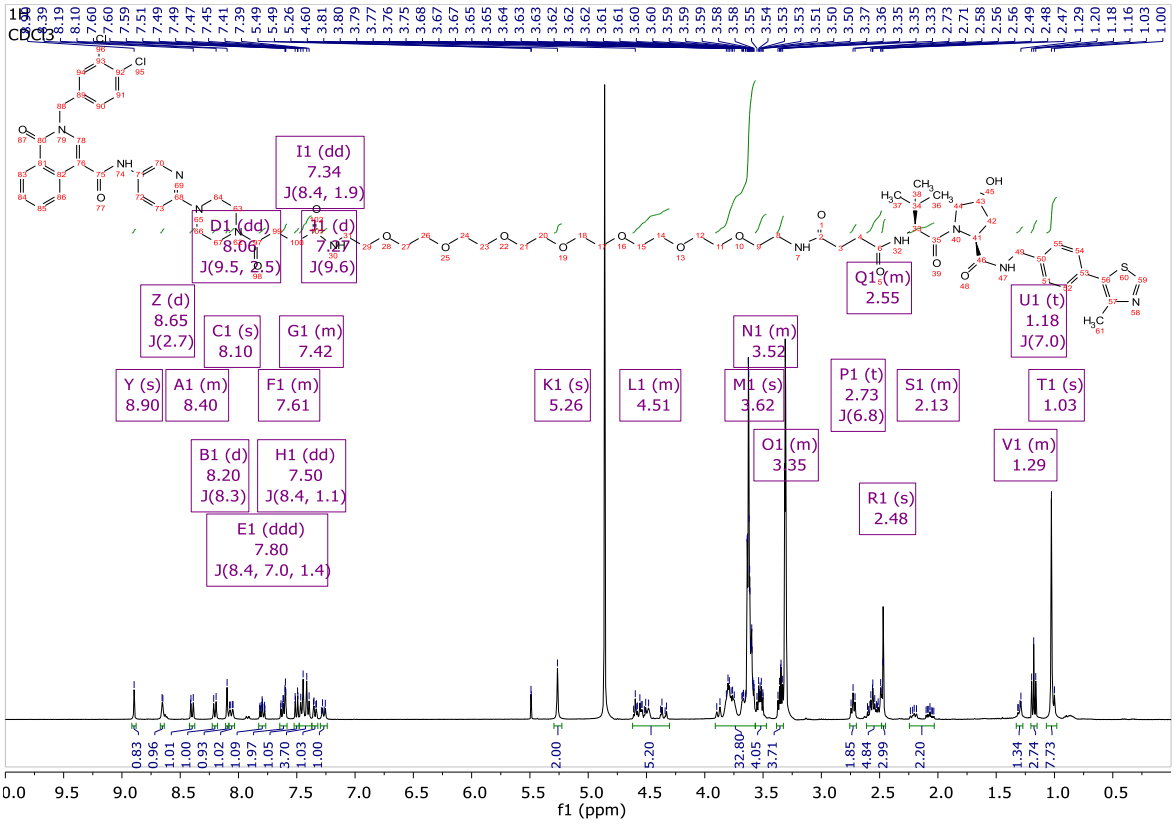

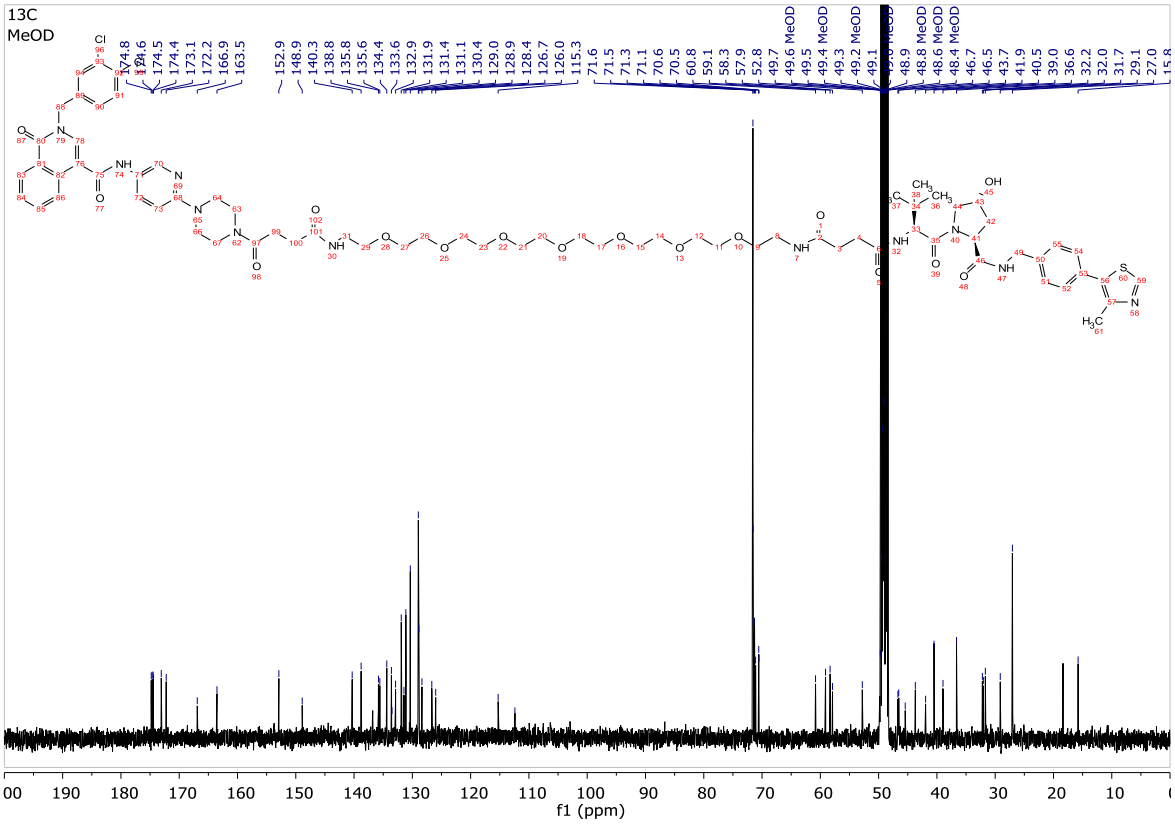

FSCN-A-CRBN-1 (3.9):

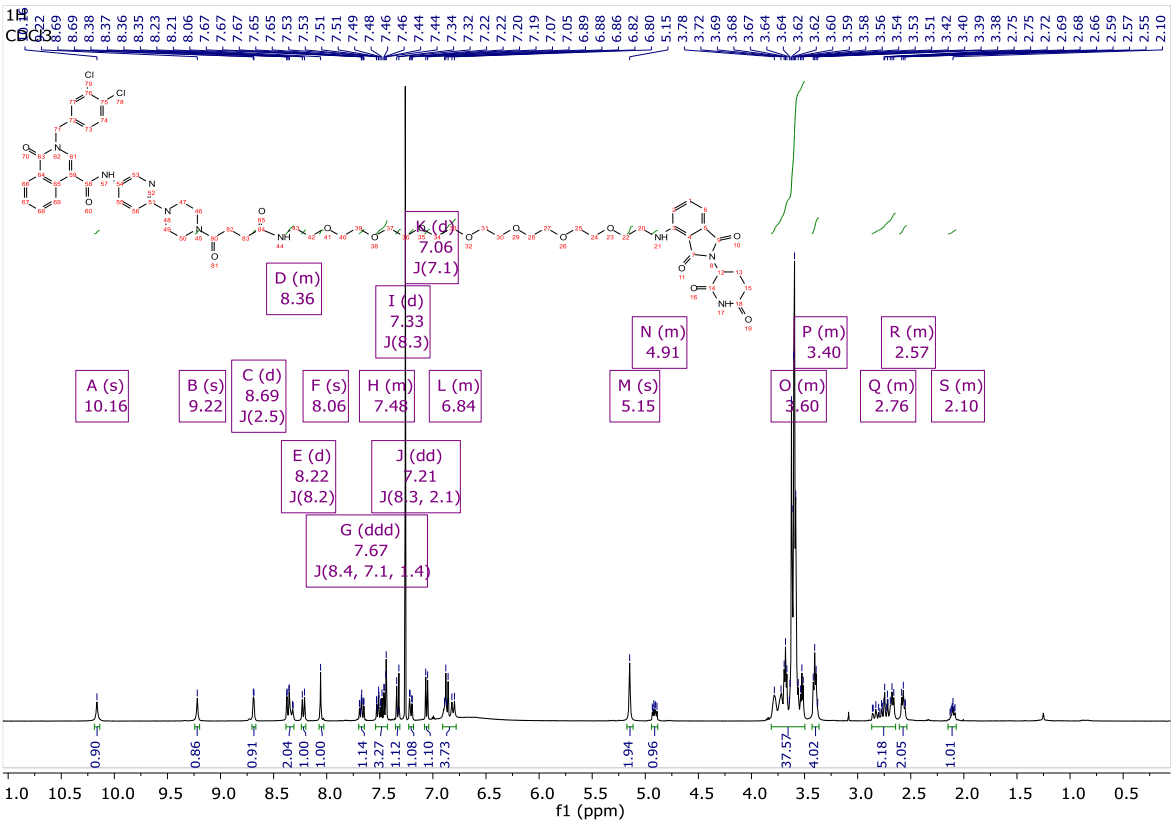

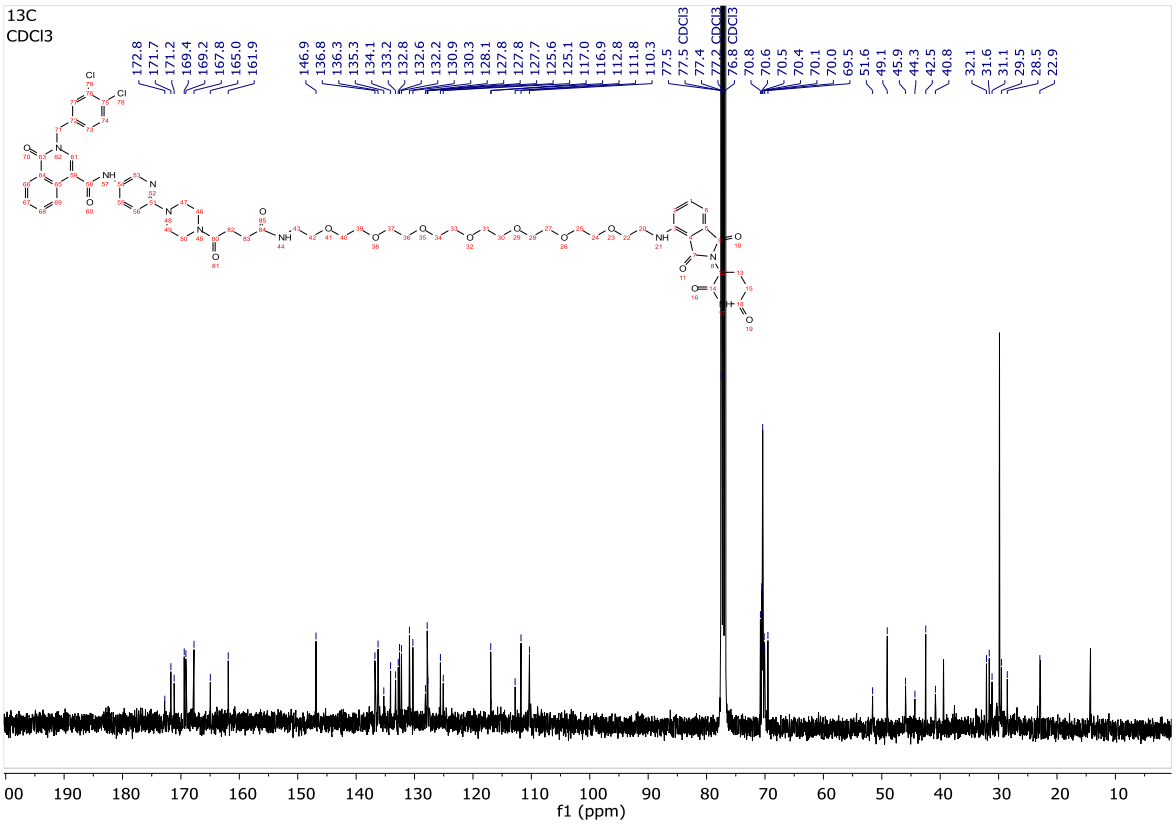

FSCN-A-CRBN-2 (3.10):

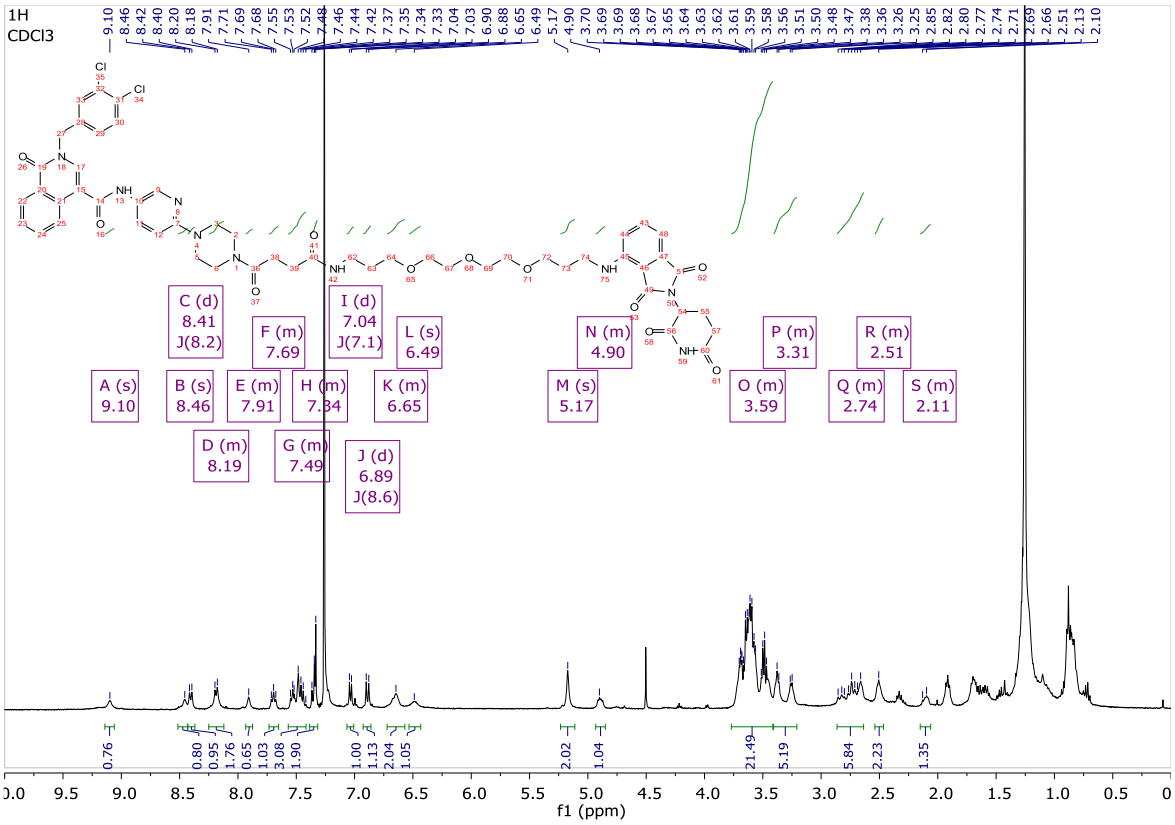

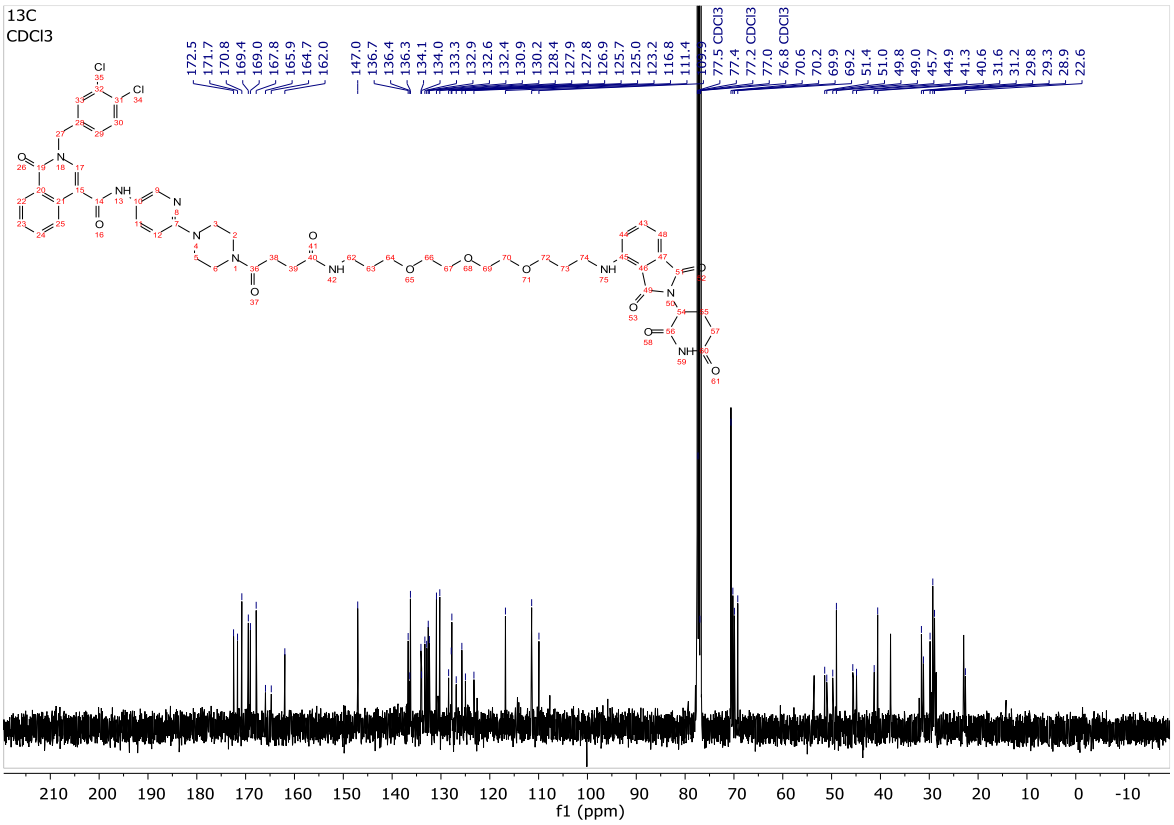

Preparation of 1st series alkylation PROTACs

- *Fascin ligand A alkylation VHL PROTACs:*

3.11:

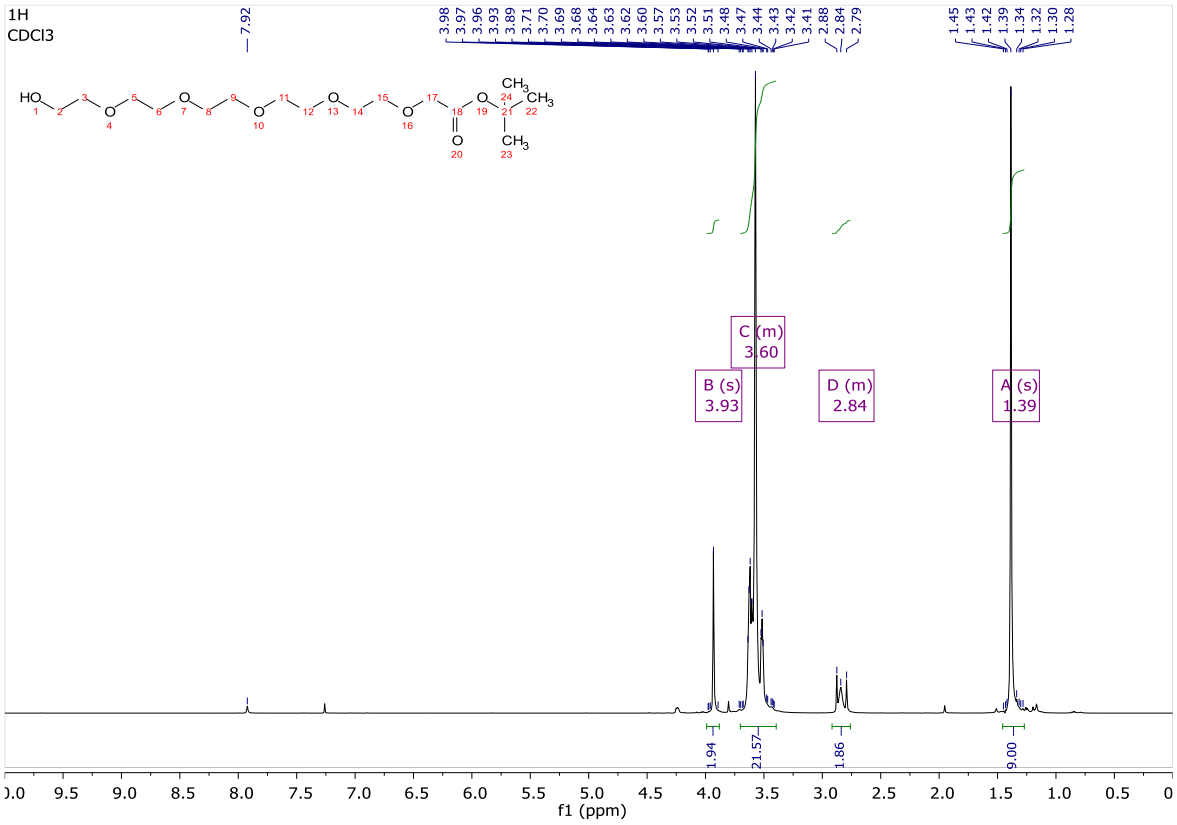

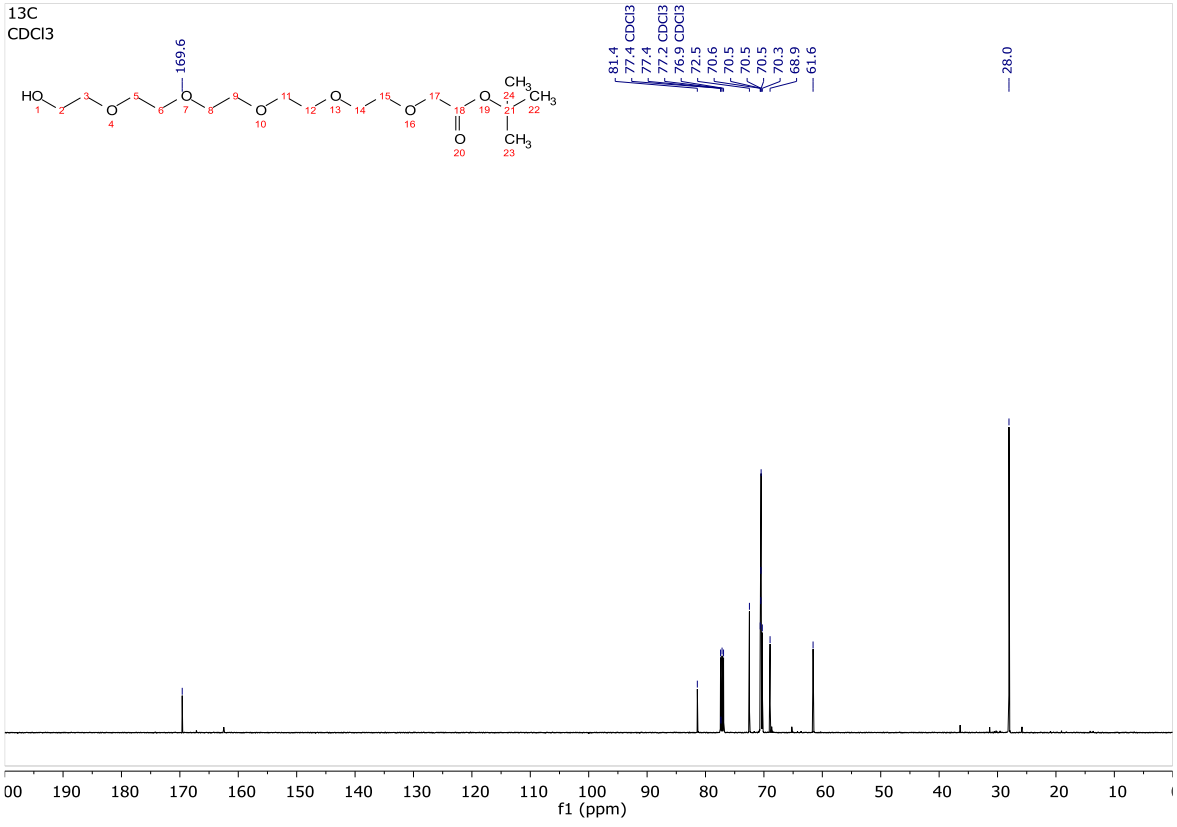

3.12:

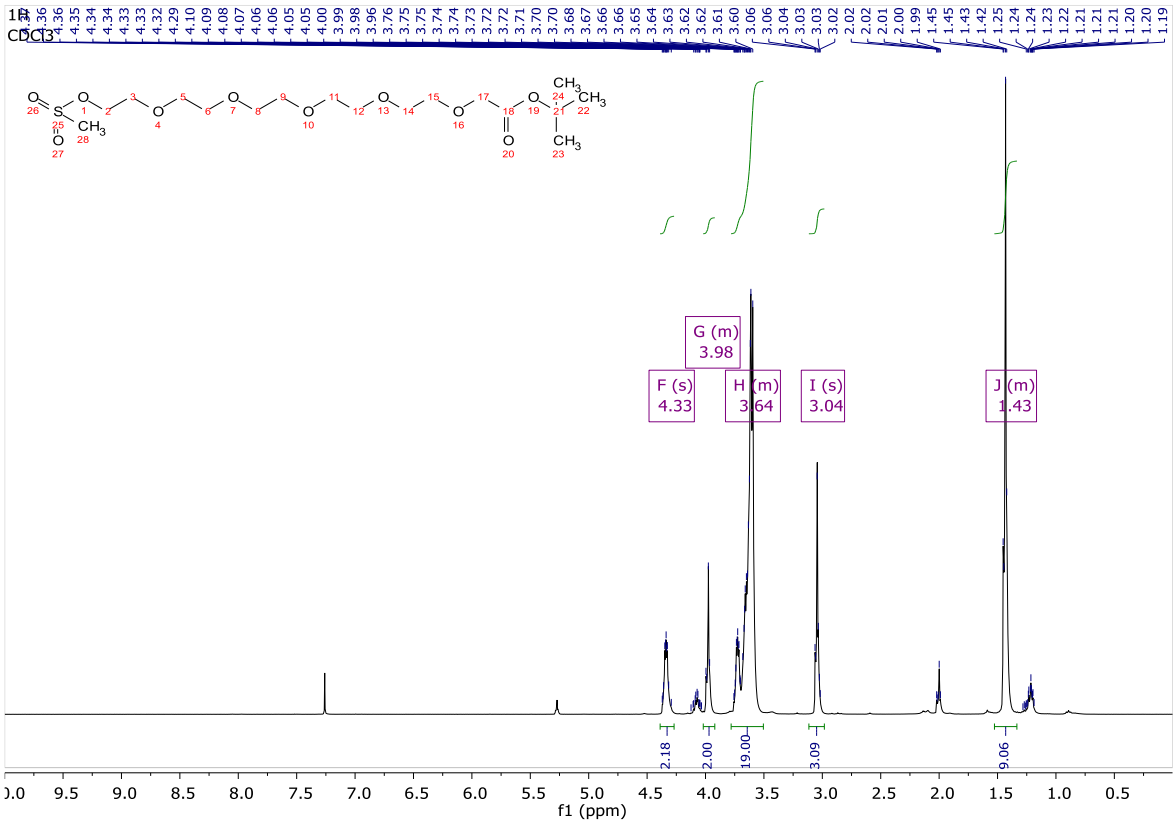
1H
CDCl3
G (m)
3.98
F (s)
4.33
H (m)
3.64
I (s)
3.04
J (m)
1.43
2.18
2.00
19.00
3.09
9.06
f1 (ppm)

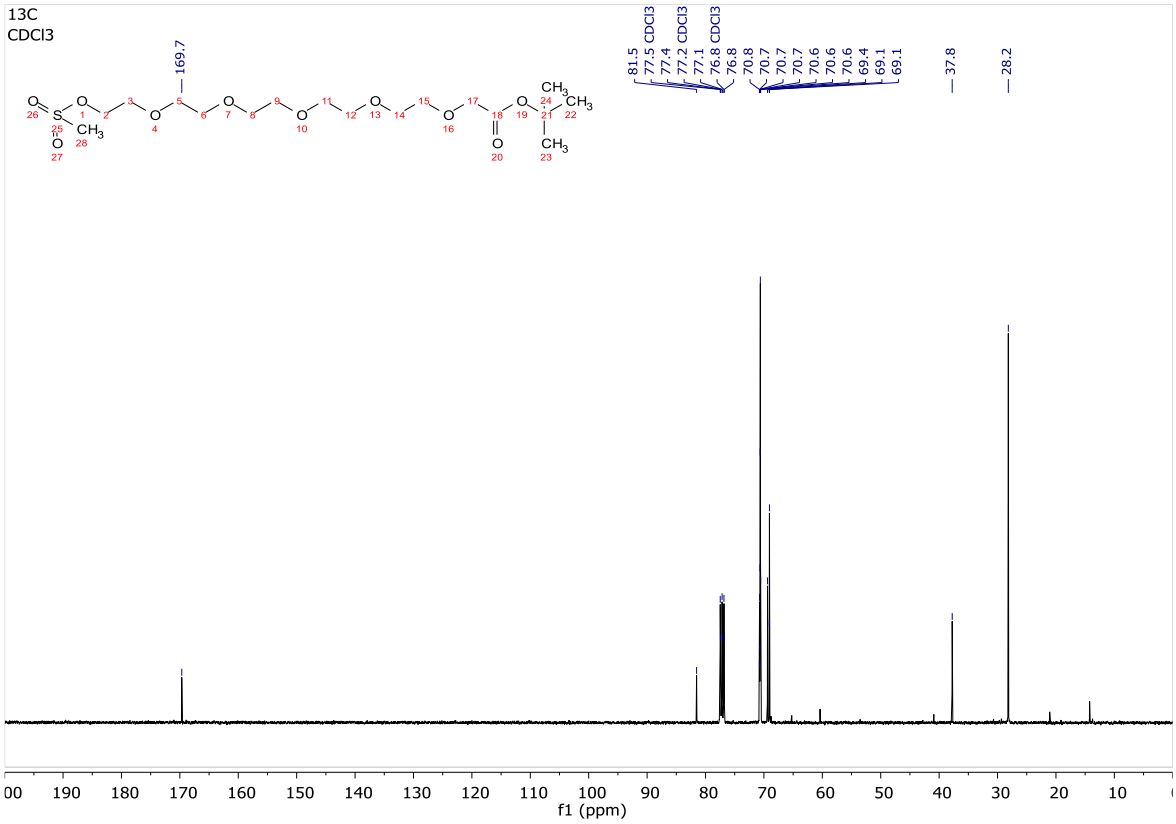
13C
CDCl3
169.7
81.5
77.5 CDCl3
77.4
77.2 CDCl3
77.1
76.8 CDCl3
76.8
70.8
70.7
70.7
70.7
70.6
70.6
70.6
69.4
69.1
69.1
37.8
28.2
f1 (ppm)

3.13:

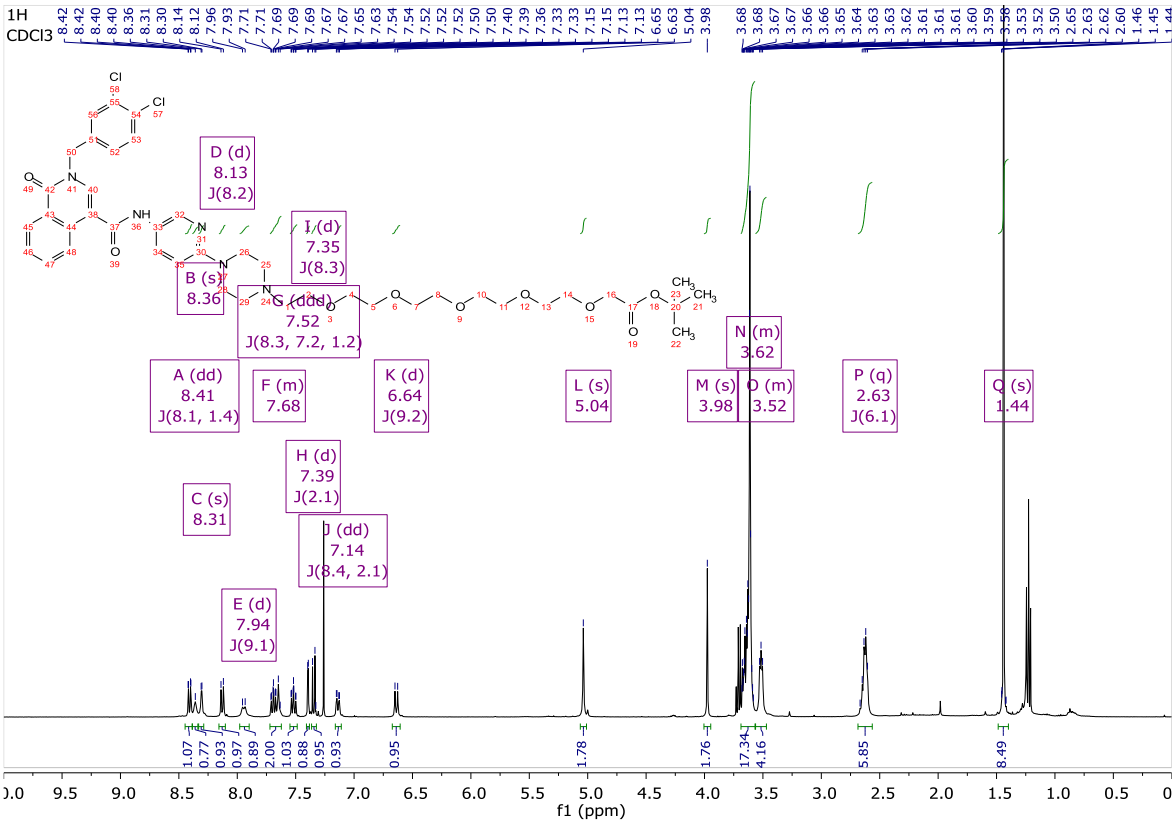
1H
CDCl3
D (d)
8.13
J(8.2)
I (d)
7.35
J(8.3)
B (s)
8.36
G (dd)
7.52
J(8.3, 7.2, 1.2)
N (m)
3.62
A (dd)
8.41
J(8.1, 1.4)
F (m)
7.68
K (d)
6.64
J(9.2)
L (s)
5.04
M (s)
3.98
O (m)
3.52
P (q)
2.63
J(6.1)
Q (s)
1.44
H (d)
7.39
J(2.1)
C (s)
8.31
J (dd)
7.14
J(8.4, 2.1)
E (d)
7.94
J(9.1)
f1 (ppm)

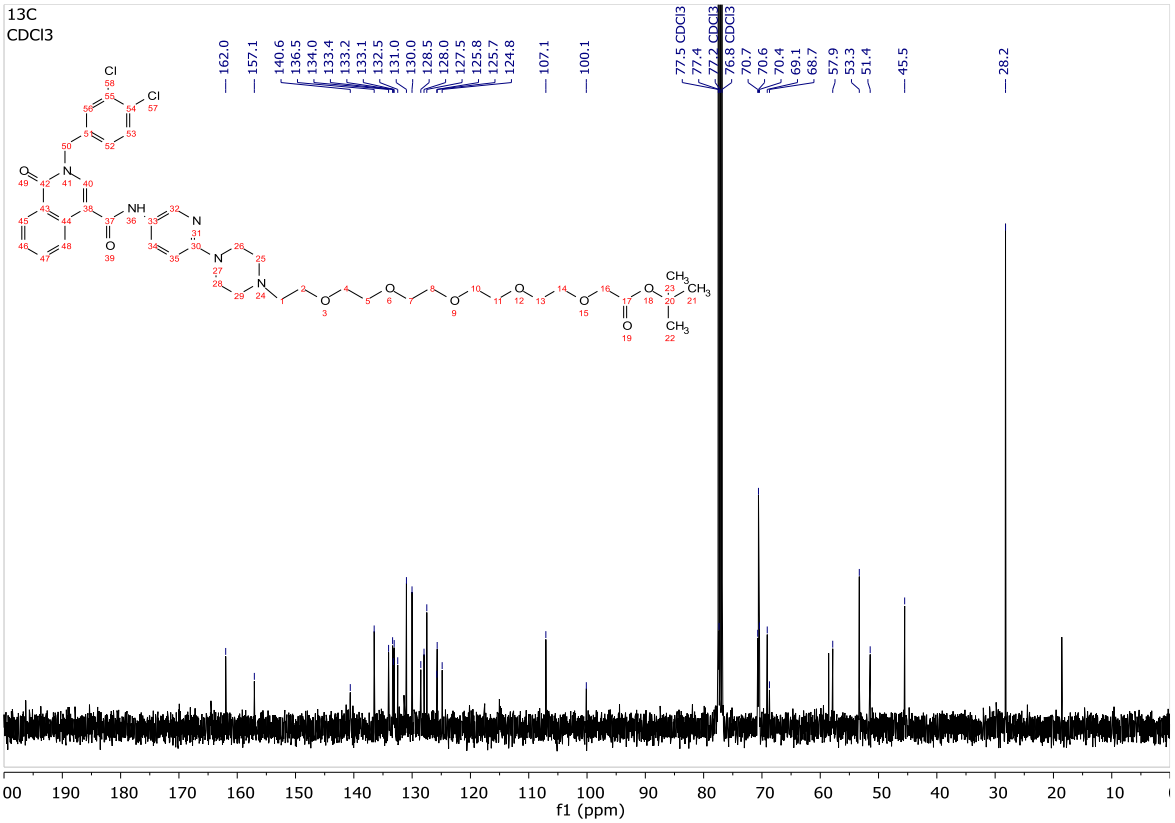
13C
CDCl3
f1 (ppm)

FSCN-A-VHL-3 (3.14):

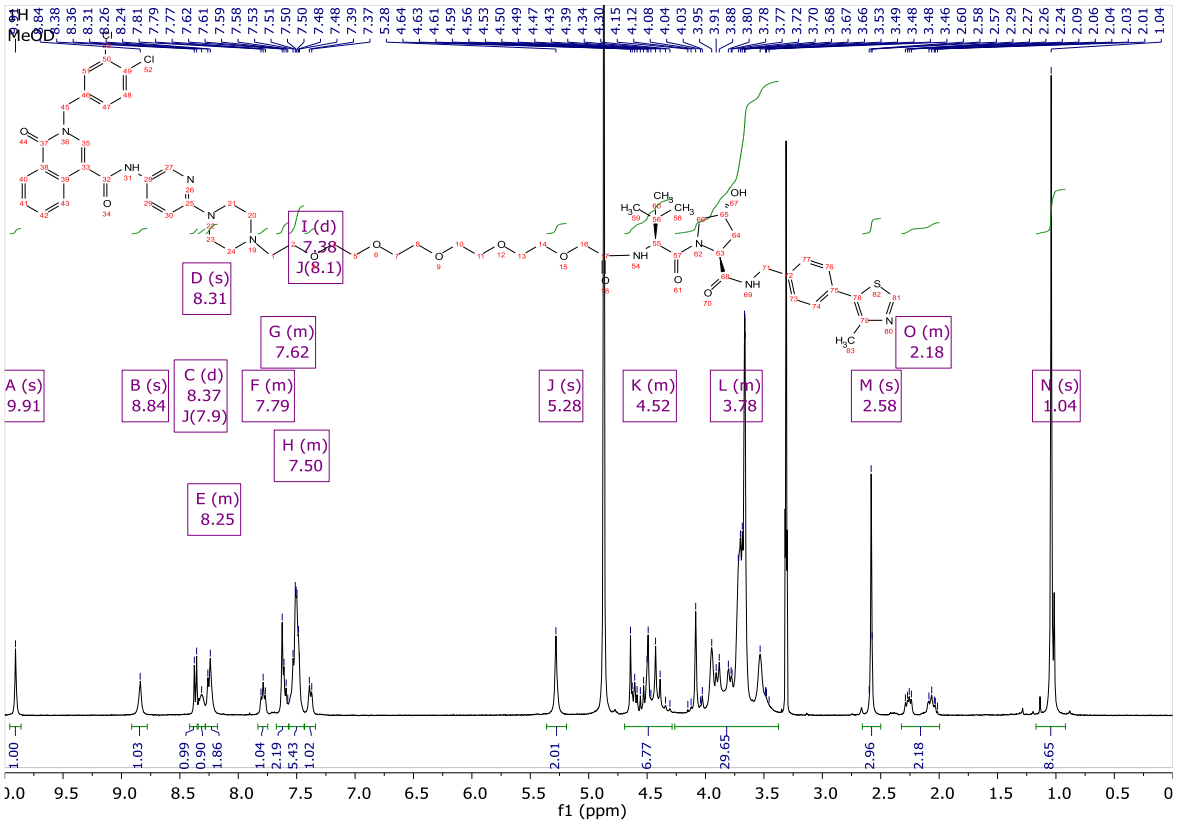

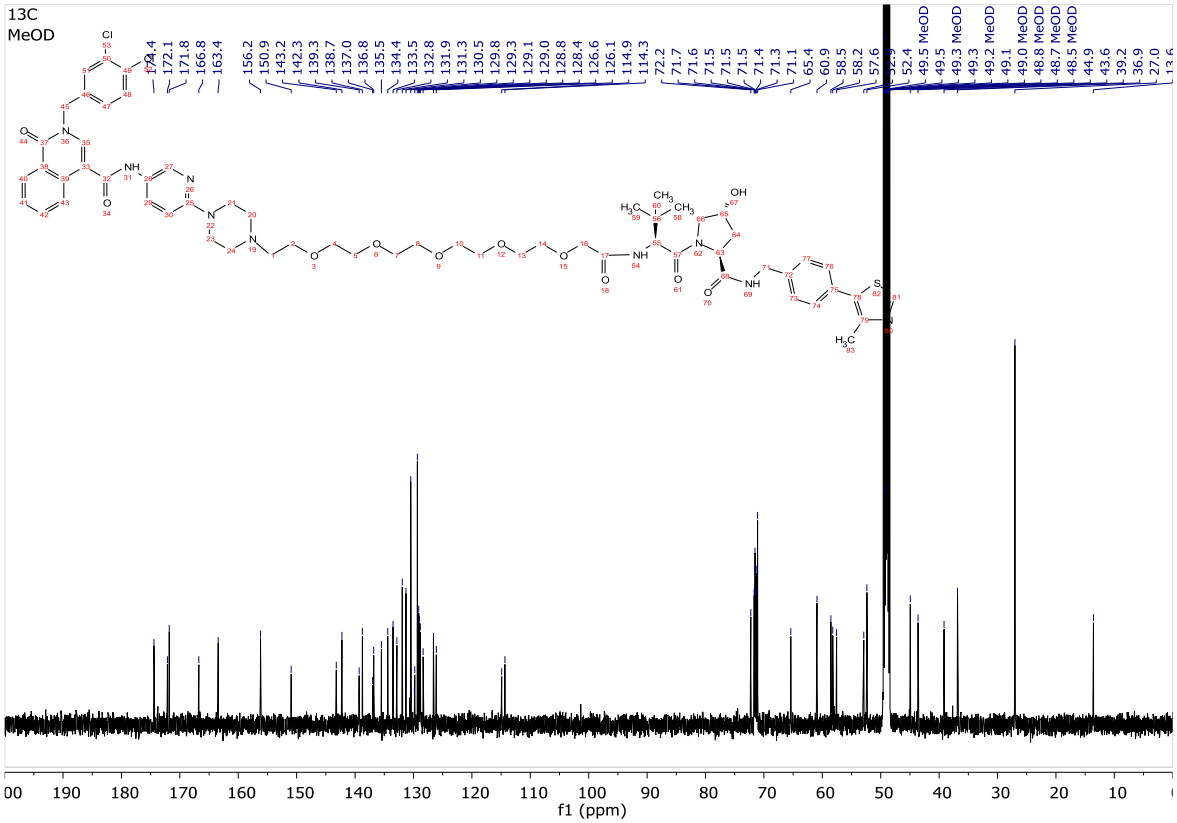

3.15:

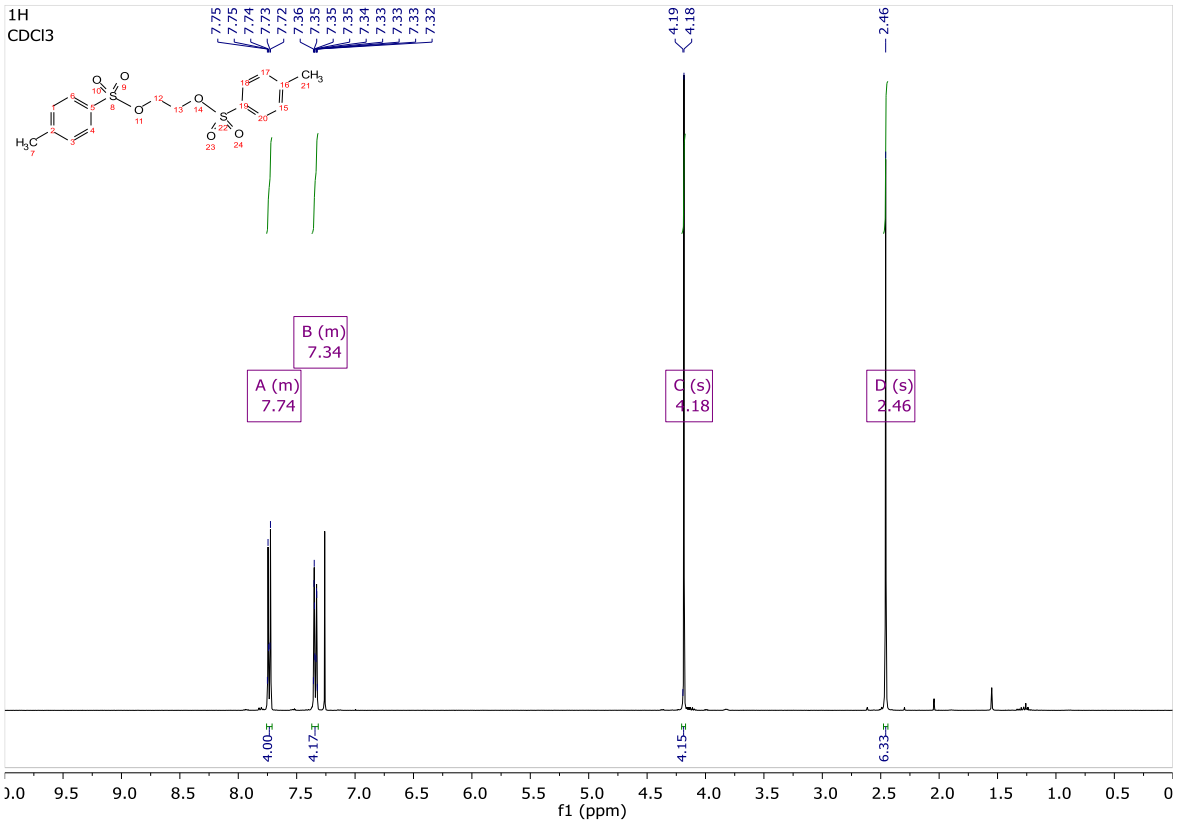
1H
CDCl3
7.75
7.75
7.74
7.73
7.72
7.36
7.35
7.35
7.35
7.34
7.33
7.33
7.33
7.32
4.19
4.18
2.46
B (m)
7.34
A (m)
7.74
C (s)
4.18
D (s)
2.46
4.00
4.17
4.15
6.33
f1 (ppm)

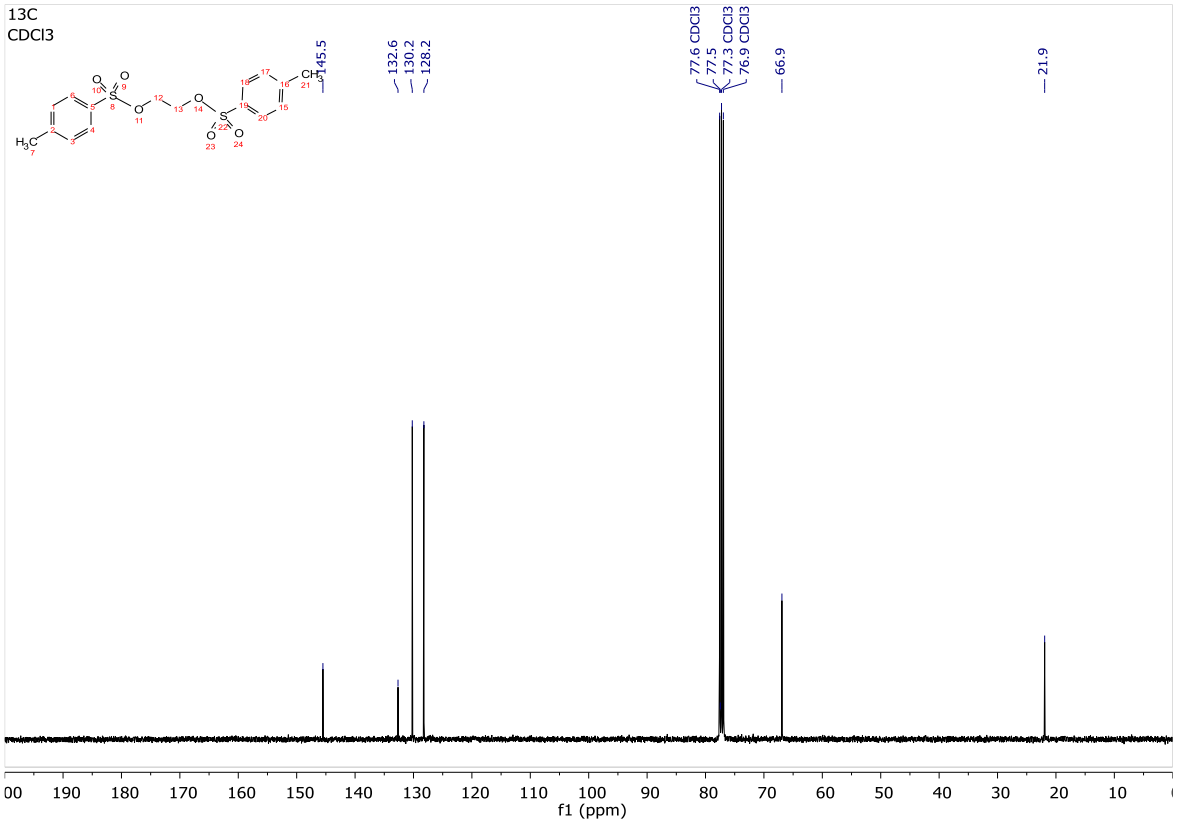
13C
CDCl3
145.5
132.6
130.2
128.2
77.6 CDCl3
77.5
77.3 CDCl3
76.9 CDCl3
66.9
21.9
f1 (ppm)

3.16:

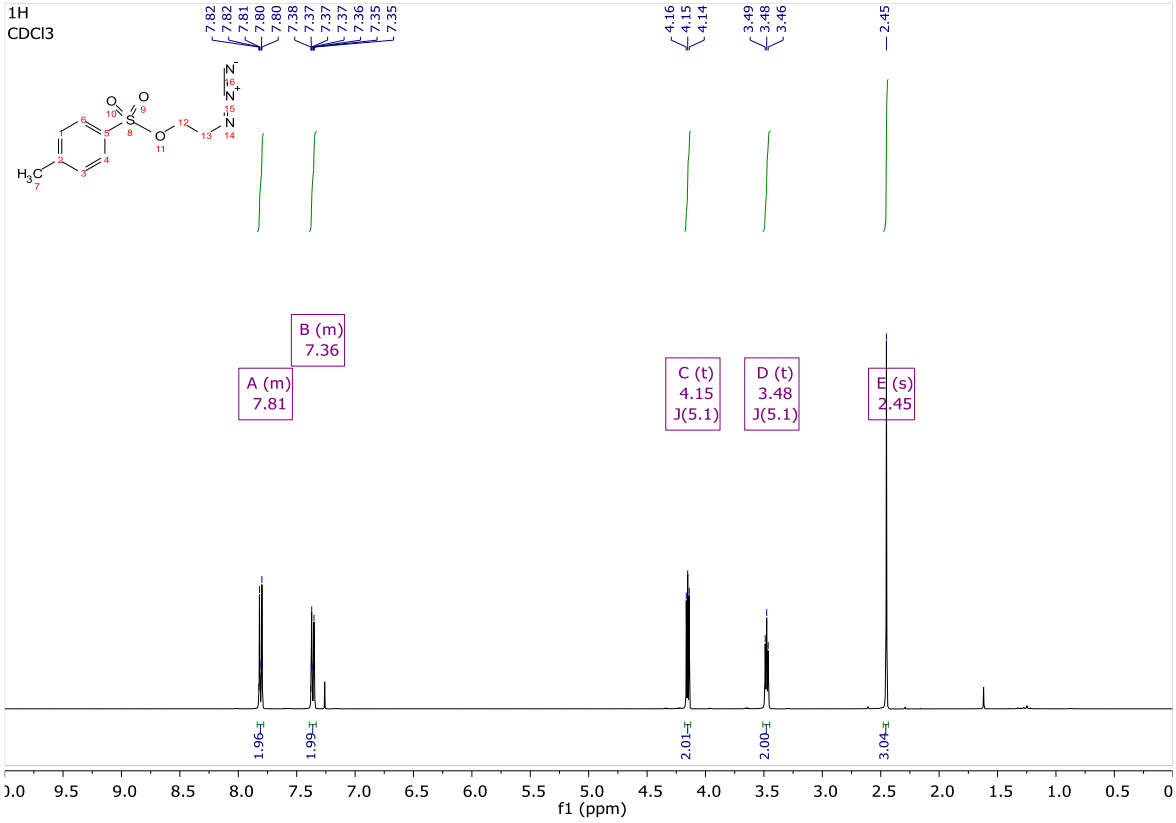
1H
CDCl3
7.82
7.82
7.81
7.80
7.80
7.38
7.37
7.37
7.37
7.36
7.35
7.35
4.16
4.15
4.14
3.49
3.48
3.46
2.45
B (m)
7.36
A (m)
7.81
C (t)
4.15
J(5.1)
D (t)
3.48
J(5.1)
E (s)
2.45
1.96
1.99
2.01
2.00
3.04
f1 (ppm)

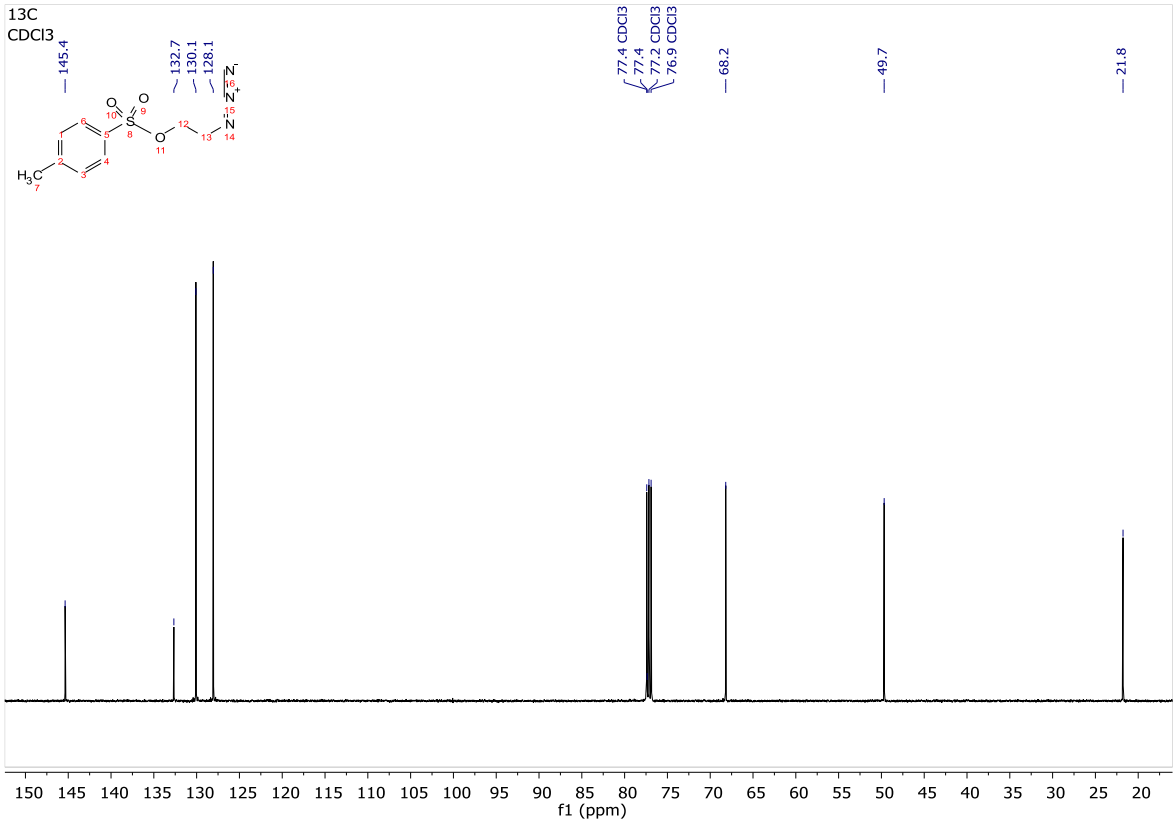
13C
CDCl3
145.4
132.7
130.1
128.1
77.4 CDCl3
77.4
77.2 CDCl3
76.9 CDCl3
68.2
49.7
21.8
f1 (ppm)

3.17:

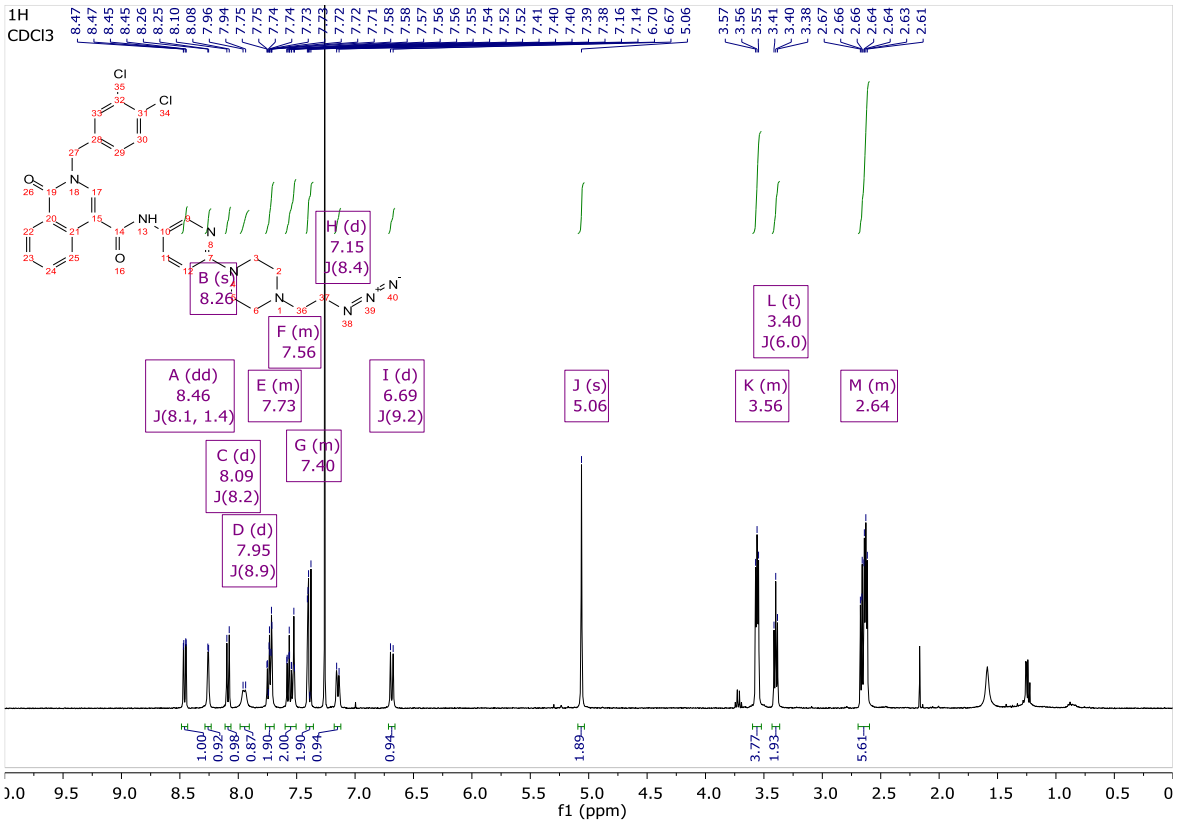
1H
CDCl3
A (dd)
8.46
J(8.1, 1.4)
B (s)
8.26
C (d)
8.09
J(8.2)
D (d)
7.95
J(8.9)
E (m)
7.73
F (m)
7.56
G (m)
7.40
H (d)
7.15
J(8.4)
I (d)
6.69
J(9.2)
J (s)
5.06
K (m)
3.56
L (t)
3.40
J(6.0)
M (m)
2.64
f1 (ppm)

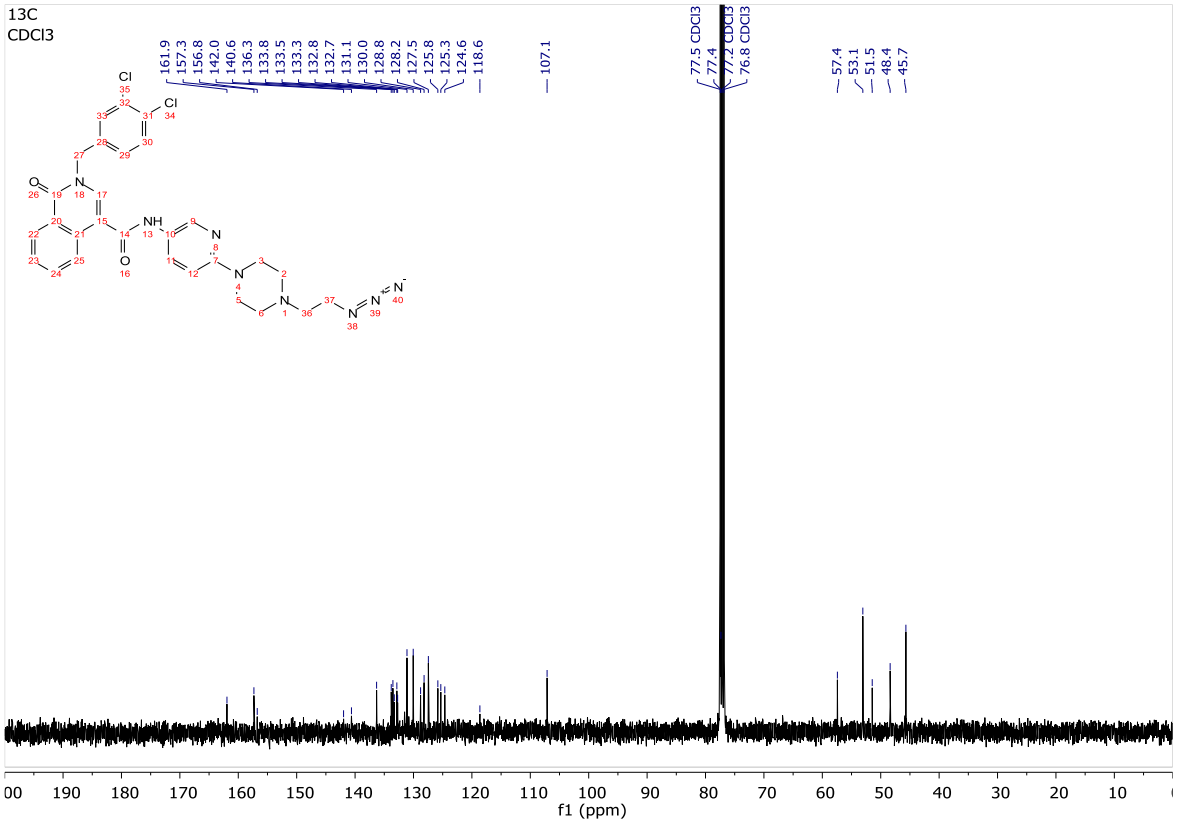
13C
CDCl3
77.5 CDCl3
77.4
77.2 CDCl3
76.8 CDCl3
f1 (ppm)

3.18:

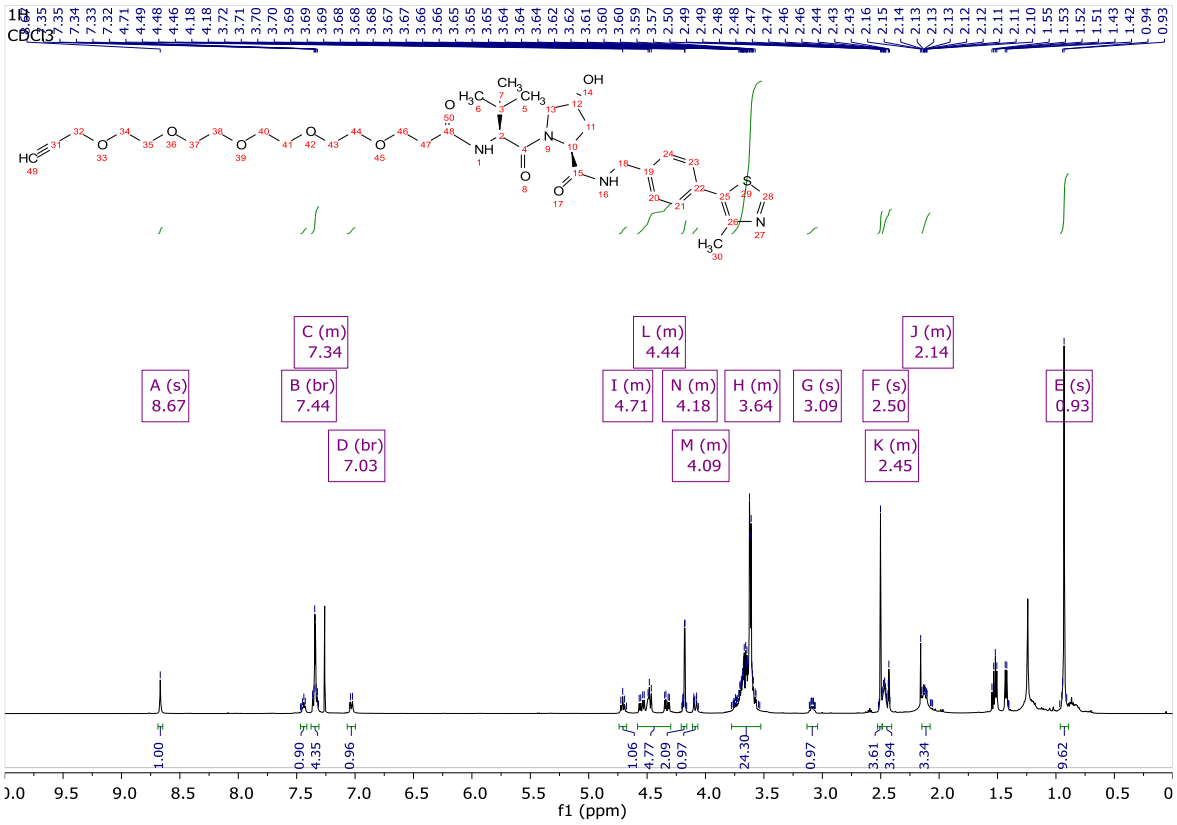
1H
CDCl3
A (s) 8.67
B (br) 7.44
C (m) 7.34
D (br) 7.03
I (m) 4.71
N (m) 4.18
M (m) 4.09
L (m) 4.44
H (m) 3.64
G (s) 3.09
F (s) 2.50
K (m) 2.45
J (m) 2.14
E (s) 0.93
f1 (ppm)

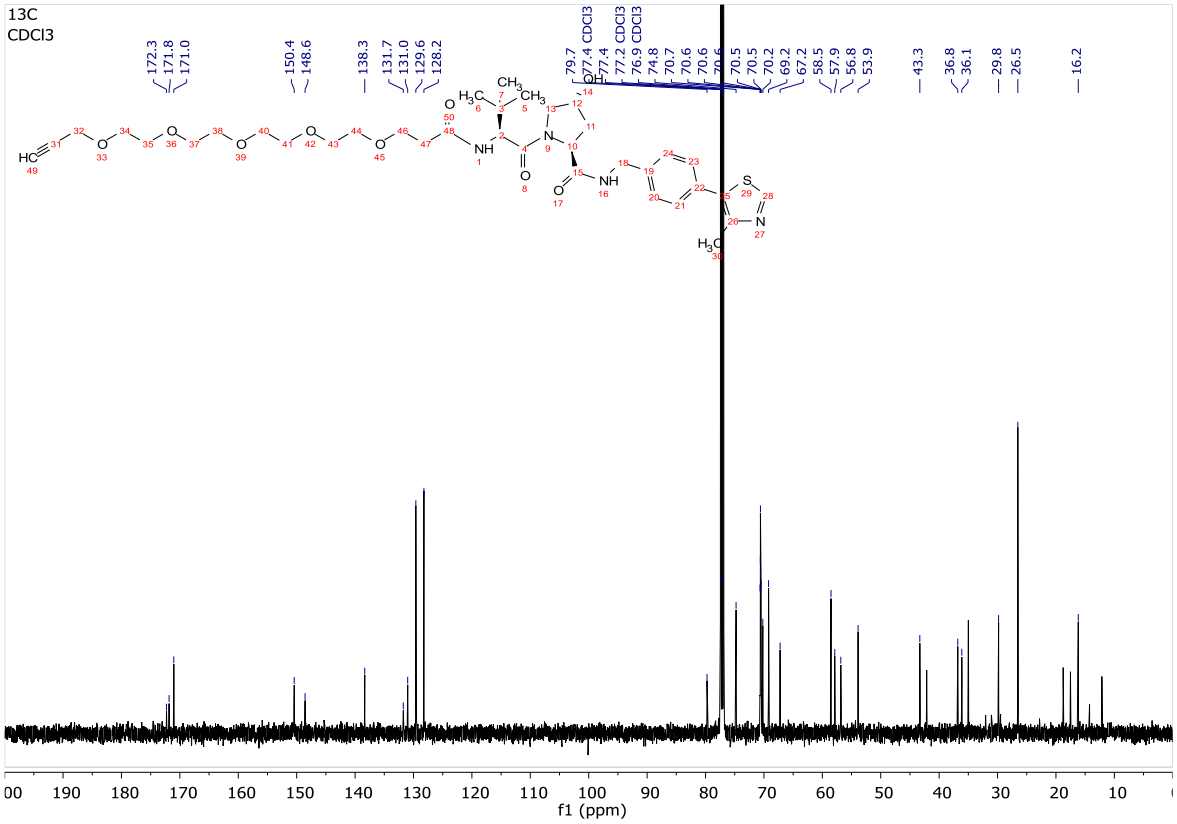
13C
CDCl3
f1 (ppm)

FSCN-A-VHL-4 (3.19):

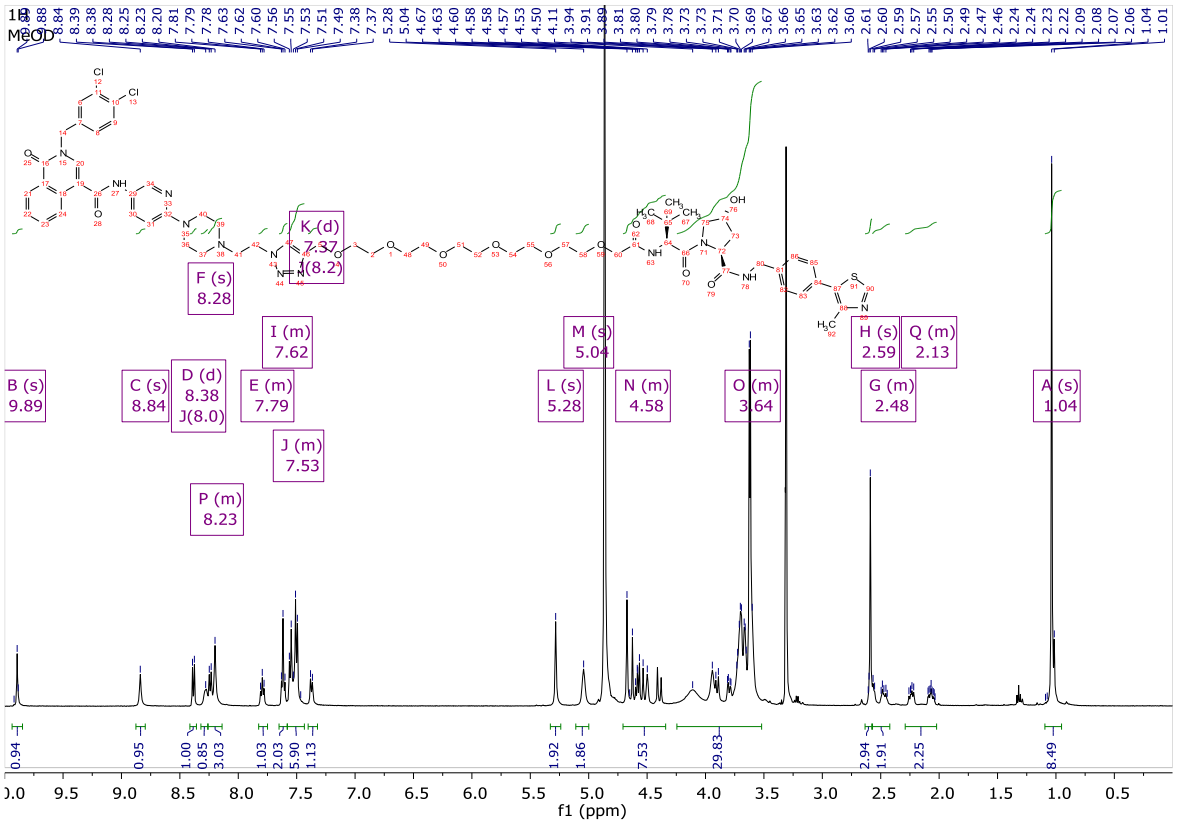

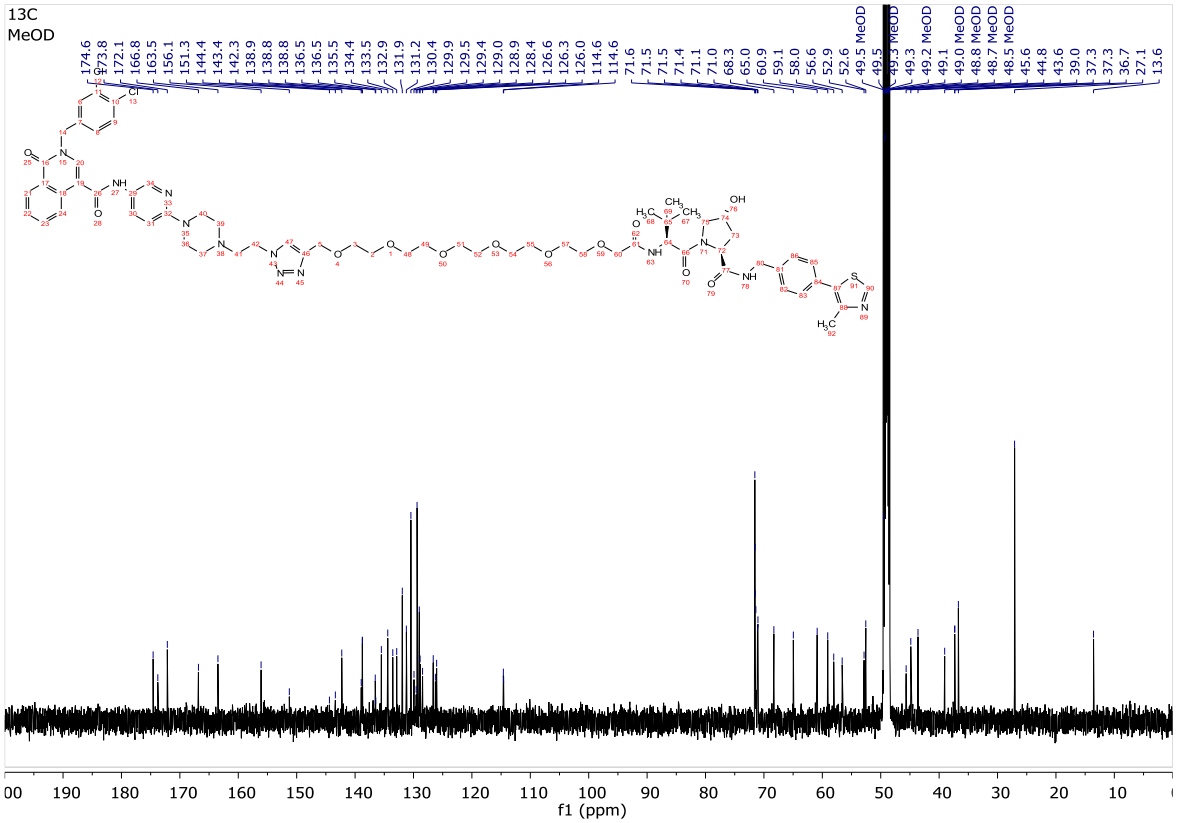

- *Fascin ligand A alkylation CRBN PROTAC:*

3.20:

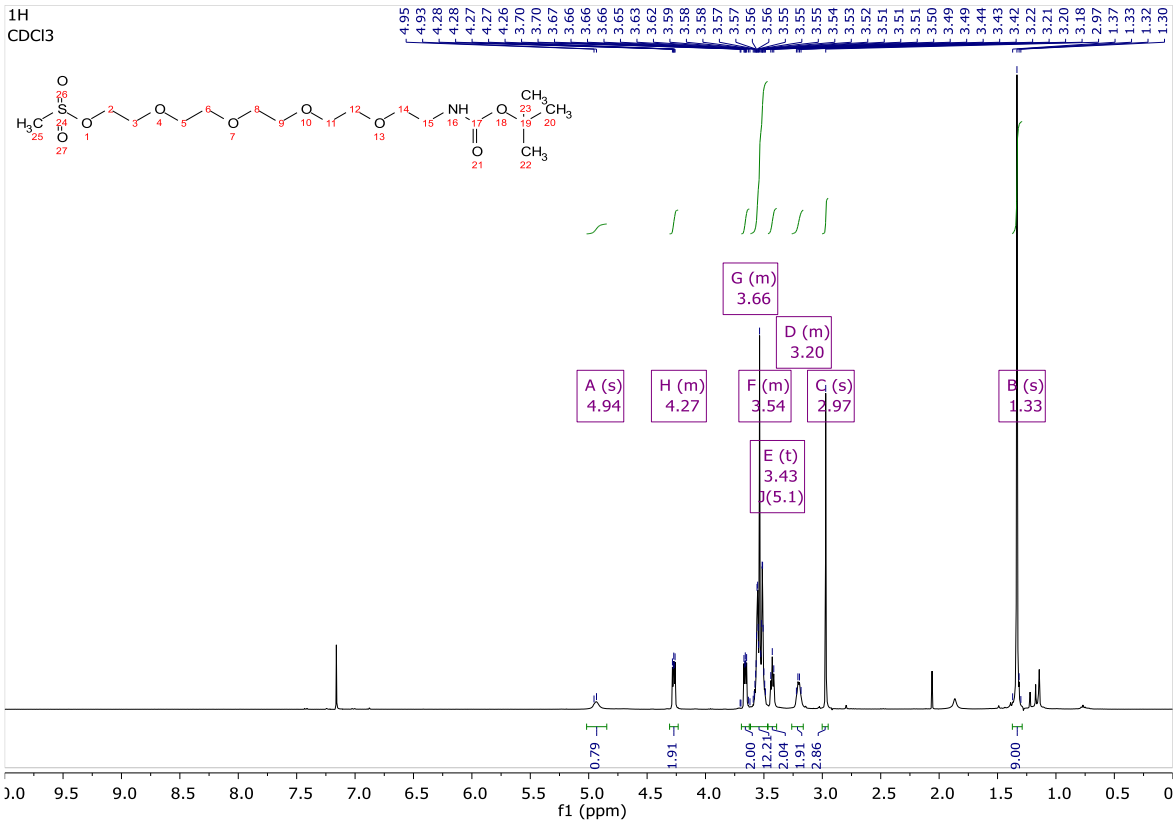

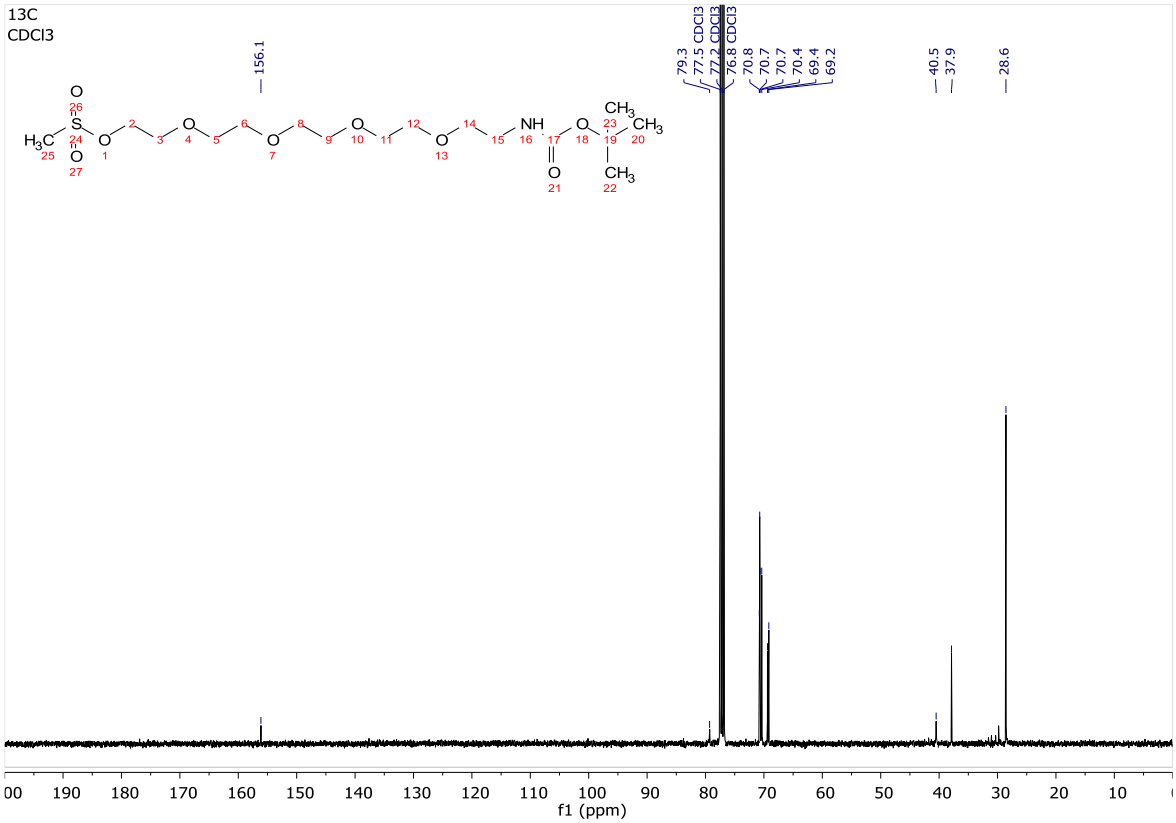

3.21:

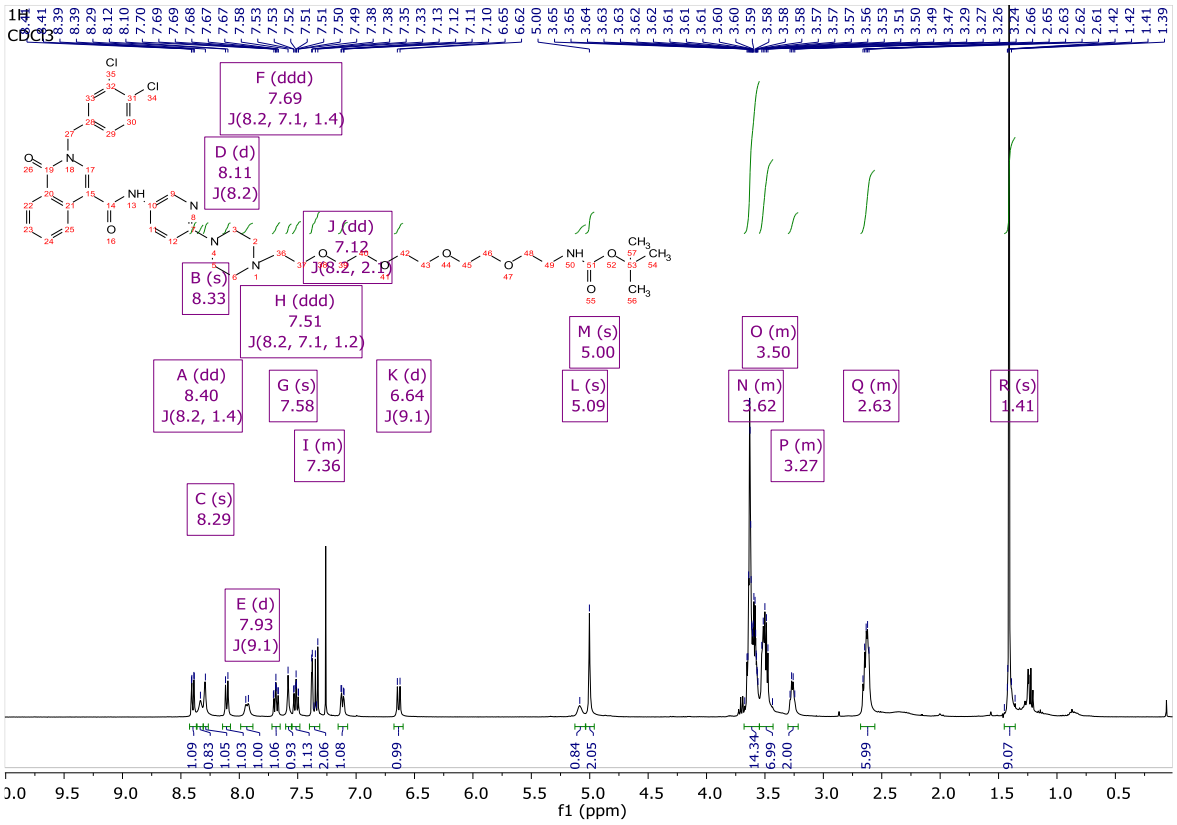
1H
CDCl3
F (ddd)
7.69
J(8.2, 7.1, 1.4)
D (d)
8.11
J(8.2)
J (dd)
7.12
J(8.2, 2.1)
B (s)
8.33
H (ddd)
7.51
J(8.2, 7.1, 1.2)
M (s)
5.00
O (m)
3.50
A (dd)
8.40
J(8.2, 1.4)
G (s)
7.58
K (d)
6.64
J(9.1)
L (s)
5.09
N (m)
3.62
Q (m)
2.63
R (s)
1.41
I (m)
7.36
P (m)
3.27
C (s)
8.29
E (d)
7.93
J(9.1)
f1 (ppm)

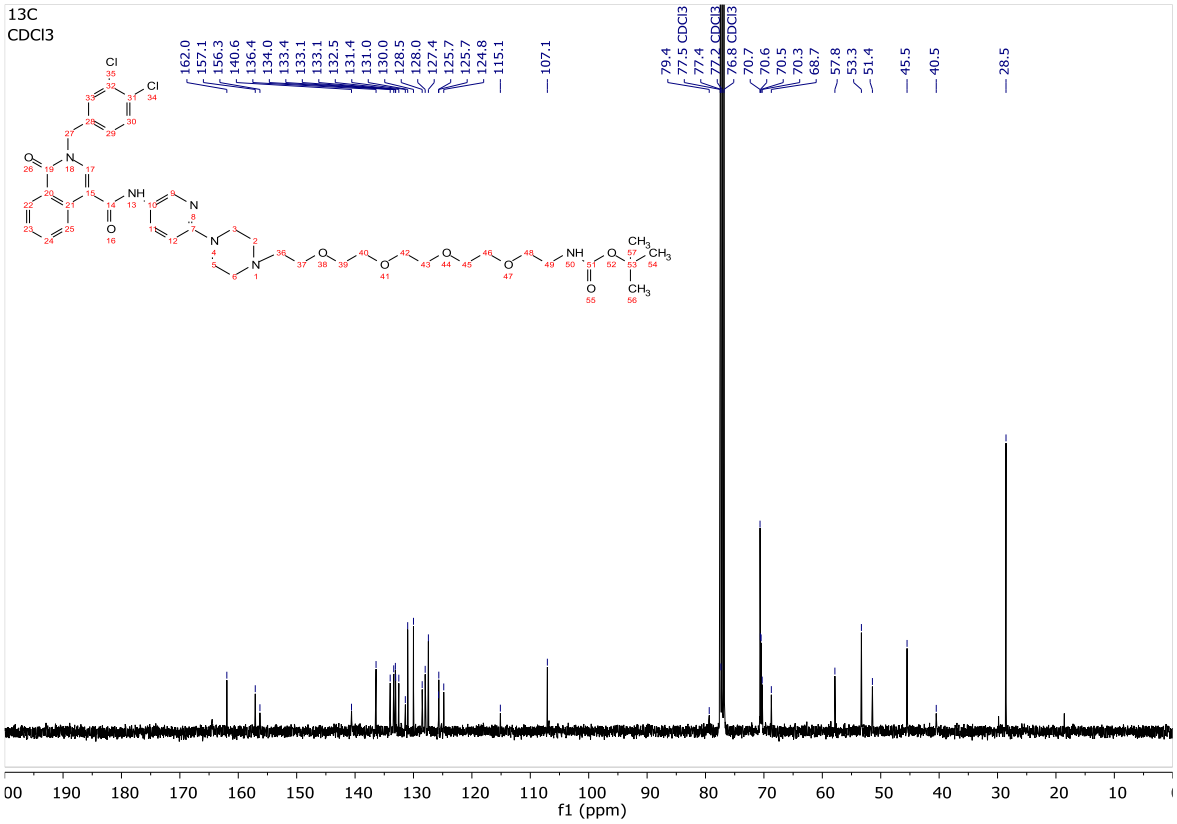
13C
CDCl3
f1 (ppm)

FSCN-A-CRBN-3 (3.22):

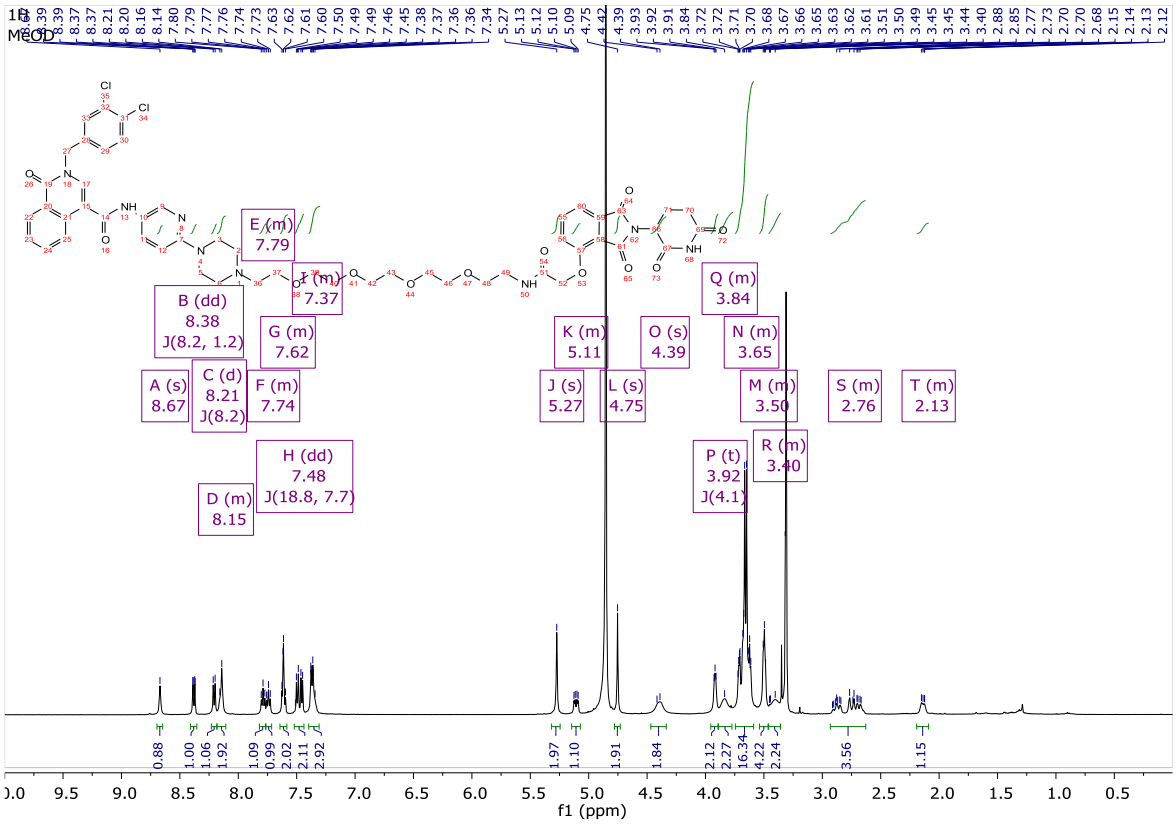

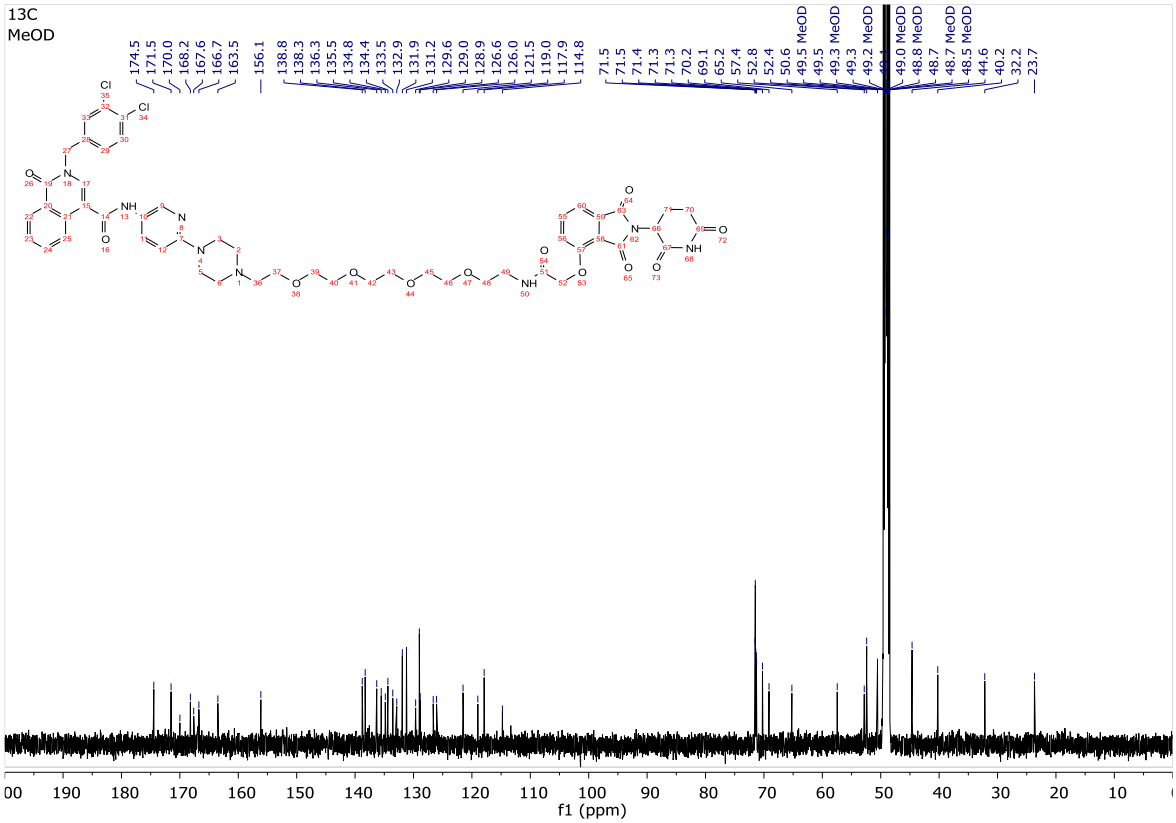

- *Fascin ligand A alkylation HyT PROTAC:*

3.23:

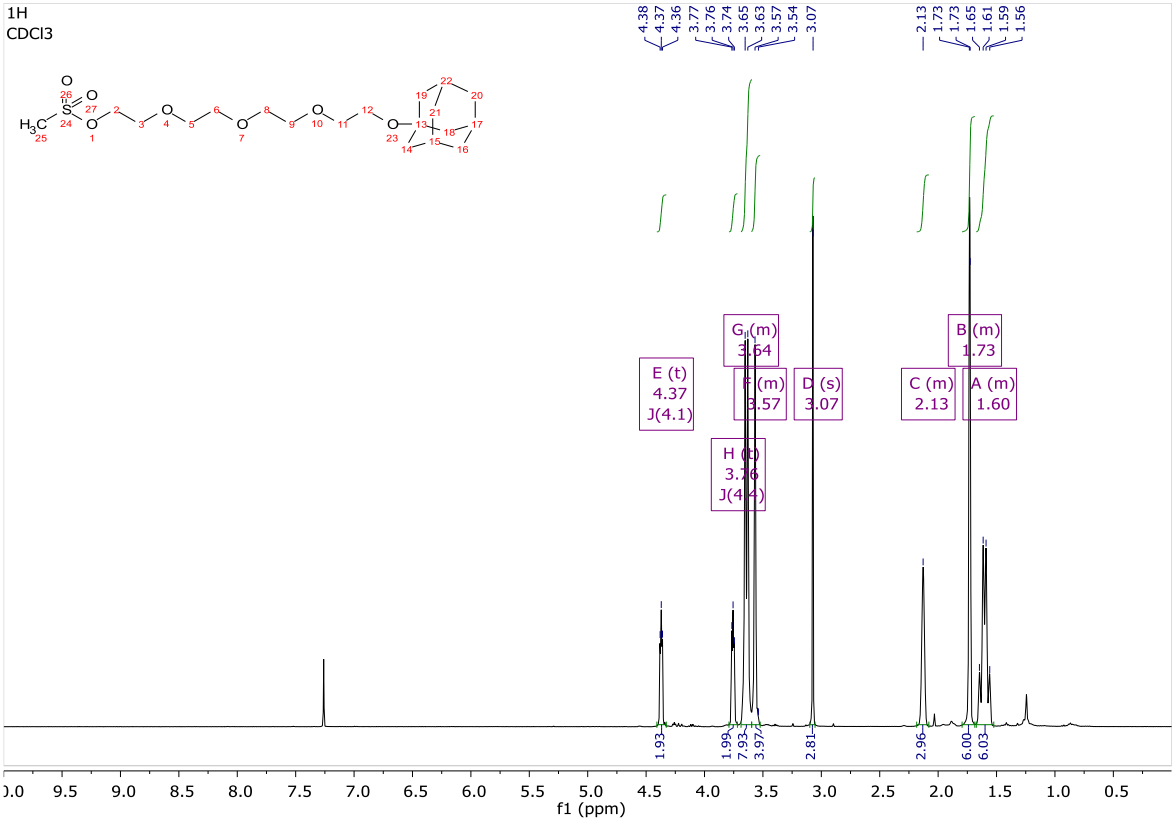

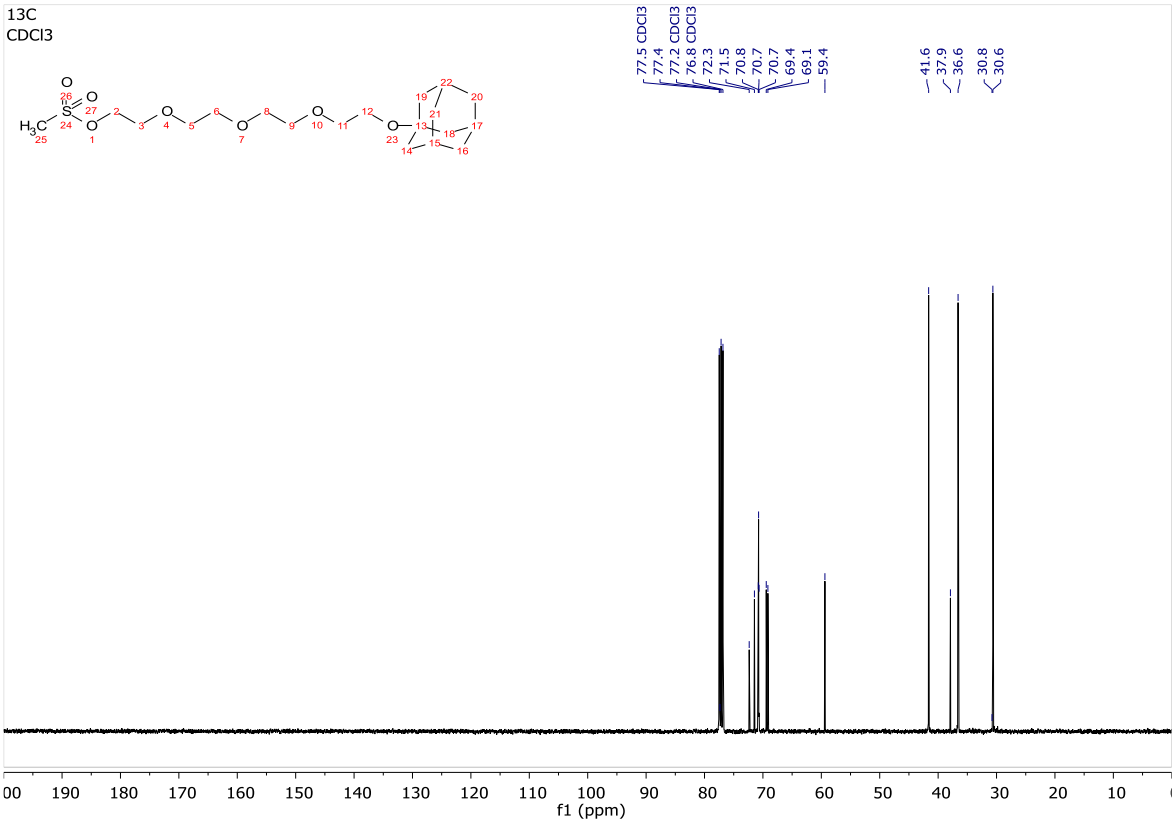

FSCN-A-HyT-1 (3.24):

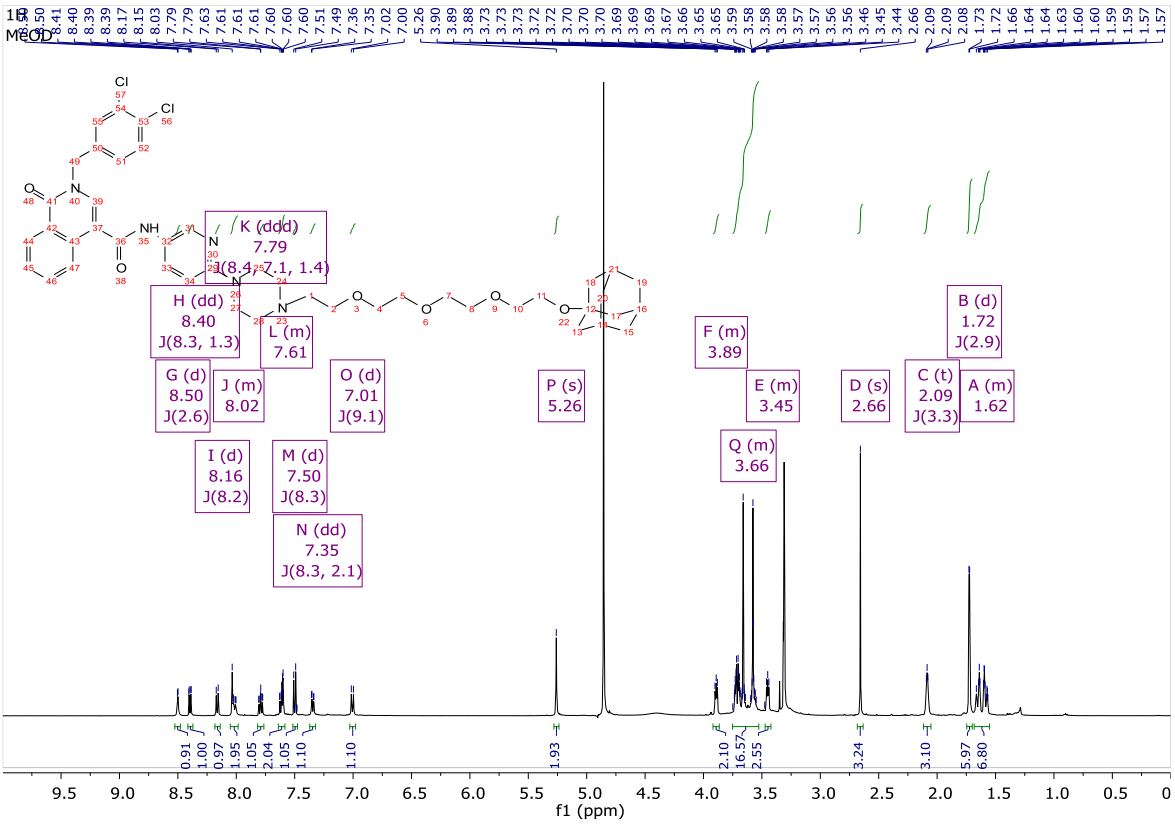

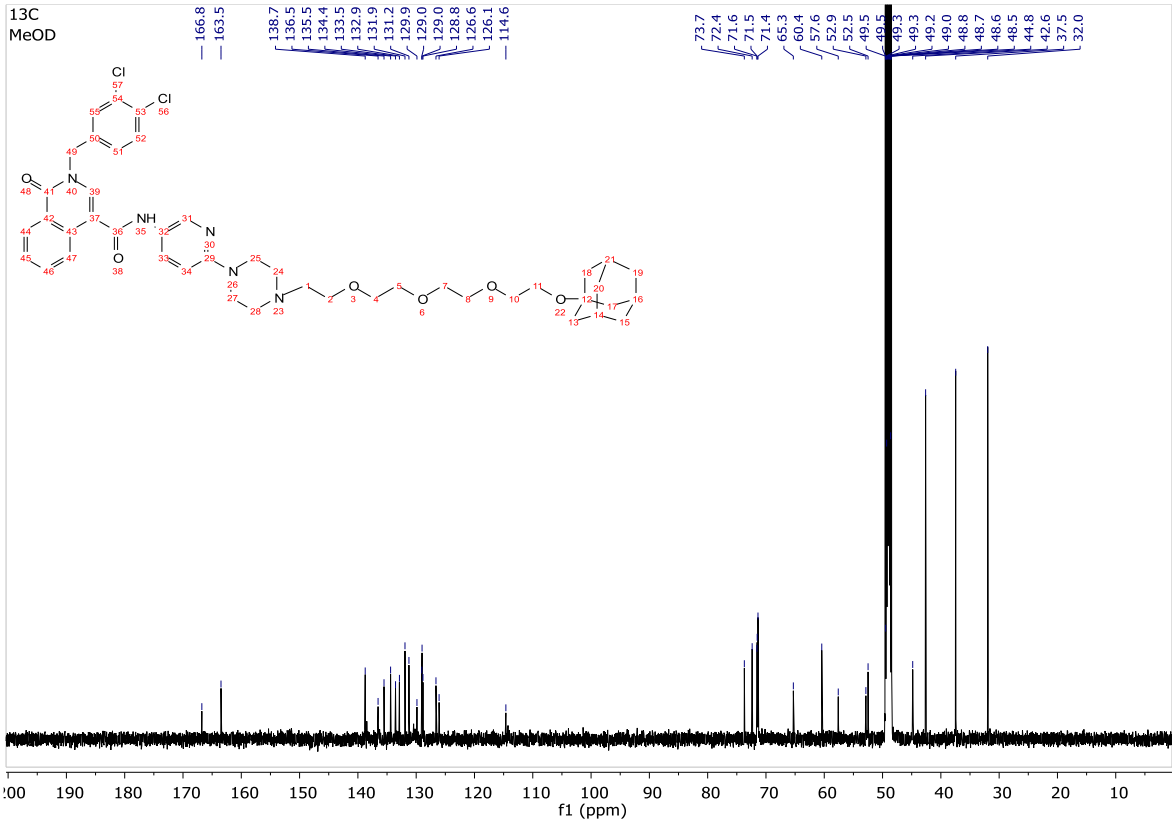

Fascin ligand B FSCN-B (1.5)

3.25:

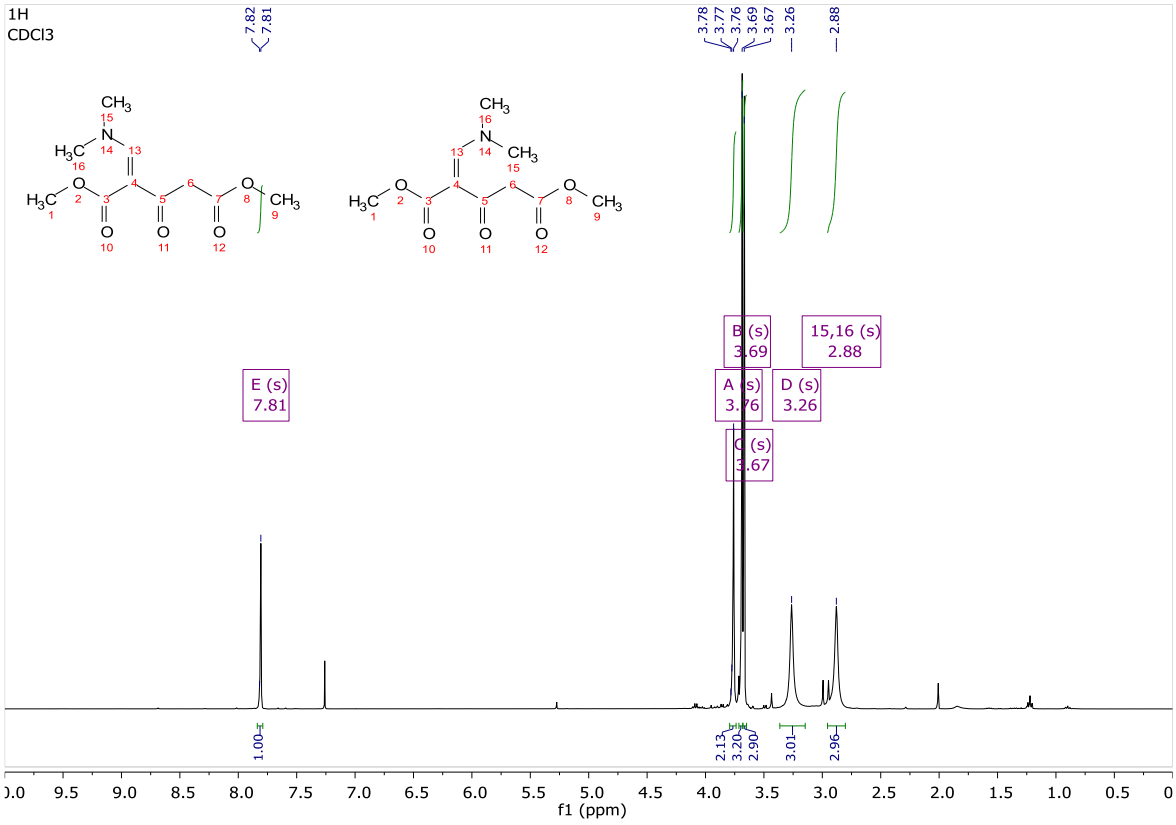

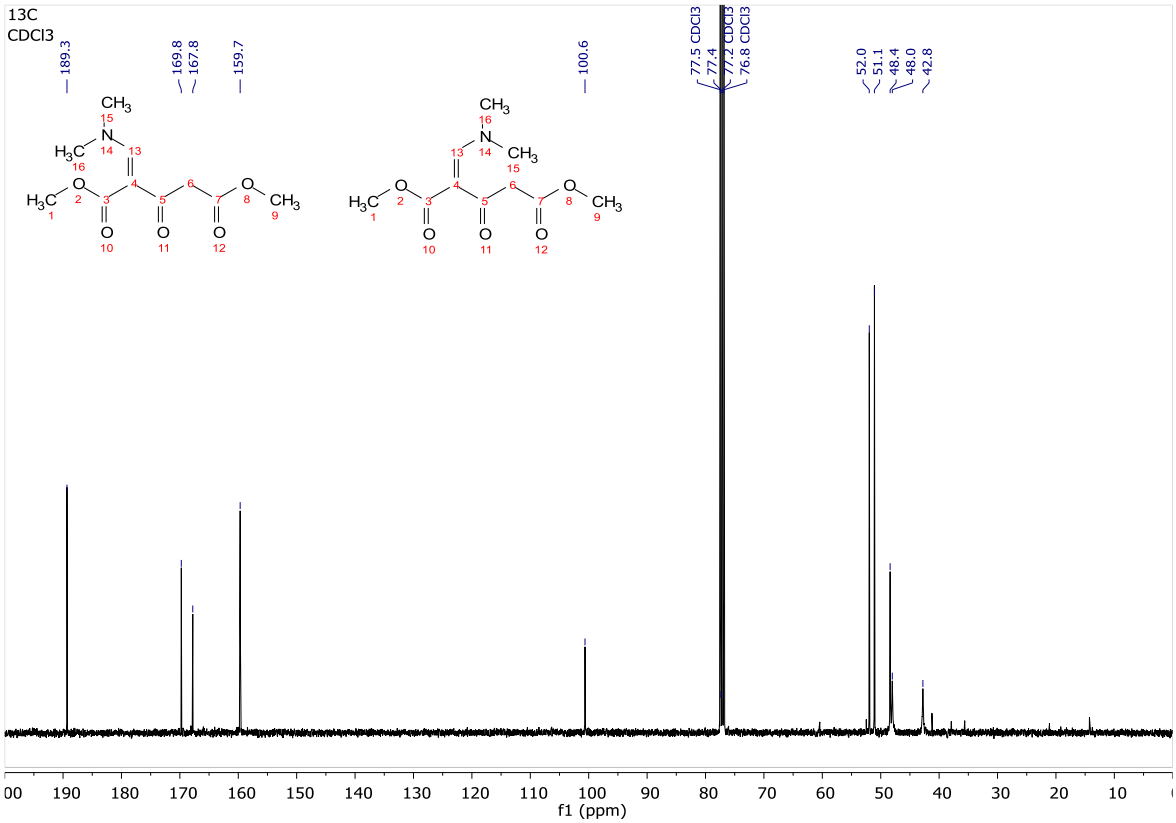

3.26a:

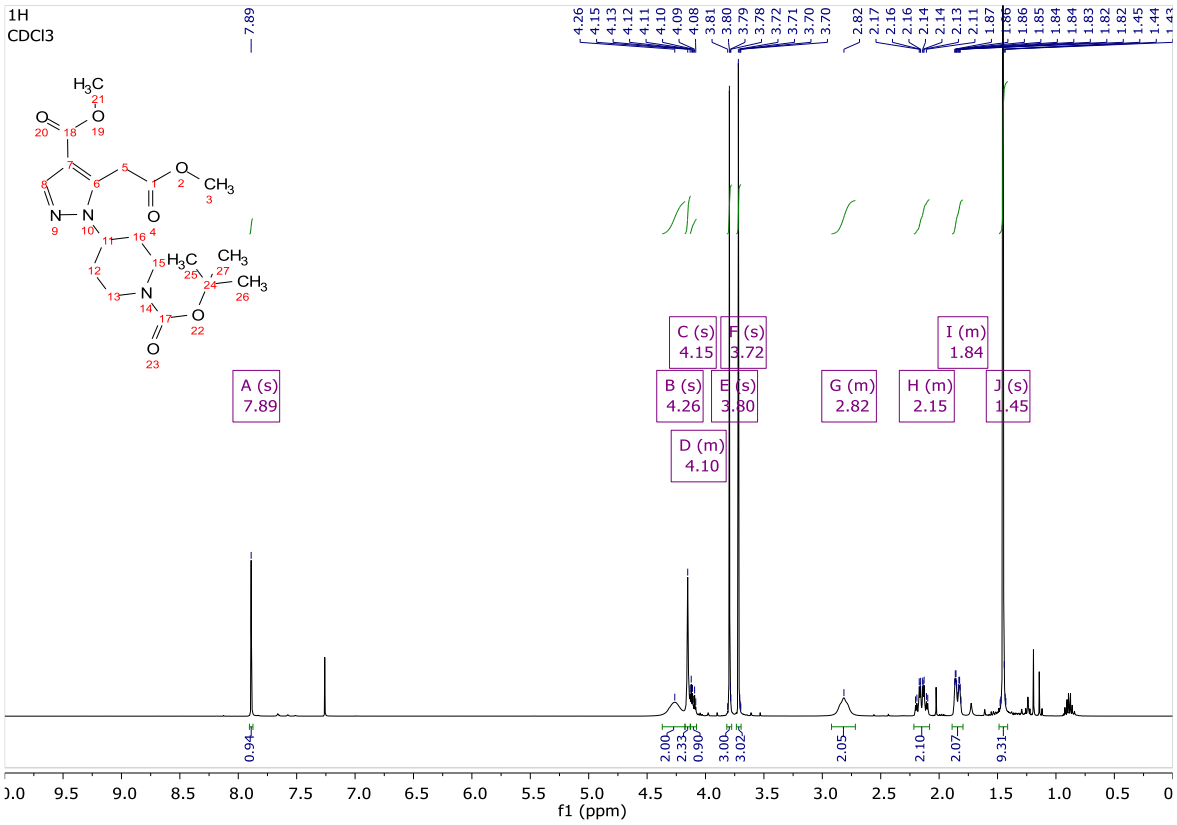
1H
CDCl3
A (s)
7.89
B (s)
4.26
C (s)
4.15
D (m)
4.10
E (s)
3.80
F (s)
3.72
G (m)
2.82
H (m)
2.15
I (m)
1.84
J (s)
1.45
f1 (ppm)

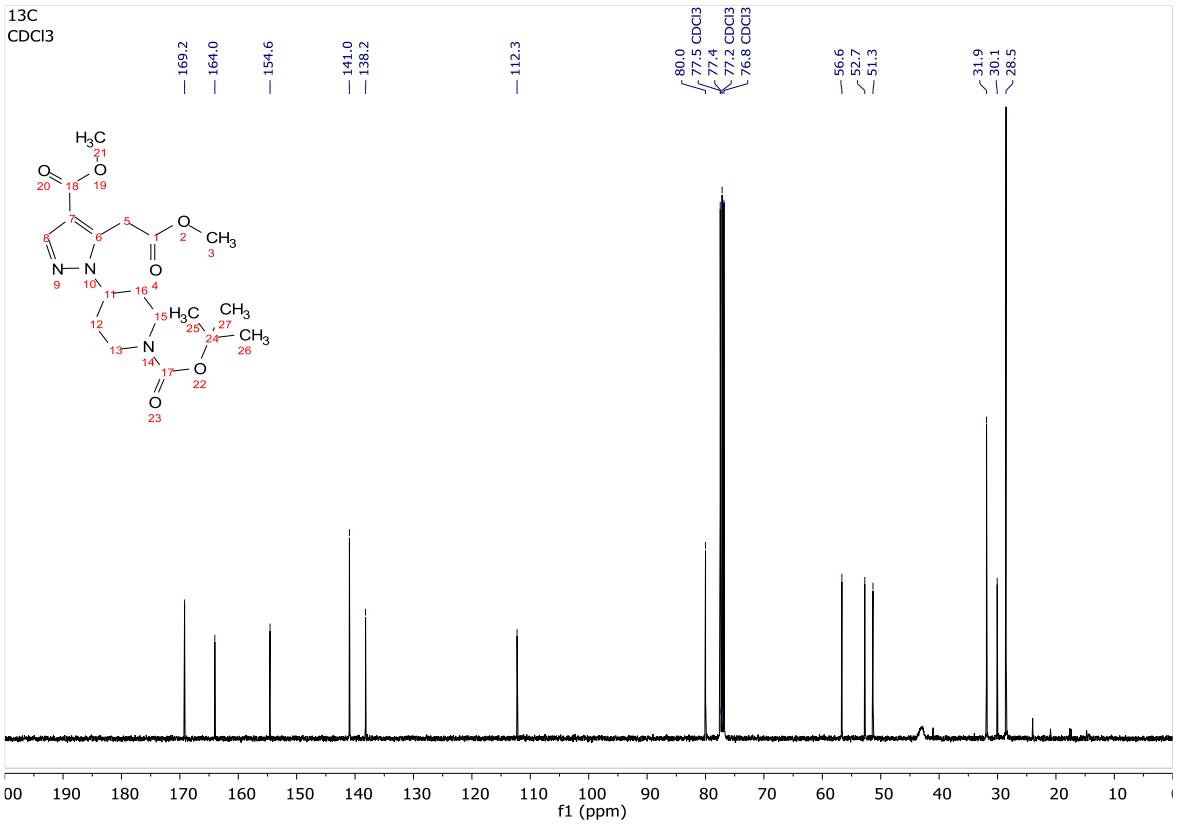
13C
CDCl3
169.2
164.0
154.6
141.0
138.2
112.3
80.0
77.5 CDCl3
77.4
77.2 CDCl3
76.8 CDCl3
56.6
52.7
51.3
31.9
30.1
28.5
f1 (ppm)

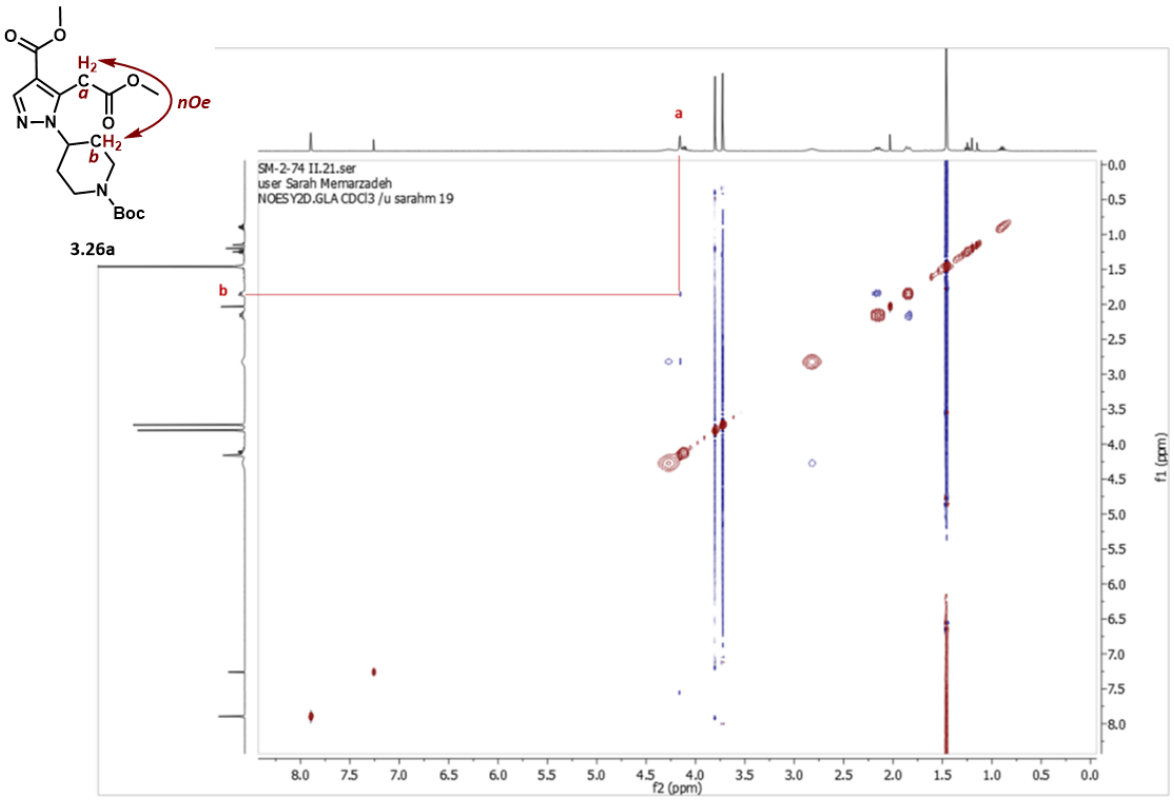
nOe
Boc
3.26a
SM-2-74 II.21.ser
user Sarah Memarzadeh
NOESY2D.GLA CDCl3 /u sarahm 19
a
b
f2 (ppm)
f1 (ppm)

3.28:

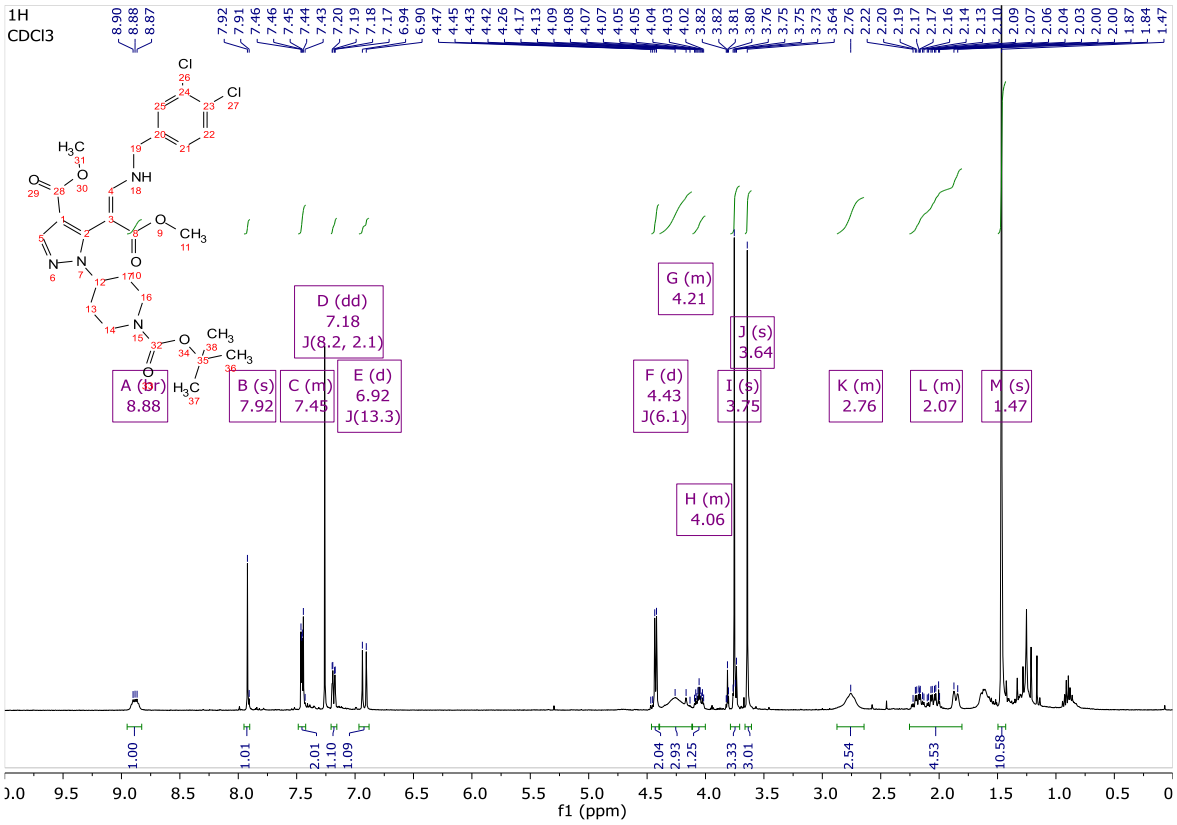
1H
CDCl3
A (br)
8.88
B (s)
7.92
C (m)
7.45
D (dd)
7.18
J(8.2, 2.1)
E (d)
6.92
J(13.3)
F (d)
4.43
J(6.1)
G (m)
4.21
H (m)
4.06
I (s)
3.75
J (s)
3.64
K (m)
2.76
L (m)
2.07
M (s)
1.47
f1 (ppm)

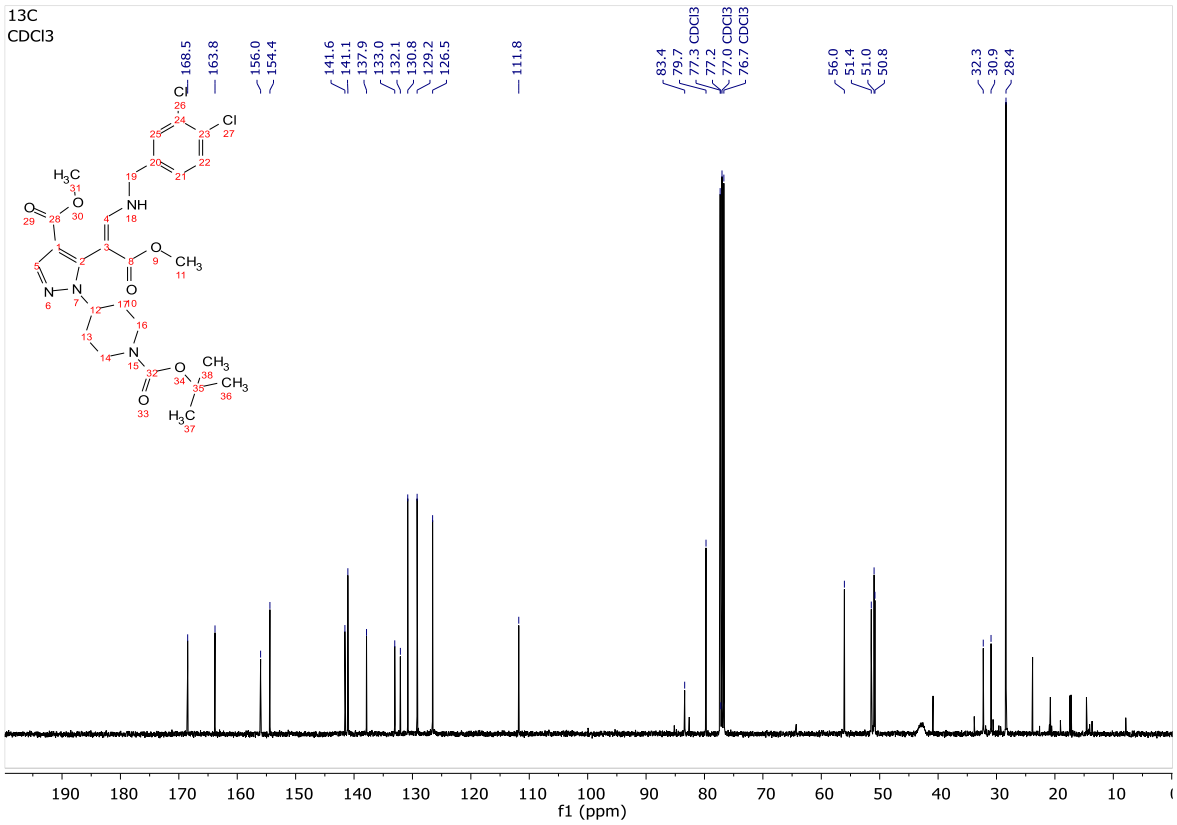
13C
CDCl3
f1 (ppm)

3.29:

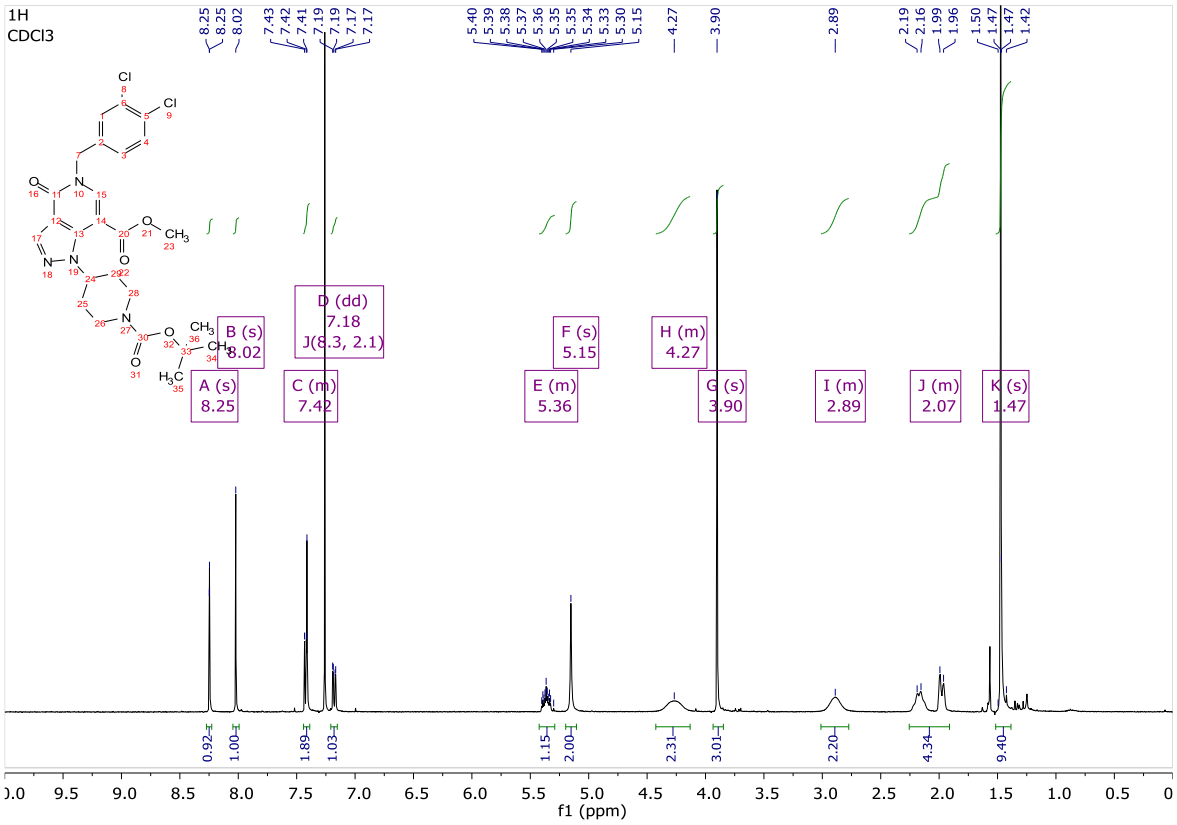
1H
CDCl3
A (s) 8.25
B (s) 8.02
C (m) 7.42
D (dd) 7.18 J(8.3, 2.1)
E (m) 5.36
F (s) 5.15
G (s) 3.90
H (m) 4.27
I (m) 2.89
J (m) 2.07
K (s) 1.47
f1 (ppm)

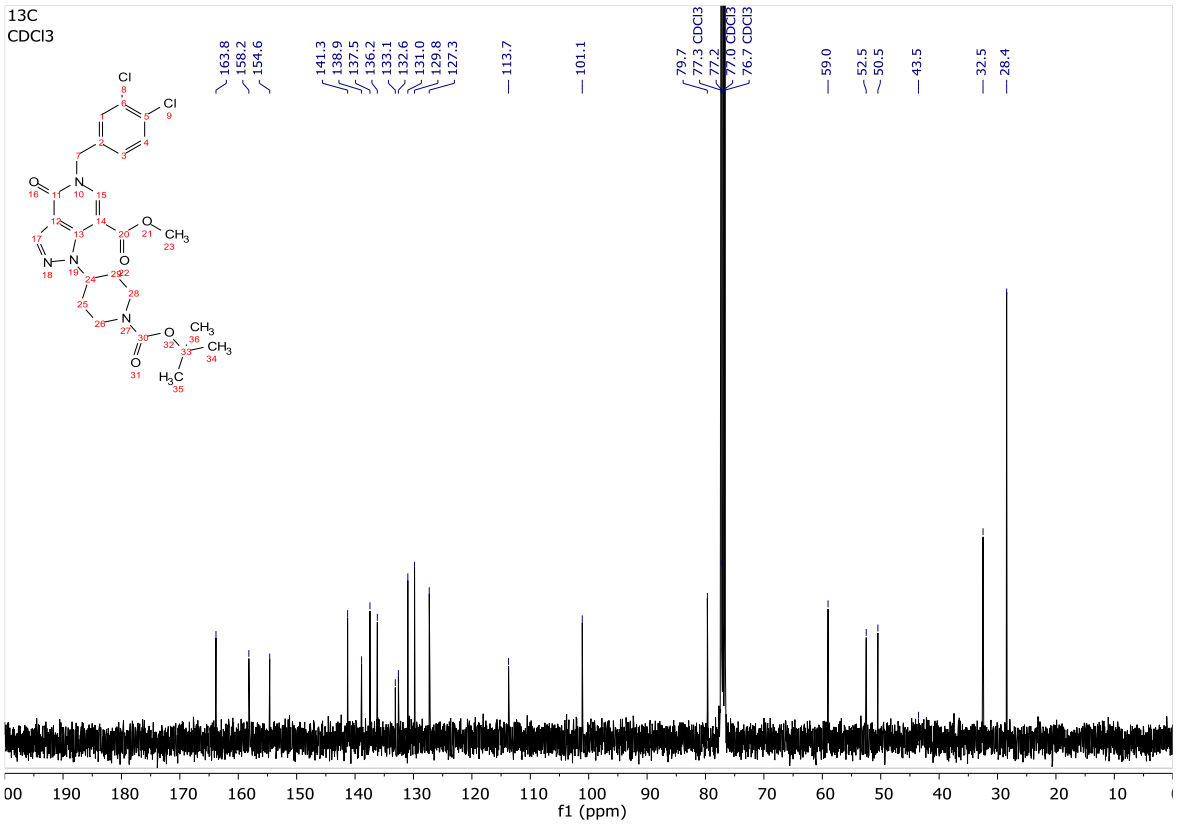
13C
CDCl3
f1 (ppm)

3.31:

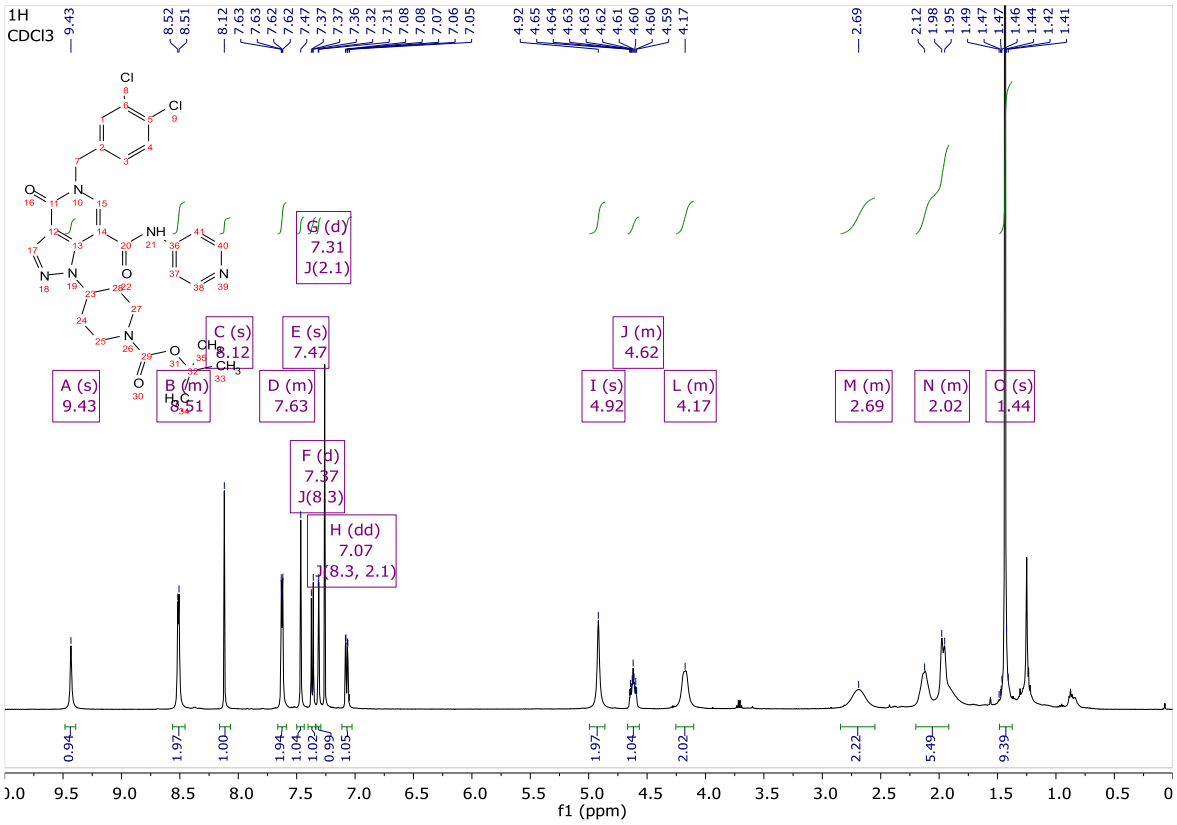
1H
CDCl3
A (s)
9.43
B (m)
8.51
C (s)
8.12
D (m)
7.63
E (s)
7.47
F (d)
7.37
J(8.3)
G (d)
7.31
J(2.1)
H (dd)
7.07
J(8.3, 2.1)
I (s)
4.92
J (m)
4.62
L (m)
4.17
M (m)
2.69
N (m)
2.02
O (s)
1.44
f1 (ppm)

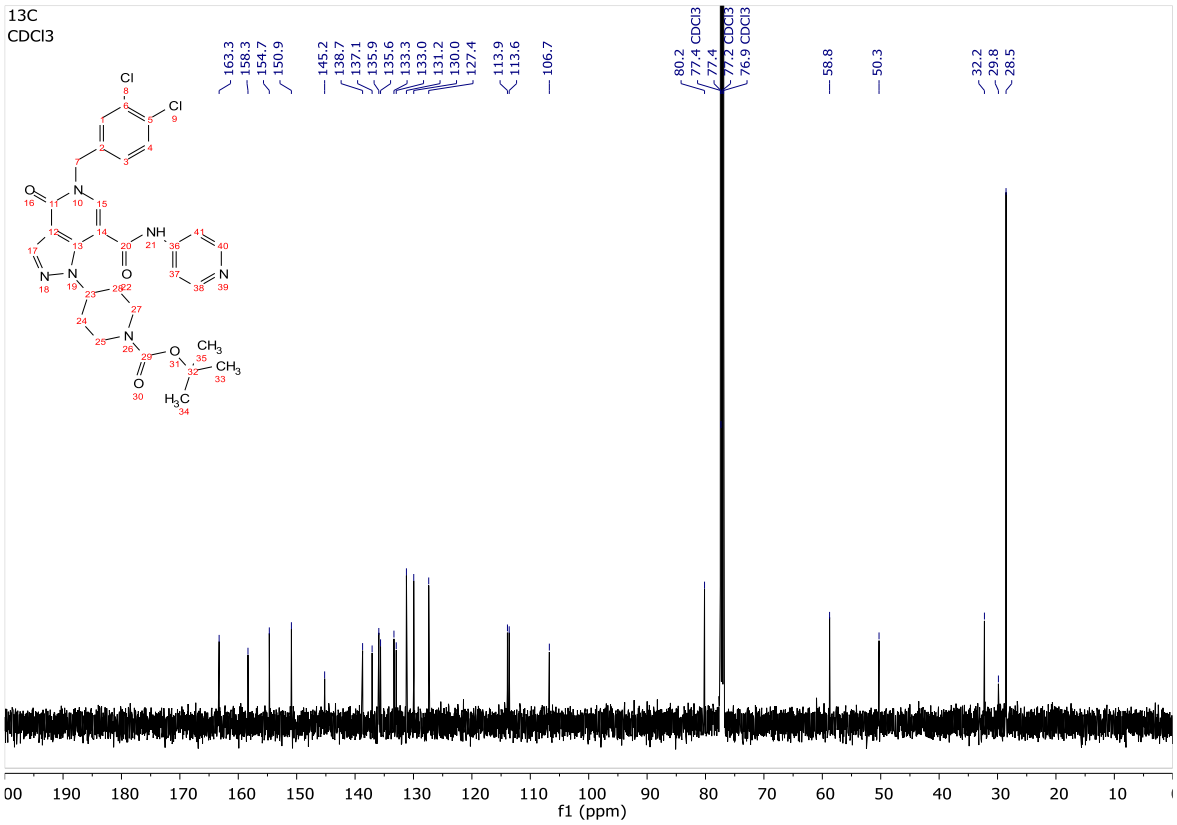
13C
CDCl3
77.4 CDCl3
77.2 CDCl3
76.9 CDCl3
f1 (ppm)

FSCN-B (1.5):

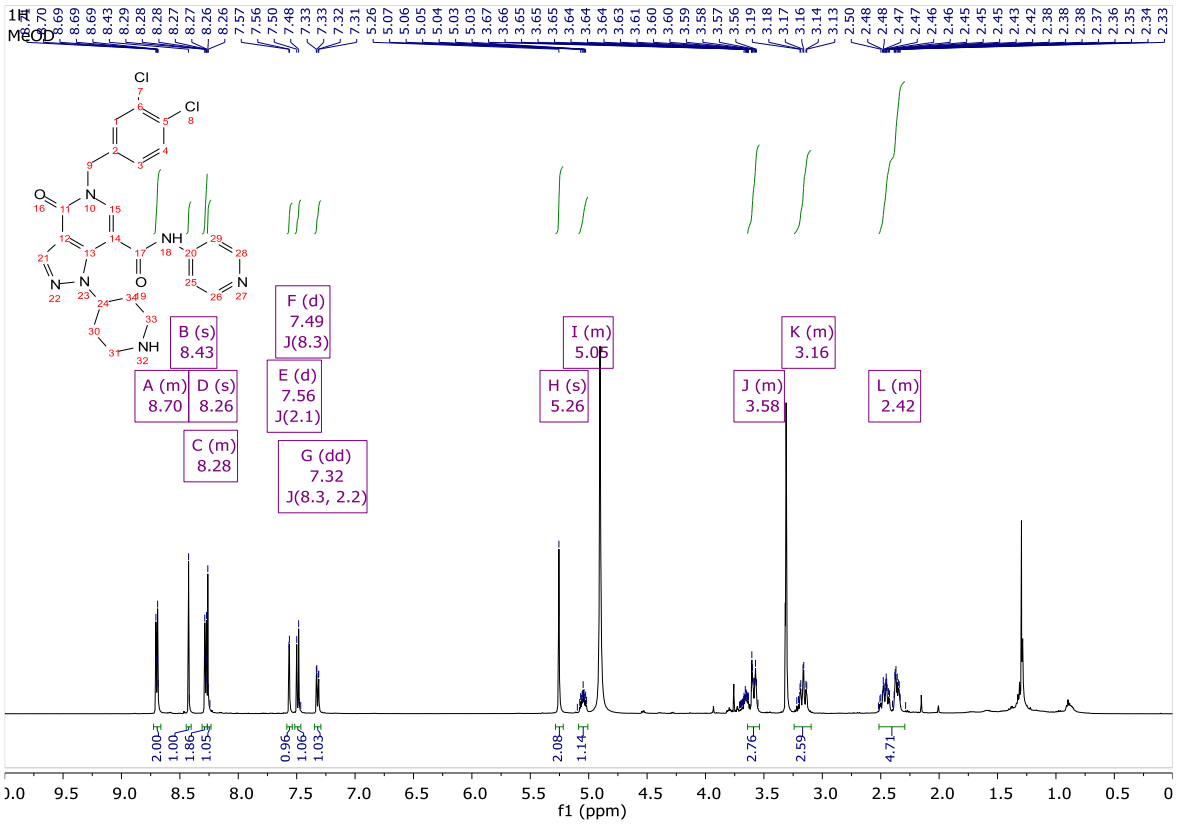
1H
MeOD
B (s) 8.43
A (m) 8.70
D (s) 8.26
C (m) 8.28
F (d) 7.49 J(8.3)
E (d) 7.56 J(2.1)
G (dd) 7.32 J(8.3, 2.2)
I (m) 5.05
H (s) 5.26
K (m) 3.16
J (m) 3.58
L (m) 2.42
f1 (ppm)

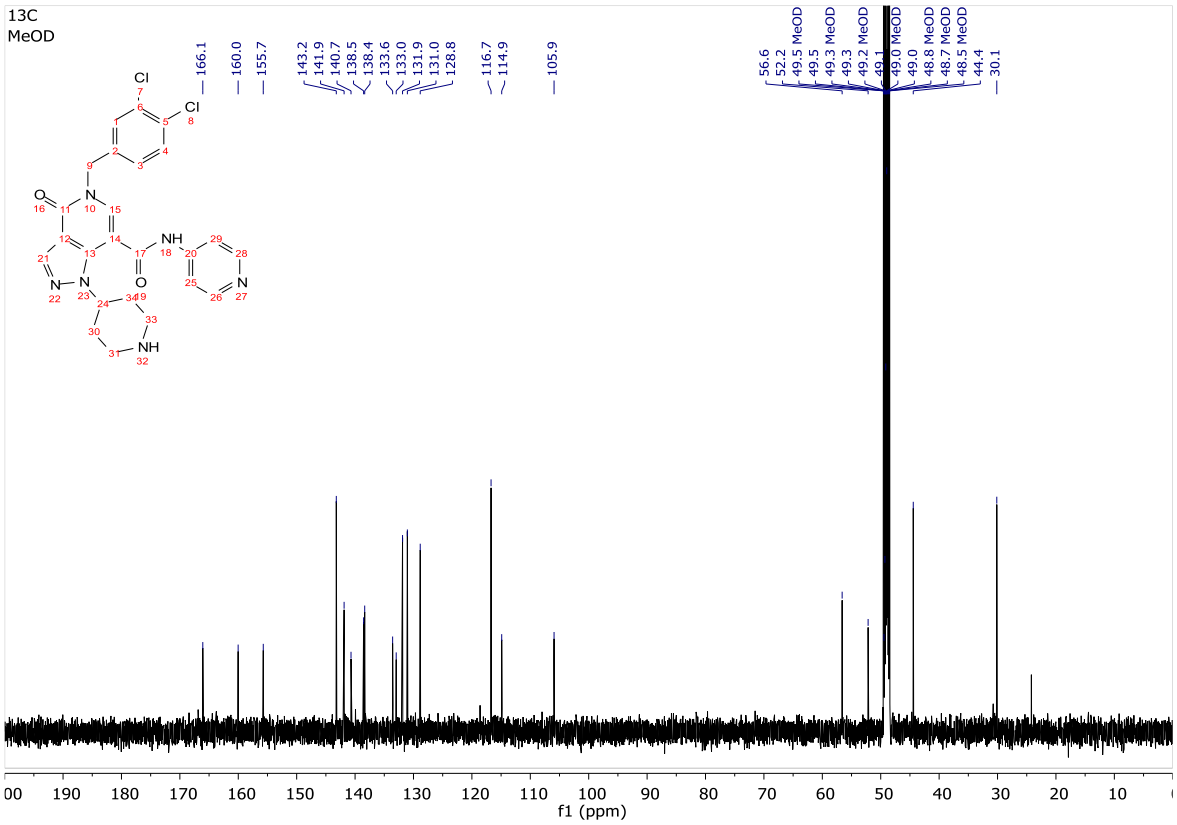
13C
MeOD
f1 (ppm)

2nd series PROTACs

- *Fascin ligand B VHL PROTACs:*

3.32:

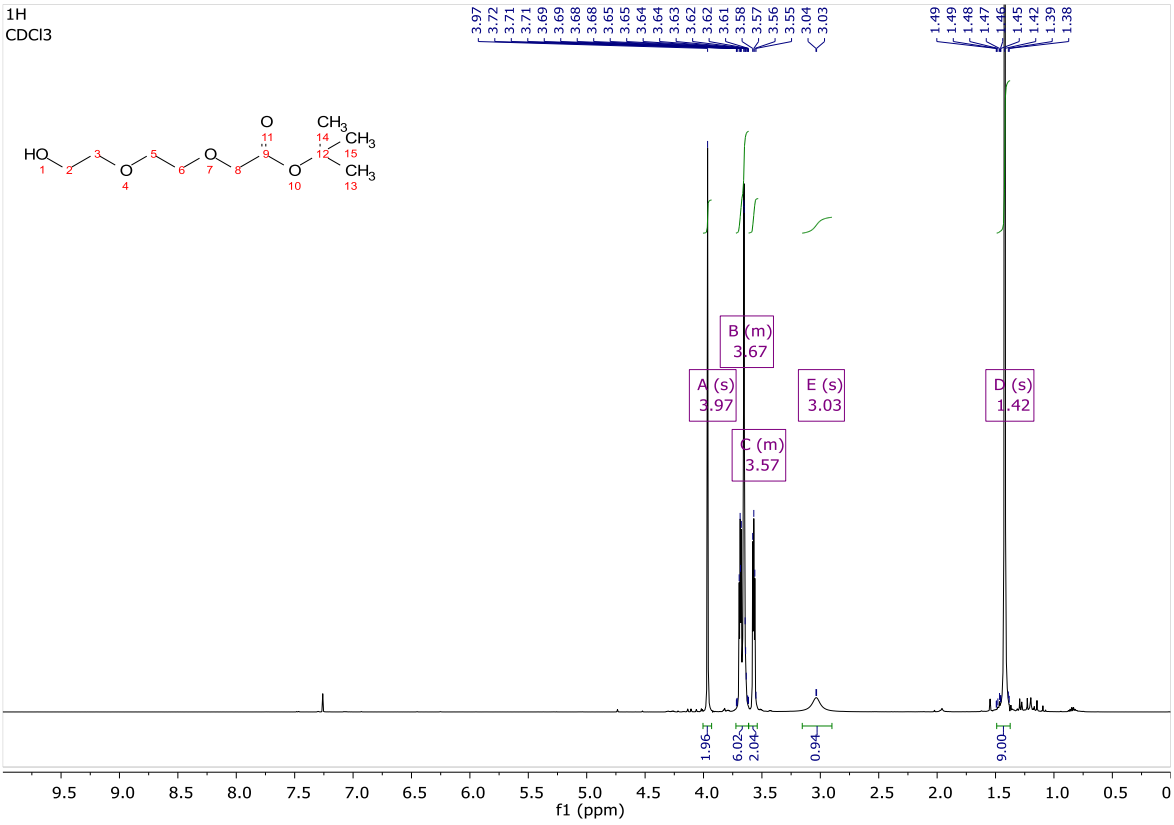

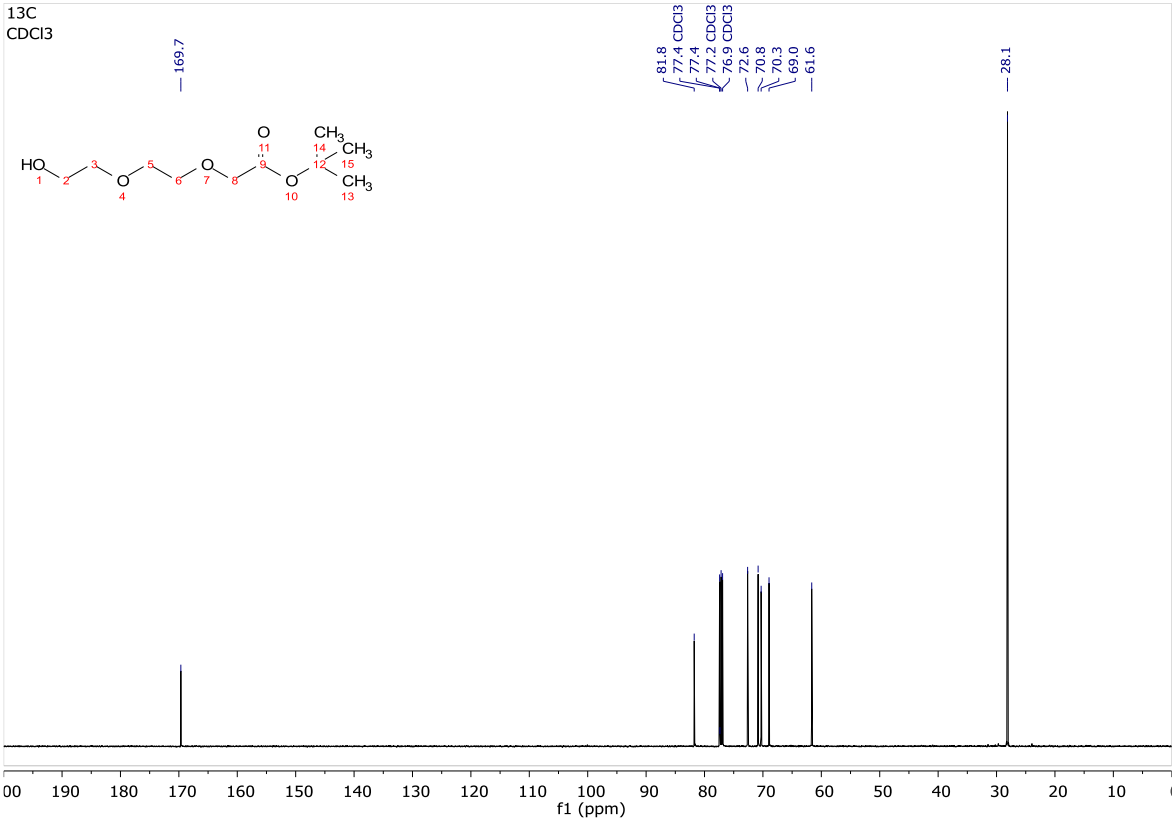

3.33:

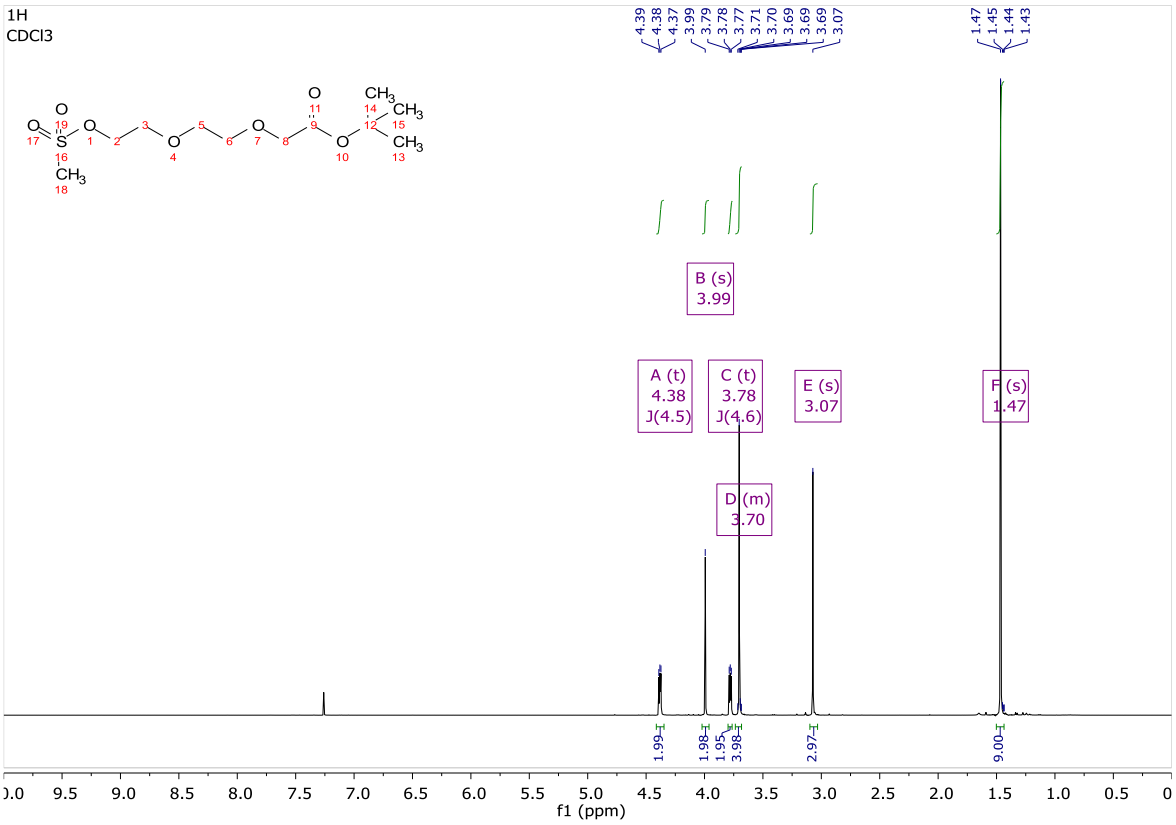
1H
CDCl3
4.39
4.38
4.37
3.99
3.79
3.78
3.77
3.71
3.70
3.69
3.69
3.69
3.07
1.47
1.45
1.44
1.43
B (s)
3.99
A (t)
4.38
J(4.5)
C (t)
3.78
J(4.6)
E (s)
3.07
F (s)
1.47
D (m)
3.70
1.99
1.98
1.95
3.98
2.97
9.00
f1 (ppm)

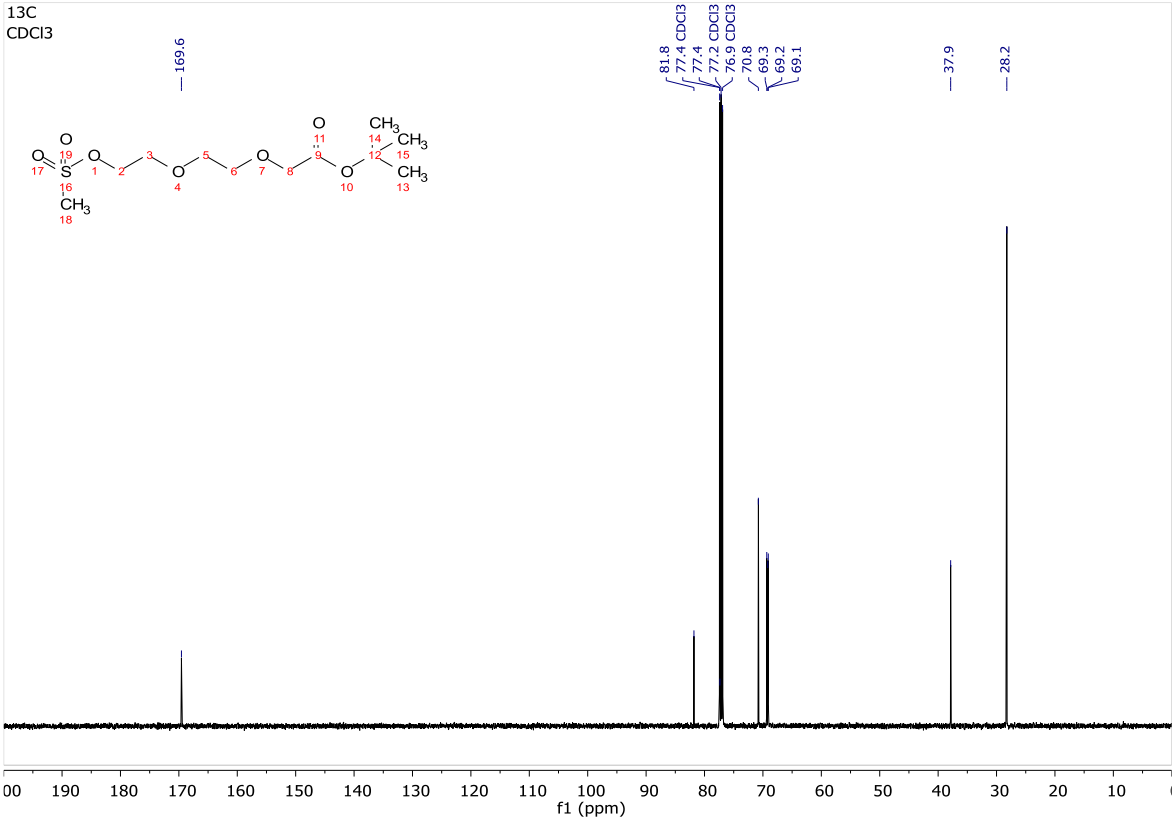
13C
CDCl3
169.6
81.8
77.4 CDCl3
77.4
77.2 CDCl3
76.9 CDCl3
70.8
69.3
69.2
69.1
37.9
28.2
f1 (ppm)

3.34a:

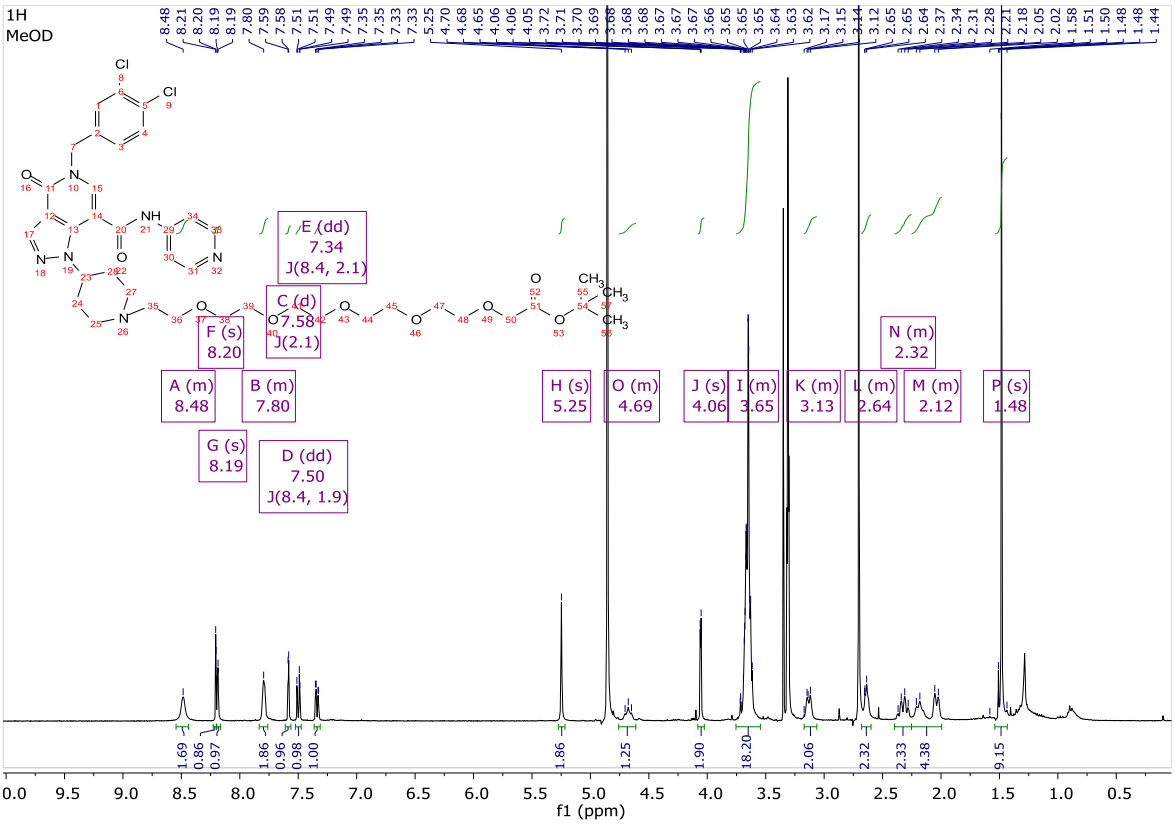
1H
MeOD
A (m) 8.48
B (m) 7.80
C (d) 7.58 J(2.1)
D (dd) 7.50 J(8.4, 1.9)
E (dd) 7.34 J(8.4, 2.1)
F (s) 8.20
G (s) 8.19
H (s) 5.25
I (m) 3.65
J (s) 4.06
K (m) 3.13
L (m) 2.64
M (m) 2.12
N (m) 2.32
O (m) 4.69
P (s) 1.48
f1 (ppm)

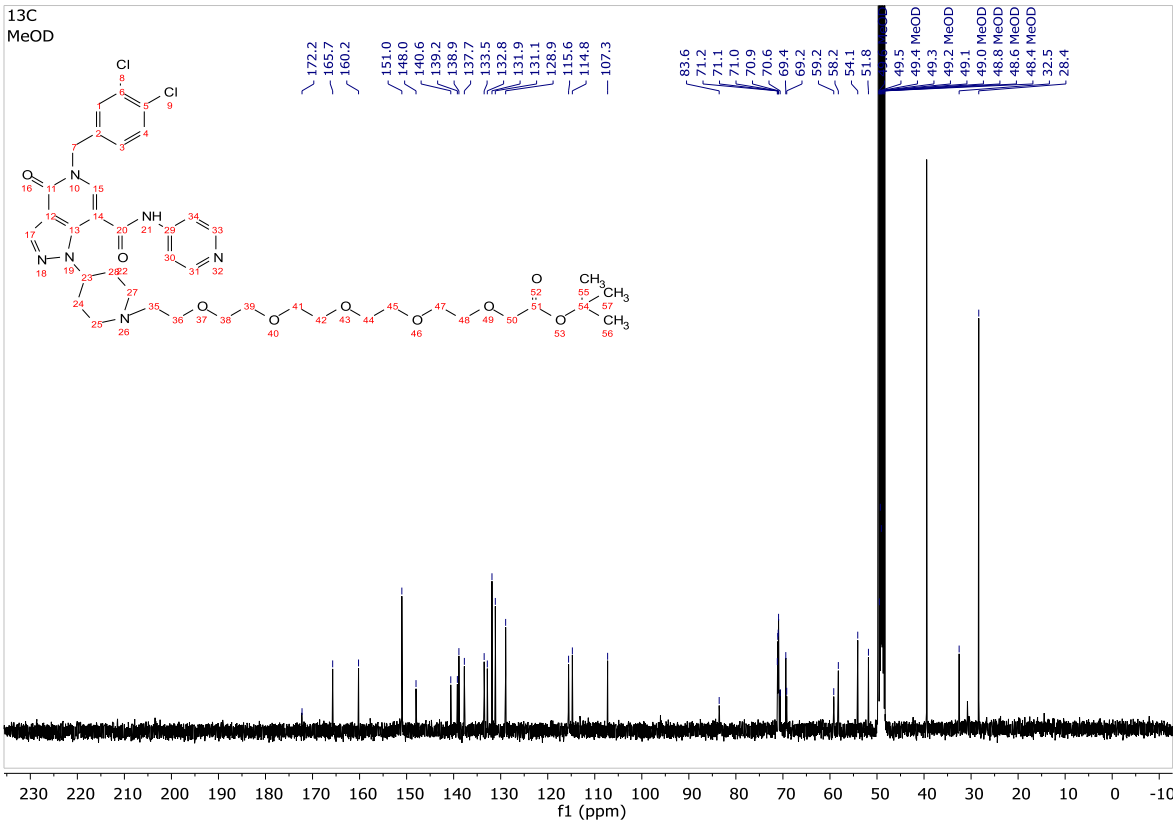
13C
MeOD
f1 (ppm)

3.34b:

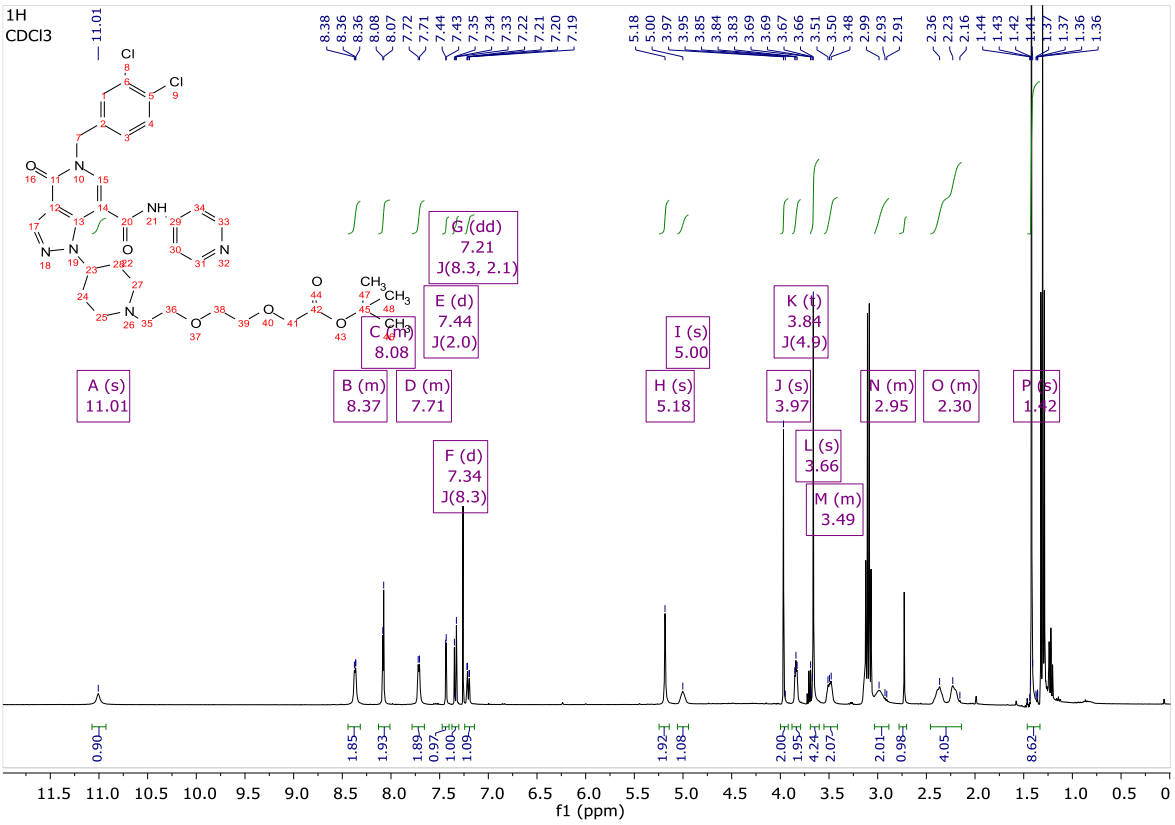
1H
CDCl3
A (s) 11.01
B (m) 8.37
C (m) 8.08
D (m) 7.71
E (d) 7.44 J(2.0)
F (d) 7.34 J(8.3)
G (dd) 7.21 J(8.3, 2.1)
H (s) 5.18
I (s) 5.00
J (s) 3.97
K (t) 3.84 J(4.9)
L (s) 3.66
M (m) 3.49
N (m) 2.95
O (m) 2.30
P (s) 1.42
f1 (ppm)

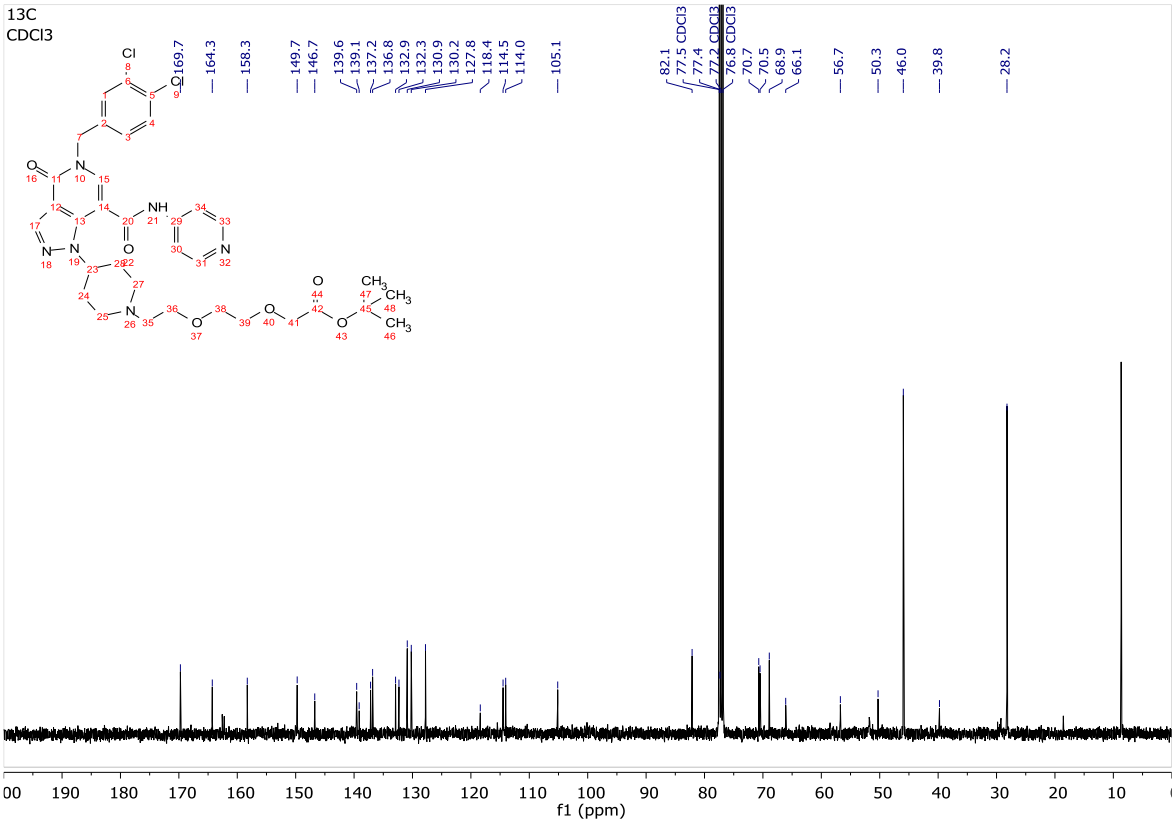
13C
CDCl3
f1 (ppm)

FSCN-B-VHL-1 (3.35):

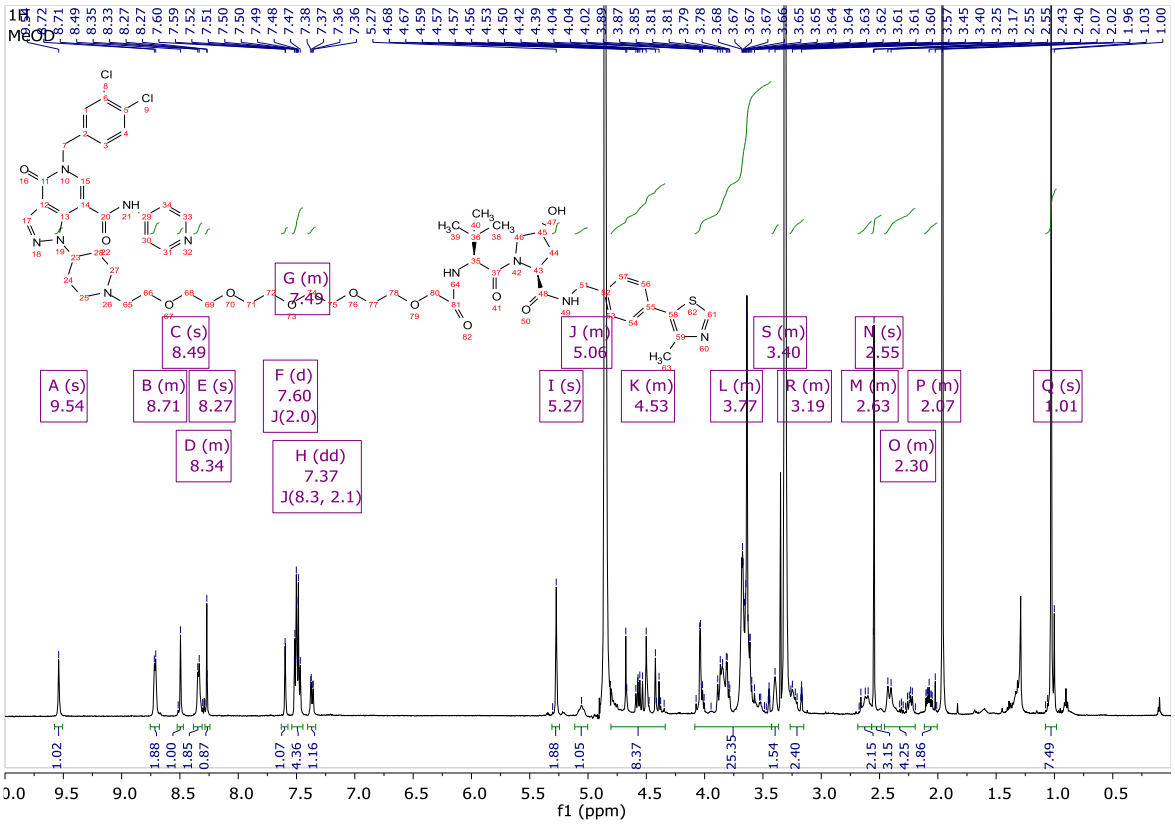

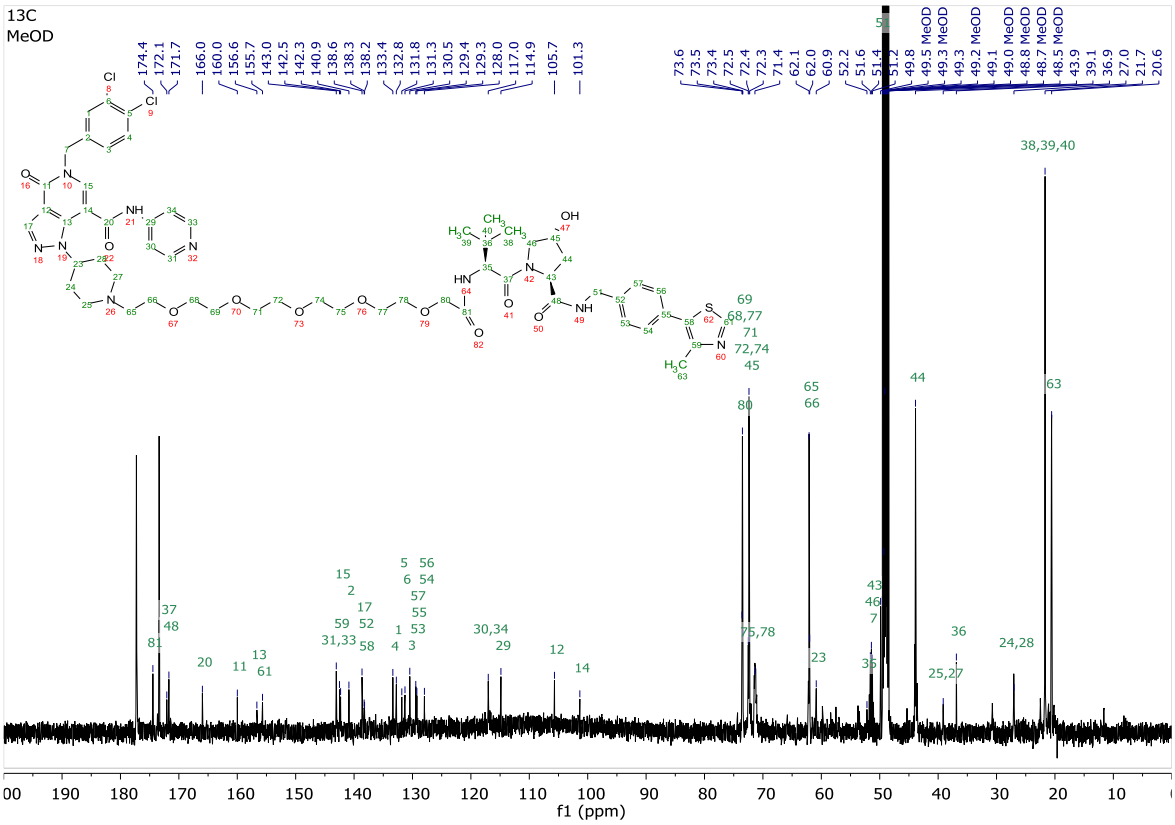

FSCN-B-VHL-2 (3.36):

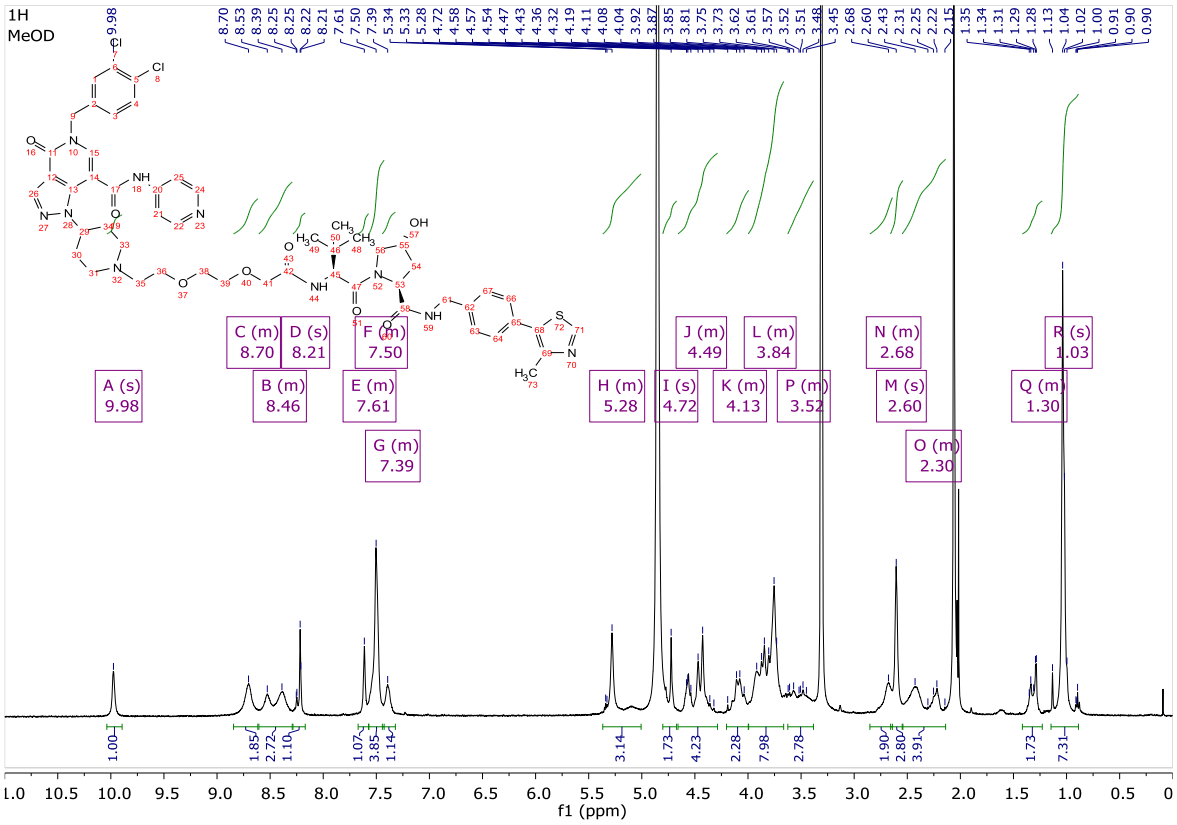

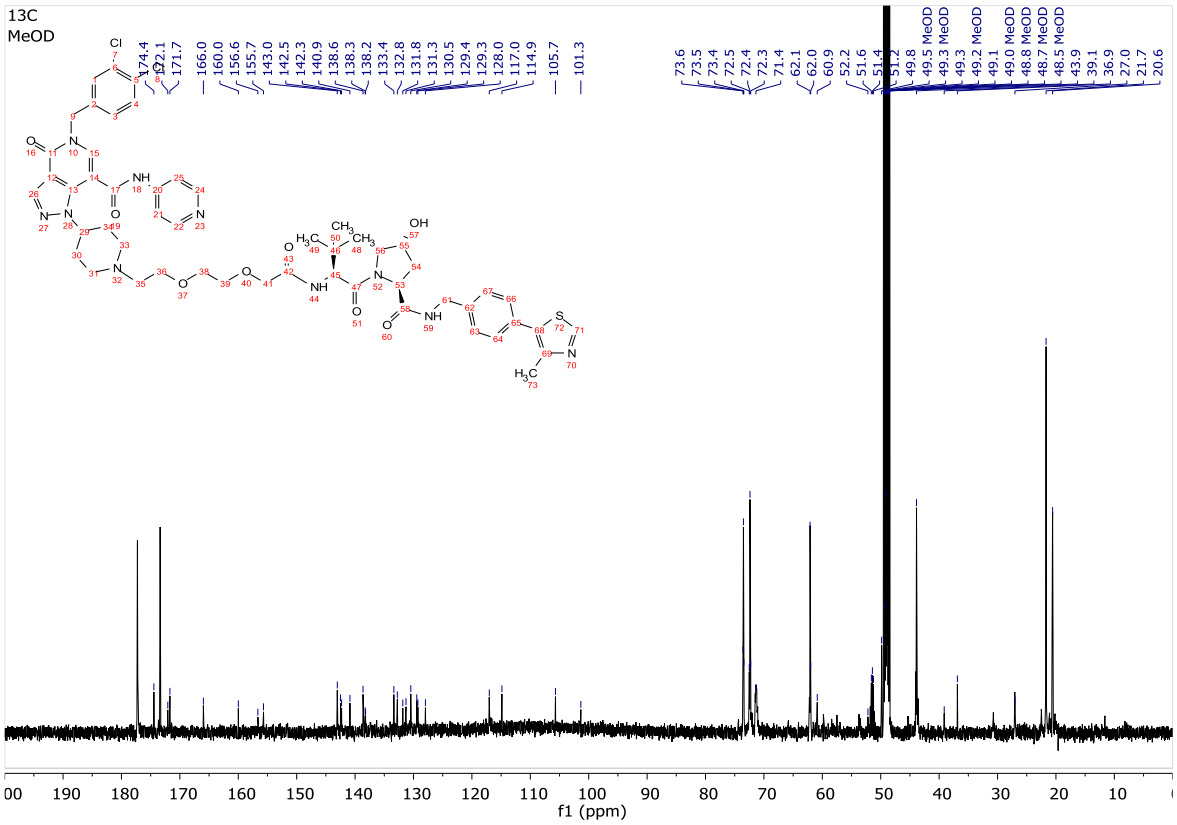

- *Fascin ligand B CRBN PROTACs:*

3.37:

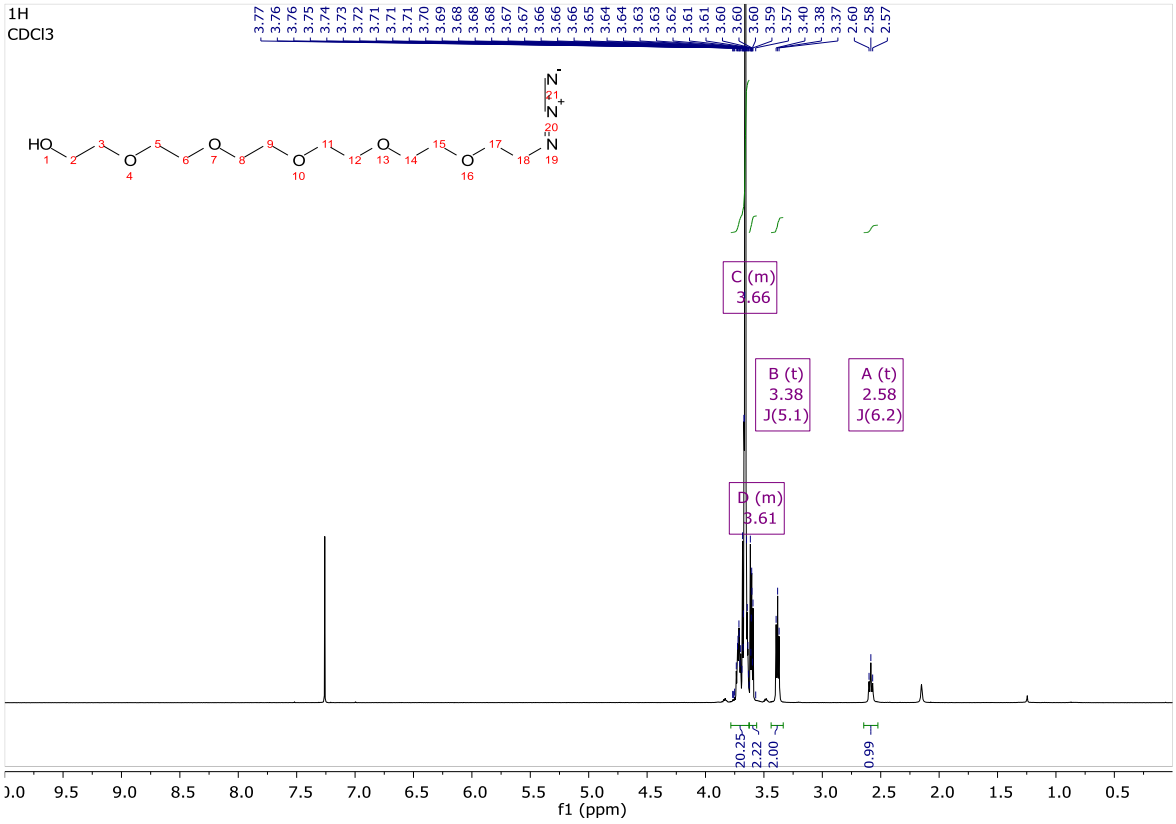

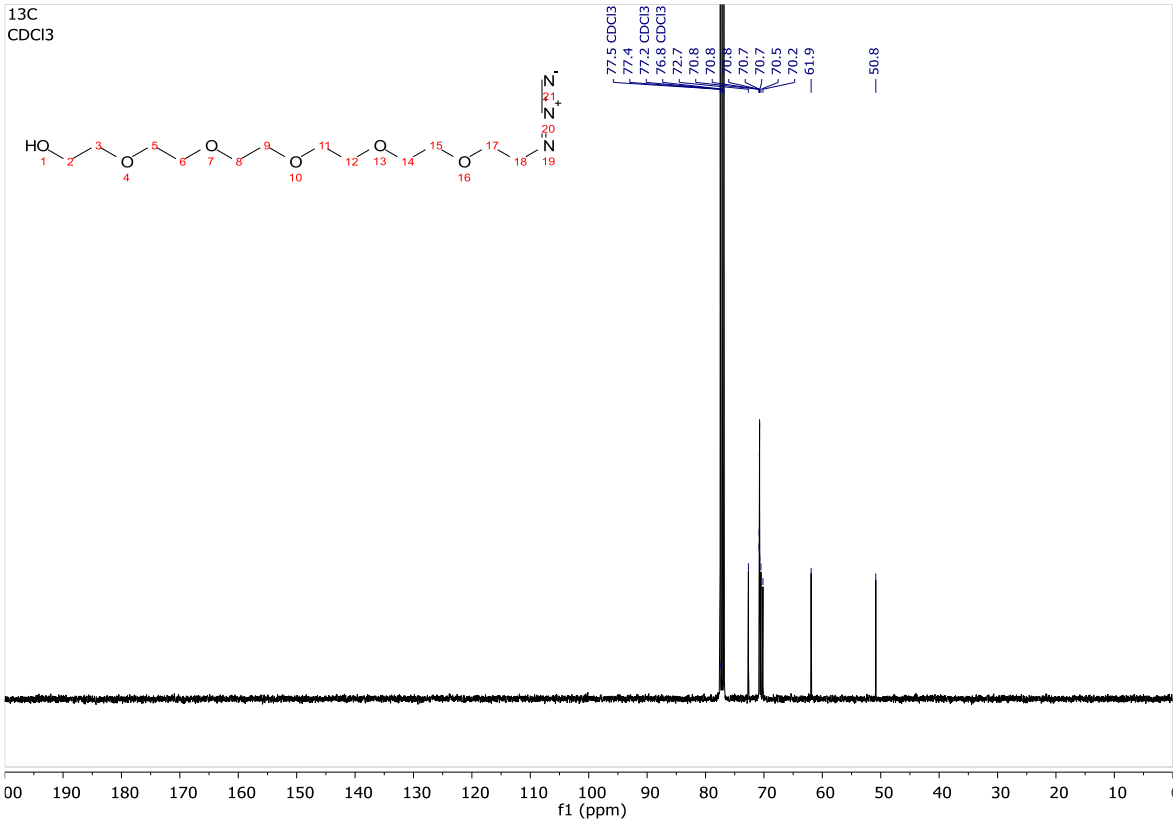

3.38:

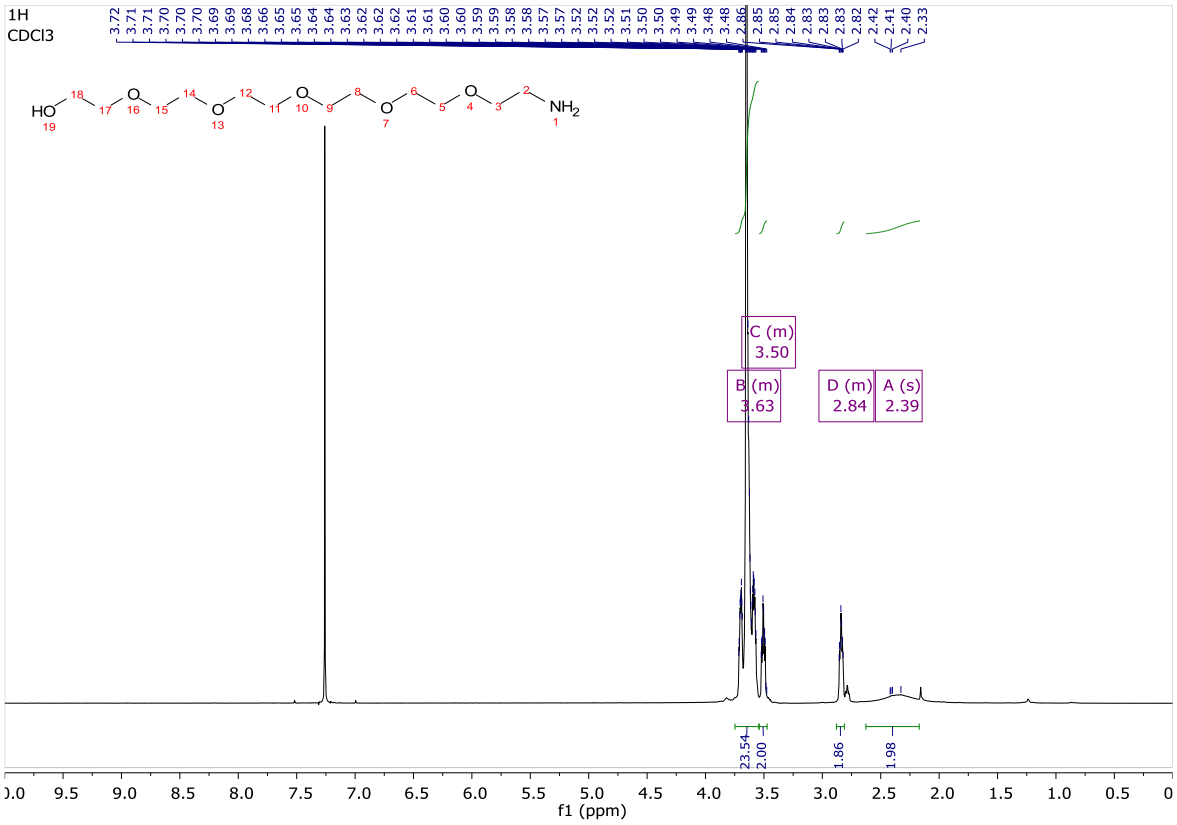
1H
CDCl3
C (m)
3.50
B (m)
3.63
D (m)
2.84
A (s)
2.39
23.54
2.00
1.86
1.98
f1 (ppm)

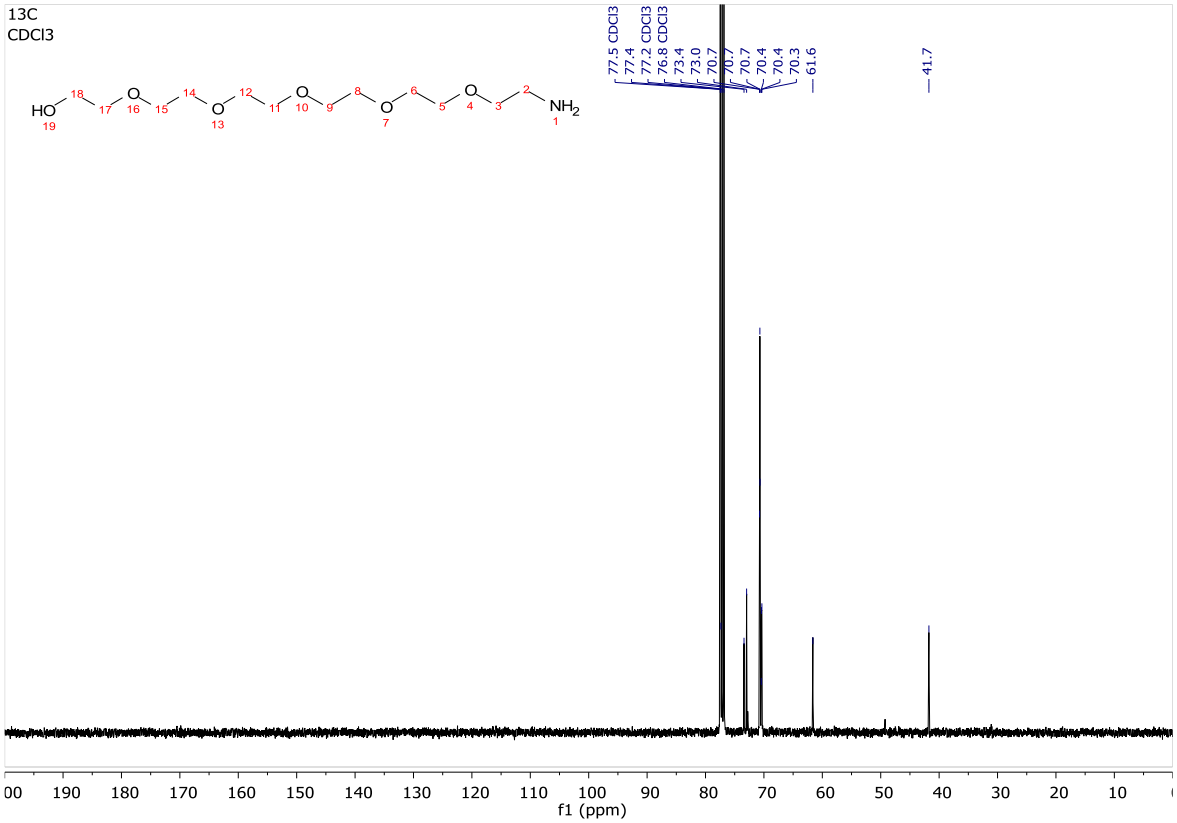
13C
CDCl3
77.5 CDCl3
77.4
77.2 CDCl3
76.8 CDCl3
73.4
73.0
70.7
70.7
70.7
70.4
70.4
70.3
61.6
41.7
f1 (ppm)

3.39:

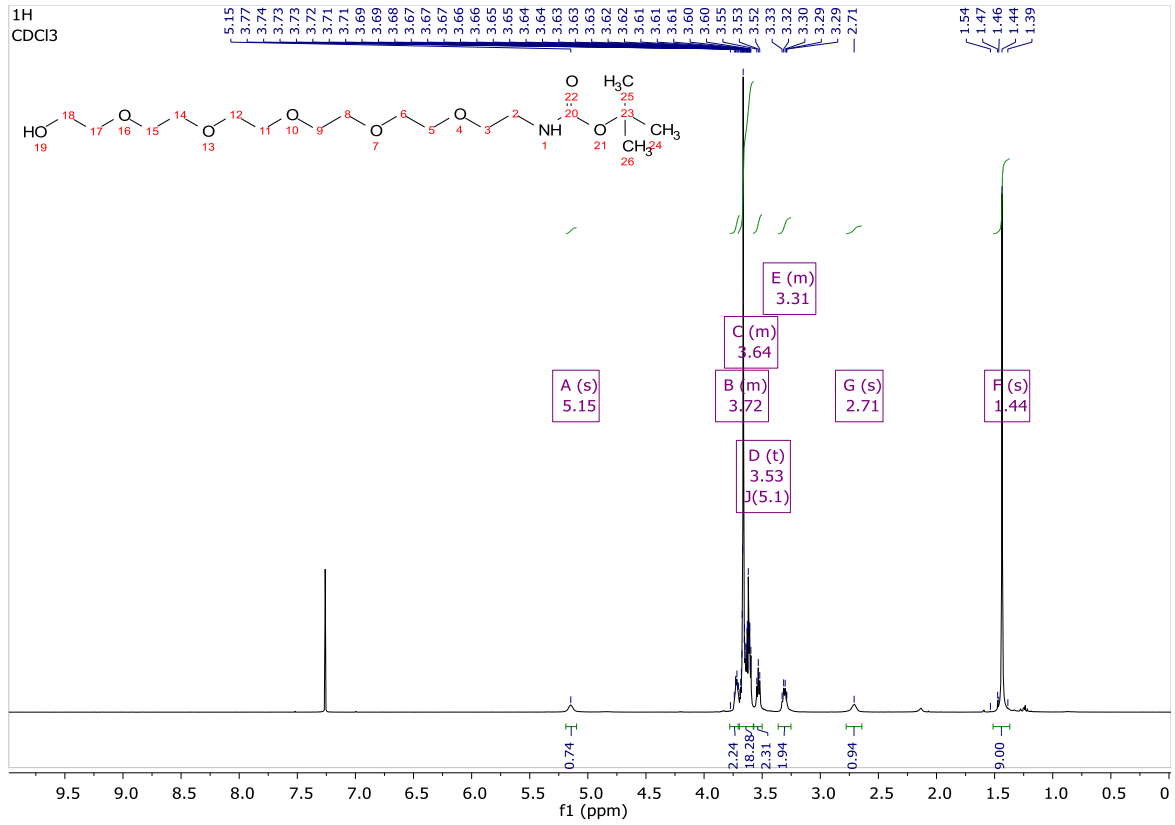
1H
CDCl3
E (m)
3.31
C (m)
3.64
A (s)
5.15
B (m)
3.72
G (s)
2.71
F (s)
1.44
D (t)
3.53
J(5.1)
f1 (ppm)

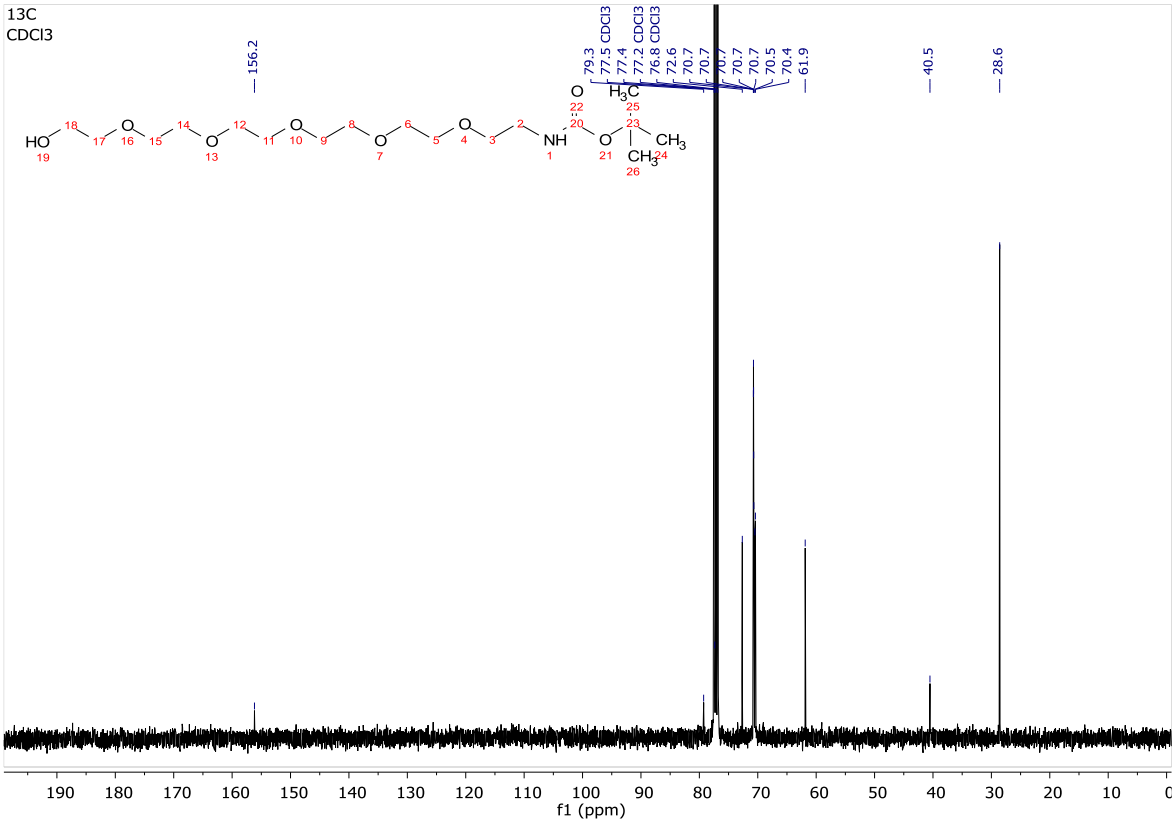
13C
CDCl3
f1 (ppm)

3.40:

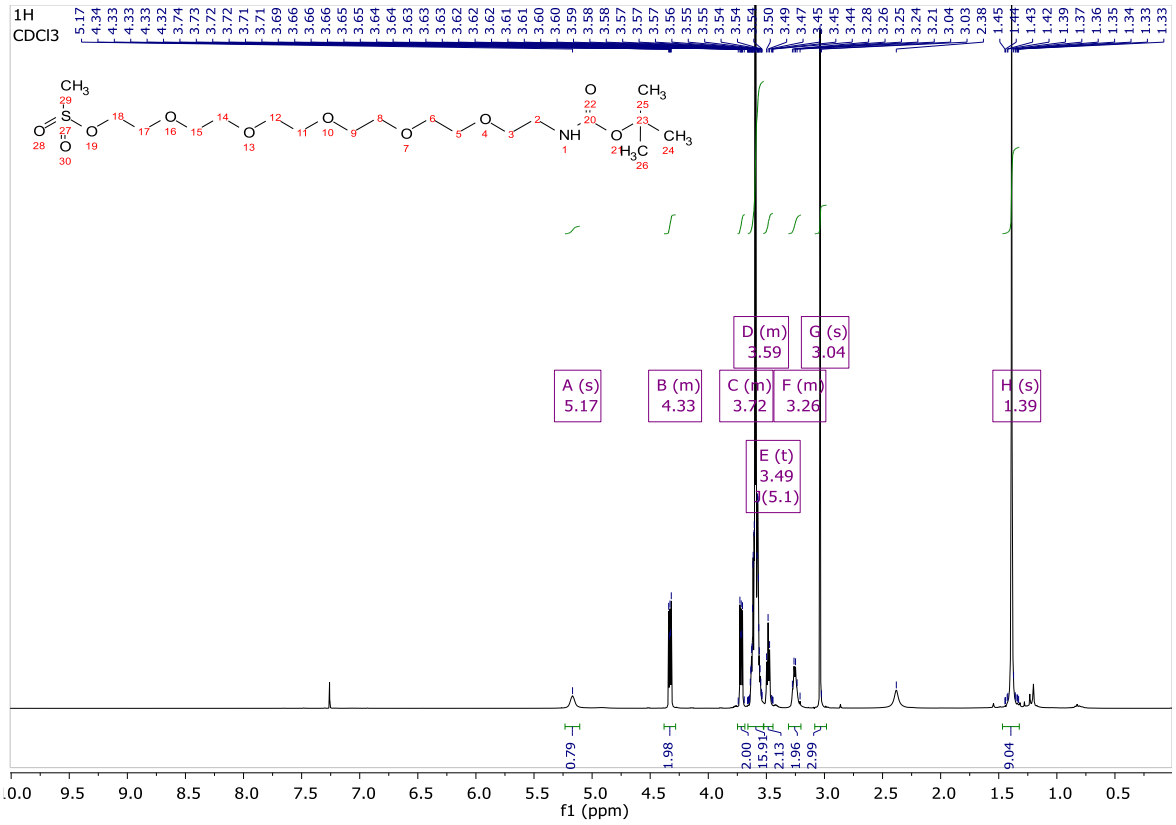
1H
CDCl3
A (s)
5.17
B (m)
4.33
C (m)
3.72
D (m)
3.59
E (t)
3.49
J(5.1)
F (m)
3.26
G (s)
3.04
H (s)
1.39
0.79
1.98
2.00
15.91
2.13
1.96
2.99
9.04
f1 (ppm)

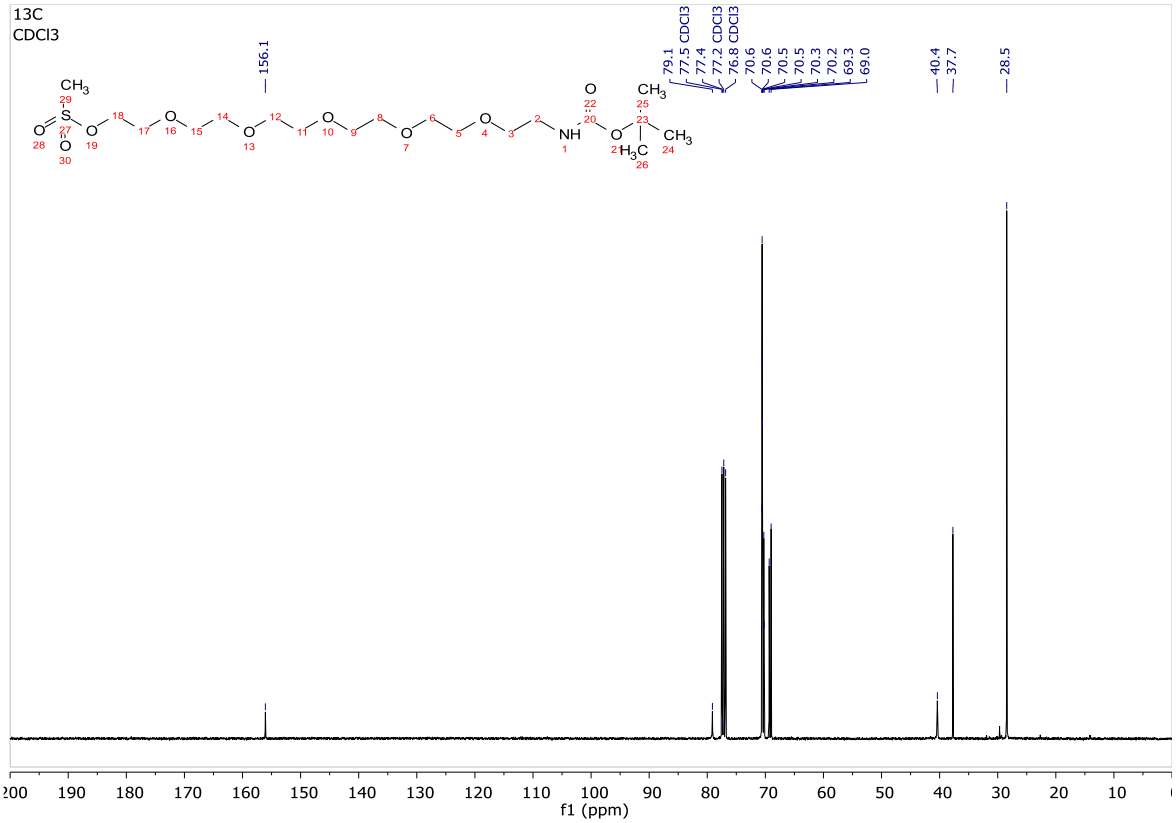
13C
CDCl3
156.1
79.1
77.5 CDCl3
77.4
77.2 CDCl3
76.8 CDCl3
70.6
70.6
70.5
70.5
70.3
70.2
69.3
69.0
40.4
37.7
28.5
f1 (ppm)

3.41:

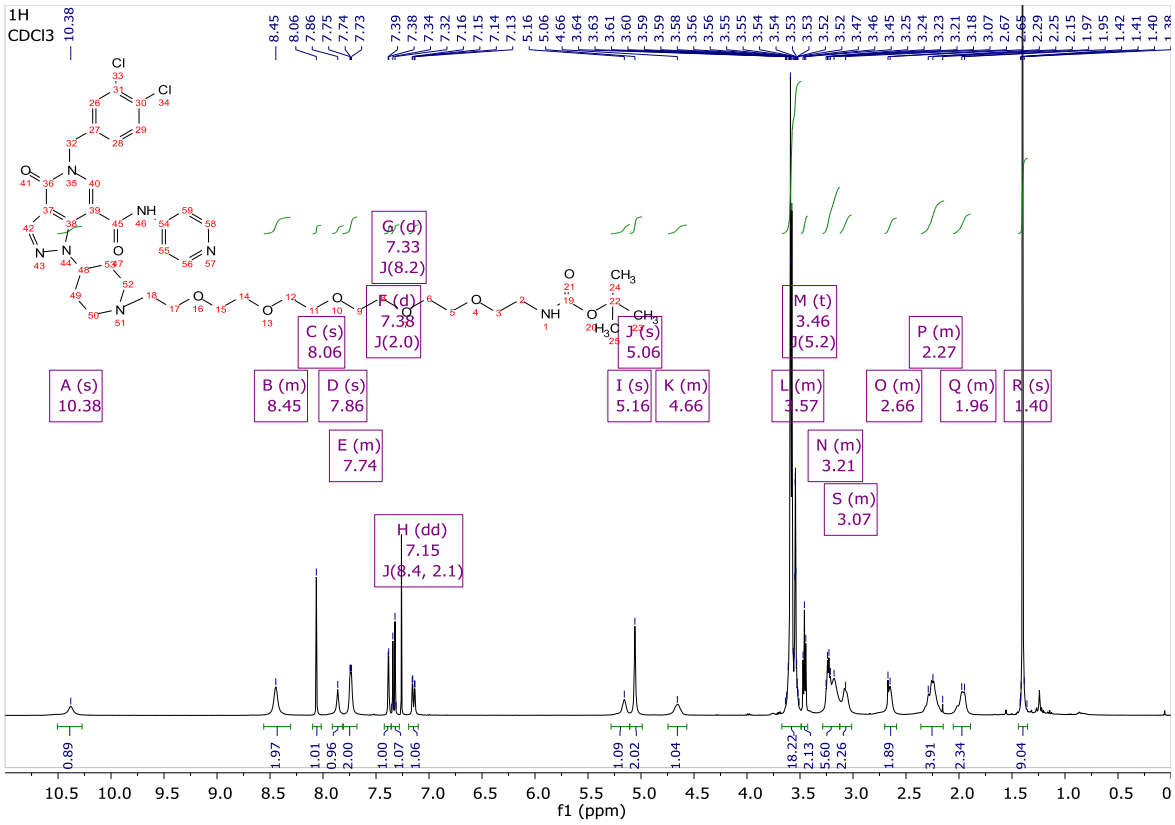
1H
CDCl3
A (s)
10.38
B (m)
8.45
C (s)
8.06
D (s)
7.86
E (m)
7.74
F (d)
7.38
J(2.0)
G (d)
7.33
J(8.2)
H (dd)
7.15
J(8.4, 2.1)
I (s)
5.16
J (s)
5.06
K (m)
4.66
L (m)
3.57
M (t)
3.46
J(5.2)
N (m)
3.21
S (m)
3.07
O (m)
2.66
P (m)
2.27
Q (m)
1.96
R (s)
1.40
f1 (ppm)

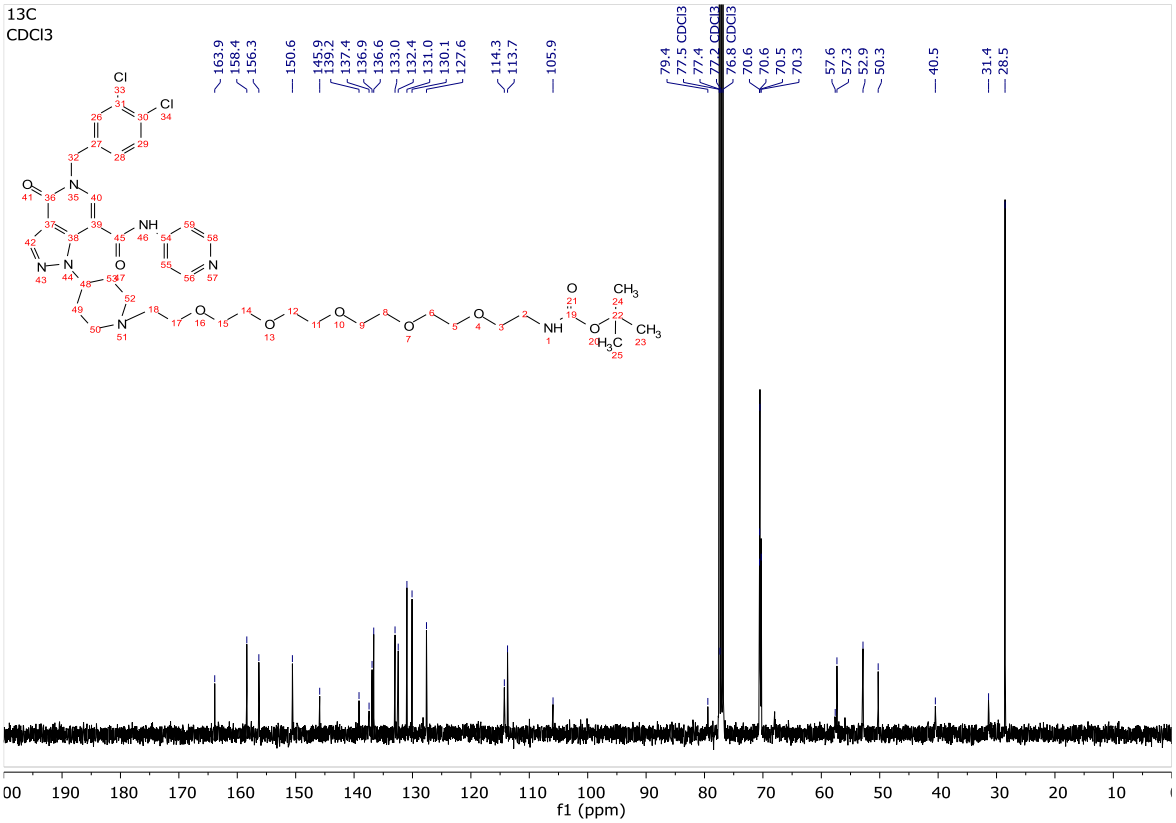
13C
CDCl3
f1 (ppm)

3.43:

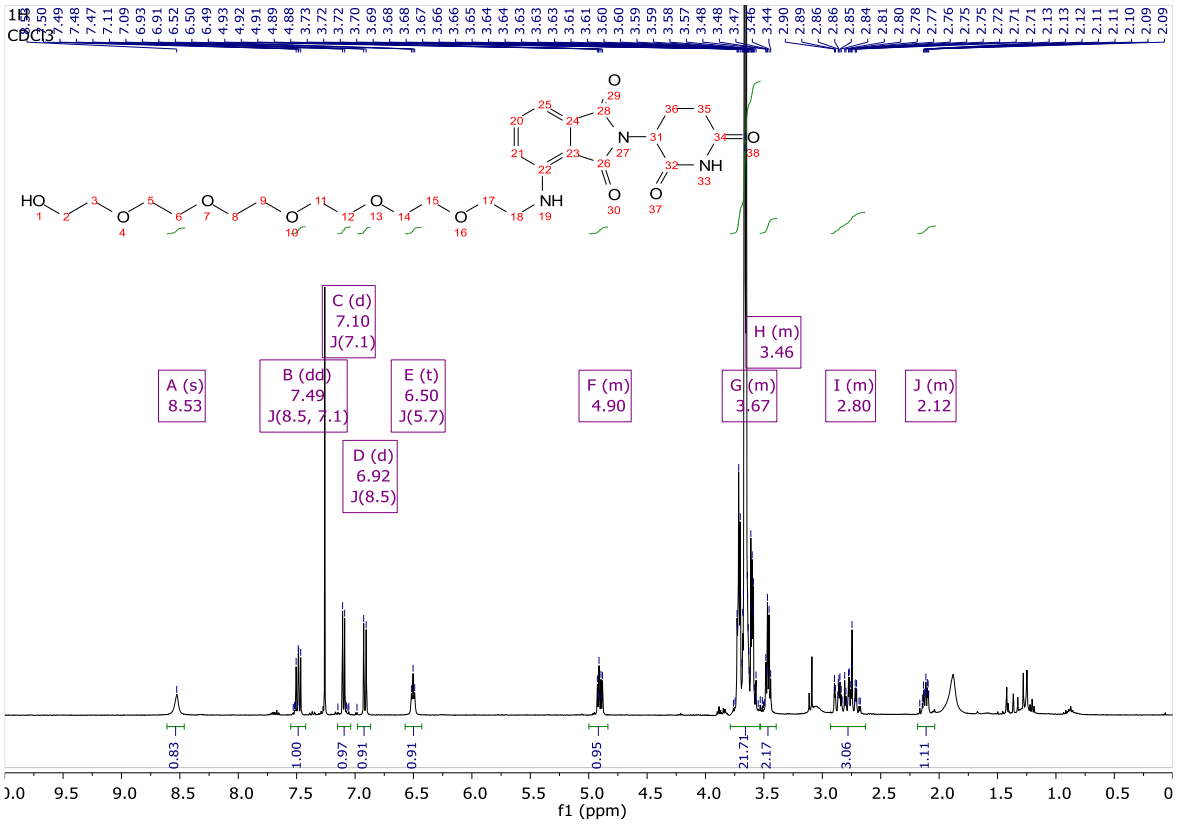
CDCl3
A (s)
8.53
B (dd)
7.49
J(8.5, 7.1)
C (d)
7.10
J(7.1)
D (d)
6.92
J(8.5)
E (t)
6.50
J(5.7)
F (m)
4.90
G (m)
3.67
H (m)
3.46
I (m)
2.80
J (m)
2.12
0.83
1.00
0.97
0.91
0.91
0.95
21.71
2.17
3.06
1.11
f1 (ppm)

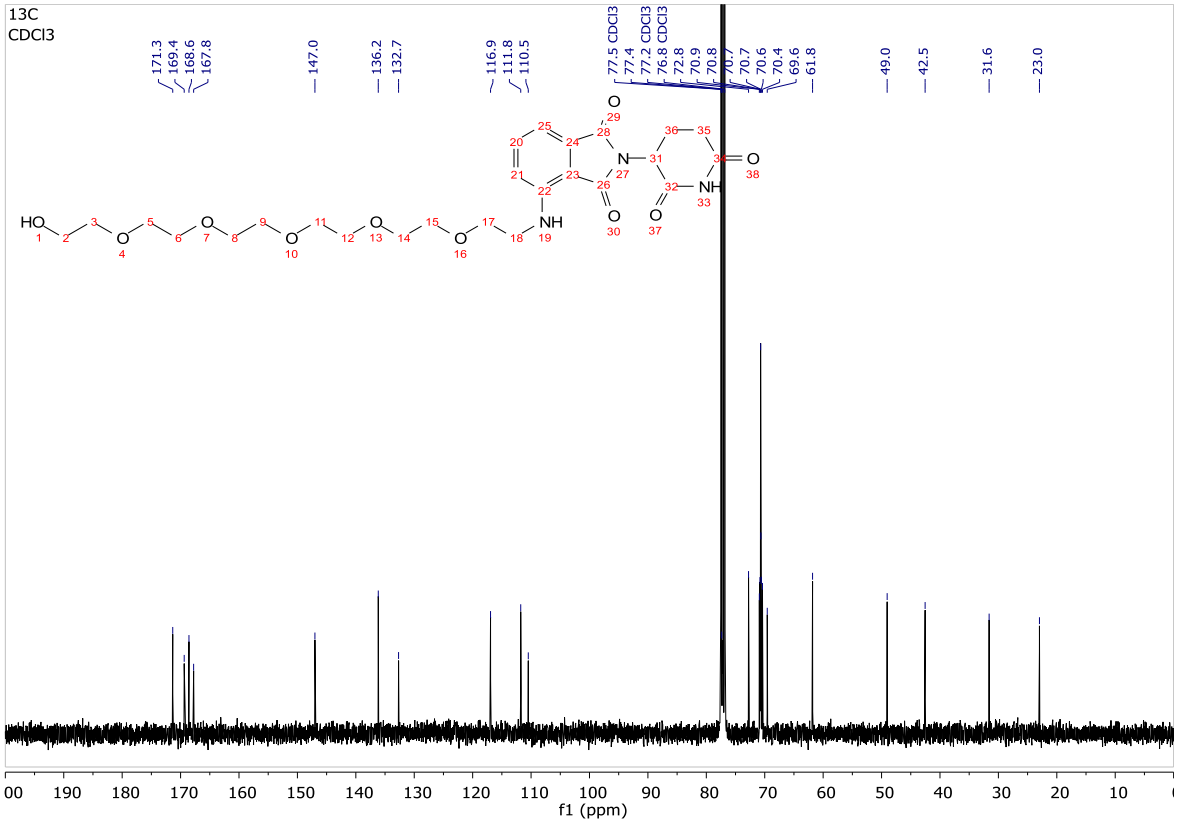
13C
CDCl3
171.3
169.4
168.6
167.8
147.0
136.2
132.7
116.9
111.8
110.5
77.5 CDCl3
77.4
77.2 CDCl3
76.8 CDCl3
72.8
70.9
70.8
70.7
70.7
70.6
70.4
69.6
61.8
49.0
42.5
31.6
23.0
f1 (ppm)

3.44:

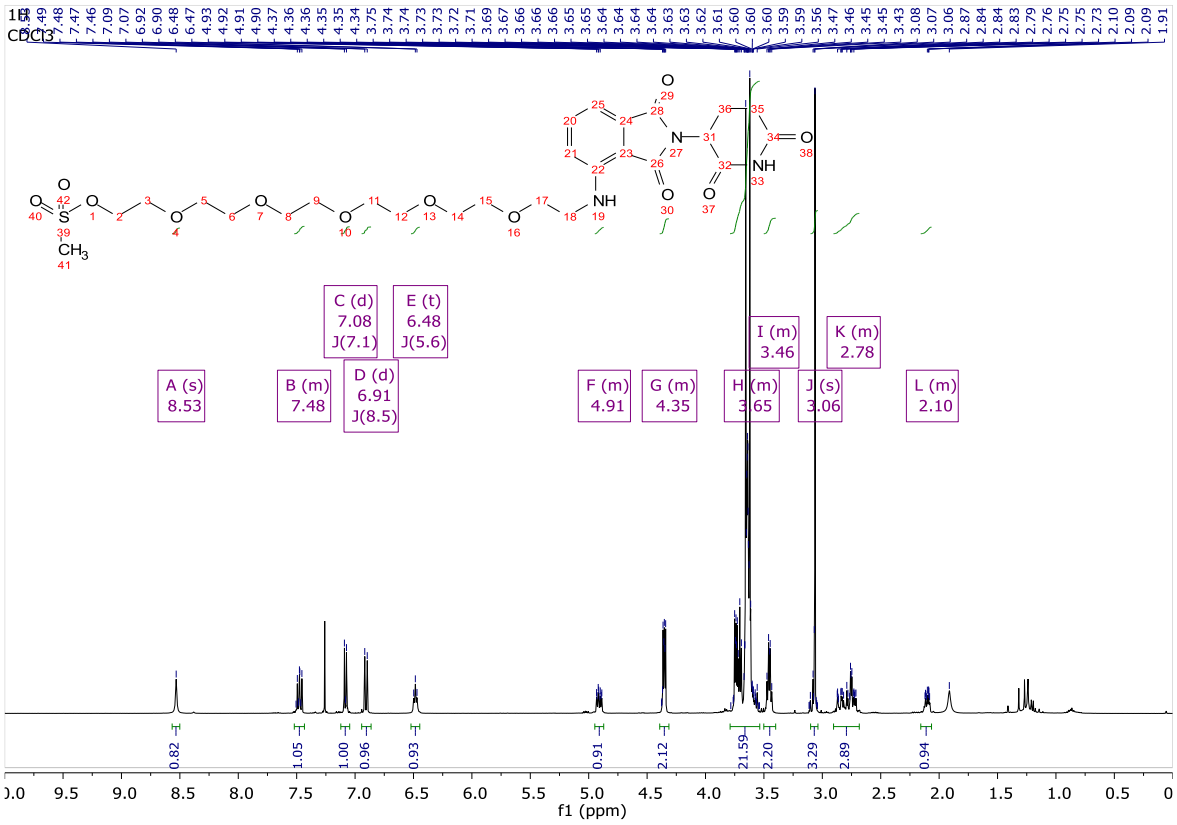
1H
CDCl3
A (s)
8.53
B (m)
7.48
C (d)
7.08
J(7.1)
D (d)
6.91
J(8.5)
E (t)
6.48
J(5.6)
F (m)
4.91
G (m)
4.35
H (m)
3.65
I (m)
3.46
J (s)
3.06
K (m)
2.78
L (m)
2.10
f1 (ppm)

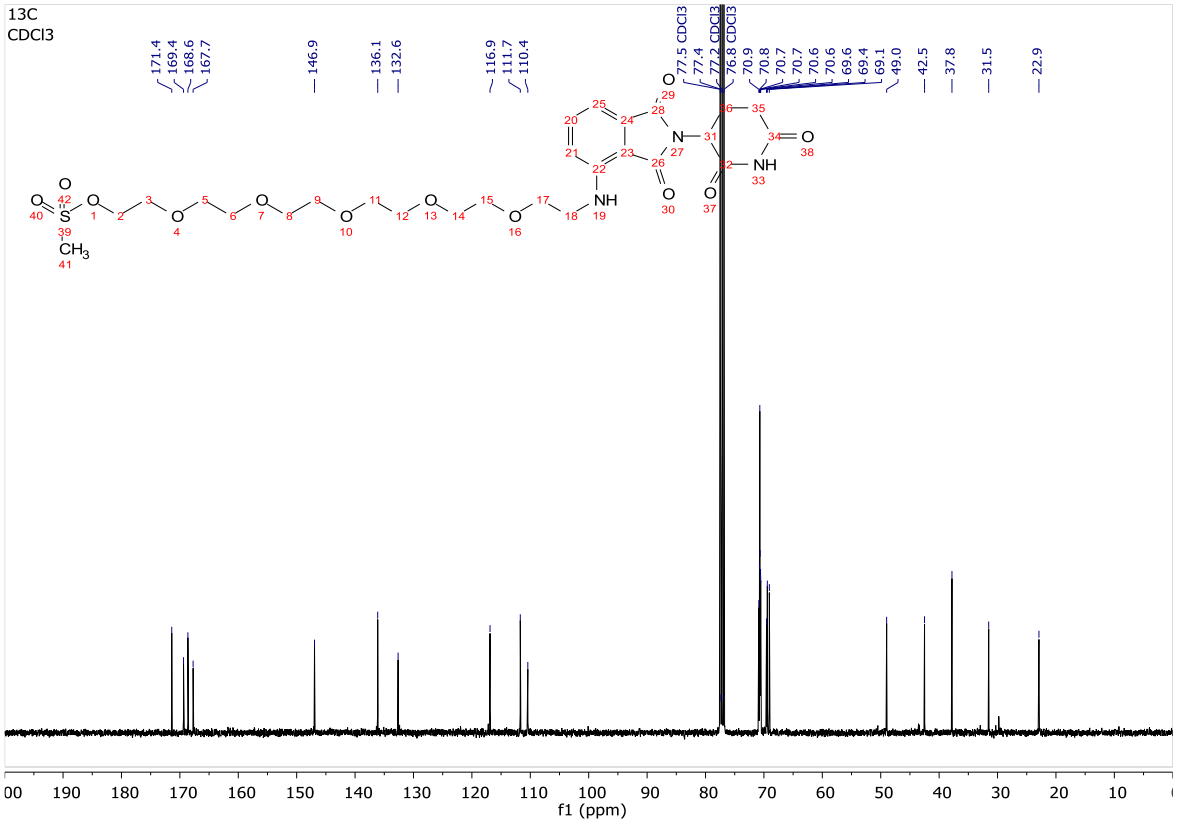
13C
CDCl3
f1 (ppm)

FSCN-B-CRBN-1 (3.42) *via* Route B:

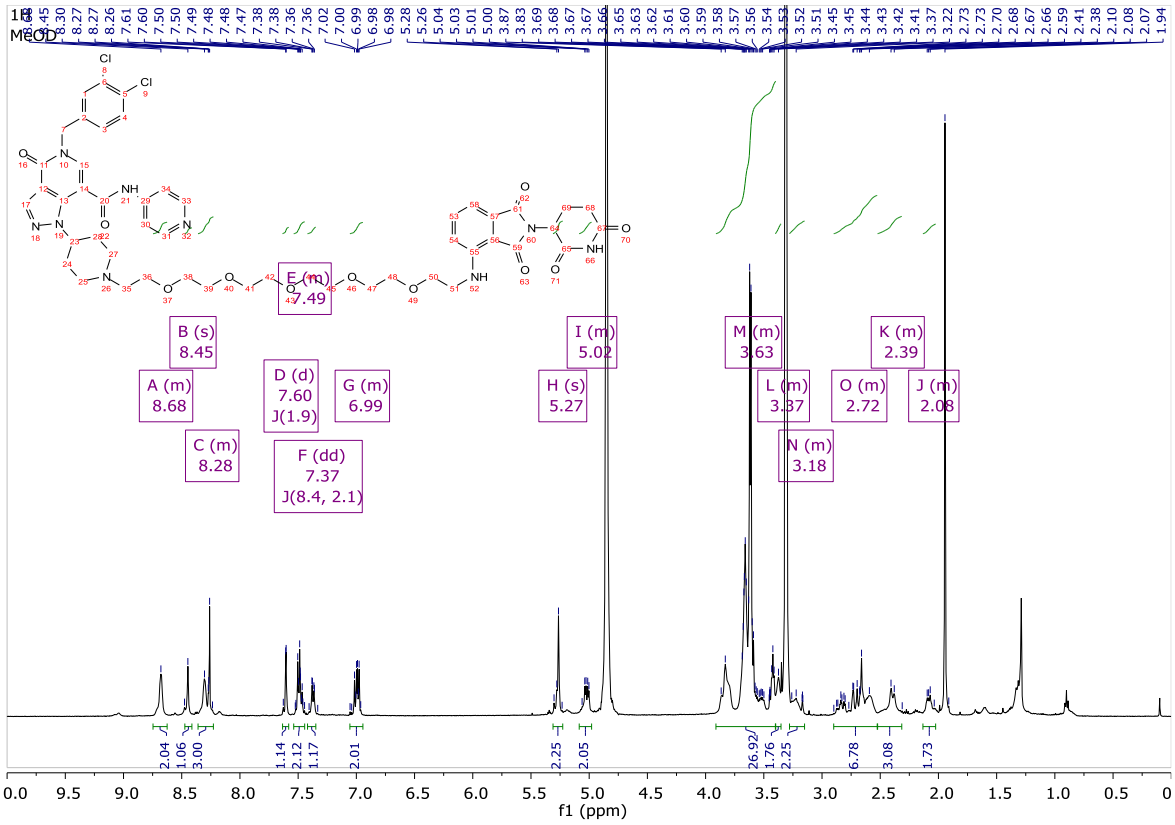

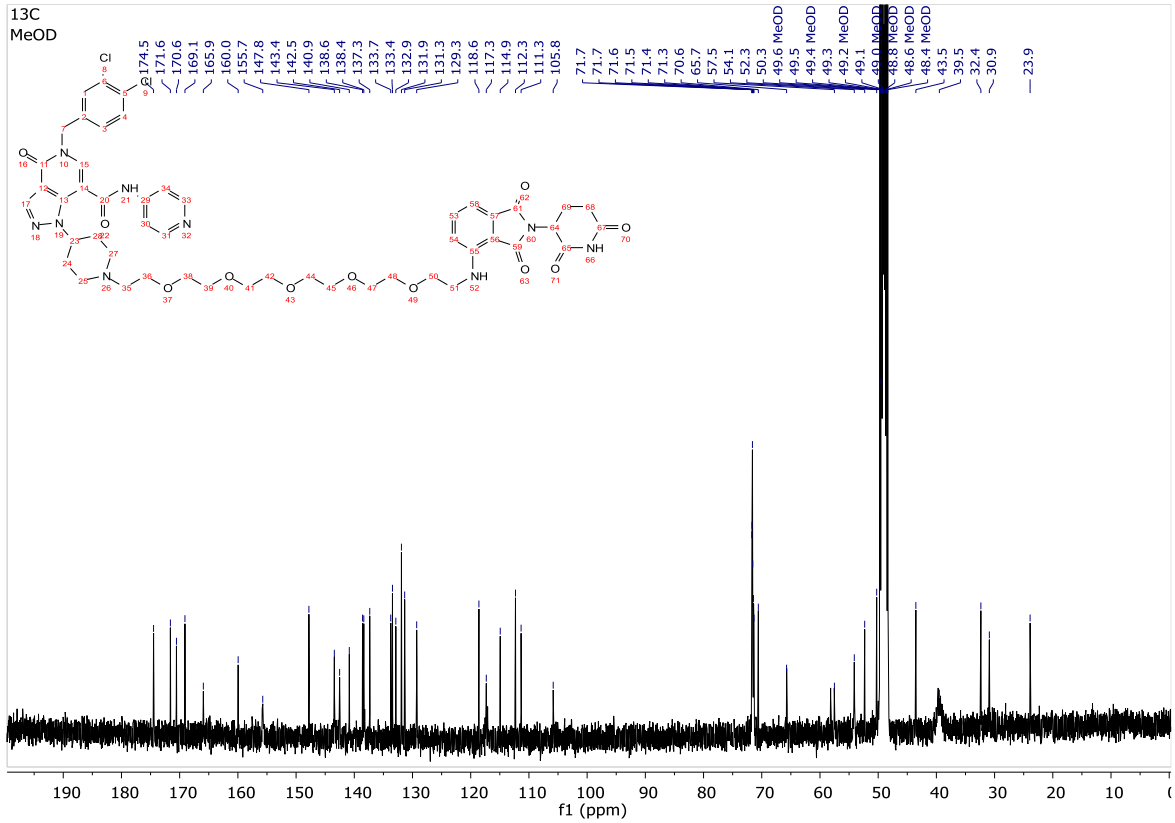

3.45:

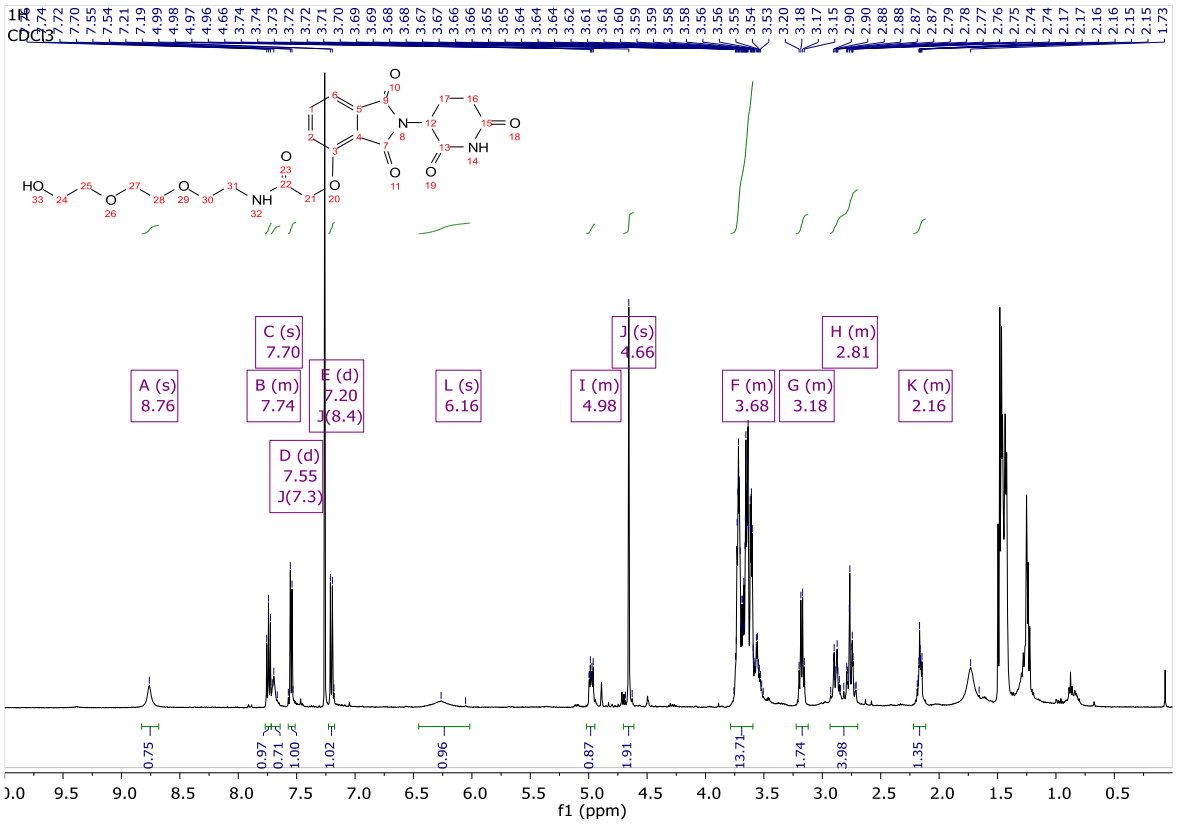
1H
CDCl3
A (s)
8.76
B (m)
7.74
C (s)
7.70
D (d)
7.55
J(7.3)
E (d)
7.20
J(8.4)
L (s)
6.16
I (m)
4.98
J (s)
4.66
F (m)
3.68
G (m)
3.18
H (m)
2.81
K (m)
2.16
f1 (ppm)

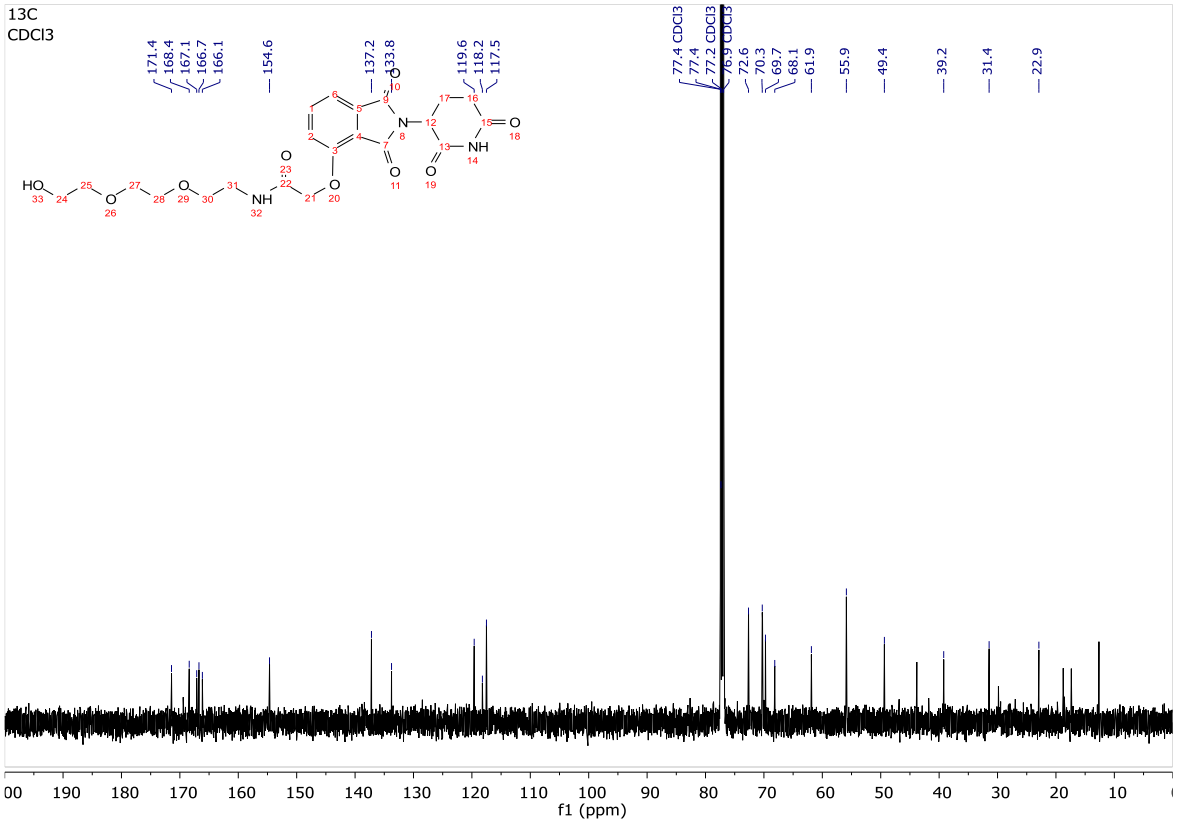
13C
CDCl3
f1 (ppm)

3.46:

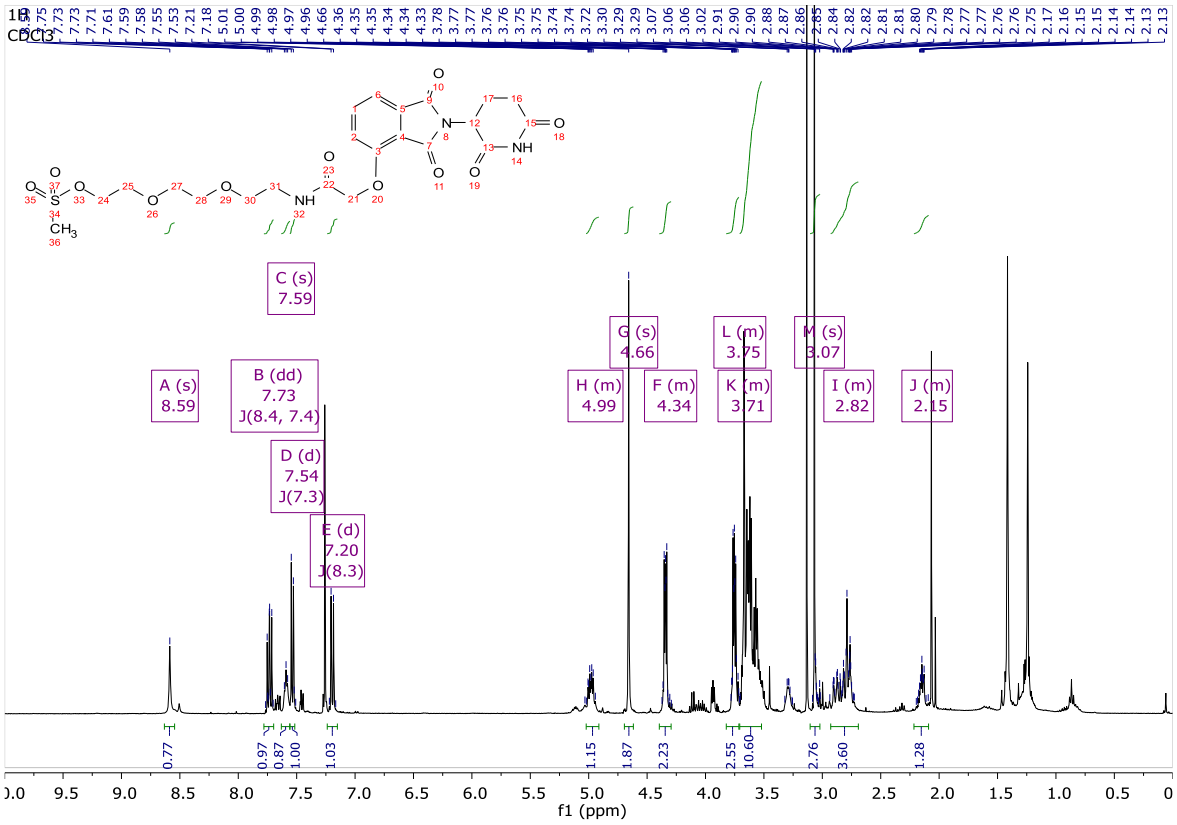
1H
CDCl3
C (s)
7.59
A (s)
8.59
B (dd)
7.73
J(8.4, 7.4)
D (d)
7.54
J(7.3)
E (d)
7.20
J(8.3)
G (s)
4.66
H (m)
4.99
F (m)
4.34
L (m)
3.75
K (m)
3.71
M (s)
3.07
I (m)
2.82
J (m)
2.15
f1 (ppm)

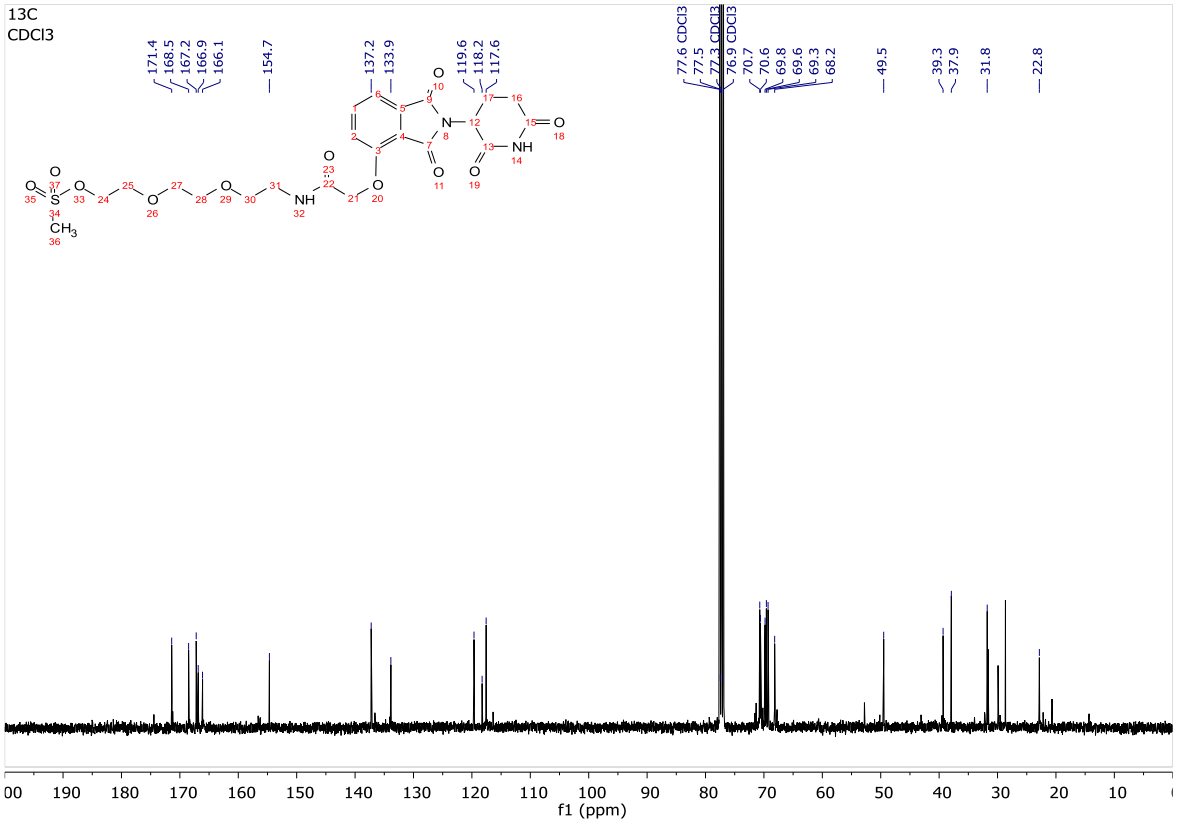
13C
CDCl3
f1 (ppm)

FSCN-B-CRBN-2 (3.47):

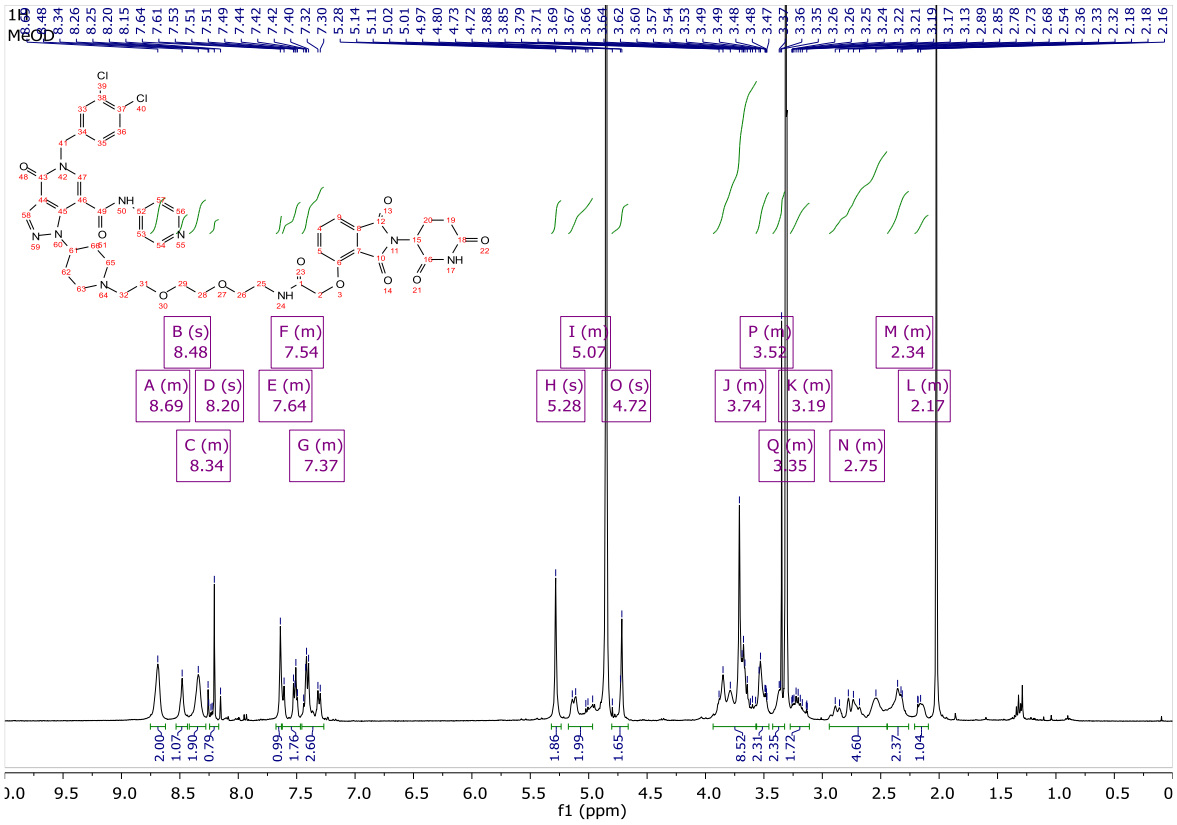

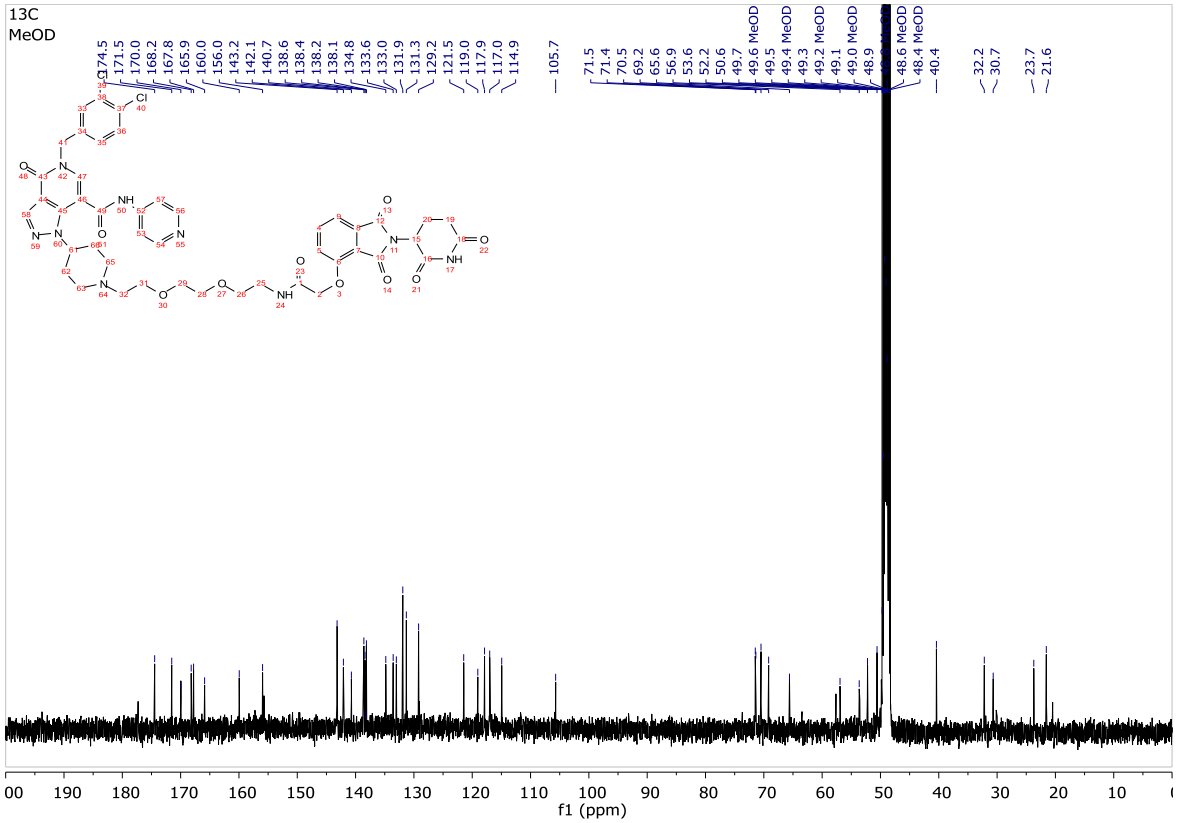

- *Fascin ligand B HyT PROTACs:*

FSCN-B-HyT-1 (3.48):

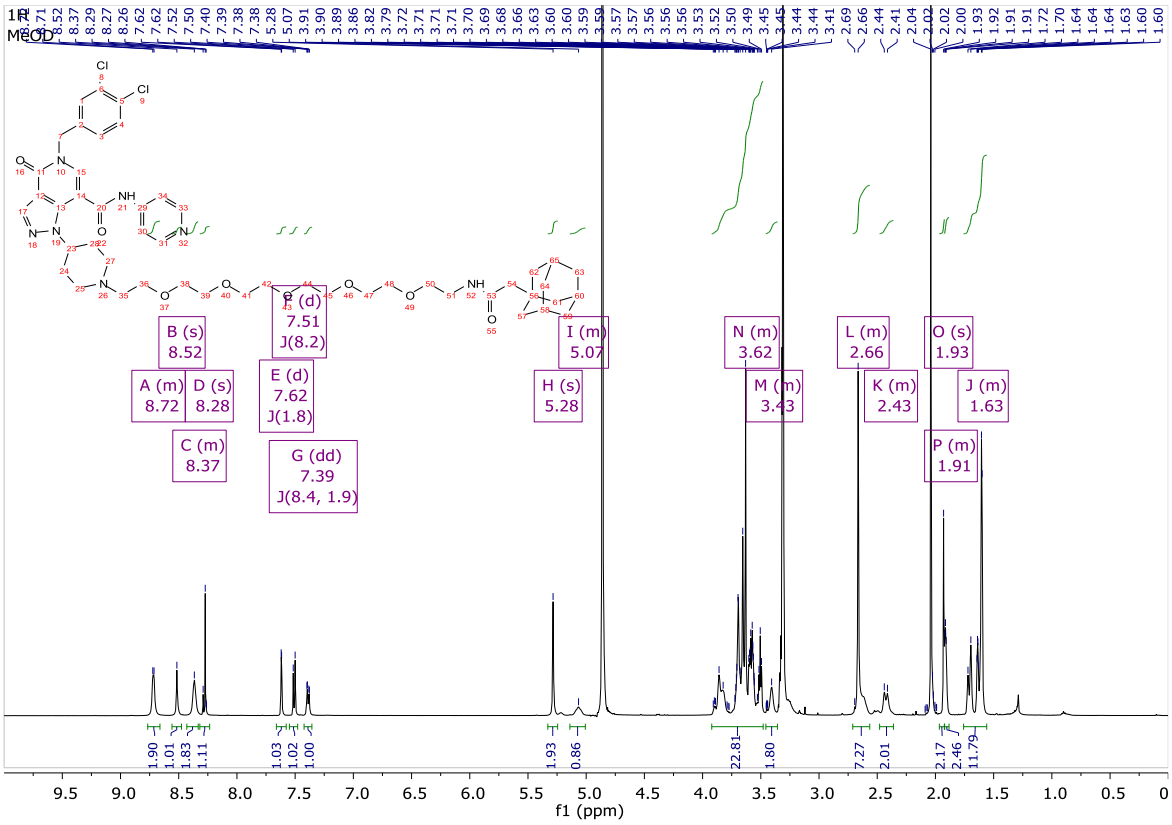

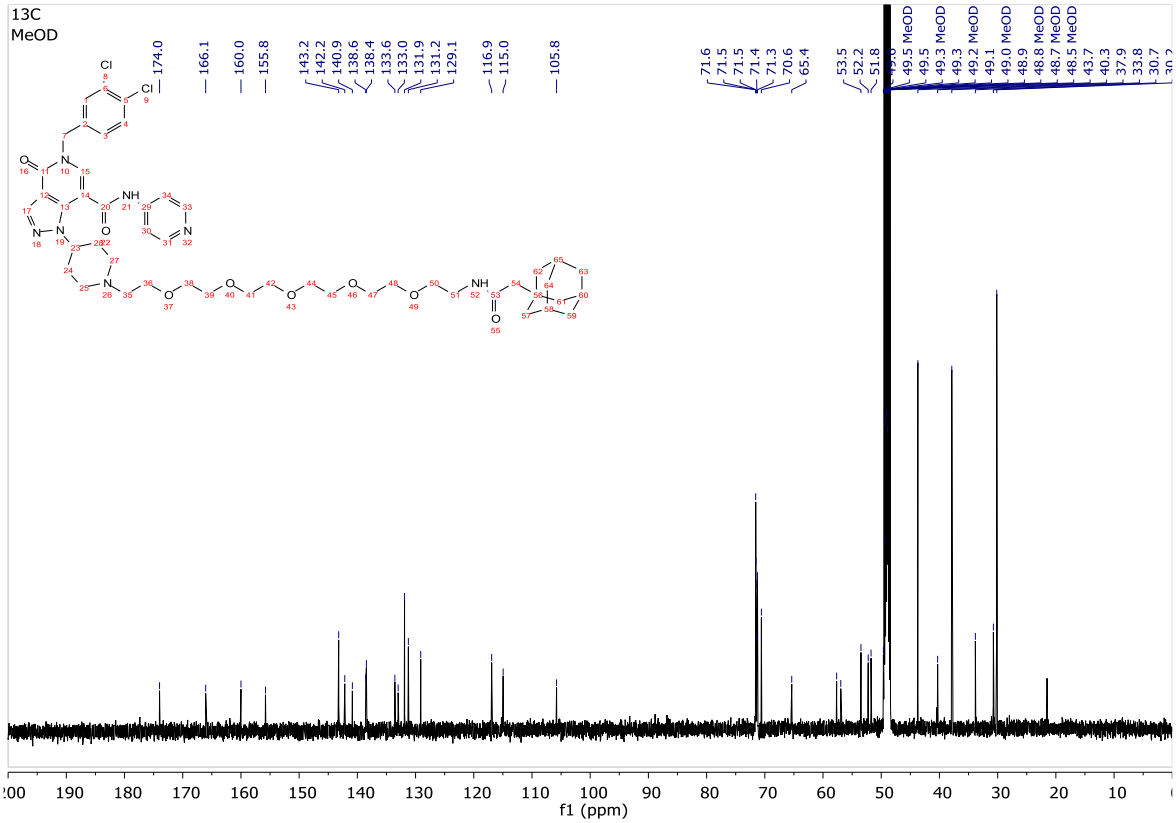

3.49:

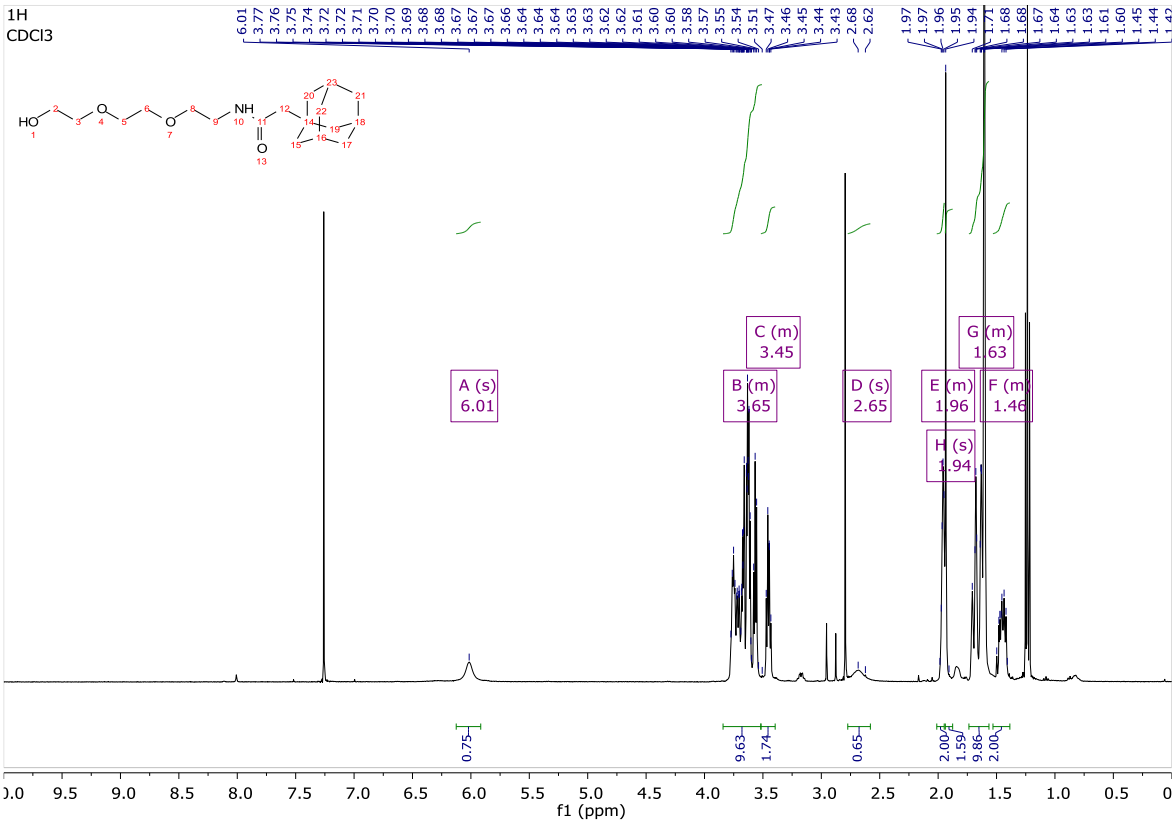
1H
CDCl3
A (s)
6.01
B (m)
3.65
C (m)
3.45
D (s)
2.65
E (m)
1.96
F (m)
1.46
G (m)
1.63
H (s)
1.94
f1 (ppm)

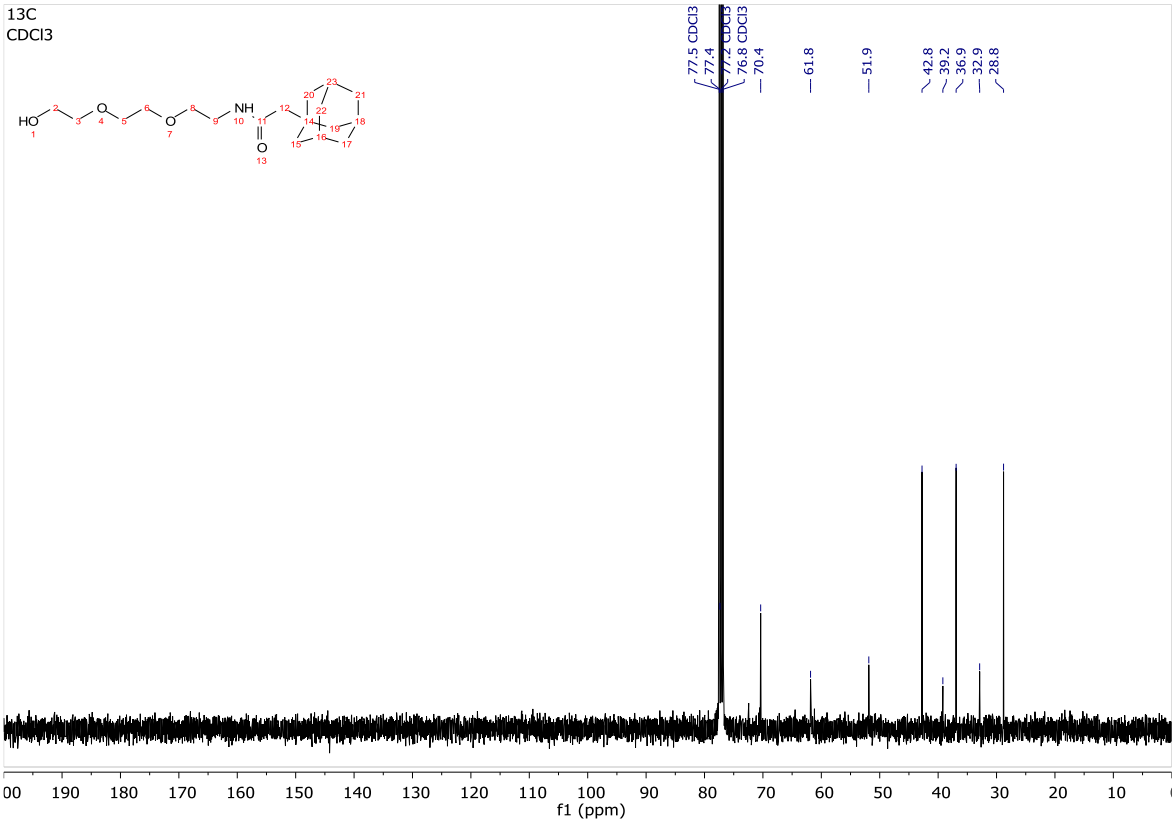
13C
CDCl3
77.5 CDCl3
77.4
77.2 CDCl3
76.8 CDCl3
70.4
61.8
51.9
42.8
39.2
36.9
32.9
28.8
f1 (ppm)

3.50:

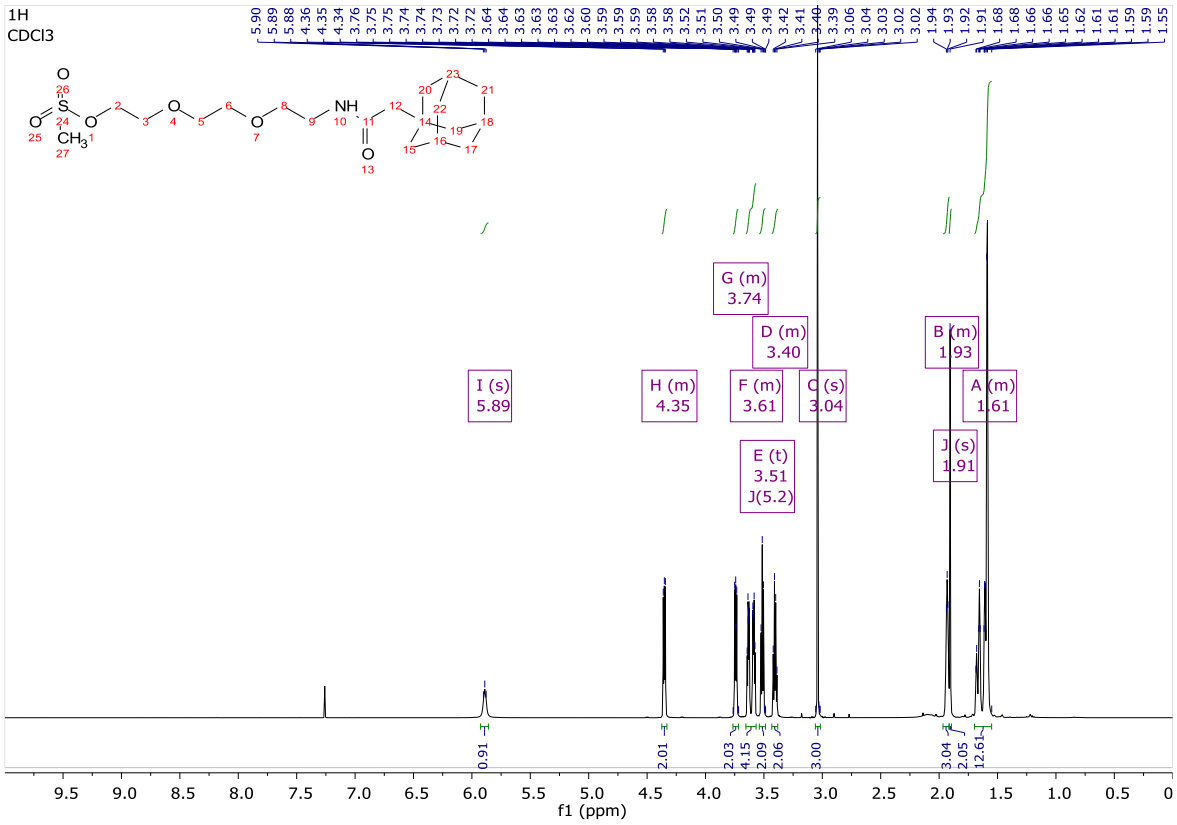
1H
CDCl3
G (m)
3.74
D (m)
3.40
B (m)
1.93
I (s)
5.89
H (m)
4.35
F (m)
3.61
C (s)
3.04
A (m)
1.61
E (t)
3.51
J(5.2)
J (s)
1.91
f1 (ppm)

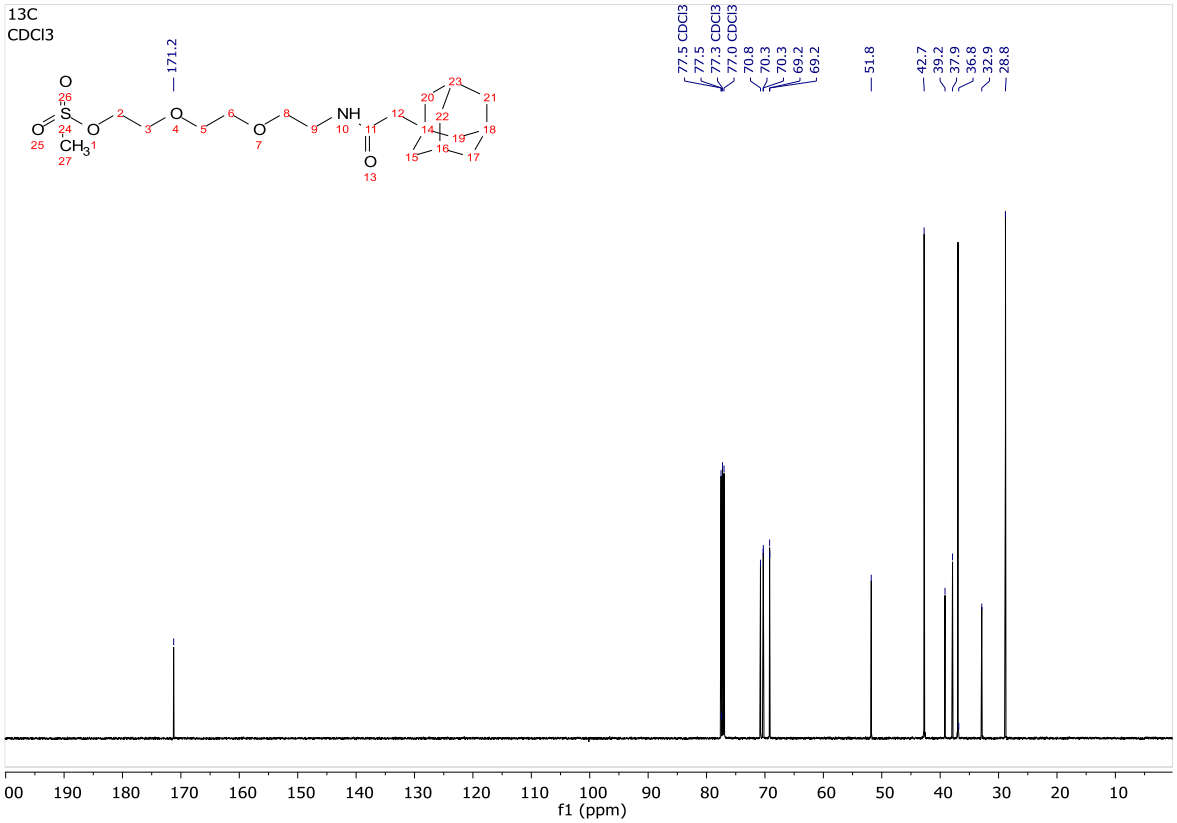
13C
CDCl3
171.2
77.5 CDCl3
77.5
77.3 CDCl3
77.0 CDCl3
70.8
70.3
70.3
69.2
69.2
51.8
42.7
39.2
37.9
36.8
32.9
28.8
f1 (ppm)

FSCN-B-HyT-2 (3.51):

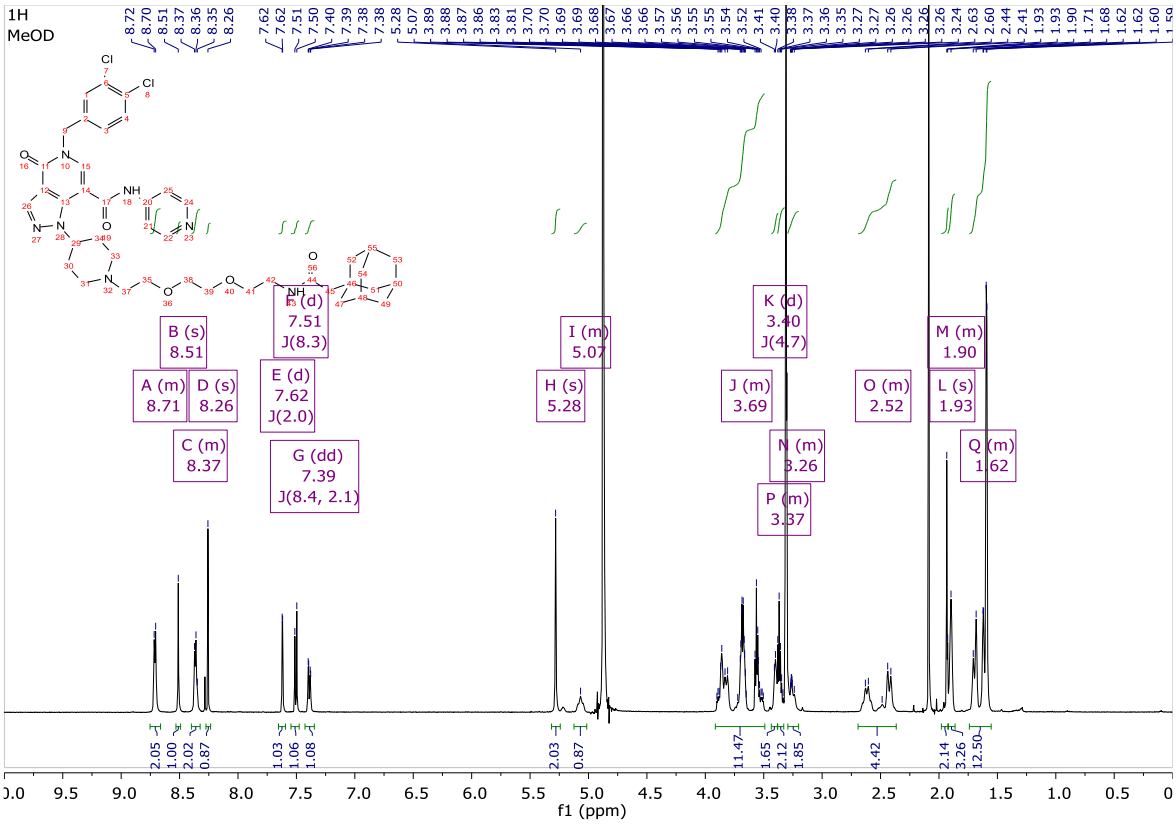

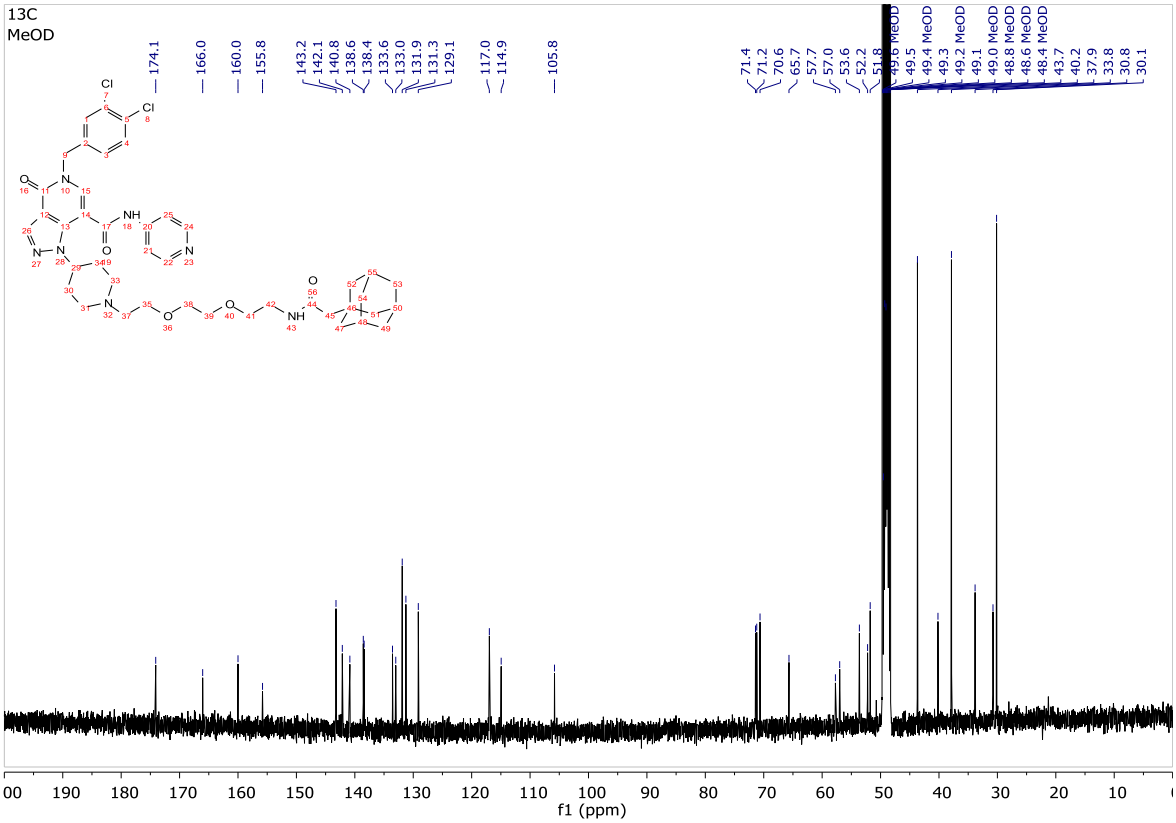

3.54:

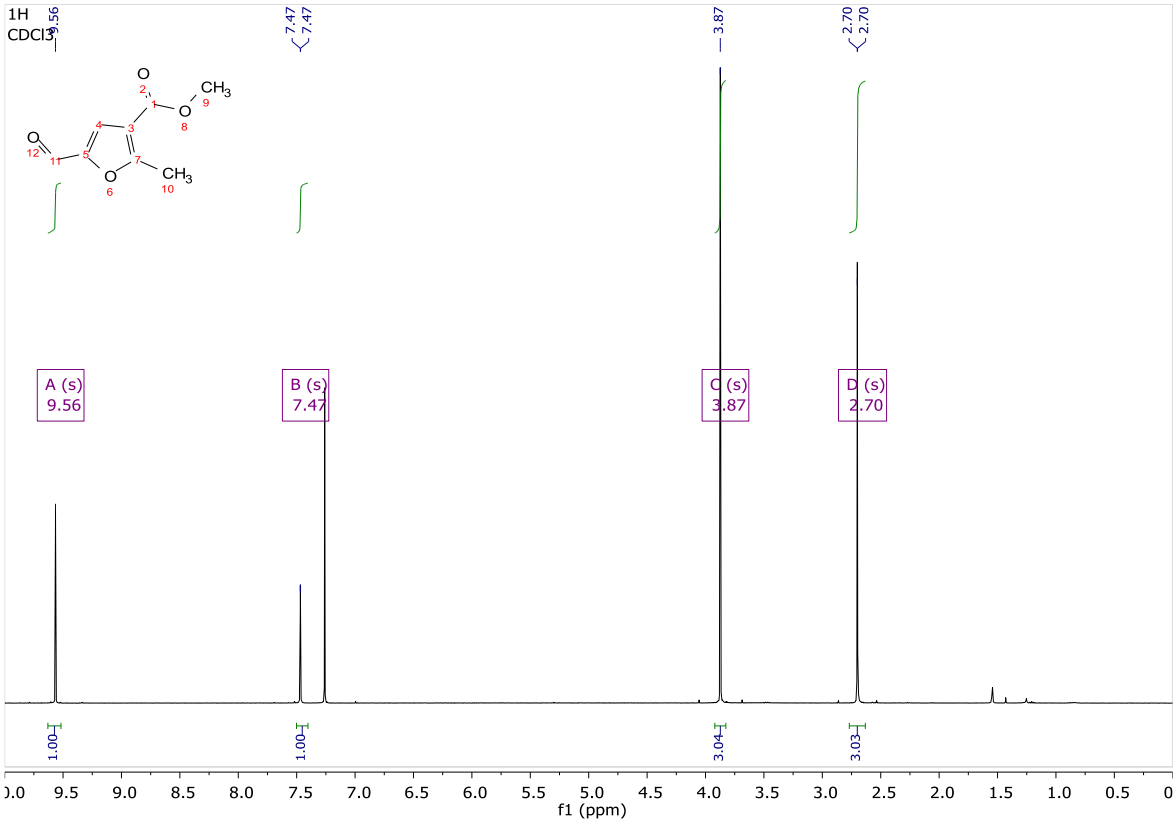
1H
CDCl3
9.56
7.47
7.47
3.87
2.70
2.70
A (s)
9.56
B (s)
7.47
C (s)
3.87
D (s)
2.70
1.00
1.00
3.04
3.03
f1 (ppm)

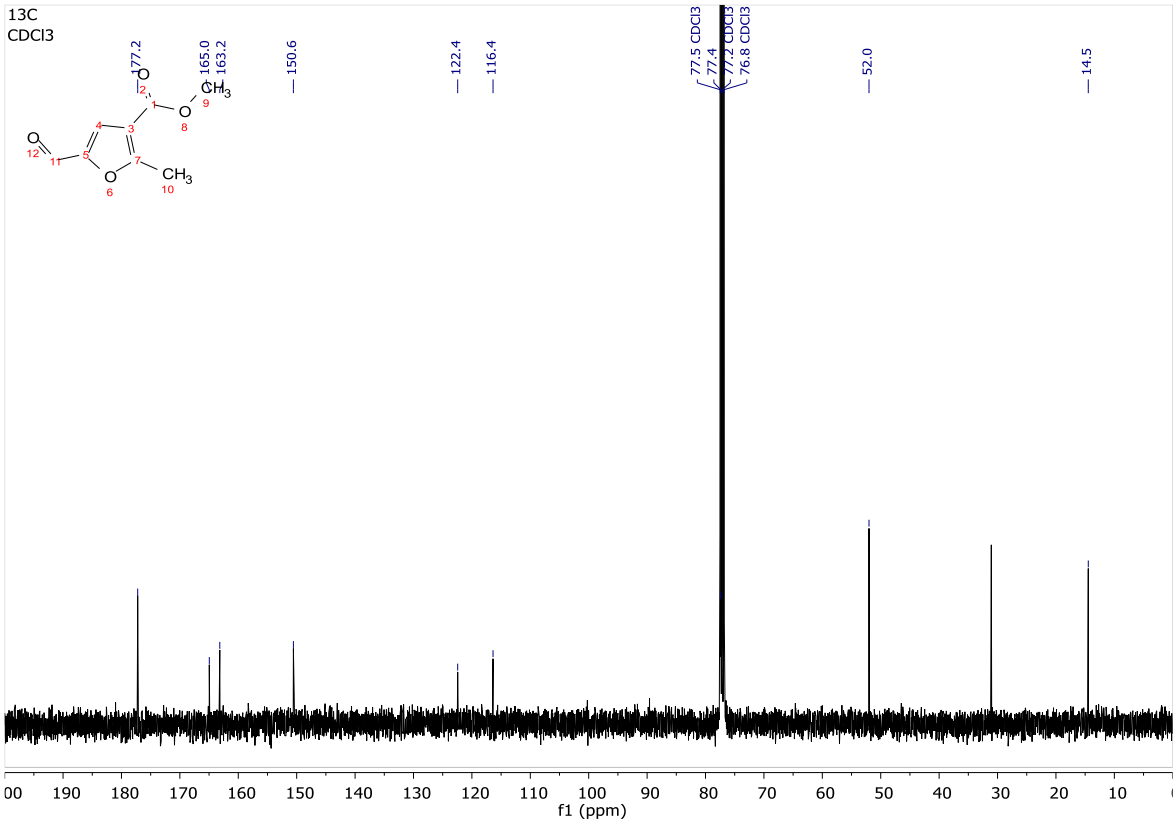
13C
CDCl3
177.2
165.0
163.2
150.6
122.4
116.4
77.5 CDCl3
77.4
77.2 CDCl3
76.8 CDCl3
52.0
14.5
f1 (ppm)

3.55:

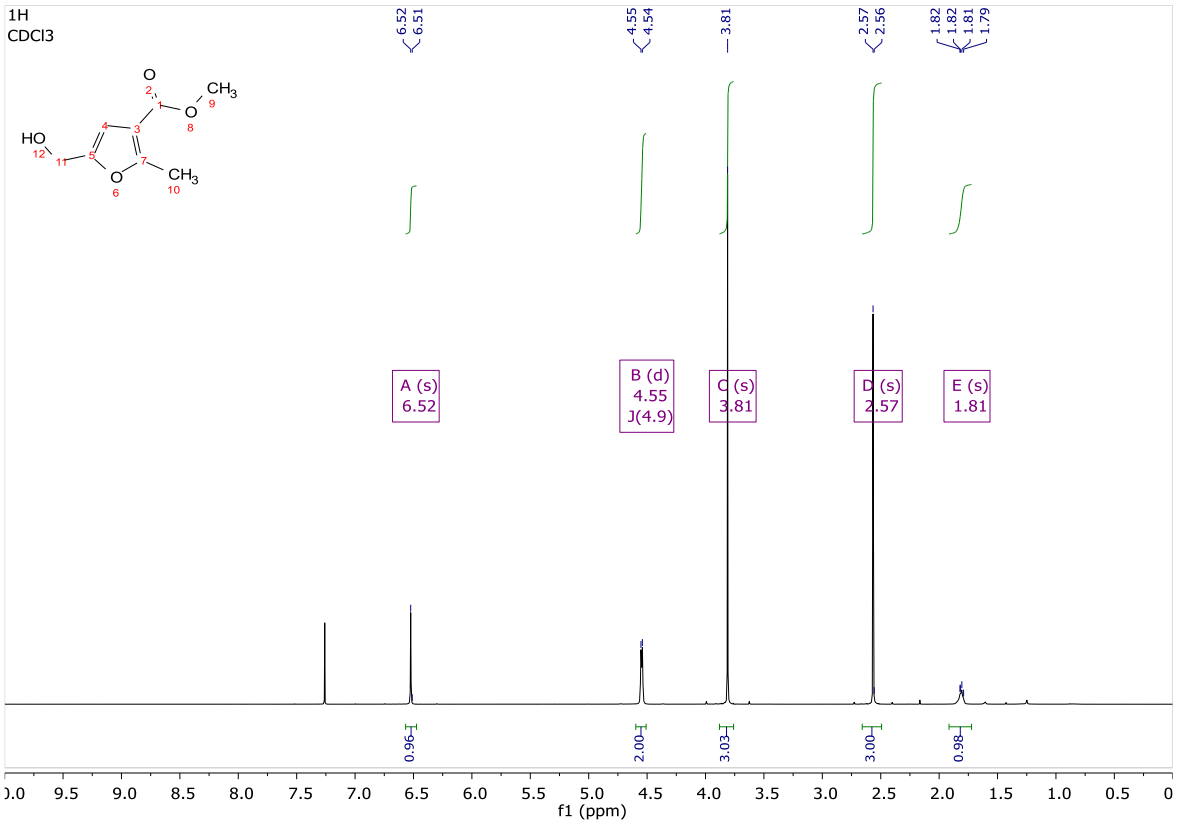
1H
CDCl3
6.52
6.51
4.55
4.54
3.81
2.57
2.56
1.82
1.82
1.81
1.79
A (s)
6.52
B (d)
4.55
J(4.9)
C (s)
3.81
D (s)
2.57
E (s)
1.81
0.96
2.00
3.03
3.00
0.98
f1 (ppm)

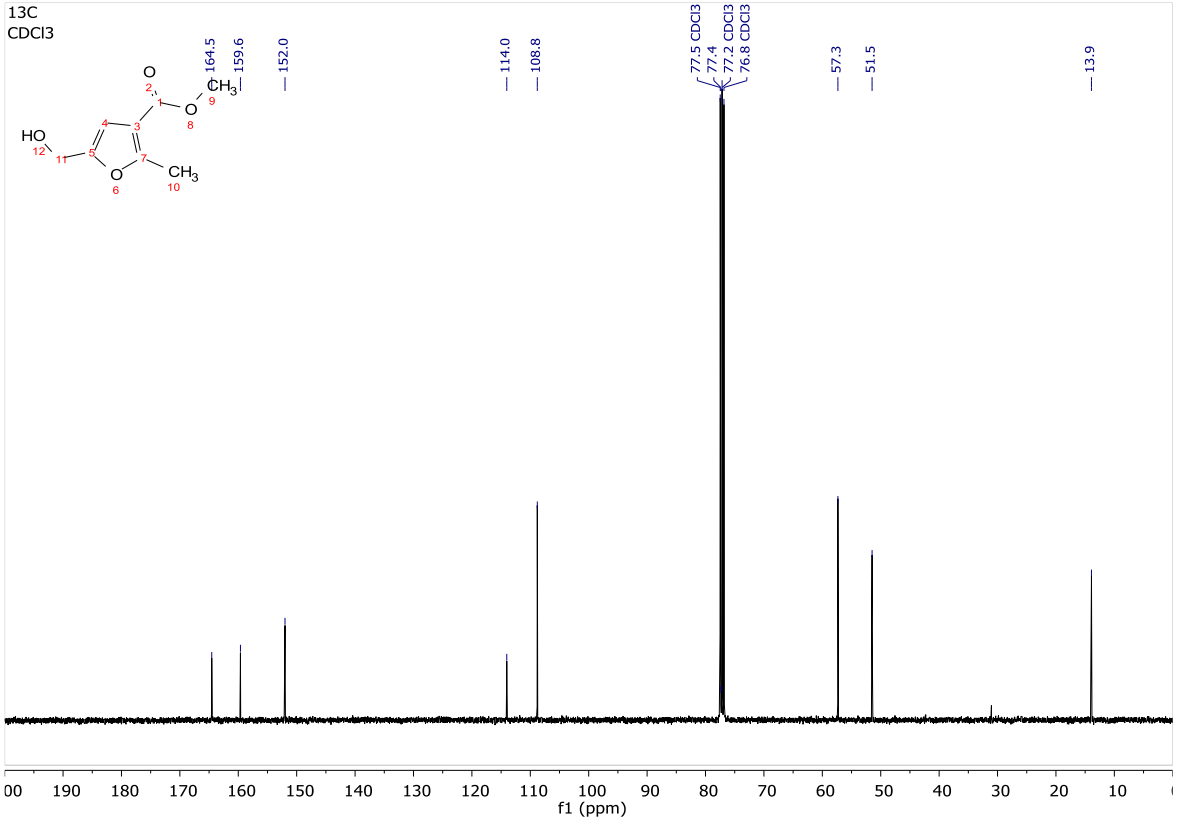
13C
CDCl3
164.5
159.6
152.0
114.0
108.8
77.5 CDCl3
77.4
77.2 CDCl3
76.8 CDCl3
57.3
51.5
13.9
f1 (ppm)

3.56a:

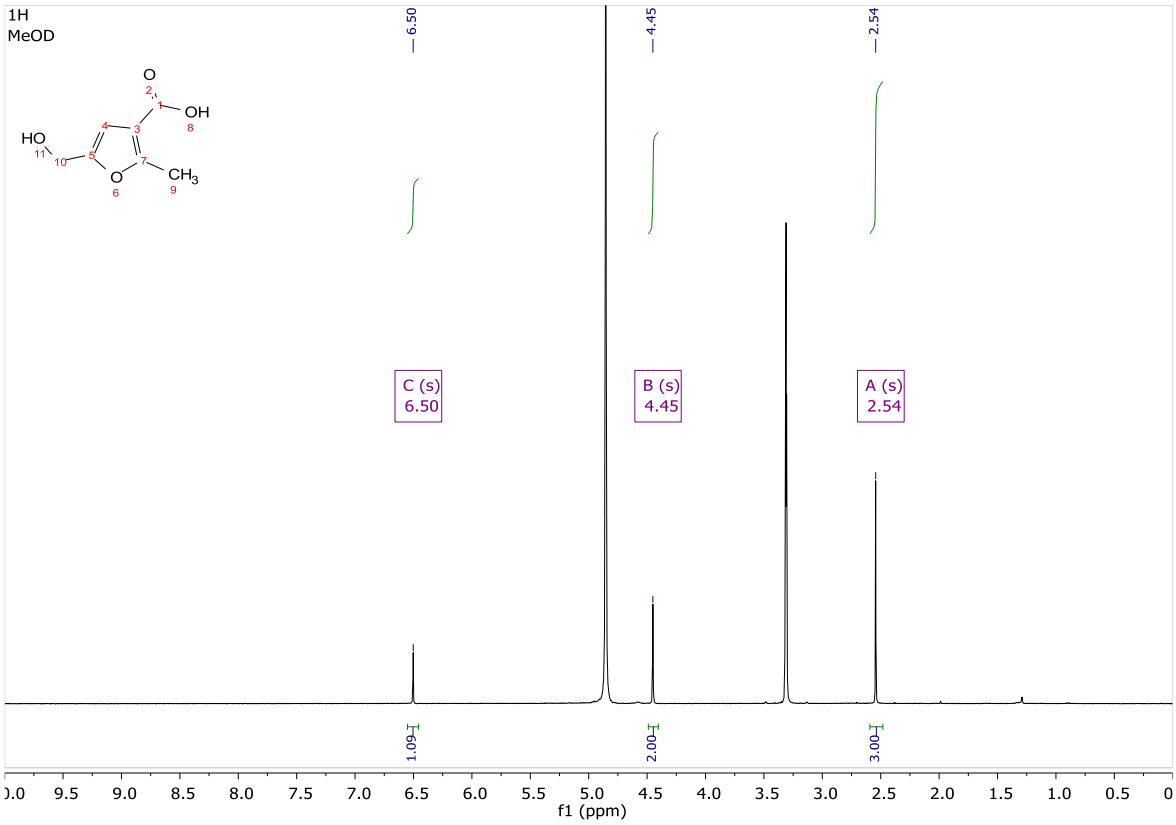
1H
MeOD
6.50
4.45
2.54
C (s)
6.50
B (s)
4.45
A (s)
2.54
1.09
2.00
3.00
f1 (ppm)

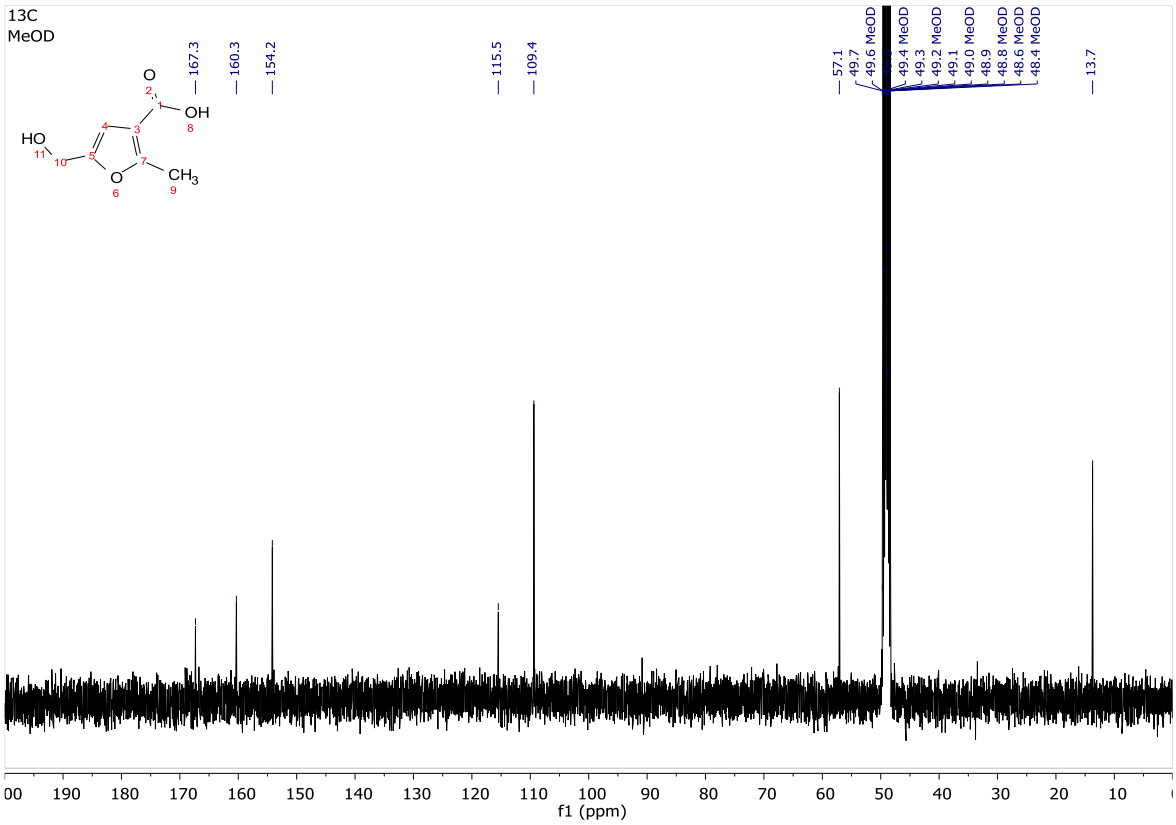
13C
MeOD
167.3
160.3
154.2
115.5
109.4
57.1
49.7
49.6 MeOD
49.4 MeOD
49.3
49.2 MeOD
49.1
49.0 MeOD
48.9
48.8 MeOD
48.6 MeOD
48.4 MeOD
13.7
f1 (ppm)

3.56b:

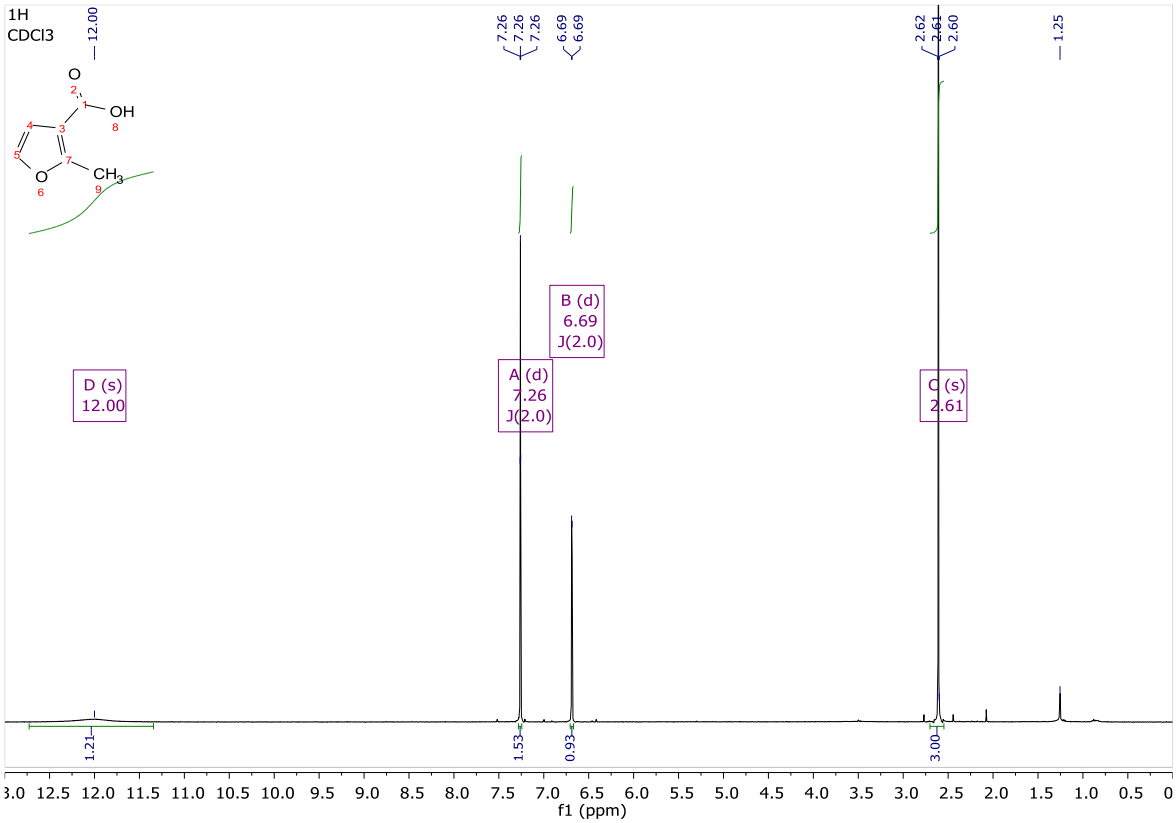
1H
CDCl3
12.00
7.26
7.26
7.26
6.69
6.69
2.62
2.61
2.60
1.25
O
OH
O
CH3
D (s)
12.00
B (d)
6.69
J(2.0)
A (d)
7.26
J(2.0)
C (s)
2.61
1.21
1.53
0.93
3.00
f1 (ppm)

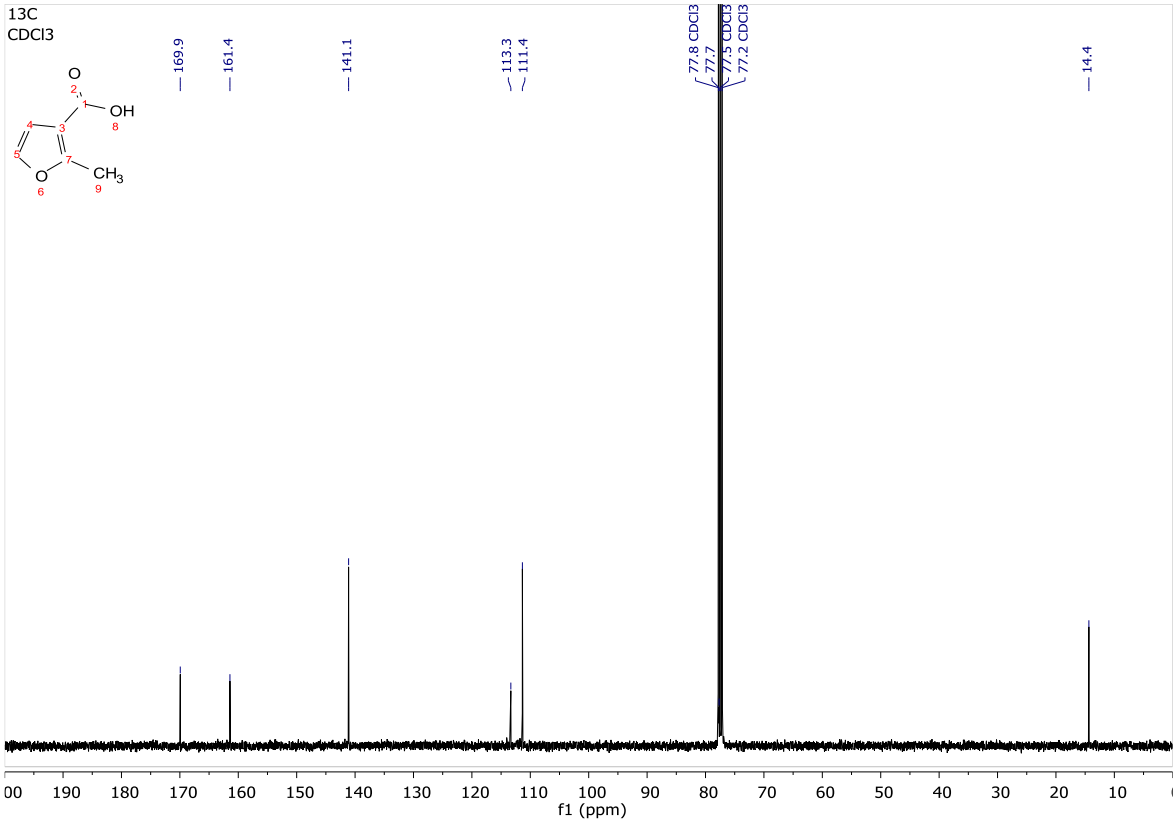
13C
CDCl3
169.9
161.4
141.1
113.3
111.4
77.8 CDCl3
77.7
77.5 CDCl3
77.2 CDCl3
14.4
O
OH
O
CH3
f1 (ppm)

3.57a:

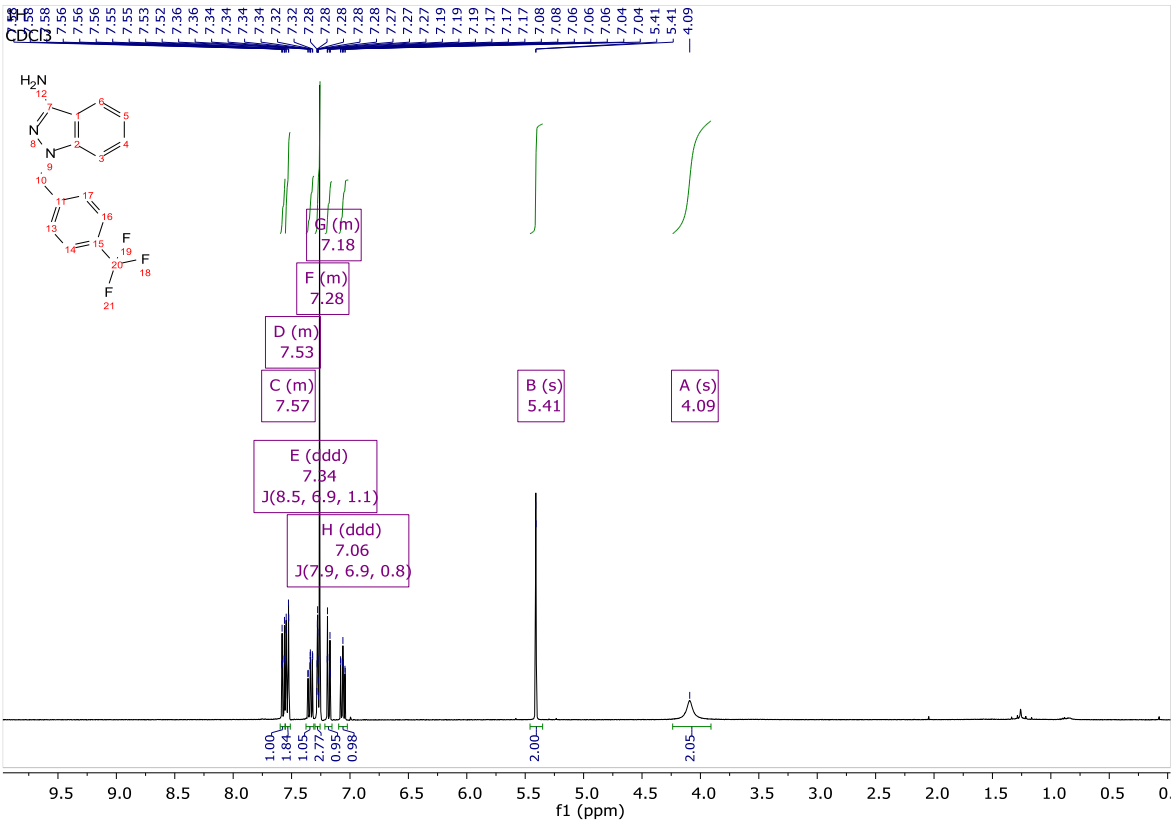
CDCl3
G (m)
7.18
F (m)
7.28
D (m)
7.53
C (m)
7.57
B (s)
5.41
A (s)
4.09
E (ddd)
7.34
J(8.5, 6.9, 1.1)
H (ddd)
7.06
J(7.9, 6.9, 0.8)
f1 (ppm)

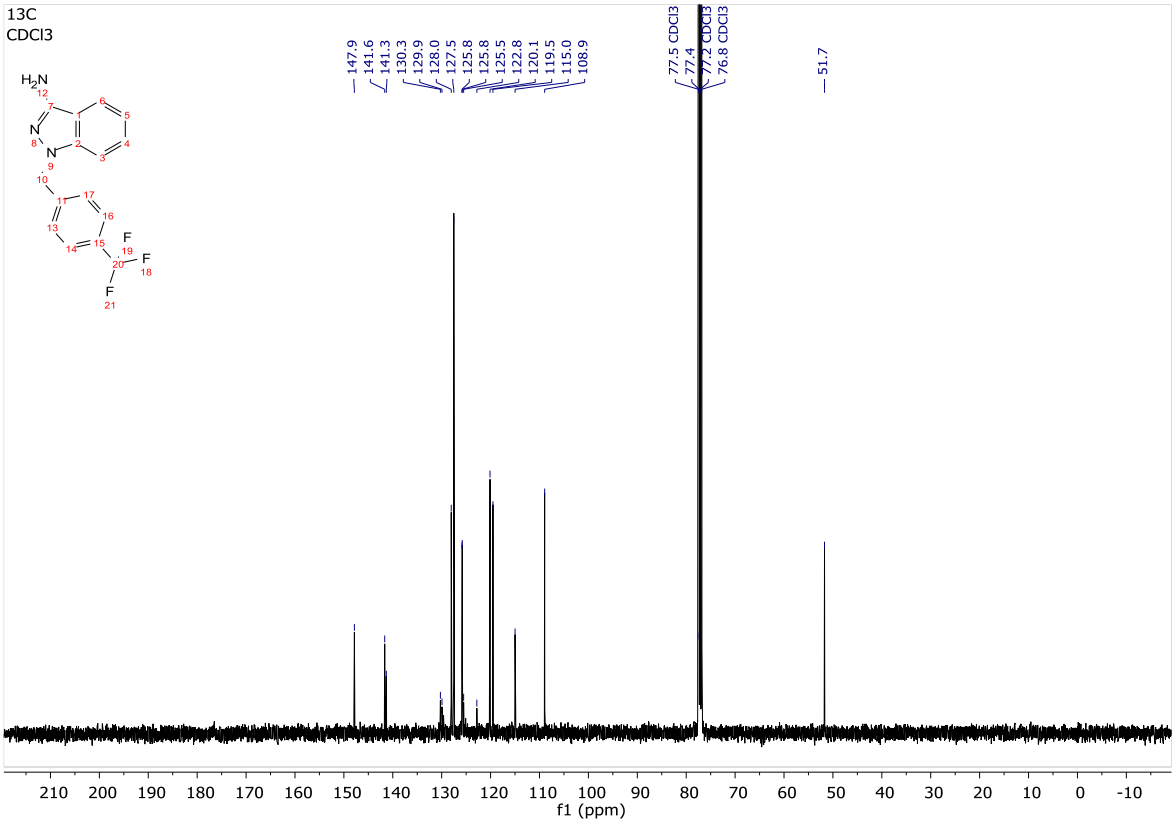
13C
CDCl3
f1 (ppm)

3.57b:

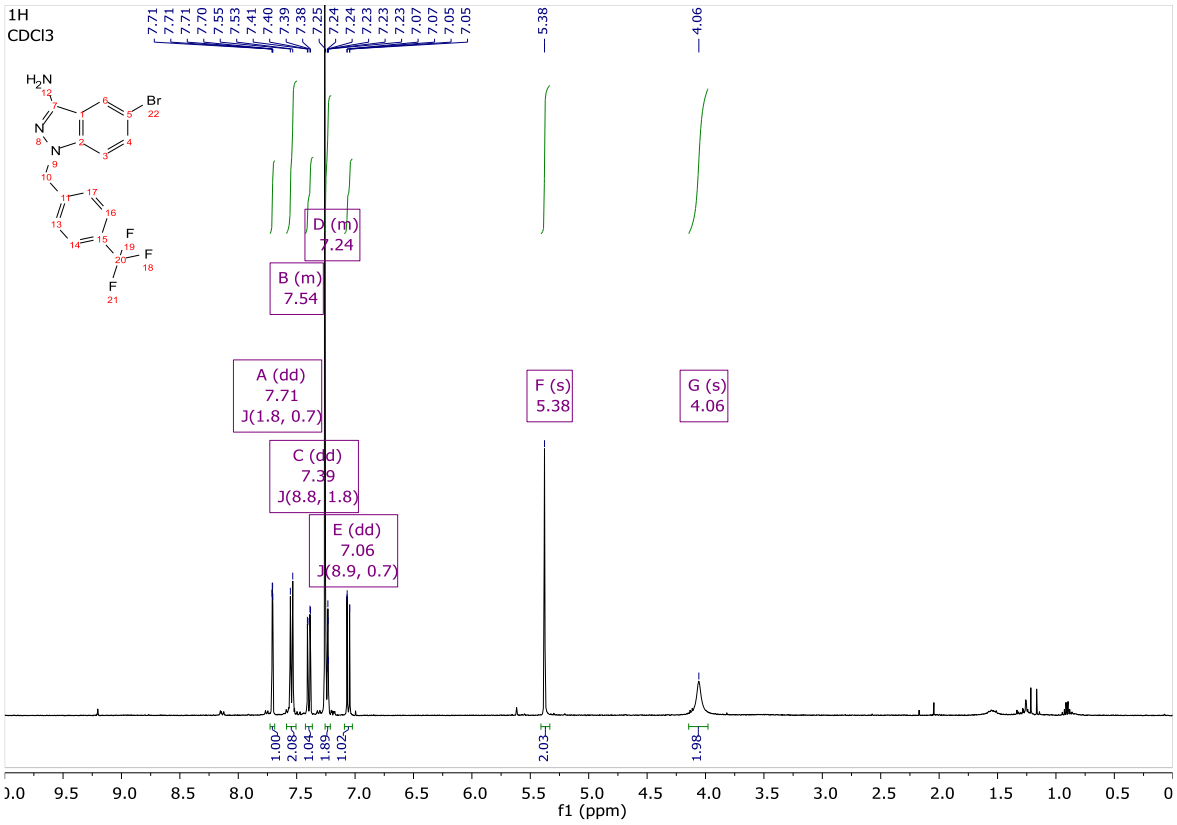
1H
CDCl3
D (m)
7.24
B (m)
7.54
A (dd)
7.71
J(1.8, 0.7)
C (dd)
7.39
J(8.8, 1.8)
E (dd)
7.06
J(8.9, 0.7)
F (s)
5.38
G (s)
4.06
f1 (ppm)

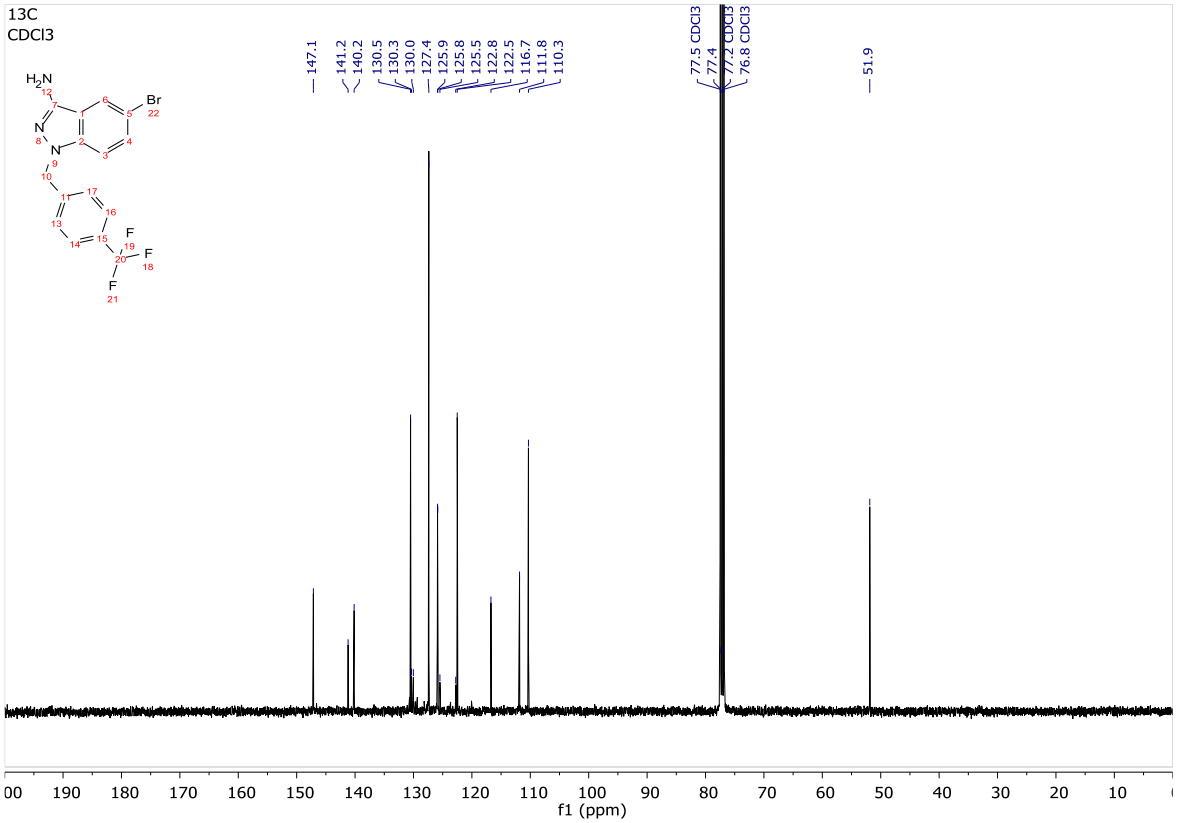
13C
CDCl3
f1 (ppm)

FSCN-C (1.7):

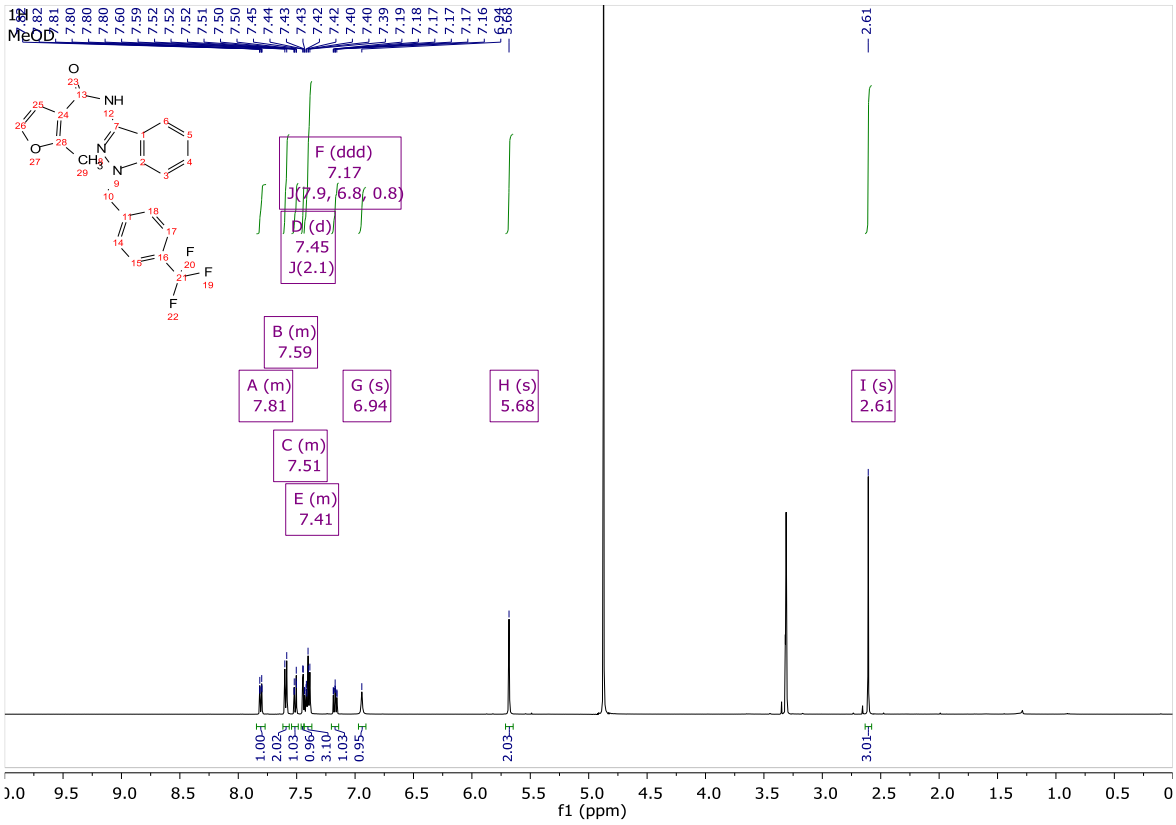
1H
MeOD
F (ddd)
7.17
J(7.9, 6.8, 0.8)
D (d)
7.45
J(2.1)
B (m)
7.59
A (m)
7.81
G (s)
6.94
H (s)
5.68
I (s)
2.61
C (m)
7.51
E (m)
7.41
f1 (ppm)

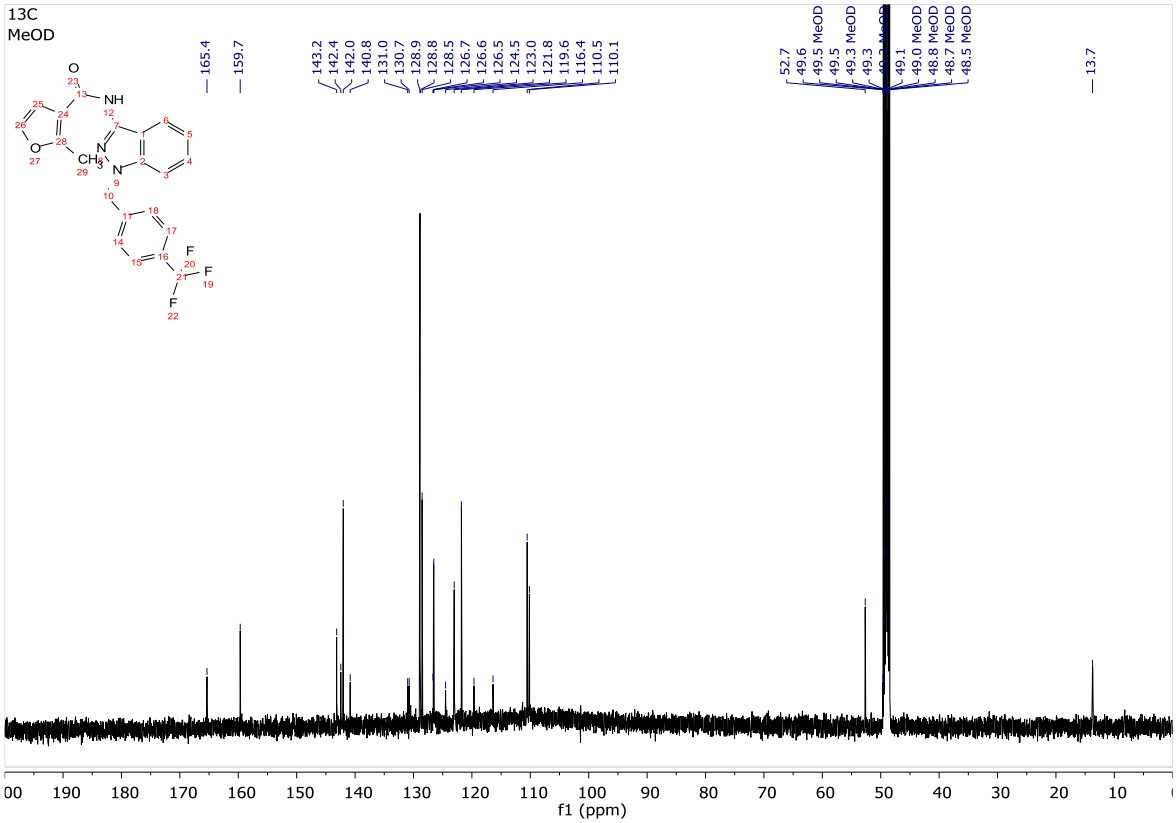
13C
MeOD
f1 (ppm)

3.52:

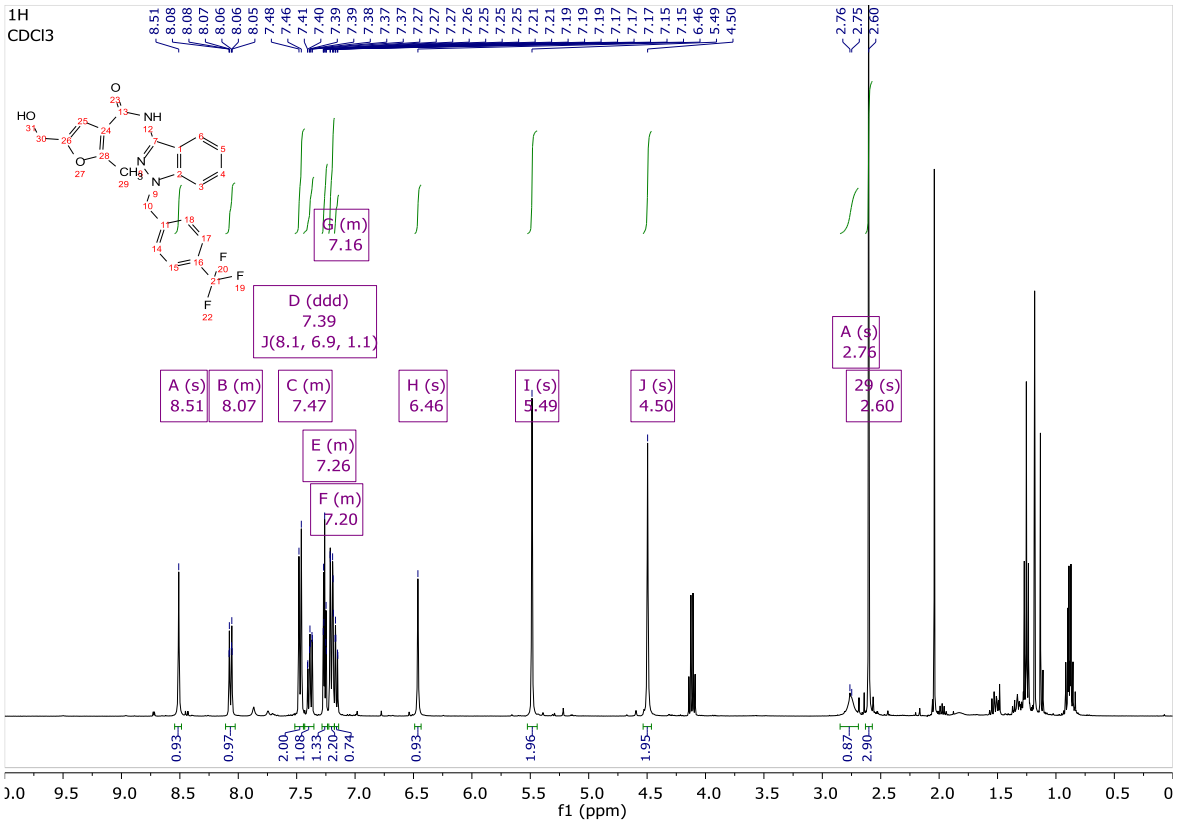
1H
CDCl3
G (m)
7.16
D (ddd)
7.39
J(8.1, 6.9, 1.1)
A (s)
8.51
B (m)
8.07
C (m)
7.47
H (s)
6.46
I (s)
5.49
J (s)
4.50
A (s)
2.75
29 (s)
2.60
E (m)
7.26
F (m)
7.20
f1 (ppm)

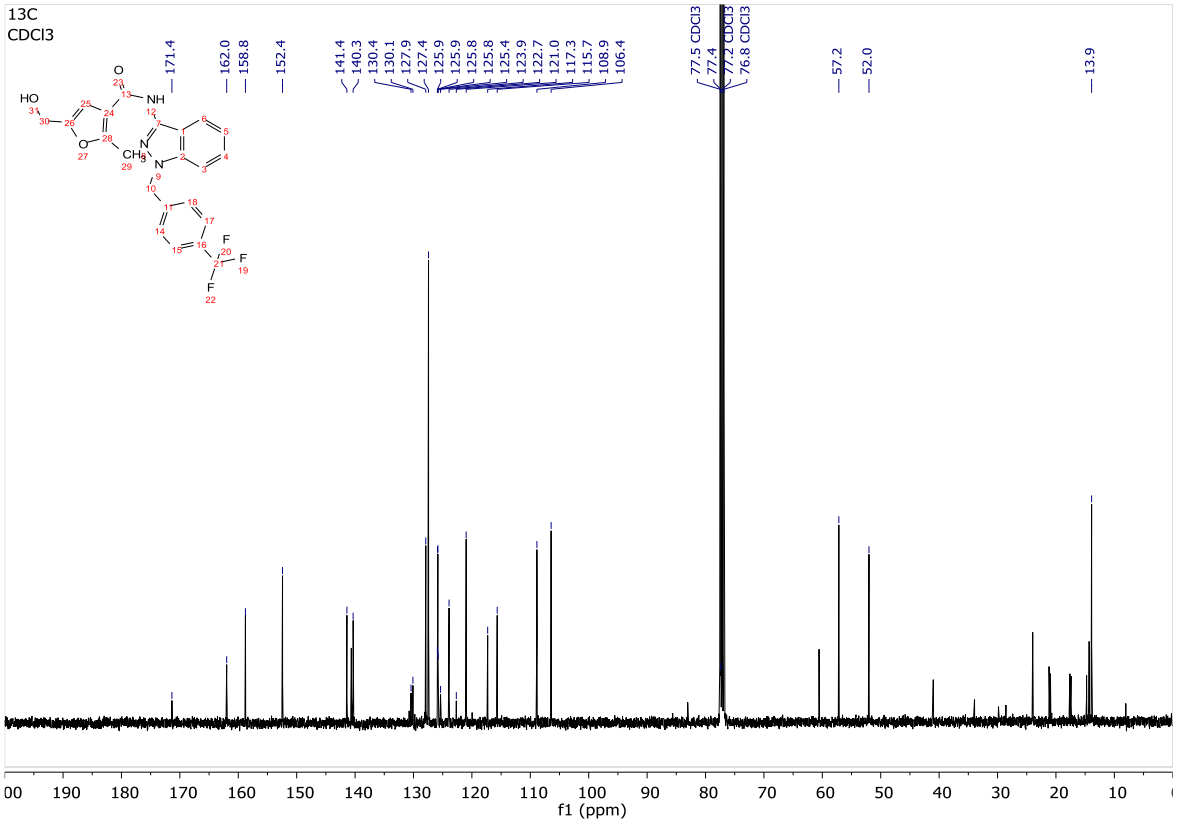
13C
CDCl3
f1 (ppm)

3.53:

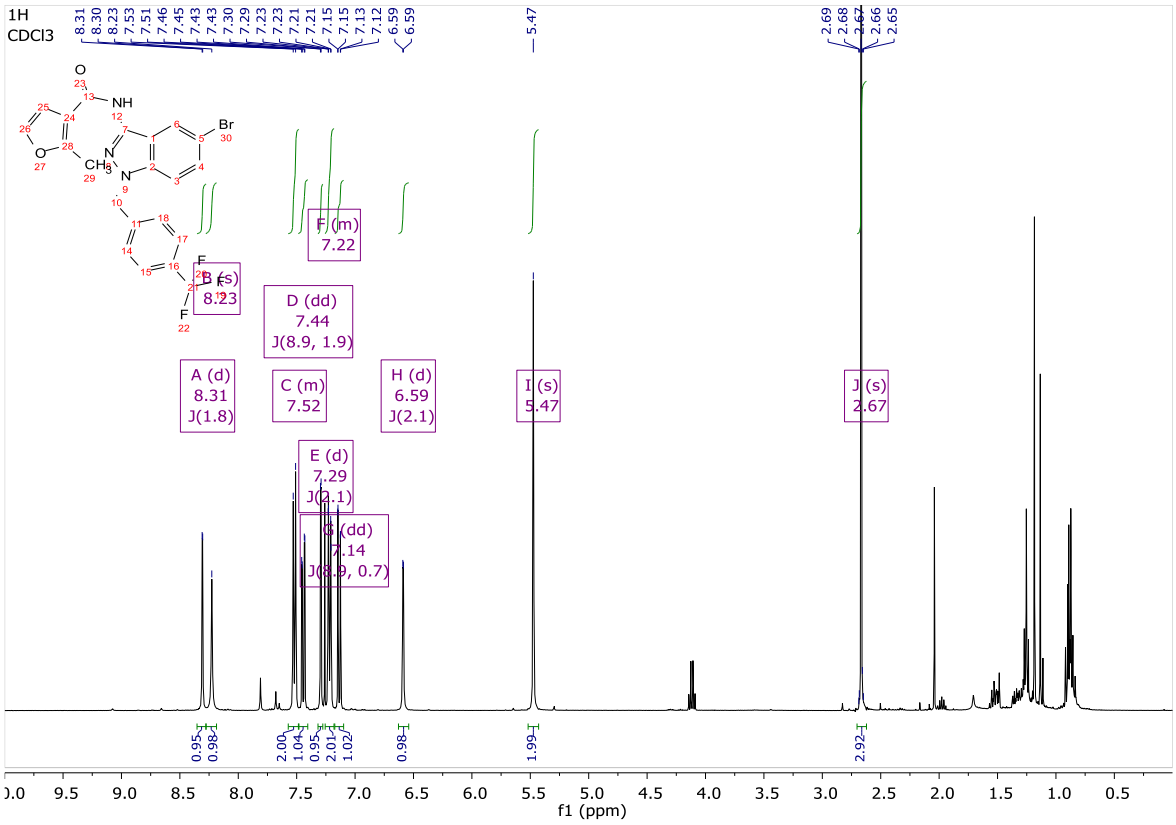
1H
CDCl3
F (m)
7.22
B (s)
8.23
D (dd)
7.44
J(8.9, 1.9)
A (d)
8.31
J(1.8)
C (m)
7.52
H (d)
6.59
J(2.1)
I (s)
5.47
J (s)
2.67
E (d)
7.29
J(2.1)
G (dd)
7.14
J(8.9, 0.7)
f1 (ppm)

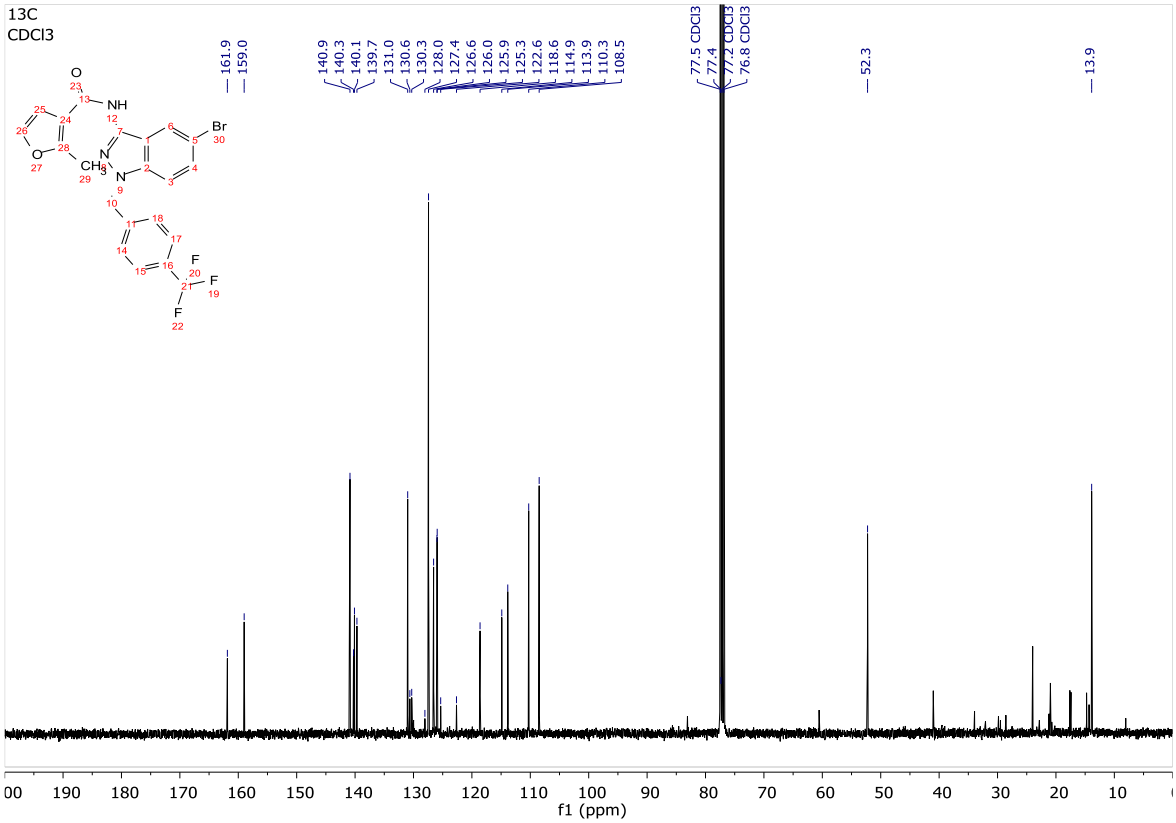
13C
CDCl3
77.5 CDCl3
77.4
77.2 CDCl3
76.8 CDCl3
52.3
13.9
f1 (ppm)

3rd series PROTACs

3.59:

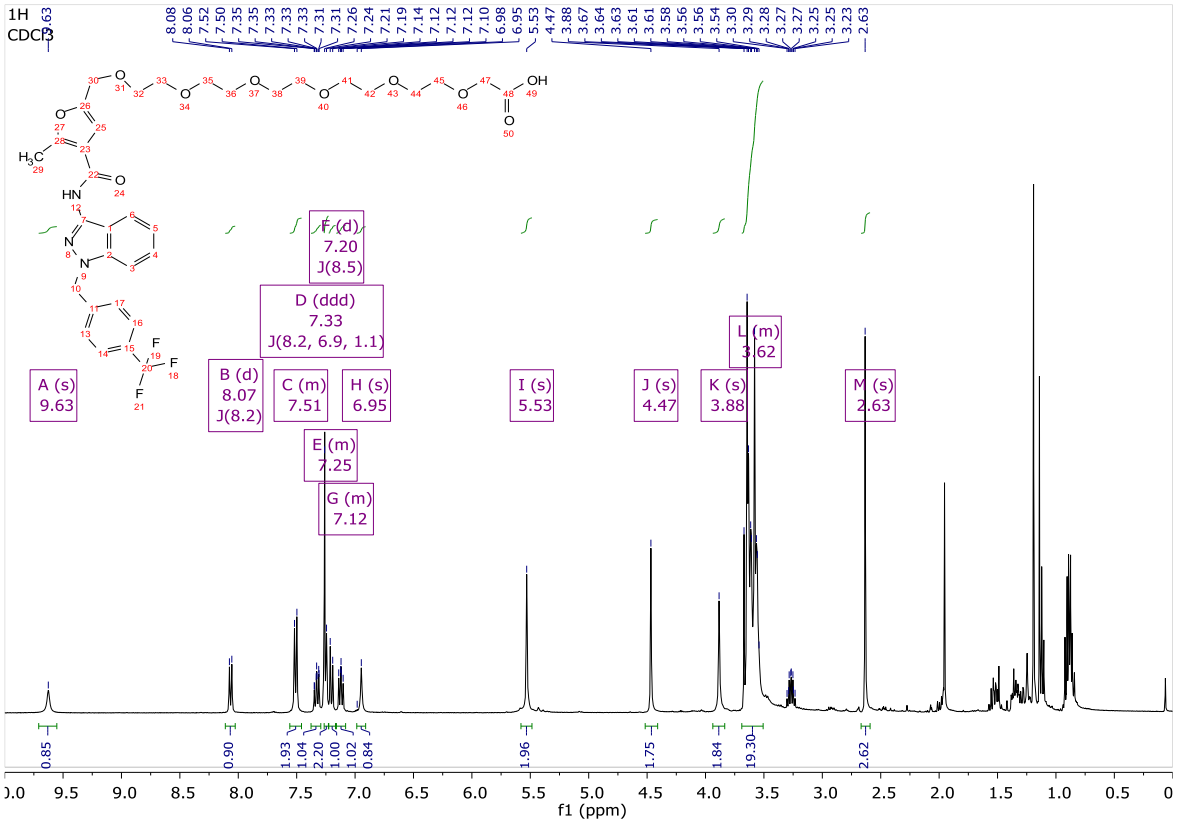

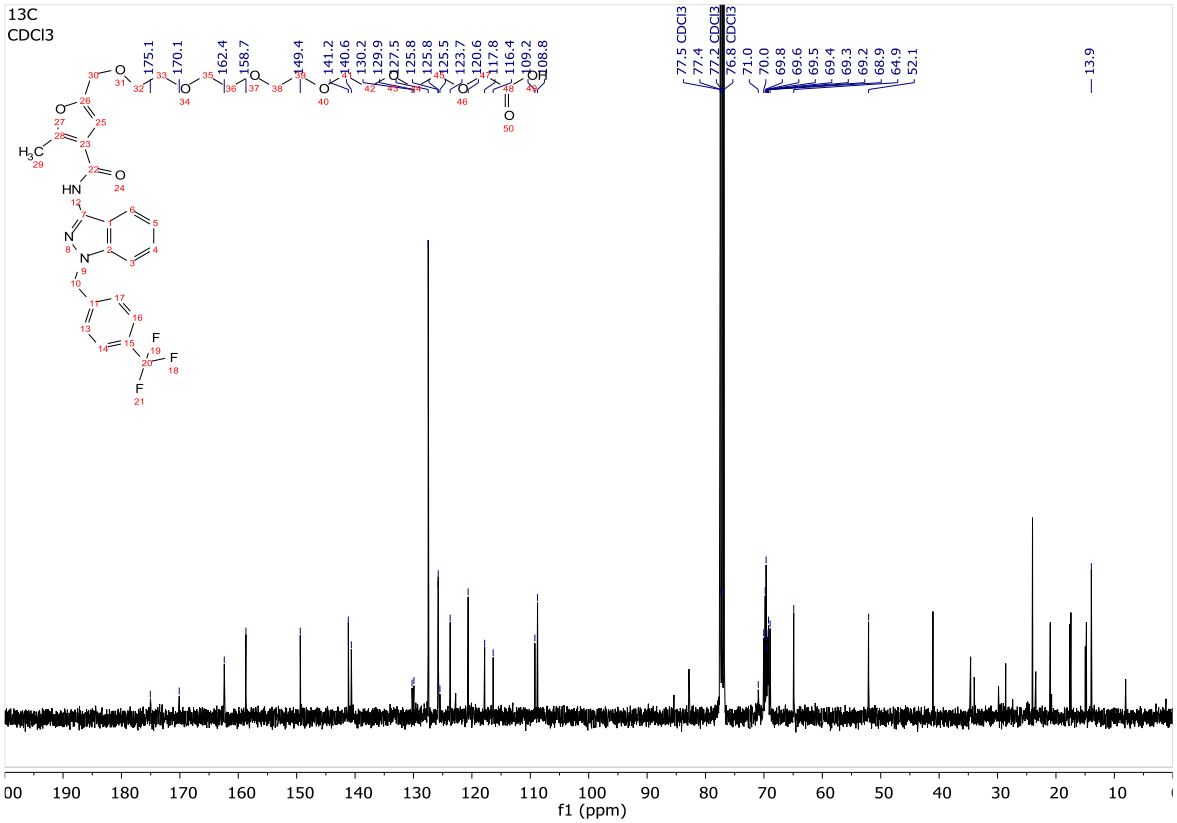

FSCN-C-VHL-1 (3.60):

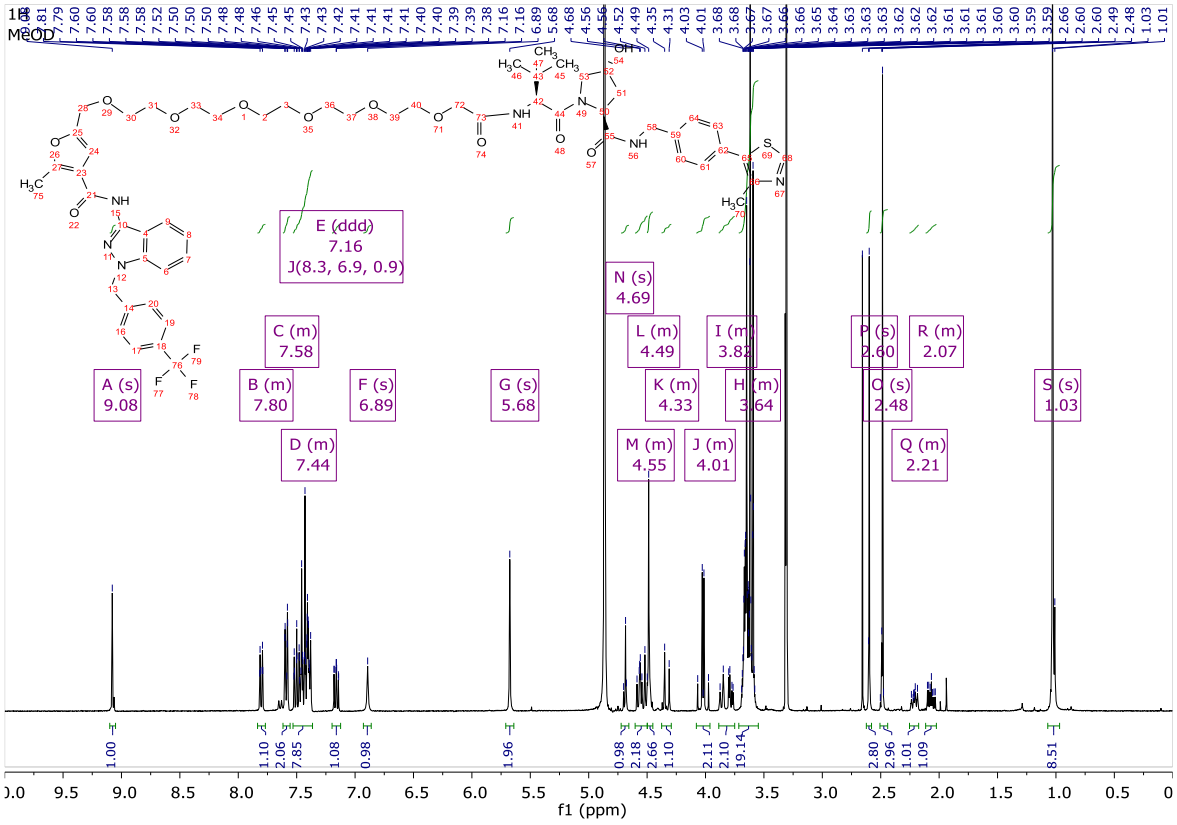

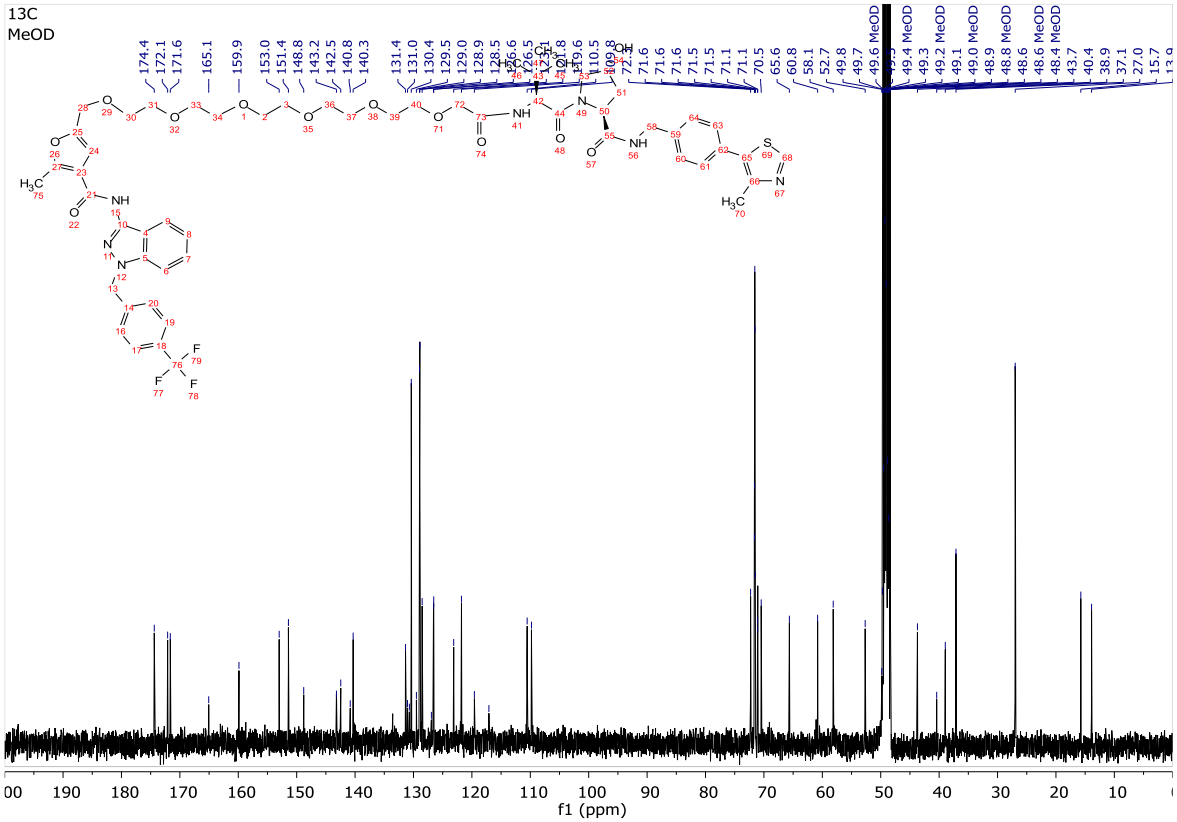

3.61c:

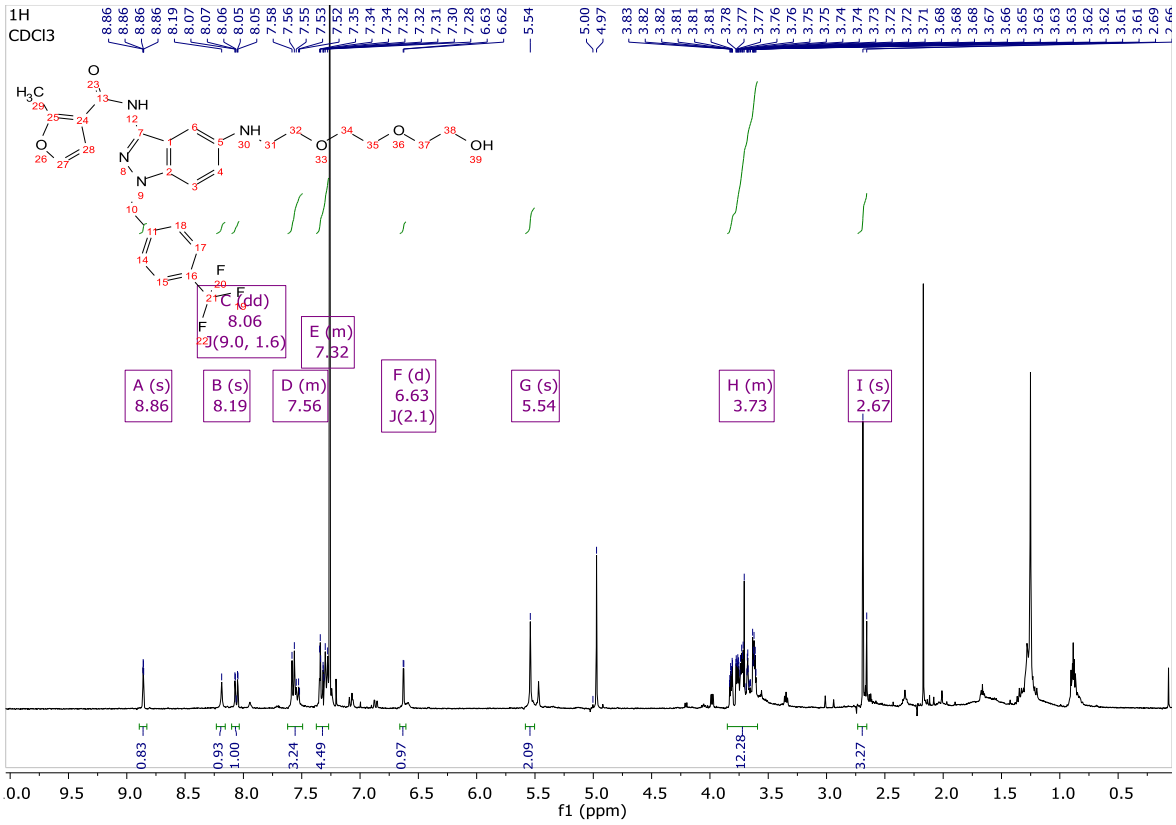
1H
CDCl3
C (dd)
8.06
J(9.0, 1.6)
E (m)
7.32
A (s)
8.86
B (s)
8.19
D (m)
7.56
F (d)
6.63
J(2.1)
G (s)
5.54
H (m)
3.73
I (s)
2.67
f1 (ppm)

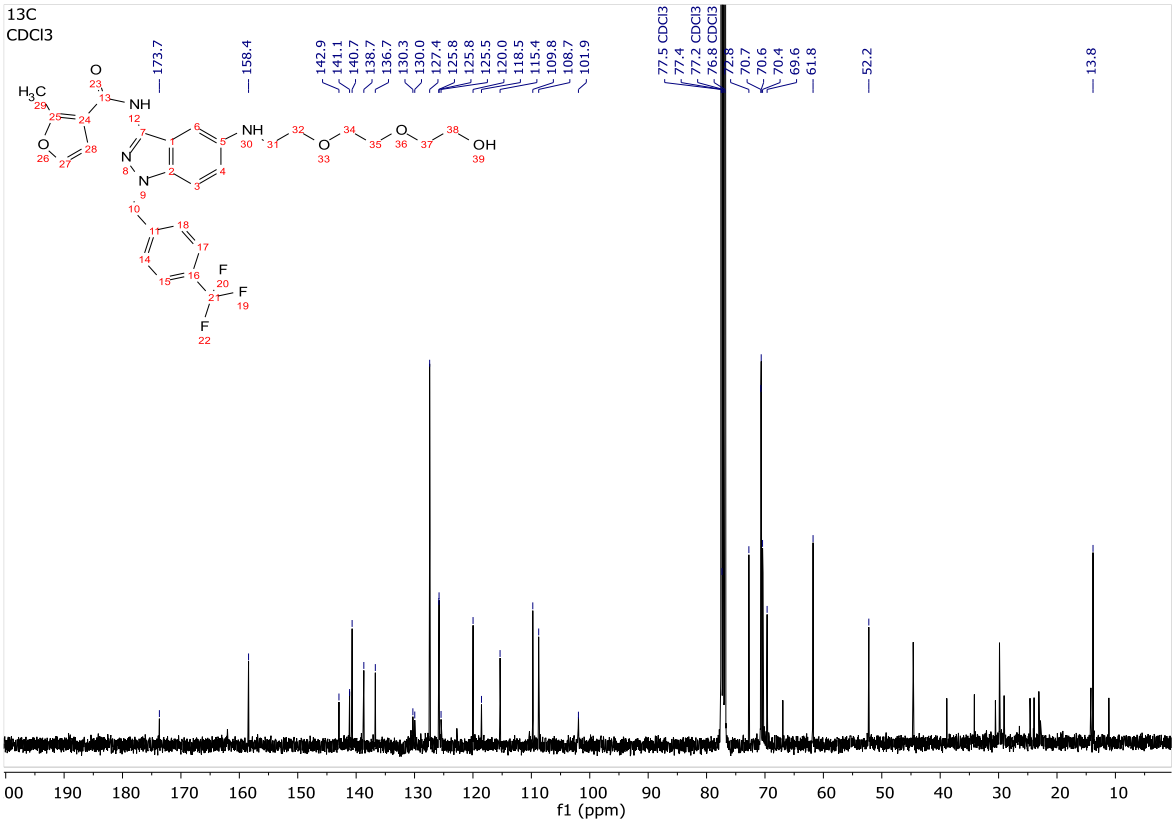
13C
CDCl3
f1 (ppm)

X-ray diffraction data for FSCN-B (1.5)

Structure report for 2019GU34 / SM-100

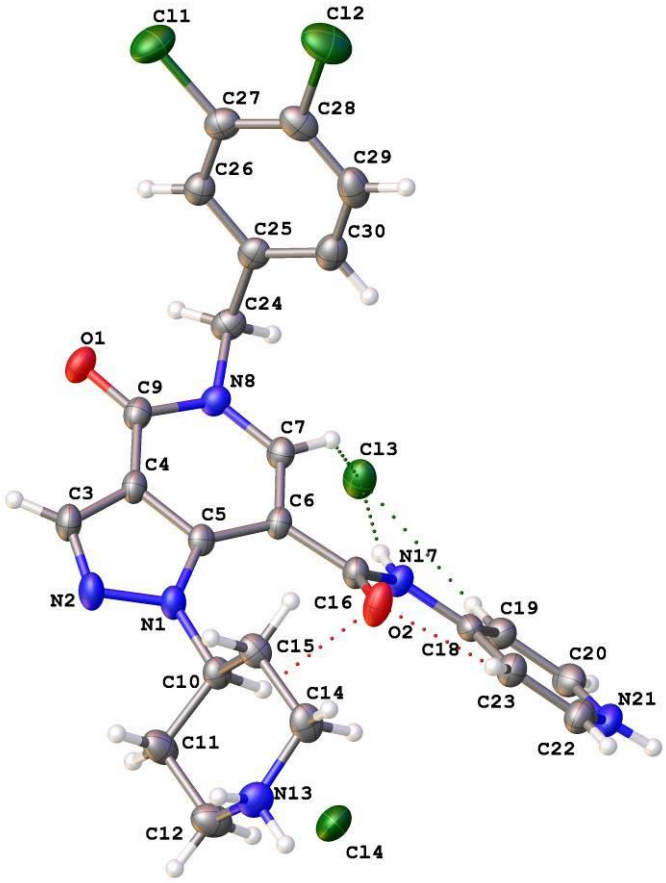

View showing the structure and atom labelling scheme for SM-100; atomic displacement ellipsoids drawn at 50% probability level. 0.5 molecule of cyclohexane (per molecule) omitted for clarity. A region of poorly defined solvent was accounted for using SQUEEZE.

Refinement

Crystal data, data collection and structure refinement details are summarized in Table 1.

Computing details

Data collection: *APEX3* Ver. 2016.9-0 (Bruker-AXS, 2016); cell refinement: *SAINT* V8.37A (Bruker-AXS, 2016); data reduction: *APEX3* Ver. 2016.9-0 (Bruker-AXS, 2016); program(s) used to solve structure: SHELXT 2014/5 (Sheldrick, 2014); program(s) used to refine structure: XL (Sheldrick, 2008); molecular graphics: Olex2 (Dolomanov *et al.*, 2009); software used to prepare material for publication: Olex2 (Dolomanov *et al.*, 2009).

References

Dolomanov, O. V., Bourhis, L. J., Gildea, R. J., Howard, J. A. K. & Puschmann, H. (2009). *J. Appl. Cryst.* **42**, 339–341.
Sheldrick, G. M. (2008). *Acta Cryst.* A**64**, 112–122.

(2019gu0034_150k_sq)

Crystal data

$C_{24}H_{24}Cl_2N_6O_2 \cdot 2(Cl) \cdot C_3H_6$	$F(000) = 1272$
$M_r = 612.37$	$D_x = 1.370$ Mg m^{-3}
Monoclinic, $P2_1/c$	Mo $K\alpha$ radiation, $\lambda = 0.71073$ Å
$a = 19.2837$ (6) Å	Cell parameters from 9975 reflections
$b = 12.1401$ (4) Å	$\theta = 2.5–26.4°$
$c = 12.6821$ (4) Å	$\mu = 0.43$ mm^{-1}
$\beta = 90.670$ (1)°	$T = 150$ K
$V = 2968.75$ (16) Å^3	Hexagonal, colourless
$Z = 4$	0.17 × 0.08 × 0.02 mm

Data collection

Bruker D8 VENTURE diffractometer	6045 independent reflections
Radiation source: microfocus sealed tube, INCOATEC Iμs 3.0	5227 reflections with $I > 2\sigma(I)$
Multilayer mirror optics monochromator	$R_{int} = 0.036$
Detector resolution: 7.4074 pixels mm^{-1}	$\theta_{max} = 26.4°$, $\theta_{min} = 2.3°$
ω and φ scans	$h = -24\rightarrow24$
Absorption correction: multi-scan *SADABS2016*/2 (Bruker,2016/2) was used for absorption correction. wR2(int) was 0.1005 before and 0.0547 after correction. The Ratio of minimum to maximum transmission is 0.8785. The $\lambda/2$ correction factor is Not present.	$k = -13\rightarrow15$
$T_{min} = 0.655$, $T_{max} = 0.745$	$l = -15\rightarrow11$
26464 measured reflections	

Refinement

Refinement on F^2	0 restraints
Least-squares matrix: full	Hydrogen site location: mixed
$R[F^2 > 2\sigma(F^2)] = 0.041$	H atoms treated by a mixture of independent and constrained refinement
$wR(F^2) = 0.114$	$w = 1/[\sigma^2(F_o^2) + (0.0514P)^2 + 2.2569P]$ where $P = (F_o^2 + 2F_c^2)/3$
$S = 1.04$	$(\Delta/\sigma)_{max} = 0.001$
6045 reflections	$\Delta\rho_{max} = 0.63$ e Å^{-3}
364 parameters	$\Delta\rho_{min} = -0.51$ e Å^{-3}

Special details

Geometry. All esds (except the esd in the dihedral angle between two l.s. planes) are estimated using the full covariance matrix. The cell esds are taken into account individually in the estimation of esds in distances, angles and torsion angles; correlations between esds in cell parameters are only used when they are defined by crystal symmetry. An approximate (isotropic) treatment of cell esds is used for estimating esds involving l.s. planes.

Fractional atomic coordinates and isotropic or equivalent isotropic displacement

parameters (Å²)

	x	*y*	*z*	U_{iso}*/U_{eq}
Cl1	0.61538 (3)	0.14297 (6)	0.35593 (5)	0.04913 (17)
Cl2	0.65465 (3)	0.17386 (6)	0.59589 (6)	0.05507 (18)
O1	0.35084 (8)	0.28542 (12)	0.31084 (10)	0.0346 (3)
O2	0.22189 (8)	0.42530 (11)	0.75366 (11)	0.0366 (3)
N1	0.22450 (8)	0.52511 (13)	0.51047 (12)	0.0251 (3)
N2	0.23855 (9)	0.57386 (14)	0.41528 (12)	0.0310 (4)
N8	0.31831 (8)	0.22513 (13)	0.47389 (12)	0.0254 (3)
N13	0.14121 (10)	0.78390 (15)	0.70033 (15)	0.0333 (4)
H13A	0.1576 (14)	0.841 (2)	0.667 (2)	0.047 (7)*
H13B	0.1138 (13)	0.812 (2)	0.750 (2)	0.043 (7)*
N17	0.18643 (8)	0.24750 (13)	0.73057 (12)	0.0248 (3)
H17	0.189583	0.190508	0.688027	0.030*
N21	0.06977 (9)	0.19182 (15)	0.99492 (14)	0.0333 (4)
H21	0.0440 (15)	0.169 (2)	1.050 (2)	0.057 (8)*
C3	0.27476 (11)	0.50159 (16)	0.36188 (15)	0.0304 (4)
H3	0.291424	0.513325	0.292591	0.036*
C4	0.28566 (10)	0.40467 (16)	0.42044 (14)	0.0246 (4)
C5	0.25282 (9)	0.42276 (15)	0.51644 (14)	0.0224 (4)
C6	0.25171 (9)	0.33618 (15)	0.59405 (14)	0.0234 (4)
C7	0.28546 (9)	0.24211 (15)	0.56696 (14)	0.0252 (4)
H7	0.286163	0.183733	0.616847	0.030*
C9	0.32094 (10)	0.30491 (16)	0.39374 (14)	0.0264 (4)
C10	0.18758 (10)	0.58969 (15)	0.58959 (14)	0.0252 (4)
H10	0.161724	0.537650	0.635941	0.030*
C11	0.13557 (11)	0.66843 (18)	0.53894 (17)	0.0355 (5)
H11A	0.160259	0.724460	0.496857	0.043*
H11B	0.103880	0.627324	0.491216	0.043*
C12	0.09428 (11)	0.7244 (2)	0.62527 (18)	0.0397 (5)
H12A	0.061125	0.777158	0.593080	0.048*
H12B	0.067355	0.668345	0.664073	0.048*
C14	0.19741 (11)	0.71327 (17)	0.74536 (16)	0.0339 (5)
H14A	0.176930	0.657091	0.792240	0.041*
H14B	0.229484	0.759190	0.788166	0.041*
C15	0.23750 (10)	0.65653 (16)	0.65859 (15)	0.0289 (4)
H15A	0.273031	0.607242	0.690025	0.035*
H15B	0.261397	0.712248	0.615092	0.035*
C16	0.21983 (10)	0.34320 (15)	0.69980 (14)	0.0251 (4)
C18	0.14867 (9)	0.23279 (15)	0.82146 (14)	0.0240 (4)
C19	0.11384 (10)	0.13246 (16)	0.83260 (16)	0.0294 (4)
H19	0.117173	0.077399	0.779677	0.035*
C20	0.07493 (10)	0.11440 (18)	0.92042 (17)	0.0331 (4)
H20	0.051361	0.046260	0.928553	0.040*
C22	0.10234 (11)	0.28820 (18)	0.98590 (16)	0.0333 (4)
H22	0.097320	0.341883	1.039772	0.040*
C23	0.14285 (10)	0.31161 (17)	0.90083 (15)	0.0295 (4)
H23	0.166474	0.380063	0.895988	0.035*
C24	0.35627 (10)	0.12076 (16)	0.45880 (16)	0.0291 (4)
H24A	0.354274	0.099690	0.383416	0.035*
H24B	0.333835	0.061656	0.499980	0.035*

C25	0.43122 (10)	0.13213 (15)	0.49381 (15)	0.0272 (4)
C26	0.48327 (10)	0.13262 (15)	0.41961 (15)	0.0279 (4)
H26	0.471904	0.125185	0.346871	0.034*
C27	0.55203 (10)	0.14396 (16)	0.45124 (17)	0.0311 (4)
C28	0.56890 (11)	0.15634 (16)	0.55653 (18)	0.0347 (5)
C29	0.51753 (12)	0.15623 (17)	0.63113 (17)	0.0372 (5)
H29	0.529197	0.164551	0.703677	0.045*
C30	0.44898 (11)	0.14397 (17)	0.60024 (16)	0.0334 (4)
H30	0.413668	0.143610	0.651852	0.040*
Cl3	0.19230 (3)	0.00421 (4)	0.60410 (4)	0.03699 (14)
Cl4	-0.00811 (3)	0.37615 (6)	0.68736 (4)	0.04690 (16)
C1S	0.53880 (17)	0.4548 (2)	0.5889 (2)	0.0631 (8)
H1SA	0.559454	0.521331	0.621734	0.076*
H1SB	0.553690	0.390097	0.630888	0.076*
C2S	0.46037 (17)	0.4638 (2)	0.5910 (3)	0.0651 (8)
H2SA	0.439625	0.393701	0.566193	0.078*
H2SB	0.445268	0.476370	0.664372	0.078*
C3S	0.43495 (16)	0.5567 (2)	0.5222 (3)	0.0623 (8)
H3SA	0.450967	0.627679	0.552145	0.075*
H3SB	0.383605	0.557082	0.520967	0.075*

Atomic displacement parameters (Å²)

	U^{11}	U^{22}	U^{33}	U^{12}	U^{13}	U^{23}
Cl1	0.0355 (3)	0.0622 (4)	0.0500 (3)	-0.0071 (3)	0.0115 (2)	-0.0092 (3)
Cl2	0.0416 (3)	0.0566 (4)	0.0665 (4)	0.0017 (3)	-0.0205 (3)	-0.0125 (3)
O1	0.0422 (8)	0.0389 (8)	0.0228 (7)	0.0013 (6)	0.0089 (6)	-0.0035 (6)
O2	0.0613 (10)	0.0258 (7)	0.0228 (7)	-0.0071 (7)	0.0084 (6)	-0.0024 (6)
N1	0.0342 (8)	0.0230 (8)	0.0181 (7)	-0.0007 (6)	-0.0009 (6)	0.0004 (6)
N2	0.0441 (10)	0.0280 (8)	0.0209 (8)	0.0002 (7)	0.0001 (7)	0.0051 (7)
N8	0.0279 (8)	0.0231 (8)	0.0253 (8)	-0.0012 (6)	0.0037 (6)	-0.0014 (6)
N13	0.0393 (10)	0.0266 (9)	0.0340 (10)	-0.0001 (8)	0.0027 (8)	-0.0058 (8)
N17	0.0310 (8)	0.0223 (8)	0.0211 (8)	-0.0015 (6)	0.0051 (6)	-0.0008 (6)
N21	0.0302 (9)	0.0419 (10)	0.0280 (9)	-0.0009 (7)	0.0074 (7)	0.0062 (8)
C3	0.0395 (11)	0.0315 (10)	0.0202 (9)	-0.0016 (8)	0.0008 (8)	0.0035 (8)
C4	0.0287 (9)	0.0278 (9)	0.0174 (8)	-0.0043 (7)	-0.0011 (7)	0.0000 (7)
C5	0.0262 (9)	0.0222 (9)	0.0188 (8)	-0.0043 (7)	-0.0028 (7)	-0.0021 (7)
C6	0.0274 (9)	0.0244 (9)	0.0184 (8)	-0.0041 (7)	0.0002 (7)	0.0004 (7)
C7	0.0290 (9)	0.0228 (9)	0.0237 (9)	-0.0028 (7)	0.0017 (7)	0.0025 (7)
C9	0.0272 (9)	0.0306 (10)	0.0214 (9)	-0.0049 (7)	0.0002 (7)	-0.0008 (7)
C10	0.0306 (9)	0.0228 (9)	0.0221 (9)	-0.0009 (7)	-0.0026 (7)	-0.0025 (7)
C11	0.0386 (11)	0.0354 (11)	0.0321 (11)	0.0075 (9)	-0.0118 (9)	-0.0077 (9)
C12	0.0353 (11)	0.0406 (12)	0.0431 (12)	0.0055 (9)	-0.0069 (9)	-0.0101 (10)
C14	0.0453 (12)	0.0275 (10)	0.0287 (10)	-0.0016 (9)	-0.0067 (9)	-0.0059 (8)
C15	0.0321 (10)	0.0246 (9)	0.0300 (10)	-0.0026 (8)	-0.0070 (8)	-0.0035 (8)
C16	0.0306 (9)	0.0245 (9)	0.0202 (9)	0.0000 (7)	0.0005 (7)	0.0015 (7)
C18	0.0229 (8)	0.0268 (9)	0.0222 (9)	0.0033 (7)	0.0009 (7)	0.0048 (7)
C19	0.0302 (10)	0.0266 (10)	0.0314 (10)	0.0005 (8)	0.0035 (8)	0.0011 (8)
C20	0.0304 (10)	0.0324 (10)	0.0365 (11)	-0.0016 (8)	0.0048 (8)	0.0066 (9)
C22	0.0347 (10)	0.0400 (12)	0.0253 (10)	-0.0005 (9)	0.0028 (8)	-0.0016 (8)
C23	0.0332 (10)	0.0296 (10)	0.0256 (10)	-0.0015 (8)	0.0023 (8)	0.0001 (8)

C24	0.0321 (10)	0.0222 (9)	0.0331 (10)	-0.0010 (8)	0.0048 (8)	-0.0042 (8)
C25	0.0342 (10)	0.0176 (8)	0.0298 (10)	0.0011 (7)	0.0034 (8)	-0.0019 (7)
C26	0.0335 (10)	0.0235 (9)	0.0269 (9)	-0.0005 (8)	0.0016 (8)	-0.0021 (7)
C27	0.0325 (10)	0.0242 (9)	0.0365 (11)	0.0001 (8)	0.0037 (8)	-0.0032 (8)
C28	0.0377 (11)	0.0242 (10)	0.0420 (12)	0.0026 (8)	-0.0100 (9)	-0.0046 (9)
C29	0.0530 (13)	0.0297 (11)	0.0287 (10)	0.0031 (9)	-0.0065 (9)	-0.0020 (8)
C30	0.0448 (12)	0.0271 (10)	0.0284 (10)	0.0021 (9)	0.0043 (9)	-0.0012 (8)
Cl3	0.0505 (3)	0.0272 (2)	0.0333 (3)	0.0011 (2)	0.0039 (2)	0.0023 (2)
Cl4	0.0459 (3)	0.0613 (4)	0.0339 (3)	0.0108 (3)	0.0136 (2)	0.0029 (3)
C1S	0.080 (2)	0.0405 (14)	0.0678 (19)	0.0002 (13)	-0.0387 (16)	0.0066 (13)
C2S	0.085 (2)	0.0412 (14)	0.0683 (19)	-0.0134 (14)	-0.0186 (16)	0.0040 (13)
C3S	0.0651 (17)	0.0421 (14)	0.079 (2)	-0.0017 (13)	-0.0270 (15)	-0.0056 (14)

Geometric parameters (Å, º) for (2019gu0034_150k_sq)

Cl1—C27	1.729 (2)	C12—H12B	0.9900
Cl2—C28	1.735 (2)	C14—H14A	0.9900
O1—C9	1.228 (2)	C14—H14B	0.9900
O2—C16	1.209 (2)	C14—C15	1.518 (3)
N1—N2	1.374 (2)	C15—H15A	0.9900
N1—C5	1.359 (2)	C15—H15B	0.9900
N1—C10	1.465 (2)	C18—C19	1.399 (3)
N2—C3	1.314 (3)	C18—C23	1.394 (3)
N8—C7	1.362 (2)	C19—H19	0.9500
N8—C9	1.405 (2)	C19—C20	1.368 (3)
N8—C24	1.477 (2)	C20—H20	0.9500
N13—H13A	0.87 (3)	C22—H22	0.9500
N13—H13B	0.89 (3)	C22—C23	1.369 (3)
N13—C12	1.492 (3)	C23—H23	0.9500
N13—C14	1.491 (3)	C24—H24A	0.9900
N17—H17	0.8800	C24—H24B	0.9900
N17—C16	1.387 (2)	C24—C25	1.513 (3)
N17—C18	1.382 (2)	C25—C26	1.384 (3)
N21—H21	0.90 (3)	C25—C30	1.396 (3)
N21—C20	1.337 (3)	C26—H26	0.9500
N21—C22	1.334 (3)	C26—C27	1.388 (3)
C3—H3	0.9500	C27—C28	1.379 (3)
C3—C4	1.406 (3)	C28—C29	1.378 (3)
C4—C5	1.396 (2)	C29—H29	0.9500
C4—C9	1.432 (3)	C29—C30	1.382 (3)
C5—C6	1.440 (3)	C30—H30	0.9500
C6—C7	1.361 (3)	C1S—H1SA	0.9900
C6—C16	1.484 (2)	C1S—H1SB	0.9900
C7—H7	0.9500	C1S—C2S	1.517 (5)
C10—H10	1.0000	C1S—C3S^{i}	1.509 (4)
C10—C11	1.522 (3)	C2S—H2SA	0.9900
C10—C15	1.527 (3)	C2S—H2SB	0.9900
C11—H11A	0.9900	C2S—C3S	1.504 (4)
C11—H11B	0.9900	C3S—H3SA	0.9900

C11—C12	1.521 (3)	C3S—H3SB	0.9900
C12—H12A	0.9900		
N2—N1—C10	118.28 (15)	C14—C15—H15A	109.8
C5—N1—N2	111.06 (15)	C14—C15—H15B	109.8
C5—N1—C10	130.51 (15)	H15A—C15—H15B	108.2
C3—N2—N1	106.05 (15)	O2—C16—N17	122.97 (17)
C7—N8—C9	122.93 (16)	O2—C16—C6	123.14 (17)
C7—N8—C24	118.59 (16)	N17—C16—C6	113.89 (15)
C9—N8—C24	118.39 (15)	N17—C18—C19	117.07 (17)
H13A—N13—H13B	104 (2)	N17—C18—C23	124.12 (17)
C12—N13—H13A	107.5 (18)	C23—C18—C19	118.80 (17)
C12—N13—H13B	106.0 (16)	C18—C19—H19	120.3
C14—N13—H13A	112.1 (18)	C20—C19—C18	119.37 (19)
C14—N13—H13B	112.7 (16)	C20—C19—H19	120.3
C14—N13—C12	113.49 (17)	N21—C20—C19	120.57 (19)
C16—N17—H17	116.8	N21—C20—H20	119.7
C18—N17—H17	116.8	C19—C20—H20	119.7
C18—N17—C16	126.44 (16)	N21—C22—H22	119.2
C20—N21—H21	111.8 (19)	N21—C22—C23	121.56 (19)
C22—N21—H21	127.0 (19)	C23—C22—H22	119.2
C22—N21—C20	121.14 (18)	C18—C23—H23	120.7
N2—C3—H3	124.3	C22—C23—C18	118.54 (19)
N2—C3—C4	111.32 (17)	C22—C23—H23	120.7
C4—C3—H3	124.3	N8—C24—H24A	109.5
C3—C4—C9	130.66 (17)	N8—C24—H24B	109.5
C5—C4—C3	105.21 (17)	N8—C24—C25	110.91 (15)
C5—C4—C9	124.12 (17)	H24A—C24—H24B	108.0
N1—C5—C4	106.34 (15)	C25—C24—H24A	109.5
N1—C5—C6	134.11 (17)	C25—C24—H24B	109.5
C4—C5—C6	119.45 (17)	C26—C25—C24	119.91 (18)
C5—C6—C16	125.82 (16)	C26—C25—C30	119.04 (19)
C7—C6—C5	115.41 (16)	C30—C25—C24	121.04 (17)
C7—C6—C16	118.73 (16)	C25—C26—H26	119.9
N8—C7—H7	117.5	C25—C26—C27	120.13 (19)
C6—C7—N8	125.08 (17)	C27—C26—H26	119.9
C6—C7—H7	117.5	C26—C27—Cl1	118.55 (16)
O1—C9—N8	120.51 (18)	C28—C27—Cl1	121.15 (17)
O1—C9—C4	126.49 (18)	C28—C27—C26	120.31 (19)
N8—C9—C4	113.00 (15)	C27—C28—Cl2	120.35 (17)
N1—C10—H10	108.3	C29—C28—Cl2	119.55 (17)
N1—C10—C11	111.73 (15)	C29—C28—C27	120.1 (2)
N1—C10—C15	111.64 (15)	C28—C29—H29	120.1
C11—C10—H10	108.3	C28—C29—C30	119.9 (2)
C11—C10—C15	108.42 (16)	C30—C29—H29	120.1
C15—C10—H10	108.3	C25—C30—H30	119.7
C10—C11—H11A	109.9	C29—C30—C25	120.53 (19)
C10—C11—H11B	109.9	C29—C30—H30	119.7
H11A—C11—H11B	108.3	H1SA—C1S—H1SB	108.0
C12—C11—C10	108.93 (17)	C2S—C1S—H1SA	109.3
C12—C11—H11A	109.9	C2S—C1S—H1SB	109.3
C12—C11—H11B	109.9	C3S^{i}—C1S—H1SA	109.3

N13—C12—C11	110.89 (18)	C3S^{i}—C1S—H1SB	109.3
N13—C12—H12A	109.5	C3S^{i}—C1S—C2S	111.6 (2)
N13—C12—H12B	109.5	C1S—C2S—H2SA	109.4
C11—C12—H12A	109.5	C1S—C2S—H2SB	109.4
C11—C12—H12B	109.5	H2SA—C2S—H2SB	108.0
H12A—C12—H12B	108.0	C3S—C2S—C1S	111.2 (3)
N13—C14—H14A	109.4	C3S—C2S—H2SA	109.4
N13—C14—H14B	109.4	C3S—C2S—H2SB	109.4
N13—C14—C15	110.95 (17)	C1S^{i}—C3S—H3SA	109.4
H14A—C14—H14B	108.0	C1S^{i}—C3S—H3SB	109.4
C15—C14—H14A	109.4	C2S—C3S—C1S^{i}	111.2 (3)
C15—C14—H14B	109.4	C2S—C3S—H3SA	109.4
C10—C15—H15A	109.8	C2S—C3S—H3SB	109.4
C10—C15—H15B	109.8	H3SA—C3S—H3SB	108.0
C14—C15—C10	109.49 (16)		
Cl1—C27—C28—Cl2	1.2 (2)	C7—C6—C16—N17	-41.4 (2)
Cl1—C27—C28—C29	-179.62 (16)	C9—N8—C7—C6	0.0 (3)
Cl2—C28—C29—C30	179.03 (16)	C9—N8—C24—C25	85.6 (2)
N1—N2—C3—C4	-0.4 (2)	C9—C4—C5—N1	-178.71 (17)
N1—C5—C6—C7	177.42 (19)	C9—C4—C5—C6	-1.9 (3)
N1—C5—C6—C16	-5.0 (3)	C10—N1—N2—C3	176.66 (16)
N1—C10—C11—C12	174.48 (17)	C10—N1—C5—C4	-176.07 (17)
N1—C10—C15—C14	-174.74 (15)	C10—N1—C5—C6	7.8 (3)
N2—N1—C5—C4	-0.8 (2)	C10—C11—C12—N13	57.7 (2)
N2—N1—C5—C6	-176.94 (19)	C11—C10—C15—C14	61.8 (2)
N2—N1—C10—C11	33.7 (2)	C12—N13—C14—C15	53.1 (2)
N2—N1—C10—C15	-87.9 (2)	C14—N13—C12—C11	-53.7 (3)
N2—C3—C4—C5	-0.1 (2)	C15—C10—C11—C12	-62.1 (2)
N2—C3—C4—C9	179.06 (19)	C16—N17—C18—C19	174.28 (17)
N8—C24—C25—C26	-109.55 (19)	C16—N17—C18—C23	-5.0 (3)
N8—C24—C25—C30	69.4 (2)	C16—C6—C7—N8	-178.49 (17)
N13—C14—C15—C10	-56.7 (2)	C18—N17—C16—O2	3.4 (3)
N17—C18—C19—C20	-179.07 (17)	C18—N17—C16—C6	-175.60 (16)
N17—C18—C23—C22	178.29 (18)	C18—C19—C20—N21	0.3 (3)
N21—C22—C23—C18	1.2 (3)	C19—C18—C23—C22	-1.0 (3)
C3—C4—C5—N1	0.5 (2)	C20—N21—C22—C23	-0.6 (3)
C3—C4—C5—C6	177.36 (17)	C22—N21—C20—C19	-0.1 (3)
C3—C4—C9—O1	1.4 (3)	C23—C18—C19—C20	0.2 (3)
C3—C4—C9—N8	-177.99 (19)	C24—N8—C7—C6	176.37 (17)
C4—C5—C6—C7	1.6 (3)	C24—N8—C9—O1	4.1 (3)
C4—C5—C6—C16	179.18 (17)	C24—N8—C9—C4	-176.45 (16)
C5—N1—N2—C3	0.7 (2)	C24—C25—C26—C27	179.46 (17)
C5—N1—C10—C11	-151.30 (19)	C24—C25—C30—C29	-178.86 (18)
C5—N1—C10—C15	87.1 (2)	C25—C26—C27—Cl1	179.47 (15)
C5—C4—C9—O1	-179.55 (19)	C25—C26—C27—C28	-0.9 (3)
C5—C4—C9—N8	1.0 (3)	C26—C25—C30—C29	0.1 (3)
C5—C6—C7—N8	-0.8 (3)	C26—C27—C28—Cl2	-178.44 (15)
C5—C6—C16—O2	-37.8 (3)	C26—C27—C28—C29	0.8 (3)
C5—C6—C16—N17	141.16 (18)	C27—C28—C29—C30	-0.2 (3)
C7—N8—C9—O1	-179.52 (17)	C28—C29—C30—C25	-0.3 (3)
C7—N8—C9—C4	0.0 (2)	C30—C25—C26—C27	0.5 (3)

C7—N8—C24—C25	-90.9 (2)	C1S—C2S—C3S—C1S^{i}	54.9 (3)
C7—C6—C16—O2	139.6 (2)	C3S^{i}—C1S—C2S—C3S	-55.2 (3)

Symmetry code: (i) -*x*+1, -*y*+1, -*z*+1.

Hydrogen-bond geometry (Å, º) for (2019gu0034_150k_sq)

D—H···*A*	*D*—H	H···*A*	*D*···*A*	*D*—H···*A*
N13—H13*A*···Cl3^{ii}	0.87 (3)	2.24 (3)	3.105 (2)	171 (2)
N13—H13*B*···Cl4^{iii}	0.89 (3)	2.33 (3)	3.155 (2)	153 (2)
N17—H17···Cl3	0.88	2.50	3.3636 (16)	167
N21—H21···Cl4^{iv}	0.90 (3)	2.10 (3)	2.9964 (18)	174 (3)
C7—H7···Cl3	0.95	2.84	3.4366 (19)	122
C10—H10···O2	1.00	2.32	2.953 (2)	120
C11—H11*B*···Cl4^{v}	0.99	2.91	3.795 (2)	150
C14—H14*B*···Cl2^{vi}	0.99	2.85	3.505 (2)	124
C14—H14*B*···N2^{vii}	0.99	2.59	3.451 (3)	145
C15—H15*A*···O2	0.99	2.55	3.071 (2)	113
C15—H15*B*···Cl1^{i}	0.99	2.97	3.744 (2)	135
C19—H19···Cl3	0.95	2.81	3.635 (2)	145
C20—H20···Cl4^{viii}	0.95	2.66	3.443 (2)	140
C22—H22···Cl3^{iv}	0.95	2.73	3.398 (2)	128
C23—H23···O2	0.95	2.18	2.789 (2)	121

Symmetry codes: (i) -*x*+1, -*y*+1, -*z*+1; (ii) *x*, *y*+1, *z*; (iii) -*x*, *y*+1/2, -*z*+3/2; (iv) *x*, -*y*+1/2, *z*+1/2; (v) -*x*, -*y*+1, -*z*+1; (vi) -*x*+1, *y*+1/2, -*z*+3/2; (vii) *x*, -*y*+3/2, *z*+1/2; (viii) -*x*, *y*-1/2, -*z*+3/2.

Document origin: *publCIF* [Westrip, S. P. (2010). *J. Apply. Cryst.*, **43**, 920-925].